Report on the Scientific Validation of PHT OLP Version 10.0

Ulrich Klaas
(ISOPHOT Data Centre at MPIA)

and

Phil Richards
(UK ISO Data Centre, CCLRC, RAL)

with contributions by:
Karsten Wilke, Csaba Kiss, Peter Ábrahám
and Mario Radovich
(ISOPHOT Data Centre at MPIA)

Version 1.0

April 09, 2002

Max-Planck-Institut für Astronomie, Heidelberg

Contents

1 Results and Achievements by PHT OLP V10.0 Scientific Validation 5

1.1 Processing and Calibration Upgrades from OLP9 to OLP10 5
1.1.1 Two-threshold deglitching for ramp processing 5
1.1.2 Glitch removal for PHT32 observations 5
1.1.3 Signal processing parameters in case of non-stabilized signals 5
1.1.4 Warning of residual drifts in FCS calibration 5
1.1.5 Further consolidation of flux dependent signal linearization and FCS characterization 7
1.1.6 Point spread function correction factors 7
1.1.7 Orbit dependent default responsivities 7
1.1.8 Application of default responsivities if FCS power is outside calibrated range 7
1.1.9 Application of average responsivities in mapping mode 7
1.1.10 Refinement of signal correction for chopped P2 photometry measurements 8
1.1.11 Extension of PHT-S dynamic spectral response calibration to longest exposure times 8
1.1.12 Relative intensity profiles for multi-aperture measurements 8
1.1.13 Statistical flat-field correction for PHT-C raster maps 8
1.1.14 On-source coordinates for rectangular chopped measurements 8
1.1.15 World coordinates in maps 9
1.2 Definition of Photometric Accuracies 10
1.3 Re-validation of Staring Mode Photometry and Achieved Accuracies 11
1.3.1 Multi-filter Staring Modes 11
1.3.2 Absolute Photometric Modes 11
1.3.3 Multi-filter Sparse Map Photometric Modes 11
1.3.4 Default Responsivity Calibration 11
1.3.5 Limitations in Staring On-Off Photometry Accuracy 11
1.4 Re-validation of Spectroscopy and Achieved Accuracies 13
1.4.1 Spectroscopy in Staring Mode on Point Sources 13
1.4.2 Spectroscopy in Staring Mode on Extended Sources 13
1.4.3 Spectroscopy in Chopped Mode 13
1.4.4 Spectroscopy in Raster Mode 13
1.5 Re-validation of Raster Mode Photometry and Achieved Accuracies 15
1.5.1 PHT22 Raster Maps 15
1.5.2 PHT03 Nodding 16
1.5.3 PHT22 Nodding 16
1.6 Validation of Chopped Photometry and Achieved Accuracies 17
1.7 Scientific Assessment of Multi-aperture Photometry 20
1.8 Scientific Assessment of Chopped High Resolution Mapping (PHT32) 21
1.9 ISOPHOT Photometric Calibration Accuracy Overview 22
1.10 General Accuracy Limitations of OLP Processing 23
1.11 Areas of Improved Processing by Interactive Data Analysis 24
1.12 Status of Scientific Validation of PHT AOTs 25

2 Known Limitations and Caveats **27**
2.1 Validity Ranges of FCS Calibration Files . . . 27
2.2 Inhomogeneous FCS Illumination of PHT-P Apertures . . . 29
2.3 Non-geometric Aperture Beam Size Scaling . . . 29
2.4 Non-linearity of Detector Responsivity with Flux . . . 30
2.5 Detector Signal Transients . . . 30
2.6 Long Term Detector Drifts . . . 31
2.7 Error Calculation and Propagation . . . 32
2.8 Limitations in Use of PHT Color Correction Factors . . . 32
2.9 Incomplete Raster Map Appearance in Case of Zero Signal Flag . . . 33
2.10 Application of Point Spread Function Fraction Factors to AAR Data Products 33
2.11 Residual Flat-field Structures in PHT22 Raster Maps . . . 34
2.12 Point Source Photometry from Staring Mode Raster Mini-Maps . . . 34
2.13 Filters with Less Reliable Photometry . . . 35
2.14 Limitations of PHT-S Dynamic Spectral Response Calibration . . . 35
2.15 Limitations in Accuracy of Spectrophotometry for Pointings not Centered in the Aperture of PHT-S . . . 36

3 Prerequisites for OLP Scientific Validation **37**

4 Overview of Software and Calibration File Changes and Updates by SVP **39**

5 Staring Mode Photometry **41**
5.1 Consistency Check of Multi-filter Photometry . . . 42
5.1.1 PHT03 and PHT22 Multi-filter Photometry: The SED of α Bootes (HR 5340) . . . 43
5.1.2 PHT03 and PHT22 Multi-filter Photometry: The SED of γ Draconis (HR 6705) . . . 49
5.1.3 PHT03 Multi-filter Photometry: The SED of Sirius (HR 2491) . . . 60
5.1.4 PHT03 Multi-filter Photometry: The SED of HR 6847 . . . 63
5.1.5 PHT03 Multi-filter Photometry: The SED of HR 7469 . . . 66
5.1.6 PHT03 Multi-filter Photometry: The SED of HD 207129 . . . 69
5.1.7 PHT03 and PHT22 Multi-filter Photometry: The SED of Arp 220 . . . 73
5.1.8 PHT03 and PHT22 Multi-filter Photometry: The SED of NGC 6240 . . . 80
5.1.9 PHT03 Multi-filter Photometry: The SED of β Pictoris (HR 2020 / HD 39060) . . . 87
5.1.10 PHT03 Multi-filter Photometry in Non-standard Apertures . . . 90
5.2 Consistency Check of Absolute Photometry . . . 97
5.2.1 PHT05 and PHT25 Absolute Photometry: The SED of γ Draconis (HR 6705) . . . 98
5.2.2 PHT05 Absolute Photometry: The SED of Sirius (HR 2491) . . . 102
5.2.3 PHT05 Absolute Photometry: The SED of α Ari (HR 617) . . . 105
5.2.4 PHT25 Absolute Photometry: The SED of Uranus . . . 108
5.2.5 PHT05 Absolute Photometry in Non-standard Apertures . . . 111
5.3 Consistency Check of Sparse Map Photometry . . . 114
5.3.1 PHT17/19 and PHT37/39 Sparse Map On-Off Mode: The SED of HR 337 . . . 115
5.3.2 PHT17/19 and PHT37/39 Sparse Map On-Off Mode: The SED of Arp 244 . . . 118
5.3.3 PHT17/19 Sparse Map On-Off Mode: The SED of BS 5062 . . . 126
5.3.4 PHT17/18/19 and PHT37/38/39 Sparse Map Sequences: The 60 μm Flux of the Faint Star HR 5981 . . . 131
5.3.5 PHT37/38/39 Sparse Map Sequence: The 90 μm Flux of the Faint Star IRC+60228 . . . 136

6 Raster Map Photometry **140**
6.1 Consistency Check of Mini-map Photometry . . . 141
6.1.1 Point Source Photometry from PHT22 Mini-Maps: The SED of HR 7980 142
6.1.2 Point Source Photometry from PHT22 Mini-Maps: The SED of HR 1654 145
6.1.3 Point Source Photometry from PHT22 Mini-Maps: The SED of HR 7310 148
6.1.4 Point Source Photometry from PHT22 Mini-Maps: The SED of Sirius (HR 2491) . . . 151
6.1.5 Point Source Photometry from PHT22 Mini-Maps: The SED of Uranus 154
6.1.6 Point Source Photometry from PHT22 Mini-Maps: The 180 μm flux of α Ari (HR 617) . . . 157
6.1.7 Point Source Photometry from PHT22 Mini-Maps: The 90 μm flux of HR 6464 . . . 160
6.1.8 Point Source Photometry from PHT22 Mini-Maps: The 60 μm flux of HR 7557 (HD 187642, α Aql) . . . 164
6.1.9 Point Source Photometry from PHT22 Mini-Maps: The 60 μm flux of HR 7469 (HD 185395) . . . 167
6.1.10 Point Source Photometry from PHT22 Mini-Maps: The 60 μm flux of HD 185144 . . . 170
6.1.11 Point Source Photometry from PHT22 Mini-Maps: The FIR SED of Vega (HR 7001) . . . 173
6.1.12 Point Source Photometry from PHT22 Mini-Maps: The FIR SED of HD 169142 . . . 176
6.1.13 Point Source Photometry from PHT22 Mini-Maps: The FIR SED of HD 216956 (Formalhaut) . . . 179
6.1.14 Point Source Photometry from PHT22 Mini-Maps: The SED of the Quasar PG 1700+518 . . . 183

7 Nodding Photometry **186**

8 Chopped Photometry **187**
8.1 Chopped Photometry Test Cases with Quasi-simultaneous Staring Mode References and Reproducibility Checks . . . 188
8.1.1 PHT03 and PHT22 Multi-filter Chopped Photometry: The SED of IRAS 03068-5346 . . . 189
8.1.2 Comparison of PHT03 and PHT22 Chopped and Staring Mode Photometry of Standard Stars from the Empirical Signal Correction Calibration Program . . . 194
8.1.3 PHT03 and PHT22 Chopped Photometric Results for the Faint Point Source Detection Limit Program . . . 206
8.1.4 PHT03 and PHT22 Chopped Photometry of Stars Observed by the MFAINT and CFAINT Programs . . . 212
8.1.5 Reproducibility Assessment of PHT03 and PHT22 Chopped Mode Photometry from CFAINT Program . . . 221
8.2 Chopped Photometry Test Cases with Staring Mode References on other Revolutions . . . 232
8.2.1 PHT03 and PHT22 Chopped Mode: The FIR Excess SED of Vega . . 233
8.2.2 PHT03 Chopped Mode: The SED of Sirius (HR 2491) . . . 238
8.2.3 PHT03 Chopped Mode: The SED of HR 337 . . . 241
8.2.4 PHT03 Chopped Mode: The SED of HR 617 . . . 244
8.2.5 PHT03 Chopped Mode: The SED of HR 6847 . . . 247
8.2.6 PHT03 and PHT22 Chopped Mode: The SED of HR 7469 . . . 251
8.2.7 PHT03 and PHT22 Chopped Mode: The SED of HR 7557 . . . 254
8.2.8 PHT22 Chopped Mode: The SED of HD 216956 (Formalhaut) . . . 257
8.2.9 PHT03 and PHT22 Chopped Mode: The SED of the Quasar PG 1700+518 260
8.3 Chopped Observations of Known Sources . . . 263
8.3.1 PHT03 and PHT22 Chopped Mode: The SEDs of Stars with Known Fluxes . . . 264

9 Multi-aperture Photometry **278**

10 Chopped High Resolution Mapping **279**

11 Staring Mode Spectroscopy **280**
11.1 Consistency Check of Calibration Method with Calibration Standards 281
11.1.1 PHT40 Spectroscopy: Consistency Check of PHT-S Dynamic Response Calibration on Calibration Stars 282
11.1.2 PHT40 Spectroscopy: Consistency Check of PHT-S Dynamic Response Calibration Extension for Measurements Greater Equal 1024 Seconds 289
11.2 Comparison with Stellar Models for Non-calibration Stars 304
11.2.1 PHT40 Spectroscopy: MIR Spectra of Stars from Staring On and Off PHT-S Measurements 305
11.3 Comparison with Ground-based Spectroscopy 310
11.3.1 PHT40 Spectroscopy: MIR Spectra of Galaxies from Staring PHT-S Measurements 311
11.3.2 PHT40 Spectroscopy: MIR Spectra of Planetary Nebulae from Staring PHT-S Measurements 315
11.4 Comparison with IRTS spectra 325
11.4.1 PHT40 Spectroscopy: Cross-calibration of IRTS and ISOPHOT-S on HR 7980 (ω Cap) 326
11.4.2 PHT40 Spectroscopy: Spectra of the Carbon Star U Cam and the S-type Star S Cas 327
11.5 Measurements out of Calibrated Range 330
11.5.1 PHT40 Spectroscopy: Stellar Spectra with Measurement Conditions outside the Calibrated Range 331

12 Chopped Mode Spectroscopy **335**
12.1 Consistency Check of Calibration Method with Calibration Standards 336
12.1.1 PHT40 Spectroscopy: Consistency Check of Chopped PHT-S Relative Spectral Response Function on Calibration Stars for Different Chopper Modes 337
12.2 Comparison with Stellar Models for Non-calibration Stars 342
12.2.1 PHT40 Spectroscopy: MIR Spectra of the Stars HD 23763, HR 7428 and HD 23441 from Chopped PHT-S Measurements 343
12.3 Comparison with Ground-based Spectroscopy 347
12.3.1 PHT40 Spectroscopy: MIR Spectra of a Symbiotic Star and a Nova from Chopped PHT-S Measurements 348
12.3.2 PHT40 Spectroscopy: MIR Spectra of Galaxies from Chopped PHT-S Measurements 351

13 Raster Mode Spectroscopy **370**

14 Conclusions and Outlook **371**

Chapter 1

Results and Achievements by PHT OLP V10.0 Scientific Validation

1.1 Processing and Calibration Upgrades from OLP9 to OLP10

In Table 1.1 we list the major calibration upgrades which were implemented for OLP10 and describe which AOTs or AOT submodes were affected by the individual upgrades. There are two calibration upgrades which are part of the formal OLP/CALG delivery, but which are standalone and are not used by the OLP processing. They are or can be used in the Interactive Analysis environment.

1.1.1 Two-threshold deglitching for ramp processing

Following the detection of a glitch along the sequence of read-outs of a ramp the threshold is reduced giving a more efficient glitch detection, in particular for glitch tails. For ramps with at least 32 read-outs the threshold is reduced from 4.0 sigmas to 1.0 sigma until the end of the ramp or when the difference is below 1.0 sigma.

1.1.2 Glitch removal for PHT32 observations

Due to the fast chopper sweeps applied in PHT32 measurements, usually each chopper plateau comprises only a small number of ramps and each ramp a small number of read-outs. Hence the OLP standard deglitching algorithm was not adequate and practically no deglitching was performed for PHT32 observations. Similar to the processing for single pointing chopped measurements, the difference signals between adjacent read-outs are used rather than the slopes of the complete ramps and the signal per chopper plateau is determined by using the robust bi-weight mean method.

1.1.3 Signal processing parameters in case of non-stabilized signals

In case of the Mann test finding a non-stabilized signal at the end of the measurement, the best parameters for deriving an average signal are: the last 7 data points or the last 8 seconds of data whichever is longer in time. So far only the last 7 data points were used, regardless whether they correspond to at least 8 seconds of data or not. Thus, it was possible, that an amount of data less than 8 seconds was averaged which is now corrected.

1.1.4 Warning of residual drifts in FCS calibration

The usual exposure time of FCS measurements is 32 s. This is sometimes too short to achieve a stabilized signal. Since the absolute signal of the FCS measurement determines the responsivity and hence the absolute flux calibration, any unstabilized FCS signal has

Table 1.1: Processing and calibration upgrades from OLP 9.0 to OLP 10.0 and impact on the different AOT modes

	calibration upgrade	**affects AOT**
1)	two-threshold deglitching for ramp processing	all AOTs, except PHT32 for staring mode only
2)	glitch removal for PHT32 observations	PHT32
3)	signal processing parameters in case of non-stabilized signals	all AOTs, except PHT32 for staring mode only
4)	warning of residual drifts in FCS calibration	all AOTs, except PHT40
5)	further consolidation of flux dependent signal linearization and FCS characterization	all AOTs, except PHT40
6)	point spread function correction factors	all AOTs, except PHT40
7)	orbit dependent default responsivities	all AOTs, except PHT40
8)	application of default responsivities if FCS power is outside calibrated range	all AOTs, except PHT40
9)	application of average responsivities in mapping mode	PHT03, PHT22, in raster mode PHT32
10)	refinement of signal correction for chopped P2 photometry measurements	PHT03, in chopped mode
11)	extension of PHT-S dynamic spectral response calibration to longest exposure times	PHT40, in staring mode
12)	relative intensity profiles for multi-aperture measurements	PHT04, in staring mode
13)	statistical flat-field correction for PHT-C raster maps	PHT22, in raster mode PHT32
14)	on-source coordinates for rectangular chopped measurements	PHT03, PHT22, PHT40, in chopped mode
15)	world coordinates in maps	PHT03, PHT22, in raster mode PHT32

direct impact on the absolute calibration accuracy. In case of unstabilzed FCS signals, warning messages are written to the headers of the SPD and AAR products.

1.1.5 Further consolidation of flux dependent signal linearization and FCS characterization

The linearization tables P%%SLINR were updated with regard to the following aspects:

a) new input calibration data on Uranus and Neptune were available;

b) the linearization solution was made independent of orbital dependence;

c) analysis of many linearized observations gave a better understanding of the linearization curves.

Since linearization curves and FCS power files are linked together, both were updated consistently, i.e. also new CalG tables P%%ILLUM, P%%FCSPOW, P%%FLAT and PPFTOF were generated. Artificial features in multi-filter measurements flagged in the caveat "Filters with less reliable photometry" of the OLP 9.0 Scientific Validation Report [1] are either removed or drastically reduced.

1.1.6 Point spread function correction factors

The point spread function correction factors of PHT-P apertures and PHT-C pixels were based on a two-mirror model with central obscuration of the primary. New psf factors (CalG files PPPSF and PCPSF) were computed taking a model for the secondary tripod into account. These updated psf factors were also used in the ISOPHOT flux calibration system 1.1.5.

1.1.7 Orbit dependent default responsivities

The relative orbit dependence of the default responsivities was based on an OLP 7 processing of the FCS measurement data base. This processing did not include linearity correction, so that some scatter in the resulting responsivities was introduced by the lack of this correction impacting also on the relative orbit shape. For P3, C100 and C200, showing strong orbit dependence of the default responsivity, the FCS measurement data set was reprocessed using the correct OLP 10 calibration. Linear least median square fits were applied to the data and bootstrapping on 500 data sets per detector and time dependence was performed to derive the uncertainties. The time dependent CalG files PPRESP_01, PPRESP_02, PC1RESP_01, PC1RESP_02, PC2RESP_01, and PC2RESP_02 were revised.

1.1.8 Application of default responsivities if FCS power is outside calibrated range

In particular for P1, tests showed that more accurate photometry results were achieved when using the default responsivity rather than the extrapolation of the FCS power curves. As soon as the FCS heating power is outside the calibrated range for the respective filter, default responsivities are used in calibration. This holds for staring, absolute, raster and chopped photometry. Information messages are written to the SPD product header.

1.1.9 Application of average responsivities in mapping mode

The linear interpolation between two bracketting FCS measurements in mapping modes was found to be not adequate to correct for long term non-linear drifts and also not to be transparent to the user which responsivity value was applied to which data point. To simplify this the responsivities are now averages of the two FCS measurements, provided both are of good quality. If both are outside the calibrated FCS heating power range, default responsivities are used (see 1.1.8). If only one good FCS measurement is available, this one will be taken. This is in particular important for sparse map measurements where the FCS settings can be different.

1.1.10 Refinement of signal correction for chopped P2 photometry measurements

P2 chopped photometry uses now orbit dependent default responsivities rather than responsivites derived from the chopped FCS measurements. A more systematic chopped signal correction could be established, showing that:

a) the signal loss grows with the chopper frequency for chopper plateaux times < 32 seconds.

b) for the same chopper plateau time the signal loss is relatively stronger for small signal differences.

CalG file PP2CHOPSIG was revised. Due to the new correction scheme, the asymmetry correction has been removed. This is the case for P1 chopped observations, too, for which no signal correction at all is applied.

1.1.11 Extension of PHT-S dynamic spectral response calibration to longest exposure times

There are no PHT-S calibration star measurements longer than 1024 s, in fact most exposures of calibration stars are less equal 512 s. The dynamic spectral response calibration was restricted to the first 1024 s. Good quality measurements of 1024 s up to 4096 s were used for self-calibration in that respect, that the flux was predicted from the first 512 s of the measurement, which is based on calibration standards, and transferred to the remaining exposure time. The consistency of the method was checked for the standard star measurements of 1024 s. Consequently the conversion factors in the CalG file PSDYNAMIC were updated and the weights in PSDYNWT adapted.

1.1.12 Relative intensity profiles for multi-aperture measurements

In ESA SP-455 (ISO Beyond Point Sources), page 41, T.G. Mueller described a method how to make scientific use out of multi-aperture measurements (PHT04), provided the source is as compact as 2 arcmin. The background signal is derived from the annulus formed by the 120 and 180 arcsec apertures of the on-source measurement. Therefore, only measurement sequences with these two apertures and at least two smaller ones are processed in this way. The background for all apertures has to be scaled with regard to the 180 arcsec aperture applying non-unity correction factors to the geometrical aperture area ratios. These were determined from consistency checks of many measurements using this method. A signal normalized to the one in the 180 arcsec aperture is constructed which is the same as the flux ratio of both apertures. In comparison with the profiles of true point sources available in the data base, the normalized psf fraction (see item 6), and the profiles of flat sky sequences, this allows to determine the extension of a source or the presence of a companion. The normalized fluxes are written to the header of the AAR product. In addition source and background signals are written to the header of the SPD product. The aperture correction factors for the background scaling have been hardcoded, no CalG file was generated.

1.1.13 Statistical flat-field correction for PHT-C raster maps

If the extent of the PHT22 or PHT32 raster map exceeds 20 raster points or plateaux, a statistical flat-field is determined from the ratio of the %10tile of the surface brightness of each pixel to the average %10tile for all pixels. These correction factors are applied to the PGAI products and are written to the product header.

1.1.14 On-source coordinates for rectangular chopped measurements

So far pointing information in the product headers is related to the telescope pointing. In the case of rectangular chopped measurements the telescope pointing is, however, in between the on-source and the off-source position and the target position is not given. This is now provided by the new pointing keywords CONSCRA and CONSCDEC which are derived from the corrected telescope pointing information CINSTRA, CINSTDEC and CINSTROL

and the chopper amplitude. The new keywords for the target position are given for all observing modes, hence their values are identical with the telescope pointing for all modes except rectangular chopped mode.

1.1.15 World coordinates in maps

In PGAI products the world coordinate set CD1_1 to CD3_3 has been added, however with the restriction that axis 3 remains an index rather than a wavelength due to the inhomegeneous spacing of the ISOPHOT filter central wavelengths. For compatibility the old keywords CDELTi and CROTAi (i=1,2,3) are still provided.

1.2 Definition of Photometric Accuracies

Global calibration accuracies have been estimated from the investigation of the test cases and the comparison with published reference photometry. They can be applied, if not one of the caveats on photometry applies, cf. Sect. 2.
The terms **absolute accuracy**, **relative accuracy** and **reproducibility** have been defined in the following context:

- **absolute accuracy** is the accuracy achieved w.r.t. the reference photometry, if the filter measurement had a corresponding FCS transfer measurement in the same filter. Hence, the quality of the FCS calibration against celestial standards is directly verified. Note that no calibration accuracy of the reference photometry (models, IRAS) has been taken into account, as this is beyond the scope of this report. A typical order of the absolute accuracy of the reference photometry is $2 - 10\%$. Table 1.2 lists the achieved values per detector and flux range.

- **relative (filter-to-filter) accuracy** is the accuracy achieved w.r.t. the reference photometry, if the filter measurement was not performed in the filter in which the FCS calibration was done. Currently, assumptions about the constancy of the responsivity over the full flux range and for all filters, and, related to that relative filter-to-filter correction factors, apply. It has been proven that this is in general not correct, and it is considered that in future OLP versions corrections for non-linearities of the responsivity with the in-band power will be applied. Hence, the relative uncertainty can be much larger than the absolute one in multi-filter measurements with certain source SEDs. Table 1.2 lists the achieved values per detector and flux range. The number of suitable test cases performed in multi-filter mode is much smaller than the number of test cases in any of the absolute measurement modes (i.e. with an FCS measurement in the respective filter). The relative filter-to-filter accuracy could only be established for a minor subset.

- absolute and relative accuracy are assumed to add to the total photometric uncertainty. In multi-filter measurements with one FCS measurement the absolute measurement uncertainty is subtracted from all measurements in non-FCS filters in order to derive the relative measurement accuracy.

- **reproducibility** is the relative consistency of measurements repeated several times with the same measurement set-up. It is a measure of the internal stability of the instrument and describes also the current limitations in signal processing. Table 1.3 lists the achieved values per detector both for a bright secondary standard and a faint source. These values were obtained from special calibration monitoring programs performed during ISO's Routine Phase [18].

1.3 Re-validation of Staring Mode Photometry and Achieved Accuracies

1.3.1 Multi-filter Staring Modes

The PHT staring photometric modes PHT03 and PHT22 OLP processing was successfully re-validated. This includes extended source photometry with PHT-C (PHT22), cf. Table 1.7. There is some improvement in both absolute and relative calibration by this OLP version, see Table 1.2. An overview on the calibration reproducibility is given in Table 1.3. For OLP 9.0 we found that for some filters and some flux ranges the photometry was less reliable. With this version the number of affected filters could be reduced and the quality be improved, but there are still some systematic outliers. This has been flagged in the Caveat Sect. 2.13 which also gives a revised assessment.

1.3.2 Absolute Photometric Modes

The PHT absolute photometric modes PHT05 and PHT25 OLP processing was successfully re-validated. The calibration accuracies of this mode are also given in Table 1.2.

1.3.3 Multi-filter Sparse Map Photometric Modes

The PHT sparse map photometric modes PHT17/18/19 and PHT37/38/39 OLP processing was successfully re-validated. The calibration accuracies of this mode are also given in Table 1.2.

1.3.4 Default Responsivity Calibration

For all three staring modes several test cases have shown considerably improved photometry when using default responsivity calibration instead of the actual responsivity calibration, if the FCS heating power was outside the calibrated range.

1.3.5 Limitations in Staring On-Off Photometry Accuracy

The scientific assessment has shown that the quoted accuracies hold down to certain flux levels only. Below those fluxes the accuracies can become considerably worse.

OLP 10 on-off photometry gives reliable accuracies at least down to the following flux limits:

1) **ISOPHOT-P1: ~0.5 Jy**
2) **ISOPHOT-P2: ~0.5 Jy**
3) **ISOPHOT-P3: ~1.5 Jy**
4) **ISOPHOT-C100: ~1.5 Jy**
5) **ISOPHOT-C200: ~2.0 Jy**

The possible reasons for these limitations are:

1) S/N limitations of the respective measurement.
2) Residual systematic calibration effects (under investigation).
3) Cirrus confusion for wavelengths longward of 80 μm.

Cirrus confusion may have a significant impact on FIR staring on-off photometry for wavelengths longward of 80 μm, in particular since only one sky reference position is used and off-positions can be several arcmin away from the on-source position. For bright backgrounds (several 10 MJy sr^{-1}) cirrus confusion noise up to several Jy can be possible. Reference [39] gives the so far best prescription how to estimate the cirrus confusion noise for a certain measurement. Refinements of the estimates for the various instrument configurations are under preparation.

Table 1.2: Absolute and relative (filter-to-filter) calibration accuracies per detector achieved for various flux ranges in multi-filter and absolute mode with OLP V10.0. Bold values indicate an improvement w.r.t. OLP V9.0.

detector	**AOT mode**	**flux range** [Jy]	**abs. accuracy** [%]	**rel. accuracy** [%]	**standard**
P1	P03 off & on	300 - 6000	≤ 5	10	α Boo
P1	P03, P05 off & on	70 - 1250	10	≤ 30	γ Dra
P1	P03, P05 off & on	50 - 1000	< 10	< 10	Sirius
P1	P05 off & on	35 - 600	< 10	–	α Ari
P1	P03 off & on	0.6 - 6.5	< 10	$<$ **10**	HD 207129
P1	P03 off & on	0.8 - 3.5	< 5	5	HR 6847
P2	P03 off & on	100 - 200	≤ 7	5	α Boo
P2	P03, P05 off & on	25 - 40	< 5	5	γ Dra
P2	P05 off & on	~ 25	< 5	–	Sirius
P2	P05 off & on	13 - 20	< 10	–	α Ari
P3	P03 off & on	10 - 25	≤ 5	$\leq$ **5**	α Boo
P3	P03, P05 off & on	~ 5	< 7	–	γ Dra
P3	P17/18/19 4 times	~ 0.15	$\leq$ **10**	–	HR 5981
C100	P22 off & on	6 - 25	6	$\leq$ **15**	α Boo
C100	P22, P25 off & on	~ 5	20	20	γ Dra
C200	P25 off & on	500 - 900	$\leq$ **5**	–	Uranus
C200	P22 off & on	2 - 5	8	20	α Boo
C200	P25 off & on	~ 0.5	10	–	γ Dra

Table 1.3: Relative Calibration Reproducibility Accuracy per Detector for Bright and Faint Fluxes from Monitoring Programs in Staring Mode.

detector	**target**	**flux** [Jy]	**relative accuracy** **1** σ [%]
P1	NGC 6543	8	5
P1	HD 172323	0.085	10
P2	NGC 6543	100	2
P2	HR 5986	0.67	12
P3	NGC 6543	100	7
P3	HR 7310	0.67	7
C100	NGC 6543	50	3
C100	HR 7310	0.21	20
C200	NGC 6543	11	10
C200	HR 6705	0.67	7

1.4 Re-validation of Spectroscopy and Achieved Accuracies

1.4.1 Spectroscopy in Staring Mode on Point Sources

The PHT OLP processing of the spectroscopic mode PHT40 staring on point sources was successfully re-validated. The dynamic spectral response function calibration on faint source level could be improved, for an overview of the calibration accuracies of this mode, see Table. 1.4.

1.4.2 Spectroscopy in Staring Mode on Extended Sources

The PHT OLP processing of the spectroscopic mode PHT40 staring on extended sources was successfully re-validated. The dynamic spectral response function calibration on faint source level could be improved, for an overview of the calibration accuracies of this mode, see Table 1.5.

1.4.3 Spectroscopy in Chopped Mode

The PHT OLP processing of the spectroscopic mode PHT40 OLP chopping was successfully re-validated. For an overview of the calibration accuracies of this mode, see Table. 1.6. The quoted accuracies apply to flux levels down to about $7 \times 10^{-14}\,\mathrm{W\,m^{-2}\,\mu m^{-1}}$ for PHT-SS, corresponding to around 400 mJy at 4 μm and $7 \times 10^{-15}\,\mathrm{W\,m^{-2}\,\mu m^{-1}}$ to $10^{-14}\,\mathrm{W\,m^{-2}\,\mu m^{-1}}$ for PHT-SL, corresponding to 150 – 210 mJy at 8 μm, for typical on-source exposure times of 512 s. These flux limits scale with the square root of the on-source exposure time.

1.4.4 Spectroscopy in Raster Mode

Due to the unpredictable illumination history the dynamic spectral response function calibration cannot be applied to the PHT40 raster mode. The application of a static spectral response function calibration and hence no transient correction limits the accuracy of this submode to 30 % absolute and 30 % relative.

Table 1.4: Absolute and relative (spectral shape) calibration accuracies per detector for staring spectrophotometry achieved for various flux ranges with OLP V10.0.

detector	**AOT mode**	**flux range** [Jy]	**abs. accuracy** [%]	**rel. accuracy** [%]	**standard**
SS	P40 off & on	2000 - 8000	< 5	< 10	HR 5340
SS	P40 off & on	800 - 2500	< 5	< 10	HR 337
SS	P40 off & on	250 - 850	< 5	< 15	HR 617
SS	P40 off & on	150 - 500	~ 5	< 10	HR 7001 (Vega)
SS	P40 off & on	120 - 400	< 5	< 10	HR 7980
SS	P40 off & on	70 - 240	~ 10	< 20	HR 7924
SS	P40 off & on	6 - 20	< 5	< 15	HR 7469
SS	P40 off & on	1 - 4	~ 5	< 10	HR 8487
SL	P40 off & on	500 - 1800	< 5	< 10	HR 5340
SL	P40 off & on	200 - 700	< 5	< 10	HR 337
SL	P40 off & on	60 - 210	< 5	< 10	HR 617
SL	P40 off & on	30 - 110	~ 5	< 10	HR 7001 (Vega)
SL	P40 off & on	30 - 110	< 5	< 10	HR 7980
SL	P40 off & on	15 - 50	~ 10	< 20	HR 7924
SL	P40 off & on	1 - 5	< 5	< 15	HR 7469
SL	P40 off & on	0.2 - 0.7	~ 10	< 20	HR 8487

Table 1.5: Calibration Accuracy for Spectrophotometry with PHT-S for Extended Sources for Various Flux Ranges with OLP V10.0. The relative accuracy is a measure of the relative spectral shape. The absolute accuracy depends highly on the exposure time, it can be as good as 10 %. The Zodiacal Light background is too faint in the SS range to be detected with sufficient S/N.

detector	**flux range** [MJy sr^{-1}]	**absolute accuracy** [%]	**relative accuracy** [%]	**standard**
SL	3 - 20	10 - < 50	20	COBE/DIRBE

Table 1.6: Absolute and relative (spectral shape) calibration accuracies per detector for chopped spectrophotometry achieved for various flux ranges with OLP V10.0. RC = rectangular chopping, TC = triangular chopping, SC = sawtooth chopping.

detector	**AOT**	**flux range** [Jy]	**abs. accuracy** [%]	**rel. accuracy** [%]	**standard**
SS	P40	4 - 15	∼5	< 10	HR 6817 (RC)
SS	P40	4 - 15	<5	< 10	HR 6817 (TC)
SS	P40	2 - 6	∼10	< 10	HR 6847 (RC)
SS	P40	2 - 6	<10	< 10	HR 6847 (TC)
SS	P40	0.4 - 1	∼10	< 10	HD 23367 (SC)
SL	P40	1 - 4	< 5	< 10	HR 6817 (RC)
SL	P40	1 - 4	< 5	< 10	HR 6817 (TC)
SL	P40	0.4 - 1.5	< 5	< 10	HR 6847 (RC)
SL	P40	0.4 - 1.5	< 10	< 10	HR 6847 (TC)
SL	P40	0.15 - 0.24	< 10	< 20	HR 23367 (SC)

1.5 Re-validation of Raster Mode Photometry and Achieved Accuracies

1.5.1 PHT22 Raster Maps

Surface brightness photometry

Surface brightness photometry of PHT-C raster maps was cross-checked with COBE/DIRBE photometry (this includes single pointing background measurements). By finding a good consistency this mode was successfully revalidated, see Table 1.7 for a summary of the results.

Table 1.7: Calibration Accuracy per Detector for Extended Sources for Various Flux Ranges with OLP V10.0. The range for which both absolute and relative accuracies can be given is covered for PHT-C by multi-filter background measurements, while the larger range is covered by raster maps.

detector	**flux range** [MJy sr^{-1}]	**absolute accuracy** [%]	**relative accuracy** [%]	**standard**
C100	5 - 15	< 25	20	COBE/DIRBE
	5 - 400	< 25	–	COBE/DIRBE
C200	4 - 10	< 25	20	COBE/DIRBE
	3 - 600	< 25	–	COBE/DIRBE

Flat-field accuracies

The flat-field accuracies could be considerably improved and residual flat-field patterns be removed by applying a statistical correction derived from the maps themselves (provided they have a minimum number of 20 raster positions). The flat-field accuracies are listed in Table 1.8).

Table 1.8: Flat-field (ff) accuracies for ISOPHOT-C P22 raster maps. The ff accuracies are determined as ratio of the standard deviation of the mean background surface brightness to the mean surface brightness value for a flat sky background field with no sources. They are filter independent. There is some trend that for the same set of raster parameters the ff accuracy improves with increasing absolute surface brightness. For C100 the ff accuracy can vary over the map area.

detector	**flat-field accuracy**	
	no pixel overlap (%)	**with pixel overlap** (%)
C100	4 - 10	3 - 6
C200	2 - 6	2 - 4

Point source photometry from mini-maps

The PHT-C staring mode raster map PHT22 OLP processing was successfully revalidated with regard to point source photometry from mini-maps. The accuracy of this photometric mode can be improved considerably when using the PCAS product, see Table 1.9 below. Using the PGAI products and aperture photometry gives an accuracy of only 30 % for point sources above 1 Jy for C100 and only 50 % for the full flux range of C200. The reason for this behaviour is not yet completely understood.

Table 1.9: Absolute calibration accuracies achieved for various flux ranges in mini-map mode using the PCAS data products and PCAS evaluation method .

detector	**flux range** [Jy]	**abs. accuracy** [%]	**standard**
C100	$1 - 5$	<10	Sirius
C100	0.9	<10	HR 7557
C100	0.5 - 1.6	**<10**	HR 1654
C100	0.4 - 1.2	**<10**	HR 7980
C100	>0.2	<30	HR 7310
C100	~ 0.12	<30	HR 6464
C100	~ 0.1	**<20**	HD 185144
C100	~ 0.05	<30	HD 185395
C200	$500 - 900$	**<10**	Uranus
C200	0.2- 0.4	**<15**	HR 1654
C200	0.25	**30**	HR 617
C200	0.15 - 0.3	**<25**	HR 7980

1.5.2 PHT03 Nodding

TBW

1.5.3 PHT22 Nodding

TBW

1.6 Validation of Chopped Photometry and Achieved Accuracies

Tables 1.10 and 1.11 present the compilation of the assessment of absolute accuracy, relative filter-to-filter accuracy, and reproducibility of chopped photometry products from the respective test cases.
It should also be noted that the SPD product contains now the so-called "chop pattern" which is a robust representation of the signal modulation for this measurement. This should be consulted to check whether the source was clearly detected.

Table 1.10: Absolute and relative (filter-to-filter) calibration accuracies per detector for chopped photometry achieved for various flux ranges in multi-filter mode with OLP V10.0.

detector	**AOT**	**flux range** [Jy]	**abs. accuracy** [%]	**rel. accuracy** [%]	**standard**
P1	P03	2 - 10	< 10	–	HR 6817
P1	P03	2.5	< 10	–	BS 5062
P1	P03	2.2	< 10	–	HR 5986
P1	P03	0.3 - 3.5	< 10	~ 25	HR 6847
P1	P03	0.06	< 25	–	HD 172323(6×)
P2	P03	20	< 15	–	Sirius
P2	P03	10	< 10	–	Vega
P2	P03	5	< 10	–	HR 7557
P2	P03	3.5	< 30	–	HR 7310
P2	P03	0.5	< 30	–	HR 5986(3×)
P2	P03	0.4	< 10	–	HR 5914
P2	P03	0.3	< 30	–	HR 5447
P2	P03	0.25	< 10	–	HR 7469
P2	P03	0.25	~ 20	–	PG 1700+518
P3	P03	7 - 19	< 25	–	HR 1457
P3	P03	7 - 9	< 15	–	Vega
P3	P03	2.5 - 8	< 10	< 20	HR 337
P3	P03	0.8 - 2.5	< 10	~ 25	HR 617
P3	P03	0.6	< 50	–	HR 7310(6×)
P3	P03	0.15 - 1	in general fluxes 40 - 70 % too low		
C100	P22	11	~ 20	–	HD 216956
C100	P22	1.5 - 2	< 20	< 20	HR 6705
C100	P22	0.4	~ 20	–	PG 1700+518
C100	P22	0.2	< 30	–	HR 7310(6×)
C200	P22	2 - 5	40	60	HR 5340
C200	P22	< 1	strong cirrus contamination for B > 5 MJy sr^{-1}		

Table 1.11: Relative Calibration Reproducibility Accuracy per Detector from Monitoring Programs in Chopped Mode. For C200 no number can be derived because of strong cirrus confusion of the target area.

detector	**target**	**flux** [Jy]	**relative accuracy** **1** σ [%]
P1	HR 6847	3.3	3
P1	HD 172323	0.064	16
P2	HR 5986	0.52	7
P3	HR 7310	0.59	12
C100	HR 7310	0.21	12

Based on this compilation and the results of the individual test case assessment the following conclusions can be drawn:

1) **ISOPHOT-P1:**
   Better than 25 % absolute over the full flux range 0.06 – 10 Jy. One open issue is the relative filter calibration for some test cases. Transient and beam effects may play a role. The relative reproducibility accuracy is 15 %.

2) **ISOPHOT-P2:**
   Better than 30 % absolute over the flux range from 0.25 – 20 Jy. There is not sufficient information on relative filter calibration accuracy. The relative reproducibility accuracy is < 10 %.

3) **ISOPHOT-P3:**
   Better than 30 % absolute in the flux range 1 – 20 Jy. Below 1 Jy, down to about 0.15 Jy, fluxes are in general too low by 40 - 70 % which might be due to a systematic calibration effect (under investigation). Due to the large apertures that may be in use, below 0.5 Jy at 100 μm cirrus confusion noise may have a significant impact on the final photometric accuracy. The relative filter calibration accuracy is ~ 25 %. The relative reproducibility accuracy is < 15 %.

4) **ISOPHOT-C100:**
   Better than 30 % absolute in the flux range 0.2 – 11 Jy. For wavelengths beyond 80 μm and expected fluxes below 0.2 Jy cirrus confusion can have a severe impact on the final calibration accuracy. Positive flux offsets at 60 μm for sources in the flux range 0.05 – 0.2 Jy might be due to a systematic calibration effect (under investigation). The relative filter calibration accuracy is ~ 20 %. The relative reproducibility accuracy is < 15 %.

5) **ISOPHOT-C200:**
   Suitable test cases are hard to find. The contamination by cirrus confusion is highest and noticable below expected fluxes of 1 Jy. The absolute accuracy for sources brighter than 1 Jy is better than 40 %. This has also an impact on the reproducibility where a strong trend was found for the test case when the chopper angle was rotating w.r.t. the sky.

Based on the results per detector listed above, chopped photometry with ISOPHOT-P and -C can be declared as scientifically valid, however, there are some restrictions and caveats. These are:

1) **Accuracies are in general poorer than for comparable staring mode measurements, in particular if the latter ones made use of optimized observing strategies.**

2) **Due to the restricted number of sky references, cirrus confusion is a limiting factor for measurements longward of 80 μm:**

   a) **For P3 measurements depending on aperture size and chopper throw below between 0.2 and 1 Jy.**

   b) **For C100 measurements (making use of the central pixel only) below 0.2 Jy.**

   c) **For C200 measurements (only 1 reference position!) below 1 – 2 Jy.**

   Reference [39] gives the so far best prescription how to estimate the cirrus confusion noise for a certain measurement. Refinements of the estimates for the various instrument configurations are under preparation.

1.7 Scientific Assessment of Multi-aperture Photometry

TBW

1.8 Scientific Assessment of Chopped High Resolution Mapping (PHT32)

TBW

1.9 ISOPHOT Photometric Calibration Accuracy Overview

Table 1.12 gives a summary overview of the achieved photometric accuracies for ISOPHOT with OLP 10. For the first time chopped observations are included. While 32 s is a standard on-source exposure time for bright sources in photometry mode, for faint sources and spectroscopy longer exposure times of at least 128 – 256 s are necessary in order to obtain a sufficient S/N. For the faint sources also the choice of an optimized observing mode was necessary, otherwise the quoted accuracies are not achieved. These accuracies are derived on a statistical basis as conservative numbers reflecting the general performance of the chain of calibration corrections for the respective wavelength or flux range. Individual measurements can have better or worse accuracies. Degradation of accuracy can happen due to unusual instrument configurations which are not properly covered by the calibration progrmas, space weather impact or a complex background structure. In the first case checking of processing warning flags in the product headers is advisable. Depending on the kind of warning interactive step-by-step processing may be necessary.

Table 1.12: ISOPHOT Photometric Calibration Accuracy Overview for OLP 10.

detector	source type point / extended	source brightness	typical on-source integration [s]	absolute accuracy [%]	reproducibility $1\,\sigma$ of 20 samples [%]	multi-filter accuracy [%]
P1	p, star	50 – 6000 Jy	32	<10	5	<20
P1	p, star	0.1 – 50 Jy	≤256	40	10	–
P1	p, chop	0.06 – 10 Jy	128	<25	<16	<25
P2	p, star	10 – 200 Jy	32	<10	2	5
P2	p, star	0.5 – 10 Jy	≤256	<15	12	–
P2	p, chop	0.2 – 20 Jy	128	<30	<10	–
P3	p, star	0.5 – 25 Jy	32	10	7	<10
P3	p, star	<0.5 Jy	≤256	20	7	–
P3	p, chop	≥0.8 Jy**	128	<25	<15	<25
C100	p, star	0.5 – 25 Jy	32	15	≥3	<25
C100	p, star	0.05 – 0.5 Jy	≤256	<25*	20	–
C100	e, star	5 – 15 MJy sr^{-1}	32	25	10	20
C100	p, chop	≥0.2 Jy**	128	<30	<15	<20
C200	p, star	1 – 900 Jy	128	10	10	20
C200	p, star	0.2 – 1 Jy	≤256	<20*	10	–
C200	e, star	4 – 10 MJy sr^{-1}	64	20	10	20
C200	p, chop	≥1.5 Jy**	128	<40	–	–
SS	p, star	1 – 6000 Jy	256	<10	–	<15
SS	p, chop	0.5 – 500 Jy	1024	<10	–	<10
SS	e, star	30 – 3000 MJy sr^{-1}	256	<10	–	<15
SL	p, star	0.3 – 1500 Jy	256	<10	–	<15
SL	p, chop	0.2 – 200 Jy	1024	<10	–	<10
SL	e, star	5 – 10000 MJy sr^{-1}	256	<10	–	<15

* for mini-map photometry using PCAS products
** for fainter fluxes careful estimate of cirrus confusion necessary

1.10 General Accuracy Limitations of OLP Processing

The previous sections provided an overview of the currently achievable average calibration accuracy using OLP products and Sect. 2 lists the conditions of limitations due to yet incomplete corrections or calibrations.
There are, however, a few general accuracy limitations which should be taken into account when using ISOPHOT OLP data products:

- **Accuracy Limitations of Celestial Standards**
  During the course of the ISO project considerable improvements for certain classes of standard sources have been achieved by new observational programmes and refined modelling. One specific case from which ISOPHOT calibration benefited a lot were the new thermophysical models of asteroids [31]. On the other hand, it has to be noted that in the FIR range the stellar spectra a very often extrapolations of measured SEDs up to at most 35 μm. In particular for faint standard stars (< 1 Jy) not much is known about the true SED in the FIR. There are indications that some standard stars do not have good flux predictions. Those will have to be identified by cross-calibration with other stars.

- **Measurement beyond Sensitivity Limit**
  There are measurements in the data base which did not apply the most optimal observing strategy (cf. [27], [28]). Then even the best reduction does not achieve a satisfying result. Sensitivity limits and the corresponding minimum exposure times are given in the above cited reference documents, which have been derived from actual ISOPHOT observations.

- **Confusion by Sky Background Structure**
  In the FIR the sky shows a significant structure, mainly due to IR cirrus (see [32] and [39] for a discussion on actual data). This sky confusion limits the ability to adequately determine a sky background and to derive accurate fluxes of faint sources. It can be partly circumvented by an optimized observing strategy (cf. [27], [28]) and by determining the sky background as close as possible to the source.

- **Processing Items which Require User Interaction**
  There are several processing steps from the raw data to the final data products for which interactive processing can provide much better results due to visual inspection of the intermediate data products and optimizing the processing parameters or due to interactive input by the user with regard to special properties of the source (extension, structure, etc.).

1.11 Areas of Improved Processing by Interactive Data Analysis

The provision of a percentage number characterizing which improvements in calibration accuracy can be obtained by careful interactive processing is currently not possible, since so far no comprehensive systematic investigation was performed. Interactive Analysis uses the same set of general calibration files (cal-G) as OLP. The limitations due to photometric bias, e.g. the accuracy of the standard source fluxes, fully apply to interactive calibration, too. One can expect, however, to achieve a higher accuracy with IA for the following cases (cf. [33] for a tutorial):

1) measurements with signal transients which do not stabilise during the measurement time, but which are long enough to perform a reasonable transient fit.

    a) PIA provides several transient correction tools. The most efficient ones are the ones for ISOPHOT-S based on the Fouks-Schubert model (full drift modelling and initial signal jump) and the empirical solution for FIR detectors (P3, C100, and C200) based on exponential functions.

    b) PIA allows to view the transient fitting and to accept or reject it.

2) correction of non-linear signal drifts in maps.

    a) The time sequence of the signals can be interactively inspected and non-linear baseline fits be applied in order to flatten the map.

3) detection of faint sources by refined deglitching and filtering.

    a) Individual ramps or signal sequences can be inspected by eye and can be deselected or corrected manually.

1.12 Status of Scientific Validation of PHT AOTs

With the finalisation of the OLP10.0 validation the validation status per AOT submode is given in Table 1.13.

Table 1.13: Scientific Validation of ISOPHOT OLP AOT Processing for the ISO Legacy Archive. The 11 AOTs have been divided into 28 submodes and the respective number of executed astronomical observations is given. An observation in multi-filter and multi-aperture mode can comprise several measurements. The sparse map modules have been counted individually. OLP Versions 5 and 6 were released during the ISO mission, OLP Version 7 is the end-of-mission pipeline, OLP Versions 8 and 9 were released during Post Operations Phase and OLP version 10 is the Legacy Archive Version. "No" means that the submode is still unvalidated in the Legacy Archive due to low priority or on-going calibration work and will be validated later during the Active Archive Phase.

AOT	observation type	submode	# of AOs	scientific validation with	comments
PHT03 (P)	multi-filter photometry	staring point source	961	V6	for standard apertures
		staring ext. source	270	no	
		nodding	230	V6	for standard apertures
		chopped	1134	V10	
		raster map	431	no	
PHT04 (P)	multi-aperture photometry	staring point source	219	V10	relative curve of growth
		staring ext. source	36	V10	for extent < 2 arcmin
		chopped	17	no	sequ: ≥ 4 aper. (120,180)
PHT05 (P)	absolute photometry	staring point source	57	V6	for standard apertures
		staring ext. source	162	no	
PHT17 (P) 18, 19	sparse map photometry	staring point source	682	V6	for standard apertures
		staring ext. source	524	no	
PHT22 (C)	multi-filter photometry	staring point source	373	V7	
		staring ext. source	123	V7	
		nodding	29	V7	
		chopped	1887	V10	limited by sky confusion
		raster map	2884	V8.4	ff quality for >20 RP
PHT25 (C)	absolute photometry	staring point source	54	V7	
		staring ext. source	149	V7	
PHT32 (C)	oversampled mapping	chopped mapping	1565	V10	partially validated w.r.t. SB, ff quality
PHT37 (C) 38, 39	sparse map photometry	staring point source	2109	V7	
		staring ext. source	710	V7	
PHT40 (S)	spectroscopy	staring point source	835	V5	
		staring ext. source	102	V6	
		chopped	412	V6	
		raster map	135	V6	
PHT50 (P)	aperture polarimetry	staring point & ext. source	15	V7	interactive processing & special FORTRAN routine
PHT51 (C)	array polarimetry	staring point & ext. source	110	V7	interactive processing & special FORTRAN routine
		raster		V7	beam effects for ext. sources?

In Table 1.14 we list the validated modes per detector sub-system. For completeness we have added the polarisation modes which can only be evaluated interactively using PIA and special FORTRAN routines.

Table 1.14: Scientifically Validated Observing Modes per Detector, June 2001

detector	**scientifically validated mode**	**AOT**
P1	absolute photometry point sources	PHT05
	staring multi-filter photometry point sources	PHT03
	faint source multi-filter nodding	PHT03
	multi-filter sparse map	PHT17/18/19
	chopped multi-filter photometry point sources	PHT03
P2	absolute photometry point sources	PHT05
	staring multi-filter photometry point sources	PHT03
	faint source multi-filter nodding	PHT03
	multi-filter sparse map	PHT17/18/19
	polarimetry (PIA)	PHT50
	chopped multi-filter photometry point sources	PHT03
P3	absolute photometry point sources	PHT05
	staring multi-filter photometry point sources	PHT03
	faint source multi-filter nodding	PHT03
	multi-filter sparse map	PHT17/18/19
	chopped multi-filter photometry point sources	PHT03
C100	absolute photometry point sources	PHT25
	absolute photometry extended sources	PHT25
	staring multi-filter photometry point sources	PHT22
	staring multi-filter extended sources	PHT22
	faint source multi-filter nodding	PHT22
	staring multi-filter raster maps	PHT22
	multi-filter sparse map	PHT37/38/39
	chopped multi-filter photometry point sources	PHT22
C200	absolute photometry point sources	PHT25
	absolute photometry extended sources	PHT25
	staring multi-filter photometry point sources	PHT22
	staring multi-filter extended sources	PHT22
	faint source multi-filter nodding	PHT22
	staring multi-filter raster maps	PHT22
	multi-filter sparse map	PHT37/38/39
	polarimetry (PIA)	PHT51
	chopped multi-filter photometry point sources	PHT22
SS/SL	staring point source spectroscopy	PHT40
	extended source spectroscopy	PHT40
	chopped point source spectroscopy	PHT40

Chapter 2

Known Limitations and Caveats

This section addresses the limitations and caveats of the PHT calibration file Version 7.0 and the OLP implementation 10.0 which have been identified during the scientific pipeline validation process. It addresses also which caveats from calibration file Version 6.0 and OLP version 9.0 have been closed out by this latest version.

2.1 Validity Ranges of FCS Calibration Files

OLP 9.0 contained the following caveats concerning the validity ranges of the FCS calibration files (cf. Report on the Scientific Validation for PHT OLP 9.0 [1]):

1 *OLP 9.0 Caveat:* A poorer calibration accuracy can be expected for observations for which the headers of the PHT data products indicate that the FCS power settings were outside the validity range given in the header of the P*FCSPOW*.FITS CAL-G files. The deviation is larger for extrapolations further away from the validity range.

2 *OLP 9.0 Caveat:* The FCS calibration for P3, C100 and C200 before revolution 94 is less well sampled with standard calibration observations, than after revolution 94. Therefore, the quality of the FCS calibration of observations before revolution 94 can be poorer as compared to observations taken later in the mission. This also applies for the FCS flat-field calibration for the C100 and C200 detectors.

For OLP 10.0 the FCS calibration files were derived once more, in order to adjust them to the refined set of signal linearization corrections. Table 2.1 lists the limits used for OLP V9.0 and OLP V10.0. There are only very minor differences. However, with OLP 10 the processing of measurements with FCS heating power outside the validity range changed. If this case occurs, then the default responsivity is used, in case of sparse maps which may have different FCS settings only the FCS with a setting inside the validity range may be used. The selected responsivity calibration (single, both, first, second, default) is indicated in the SPD product file header (type PP1S, PP2S, PP3S, PC1S, PC2S depending on selected detector P1, P2, P3, C100 or C200). For P1 and P2 detectors there is no impact on calibration quality by using default responsivities. For the FIR detectors P3, C100, and C200 peculiar space weather conditions may lead to responsivities which are 30–50 % off the default value.

Therefore, for OLP Version 10.0 the following caveats apply, provided **the measurement was executed with AOTs P03, P04, P05, P17/18/19, P22, P25, P32, or P37/38/39**:

Caveat 1: A poorer calibration accuracy may be expected for observations with detectors P3, C100 or C200 for which the headers of the PHT SPD data products indicate that the FCS power settings were outside the validity range given in the header of the P*FCSPOW*.FITS CAL-G files and default responsivities were used. Due to the dependence of the FIR detector responsivities on space weather conditions calibration offsets by 30–50 % are possible.

Due to a change in the illumination characteristics of the long wavelength section of the FCS in the beginning of revolution 94, the FCS power files for the FIR detectors P3, C100, and C200 are time dependent. Before revolution 94 the coverage of the calibration curves by standard sources is less good than for the rest of the mission. This affects only a small number of Routine Phase observations (from rev. 79 to rev. 93):

Caveat 2: The FCS calibration for P3, C100 and C200 before revolution 94 is less well sampled with standard calibration observations, than after revolution 94. Therefore, the quality of the FCS calibration of observations before revolution 94 can be poorer as compared to observations taken later in the mission. This also applies for the FCS flat-field calibration for the C100 and C200 detectors.

Table 2.1 compares the valid ranges of the main FCS, FCS1, for OLP V9.0 and OLP V10.0 (in mW of electrical FCS power). The ranges are practically identical, since from OLP V8.4 onwards the full calibration data sets has been used and the maximum ranges were established with OLP 9.0. Note that strictly speaking for PHT-P the power range is associated with the corresponding standard aperture (cf. Sect. 2.2 for a table of the standard apertures per PHT-P filter and additional caveat).

Table 2.1: Validity Ranges of FCS Tables (for FCS1 only). The validity range is given by the calibrated electrical heating power range (in mW) for each filter.

	up to revolution 93				**after revolution 93**			
	OLP V9.0		**OLP V10.0**		**OLP V9.0**		**OLP V10.0**	
Filter	**min**	**max**	**min**	**max**	**min**	**max**	**min**	**max**
P_3.29	17.48	50.00	17.48	50.00	17.48	50.00	17.48	50.00
P_3.6	9.49	50.01	9.49	50.01	9.49	50.01	9.49	50.01
P_4.85	12.36	35.34	12.36	35.34	12.36	35.34	12.36	35.34
P_7.3	7.48	22.13	7.59	22.13	7.48	22.13	7.59	22.13
P_7.7	8.58	24.41	8.58	24.41	8.58	24.41	8.58	24.41
P_10	5.45	11.49	5.45	11.49	5.45	11.49	5.45	11.49
P_11.3	4.81	11.78	4.81	11.78	4.81	11.78	4.81	11.78
P_11.5	3.50	9.68	3.53	9.68	3.50	9.68	3.53	9.68
P_12.8	3.65	7.63	3.65	7.63	3.65	7.63	3.65	7.63
P_16	2.66	6.58	2.66	6.58	2.66	6.58	2.66	6.58
P_20	1.72	4.00	1.72	4.00	1.72	4.00	1.72	4.00
P_25	1.40	3.61	1.40	3.61	1.40	3.61	1.40	3.61
P_60	1.05	2.98	0.93	2.98	0.42	2.13	0.42	2.13
P_100	0.42	1.84	0.42	1.84	0.27	1.84	0.27	1.84
C_50	1.03	4.23	1.03	4.23	0.59	5.27	0.59	5.27
C_60	1.09	3.88	1.09	3.88	0.39	6.39	0.39	6.39
C_70	0.74	4.03	0.74	4.03	0.43	3.15	0.43	3.15
C_90	0.46	1.93	0.46	1.93	0.29	4.40	0.29	4.40
C_100	0.46	2.03	0.46	2.03	0.20	3.79	0.20	3.79
C_105	0.40	2.22	0.40	2.22	0.20	5.84	0.20	5.84
C_120	0.31	1.86	0.31	1.86	0.24	3.47	0.24	3.47
C_135	0.27	1.34	0.27	1.34	0.17	2.60	0.17	2.60
C_160	0.22	1.16	0.22	1.16	0.07	2.45	0.07	2.45
C_180	0.27	1.90	0.27	1.90	0.12	2.88	0.12	2.88
C_200	0.22	0.81	0.22	0.81	0.13	5.78	0.13	5.78

2.2 Inhomogeneous FCS Illumination of PHT-P Apertures

The illumination of the both the PHT-P apertures and the PHT-C arrays by the internal Fine Calibration Source (FCS) is not flat. As a result the illumination of the detector does not scale with the area of the aperture. This effect is corrected for in the case of PHT-C by the so-called illumination matrix (PC1ILLUM and PC2ILLUM cal-G files). Currently, for PHT-P linearity with the aperture area is assumed and the corresponding PHT-P CAL-G files (PP1FCSAP, PP2FCSAP and PP3FCSAP) only contain correction factors of 1 (i.e. they do not imply any correction).

Table 2.2: ISOPHOT Standard Calibration Apertures

Filter	**Standard Aperture**
P_3.29	23"
P_3.6	23"
P_4.85	23"
P_7.3	23"
P_7.7	23"
P_10	52"
P_11.3	52"
P_11.5	52"
P_12.8	52"
P_16	52"
P_20	79"
P_25	79"
P_60	180"
P_100	180"

Therefore the following caveat remains in place, for **measurements executed with AOTs P03, P04, P05 or P17/18,19**:

Caveat 3: In case the FCS calibration of an observation is performed in a non-standard aperture of this filter (cf. Table 1) strong deviations (factor $\simeq 2$) of the correct responsivity and thus the derived fluxes can occur. The deviations are strongest for the usage of the largest apertures in combination with P1 filters.

2.3 Non-geometric Aperture Beam Size Scaling

By evaluation of multi-aperture measurements on flat backgrounds it has been found that in some filters strong non-linear behaviour w.r.t. the geometrical aperture area occurs (in particular for the largest apertures, ≥ 120", of the 11.5 micron filter). This means, that, if observations are performed in apertures deviating strongly from the ones used in calibration (cf. Table 2.2), deviations from the correct flux can occur. This is especially of importance for multi-aperture measurements, because often background measurements are performed in different (larger) apertures than the related source observations and are scaled to the corresponding on-source aperture size.
The extended source calibration and the correction for non-geometric beam size effects of ISOPHOT-P is not yet finalized. Currently, the s/w uses the geometrical beam sizes only.

Therefore the following caveat still applies for **measurements executed with AOTs P03, P04, P05 or P17/18/19**:

Caveat 4: If observations are performed in apertures, which are different in diameter from the ones used in standard calibration, deviations from the correct flux calibration can occur. This implies especially for extended source or background observations using the largest apertures with P1 and P2.

2.4 Non-linearity of Detector Responsivity with Flux

The non-linearity of the detector systems with incident flux has been characterized in the calibration files PP1SLINR, PP2SLINR, PP3SLINR, PC1SLINR, PC2SLINR. They provide a linearization of the detector signals so that the responsivity becomes homogeneous for the full applicable flux range.
The linearity calibration is only valid for certain signal ranges. Table 2.3 lists the lower and upper signal limits as given in the headers of the calibration files PP1SLINR, PP2SLINR, PP3SLINR, PC1SLINR, PC2SLINR. The polynomial approximations to the non-linearity curves are not extrapolated beyond the calibrated signal ranges but are kept at the level of the boundary. In different filters different relative signal ranges may be covered so that in some cases with signals at the boundaries of the calibrated ranges some unsteadiness may be introduced.

Table 2.3: Calibrated Signal Ranges of Non-linearity Correction Tables

Detector	**Filter**	**Lower Limit** [V/s]	**Upper Limit** [V/s]
P1	3.3	0.000	55.4
P1	3.6	0.000	166.2
P1	4.8	0.000	126.8
P1	7.3	0.000	95.5
P1	7.7	0.000	27.1
P1	10.0	0.000	23.5
P1	11.3	0.000	2.9
P1	12.0	0.024	35.7
P1	12.8	0.031	11.3
P1	15.0	0.020	3.7
P2	20.0	0.075	9.5
P2	25.0	0.099	10.9
P3	60.0	0.247	56.9
P3	100.0	0.266	68.1
C100	60.0	0.000	55.4
C100	65.0	0.000	45.0
C100	80.0	0.202	32.2
C100	90.0	0.000	44.8
C100	100.0	0.000	36.5
C100	105.0	0.000	34.6
C200	120.0	0.000	25.2
C200	150.0	0.000	33.3
C200	170.0	0.000	23.9
C200	180.0	0.000	21.1
C200	200.0	0.000	7.3

2.5 Detector Signal Transients

PHT OLP does not use physical (Fouks) or empirical (exponential, signal jump) signal transient correction functions, as they are available in the PIA, because those require still a highly interactive mode. Currently OLP detects detector transients by statistical trend

analysis methods and discards parts of a measurement found to be affected by drifts. This method works reasonably well, if a given measurement reaches stability, i.e. for bright sources and for very long observations. The condition that stability is achieved is that the variation of the signals during the considered time interval is less than 5%. Then the signals within the stability period are used to derive the final signal per chopper plateau. In case this criterium is not met, OLP uses the weighted mean of the last 8 signals.
For ISOPHOT-S measurements there is an intrinsic transient correction by the calibration method, both for staring and chopped measurements. In particular for the staring measurements the temporal behaviour of the transient is corrected for by considering the standard star measurement at the same time suffering the same transient effect due to the selection of a standard star or, in case of faint sources, sky background close in flux. Only in case of ISOPHOT-S raster maps a static spectral response function is applied, so that transient effects play a role.

Therefore, the following caveat applies for **measurements executed with AOTs P03, P04, P05, P17/18/19, P22, P25, P37/38/39, raster mode of P40**:

Caveat 5: The transient correction only works satisfactory for ISOPHOT-P and -C measurements longer than the detector transient time constant at a given illumination. The transients are very often the limiting factor for the achieved accuracy. Measurements flagged by the OLP software as *"plateau data affected by residual drift"* can show strong deviations (residual drift is greater than 5%) from the correct result. Raster measurements with ISOPHOT-S suffer transient effects, since a static spectral response function is applied.

Note: The quality of an observation, w.r.t. drift and other criteria is coded into the SPD field **PxxSFLAG** where xx identifies the detectors as follows: C1, C2, P1, P2, P3, SS and SL. The flags are given for each chopper plateau individually and are defined in the OLP include file SPP_PIX_FLAGS_PAR.INC. The following table gives an overview:

Table 2.4: Quality flags for PHT SPD Data

Flag	Description
0	normal
1	calibration measurement saturated
2	part of plateau data affected by drifts
3	all ramps on plateau rejected
4	plateau data affected by residual drift
5	zero standard deviation
7	zero signal for plateau

2.6 Long Term Detector Drifts

For single pointing measurements with one FCS measurement per detector no attempt is made by PHT OLP software to correct for long term detector responsivity drifts, i.e. stability of the detector responsivity during the execution time of an AOT is assumed. Investigation of PHT-C maps has shown that the detector long term drift is not linear, but very often shows an exponential behaviour due to switch-on effects. Therefore, models of the detector behaviour or baseline fits would be required for optimum results.
Due to the very often inapproriate linear interpolation with time of the responsivity values derived from the two bracketing FCS measurements for raster pointing observations and sparse maps, this processing feature has been removed with OLP 10. The average of the two responsivity values is used, provided both have neither a R/T problem nor are outside

the validity range of the FCS heating power (see Sect. 2.1). This calibration procedure is also more transparent to the user of the data products.

Therefore, the following caveat applies to long exposures in **measurements executed with AOTs P03, in particular raster maps, P04, P17/18/19, P22, in particular raster maps, P32, P37/38/39**:

Caveat 6: PHT OLP does not correct for long term detector drifts within an AOT. In case of maps with bracketing FCS measurements only the average responsivity value is used.

2.7 Error Calculation and Propagation

Uncertainties provided by OLP 10.0 are still pure statistical errors from signal evaluation. In order to assess all other uncertainties it is necessary to refer to the related documentation on PHT calibration in combination with the OLP products. (cf. documents ISOPHOT Handbook [2] and ISOPHOT Error Budgets [3]).

Caveat 7: The PHT OLP software does only provide an uncertainty from the statistical signal evaluation. It does not give any estimates of the systematic uncertainties of all performed calibration steps. Therefore, OLP 10 uncertainties are **minimal** errors. It is essential to refer to special documentation which provide an overview of the uncertainties introduced step by step. These depend on the exact observing conditions and evaluation steps which may even not be completed inside OLP (e.g. background subtraction in maps or from independent staring measurements).

2.8 Limitations in Use of PHT Color Correction Factors

Color correction factors are in general not applied by PHT OLP, the quoted fluxes in the data products always refer to the standard SED $F_\nu \cdot \nu = \text{constant}$. Color correction can be performed inside PIA. The color correction factors have been calculated from the bandpass transmission files currently available, which have typically about 300 data points equally spaced in wavelength. Two different interpolation and integration methods have been used to derive the color correction factors and they give equal results except for the cases where steep Wien branches are convolved with the bandpass transmission numbers. Furthermore, the bandpass transmission files used are centered on the main throughput range. All wavelengths for which the transmission was below 10^{-4} have been excluded.

Therefore, the following caveats still apply for color correction factors:

Caveat 8: Color correction factors above 2 should be considered as less accurate and factors above 4 only as an indication of the order of the correction, as they clearly depend on the integration and interpolation method used. This applies in particular for SEDs of cold sources in combination with the P1 filters which fall onto the steep Wien branch of these SEDs. In these cases it is recommended to establish the color correction factor yourself.

The relative spectral system responses of all ISOPHOT-P and -C bandpasses (the same ones which the tabulated color correction factors are based on) are provided in the two CAL-G files PPFILTRAN.FITS and PCFILTRAN.FITS. This enables observers to calculate color correction factors for any SED shape not covered by the dedicated color correction CAL-G files.

2.9 Incomplete Raster Map Appearance in Case of Zero Signal Flag

For PHT-P raster maps **executed with AOT P03** the following caveat applies:

Caveat 9: In case the total flux on the detector is very small, resulting in close to zero or even negative signals at the end of the DERIVE_SPD processing stage, OLP sets the "zero signal flag" for the corresponding plateaux times and does not continue to process these data sections in DERIVE_AAR (cf. description of SPD product types, coding of pixel status flag PPxSFLAG; a listing of the quality flags is given in Table 2.4). This leads then to incomplete appearing map products PGAI. The most likely cases are for the short wavelength filters of PHT-P1, where the sky background (Zodiacal Light) shows a minimum, in particular in combination with small aperture sizes.

2.10 Application of Point Spread Function Fraction Factors to AAR Data Products

For **measurements executed with AOTs P03 (single pointing), P04, P05, P17/18/19, P22 (single pointing), P25, P37/38/39** it should be noted that:

Caveat 10: The point spread function fraction correction factors are applied to all data products associated to point source photometry, like PPAP and PCAP, regardless whether a background subtraction was performed or not. For staring mode observations without background subtraction this has to be accounted for when subtracting the separate background measurement.

The background measurement can be either a point source photometry (in Jy), of type PPAP or PCAP:

$F_{src+back} = F_{on} \; / \; f_{psf}$
$F_{back} = F_{off} \; / \; f_{psf}$
$\rightarrow F_{src} = F_{src+back} - F_{back} = (F_{on} - F_{off}) \; / \; f_{psf}$

or an extended source measurement of type PPAE or PCAE (in $MJy\,sr^{-1}$; for the conversion of in-band power to surface brightness, cf. chapter 8.4.10 in [2]):

$F_{src+back} = F_{on} \; / \; f_{psf}$
$B_{back} = (F_{off_pix} \; / \; ((1\text{-}\varepsilon^2) \cdot \Omega)$
$\rightarrow F_{src} = F_{src+back} - F_{back} = (F_{on} - n_{pix} \cdot (B_{back} \cdot (1\text{-}\varepsilon^2) \cdot \Omega)) \; / \; f_{psf}$

F_{on}, F_{off}, F_{off_pix} are fluxes in the aperture uncorrected for point source function effects (the latter one for one single pixel of the array). B_{back} is the surface brightness of the background.

Please note the following definitions with regard to application of f_{psf}-factors to header keywords :

1) For PPAP and PPAE:
   $f_{psf} = f_{psf}^{aperture}$
   $n_{pix} = 1$

2) For PCAP and PCAE staring modes:
   total flux of the array is used!
   $f_{psf} = f_{psf}^{array}$
   converted flux from surface brightness has to be multiplied with number of pixels, because the solid angle Ω is defined per pixel!
   $n_{pix} = 9$ for C100, $n_{pix} = 4$ for C200

3) For C100 PCAP and PCAE chopped mode (PHT22):
$f_{psf} = f_{psf}^{pixel}$
because only the central pixel is used!
$n_{pix} = 1$
Note that f_{psf}^{array} is applied to the data fields PCAPSRCE for consistency with the staring mode!

4) For C200 PCAP and PCAE chopped mode (PHT22):
$f_{psf} = f_{psf}^{array}$
$n_{pix} = 4$

2.11 Residual Flat-field Structures in PHT22 Raster Maps

As part of the scientific validation of PHT22 raster maps for OLP V8.4 and 9.0 the flat-field accuracies for maps having a wide range of selected raster parameters, with and without pixel overlap, and a wide range of sky background brightness had been assessed. It was found that in case of no pixel overlap flat field accuracies both for C100 and C200 were in general worse than 8 % (standard deviation of the mean sky background versus mean sky background). This limit was due to systematic flat-field residuals of the arrays and could be recognized as systematically repeated patterns in most of the maps. In addition, for C100 maps, temporal variations of these flat-field structures were found. This is linked to non-linear detector drifts as flagged in Sect. 2.6. Therefore, for OLP 9.0- the following caveat was imposed on mapping products PGAI:

- *OLP 9.0 Caveat:* Systematic flat-field residuals in maps with no pixel overlap which account to between 10 and 20 % as well as temporal variations of the flat-field in case of C100 maps limit the ability of faint source detections and photometry on low sky background levels.

With OLP 10 a statistical flat-field method was introduced which removes the systematic flat-field residuals for maps with more than 20 raster points. Since smaller raster maps are usually performed for photometry of individual sources centered in the map (so-called mini-map photometry) for which dedicated analysis methods have been developped (so-called PCAS method), this OLP 9.0 Caveat has been significantly toned down.

Therefore the following caveat applies to **measurements executed with AOT P22 in raster mode**:

Caveat 11: Temporal variations of the flat-field in case of C100 maps limit the ability of faint source detections and photometry on low sky background levels.

2.12 Point Source Photometry from Staring Mode Raster Mini-Maps

For photometry from mini-maps (staring raster maps with restricted grid size, typical 3×3 for C100 or 2×2 for C200) **executed with AOT P22 in raster mode** the following caveat applies:

Caveat 12: Aperture photometry on PGAI map products gives reliable fluxes only for a rather limited flux range. These products should mainly be used for a check what can be seen in the maps (source detected, structures around ...). For reliable photometry over a wide flux range the PCAS products (photometry per raster point) should be used.

2.13 Filters with Less Reliable Photometry

The investigation of test cases, mainly staring mode photometry, during Scientific Validation of OLP 9.0 had shown several systematic artifacts in the resulting SEDs which were flagged:

- *OLP 9.0 Caveat:* Several filters display systematic flux offsets in multi-filter SEDs. Since in most cases they do not show up over the full flux range, most of the artifacts may be related to a poor linearisation correction for this filter. The filters and the flux levels for which these artifacts were found are listed below.

1) P1 12.8 μm filter: positive flux offset from +15 % at flux level 100 Jy to factor of 3 at background level.

2) P1 3.3 and 11.3 μm filters.

3) P2 20 μm filter: -40 % at background level.

4) C100 65 and 80 μm filters: +20 - +40 % at background level (restricted to multi-filter cases?).

In preparation of OLP 10.0 quite some effort has been spent to remove these artifacts. However, finally it has not been possible to resolve all issues.

Therefore, the general caveat still applies for **measurements executed with AOTs P03, P05, P17/18/19, P22 and P37/38/39**:

Caveat 13: Several filters display systematic flux offsets in multi-filter SEDs. The filters and the flux levels for which these artifacts were found are listed below.

1) P1 12.8 μm filter: positive flux offset from +10 % at flux level 50 Jy to factor of 2 at background level.

2) C100 65 and 80 μm filters: +15 - +30 % at background level (restricted to multi-filter cases?).

3) Background measurements in the shortest wavelength PHT-P filters (3.3, 3.6, 4.8 μm) in apertures considerably smaller than the 180 arcsec aperture (this comprises the default aperture for these filters which is the 23 arcsec aperture) usually do not give any meaningful results, because the measurement is dominated by dark signal.

2.14 Limitations of PHT-S Dynamic Spectral Response Calibration

The nature of the PHT-S dynamic spectral response calibration implies the following two restrictions for **measurements executed with AOT P40 in staring mode**:

Caveat 14: The transient behaviour of the PHT-S detectors is temperature dependent. The calibration was established for a certain temperature range which the calibration standard measurements are located in. Since PHT-S was not actively temperature controlled fluctuations of the detector temperature outside the calibrated range (2.7 K < T < 3.1 K) can occur. In this case absolute and relative spectral shape accuracies are worse than the quoted one due to different signal transient behaviour. These observations are flagged by a warning message in the PSSS and/or PSLS product headers.

The warning message is the following:

```
COMMENT ************************************************
COMMENT !!!WARNING!!!
COMMENT Detector temperature outside valid range
COMMENT ************************************************
```

Caveat 15: For certain wavelength ranges fluxes of some targets can be outside the range covered by standard stars. In this case a worsening of the relative spectral shape accuracy is possible. These observations are flagged by a warning message in the PSSS and/or PSLS product headers.

The warning message is the following:

```
COMMENT ************************************************
COMMENT !!!WARNING!!!
COMMENT Flux for pixel i out of cal range
COMMENT ************************************************
```

From the scientific validation assessment performed in this report the following two general caveats have been derived:

Caveat 16: The Zodical Light level is below the sensitivity limit of PHT-SS (short wavelength array). (The Zodiacal Light intensity is less than $1\,\mathrm{MJy\,sr^{-1}}$ for 2.5 to 4.9 μm).

Caveat 17: Quoted absolute accuracies are only valid for Zodiacal Light level in the PHT-SL range (Zodiacal Light intensity $\sim$ 5 - $20\,\mathrm{MJy\,sr^{-1}}$ for 5.8 to 11.6 μm), if the exposure time is greater equal 1024 seconds.

2.15 Limitations in Accuracy of Spectrophotometry for Pointings not Centered in the Aperture of PHT-S

The quoted accuracies for spectrophotometry of point sources with PHT-S are only valid, if the source was located within ± 3 arcsec of the centre of the PHT-S aperture. Due to a steep beam profile, in particular in cross-dispersion (spatial) direction, i.e. in S/C y-axis direction, both a significant absolute flux offset and a change of the relative spectral shape can occur. The latter is also often visible due to flux jumps at the borders of the order sorting filter ranges which are at 3.7 μm for the PHT-SS array and 8.8 mum for the PHT-SL array. It is therefore advisable to cross check the PHT-S pointing with a source data base and determine the offset (e.g. the offset via the SIMBAD reference position as offered by the ISO Data Archive interface).

Therefore, the following caveat applies for **measurements executed with AOT P40**:

Caveat 18: The accuracies for PHT-S point source spectrophotometry are only valid, if the source was centered within ± 3 arcsec of the aperture. Off-pointings can lead to significant flux losses and modifications of the spectral shape. Conspicuous artifacts are flux jumps at the wavelengths of the order sorting filter transitions at 3.7 μm for the SS array and 8.8 mum for the SL array.

Chapter 3

Prerequisites for OLP Scientific Validation

The scientific validation of the PHT pipeline follows the guidelines as out-lined in the e-mail by the ISO Project Scientist Martin Kessler, "Scope of OLP Scientific Validation - IDT AI #8/16" from 18-JUL-1995. The major goals of the scientific validation process according to this note are to:

- confirm that the applied processing has had the expected effect(s) on the data;
- establish that sufficient processing has been applied to the data so that the products are usable by the observer;
- demonstrate that the processing is reliable, stable and repeatable;
- establish the level of accuracy of the calibration;
- document any known caveats or concerns with the processing and/or calibration;
- demonstrate that, with the aid of the relevant ISO Data Users Manual (IDUM, now part of the ISO Handbooks), observers can further process products to a publish-able form.

The scientific validation process is restricted to PHT Standard Processed Data (SPD) and Auto-Analysis Products. Edited Raw Data (ERD) were declared scientifically valid for data products generated with OLP version 4.0 or higher, during the "OLP V4.0 AND BEYOND REVIEW MEETING" on the 24th of April 1996. Therefore, all tests outlined here assume the correctness of all ERD data.
All test data sets were processed with the IDC test pipeline version 10.0beta. Re-processing with a delta version of 10.0beta at RAL was performed as necessary in order to validate OLP modules which have been improved during the validation process.
The report refers to several sets of data products. The PHT OLP 10 Scientific Validation was split over 7 periods, the three most important ones for the results presented in this report were period 2 (using OLP 10.0b5), period 3 (using OLP 10.0b7) and period 4 (using OLP 10.0b8). The later periods were quite short verifying only very specific aspects (corresponding to OLP 10.0b9, OLP 10.0b11 and OLP 10.0b12).
In the following we provide an overview:
OLP 10.0 products were also obtained by on-the-fly re-processing after official release of the OLP 10 software.

Table 3.1: Usage of data sets during OLP 10 scientific validation

data set	**used in period and purpose**	**period**
OLP 10.0b1&b3	main set during SVP1	17/01-02/02/2001
OLP 10.0b5	main set during SVP2	13/02-14/03/2001
OLP 10.0b7	main set during SVP3	23/03-16/04/2001
OLP 10.0b8	main set during SVP4	23/03-03/05/2001
OLP 10.0b9	set during SVP5	09/05-23/05/2001
OLP 10.0b11	set during SVP6	25/05-31/05/2001
OLP 10.0b12	set during SVP7	05/06/2001

Chapter 4

Overview of Software and Calibration File Changes and Updates by SVP

In preparation of the PHT OLP 10.0 Scientific Validation the Software Change Requests (SCREWs) and Software Problem Reports (SPRs) as listed in Table 4.1 were addressed.

Table 4.1: Upgrades and Fixes in Preparation of OLP 10.0 Scientific Validation

Issue	**CI**	**SCREW**	**SPR**
Wrong Target Coordinates in BPs	OLP	414	
World coordinates in PHT maps	OLP	442	
Two-threshold deglitching for PHT OLP ramp processing	OLP	458	
Background subtracted normalized source signal for PHT-P multi-aperture measurements	OLP	459	
Glitch removal for P32 observations	OLP	461	
Statistical flat-field correction for P22 and P32 maps	OLP	462	
Changes to chopped photometry processing	OLP/CALG	463	
Application of average and default responsivities	OLP	464	
Warning of residual drifts in FCS calibration measurements	OLP	465	
Upgrade of PHT signal linearization files	CALG		3496
Upgrade of the point spread function correction files	CALG		3497
Upgrade of FCS calibration files	CALG		3498
Upgrade of orbit dependent default responsivity files	CALG		3499
Upgrade of PHT-S dynamic spectral response calibration files	CALG		3500
Signal processing parameters in case of Mann test failure	OLP		3503
Filter-to-filter flat-field corrections for median values	OLP		3504
Redundant code for staring mode in PHT DERIVE_SPD	OLP		3505

Table 4.2 lists the items which were fixed during the Scientific Validation periods (see Sect. 3).

Table 4.2: Problems found during OLP 10.0 Scientific Validation

Problem	**CI**	**SPR**
PHT DERIVE_SPD failures in processing some P32 observations	OLP	3509
Undefined calibration values in FCS power files	CALG	3524
Error in plateau averaging (PHT DERIVE_SPD)	OLP	3532
Upgrade of CalG file PP2CHOPSIG.FITS	CALG	3543
New SPP failure during Bulk Reprocessing	OLP	3550
New SPP failure during Bulk Reprocessing	OLP	3551
New AAP failure during BKRP (TDT 178017080)	OLP	3559
SPP high performance arithmetic trap error again during BKRP	OLP	3565
Discrepancy in chopped PHT-S extended source spectra	OLP	3572
Use of default responsivity when PHT FCS out of cal range	OLP	3573
Filter ordering in CALG file PPPSF.FITS	CALG	3576
Photometric calibration of P1 12.8 micron filter	CALG	3577
PHT P04 - source signal ratios not as expected	OLP	3578
Improved default responsivities for C100 and C200	CALG	3580
PHT P04 - update aperture correction factors	OLP	3600
Further upgrade of PHT default responsivities	CALG	3601
Zero default responsivity uncertainties in PHT SPD	OLP	3604
Responsivity information in SPD header for absolute photometry	OLP	3614
Implementation error in PHT 2-threshold deglitching	OLP	3624
Correct plateau time in P32 SPD products	OLP	3634
Minor changes to the PHT absolute photometry headers	OLP	3635
Error in calculation of plateau time for P32	OLP	3643
Minor changes to PGAI, PGAU and PGAT headers	OLP	3651

Following the release of OLP 10 in June 2001, the subsequent bulk re-processing showed some problems which were not caught during the scientific validation periods. These (see Table 4.3) were fixed for OLP 10.1.

Table 4.3: Problems fixed for OLP 10.1

Problem	**CI**	**SPR**
PHT Sparse Maps new error during BKRP OLPv10	OLP	3697
Reopening of SPR3113	OLP	3699

Chapter 5

Staring Mode Photometry

5.1 Consistency Check of Multi-filter Photometry

Summary

- Staring mode multi-filter photometry was successfully revalidated.
- Calibration accuracies achieved by OLP V9 have been consolidated and slightly improved, in particular for the relative filter-to-filter calibration. Calibration accuracies are provided in the general overview in Sect. 1.3.
- We notice the peculiar behaviour of some filters for some flux ranges:
  - Photometry in the 12.8 μm filter shows a strong positive offset from background level up to fluxes of a few Jy.
  - Surface brightness photometry in the 65 and 80 μm filters shows a systematic offset.
  - Background flux measurements with the shortest wavelength PHT-P filters (3.3 – 4.8 μm) in apertures considerably smaller than 180 arcsec usually do not give meaningful results, because the measurement is dominated by dark signal.
- We note a lower flux limit for reliable photometry with the standard on-off staring mode. This is for:
  - P1 : $\approx$ 0.5 Jy
  - P2 : $\approx$ 0.5 Jy
  - P3 : $\approx$ 1.5 Jy
  - C100: $\approx$ 1.5 Jy
  - C200: $\approx$ 2.0 Jy
- We note systematic offsets for PHT-P photometry in smaller apertures than non-standard ones. Currently no systematic assessment of these offsets is available.

5.1.1 PHT03 and PHT22 Multi-filter Photometry: The SED of α Bootes (HR 5340)

Motivation

TDTs 45200201(background, PHT-P), 45200202(α Boo, PHT-P), 45200203(background, PHT-C), 45200204(α Boo, PHT-C) is one of the key OLP validation cases [1]. The staring mode AOTs PHT-03 and PHT-22 use all available PHT filters (but the 3.6 and 4.85 μm filters had to be excluded from the analysis, because the source saturates the measurement) on a stellar (declining) SED. α Bootes is one of the most important stellar PHT calibration standards and there are detailed models available from M. Cohen (composite spectrum from 1 to 35 μm and extrapolations to 300 μm). This test case is very suitable for a test of both the absolute calibration and the relative filter-to-filter calibration. It should be noted that this multi-filter measurement was not used for the establishment of the FCS calibration curve.

Method

We compare the background subtracted, color corrected flux values of both OLP V9.0b6 and OLP V10.0b7 results against the model prediction.

Results

The comparison of the OLP V9.0b6 and OLP V10.0b7 photometry with the model is given in part 1 of the evaluation log section. We estimate the absolute photometric accuracy per detector assembly for this target as the deviation from the model flux in the filter in which the FCS calibration was done, and the relative filter-to-filter accuracy as the peak-to-peak variation of the other filters around this offset. Note that for P1 the FCS calibration was actually done in the 3.6 μm filter, but for this filter the sky measurement is heavily saturated. The derived absolute and relative photometric accuracies are presented in Tab. 5.1.
Fig. 5.1 shows the PHT photometric data points in comparison to the model and IRAS photometry (color corrected) from 3.3 to 200 μm for OLP 9.0b6 and OLP 10.0b7, respectively.

Table 5.1: Absolute and relative calibration accuracies per detector achieved for HR 5340 observation with OLP V10.0b7

detector	**absolute accuracy** [%]	**relative accuracy** [%]
P1	< 5 at 3.3 μm	10
P2	< 7 at 20 μm	< 5
P3	< 5 at 60 μm	< 5
C100	6 at 90 μm	<15
C200	8 at 170 μm	20
		< 10 for $\lambda <170$ μm

The fluxes in the two longest wavelength C200 filters remain too low by 25 to 30 %. As already outlined in the previous report (cf. [1]) this flux fall-off seems to be related to the absolute level of the background (for source-to-background ratios see last table in evaluation log, item 2).
Part 2 of the evaluation log section and Fig. 5.2 provide the surface brightness photometry of the background position and the comparison with COBE.
From Table 5.2 it can be seen that the consistency with COBE has improved and looks much smoother. We still notice systematic offsets in the 65 and 80 filters relative to the COBE reference. The slope of the background SED in the C200 range appears still to be too shallow with regard to COBE.

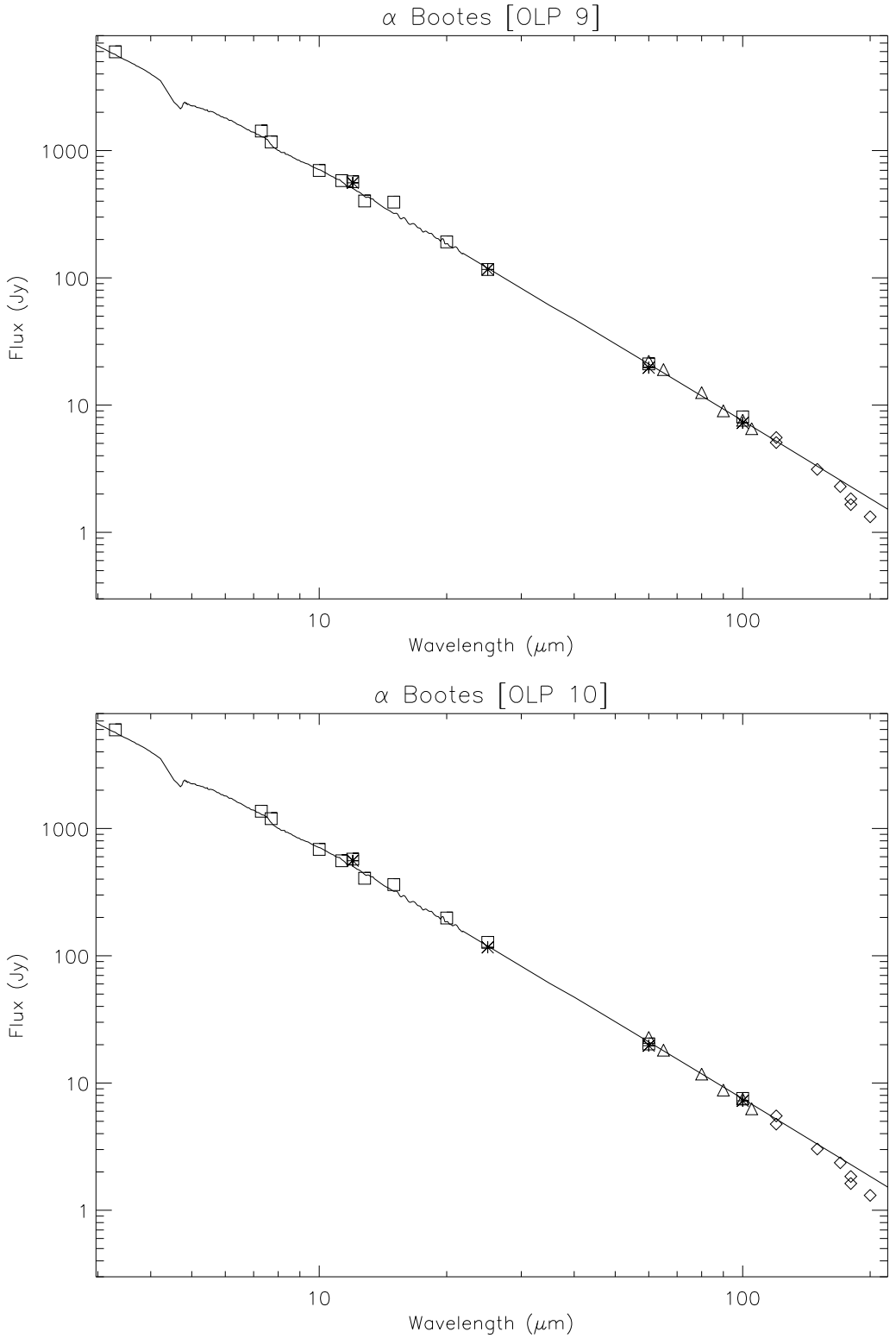

Figure 5.1: Comparison of PHT-P and PHT-C photometry, using the full ISOPHOT filter set, with the composite spectrum and out to 300 μm extrapolated SED of α Boo (HR 5340) provided by M. Cohen and with IRAS photometry for OLP 9.0b6 (upper panel) and OLP 10.0b7 (lower panel). All photometric points are color corrected for a 4000 K BB. The meaning of the symbols is the following: solid line: model, asterisk: IRAS, square: PHT-P (P03 AOT), triangle: C100 (P22 AOT), diamond: C200 (P22 AOT).

Table 5.2: Consistency check of α Boo background position surface brightness results with COBE/DIRBE annual maps.

wavelength μm	**consistency w.r.t. COBE OLP V9.0b6** [%]	**consistency w.r.t. COBE OLP V10.0b7** [%]
60	+13.0	+ 6.7
100	+43.5	+25.9
150	-19.6	-25.8
200	+47.5	+38.1

Conclusions

- PHT photometry gives a good representation of the SED from 3.3 to 170 μm; it is quite similar to the OLP 9.0 result.
- There is still a flux fall-off at the longest wavelengths, where the source flux makes up only 20 % of the background. A reason may be that the background flux is derived too high which is supported by the consistency check with COBE/DIRBE photometry.
- The FIR background SED looks smoother compared to the OLP 9.0 one.

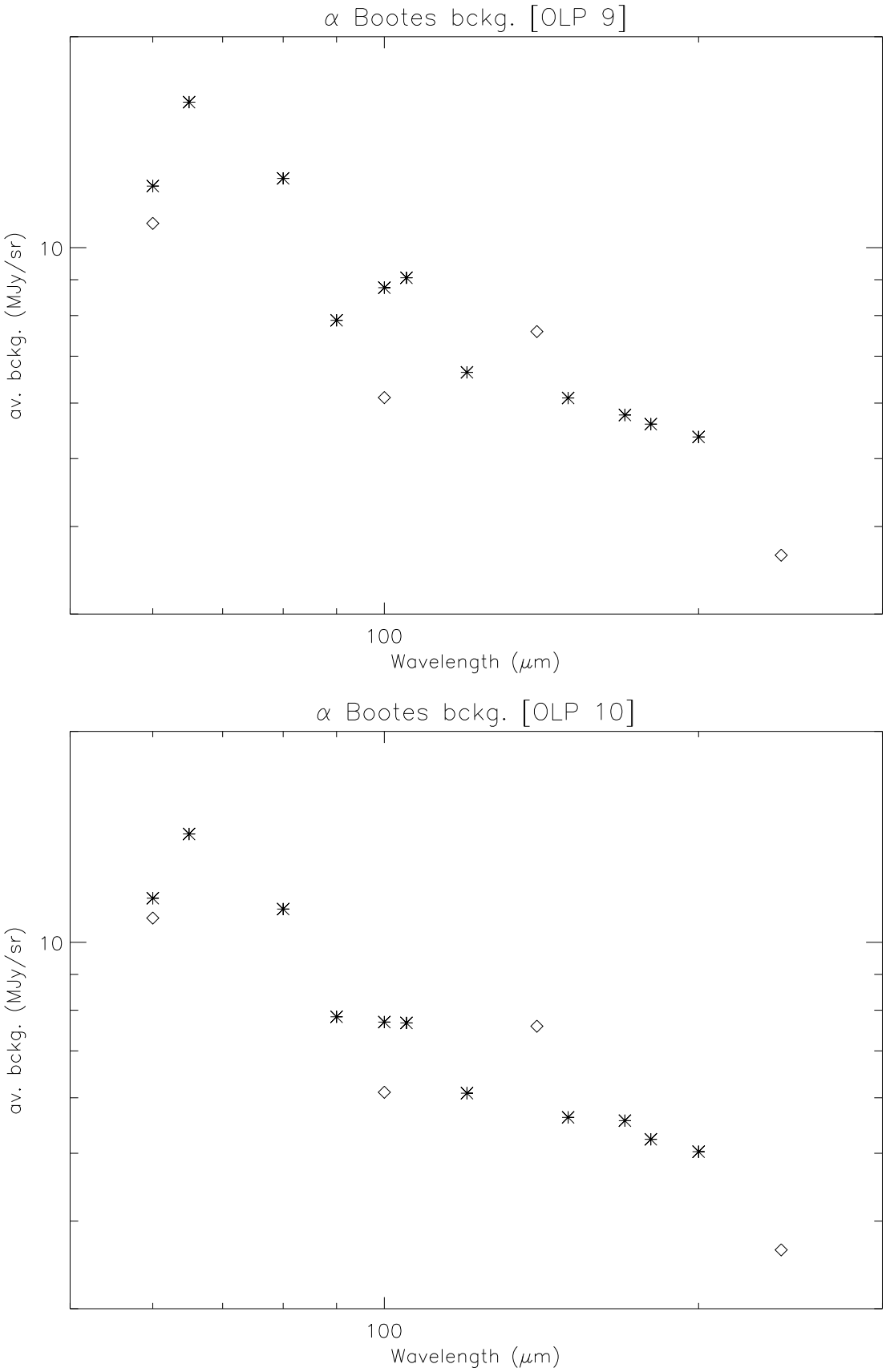

Figure 5.2: Comparison of OLP V9.0b6 and OLP V10.0b7 surface brightness (asterisk) with COBE annual map fluxes (diamond).

Evaluation Log

1) Point source photometry for Alpha Bootes in comparison with IRAS and Cohen model. Fluxes are in Jy.

Measurements:

PHT-P:	ppap45200202 (src+back)
	ppae45200201 (back)
PHT-C:	pcap45200204 (src+back)
	pcae45200203 (back)
(b)	pcap62900721 (src+back)
(b)	pcap62900720 (back)

Colour correction: black body, T = 4000 K

Model: Cohen

Det	cwl (μm)	OLP 9	OLP 10	IRAS	Model	Δ (OLP 9)	Δ (OLP 10)
P1	3.3	5968.594	5956.200		5695.470	4.80	4.58
P1	7.3	1423.773	1366.706		1291.496	10.24	5.82
P1	7.7	1169.081	1195.772		1116.581	4.70	7.09
P1	10.0	697.696	685.298		708.004	-1.46	-3.21
P1	11.3	580.845	557.764		570.349	1.84	-2.21
P1	12.0	568.950	574.434	558.500	507.360	12.14	13.22
P1	12.8	401.790	406.382		435.541	-7.75	-6.69
P1	15.0	393.588	362.336		320.700	22.73	12.98
P2	20.0	191.659	197.972		185.467	3.34	6.74
P2	25.0	116.274	127.366	116.400	119.146	-2.41	6.90
P3	60.0	21.082	20.261	19.650	21.030	0.25	-3.66
C1	60.0	22.120	22.802	19.650	21.030	5.18	8.42
C1	65.0	19.023	18.125		17.910	6.21	1.20
C1	80.0	12.532	11.757		11.800	6.20	-0.36
C1	90.0	9.012	8.800		9.303	-3.12	-5.41
P3	100.0	8.077	7.566	7.250	7.521	7.40	0.60
C1	100.0	7.596	7.485	7.250	7.521	1.00	-0.47
C1	105.0	6.529	6.269		6.814	-4.19	-7.99
C2	120.0	5.078	4.756		5.201	-2.37	-8.55
C2b	120.0	5.559	5.514		5.201	6.88	6.01
C2	150.0	3.126	3.032		3.310	-5.55	-8.41
C2	170.0	2.290	2.363		2.568	-10.82	-7.99
C2	180.0	1.654	1.623		2.286	-27.66	-28.99
C2b	180.0	1.836	1.842		2.286	-19.69	-19.42
C2	200.0	1.326	1.309		1.845	-28.15	-29.03

2) surface brightness photometry of Alpha Bootes background

λ	OLP9 (MJy/sr)	OLP10 (MJy/sr)	COBE (MJy/sr)
60.0	12.24	11.56	10.83
65.0	16.13	14.28	
80.0	12.56	11.16	
90.0	7.88	7.83	
100.0	8.77	7.69	6.11
105.0	9.06	7.67	
120.0	6.64	6.09	
150.0	6.10	5.63	7.59
170.0	5.77	5.57	
180.0	5.60	5.24	
200.0	5.37	5.03	3.64

λ	background flux (Jy)	expected source flux (Jy)	Source/background
60.0	8.02	21.03	2.62
65.0	9.87	17.91	1.81
80.0	7.58	11.80	1.56
90.0	5.56	9.30	1.67
100.0	5.96	7.52	1.26
105.0	6.27	6.81	1.09
120.0	12.01	5.20	0.43
150.0	10.21	3.31	0.32
170.0	10.80	2.57	0.24
180.0	9.40	2.29	0.24
200.0	8.13	1.85	0.23

5.1.2 PHT03 and PHT22 Multi-filter Photometry: The SED of γ Draconis (HR 6705)

Motivation

The star γ Draconis (HR 6705) is one of the most important calibration stars for ISOPHOT. Also several AOT commissioning observations were performed on this star. The set of observations comprises multi-filter photometry, absolute photometry, and multi-filter PHT-C100 photometry with different reset interval settings, cf. [4] for more details. It is one of the key OLP validation cases [1]. The staring mode AOTs PHT-03 and PHT-22 use all available PHT filters out to 200 μm complementing the α Bootes observations towards the fainter flux end. There are detailed models available from M. Cohen (composite spectrum from 1 to 35 μm and extrapolations to 300 μm). This test case is very suitable for a test of both the absolute calibration and the relative filter-to-filter calibration. Furthermore, the last C100 measurements of TDT 35602204, including the C100 FCS measurement failed due to a R/T problem (therefore repetition by TDT 39802003). The available C100 measurements of TDT 35602204 are calibrated with the C100 default responsivities.

Method

We compare the background subtracted, color corrected flux values of both OLP V9.0b6 and OLP V10.0b8 results against the model prediction.

Results

The comparison of the OLP9.0b6 and OLP10.0b8 photometry with the model is given in part 1 of the evaluation log section with the model. We estimate the absolute photometric accuracy per detector assembly for this target as the deviation from the model flux in the filter in which the FCS calibration was done, and the relative filter-to-filter accuracy as the peak-to-peak variation of the other filters around this offset. Fig. 5.3 shows the PHT photometric data points in comparison to the model and IRAS photometry (color corrected) for OLP 9.0b6 and OLP 10.0b8, respectively.
The multi-filter photometry results show some features which are quite similar for both OLP versions:

- The 15 μm flux shows a high excess of 70 % with regard to the model. We could clarify that this to a large extent due to detector transients. There is a second measurement (TDT 39801901) which was only repeated at 3.6 and 15 μm, but with longer exposure times. While the 3.6 μm fluxes coincide within 1 %, the 15 μm flux of the longer exposure is only off by <30 %, so that at least 40 % of the flux excess of the first measurement can be accounted for by transients. This is one of the few examples we encountered during OLP scientific validation with such a high impact by transients.

- The C100 filters are systematically too high by 20 to 45 %, except the 105 μm filter which is significantly too low. Again, this filter was the first filter in the multi-filter sequence performed on rev. 398. It is hard to believe the the flux deficiency in the 105 μm filter is due to background features, since the adjacent 100 μm filter does not show this problem.

- Like the 105 μm filter for C100 the P3 100 μm filter shows a similar drastic fall-off in flux.

- All C200 fluxes are too low and from 170 μm onwards are even negative. This is in contrast to the excellent absolute photometry performance at 170 μm (cf. Sect. 5.2.1).

The photometric accuracies are presented in Tab. 5.3. The 15 μm, 100 μm (P3) and 105 μm (C100) results from the multi-filter measurements on revs. 356 and 398 have not been taken into account. Also the C200 multi-filter measurements from rev. 356 could not be used to establish quantitative numbers.
The first attempt to perform a C100 multi-filter sequence on γ Dra on rev. 356 failed due to a telemetry drop which caused non-execution of the three last filter measurements and the FCS calibration measurement. However, the first three filter measurements at 105, 90,

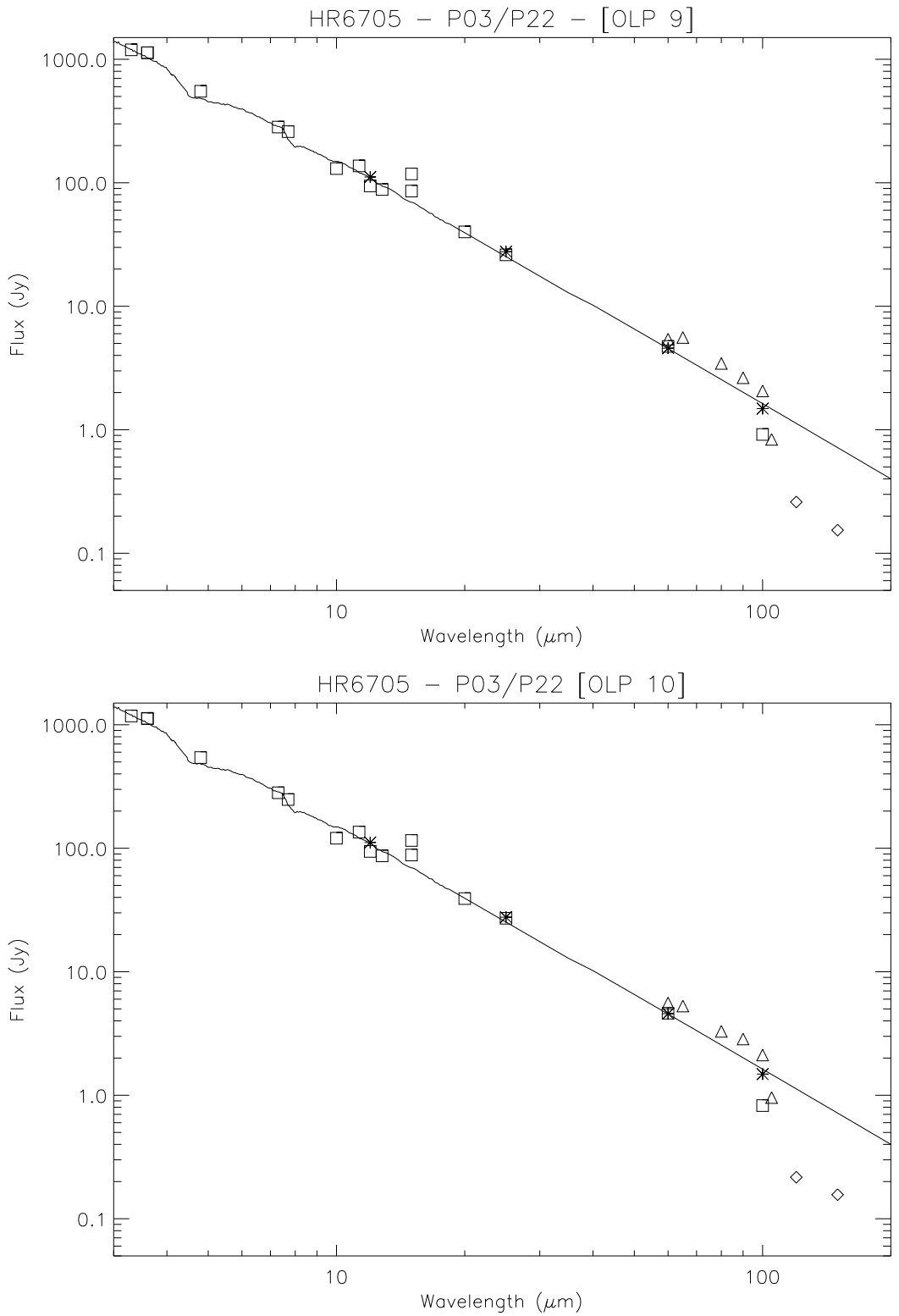

Figure 5.3: Comparison of PHT-P and PHT-C multi-filter photometry (P03/P22), using the full ISOPHOT filter set, with the composite spectrum and out to 300 μm extrapolated SED of γ Dra (HR 6705) provided by M. Cohen and with IRAS photometry for OLP 9.0b6 (upper panel) and OLP 10.0b8 (lower panel). All photometric points are color corrected for a 4000 K BB. The meaning of the symbols is the following: solid line: model, asterisk: IRAS, square: PHT-P (P03 AOT), triangle: C100 (P22 AOT), diamond: C200 (P22 AOT).

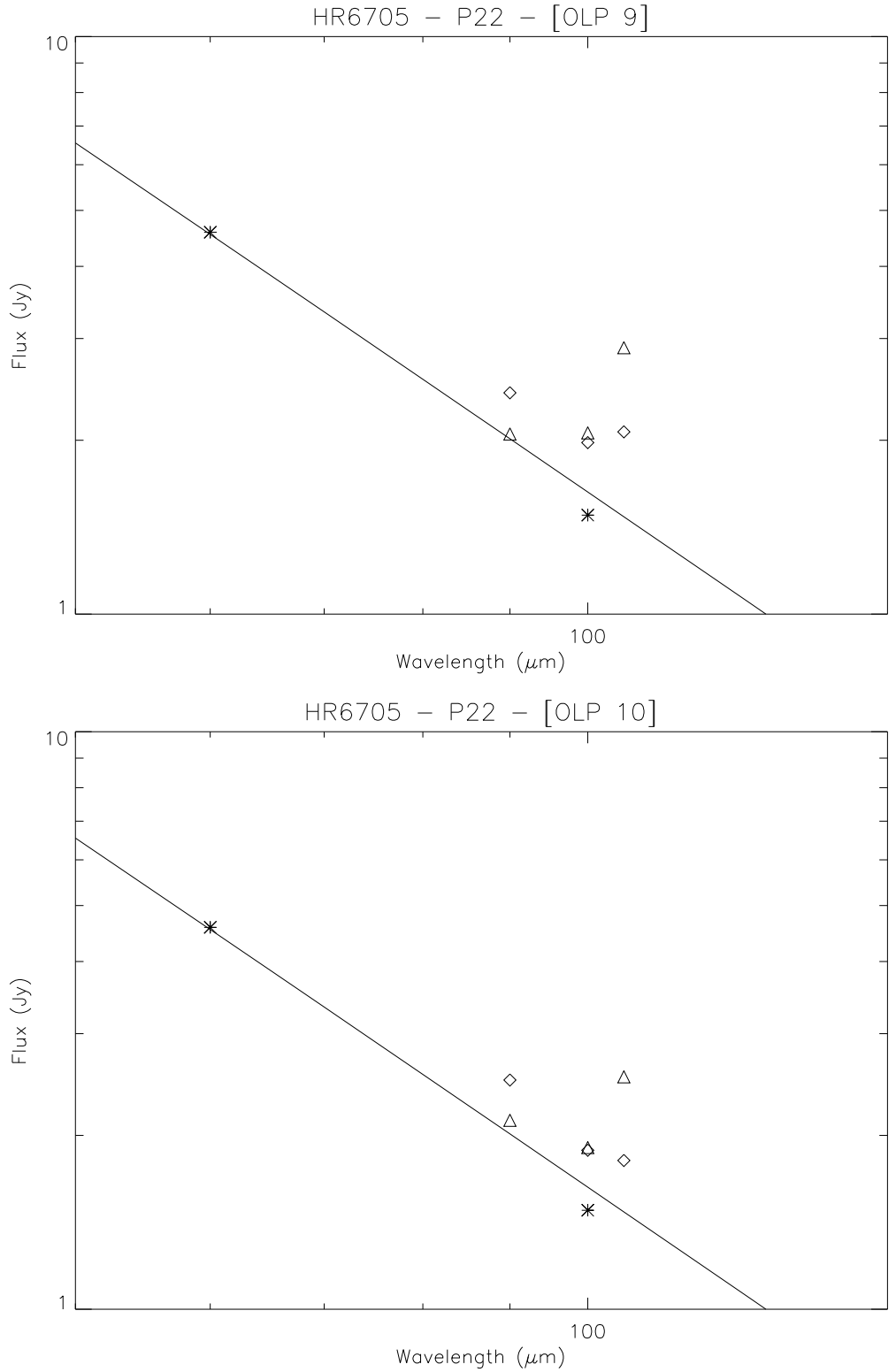

Figure 5.4: Comparison of PHT-C multi-filter photometry (P22) with the composite spectrum and out to 300 μm extrapolated SED of γ Dra (HR 6705) provided by M. Cohen and with IRAS photometry for OLP 9.0b6 (upper panel) and OLP 10.0b5 (lower panel). All photometric points are color corrected for a 4000 K BB. The meaning of the symbols is the following: solid line: model, asterisk: IRAS, square: triangle: C100 (reset interval setting #1), diamond: C100 (reset interval setting #2).

Table 5.3: Absolute and relative calibration accuracies per detector achieved for HR 6705 observation with OLP V10.0b8

detector	**absolute accuracy** [%]	**relative accuracy** [%]
P1	10 at 3.6 μm	<30
P2	< 2 at 20 μm	5
P3	< 2 at 60 μm	–
C100	20 at 60 μm	20

and 65 μm are available and are calibrated using the orbit dependent default responsivity calibration. The background is subtracted using the associated background measurement from' rev. 356 which is calibrated using the actual responsivity of its FCS measurement. Fig. 5.5 displays the result. We can see that the 65 and 90 μm filter are reasonably well calibrated (they are 15 % below the model, while the corresponding measurements using the actual responsivity from rev. 398 yield a too high flux by 30 to 40 %). On the other hand, the 105 μm filter shows a negative flux, which could be due to the derived background flux. From the consistency with the model in the 2 filters we conclude that the default responsivity calibration processing is consistently implemented.
Part 4 of the evaluation log section and Figs. 5.6 and 5.7 provide the surface brightness photometry of the background position and the comparison with COBE both for multi-filter photometry mode.
From Table 5.4 it can be seen that the consistency of the surface brightness measurements from the multi-filter photometry on the two revolutions 356 and 398 with COBE is in general within 30 C100 and C200, the ISOPHOT fluxes are in general higher, the DIRBE 140 μm filter surface brightness is too high. The filter sequence on rev. 356 (Fig. 5.6) provides a reasonably smooth background SED, also in the PHT-P range. The 3.3 μm (practically no flux within the selected aperture), 7.7 μm and 12.8 μm filters stick out, the offset of the 12.8 μm filter is reduced w.r.t. OLPV9.0. Also the 65 μm surface brightness is significantly above the ones of the other C100 filters.

Table 5.4: Consistency check of γ Dra background position surface brightness results from multi-filter photometry with COBE/DIRBE annual maps.

wavelength μm	**consistency w.r.t. COBE OLP V9.0b6** [%]	**consistency w.r.t. COBE OLP V10.0b8** [%]
12 (P,rev 356)	+32.5	+23.5
25 (P,rev 356)	-12.0	-27.5
60 (P,rev 356)	+0.8	-0.2
60 (C,rev 356)	-0.8	+28.2
60 (C,rev 398)	+13.4	+6.0
100 (P,rev 356)	+5.8	+23.1
100 (C,rev 356)	+21.1	+45.0
100 (C,rev 398)	+41.5	+22.3
150 (C,rev 356)	-8.5	-14.7
200 (C,rev 356)	+23.1	+14.2

Conclusions

- In the P1 and P2 part of the SED we do not recognize significant changes from OLP 9 to OLP 10. The large offset of the 15 μm flux from the rev. 356 measurement can

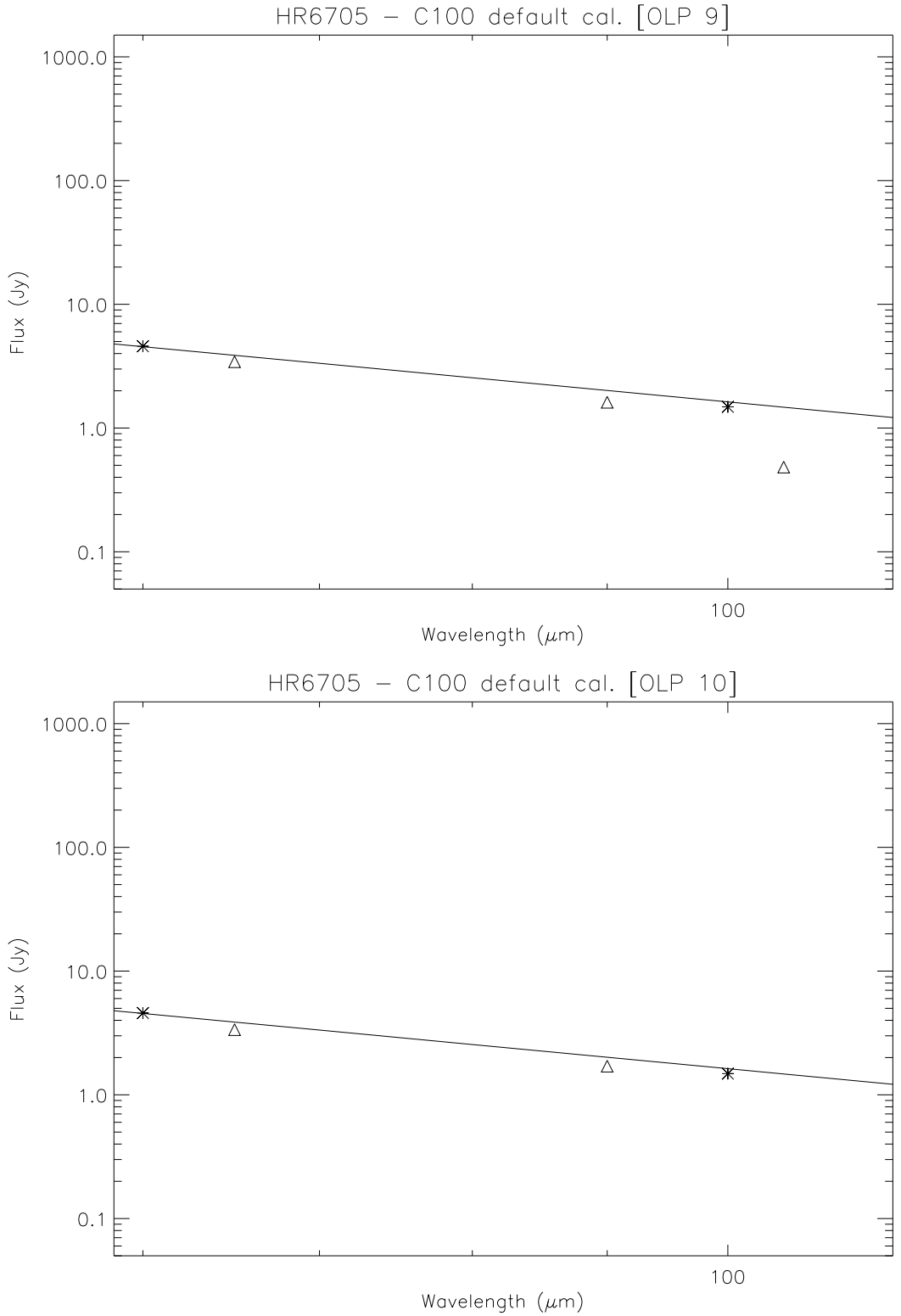

Figure 5.5: Comparison of the (incomplete due to telemetry drop) C100 PHT-C multi-filter photometry (P22) from rev. 356, using the default responsivity calibration (C100 FCS measurement failed due to the telemetry drop), with the out to 300 μm extrapolated SED of γ Dra (HR 6705) provided by M. Cohen and with IRAS photometry for OLP 9.0b6 (upper panel) and OLP 10.0b8 (lower panel). All photometric points are color corrected for a 4000 K BB. The meaning of the symbols is the following: solid line: model, asterisk: IRAS, triangle: C100 (P22 AOT).

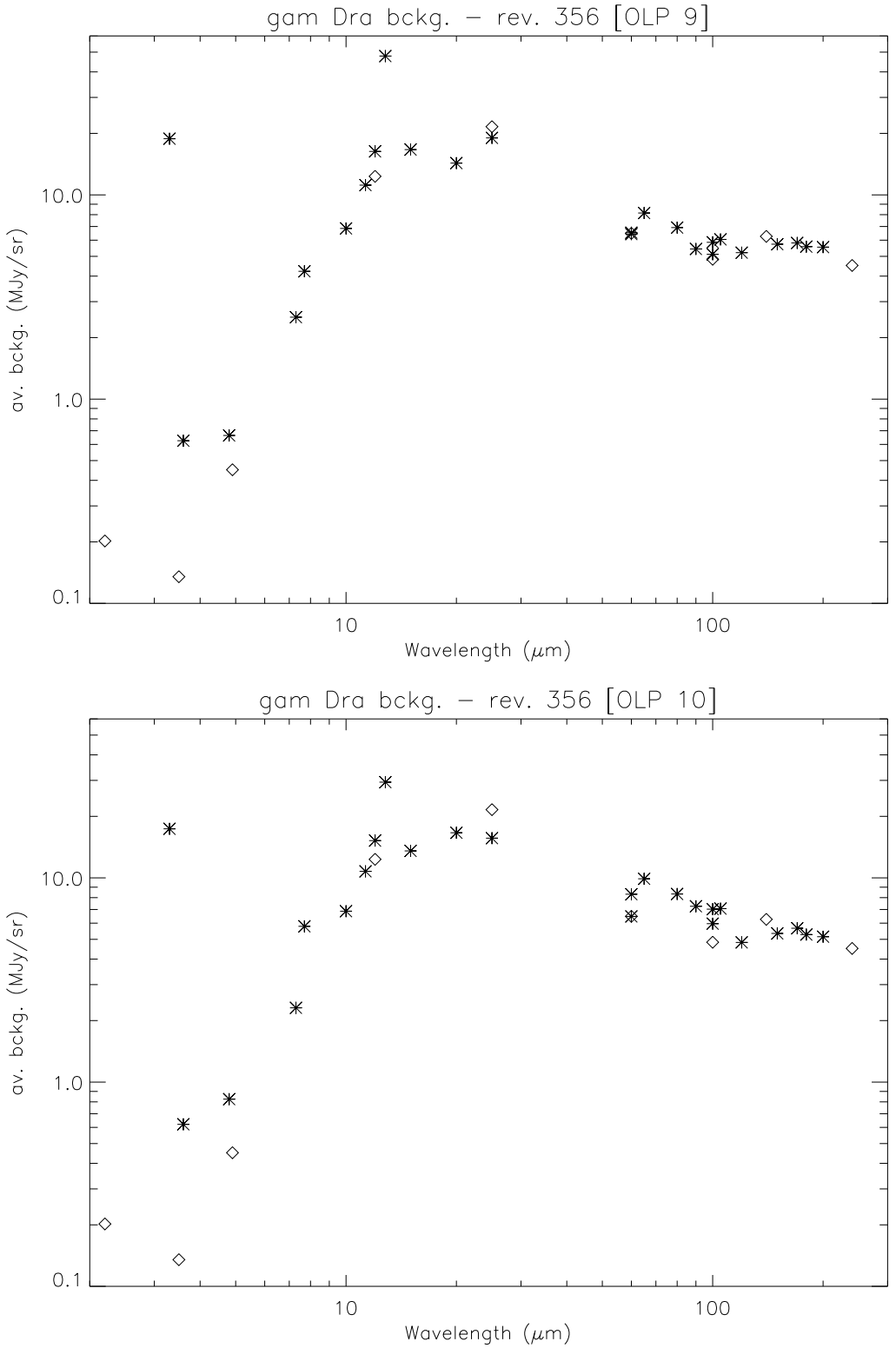

Figure 5.6: Comparison of OLP V9.0b6 and OLP V10.0b8 surface brightness, determined with the multi-filter photometry modes P03 & P22 (asterisk) on revolution 356, with COBE annual map fluxes (diamond).

be attributed to 60% to transient effects, which is exceptional among the considered OLP test cases.

- For P3 a good relative filter-to-filter calibration reported is lost, presumably by a too high background value derived for the 100 μm filter.

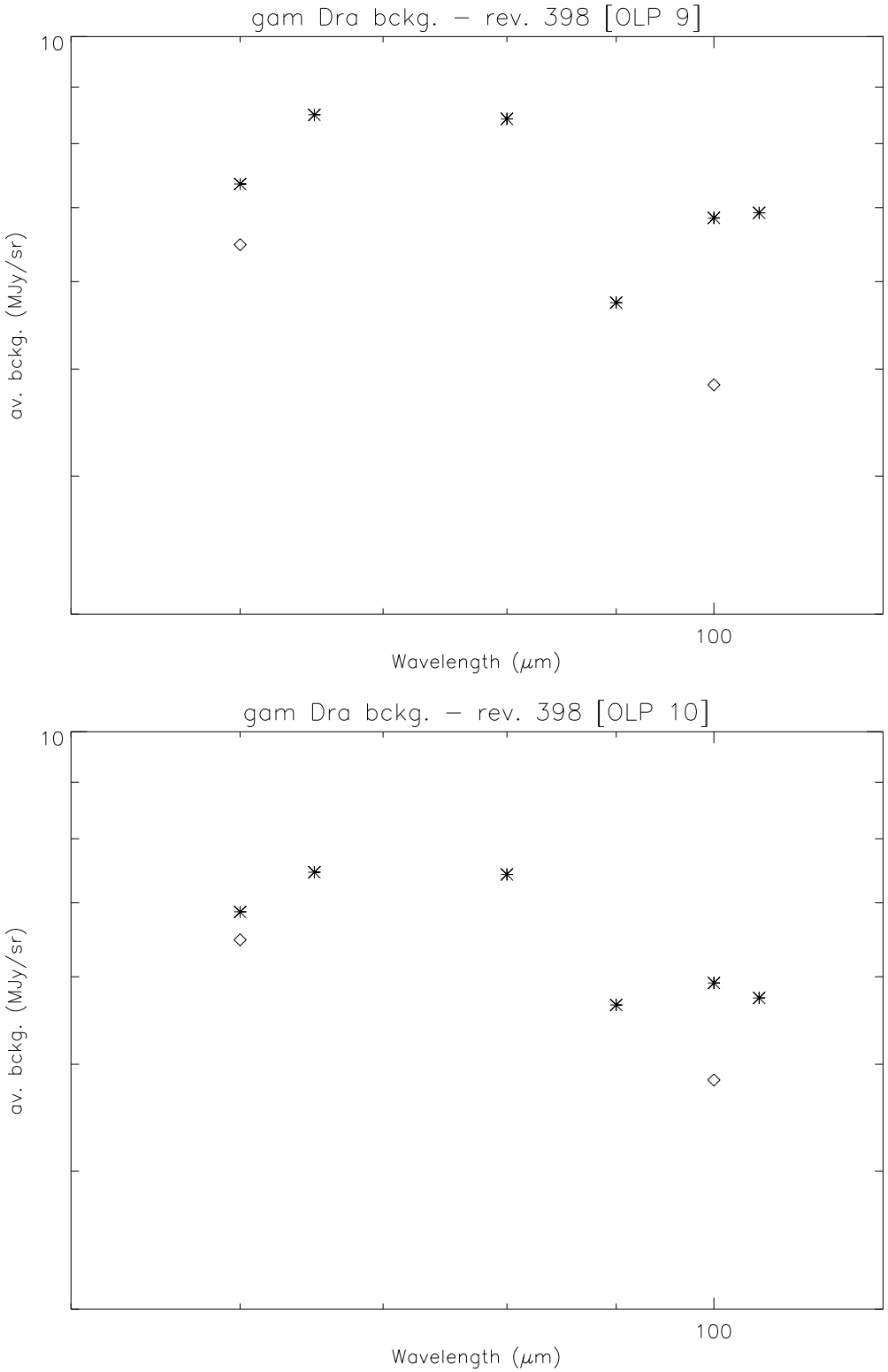

Figure 5.7: Comparison of OLP V9.0b6 and OLP V10.0b8 C100 surface brightness, determined with the multi-filter photometry mode P22 (asterisk) on revolution 398, with COBE annual map fluxes (diamond).

- For C100 the positive offset in flux of $20-40\,\%$ for all filters remains. A default responsivity calibration for C100 gives reasonably accurate photometry, however the fluxes are lower than the model in contrary to the fluxes derived with actual responsivity calibration. An exception is the $105\,\mu$m filter which shows a strong flux fall-off and

negative value, respectively for the actual and default responsivity calibration method. Very likely this is caused by the background subtraction.

- For C200 in multi-filter mode no useful results could be achieved. The fluxes are all too low or even negative.
- The consistency check of surface brightness photometry with COBE/DIRBE yields in general 30 %. The multi-filter background SEDs look relatively smooth, however some filters are systematically sticking out (as for other test cases): significant positive offsets of surface brightness are found for the 3.3 (presumably due to practically negligible flux and high dark noise), 12.8 and 65 μm filters.

Evaluation Log

1) P03 and P22 multi-filter photometry

Measurements:

PHT-P:	ppap35602102 (src+back)	FCS = 3.6, 20, 60 um
	ppap39801901 (src+back)	FCS = 3.6 um (3.6 & 15 um only)
	ppae35602101 (back)	FCS = 12, 20, 100 um
PHT-C1:	pcap39802003 (src+back)	FCS = 60 um
	pcae39802002 (back)	FCS = 90 um
PHT-C2:	pcap35602204 (src+back)	FCS = 170 um
	pcae35602203 (back)	FCS = 170 um

Colour correction: black body, T = 4000 K

Model: Cohen

Det	cwl (μm)	OLP 9	OLP 10	IRAS	Model	Δ (OLP 9)	Δ (OLP 10)
P1	3.3	1192.860	1178.314		1203.159	-0.86	-2.06
P1	3.6	1128.218	1119.692		1030.575	9.47	8.65
P1b	3.6	1130.687	1127.821		1030.575	9.71	9.44
P1	4.8	550.869	542.802		482.322	14.21	12.54
P1	7.3	282.687	281.693		285.925	-1.13	-1.48
P1	7.7	259.463	248.182		224.074	15.79	10.76
P1	10.0	130.315	120.590		149.024	-12.55	-19.08
P1	11.3	136.942	135.215		120.822	13.34	11.91
P1	12.0	94.265	94.278	111.479	108.718	-13.29	-13.28
P1	12.8	88.252	86.744		93.877	-5.99	-7.60
P1	15.0	117.956	115.654		69.510	69.70	66.39
P1b	15.0	85.706	88.212		69.510	23.30	26.91
P2	20.0	39.997	39.144		39.387	1.55	-0.62
P2	25.0	26.089	27.105	27.671	25.229	3.41	7.43
C1	60.0	5.410	5.583	4.583	4.545	19.03	22.84
P3	60.0	4.729	4.615	4.583	4.545	4.05	1.54
C1	65.0	5.588	5.277		3.872	44.32	36.29
C1	80.0	3.444	3.290		2.550	35.06	29.02
C1	90.0	2.637	2.853		2.012	31.05	41.81
C1	100.0	2.062	2.116	1.483	1.627	26.76	30.08
P3	100.0	0.916	0.825	1.483	1.627	-43.71	-49.29
C1	105.0	0.836	0.958		1.474	-43.30	-35.04
C2	120.0	0.260	0.217		1.126	-76.90	-80.74
C2	150.0	0.154	0.157		0.717	-78.54	-78.16
C2	170.0	-0.327	-0.311		0.556	-158.84	-155.86
C2	180.0	-1.183	-1.141		0.495	-338.70	-330.31
C2	200.0	-0.209	-0.056		0.400	-152.14	-114.07

2) P22 multi-filter photometry with different reset interval settings

Measurements:

PHT-C (a):	pcap67100802 (src+back)	FCS = 90 um
	pcap67100801 (back)	FCS = 90 um
PHT-C (b):	pcap67100911 (src+back)	FCS = 90 um
	pcap67100910 (back)	FCS = 90 um

Colour correction: black body, T = 4000 K

Model: Cohen

Det	cwl (μm)	OLP 9	OLP 10	IRAS	Model	Δ (OLP 9)	Δ (OLP 10)
C1a	90.0	2.050	2.124		2.012	1.91	5.57
C1a	100.0	2.059	1.905	1.483	1.627	26.57	17.11
C1a	105.0	2.893	2.526		1.474	96.24	71.37
C1b	90.0	2.417	2.494		2.012	20.10	23.96
C1b	100.0	1.981	1.885	1.483	1.627	21.77	15.83
C1b	105.0	2.068	1.810		1.474	40.29	22.77

3) C100 on-source default calibration

Measurements:

PHT-C1:	pcap35602204 (src+back)	no FCS (orbit dep. default R)
	pcae35602203 (back)	FCS = 90 um

Colour correction: black body, T = 4000 K

Model: Cohen

Det	cwl (μm)	OLP 9	OLP 10	IRAS	Model	Δ (OLP 9)	Δ (OLP 10)
C1	65.0	3.433	3.362		3.872	-11.33	-13.18
C1	90.0	1.614	1.704		2.012	-19.76	-15.30
C1	105.0	0.483	-0.225		1.474	-67.21	-115.29

4) Surface brightness on background positions:

a) multi-filter photometry on revolution 356 (not colour corrected)

λ	OLP9 (MJy/sr)	OLP10 (MJy/sr)	COBE (MJy/sr)
3.3	18.83	17.38	
3.6	0.63	0.62	
4.8	0.66	0.83	
7.3	2.52	2.31	
7.7	4.22	5.79	
10.0	6.85	6.87	
11.3	11.16	10.76	
12.0	16.32	15.21	12.32
12.8	47.79	29.41	
15.0	16.65	13.55	
20.0	14.30	16.62	
25.0	19.00	15.65	21.58
60.0	6.53	6.47	6.48
100.0	5.12	5.96	4.84
60.0	6.43	8.31	6.48
65.0	8.15	9.90	
80.0	6.92	8.34	
90.0	5.43	7.26	
100.0	5.86	7.02	4.84
105.0	6.05	7.07	
120.0	5.21	4.83	
150.0	5.73	5.34	6.26
170.0	5.81	5.66	
180.0	5.58	5.28	
200.0	5.55	5.15	4.51

b) multi-filter C100 photometry on revolution 398 (not colour corrected)

λ	OLP9 (MJy/sr)	OLP10 (MJy/sr)	COBE (MJy/sr)
60.0	7.35	6.87	6.48
65.0	8.50	7.46	
80.0	8.42	7.43	
90.0	5.74	5.66	
100.0	6.85	5.92	4.84
105.0	6.93	5.74	

5.1.3 PHT03 Multi-filter Photometry: The SED of Sirius (HR 2491)

Motivation

Beside Vega (HR 7001), Sirius is the main primary stellar standard with a model provided by M. Cohen (1-300 μm, R = 4000 up to 35 μm, delivered 12-Jan-1996). Therefore, a dedicated cross-calibration program was performed on this star using absolute photometry complemented by multi-filter photometry out to 25 μm.

Method

We compare the color corrected flux values of both OLP V9.0b6 and OLP V10.0b7 results against the model prediction by Cohen and IRAS photometry.

Results

The comparison of the OLP V9.0b6 and OLP V10.0b7 photometry with the model is given in part 1 of the evaluation log section. We estimate the absolute photometric accuracy per detector assembly for this target as the deviation from the model flux in the filter in which the FCS calibration was done, and the relative filter-to-filter accuracy as the peak-to-peak variation of the other filters around this offset. Two multi-filter sequences were performed, one from 3.3 to 12 μm with absolute calibration at 3.3 μm, and the other one from 11.3 to 15 μm with absolute calibration at 12.8 μm. The photometric accuracies are presented in Tab. 5.5. Fig. 5.8 shows the PHT photometric data points in comparison to the model and IRAS photometry (color corrected) for OLP 9.0b6 and OLP 10.0b7, respectively. The systematic offset beyond 10 μm is caused by the fact that no background measurement is available and hence the background, which is noticable here, is not subtracted. Therefore, the calibration accuracies for these wavelengths are actually better, since the background is estimated to account for nearly the whole offset.

Table 5.5: Absolute and relative calibration accuracies per detector achieved for Sirius observation with OLP V10.0b7

detector	**absolute accuracy** [%]	**relative accuracy** [%]
P1*	< 8 at 3.3 μm	7
P1*	< 5 at 12.8 μm	< 5

* no subtraction of ZL background performed!

Conclusions

- The accuracy of P1 multi-filter photometry is better than 10 % absolute and better than 10 % relative.

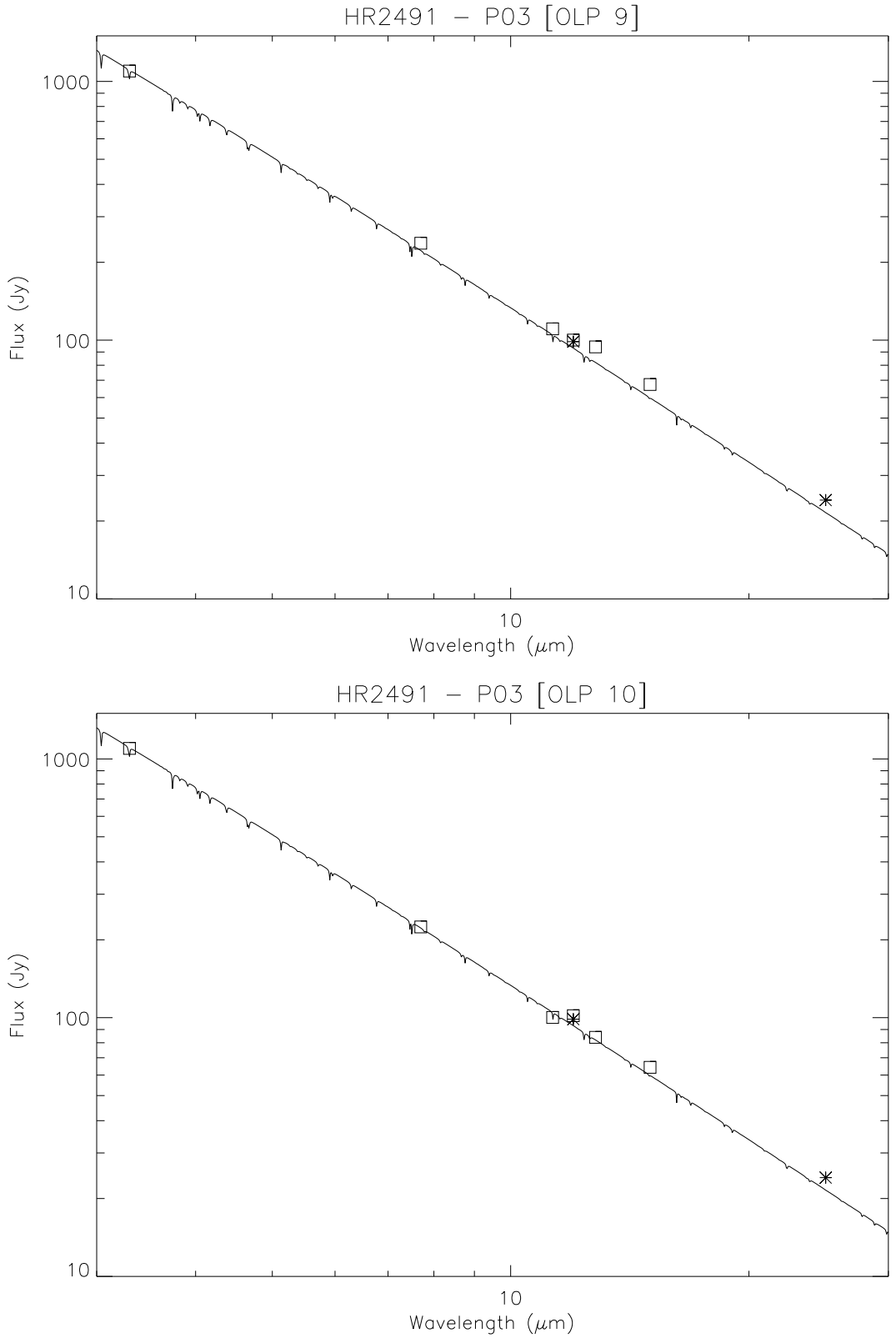

Figure 5.8: Comparison of PHT-P multi-filter photometry with the composite spectrum of Sirius (HR 2491) provided by M. Cohen and with IRAS photometry for OLP 9.0b6 (upper panel) and OLP 10.0b7 (lower panel). All photometric points are color corrected for a 10000 K BB. The meaning of the symbols is the following: solid line: model, asterisk: IRAS, square: PHT-P (P03 AOT).

Evaluation Log

1) P03 multi-filter photometry

Measurements:
PHT-P1: ppap70705302 (src+back) FCS = 3.3 um
ppap70705301 (src+back) FCS = 12.8 um

Colour correction: black body, T = 10000 K

Model: Cohen

Det	cwl (μm)	OLP 9	OLP 10	IRAS	Model	Δ (OLP 9)	Δ (OLP 10)
ppap70705301:							
P1	11.3	110.563	100.210		100.654	9.84	-0.44
P1	12.8	94.161	83.962		82.001	14.83	2.39
P1	15.0	67.398	64.277		59.566	13.15	7.91
ppap70705302:							
P1	3.3	1096.323	1097.842		1021.900	7.28	7.43
P1	7.7	236.889	224.212		222.038	6.69	0.98
P1	12.0	100.059	101.767	98.690	93.157	7.41	9.24

5.1.4 PHT03 Multi-filter Photometry: The SED of HR 6847

Motivation

HR 6847 is a standard star 300 times fainter than Sirius. A similar multi-filter observation as for Sirius was performed for this star.

Method

We compare the color corrected flux values of both OLP V9.0b6 and OLP V10.0b5 results against the model prediction by Hammersley and IRAS photometry.

Results

The comparison of the OLP V9.0b6 and OLP V10.0b5 photometry with the model is given in part 1 of the evaluation log section. We estimate the absolute photometric accuracy per detector assembly for this target as the deviation from the model flux in the filter in which the FCS calibration was done, and the relative filter-to-filter accuracy as the peak-to-peak variation of the other filters around this offset. The photometric accuracies are presented in Tab. 5.6. We do not consider the results for the 12.0 μm filter. Fig. 5.9 shows the PHT photometric data points in comparison to the model and IRAS photometry (color corrected) for OLP 9.0b6 and OLP 10.0b5, respectively.

Table 5.6: Absolute and relative calibration accuracies per detector achieved for HR 6847 observation with OLP V10.0b5

detector	**absolute accuracy** [%]	**relative accuracy** [%]
P1	< 5 at 3.6 μm	5

Conclusions

- The accuracy of the P1 multi-filter photometry is better than 5 % absolute and better than 5 % relative. This does, however, not consider the performance in the 12 μm filter. Whether the zero flux result is due to a transient effect or a calibration issue remains open.

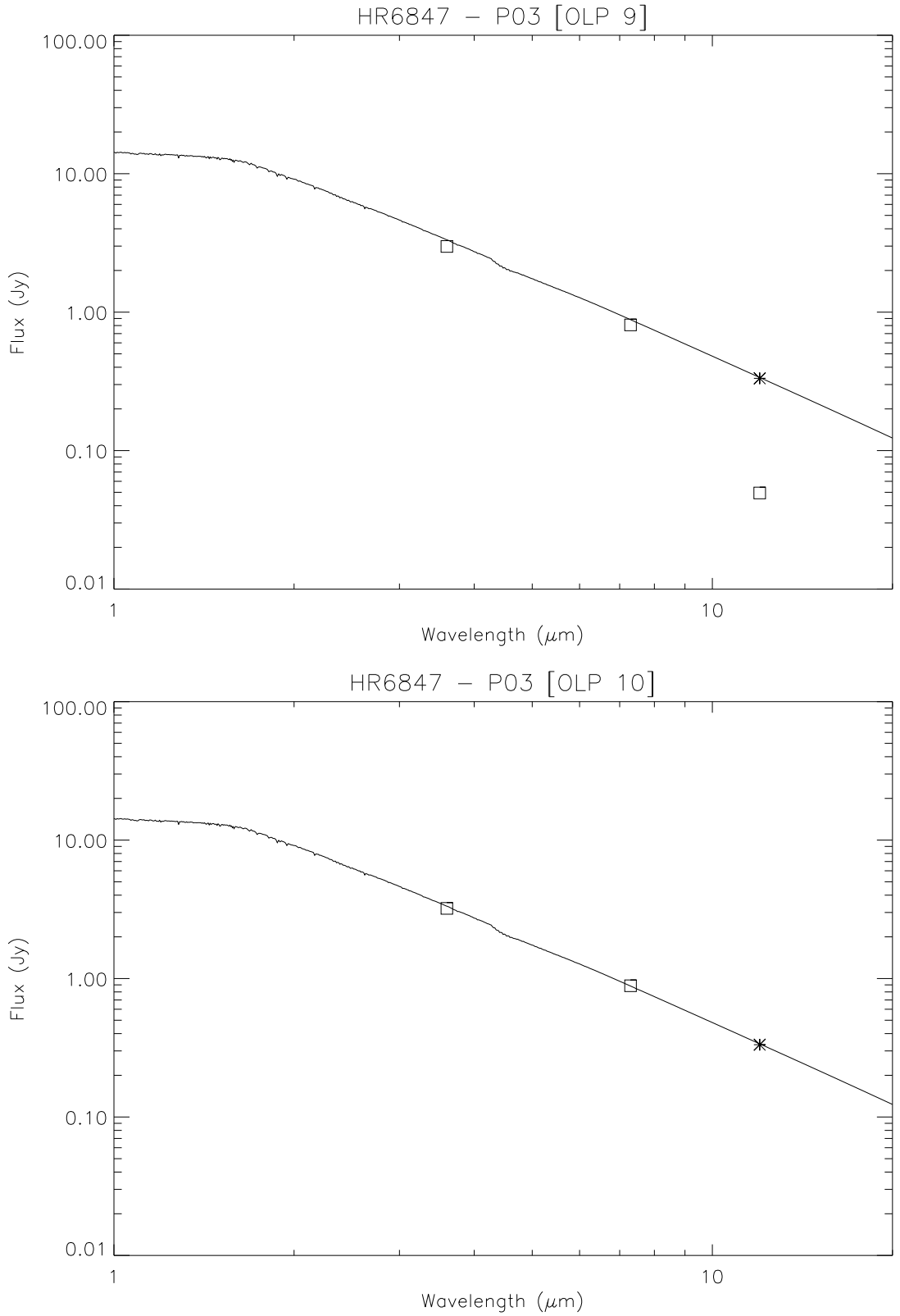

Figure 5.9: Comparison of PHT-P multi-filter photometry with the model of HR 6847 provided by P. Hammersley and with IRAS photometry for OLP 9.0b6 (upper panel) and OLP 10.0b5 (lower panel). All photometric points are color corrected for a 5720 K BB. The meaning of the symbols is the following: solid line: model, asterisk: IRAS, square: PHT-P (P03 AOT).

Evaluation Log

1) P03 multi-filter photometry

Measurements:
PHT-P: ppap70601102 (src+back) FCS = 3.6 um
ppap70601101 (back) FCS = 3.6 um

Colour correction: black body, T = 5720 K

Model: Hammersley

Det	cwl (μm)	OLP 9	OLP 10	IRAS	Model	Δ (OLP 9)	Δ (OLP 10)
P1	3.6	2.982	3.210		3.333	-10.52	-3.67
P1	7.3	0.809	0.887		0.883	-8.41	0.50
P1	12.0	0.049	0.006	0.333	0.337	-85.35	-98.28

5.1.5 PHT03 Multi-filter Photometry: The SED of HR 7469

Motivation

HR 7469 is a faint standard star in the $20 - 25\,\mu$m range.

Method

We compare the color corrected flux values of both OLP V9.0b6 and OLP V10.0b5 results against the model prediction by Hammersley and IRAS photometry.

Results

The comparison of the OLP V9.0b6 and OLP V10.0b5 photometry with the model is given in part 1 of the evaluation log section. Fig. 5.10 shows the PHT photometric data points in comparison to the model and IRAS photometry (color corrected) for OLP 9.0b6 and OLP 10.0b5, respectively. The resulting fluxes are by far too low. The total flux is $5 - 10$ times stronger than the expected source flux. Therefore, the likely reason is that the uncertainty of the background measurement causes the small differential source flux.

Conclusions

- No reasonable calibration accuracies can be derived for this faint calibration standard. The uncertainties in the background measurement and subtraction determine the achieved accuracy.

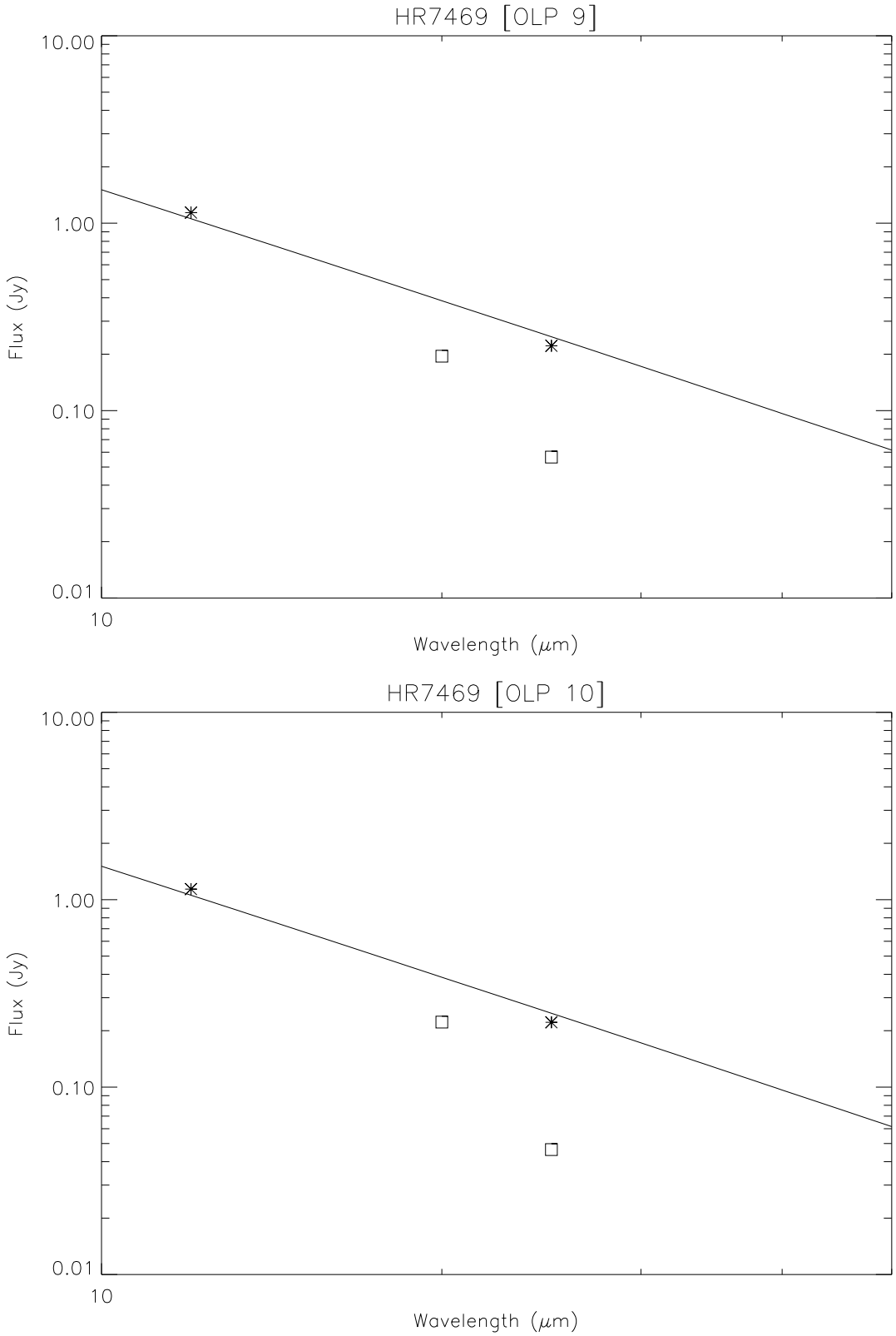

Figure 5.10: Comparison of PHT-P multi-filter photometry with the model of HR 7469 provided by P. Hammersley and with IRAS photometry for OLP 9.0b6 (upper panel) and OLP 10.0b5 (lower panel). All photometric points are color corrected for a 6622 K BB. The meaning of the symbols is the following: solid line: model, asterisk: IRAS, square: PHT-P (P03 AOT).

Evaluation Log

1) P03 multi-filter photometry

Measurements:

PHT-P:	ppap71300502 (src+back)	FCS = 25 um
	ppap71300501 (back)	FCS = 25 um

Colour correction: black body, T = 6622 K

Model: Hammersley

Det	cwl (μm)	OLP 9	OLP 10	IRAS	Model	Δ (OLP 9)	Δ (OLP 10)
P2	20.0	0.195	0.222		0.386	-49.39	-42.36
P2	25.0	0.056	0.046	0.222	0.248	-77.21	-81.27

5.1.6 PHT03 Multi-filter Photometry: The SED of HD 207129

Motivation

HD 207129 is a star with a FIR excess. Out to 25 μm the SED behaves like the one of an early G-star. It is somewhat brighter than HR 6847 (Sect. 5.1.4) in the P1 range and somewhat fainter than HR 7469 (Sect. 5.1.5) in the P2 range.

Method

We compare the color corrected flux values of both OLP V9.0b6/9.01 and OLP V10.0b5 results against the scaled model predictions of HD 168009 and HD 172323 by Hammersley and IRAS photometry.

Results

The comparison of the OLP V9.0b6 and OLP V10.0b5 photometry with the model is given in part 1 of the evaluation log section. We estimate the absolute photometric accuracy per detector assembly for this target as the deviation from the model flux in the filter in which the FCS calibration was done, and the relative filter-to-filter accuracy as the peak-to-peak variation of the other filters around this offset. The photometric accuracies are presented in Tab. 5.7. Figs. 5.11 and 5.12 show the PHT photometric data points in comparison to the model and IRAS photometry (color corrected) for OLP 9.0b6/9.01 and OLP 10.0b5, respectively.

Table 5.7: Absolute and relative calibration accuracies per detector achieved for HD 207129 observation with OLP V10.0b5

detector	**absolute accuracy** [%]	**relative accuracy** [%]
P1	< 10 at 3.6 μm	< 10

Conclusions

- The accuracy of the P1 multi-filter photometry is better than 10 % absolute and better than 10 % relative. In particular the relative filter-to-filter calibration of the 7.7 μm filter has been improved w.r.t. the OLP V9.
- For the P2 fluxes a similar flux fall-off behaviour as in the case of HR 7469 is observed.

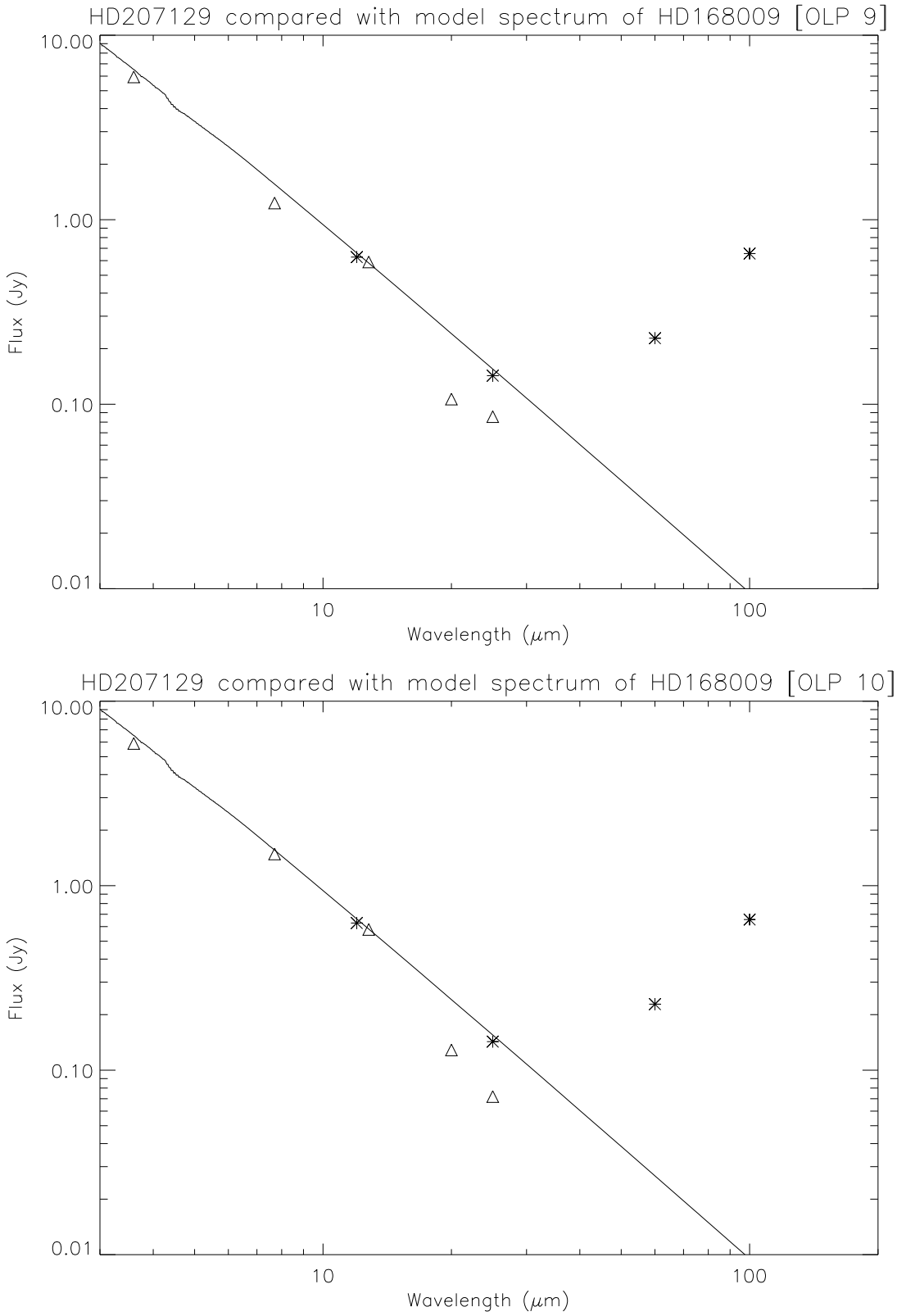

Figure 5.11: Comparison of PHT-P multi-filter photometry of HD207129 (G0V, m_v = 5.58 mag) with the scaled model of HD 168009 (G2V, m_v = 6.309 mag) provided by P. Hammersley and with IRAS photometry for OLP 9.0b6/9.01 (upper panel) and OLP 10.0b5 (lower panel). All photometric points are color corrected for a 5720 K BB. The meaning of the symbols is the following: solid line: model, asterisk: IRAS, square: PHT-P (P03 AOT).

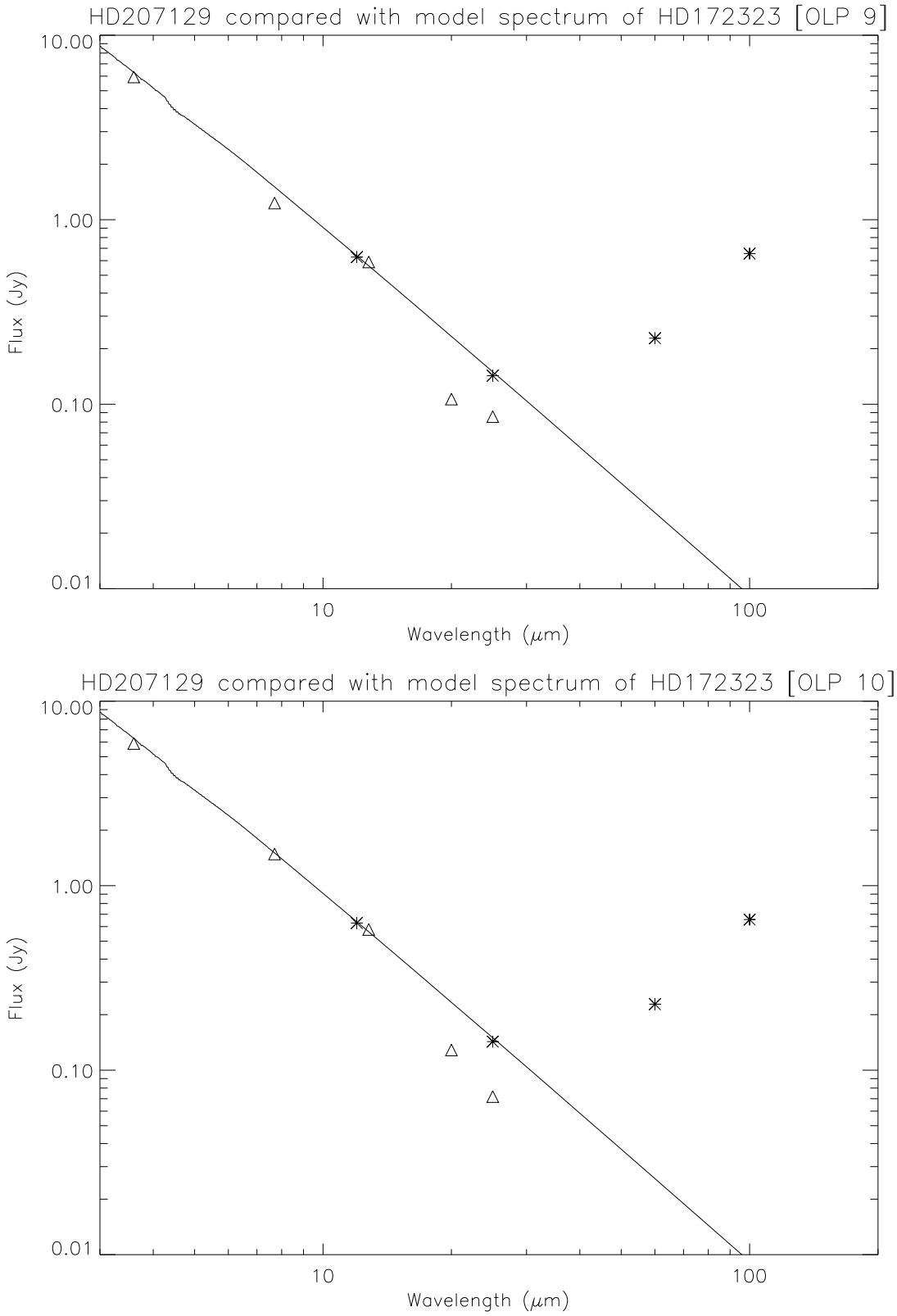

Figure 5.12: Comparison of PHT-P multi-filter photometry of HD207129 (G0V, m_v = 5.58 mag) with the scaled model of HD 172323 (G2V, m_v = 9.908 mag) provided by P. Hammersley and with IRAS photometry for OLP 9.0b6/9.01 (upper panel) and OLP 10.0b5 (lower panel). All photometric points are color corrected for a 5720 K BB. The meaning of the symbols is the following: solid line: model, asterisk: IRAS, square: PHT-P (P03 AOT).

Evaluation Log

1) P03 multi-filter photometry versus scaled HD 168009 model

Measurements:
PHT-P : PPAP55302204 (src+back) FCS = 3.6
PHT-P : PPAP55302201 (back) FCS = 3.6
PHT-P : PPAP55302203 (src+back) FCS = 12.8, 20 um
PHT-P : PPAP55302202 (back) FCS = 12.8, 20 um
Colour correction: black body, T = 5720 K

Model: Hammersley (HD168009) scaled with V-mag 5.58mag(star)/6.309mag(ref)

Det	cwl (μm)	OLP 9	OLP 10	IRAS	Model	Δ (OLP 9)	Δ (OLP 10)
P1	3.6	5.942	5.898		6.522	-8.89	-9.57
P1	7.7	1.232	1.486		1.558	-20.96	-4.68
P1	12.8	0.590	0.579		0.582	1.37	-0.57
P2	20.0	0.107	0.129		0.241	-55.82	-46.67
P2	25.0	0.086	0.072	0.143	0.155	-44.81	-53.63

2) P03 multi-filter photometry versus scaled HD 172323 model

Measurements:
PHT-P : PPAP55302204 (src+back) FCS = 3.6
PHT-P : PPAP55302201 (back) FCS = 3.6
PHT-P : PPAP55302203 (src+back) FCS = 12.8, 20 um
PHT-P : PPAP55302202 (back) FCS = 12.8, 20 um
Colour correction: black body, T = 5720 K

Model: Hammersley (HD172323) scaled with V-mag 5.58mag(star)/8.07mag(ref)

Det	cwl (μm)	OLP 9	OLP 10	IRAS	Model	Δ (OLP 9)	Δ (OLP 10)
P1	3.6	5.942	5.898		6.300	-5.68	-6.38
P1	7.7	1.232	1.486		1.505	-18.17	-1.32
P1	12.8	0.590	0.579		0.562	4.95	2.94
P2	20.0	0.107	0.129		0.233	-54.26	-44.79
P2	25.0	0.086	0.072	0.143	0.150	-42.87	-52.00

5.1.7 PHT03 and PHT22 Multi-filter Photometry: The SED of Arp 220

Motivation

TDTs 47600413(background, PHT-P), 47600414(Arp 220, PHT-P), 47600415(background, PHT-C), 47600416(Arp 220, PHT-C) is one of the key OLP validation cases [1]. The staring mode AOTs PHT-03 and PHT-22 in all PHT filters measure a galaxy SED which is steeply rising between 10 and 60 μm and gradually declining beyond 100 μm, hence has a very different shape than a stellar atmosphere SED. It can therefore be used for a check of the robustness of the relative filter-to-filter calibration and the color correction factors applied to modified Black Bodies in the temperature range 50 – 120 K. Arp 220 is significantly bright over the full wavelength range from 3.3 to 200 μm. Its photometric properties are discussed in detail in "Infrared spectral energy distributions of the interacting galaxies Arp 244, NGC 6240 and Arp 220" [15].

Method

We compare the background subtracted flux values of both OLP V9.0b6 and OLP V10.0b7/b8 results against the IRAS photometry and a model fit based on the OLP V6.x calibration.

Results

Fig. 5.13 shows the derived SED for Arp 220. The model fit from [15] is plotted as a guide line to easier recognize the changes w.r.t. OLP V9.0. Note that this fit cannot serve as reference photometry.
We have color corrected the photometry w.r.t. modified blackbodies with emissivities $\propto \lambda^{-1}$ for the 12.8 to 200 μm range (for details, see part 2 of the evaluation log section). This color corrected SED is shown in Fig. 5.14.
We notice the following results:

- The C100 photometry is now more consistent with P3 and C200 photometry, still a bit higher than IRAS. The SED looks very smooth from 60 to 200 μm, except for the dip at 90 μm.
- The P2 20 μm flux looks improved, the 12.8 μm flux is still too high, but reduced now.

In Fig. 5.15 we plot the derived multi-filter surface brightness values in comparison with COBE photometry.
The Arp 220 background SED looks very smooth now and consistent with the COBE/DIRBE photometry, including the PHT-P part. Only the 3.3 μm (practically no flux for the selected aperture) and still the 12.8 μm filter points stick out significantly. Also the 65 and 80 μm surface brightness show a positive offset like for many other test cases.

Conclusions

- The C100 photometry is now more consistent with P3 and C200 photometry, still a bit higher than IRAS. The SED looks very smooth from 60 to 200 μm, except for the dip at 90 μm.
- Surface brightness photometry for PHT-P looks very good, except for the 3.3 μm and 12.8 μm filters which show also problems for the point source photometry.
- Surface brightness photometry for PHT-C confirms the systematic excess for the 65 and 80 μm fluxes.

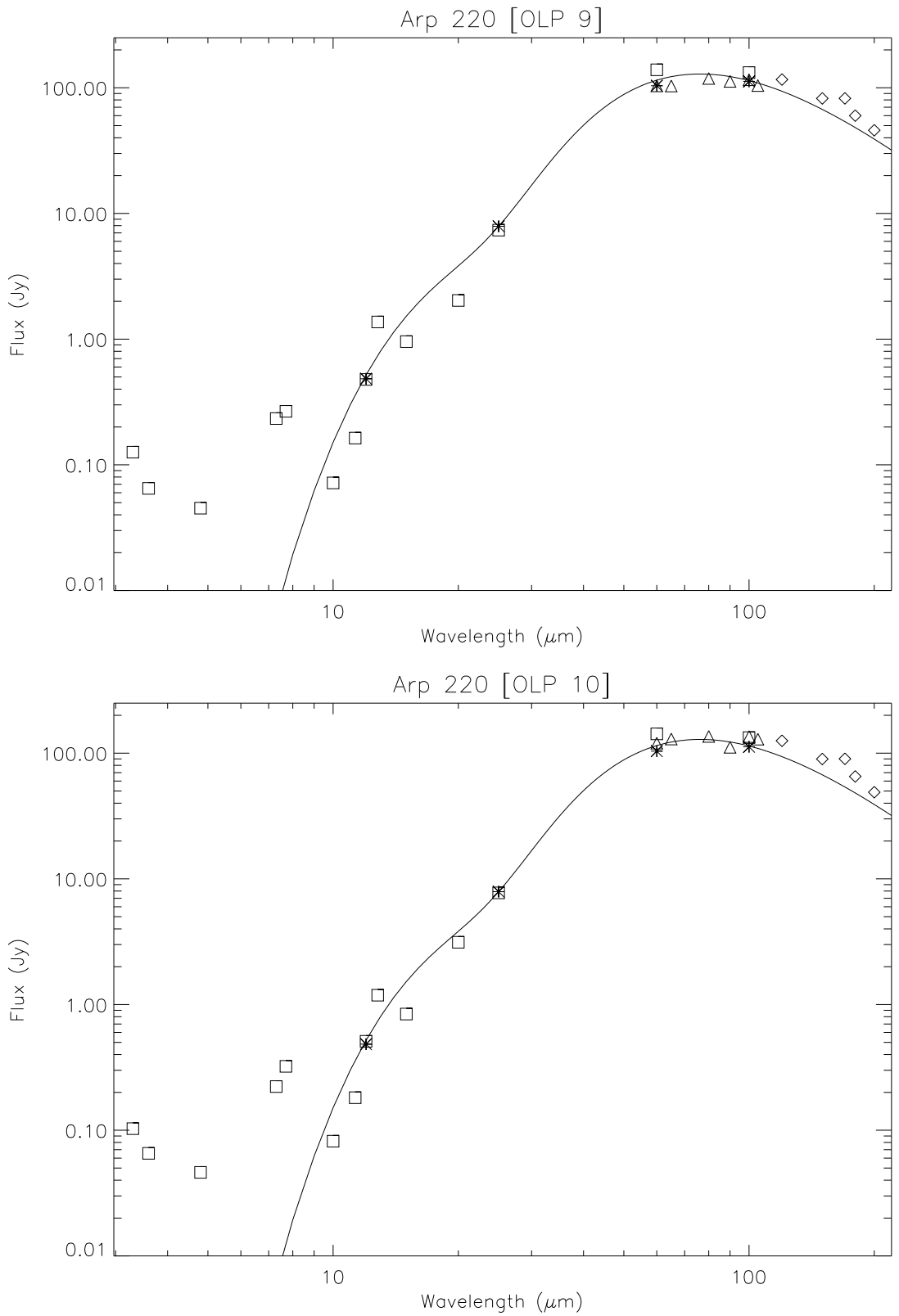

Figure 5.13: Comparison of PHT-P and PHT-C photometry, using the full ISOPHOT filter set, with IRAS photometry and the model fit as described in [15]. Note that this model fit only serves as a guide for the eye to recognize more easily the changes between the two versions. It is not an absolute photometric reference. No color correction has been applied. The meaning of the symbols is the following: solid line: model, asterisk: IRAS, square: PHT-P (P03 AOT), triangle: C100 (P22 AOT), diamond: C200 (P22 AOT).

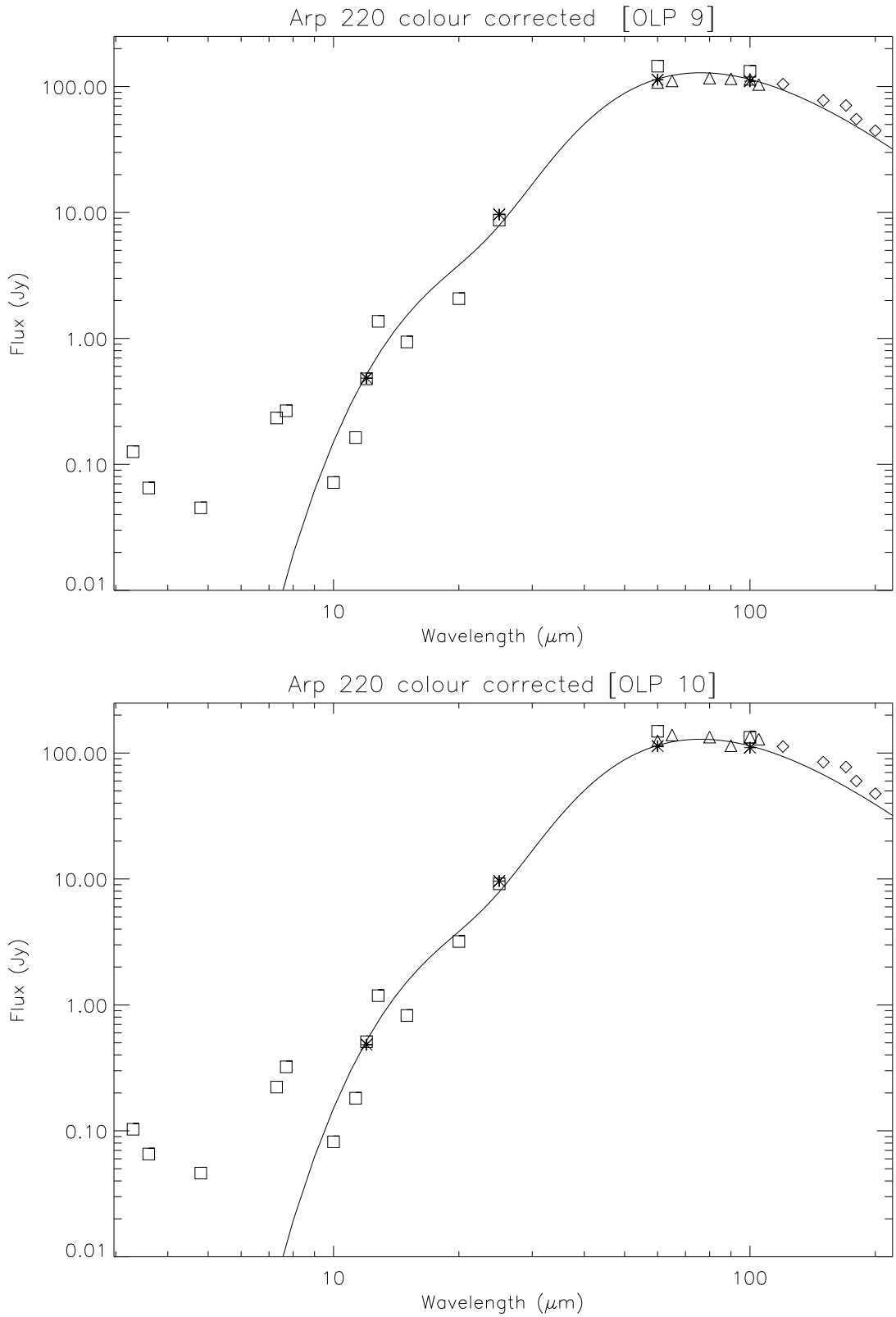

Figure 5.14: Comparison of PHT-P and PHT-C photometry, using the full ISOPHOT filter set, with IRAS photometry and the model fit as described in [15]. Note that this model fit only serves as a guide for the eye to recognize more easily the changes between the two versions. It is not an absolute photometric reference. Color correction according to the model parameters, modified BBs $\propto \lambda^{-1}$ with T1 = 120 K and T2 = 47 K, has been applied . The meaning of the symbols is the following: solid line: model, asterisk: IRAS, square: PHT-P (P03 AOT), triangle: C100 (P22 AOT), diamond: C200 (P22 AOT).

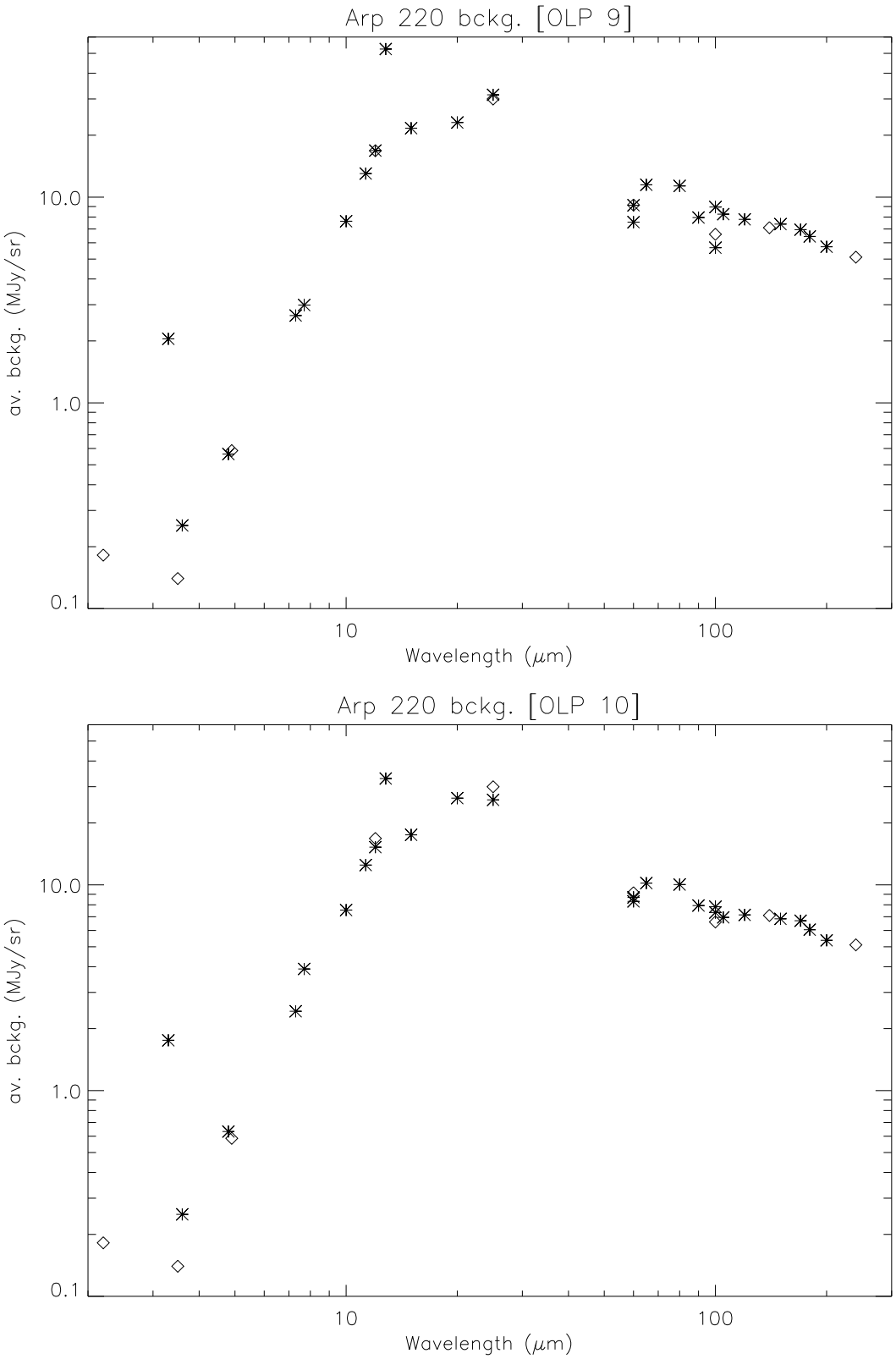

Figure 5.15: Comparison of PHT surface brightness photometry with COBE, both for OLP 9.0b6 and OLP 10.0b8. Asterisk: PHT-P and PHT-C photometry, diamond: COBE.

Evaluation Log

1) point source photometry of Arp 220 (not colour corrected)

Measurements:

PHT-P:	ppap47600414 (src+back)	FCS = 3.3, 25, 100 um
	ppae47600413 (back)	FCS = 3.3, 20, 100 um
PHT-C:	pcap47600416 (src+back)	FCS = 90, 170 um
	pcae47600415 (back)	FCS = 90, 170 um

Model: Sum of 2 modified bb, em. $\propto \lambda^{-1}$, T1 = 120 K, T2 = 47 K

Det	cwl (μm)	OLP 9	OLP 10	IRAS	Model	Δ (OLP 9)	Δ (OLP 10)
P1	3.3	0.126	0.103		-0.001	-17651.58	-14428.86
P1	3.6	0.065	0.066		-0.001	-11136.64	-11236.93
P1	4.8	0.045	0.046		-0.000	-66302.65	-67769.79
P1	7.3	0.233	0.223		0.009	2601.82	2477.23
P1	7.7	0.266	0.322		0.015	1702.32	2080.86
P1	10.0	0.072	0.082		0.151	-52.50	-45.82
P1	11.3	0.163	0.181		0.367	-55.48	-50.51
P1	12.0	0.478	0.510	0.484	0.519	-8.03	-1.87
P1	12.8	1.369	1.186		0.746	83.47	58.92
P1	15.0	0.956	0.840		1.525	-37.31	-44.91
P2	20.0	2.031	3.130		3.827	-46.93	-18.21
P2	25.0	7.365	7.732	7.910	7.902	-6.80	-2.14
P3	60.0	138.928	142.427	103.800	114.880	20.93	23.98
C1	60.0	103.544	119.999	103.800	114.880	-9.87	4.46
C1	65.0	103.301	129.594		122.541	-15.70	5.76
C1	80.0	118.510	135.788		128.115	-7.50	5.99
C1	90.0	112.382	111.315		122.723	-8.43	-9.30
P3	100.0	132.026	133.025	112.400	113.981	15.83	16.71
C1	100.0	115.721	135.560	112.400	113.981	1.53	18.93
C1	105.0	104.062	129.161		109.033	-4.56	18.46
C2	120.0	116.298	125.452		93.777	24.02	33.78
C2	150.0	82.277	89.842		67.225	22.39	33.64
C2	170.0	82.373	90.209		53.793	53.13	67.70
C2	180.0	59.993	65.269		48.236	24.37	35.31
C2	200.0	45.902	48.898		39.038	17.58	25.26

2) point source photometry of Arp 220 (colour corrected from 10 to 200 = μm)

Measurements:

PHT-P:	ppap47600414 (src+back)	FCS = 12, 25, 100 um
	ppae47600413 (back)	FCS = 12, 20, 100 um
PHT-C:	pcap47600416 (src+back)	FCS = 90, 170 um
	pcae47600415 (back)	FCS = 90, 170 um

Colour correction: according to model

Model: Sum of 2 modified bb, em. $\propto \lambda^{-1}$, T1 = 120 K, T2 = 47 K

Det	cwl (μm)	OLP 9	OLP 10	IRAS	Model	Δ (OLP 9)	Δ (OLP 10)
P1	3.3	0.126	0.103		-0.001	-17651.58	-14428.86
P1	3.6	0.065	0.066		-0.001	-11136.64	-11236.93
P1	4.8	0.045	0.046		-0.000	-66302.65	-67769.79
P1	7.3	0.233	0.223		0.009	2601.82	2477.23
P1	7.7	0.266	0.322		0.015	1702.32	2080.86
P1	10.0	0.072	0.082		0.151	-52.50	-45.82
P1	11.3	0.163	0.181		0.367	-55.48	-50.51
P1	12.0	0.478	0.510	0.484	0.519	-8.03	-1.87
P1	12.8	1.367	1.184		0.746	83.10	58.60
P1	15.0	0.938	0.824		1.525	-38.48	-45.93
P2	20.0	2.070	3.191		3.827	-45.90	-16.63
P2	25.0	8.716	9.151	9.631	7.902	10.30	15.81
P3	60.0	145.019	148.816	113.300	114.880	26.23	29.54
C1	60.0	107.634	124.739	113.300	114.880	-6.31	8.58
C1	65.0	110.838	139.049		122.541	-9.55	13.47
C1	80.0	116.758	133.781		128.115	-8.86	4.42
C1	90.0	115.263	114.170		122.723	-6.08	-6.97
P3	100.0	132.159	133.285	110.400	113.981	15.95	16.94
C1	100.0	114.123	133.688	110.400	113.981	0.12	17.29
C1	105.0	103.751	128.774		109.033	-4.84	18.11
C2	120.0	104.490	112.715		93.777	11.42	20.19
C2	150.0	77.547	84.677		67.225	15.35	25.96
C2	170.0	70.828	77.565		53.793	31.67	44.19
C2	180.0	55.090	59.935		48.236	14.21	24.26
C2	200.0	44.652	47.566		39.038	14.38	21.85

3) Surface brightness photometry of Arp 220 background

λ	OLP9 (MJy/sr)	OLP10 (MJy/sr)	COBE (MJy/sr)
3.3	2.05	1.76	
3.6	0.25	0.25	
4.8	0.56	0.63	
7.3	2.66	2.43	
7.7	2.99	3.90	
10.0	7.63	7.55	
11.3	13.02	12.48	
12.0	16.84	15.25	16.81
12.8	52.47	32.87	
15.0	21.64	17.50	
20.0	23.06	26.40	
25.0	31.44	25.90	29.99
60.0	7.56	8.31	9.15
100.0	5.68	7.34	6.60
60.0	9.13	8.69	9.15
65.0	11.48	10.20	
80.0	11.34	10.03	
90.0	7.96	7.93	
100.0	8.95	7.83	6.60
105.0	8.27	6.95	
120.0	7.80	7.15	
150.0	7.39	6.84	7.10
170.0	6.95	6.70	
180.0	6.44	6.05	
200.0	5.74	5.38	5.11

5.1.8 PHT03 and PHT22 Multi-filter Photometry: The SED of NGC 6240

Motivation

TDTs 47600509(background, PHT-P), 47600510(NGC 6240, PHT-P), 47600511(background, PHT-C), 47600512(NGC 6240, PHT-C) is another one of the key OLP validation cases [1]. Like for Arp 220, the staring mode AOTs PHT-03 and PHT-22 in all PHT filters measure a galaxy SED which is steeply rising between 8 and 60 μm and gradually declining beyond 100 μm, hence has a very different shape than a stellar atmosphere SED. It can therefore be used for a check of the robustness of the relative filter-to-filter calibration and the color correction factors applied to modified Black Bodies in the temperature range $40 - 140$ K. It is 3 times fainter than Arp 220 and does not reach possible upper boundary conditions with regard to the C100 fluxes like Arp 220. Its photometric properties are discussed in detail in "Infrared spectral energy distributions of the interacting galaxies Arp 244, NGC 6240 and Arp 220" [15].

Method

We compare the background subtracted flux values of both OLP V9.0b6 and OLP V10.0b7 results against the IRAS photometry and a model fit based on the OLP V6.x calibration.

Results

Fig. 5.16 shows the derived SED for NGC 6240. The model fit from [15] is plotted as a guide line to easier recognize the changes w.r.t. OLP V9.0. Note that this fit cannot serve as reference photometry.
We have color corrected the photometry w.r.t. modified blackbodies with emissivities $\propto \lambda^{-1}$ for the 12.8 to 200 μm range (for details, see part 2 of the evaluation log section). This color corrected SED is shown in Fig. 5.17.
We notice the following results:

- Photometry with C100 and C200 yields a relatively smooth SED.
- There is now a good consistency with IRAS at 25, 60 and 100 μm, while the 12 μm ISOPHOT flux is higher than the IRAS one.
- Again we find this positive flux excess for the 12.8 μm filter.

In Fig. 5.18 we plot the derived multi-filter surface brightness values in comparison with COBE photometry.
Like for the background close to Arp 220, the PHT-P background photometry is very consistent with COBE/DIRBE, except for the 3.3 and 12.8 μm filters. For C100 we see again the excess for the 65 and 80 μm filters.

Conclusions

The second bright galaxy example, NGC 6240, confirms essential findings of the Arp 220 test case:

- The C100 and C200 photometry has a good quality in this flux range.
- There is still a calibration problem with the 12.8 filter on the flux level $<$ a few Jy down to the background level, though reduced w.r.t. the OLP V9.
- There is also a calibration offset for the background level of the not so commonly used filters at 65 and 80 μm, showing a systematic surface brightness excess which is confirmed by other test cases.

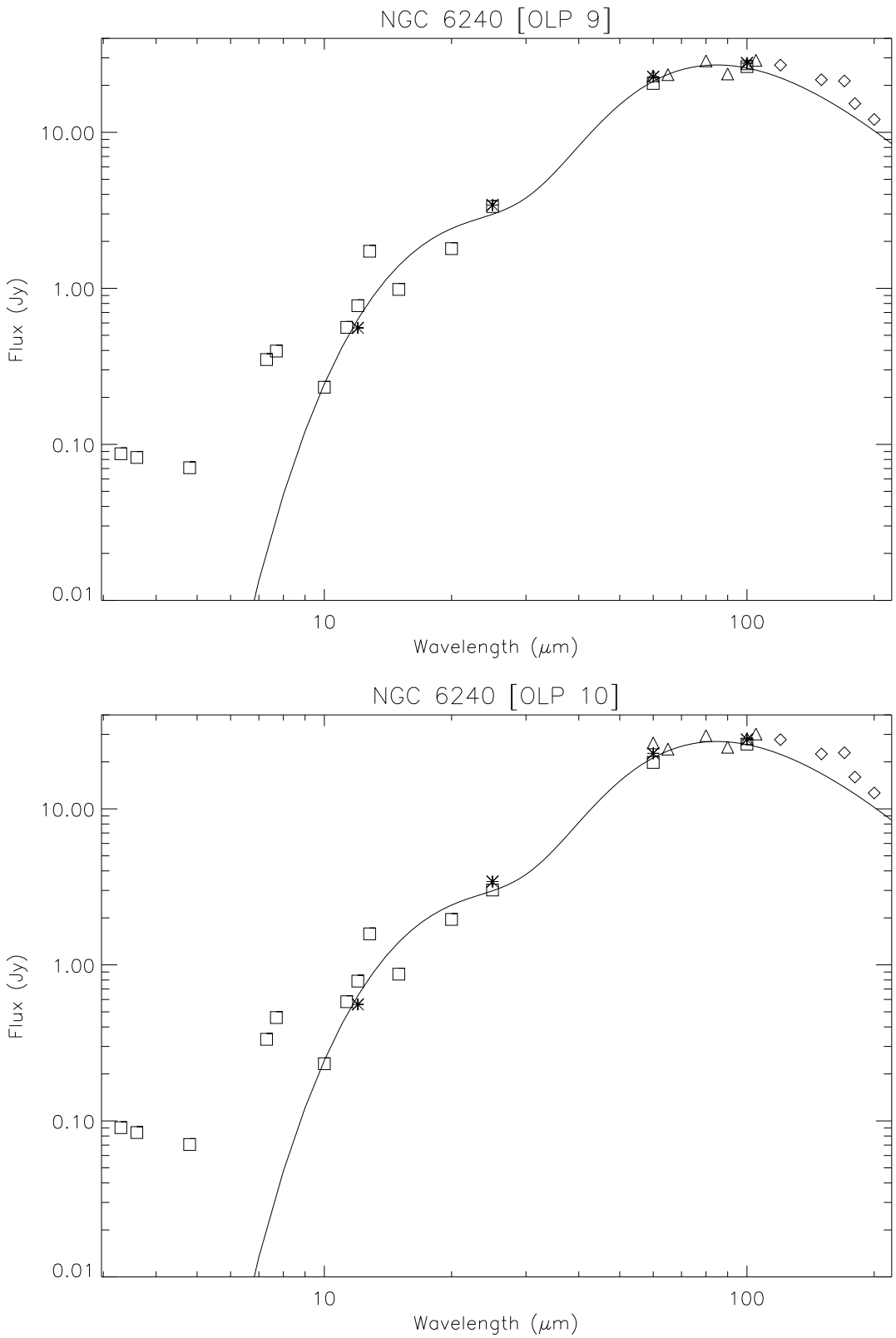

Figure 5.16: Comparison of PHT-P and PHT-C photometry, using the full ISOPHOT filter set, with IRAS photometry and the model fit as described in [15]. Note that this model fit only serves as a guide for the eye to recognize more easily the changes between the two versions. It is not an absolute photometric reference. No color correction has been applied. The meaning of the symbols is the following: solid line: model, asterisk: IRAS, square: PHT-P (P03 AOT), triangle: C100 (P22 AOT), diamond: C200 (P22 AOT).

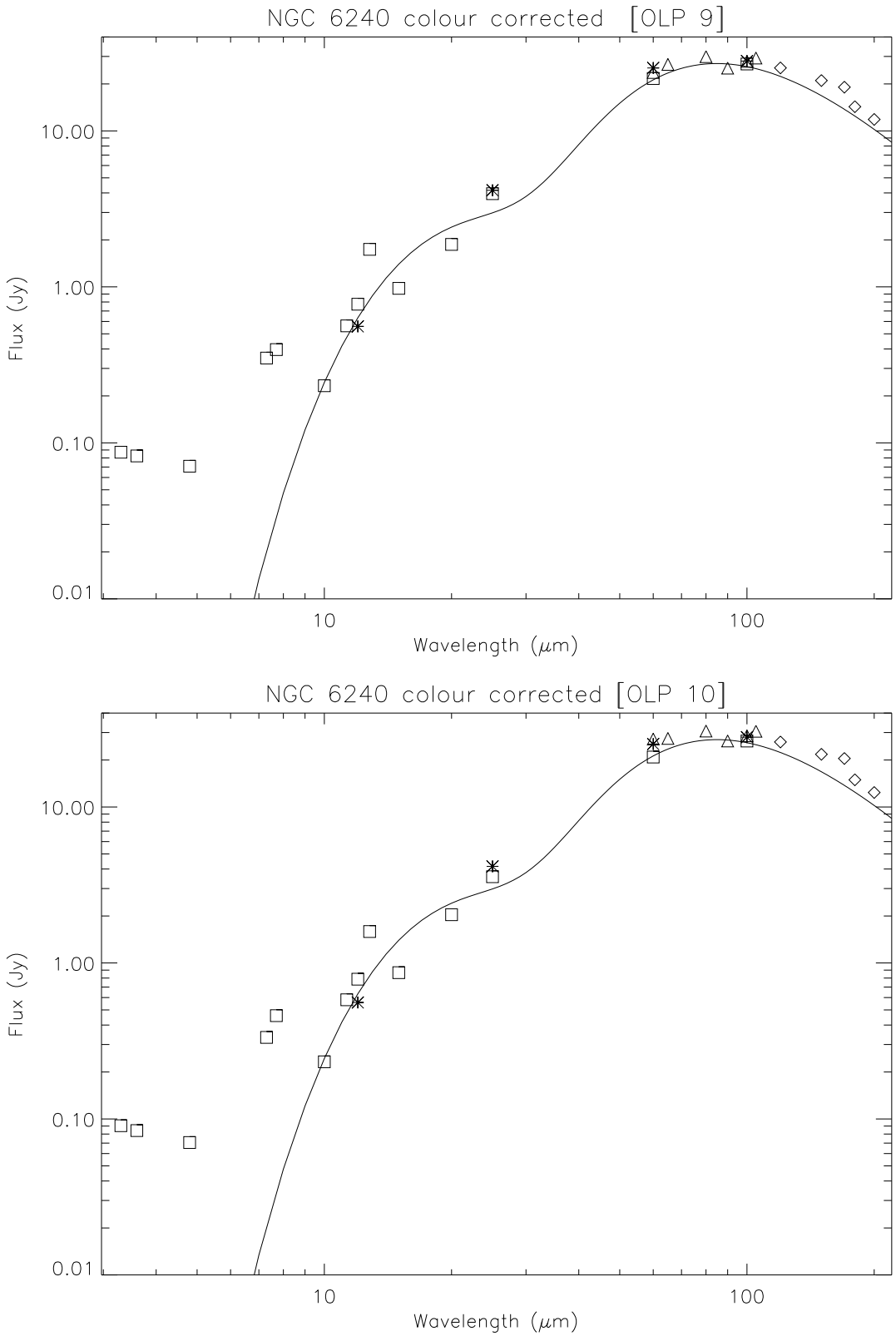

Figure 5.17: Comparison of PHT-P and PHT-C photometry, using the full ISOPHOT filter set, with IRAS photometry and the model fit as described in [15]. Note that this model fit only serves as a guide for the eye to recognize more easily the changes between the two versions. It is not an absolute photometric reference. Color correction according to the model parameters, modified BBs $\propto \lambda^{-1}$ with T1 = 140 K and T2 = 42 K, has been applied . The meaning of the symbols is the following: solid line: model, asterisk: IRAS, square: PHT-P (P03 AOT), triangle: C100 (P22 AOT), diamond: C200 (P22 AOT).

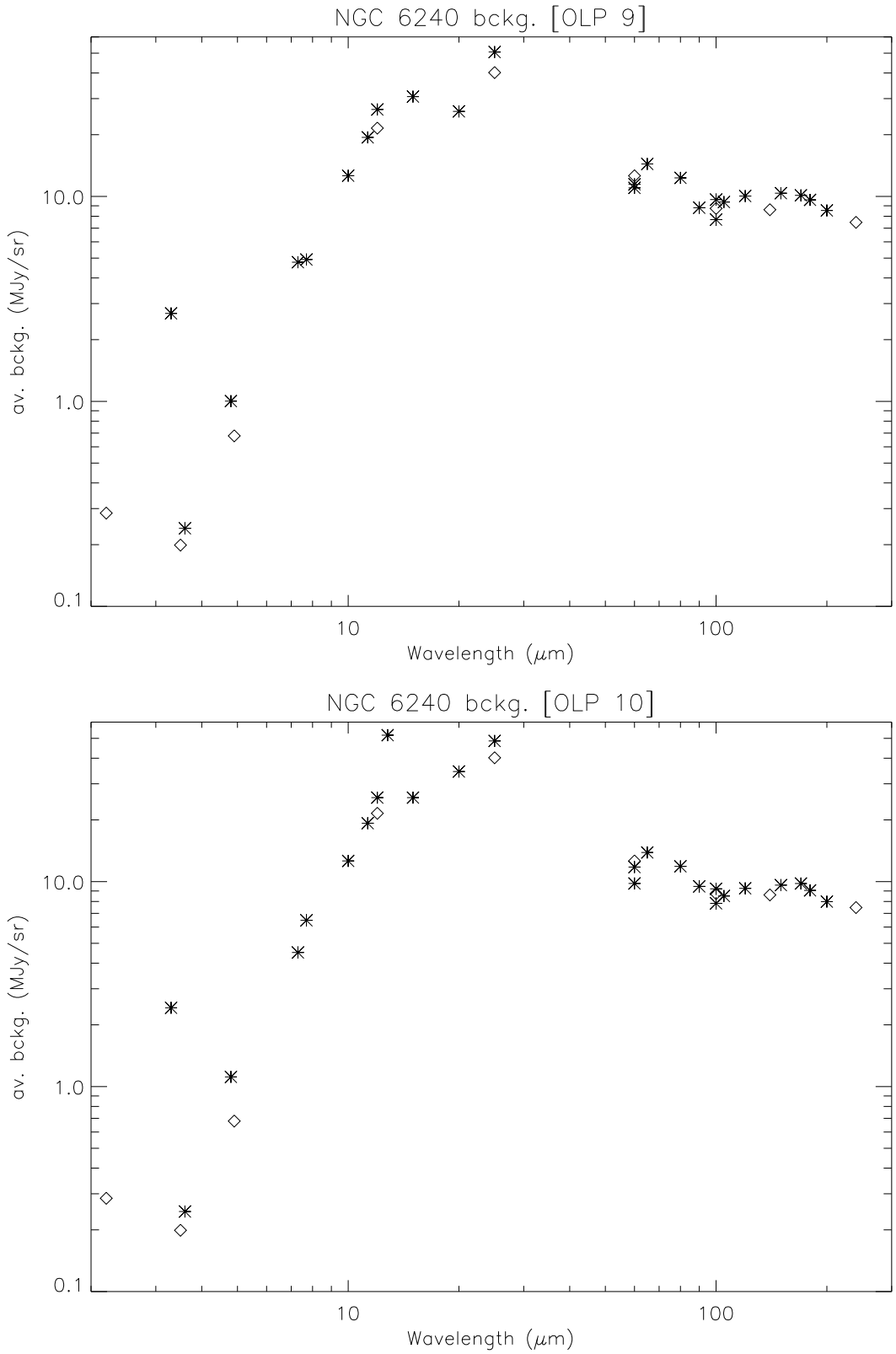

Figure 5.18: Comparison of PHT surface brightness photometry with COBE, both for OLP 9.0b6 and OLP 10.0b5. Asterisk: PHT-P and PHT-C photometry, diamond: COBE.

Evaluation Log

1) point source photometry of NGC 6240 (not colour corrected)

Measurements:

PHT-P:	ppap47600510 (src+back)	FCS = 12, 25, 100 um
	ppae47600509 (back)	FCS = 12, 20, 100 um
PHT-C:	pcap47600512 (src+back)	FCS = 90, 170 um
	pcae47600511 (back)	FCS = 90, 170 um

Model: Sum of 2 modified bb, em. $\propto \lambda^{-1}$, T1 = 140 K, T2 = 42 K

Det	cwl (μm)	OLP 9	OLP 10	IRAS	Model	Δ (OLP 9)	Δ (OLP 10)
P1	3.3	0.087	0.090		-0.003	-2678.47	-2778.44
P1	3.6	0.082	0.084		-0.003	-3094.97	-3159.19
P1	4.8	0.071	0.071		-0.000	-27788.84	-27700.53
P1	7.3	0.349	0.333		0.024	1375.15	1306.94
P1	7.7	0.396	0.459		0.037	959.59	1127.87
P1	10.0	0.232	0.232		0.244	-4.75	-4.79
P1	11.3	0.562	0.581		0.482	16.55	20.36
P1	12.0	0.774	0.787	0.558	0.634	22.12	24.20
P1	12.8	1.730	1.580		0.830	108.38	90.36
P1	15.0	0.985	0.872		1.399	-29.61	-37.68
P2	20.0	1.797	1.956		2.417	-25.65	-19.05
P2	25.0	3.345	3.018	3.417	2.983	12.15	1.18
P3	60.0	20.576	19.847	22.680	21.233	-3.09	-6.53
C1	60.0	23.005	26.455	22.680	21.233	8.35	24.59
C1	65.0	23.428	24.155		23.504	-0.33	2.77
C1	80.0	28.704	29.452		26.842	6.94	9.72
C1	90.0	23.668	24.824		26.852	-11.86	-7.55
P3	100.0	26.358	25.995	27.780	25.814	2.11	0.70
C1	100.0	27.507	28.182	27.780	25.814	6.56	9.17
C1	105.0	28.923	30.178		25.058	15.43	20.43
C2	120.0	26.965	27.770		22.343	20.69	24.29
C2	150.0	21.736	22.494		16.814	29.27	33.78
C2	170.0	21.335	22.882		13.752	55.14	66.39
C2	180.0	15.290	15.981		12.442	22.90	28.45
C2	200.0	12.086	12.639		10.220	18.26	23.67

2) point source photometry of NGC 6240 (colour corrected from 12.8 to 200 μm)

Measurements:

PHT-P:	ppap47600510 (src+back)	FCS = 12, 25, 100 um
	ppae47600509 (back)	FCS = 12, 20, 100 um
PHT-C:	pcap47600512 (src+back)	FCS = 90, 170 um
	pcae47600511 (back)	FCS = 90, 170 um

Colour correction: according to model

Model: Sum of 2 modified bb, em. $\propto \lambda^{-1}$, T1 = 140 K, T2 = 42 K

Det	cwl (μm)	OLP 9	OLP 10	IRAS	Model	Δ (OLP 9)	Δ (OLP 10)
P1	3.3	0.087	0.090		-0.003	-2678.47	-2778.44
P1	3.6	0.082	0.084		-0.003	-3094.97	-3159.19
P1	4.8	0.071	0.071		-0.000	-27788.84	-27700.53
P1	7.3	0.349	0.333		0.024	1375.15	1306.94
P1	7.7	0.396	0.459		0.037	959.59	1127.87
P1	10.0	0.232	0.232		0.244	-4.75	-4.79
P1	11.3	0.562	0.581		0.482	16.55	20.36
P1	12.0	0.774	0.787	0.558	0.634	22.12	24.20
P1	12.8	1.740	1.590		0.830	109.64	91.51
P1	15.0	0.979	0.867		1.399	-30.03	-38.05
P2	20.0	1.872	2.038		2.417	-22.55	-15.68
P2	25.0	3.958	3.571	4.162	2.983	32.72	19.74
P3	60.0	21.659	20.891	25.310	21.233	2.01	-1.61
C1	60.0	23.692	27.245	25.310	21.233	11.58	28.31
C1	65.0	26.683	27.511		23.504	13.52	17.05
C1	80.0	29.900	30.679		26.842	11.39	14.29
C1	90.0	25.259	26.493		26.852	-5.93	-1.34
P3	100.0	26.841	26.471	28.030	25.814	3.98	2.55
C1	100.0	27.926	28.611	28.030	25.814	8.18	10.83
C1	105.0	29.304	30.576		25.058	16.95	22.02
C2	120.0	25.343	26.100		22.343	13.43	16.82
C2	150.0	21.021	21.755		16.814	25.02	29.38
C2	170.0	19.066	20.449		13.752	38.64	48.69
C2	180.0	14.290	14.935		12.442	14.86	20.04
C2	200.0	11.837	12.379		10.220	15.83	21.13

3) Surface brightness photometry of NGC 6240 background

λ	OLP9 (MJy/sr)	OLP10 (MJy/sr)	COBE (MJy/sr)
3.3	2.69	2.42	
3.6	0.24	0.25	
4.8	1.00	1.12	
7.3	4.77	4.51	
7.7	4.92	6.47	
10.0	12.62	12.62	
11.3	19.41	19.27	
12.0	26.56	25.69	21.54
12.8	74.62	51.79	
15.0	30.68	25.69	
20.0	25.98	34.44	
25.0	50.62	48.56	40.18
60.0	11.01	9.80	12.61
100.0	7.70	7.83	8.74
60.0	11.46	11.78	12.61
65.0	14.40	13.87	
80.0	12.32	11.87	
90.0	8.81	9.47	
100.0	9.65	9.22	8.74
105.0	9.39	8.51	
120.0	10.04	9.27	
150.0	10.37	9.61	8.61
170.0	10.12	9.79	
180.0	9.62	9.06	
200.0	8.54	7.99	7.47

5.1.9 PHT03 Multi-filter Photometry: The SED of β Pictoris (HR 2020 / HD 39060)

Motivation

HR 2020 / HD 39060 (also β Pictoris) is a well known Vega-type star with strong IR excess. Shortward of 10 μm its SED can be compared with standard stars of spectral type G8, longward of 10 μm with IRAS photometry.

Method

We compare the color corrected flux values of both OLP V9.0b6 and OLP V10.0b5 results against the scaled model predictions of HR 5062 by Hammersley and IRAS photometry. The color correction close to 10 μm is difficult considering the composite of a 8000 K photosphere and a 65 K modified BB dust disk.

Results

The comparison of the OLP V9.0b6 and OLP V10.0b5 photometry with the model is given in part 1 of the evaluation log section. Figs. 5.19 shows the PHT photometric data points in comparison to the model and IRAS photometry (color corrected) for OLP 9.0b6 and OLP 10.0b5, respectively.
We note the following:

- The 4.8 μm flux is too low by 40 %, presumably due to a too high background flux. This seems to be supported by the fact that the absolute calibration of the P1 filters on-source is done in the 4.8 μm filter.
- In the IR excess part we find a good consistency with IRAS, in particular for the 25 μm filter.
- This is another test case where the 12.8 μm filter sticks out too high.

Conclusions

- The SED of the source is reproduced, except for the 4.8 and 12.8 μm filters. The too low 4.8 μm flux seems to be caused by a too high 4.8 μm background, the too high 12.8 μm flux confirms the results for other test cases, pointing towards a systematic calibration effect.

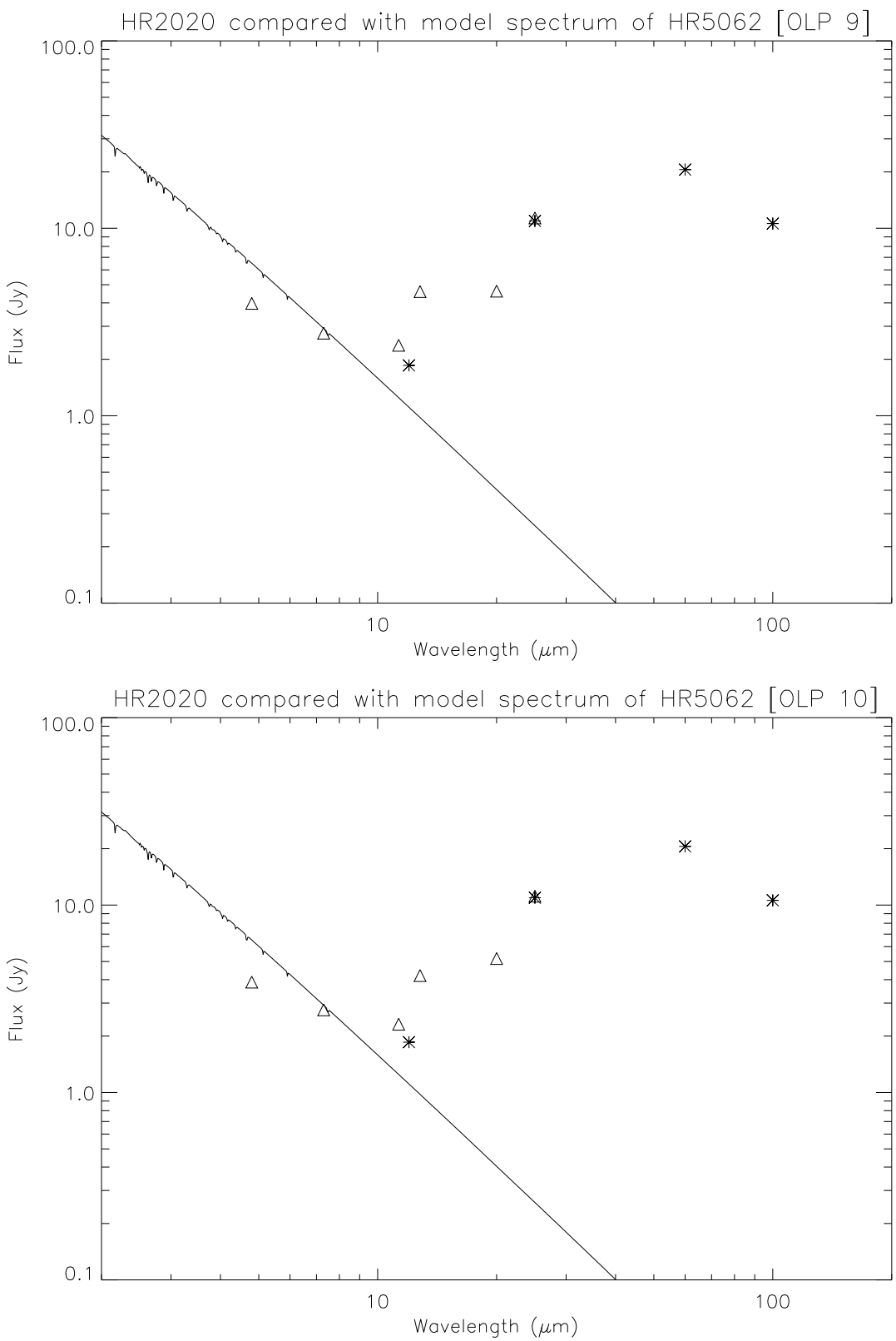

Figure 5.19: Comparison of PHT-P multi-filter photometry of β Pic (G8V + IR excess $m_v = 3.861$ mag) with the scaled model of HR 5062 (G8V, $m_v = 4.005$ mag) provided by P. Hammersley and with IRAS photometry for OLP 9.0b6 (upper panel) and OLP 10.0b5 (lower panel). All photometric points are color corrected for a mixture of a 8000 K BB and 65 K modified ($\varepsilon \propto \lambda^{-1}$) BB. The meaning of the symbols is the following: solid line: model, asterisk: IRAS, square: PHT-P (P03 AOT).

Evaluation Log

1) P03 multi-filter photometry versus scaled HR 5062 model (Note: Δ values $> 10\,\mu$m give deviations from photospheric model, not calibration accuracies!)

Measurements:
PHT-P: PPAP76602301 (src+back) FCS = 4.8, 25 um
PPAE76602302 (back) FCS = 12.8, 25 um
Colour correction: mixture of 8000 K BB & 65 K modified ($\varepsilon \propto \lambda^{-1}$)
Model: Hammersley (HR5062) scaled with V-mag 3.861mag(star)/4.005mag(ref)

Det	cwl (μm)	OLP 9	OLP 10	IRAS	Model	Δ (OLP 9)	Δ (OLP 10)
P1	4.8	3.977	3.881		6.516	-38.96	-40.44
P1	7.3	2.757	2.758		2.922	-5.66	-5.61
P1	11.3	2.374	2.311		1.249	90.15	85.11
P1	12.8	4.595	4.206		0.978	369.91	330.14
P2	20.0	4.621	5.184		0.403	1045.58	1185.20
P2	25.0	11.352	11.153	10.947	0.259	4286.12	4209.28

5.1.10 PHT03 Multi-filter Photometry in Non-standard Apertures

Motivation

In this section we want to explore what impact the usage of non-standard apertures can have on the final accuracy. We investigate here measurements of four standard stars with the same filter/aperture combinations. The apertures are considerably smaller than the standard aperture of the corresponding filter: 13.8 arcsec at 10 μm vs. 52 arcsec, 18 arcsec at 15 μm vs. 52 arcsec, 23 arcsec at 25 μm vs. 79 arcsec.

Method

We compare the color corrected flux values of both OLP V9.0b6 and OLP V10.0b5/b7 results against the model predictions and IRAS photometry.

Results

The comparison of the OLP V9.0b6 and OLP V10.0b5/b7 photometry with the model is given in parts 1 to 4 of the evaluation log section. Figs. 5.20 to 5.23 shows the PHT photometric data points in comparison to the model and IRAS photometry (color corrected) for OLP 9.0b6 and OLP 10.0b5/b7, respectively.
We note the following:

- For the three bright stars the three photometric points show a very similar oblique shape relative to the model SED. The 10 μm point is always too low (-30 % to -10 %), the 15 and 25 μm points are always too high (+15 % to +60 %; the Vega 25 μm flux which includes the IR excess has not been taken into account).
- For the faintest source of this sample the typical shape is not reproduced, pointing to a counter effect by some other calibration issue. The 25 μm flux shows a similar behaviour as other sources fainter than 1 Jy.

Conclusions

- Usage of non-standard apertures (in this case significantly smaller ones) results in systematic calibration offsets, which depend on the filter wavelengths.
- The offset at 10 μm for a 13.8 arcsec aperture vs. a 52 arcsec standard aperture is on average -20 % $\pm$ 10 %.
- The offset at 15 μm for a 18 arcsec aperture vs. a 52 arcsec standard aperture is on average +30 % $\pm$ 15 %.
- The offset at 25 μm for a 23 arcsec aperture vs. a 79 arcsec standard aperture is on average +50 % $\pm$ 5 %.
- In the case of these small apertures pointing offsets may cause some of the scatter.

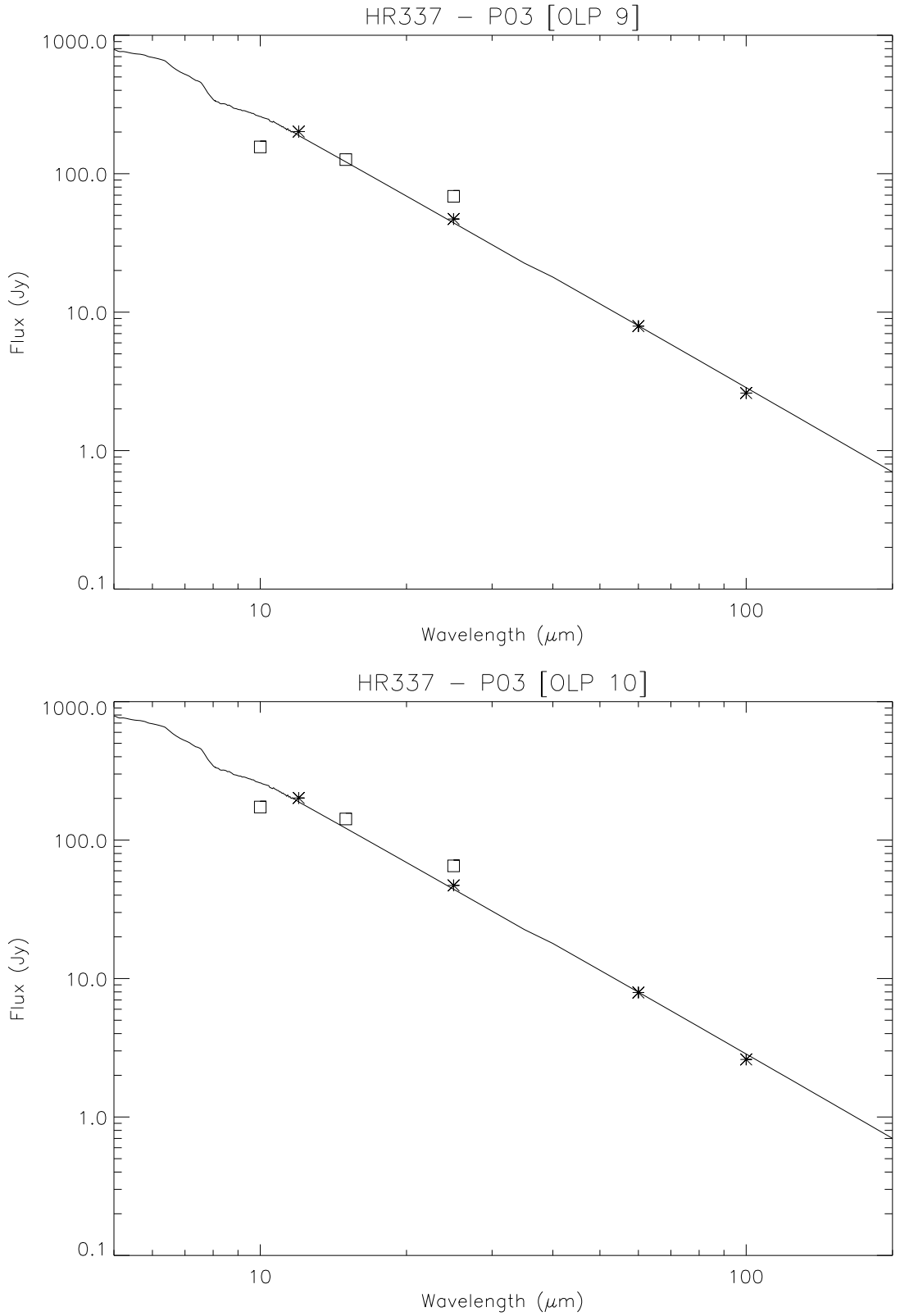

Figure 5.20: Comparison of PHT-P multi-filter photometry with the model of HR 337 provided by M. Cohen and with IRAS photometry for OLP 9.0b6 (upper panel) and OLP 10.0b7 (lower panel). All photometric points are color corrected for a 3839K BB. The meaning of the symbols is the following: solid line: model, asterisk: IRAS, square: PHT-P (P03 AOT).

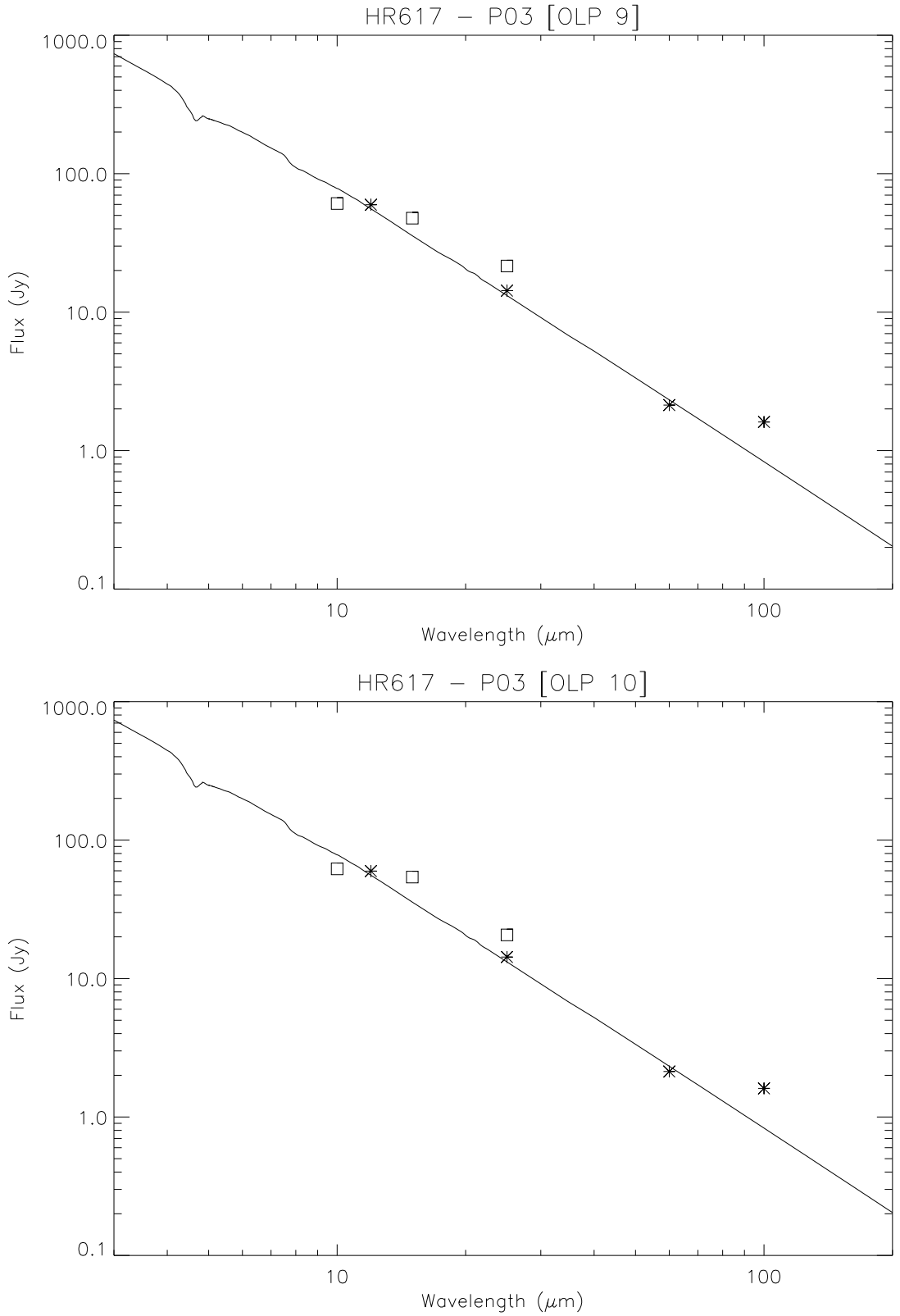

Figure 5.21: Comparison of PHT-P multi-filter photometry with the model of HR 617 provided by M. Cohen and with IRAS photometry for OLP 9.0b6 (upper panel) and OLP 10.0b5 (lower panel). All photometric points are color corrected for a 4000K BB. The meaning of the symbols is the following: solid line: model, asterisk: IRAS, square: PHT-P (P03 AOT).

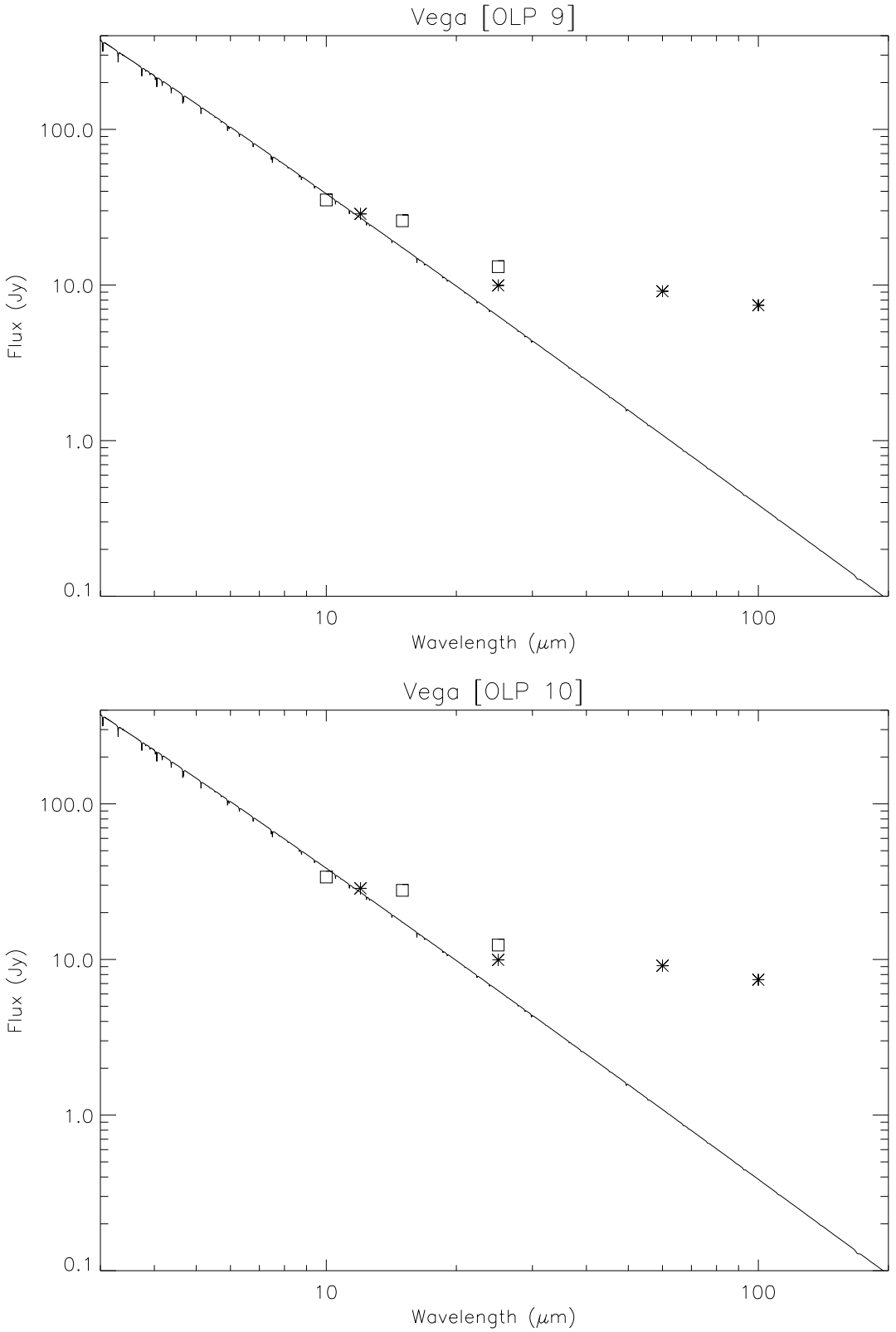

Figure 5.22: Comparison of PHT-P multi-filter photometry with the model of Vega provided by M. Cohen and with IRAS photometry for OLP 9.0b6 (upper panel) and OLP 10.0b5 (lower panel). All photometric points are color corrected for a mixture of 10000 K BB and a 80 K modified ($\varepsilon \propto \lambda^{-1}$) BB. The meaning of the symbols is the following: solid line: model, asterisk: IRAS, square: PHT-P (P03 AOT).

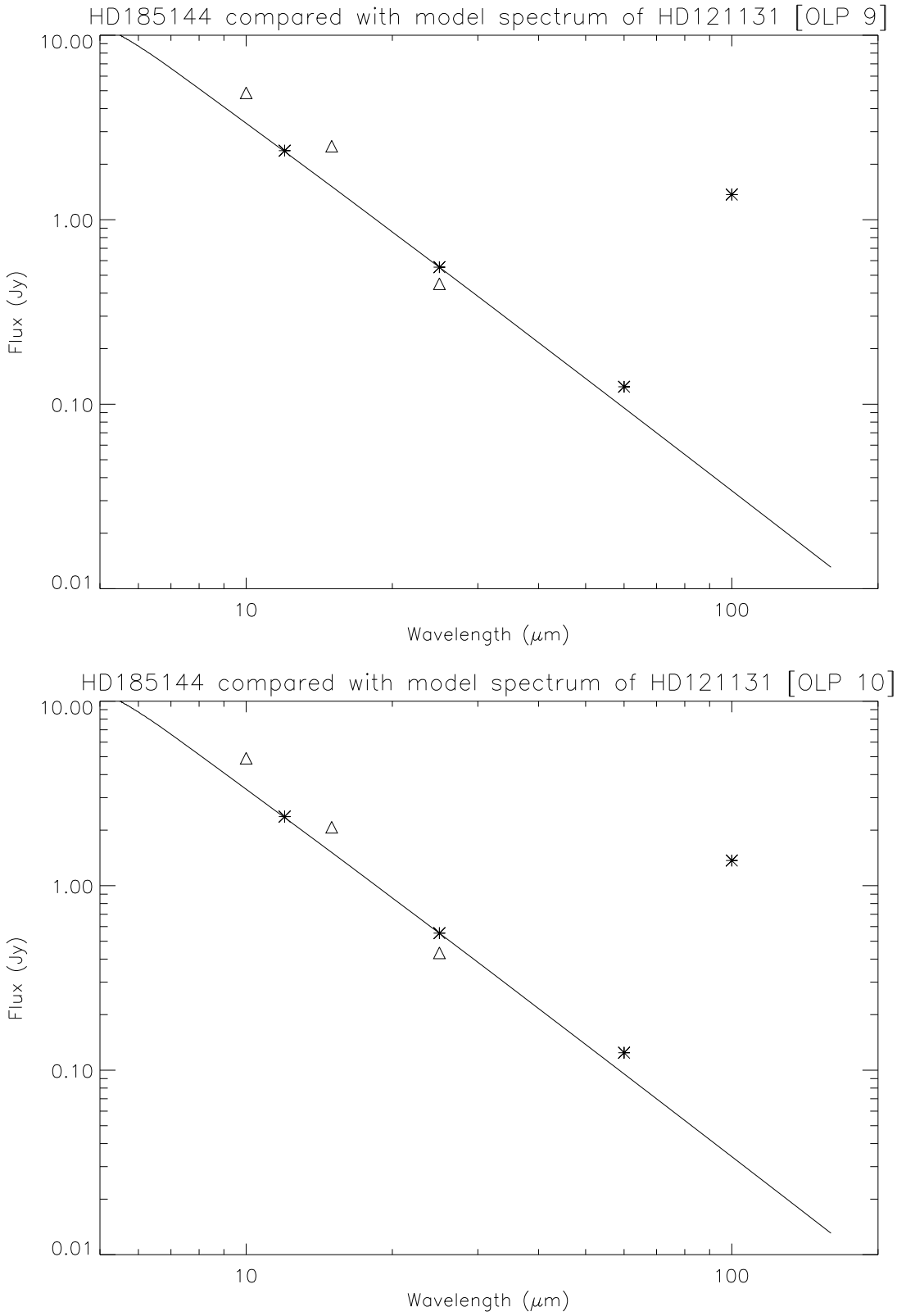

Figure 5.23: Comparison of PHT-P multi-filter photometry of HD185144 (K0V, m_v = 4.70 mag) with the model of HD121131 (K1V, m_v = 8.34 mag) provided by P. Hammersley and with IRAS photometry for OLP 9.0b6 (upper panel) and OLP 10.0b5 (lower panel). All photometric points are color corrected for a 5103 K BB. The meaning of the symbols is the following: solid line: model, asterisk: IRAS, square: PHT-P (P03 AOT).

Evaluation Log

1) P03 point source photometry for HR337

Measurements:
PHT-P1/P2: ppap42301605 (P03 src+back) FCS = 10,25 um
ppap42301656 (P03 back) FCS = 10,25 um
Colour correction: black body, T = 3839 K

Model: Cohen

Det	cwl (μm)	OLP 9	OLP 10	IRAS	Model	Δ (OLP 9)	Δ (OLP 10)
P1	10.0	156.132	173.294		258.884	-39.69	-33.06
P1	15.0	126.426	142.124		121.759	3.83	16.73
P2	25.0	68.664	65.106	47.057	44.169	55.46	47.40

2) P03 point source photometry for HR617

Measurements:
PHT-P: ppap45002408 (src+back) FCS = 10, 25 um
ppap45002458 (back) FCS = 10, 25 um
Colour correction: black body, T = 4000 K

Model: Cohen

Det	cwl (μm)	OLP 9	OLP 10	IRAS	Model	Δ (OLP 9)	Δ (OLP 10)
P1	10.0	60.896	61.996		78.282	-22.21	-20.80
P1	15.0	47.727	54.064		35.649	33.88	51.66
P2	25.0	21.539	20.658	14.293	13.180	63.43	56.74

3) P03 point source photometry for Vega

Measurements:
PHT-P: ppap08500240 (src+back) FCS = 10, 25 um
ppap08500274 (back) FCS = 10, 25 um
Colour correction: mixture of 10000 K BB & 80 K modified ($\varepsilon \propto \lambda^{-1}$) BB
Model: Cohen

Det	cwl (μm)	OLP 9	OLP 10	IRAS	Model	Δ (OLP 9)	Δ (OLP 10)
P1	10.0	35.176	33.864		38.570	-8.80	-12.20
P1	15.0	25.866	27.827		17.356	49.03	60.33
P2	25.0	13.119	12.379	9.938	6.301	108.22	96.48

4) P03 point source photometry of HD 185144 versus scaled HD 121131 model

Measurements:
PHT-P : PPAP08000342 (src+back) FCS = 10, 25 um
PHT-P : PPAP08000375 (back) FCS = 10, 25 um
Colour correction: black body, T = 5103 K

Model: Hammersley (HD121131) scaled with V-mag 4.70mag(star)/8.34mag(ref)

Det	cwl (μm)	OLP 9	OLP 10	IRAS	Model	Δ (OLP 9)	Δ (OLP 10)
P1	10.0	4.872	4.906		3.334	46.14	47.18
P1	15.0	2.501	2.073		1.514	65.15	36.93
P2	25.0	0.449	0.432	0.553	0.552	-18.63	-21.73

5.2 Consistency Check of Absolute Photometry

Summary

- Staring mode absolute photometry was successfully revalidated.
- Calibration accuracies achieved by OLP V9 have been consolidated and slightly improved.
- We noticed a somewhat degraded performance for the 11.3 and 12.8 μm filter and possibly for the 4.8 μm filter.
- Use of default responsivity calibration for P1 and C200 measurements with FCS set-up outside the calibrated range gives reliable photometry.

5.2.1 PHT05 and PHT25 Absolute Photometry: The SED of γ Draconis (HR 6705)

Motivation

The star γ Draconis (HR 6705) is one of the most important calibration stars for ISOPHOT. Also several AOT commissioning observations were performed on this star. The set of observations comprises multi-filter photometry, absolute photometry and multi-filter PHT-C100 photometry with different reset interval settings, cf. [4] for more details. It is one of the key OLP validation cases [1]. The staring mode AOTs PHT-03 and PHT-22 use all available PHT filters out to 200 μm complementing the α Bootes observations towards the fainter flux end. There are detailed models available from M. Cohen (composite spectrum from 1 to 35 μm and extrapolations to 300 μm). This test case is very suitable for a test of both the absolute calibration and the relative filter-to-filter calibration.

Method

We compare the background subtracted, color corrected flux values of both OLP V9.0b6 and OLP V10.0b5 results against the model prediction.

Results

The comparison of the OLP9.0b6 and OLP10.0b5 photometry with the model is given in part 1 of the evaluation log section. We estimate the absolute photometric accuracy per detector assembly for this target as the deviation from the model flux. Fig. 5.24 shows the PHT photometric data points in comparison to the model and IRAS photometry (color corrected) for OLP 9.0b6 and OLP 10.0b5, respectively.
The absolute photometry results as shown in Fig. 5.24 are practically unchanged and the achieved absolute photometry is better than 15 % for all detectors.
Part 2 of the evaluation log section and Fig. 5.25 provide the surface brightness photometry of the background position and the comparison with COBE for the absolute photometry mode.
From Table 5.8 it can be seen that the consistency of the surface brightness measurements from the absolute photometry with COBE is better than 20

Table 5.8: Consistency check of γ Dra background position surface brightness results from absolute photometry with COBE/DIRBE annual maps.

wavelength μm	**consistency w.r.t. COBE OLP V9.0b6** [%]	**consistency w.r.t. COBE OLP V10.0b5** [%]
12 (P)	+32.0	+21.7
25 (P)	-1.3	-4.3
60 (P)	+7.5	+2.0
60 (C)	+3.5	+1.1

Conclusions

- Absolute photometry gives an accuracy of better than 15 % for all detectors, even for the 170 μm filter of C200 in stark contrast to the multi-filter measurement.
- The surface brightness photometry of the background position is consistent with COBE/DIRBE photometry within 20 %.

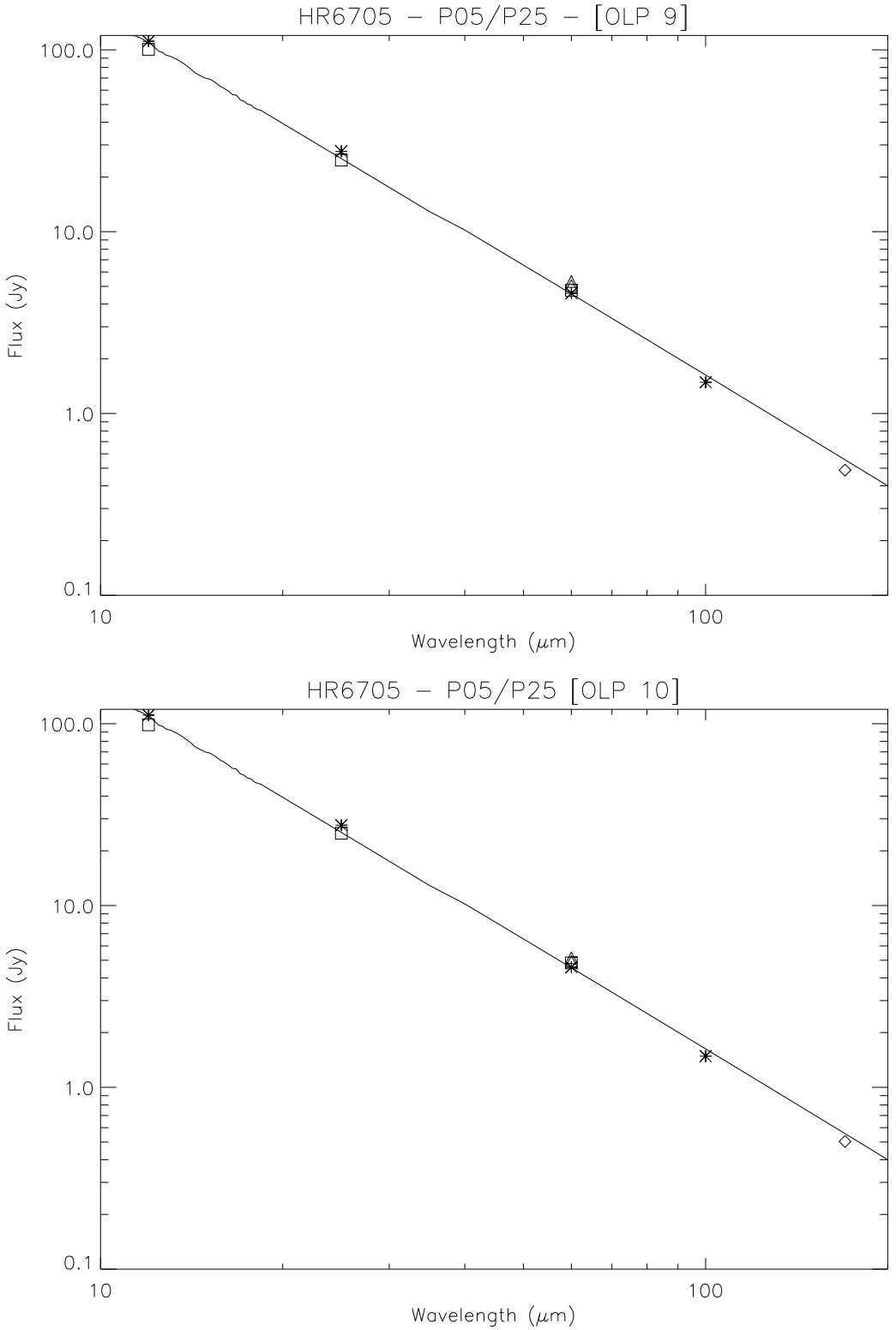

Figure 5.24: Comparison of PHT-P and PHT-C absolute photometry (P05/P25), with the composite spectrum and out to 300 μm extrapolated SED of γ Dra (HR 6705) provided by M. Cohen and with IRAS photometry for OLP 9.0b6 (upper panel) and OLP 10.0b5 (lower panel). All photometric points are color corrected for a 4000 K BB. The meaning of the symbols is the following: solid line: model, asterisk: IRAS, square: PHT-P (P05 AOT), triangle: C100 (P25 AOT), diamond: C200 (P25 AOT).

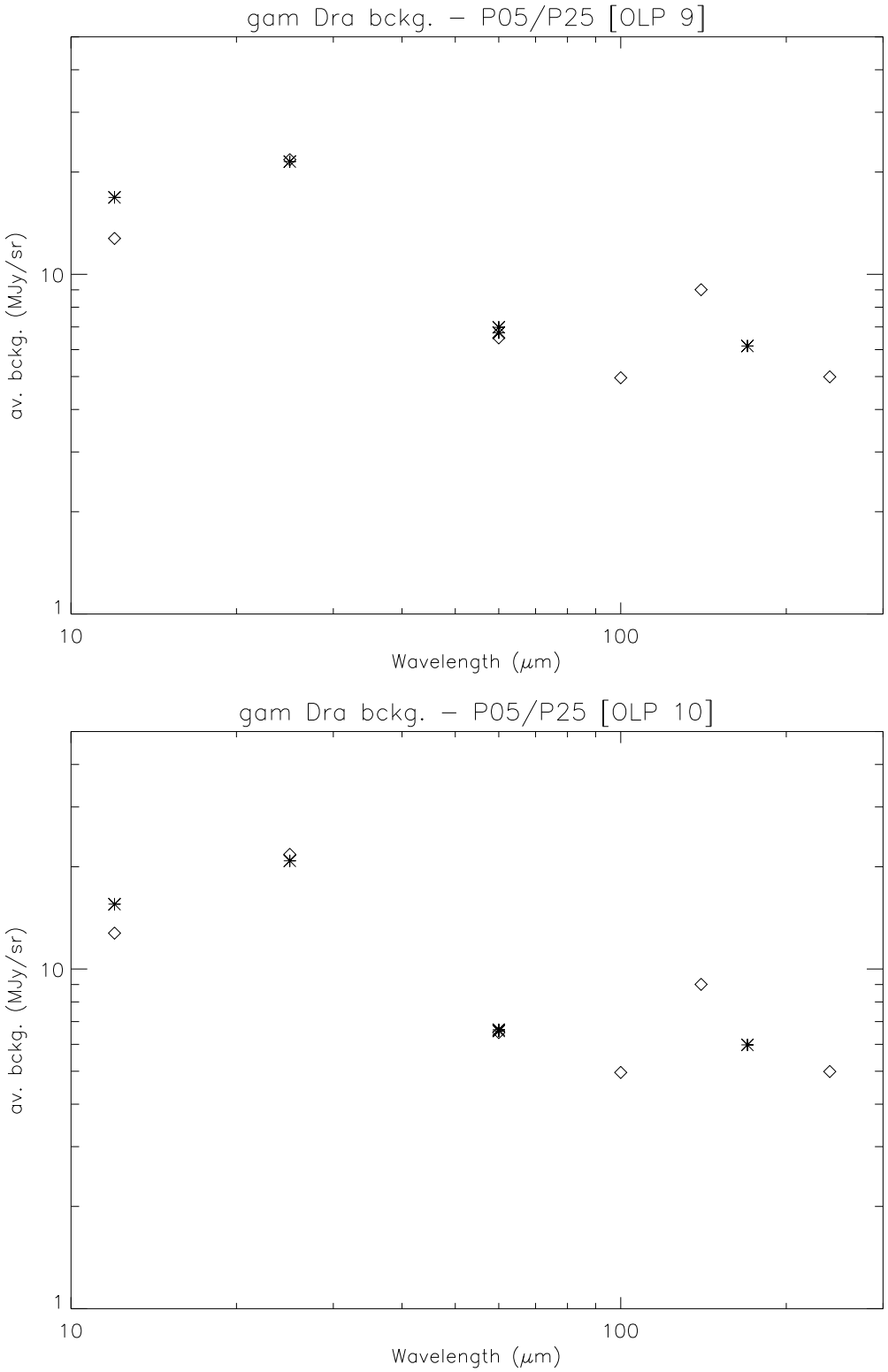

Figure 5.25: Comparison of OLP V9.0b6 and OLP V10.0b5 surface brightness, determined with the absolute photometry mode P05/P25 (asterisk) on revolution 353, with COBE annual map fluxes (diamond).

Evaluation Log

1) P05 and P25 absolute photometry

Measurements:

PHT-P1:	ppap35300302 (src+back)
	ppae35300301 (back)
PHT-P2:	ppap35300304 (src+back)
	ppae35300303 (back)
PHT-P3:	ppap35300306 (src+back)
	ppae35300305 (back)
PHT-C1:	pcap35300309 (src+back)
	pcae35300310 (src+back, b)
	pcae35300308 (back)
PHT-C2:	pcap35300312 (src+back)
	pcae35300311 (back)

Colour correction: black body, T = 4000 K

Model: Cohen

Det	cwl (μm)	OLP 9	OLP 10	IRAS	Model	Δ (OLP 9)	Δ (OLP 10)
P1	12.0	100.697	98.614	111.479	108.718	-7.38	-9.29
P2	25.0	24.748	24.987	27.671	25.229	-1.91	-0.96
P3	60.0	4.759	4.836	4.583	4.545	4.71	6.40
C1	60.0	5.323	5.158	4.583	4.545	17.11	13.49
C1b	60.0	5.056	4.923	4.583	4.545	11.25	8.32
C2	170.0	0.488	0.504		0.556	-12.28	-9.44

2) Surface brightness on background position from absolute photometry on revolution 353

λ	OLP9 (MJy/sr)	OLP10 (MJy/sr)	COBE (MJy/sr)
12.0	16.83	15.52	12.75
25.0	21.47	20.82	21.75
60.0	6.99	6.63	6.50
60.0	6.73	6.57	6.50
170.0	6.15	5.98	

5.2.2 PHT05 Absolute Photometry: The SED of Sirius (HR 2491)

Motivation

Beside Vega (HR 7001), Sirius is the main primary stellar standard with a model provided by M. Cohen (1-300 μm, R = 4000 up to 35 μm, delivered 12-Jan-1996). Therefore, a dedicated cross-calibration program was performed on this star using absolute photometry complemented by multi-filter photometry out to 25 μm.

Method

We compare the color corrected flux values of both OLP V9.0b6 and OLP V10.0b5 results against the model prediction by Cohen and IRAS photometry. At 25 μm a background measurement was performed and the not negligible background flux is subtracted from the on-target flux to get an accurate source flux.

Results

The comparison of the OLP9.0b6 and OLP10.0b5 photometry with the model is given in part 1 of the evaluation log section. We estimate the absolute photometric accuracy per detector assembly for this target as the deviation from the model flux. Fig. 5.26 shows the PHT photometric data points in comparison to the model and IRAS photometry (color corrected) for OLP 9.0b6 and OLP 10.0b5, respectively. The absolute photometry results are practically unchanged and the achieved absolute photometry is better than 6 % for both P1 and P2 detectors.

Conclusions

- The accuracy of the absolute photometry on Sirius is better than 6 % for the wavelength range 3.3 to 25 μm.

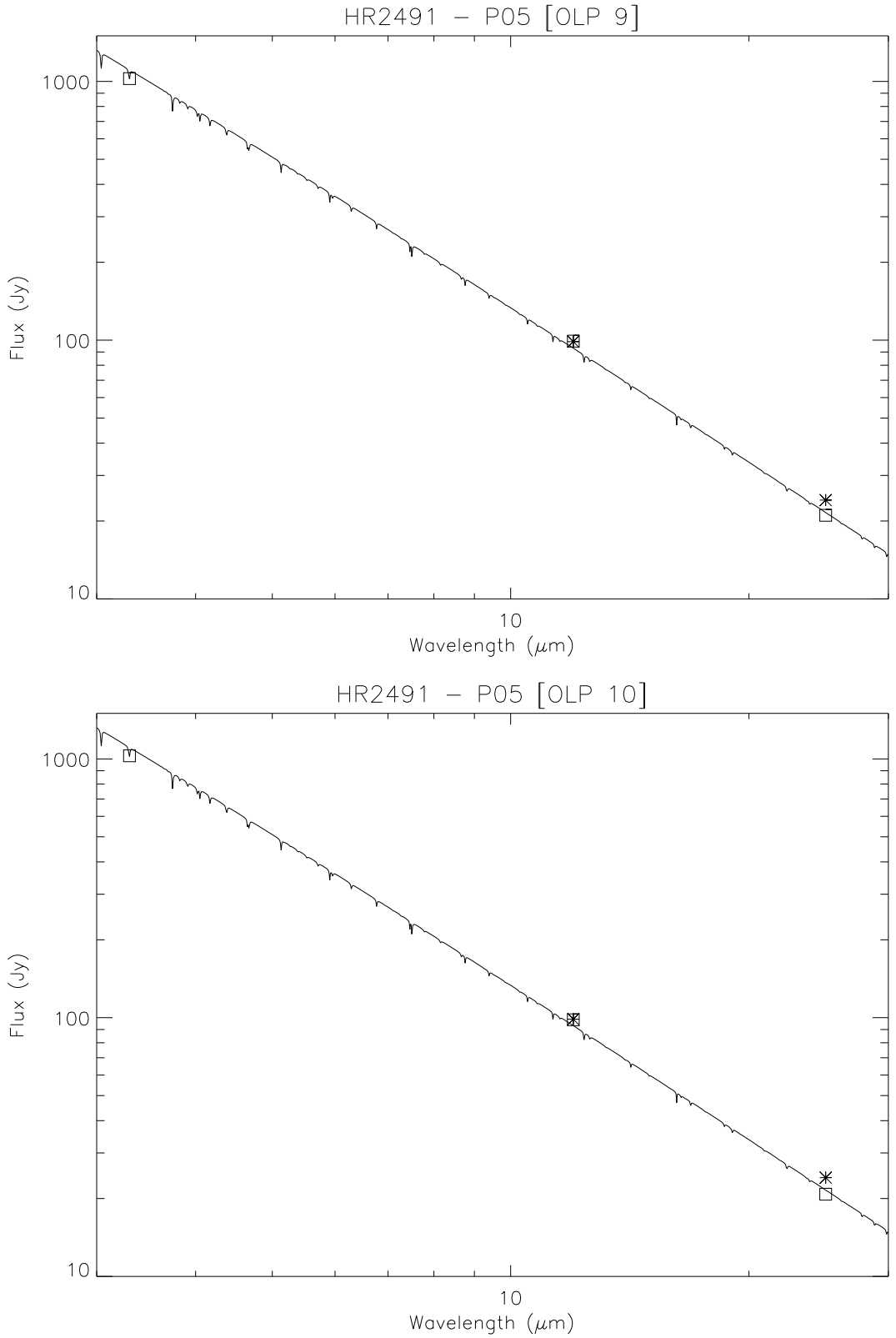

Figure 5.26: Comparison of PHT-P absolute photometry with the composite spectrum of Sirius (HR 2491) provided by M. Cohen and with IRAS photometry for OLP 9.0b6 (upper panel) and OLP 10.0b5 (lower panel). All photometric points are color corrected for a 10000 K BB. The meaning of the symbols is the following: solid line: model, asterisk: IRAS, square: PHT-P (P05 AOT).

Evaluation Log

1) P05 absolute photometry

Measurements:
PHT-P1: ppap70705310 (src+back)
ppap70705313 (src+back)
PHT-P2: ppap70705307 (src+back)
ppap70705711 (back, P03)

Colour correction: black body, T = 10000 K

Model: Cohen

Det	cwl (μm)	OLP 9	OLP 10	IRAS	Model	Δ (OLP 9)	Δ (OLP 10)
ppap70705310:							
P1	3.3	1025.462	1028.105		1021.900	0.35	0.61
ppap70705313:							
P1	12.0	99.117	98.133	98.690	93.157	6.40	5.34
ppap70705707:							
P2	25.0	21.043	20.787	24.092	21.541	-2.31	-3.50

5.2.3 PHT05 Absolute Photometry: The SED of α Ari (HR 617)

Motivation

For the star α Ari a complete suite of absolute photometry measurements was performed out to 100 μm. We can therefore test the absolute calibration accuracies of all PHT-P filters in the flux range covered by this star. The star is about half as bright as Sirius and γ Dra. In this version of the report we restrict the analysis to a wavelength up to 25 μm, since we do not perform any background subtraction and the contribution by the background becomes noticable from 20 μm onwards. The background measurements for the star are covered by nodding observations which will be analyzed in a later version of the report.

Method

We compare the color corrected flux values of OLP V9.01 and OLP V10.0b7 results against the model prediction by Cohen and IRAS photometry.

Results

The comparison of the OLP9.0b6 and OLP10.0b7 photometry with the model is given in part 1 of the evaluation log section. We estimate the absolute photometric accuracy per detector assembly for this target as the deviation from the model flux. Fig. 5.27 shows the PHT photometric data points in comparison to the model and IRAS photometry (color corrected) for OLP 9.0b6 and OLP 10.0b7, respectively.. For P1 we find very accurate absolute photometry of better than 10 % for the 3.3, 3.6, 7.3, 7.7, 10, 12, and 15 μm filter. The plot shows that inside the 4.8 μm range there is a noticable absorption feature, so the color correction with a pure black body is not correct and the effect by the different SED needs to be investigated. The 11.3 and 12.8 μm filters show clear offsets, which are probably due to intrinsic calibration uncertainties. For the 12.8 mum filter photometry we find a performance improvement w.r.t. OLP V9, yet the flux is a few per cent too high at a flux level of 50 Jy in trend with the systematic strong positive offsets found at flux levels of a few Jy down to the sky background level. For P2 it becomes noticable that no background subtraction has been performed. From a background estimate at 25 μm using COBE/DIRBE fluxes, the contribution to the total flux is around 25 % which would give a final consistency with the model of 7 %. Therefore also the P2 absolute photometry is better than 10 % for the examined flux range.

Conclusions

- We find very accurate absolute photometry results with accuracies better than 10 % over the full P1 filter range, except for the three filters 4.8, 11.3 and 12.8 μm. The 4.8 μm filter color correction appears to be not appropriate due to an underlying strong absorption feature. The performance of the 12.8 μm filter photometry has been improved w.r.t. OLP V9.
- The conclusions for P2 absolute photometry are currently restricted due to the not yet performed proper background subtraction; data on the background level are available from parallelly performed nodding observations. Estimations using COBE/DIRBE photomery at 25 μm lead to the conclusion, that the P2 absolute photometry is as accurate as 10 %, too.

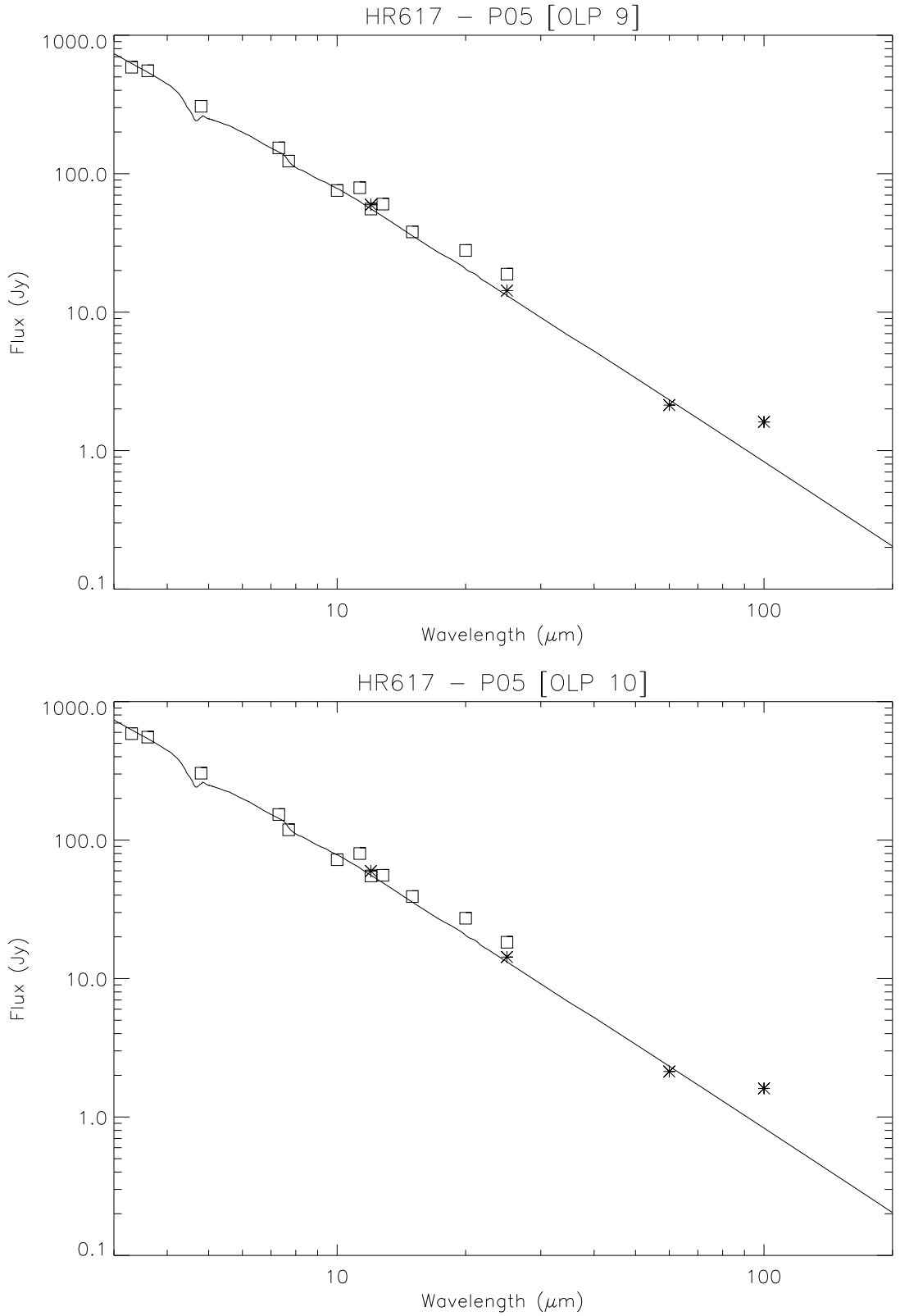

Figure 5.27: Comparison of PHT-P absolute photometry with the composite spectrum of α Ari (HR 617) plus extrapolation out to 300 μm provided by M. Cohen and with IRAS photometry for OLP 9.01 (upper panel) and OLP 10.0b7 (lower panel). All photometric points are color corrected for a 4000 K BB. The meaning of the symbols is the following: solid line: model, asterisk: IRAS, square: PHT-P (P05).

Evaluation Log

1) P05 absolute photometry (no background subtraction yet!)

Measurements:

PHT-P1:	ppap80400408 (src+back)	3.3 um
	ppap80400411 (src+back)	3.6 um
	ppap80400410 (src+back)	4.8 um
	ppap80400409 (src+back)	7.3 um
	ppap80400407 (src+back)	7.7 um
	ppap80400406 (src+back)	10 um
	ppap80400405 (src+back)	11.3 um
	ppap80400404 (src+back)	12 um
	ppap80400403 (src+back)	12.8 um
	ppap80400401 (src+back)	15 um
PHT-P2:	ppap79001603 (src+back)	20 um
	ppap79001601 (src+back)	25 um

Colour correction: black body, T = 4000 K

Model: Cohen

Det	cwl (μm)	OLP 9	OLP 10	IRAS	Model	Δ (OLP 9)	Δ (OLP 10)
P1	3.3	587.522	587.259		625.866	-6.13	-6.17
P1	3.6	554.100	554.082		540.252	2.56	2.56
P1	4.8	306.897	304.284		255.084	20.31	19.29
P1	7.3	153.658	153.061		143.409	7.15	6.73
P1	7.7	123.353	118.696		123.240	0.09	-3.69
P1	10.0	75.639	72.144		78.282	-3.38	-7.84
P1	11.3	79.202	79.992		62.951	25.82	27.07
P1	12.0	55.597	55.120	59.690	55.717	-0.22	-1.07
P1	12.8	60.326	55.698		49.125	22.80	13.38
P1	15.0	37.969	39.111		35.649	6.51	9.71
P2	20.0	27.906	27.253		20.520	35.99	32.81
P2	25.0	18.821	18.287	14.293	13.180	42.80	38.75

5.2.4 PHT25 Absolute Photometry: The SED of Uranus

Motivation

This is a check-out of the C200 absolute photometry mode for the brightest celestial standard, Uranus. For these measurements, the FCS heating power set-ups on-source were such, that they were outside the calibrated range.

Method

We compare the color corrected flux values of both OLP V9.0b6 and OLP V10.0b8 results against the model predictions by Abbas and Griffin & Orton, respectively.

Results

The comparison of the OLP9.0b6 and OLP10.0b8 photometry with the model is given in part 1 of the evaluation log section. We estimate the absolute photometric accuracy per detector assembly for this target as the deviation from the model flux. Fig. 5.28 shows the PHT photometric data points in comparison to the model for OLP 9.0b6 and OLP 10.0b8, respectively. Despite the fact that in OLP10 default responsivities are used in this absolute photometry mode, we note an improvement of the absolute calibration to better than 5 %.

Conclusions

- The C200 absolute photometry in the bright flux range is as accurate as 5 %.
- The C200 default responsivity calibration does not show any degradance in performance w.r.t. the actual responsivity calibration.

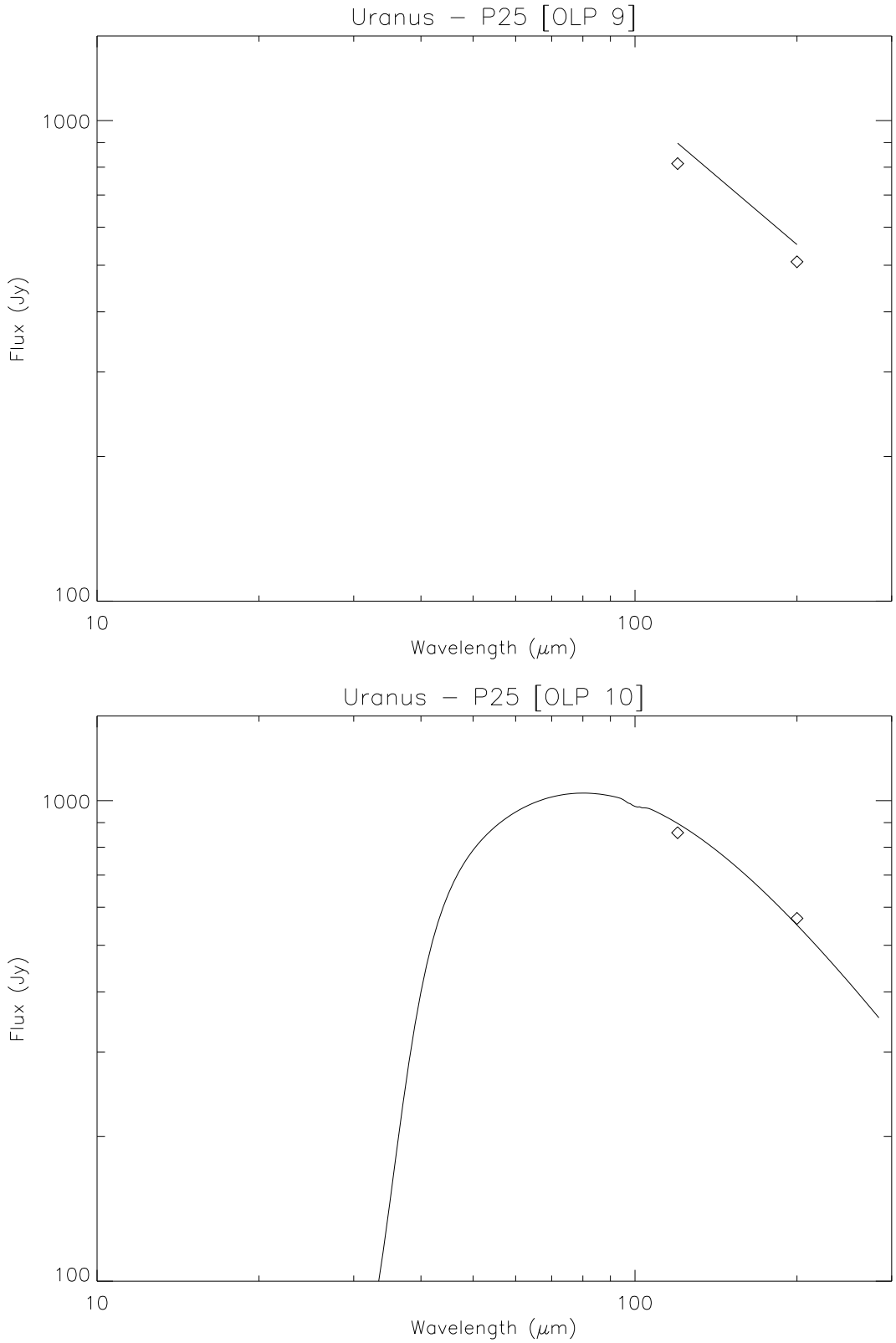

Figure 5.28: Comparison of PHT-C200 absolute photometry with the spectrum of Uranus provided by M. Griffin & G. Orton (used for OLP 10) and M. Abbas (used for OLP 9) for OLP 9.0b6 (upper panel) and OLP 10.0b8 (lower panel). All photometric points are color corrected for a 60 K BB. The meaning of the symbols is the following: solid line: model, diamond: PHT-C200 (P25 AOT).

Evaluation Log

1) P25 absolute photometry

Measurements:
PHT-C (120 um): pcap55204907 (src+back)
pcae55204906 (back)
PHT-C (200 um): pcap55204703 (src+back)
pcae55204702 (back)

Colour correction: black body, T = 60 K

Model: Griffin & Orton (OLP 10) – Abbas (OLP 9)

Det	cwl (μm)	OLP 9	OLP 10	Model	Δ (OLP 9)	Δ (OLP 10)
C2	120.0	813.865	857.617	896.663	-9.33	-4.35
C2	200.0	508.472	568.809	551.134	-7.89	3.21

5.2.5 PHT05 Absolute Photometry in Non-standard Apertures

Motivation

In this section we want to explore what impact the usage of non-standard apertures can have on the final accuracy. We investigate here measurements of standard stars in apertures which are considerably different from the standard aperture of the corresponding filter, see Table 2.2.

Method

We compare the color corrected flux values of both OLP V9.0b6 and OLP V10.0b7 results against the model predictions and IRAS photometry.

Results

Fig. 5.29 shows absolute photometry on the standard star HR 6847 performed with the 180 arcsec aperture at 3.6 μm. The sky background at this wavelength is negligible, so that no background needs to be subtracted. As can be seen from the figure 5.29 and the evaluation log, for OLP 9.0b6 the resulting flux was a factor of 2 higher than the model flux. This flux offset may be explained in the first instance as due to a beam effect, however the SPD product contains the warning that the selected FCS power was outside the calibrated range. In OLP 10 these cases were calibrated with default responsivities and Fig. 5.29 shows very good agreement with the model for OLP 10.0b7. In Section 5.1.4 we have investigated multi-filter photometry of the same star, including the 3.6 μm filter. For this measurement the 79 arcsec aperture had been used yielding an excellent agreement with the model flux. Therefore, for point sources which are far above the background the use of the bigger aperture does not have any impact on the accuracy of the sky measurement; this conclusion does not necessarily hold for the FCS measurement where default responsivities were used now. Due to the small variation of the P1 detector responsivities, the default responsivity yields a good photometric accuracy.

Conclusions

- Previous offset of photometry in a non-standard aperture could be traced as a consequence of insufficient actual responsivity calibration outside the calibrated FCS power range.
- Use of the default responsivity gives good accuracy for P1 photometry.

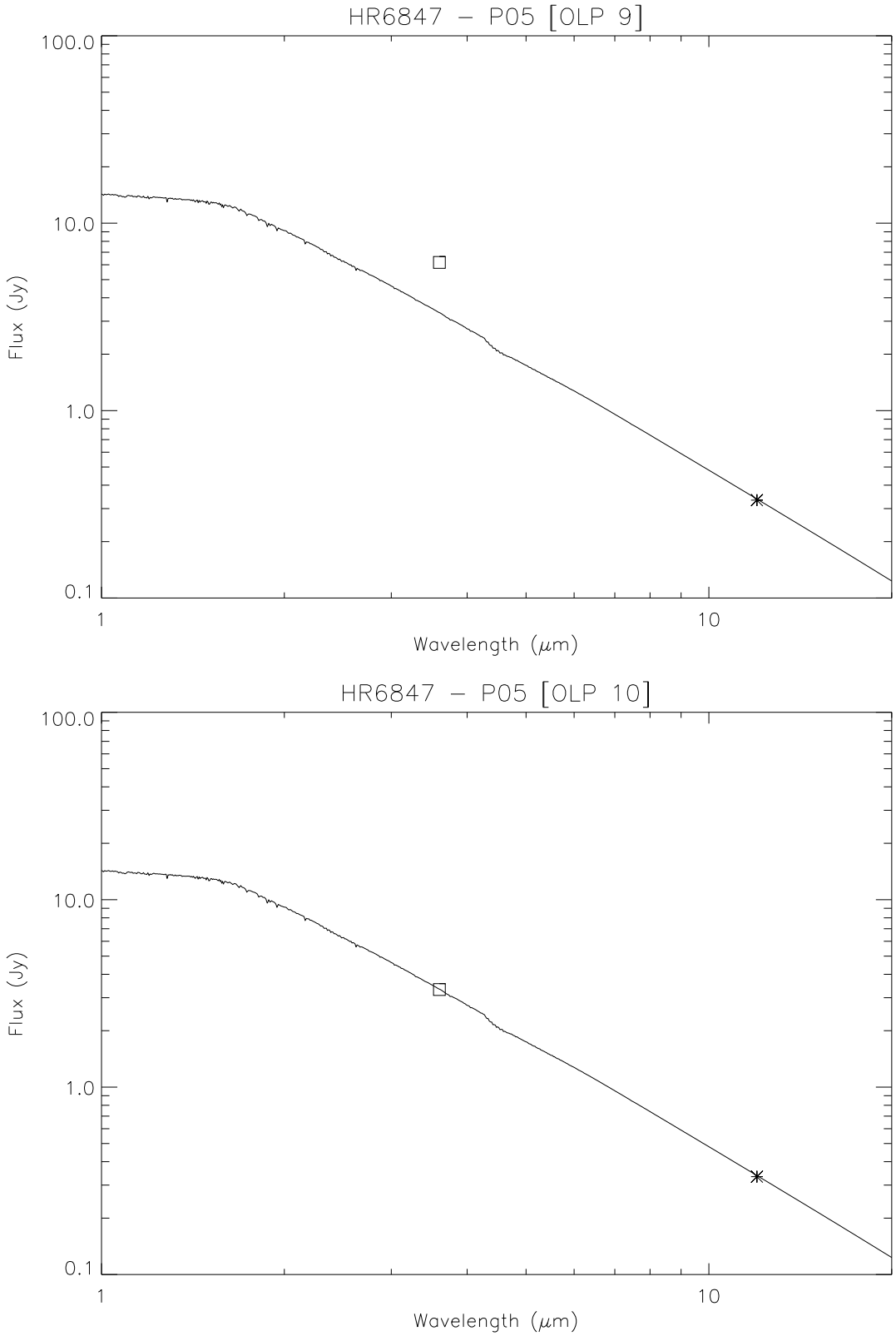

Figure 5.29: Comparison of PHT-P multi-filter photometry with the model of HR 6847 provided by P. Hammersley and with IRAS photometry for OLP 9.0b6 (upper panel) and OLP 10.0b7 (lower panel). All photometric points are color corrected for a 5720 K BB. The meaning of the symbols is the following: solid line: model, asterisk: IRAS, square: PHT-P (P05 AOT).

Evaluation Log

1) P05 absolute photometry

Measurements:
PHT-P1: ppap82501010 (src+back) 3.6 um

Colour correction: black body, T = 5720 K

Model: Hammersley

Det	cwl (μm)	OLP 9	OLP 10	IRAS	Model	Δ (OLP 9)	Δ (OLP 10)
P1	3.6	6.175	3.316		3.333	85.27	-0.51

5.3 Consistency Check of Sparse Map Photometry

Summary

- Sparse map multi-filter photometry was successfully revalidated.
- Calibration accuracies achieved by OLP V9 have been consolidated and slightly improved. Calibration accuracies are provided in the general overview in Sect. 1.3.
- We note a significant improvement for measurements where the FCS heating power was outside the calibrated range. Deselecting the one which is outside the calibrated range or switching to default responsivity gives now reasonable photometric accuracies (provided no other caveat applies, like the use of non-standard apertures).
- Sparse map sequences had been used as quasi-nodding measurements for faint sources. While we found accurate photometry for a P3 test case, the C100 test cases yielded too high fluxes. It is difficult to conclude on a general systematic calibration effect, because there may be several reasons for the deviating results. One is cirrus confusion which contaminates the background measurement. It should also be investigated whether the restriction to pixel 5 would improve the results.

5.3.1 PHT17/19 and PHT37/39 Sparse Map On-Off Mode: The SED of HR 337

Motivation

For the calibration star HR 337 a small verification program of the reset interval correction calibration was worked out which was executed in form of sparse maps. Following the off-source pointing, the first on-source pointing is with the nominal reset interval length derived for the specified source flux. In the following two sparse map modules the reset interval length is either longer or shorter by factors two to four. The last sparse map module is again performed with the nominal reset interval length, in order to check for possible detector drifts. Ideally, the fluxes from all on-source modules should be the same. The sparse map sequences are for P3, C100 and C200.

Method

We compare the background subtracted, color corrected flux values of OLP V9.0b6/V9.01 and OLP V10.0b5 against the model prediction.

Results

In the P3 sparse map photometry the first pair of measurements has a somewhat degraded accuracy in OLP 10b5. It might be due to the fact, that in OLP10 the responsivities are averaged and not interpolated anymore and that in this specific case the interpolation had compensated some responsivity drift in the OLP 9 porcessing. Otherwise there are consistent results for all selected reset interval settings. We derive $< 10\,\%$ absolute and $< 10\,\%$ relative filter-to-filter accuracy.
The C100 sparse map photometry is significantly improved absolutely and is more consistent among the various measurements with OLP 10b5. We derive $< 15\,\%$ absolute and $< 10\,\%$ relative filter-to-filter accuracy.
The situation for the C200 sparse map photometry is unchanged from OLP 9 to OLP 10. For the nominal reset interval setting the flux is systematically too high by 60 %. It is similar for the factor of 2 longer reset interval setting. The very short reset interval of only 1/2 s shows a clear outlier, in particular, as the bracketing measurements with nominal reset interval length give reproducible results.

Conclusions

- The small test data set on P3 reset interval correction gives good consistency (flux values are within 10 %) and good absolute (10 %) and relative filter-to-filter calibration.
- The small test data set on C100 reset interval correction gives reasonable consistency (flux values are within 20 %) and absolute and relative filter-to-filter accuracies of $<$ 15 % and $< 10\,\%$, respectively. and relative filter-to-filter calibration.
- The small test data set on C200 shows a systematic outlier of a rather short reset interval setting with regard to the considerably longer nominal reset interval settings. Therefore some caveat about the C200 reset interval may be appropriate, although the inspection of the C200 reset interval correction coefficients did not show any obvious flaw. This has to be followed up by interactive processing.

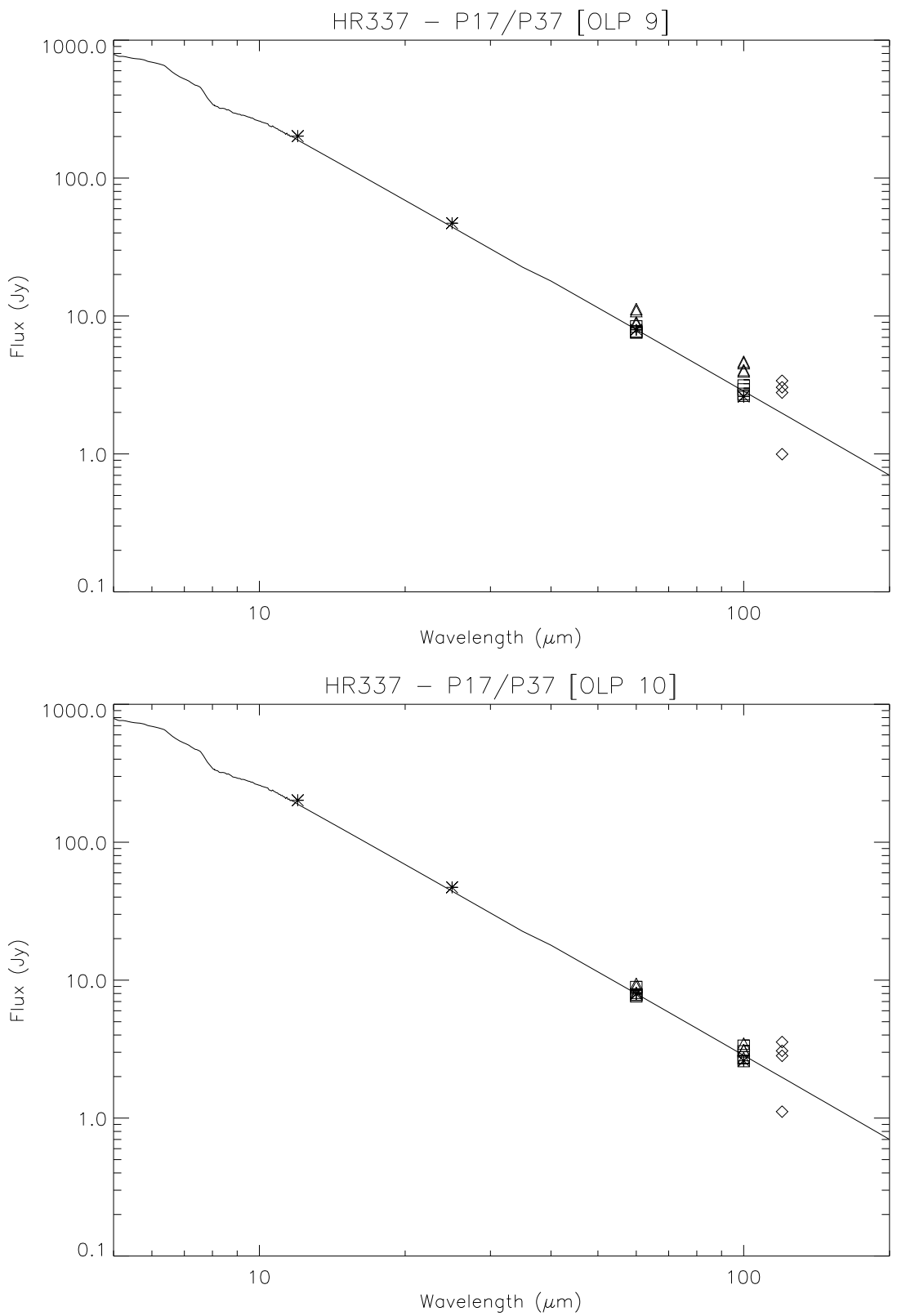

Figure 5.30: Comparison of PHT-P and PHT-C sparse map photometry with the model spectrum of HR 337 provided by M. Cohen and with IRAS photometry for OLP 9.0b6/9.01 (upper panel) and OLP 10.0b5 (lower panel). All photometric points are color corrected for a 3839 K BB. The meaning of the symbols is the following: solid line: model, asterisk: IRAS, square: PHT-P (P17/18/19 AOTs), triangle: PHT-C100 (P37/38/39 AOT), diamond: PHT-C200 (P37/38/39 AOT).

Evaluation Log

1) point source photometry of HR 337

Measurements:

PHT-P3:	ppae80400601 (P17 back)	FCS = 60 um
	ppap80400602 (P18 src+back)	RI = 1/4s
	ppap80400603 (P18 src+back)	RI = 1/2s
	ppap80400604 (P18 src+back)	RI = 1/16s
	ppap80400605 (P19 src+back)	RI = 1/4s, FCS = 60um
PHT-C100:	pcae80400706 (P37 back)	FCS = 60 um
	pcap80400707 (P38 src+back)	RI = 1/4s
	pcap80400708 (P38 src+back)	RI = 1/2s
	pcap80400709 (P38 src+back)	RI = 1/16s
	pcap80400710 (P39 src+back)	RI = 1/4s, FCS = 60um
PHT-C200:	pcae80400811 (P37 back)	FCS = 120 um
	pcap80400812 (P38 src+back)	RI = 4s
	pcap80400813 (P38 src+back)	RI = 8s
	pcap80400814 (P38 src+back)	RI = 1/2s
	pcap80400815 (P39 src+back)	RI = 4s, FCS = 120um

Colour correction: black body, T = 3839 K

Model: Cohen

Det	cwl (μm)	OLP 9	OLP 10	IRAS	Model	Δ (OLP 9)	Δ (OLP 10)
P3	60.0	8.395	8.897	7.924	7.972	5.30	11.60
P3	100.0	3.131	3.343	2.603	2.851	9.82	17.26
P3	60.0	7.591	7.845	7.924	7.972	-4.77	-1.60
P3	100.0	2.933	3.046	2.603	2.851	2.88	6.82
P3	60.0	7.749	7.867	7.924	7.972	-2.79	-1.32
P3	100.0	2.724	2.753	2.603	2.851	-4.44	-3.42
P3	60.0	7.683	7.644	7.924	7.972	-3.62	-4.11
P3	100.0	2.644	2.594	2.603	2.851	-7.26	-9.02
C1	60.0	8.985	8.981	7.924	7.972	12.71	12.66
C1	100.0	3.963	3.465	2.603	2.851	38.99	21.54
C1	60.0	8.767	7.863	7.924	7.972	9.97	-1.37
C1	100.0	4.056	3.119	2.603	2.851	42.27	9.41
C1	60.0	11.231	9.400	7.924	7.972	40.88	17.91
C1	100.0	4.550	3.105	2.603	2.851	59.59	8.92
C1	60.0	10.861	8.109	7.924	7.972	36.24	1.72
C1	100.0	4.664	2.719	2.603	2.851	63.60	-4.64
C2	120.0	3.041	3.075		1.973	54.13	55.83
C2	120.0	2.783	2.829		1.973	41.05	43.38
C2	120.0	0.996	1.114		1.973	-49.51	-43.55
C2	120.0	3.394	3.560		1.973	72.03	80.44

5.3.2 PHT17/19 and PHT37/39 Sparse Map On-Off Mode: The SED of Arp 244

Motivation

The observations of Arp 244 complement the evaluation of galaxy SEDs, since the measurements were performed in sparse map off-on mode (PHT17/PHT19 for PHT-P observations and PHT37/PHT39 for PHT-C observations, respectively; note that the 25 μm observations failed due to R/T problems). Furthermore, the observations were performed in the Performance Verification Phase, so that the pre-rev. 94 FCS calibration is applied for the FIR detectors (C100 and C200). Since the object is extended, the 180 arcsec aperture was used for the PHT-P observations. This gives some feedback on the surface brightness calibration using the maximum aperture size with regard to the standard aperture for this filter. Also, the C100 and C200 sparse map elements have FCS calibrations with different heating powers or in different filters so that they are test case for the check-out of the SCREW-464 (application of average and default responsivities) implementation.
The photometric properties of this object are discussed in detail in "Infrared spectral energy distributions of the interacting galaxies Arp 244, NGC 6240 and Arp 220" [15].

Method

We compare the background subtracted flux values of both OLP V9.0b6 and OLP V10.0b5 results against the IRAS photometry and a model fit based on the OLP V6.x calibration. As the source is extended, we do not use IRAS PSC or FSC photometry, but total fluxes as given in [29].

Results

Fig. 5.31 shows the derived SED for Arp 244. The model fit from [15] is plotted as a guide line to easier recognize the changes w.r.t. OLP V9.0b6. Note that this fit cannot serve as reference photometry.
We have color corrected the photometry w.r.t. modified blackbodies with emissivities $\propto \lambda^{-1}$ for the 12.8 to 200 μm range (for details, see part 2 of the evaluation log section). This color corrected SED is shown in Fig. 5.32.
We notice the following results:

- The OLP 9 C100 photometry gave by far too low fluxes. At 60 μm only 1/3 of the IRAS flux was derived. Approximately the same factor was suggested for the 90 μm filter from the comparison of model fit with IRAS 100 mum photometry. The FCS calibration filter is the 90 μm filter. For the C100 sparse map on-source, the OLP 9 SPD product PC1S06903806.FITS contained the following warning:

```
FILTER2 = 'C100_90_UM'         / Filter
 ...
CALP1F2 = 'Both    '           / Cal used in SPD calculations
CALP2F2 = 'Both    '           / Cal used in SPD calculations
CALP3F2 = 'Both    '           / Cal used in SPD calculations
CALP4F2 = 'Both    '           / Cal used in SPD calculations
CALP5F2 = 'Both    '           / Cal used in SPD calculations
CALP6F2 = 'Both    '           / Cal used in SPD calculations
CALP7F2 = 'Both    '           / Cal used in SPD calculations
CALP8F2 = 'Both    '           / Cal used in SPD calculations
CALP9F2 = 'Both    '           / Cal used in SPD calculations
CALFILT =                    8 / Filter for cal measurement
TRS1S2  =                    2 / Selected TRS for FCS1
POW1S2  =              2.45421 / Selected power for FCS1
POW1M2  =              2.45422 / Measured power for FCS1
CALPOW2 =             4.97E-14 / In-band power on detector for cal (Watts)
COMMENT ************************************************
COMMENT The selected FCS power was outside the calibrated range.
COMMENT ************************************************
```

This meant that the optical power by the FCS illumination was estimated a factor of 3 too low and hence the detector responsivity determined a factor of ~ 3 too high. The upper limt of the calibrated range is 1.93 mW, as can be seen from Table 2.1 in Sect. 2.1. OLP 10 now recognizes the measurement which is outside the calibrated range and uses only the first FCS measurement of the sparse map which is related to the off-source measurement and which is inside the calibrated range. The OLP 10 SPD product contains the following information:

```
FILTER2 = 'C100_90_UM'         / Filter
...
CALP1F2 = 'First   '           / Cal used in SPD calculations
CALP2F2 = 'First   '           / Cal used in SPD calculations
CALP3F2 = 'First   '           / Cal used in SPD calculations
CALP4F2 = 'First   '           / Cal used in SPD calculations
CALP5F2 = 'First   '           / Cal used in SPD calculations
CALP6F2 = 'First   '           / Cal used in SPD calculations
CALP7F2 = 'First   '           / Cal used in SPD calculations
CALP8F2 = 'First   '           / Cal used in SPD calculations
CALP9F2 = 'First   '           / Cal used in SPD calculations
CALFIL2 =                     8 / Filter for cal measurement
TRS1S2  =                     2 / Selected TRS for FCS1
POW1S2  =               2.45421 / Selected power for FCS1
POW1M2  =               2.45422 / Measured power for FCS1
CALPOW2 =             4.98E-14 / In-band power on detector for cal (Watts)
COMMENT ************************************************
COMMENT The selected FCS power was outside the calibrated range.
COMMENT ************************************************
```

The C100 photometry is now recovered and quite consistent with the IRAS results.

- The C200 photometric points appear to be a bit too high with regard to IRAS photometry. Some caution is however necessary here, since beam size effects due to the extension of the object may play a role. Since all flux is considered to come from a point source the PSF correction factors are presumably too strong for this object.

In Fig. 5.33 we plot the derived multi-filter surface brightness values in comparison with COBE photometry. The PHT-P surface brightness photometry seems to be systematically below the COBE fluxes. Since for the Arp 220 background with a quite similar brightness the matching was quite good, this could indicate the order of a correction factor using the large 180 arcsec aperture - about 30 % -, but clearly more statistics is needed here. The FIR background photometry from C100 and C200 is now quite consistent with COBE/DIRBE, except the rather flat behaviour out to 200 μm.

Conclusions

- For this pre-rev 94 test case the C100 FCS calibration was outside the calibrated range. Consequently, for OLP 9, the source flux was a factor of $2.5 - 3$ too low, which was due to a poor definition of the FCS extrapolation for the 90 μm filter. For OLP 10, the poor FCS measurement is deselected and only the first one from the off-target position which has different FCS power settings which are inside the calibrated range is used. This yields quite reasonable fluxes at 60 and 90 μm
- The C100 fluxes appear somewhat too high w.r.t. the C100 fluxes. This could be due to beam size effects and the contribution by an extended component. The C200 fluxes are derived under the assumption that the total flux comes from a point source and corresponding PSF correction factors are applied. In case there is flux from an extended component, these correction factors are too strong.
- PHT-P surface brightness photometry (not validated yet) gives too low values compared with COBE/DIRBE. This seems to indicate the order of correction (~ 30 %) taking into account the effective solid angle ratio between the 180 arcsec aperture and the standard aperture for these filters (52 arcsec).

- The $60 - 200\,\mu$m surface brightness is now quite consistent with COBE/DIRBE (20 % at $60\,\mu$m) except the rather flat shape out to $200\,\mu$m while DIRBE indicates a drop in flux, however this discrepancy might be due to local cirrus properties.

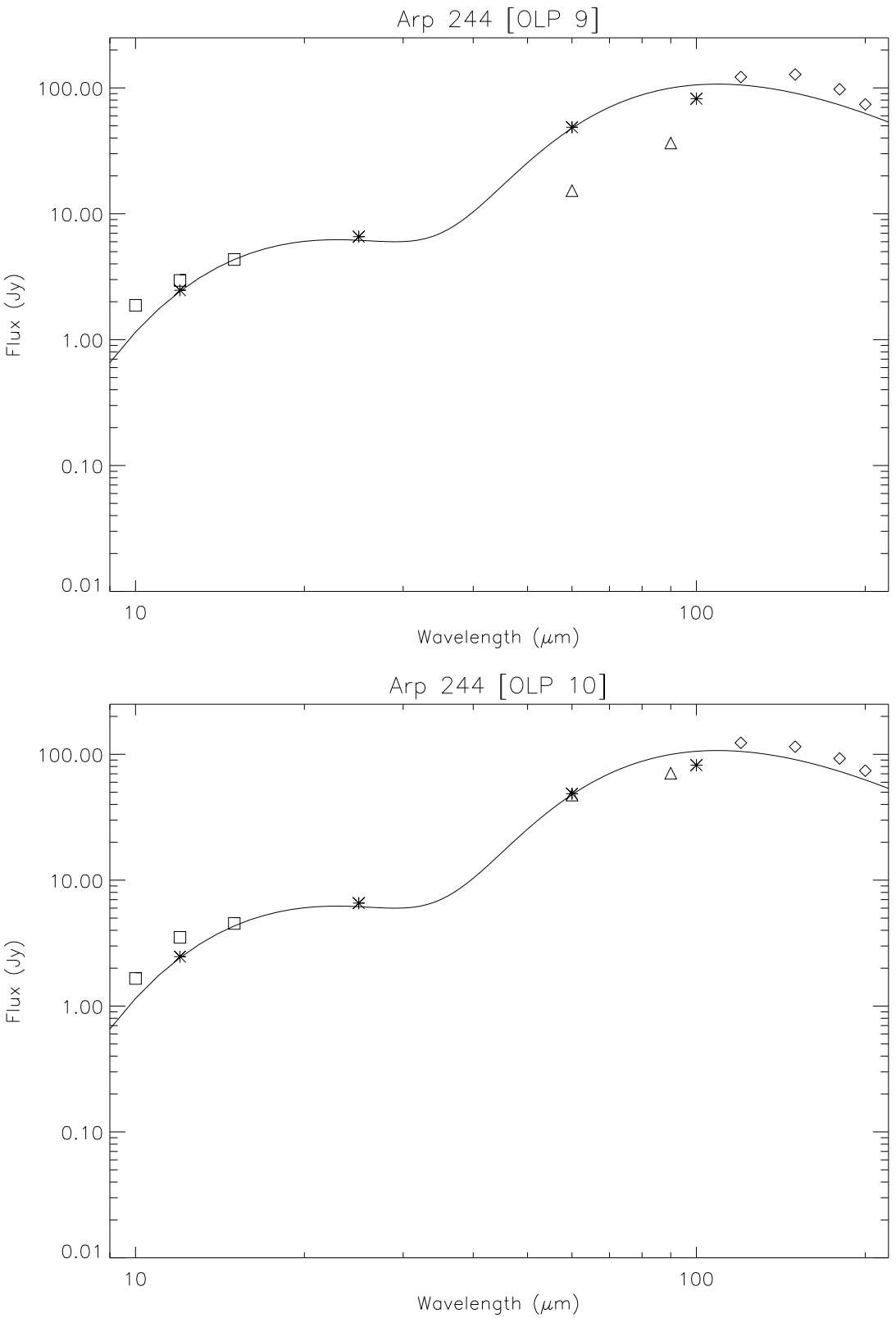

Figure 5.31: Comparison of PHT-P and PHT-C photometry with IRAS photometry and the model fit as described in [15]. Note that this model fit only serves as a guide for the eye to recognize more easily the changes between the two versions. It is not an absolute photometric reference. No color correction has been applied. The meaning of the symbols is the following: solid line: model, asterisk: IRAS, square: PHT-P (P03 AOT), triangle: C100 (P22 AOT), diamond: C200 (P22 AOT).

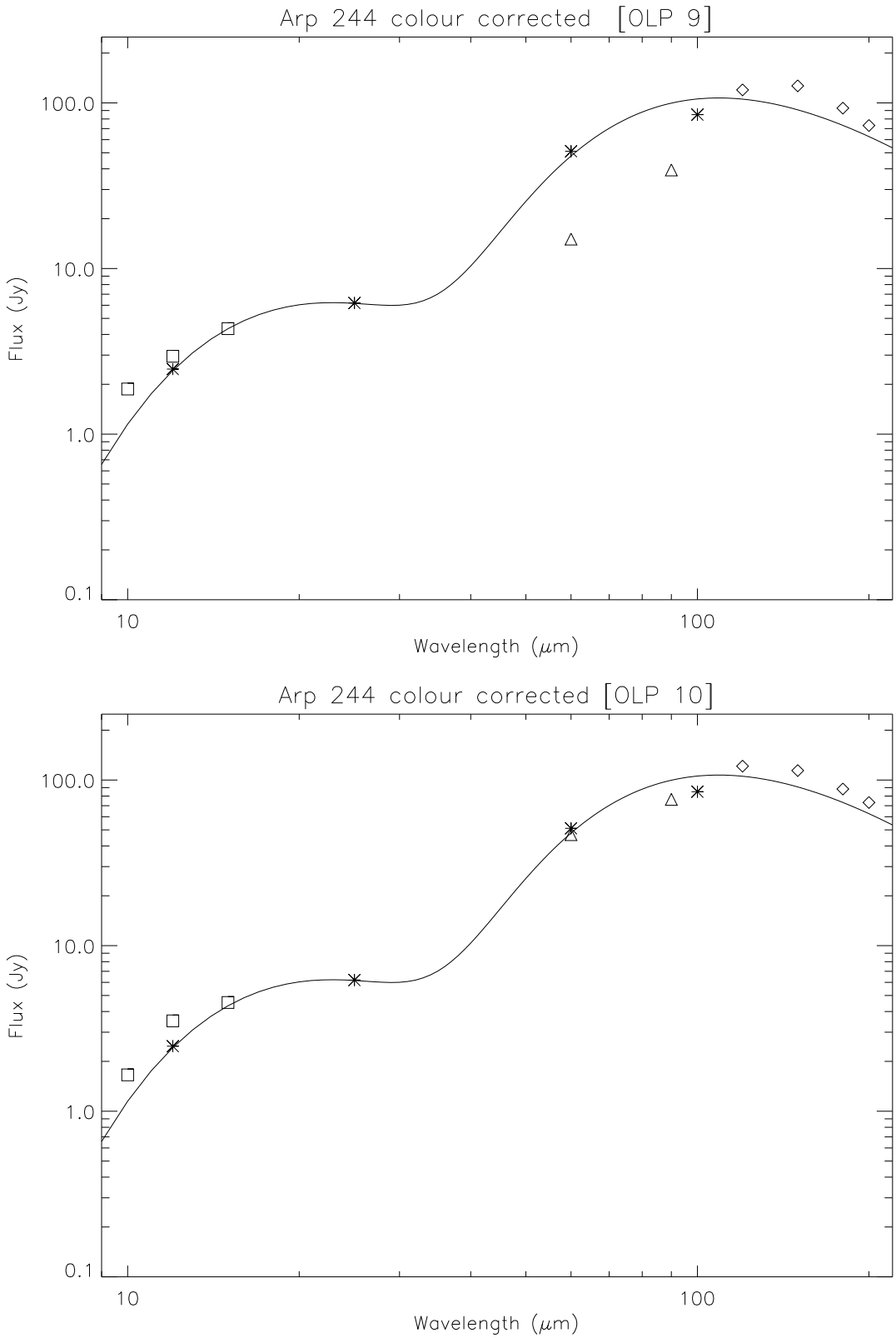

Figure 5.32: Comparison of PHT-P and PHT-C photometry with IRAS photometry and the model fit as described in [15]. Note that this model fit only serves as a guide for the eye to recognize more easily the changes between the two versions. It is not an absolute photometric reference. Color correction according to the model parameters, modified BBs $\propto \lambda^{-1}$ with T1 = 160 K and T2 = 33 K, has been applied. The meaning of the symbols is the following: solid line: model, asterisk: IRAS, square: PHT-P (P03 AOT), triangle: C100 (P22 AOT), diamond: C200 (P22 AOT).

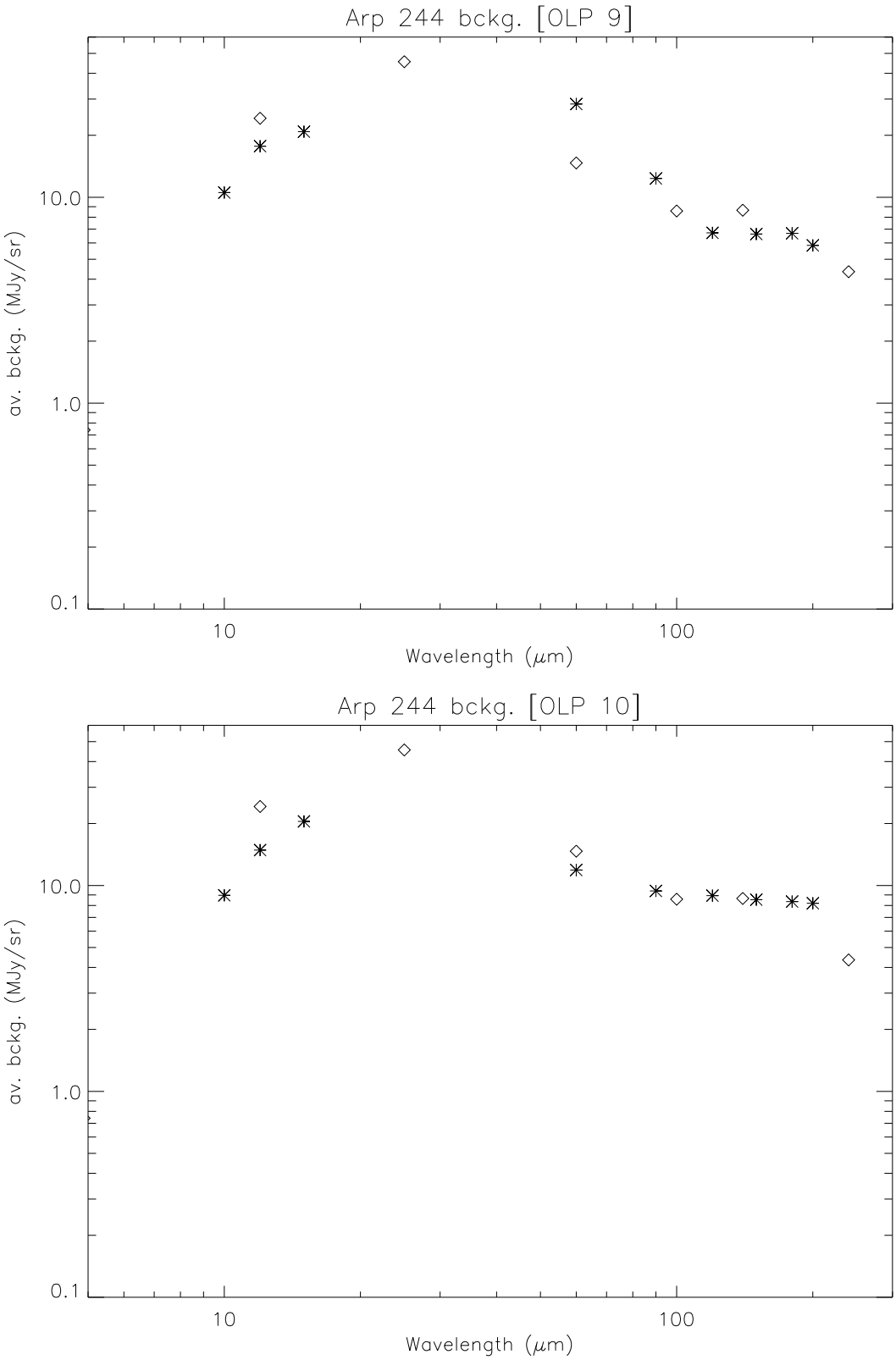

Figure 5.33: Comparison of PHT surface brightness photometry with COBE, both for OLP 9.0b6 and OLP 10.0b5. Asterisk: PHT-P and PHT-C photometry, diamond: COBE.

Evaluation Log

1) point source photometry of Arp 244 (not colour corrected)

Measurements:

PHT-P:	ppap06903802 (P19 src+back)	FCS = 15 um
	ppae06903801 (P17 back)	FCS = 15 um
PHT-C:	pcap06903806 (P39 C100 src+back)	FCS = 90 um
	pcae06903805 (P37 C100 back)	FCS = 90 um
	pcap06903808 (P39 C200 src+back)	FCS = 150 um
	pcae06903807 (P37 C200 back)	FCS = 180 um

Model: Sum of 2 modified bb, em. $\propto \lambda^{-1}$, T1 = 160 K, T2 = 33 K

Det	cwl (μm)	OLP 9	OLP 10	IRAS	Model	Δ (OLP 9)	Δ (OLP 10)
P1	10.0	1.873	1.657		1.150	62.85	44.10
P1	12.0	2.952	3.513	2.470	2.420	21.97	45.12
P1	15.0	4.331	4.531		4.334	-0.06	4.56
C1	60.0	15.248	47.405	48.680	47.813	-68.11	-0.85
C1	90.0	36.491	70.769		99.706	-63.40	-29.02
C2	120.0	121.987	123.425		105.397	15.74	17.10
C2	150.0	127.830	114.981		90.809	40.77	26.62
C2	180.0	97.579	92.595		73.181	33.34	26.53
C2	200.0	73.997	74.127		62.622	18.16	18.37

2) point source photometry of Arp 244 (colour corrected from 12.8 to 200 μm)

Measurements:

PHT-P:	ppap06903802 (P19 src+back)	FCS = 15 um
	ppae06903801 (P17 back)	FCS = 15 um
PHT-C:	pcap06903806 (P39 C100 src+back)	FCS = 90 um
	pcae06903805 (P37 C100 back)	FCS = 90 um
	pcap06903808 (P39 C200 src+back)	FCS = 150 um
	pcae06903807 (P37 C200 back)	FCS = 180 um

Colour correction: according to model

Model: Sum of 2 modified bb, em. $\propto \lambda^{-1}$, T1 = 160 K, T2 = 33 K

Det	cwl (μm)	OLP 9	OLP 10	IRAS	Model	Δ (OLP 9)	Δ (OLP 10)
P1	10.0	1.873	1.657		1.150	62.85	44.10
P1	12.0	2.952	3.513	2.470	2.420	21.97	45.12
P1	15.0	4.335	4.536		4.334	0.04	4.66
C1	60.0	15.053	46.796	51.081	47.813	-68.52	-2.13
C1	90.0	39.386	76.384		99.706	-60.50	-23.39
C2	120.0	119.853	121.266		105.397	13.72	15.06
C2	150.0	126.803	114.057		90.809	39.64	25.60
C2	180.0	93.021	88.270		73.181	27.11	20.62
C2	200.0	73.025	73.154		62.622	16.61	16.82

3) Surface brightness photometry of Arp 244 background

λ	OLP9 (MJy/sr)	OLP10 (MJy/sr)	COBE (MJy/sr)
10.0	10.54	8.96	
12.0	17.71	14.86	24.20
15.0	20.84	20.48	
60.0	28.38	11.89	14.68
90.0	12.34	9.41	
120.0	6.72	8.93	
150.0	6.63	8.53	8.65
180.0	6.68	8.36	
200.0	5.84	8.20	4.35

5.3.3 PHT17/19 Sparse Map On-Off Mode: The SED of BS 5062

Motivation

The sparse map observations of the star BS 5062 are an important check of SCREW-464 implementation (application of average and default responsivities), because for the off-measurement the FCS calibration is in a different filter (4.8 μm) and with a different heating power than for the on-measurement (3.6μm).

Method

We compare the background subtracted, color corrected flux values of both OLP V9.0b6 and OLP V10.0b5 results against the model prediction.

Results

The comparison of OLP 9.0b6 and OLP 10.0b5 with the model is given in part 1 of the evaluation log. Fig. 5.34 shows the PHT photometric data points in comparison with the model and IRAS photometry (color corrected). The OLP 9 photometry was about a factor of 10 below the model expectation for the following reason:

```
CALP1F2 = 'Both    '           / Cal used in SPD calculations
AORI2   =             0.006886 / Reset interval correction offset, A0 (V/s)
AORIU2  =             0.002526 / Unc. in reset interval cor. offset, A0 (V/s)
A1RI2   =             0.913772 / Reset interval correction slope, A1
A1RIU2  =             0.022913 / Unc. in reset interval cor. slope, A1
CALFILT =                    3 / Filter for cal measurement
TRS1S2  =                    1 / Selected TRS for FCS1
POW1S2  =              6.21490 / Selected power for FCS1
POW1M2  =              6.21490 / Measured power for FCS1
CALPOW2 =             2.56E-17 / In-band power on detector for cal (Watts)
COMMENT ************************************************
COMMENT The selected FCS power was outside the calibrated range.
COMMENT ************************************************
CALAP2  =                    1 / Aperture used for cal (CHW position)
CALPOL2 =                    4 / Polarizer used for cal (CHW position)
CALTYP2 =                    2 / Type of processing for cal measurement
RS1P1F2 =            38.268124 / Responsivity (A/W) for first cal measurement
RU1P1F2 =             8.697465 / Uncertainty in responsivity for first cal
RS2P1F2 =             0.655455 / Responsivity (A/W) for second cal measurement
RU2P1F2 =             0.006411 / Uncertainty in responsivity for second cal
RESPDEF =                    F / TRUE if default responsivity is used.
```

A check with Table 2.1 in the Caveat Section 2.1 shows that the selected FCS power for the 4.8 μm filter off-measurement of 6.2 mW is far below the lower limit of the calibrated FCS range in this filter of 12.36 mW. The combination of the lower quality FCS extrapolation and low signal levels (as reflected by the high uncertainty of 25 %) lead to an anomalously high responsivity value of 38.3 A/W (versus 1.1 A/W default responsivity). The interpolation between the "wrong" off-responsivity and the on-responsivity leads then to the too low fluxes, also for the background measurements, as shown in Fig. 5.35. This was changed in OLP 10 and only actual FCS responsivities inside the calibrated range or default responsivities are used. Using only the actual responsivity value of the on-measurement leads to fluxes which are 40 to 60 % too high, which corresponds more or less to the ratio of default to actual response (1.1/0.655 = 1.68). The default responsivity would give accurate fluxes here. One reason for this discrepancy might be that a larger aperture (52") instead of the default one (23") was used. The usage of only the second responsivity value also restores the relative spectral shape between 3.6 and 4.8 μm.

```
CALP1F1 = 'Second  '           / Cal used in SPD calculations
AORI1   =             0.003640 / Reset interval correction offset, A0 (V/s)
AORIU1  =             0.001315 / Unc. in reset interval cor. offset, A0 (V/s)
```

```
A1RI1   =             0.957484 / Reset interval correction slope, A1
A1RIU1  =             0.000396 / Unc. in reset interval cor. slope, A1
CALFIL1 =                    3 / Filter for cal measurement
TRS1S1  =                    1 / Selected TRS for FCS1
POW1S1  =              6.21490 / Selected power for FCS1
POW1M1  =              6.21490 / Measured power for FCS1
CALPOW1 =             5.17E-17 / In-band power on detector for cal (Watts)
COMMENT ************************************************
COMMENT The selected FCS power was outside the calibrated range.
COMMENT ************************************************
CALAP1  =                    1 / Aperture used for cal (CHW position)
CALPOL1 =                    4 / Polarizer used for cal (CHW position)
CALTYP1 =                    2 / Type of processing for cal measurement
RSP1F1  =             0.669281 / Responsivity (A/W) for measurement
RUP1F1  =             0.006489 / Uncertainty in responsivity
RS1P1F1 =            16.209707 / Responsivity (A/W) for first cal measurement
RU1P1F1 =             6.520762 / Uncertainty in responsivity for first cal
RQ1P1F1 =                    9 / Quality flag for cal
RS2P1F1 =             0.669281 / Responsivity (A/W) for second cal measurement
RU2P1F1 =             0.006489 / Uncertainty in responsivity for second cal
RQ2P1F1 =                    2 / Quality flag for cal
FILTER2 = 'P1_3P6_UM'          / Filter
EXFLUX2 =              1.01284 / Expected source flux (log base 10 Jy)
UNCFLX2 =              0.70757 / Uncertainty in flux (log base 10 Jy)
MXBACK2 =             -1.22185 / Maximum background (log base 10 MJy/ster)
CALP1F2 = 'Second  '           / Cal used in SPD calculations
AORI2   =             0.002936 / Reset interval correction offset, A0 (V/s)
AORIU2  =             0.001440 / Unc. in reset interval cor. offset, A0 (V/s)
A1RI2   =             0.970345 / Reset interval correction slope, A1
A1RIU2  =             0.000367 / Unc. in reset interval cor. slope, A1
CALFIL2 =                    2 / Filter for cal measurement
TRS1S2  =                    1 / Selected TRS for FCS1
POW1S2  =             20.20757 / Selected power for FCS1
POW1M2  =             20.19536 / Measured power for FCS1
CALPOW2 =             4.75E-14 / In-band power on detector for cal (Watts)
CALAP2  =                    1 / Aperture used for cal (CHW position)
CALPOL2 =                    4 / Polarizer used for cal (CHW position)
CALTYP2 =                    2 / Type of processing for cal measurement
FCSDRIFT=                    F / TRUE if residual drift in FCS measurement
RESPDEF =                    F / TRUE if default responsivity is used.
```

Fig. 5.35 shows the comparison of OLP 9.0b6 and OLP 10.0b5 surface brightness photometry with COBE/DIRBE. While the former one was about a factor 10 too low w.r.t. COBE/DIRBE, mainly caused by the poor responsivity determination of the FCS measurement of the off-target position, the latter one is about a factor 10 too high w.r.t. COBE/DIRBE. Some factor comes in due too the obviously small responsivity value on-target which causes the source flux to be about 50 % too high, however, the major factor must be due to another calibration issue which could be the signal linearization.

Conclusions

- For the specific test case a poor photometry was achieved For OLP 9 due to the combination of a FCS measurement with heating power outside the calibrated range leading to an extremely high responsivity value and a FCS measurement with a heating power inside the calibrated range. OLP 10 improves the source photometry considerably, although an offset of about 40 % in absolute flux calibration remains. This is just the ratio between actual responsivity and default responsivity. One reason for this discrepancy may be the use of a non-standard aperture (52" vs. 23" default for these filters).

- For the surface brightness photometry now afctor of 10 too high values with respect to COBE/DIRBE are achieved. This cannot be explained by the responsivity alone.

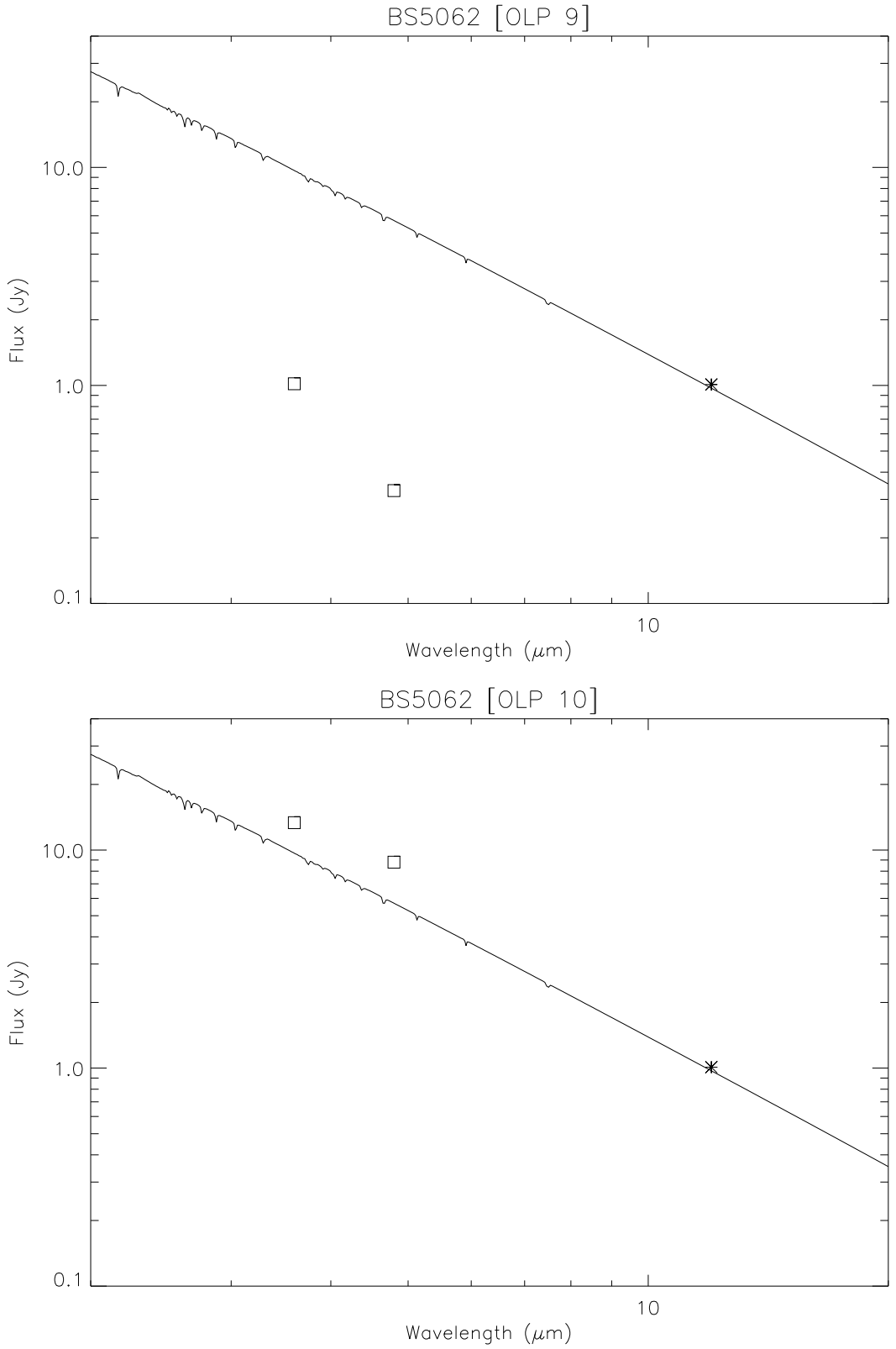

Figure 5.34: Comparison of PHT-P sparse map photometry with the model spectrum of BS 5062 provided by P. Hammersley and with IRAS photometry for OLP 9.0b6 (upper panel) and OLP 10.0b5 (lower panel). All photometric points are color corrected for a 8100 K BB. The meaning of the symbols is the following: solid line: model, asterisk: IRAS, square: PHT-P (P17/19 AOT).

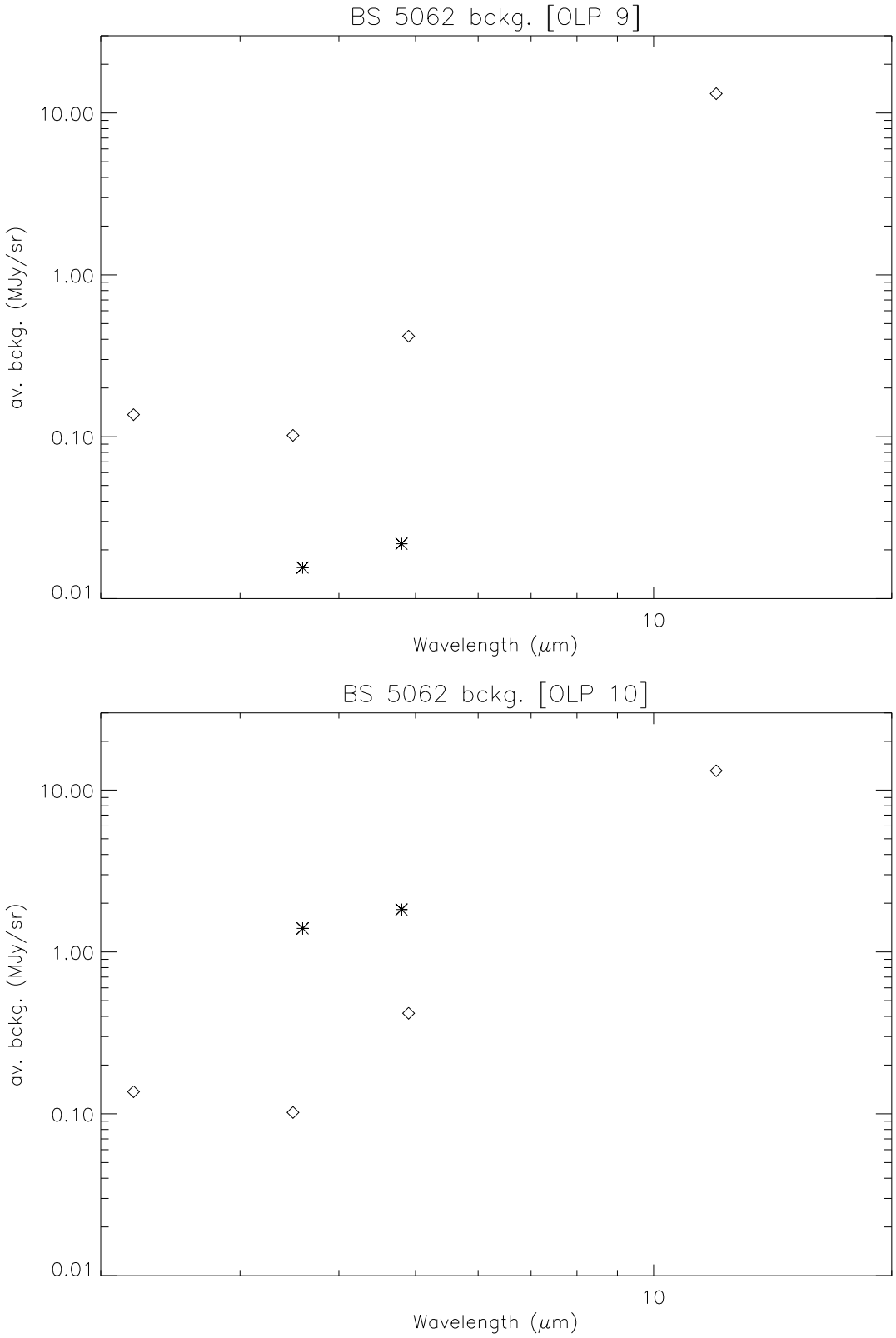

Figure 5.35: Comparison of PHT surface brightness photometry with COBE, both for OLP 9.0b6 and OLP 10.0b5. Asterisk: PHT-P photometry, diamond: COBE.

It points to a weakness of some other calibration item, and the signal linearization for the 3.6 and 4.8 μm filters should be inspected.

Evaluation Log

1) point source photometry of BS 5062

Measurements:
PHT-P: ppap19500981 (P19 src+back) FCS = 3.6 um
ppae19500980 (P17 back) FCS = 4.8 um

Colour correction: black body, T = 8087K

Model: Hammersley

Det	cwl (μm)	OLP 9	OLP 10	IRAS	Model	Δ (OLP 9)	Δ (OLP 10)
P1	3.6	1.018	13.352		9.674	-89.48	38.02
P1	4.8	0.329	8.800		5.705	-94.23	54.23

2) Surface brightness photometry of BS 5062 background

λ	OLP9 (MJy/sr)	OLP10 (MJy/sr)	COBE (MJy/sr)
3.6	0.02	1.40	
4.8	0.02	1.83	

5.3.4 PHT17/18/19 and PHT37/38/39 Sparse Map Sequences: The 60 μm Flux of the Faint Star HR 5981

Motivation

The sparse map sequences on HR 5981 belong to the measurements of the faint source detection program which was set up to find the optimal observing mode for the faintest sources. The telescope nodding mode was not yet existing at this time and the sparse map implementations considered here are quite similar to this observing mode. For HR 5981 both a PHT-P and a PHT-C sequence, each of them at 60 μm, was performed.

Method

We compare the background subtracted, color corrected flux values of both OLP V9.0b6 and OLP V10.0b5 results against the model prediction.

Results

The comparison of OLP 9.0b6 and OLP 10.0b5 with the model is given in part 1 of the evaluation log. Fig. 5.36 shows the flux sequence for the P3 detector. The source is clearly detected. Neither any systematic trend nor any systematic gradient between background positions #1 and #2 can be recognized. Therefore, the final flux was derived as the difference of the average of the 4 on-source fluxes and the average of the 5 off-source fluxes. Fig. 5.37 shows the corresponding sequence for the C100 detector. The dummy measurement clearly falls out due to the too short exposure time. The OLP 10 sequence shows a clearer source detection pattern than the OLP 9 sequence. Again, no clear drift or gradient can be recognized, so that the resulting source flux was obtained in the same way as for P3. Fig. 5.38 shows the PHT photometric data points in comparison with the model and IRAS photometry (color corrected). We note a quite good performance of the P3 photometry (better than IRAS), but the C100 photometry yields a flux which is a factor 2 too high.

Conclusions

- Use of average responsivities instead of interpolated responsivites does not show any degradation of accuracy for this faint source test case.
- The P3 photometry was slightly improved yielding now an absolute calibration accuracy of $< 10\,\%$.
- The C100 photometry shows a calibration offset of about a factor of 2.

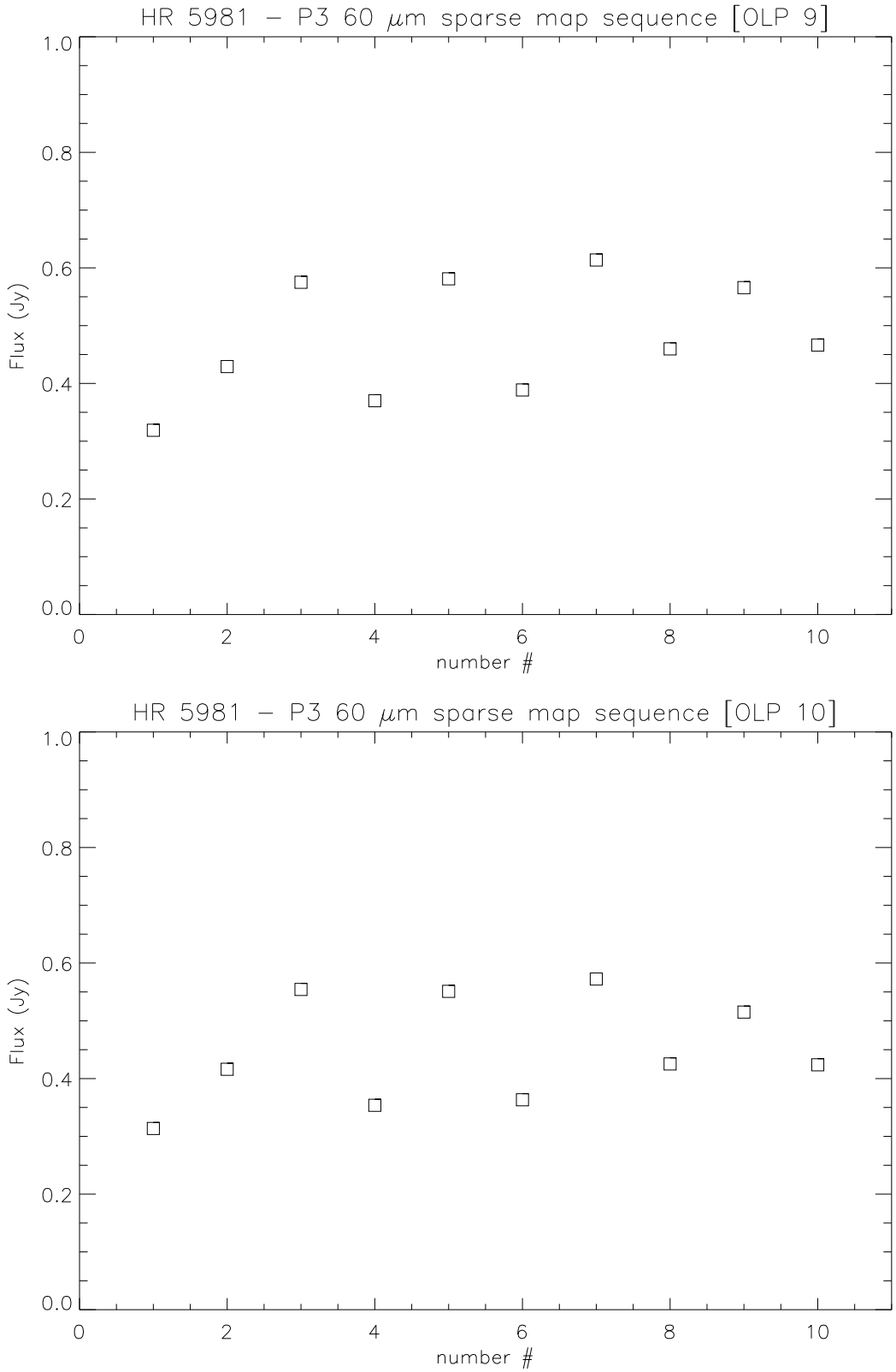

Figure 5.36: Flux sequence of the PHT-P sparse map on HR 5981 at 60 μm. The first point is the dummy measurement with a short exposure which was used to start the true sequence with a FCS exposure. Starting from the 2nd measurement the sequence was background position #1 – source – background position #2 – source – background position #1 – source – background position #2 – source – background position #1.

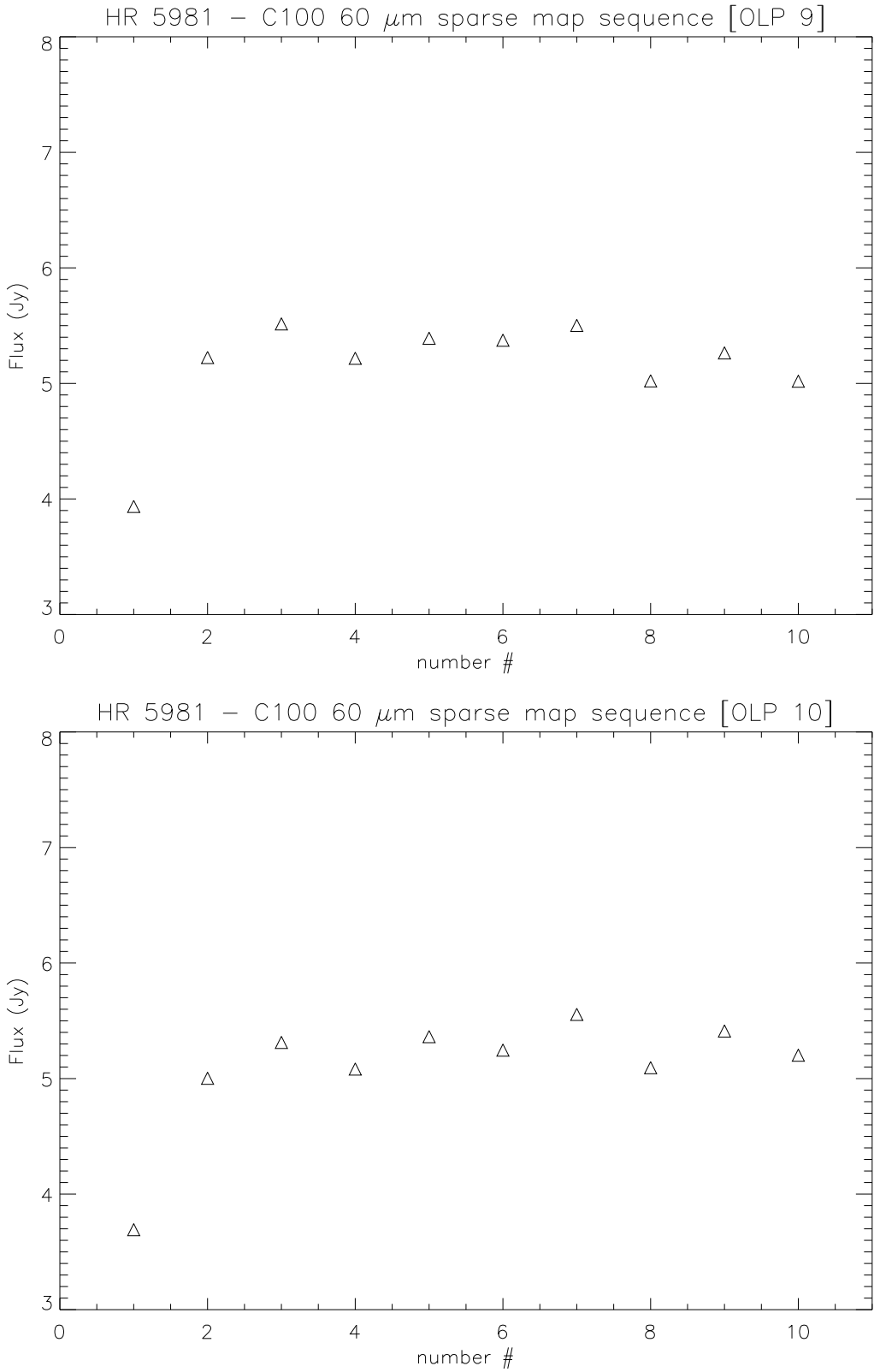

Figure 5.37: Flux sequence of the PHT-C sparse map on HR 5981 at 60 μm. The first point is the dummy measurement with a short exposure which was used to start the true sequence with a FCS exposure. Starting from the 2nd measurement the sequence was background position #1 – source – background position #2 – source – background position #1 – source – background position #2 – source – background position #1.

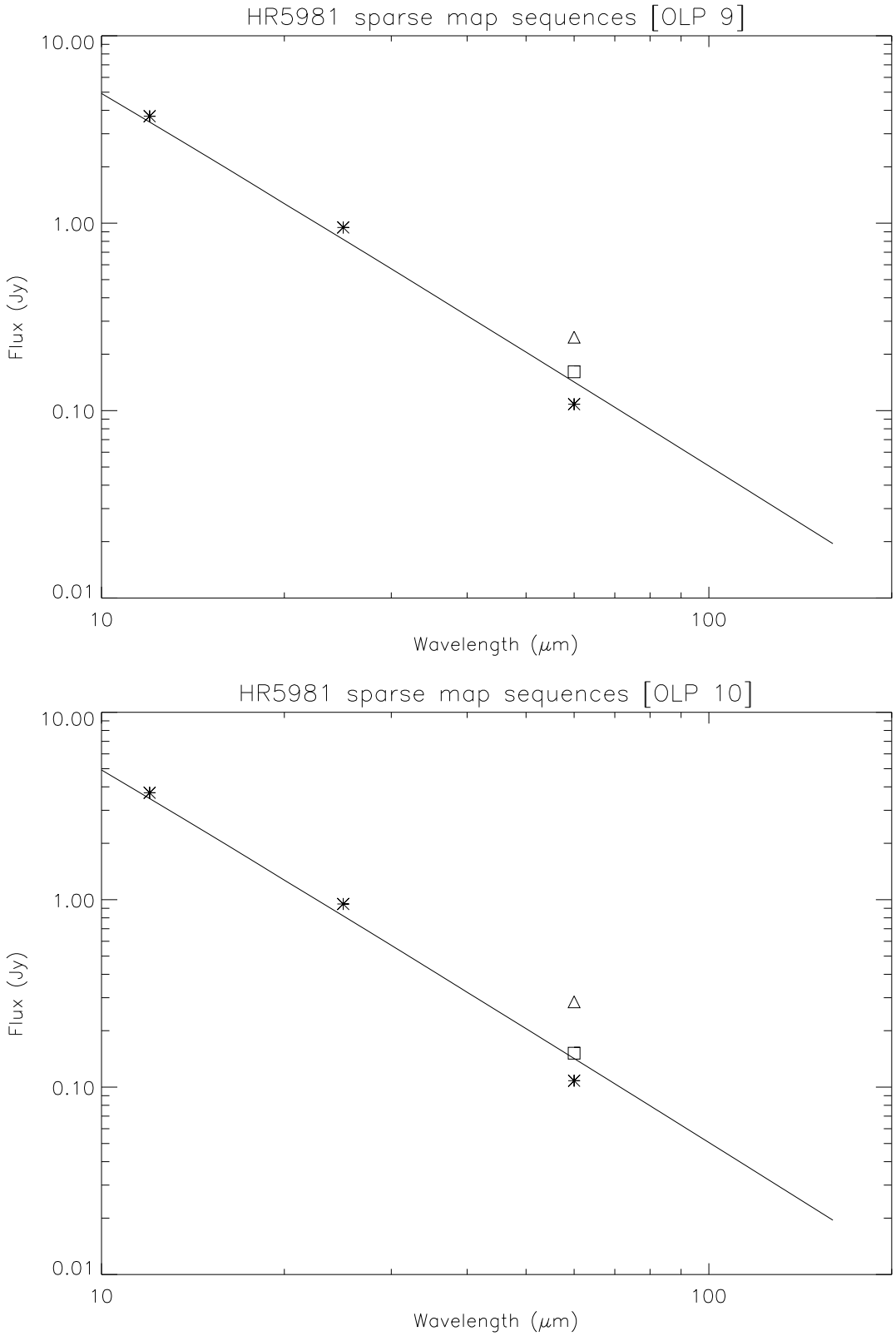

Figure 5.38: Comparison of PHT-P and PHT-C sparse map photometry with the model spectrum of HR 5981 provided by P. Hammersley and with IRAS photometry for OLP 9.0b6 (upper panel) and OLP 10.0b5 (lower panel). All photometric points are color corrected for a 4050 K BB. The meaning of the symbols is the following: solid line: model, asterisk: IRAS, square: PHT-P (P17/18/19 AOT), triangle: PHT-C (P37/38/39 AOT).

Evaluation Log

1) point source photometry of HR 5981

Measurements:

PHT-P3 :	ppap39200516	(P17, dummy, FCS = 60 um)
	ppap39200517	(P18, back1)
	ppap39200518	(P18, source)
	ppap39200519	(P18, back2)
	ppap39200520	(P18, source)
	ppap39200521	(P18, back1)
	ppap39200522	(P18, source)
	ppap39200523	(P18, back2)
	ppap39200524	(P18, source)
	ppap39200525	(P19, back1, FCS = 60 um)
PHT-C1 :	pcap39200303	(P37, dummy, FCS = 60 um)
	pcap39200304	(P38, back1)
	pcap39200305	(P38, source)
	pcap39200306	(P38, back2)
	pcap39200307	(P38, source)
	pcap39200308	(P38, back1)
	pcap39200309	(P38, source)
	pcap39200310	(P38, back2)
	pcap39200311	(P38, source)
	pcap39200312	(P39, back1, FCS = 60 um)

Colour correction: black body, T = 4048 K

Model: Hammersley

Det	cwl (μm)	OLP 9	OLP 10	IRAS	Model	Δ (OLP 9)	Δ (OLP 10)
P3	60.0	0.161	0.152	0.108	0.142	13.33	6.73
C1	60.0	0.247	0.285	0.108	0.142	73.47	100.64

5.3.5 PHT37/38/39 Sparse Map Sequence: The 90 μm Flux of the Faint Star IRC+60228

Motivation

The sparse map sequences on IRC +60228 belong to the measurements of the faint source detection program which was set up to find the optimal observing mode for the faintest sources. The telescope nodding mode was not yet existing at this time and the sparse map implementation considered here is quite similar to this observing mode.

Method

We compare the background subtracted, color corrected flux values of both OLP V9.0b6 and OLP V10.0b5 results against the model prediction.

Results

The comparison of OLP 9.0b6 and OLP 10.0b5 photometry with the model is given in part 1 of the evaluation log. Fig. 5.39 shows the flux sequence for the C100 detector. The source is clearly detected. No systematic gradient between background positions #1 and #2 can be recognized. However, there is a slight systematic upward drift with time for the OLP V10 product. It should be noted here that OLP V10 uses the average of the responsivity values from the two bracketting FCS measurements. In the contrary, the OLP V9 product shows a downward trend. Here the FCS measurements had been used to interpolate the responsivity values used for the intermediate measurements which led to a slight overcorrection. Fig. 5.40 shows the PHT photometric data points in comparison with the model and IRAS photometry (color corrected). As for the previous C100 faint source test case on HR 5981 5.3.4 we note here also a positive offset which is here in the order of 60–70 %. IRAS was cirrus confusion noise limited at 100 μm, so that part of the offset of the ISOPHOT photometry may be explained due to cirrus confusion.

Conclusions

- Use of average responsivities instead of interpolated responsivites does not show any degradation of accuracy for this faint source test case.
- The C100 photometry shows a calibration offset of about a factor of 2. Since the source is expected to be fainter than 100 mJy and the measurement is in a cirrus sensitive wavelength range the limited calibration accuracy may be caused by cirrus confusion.

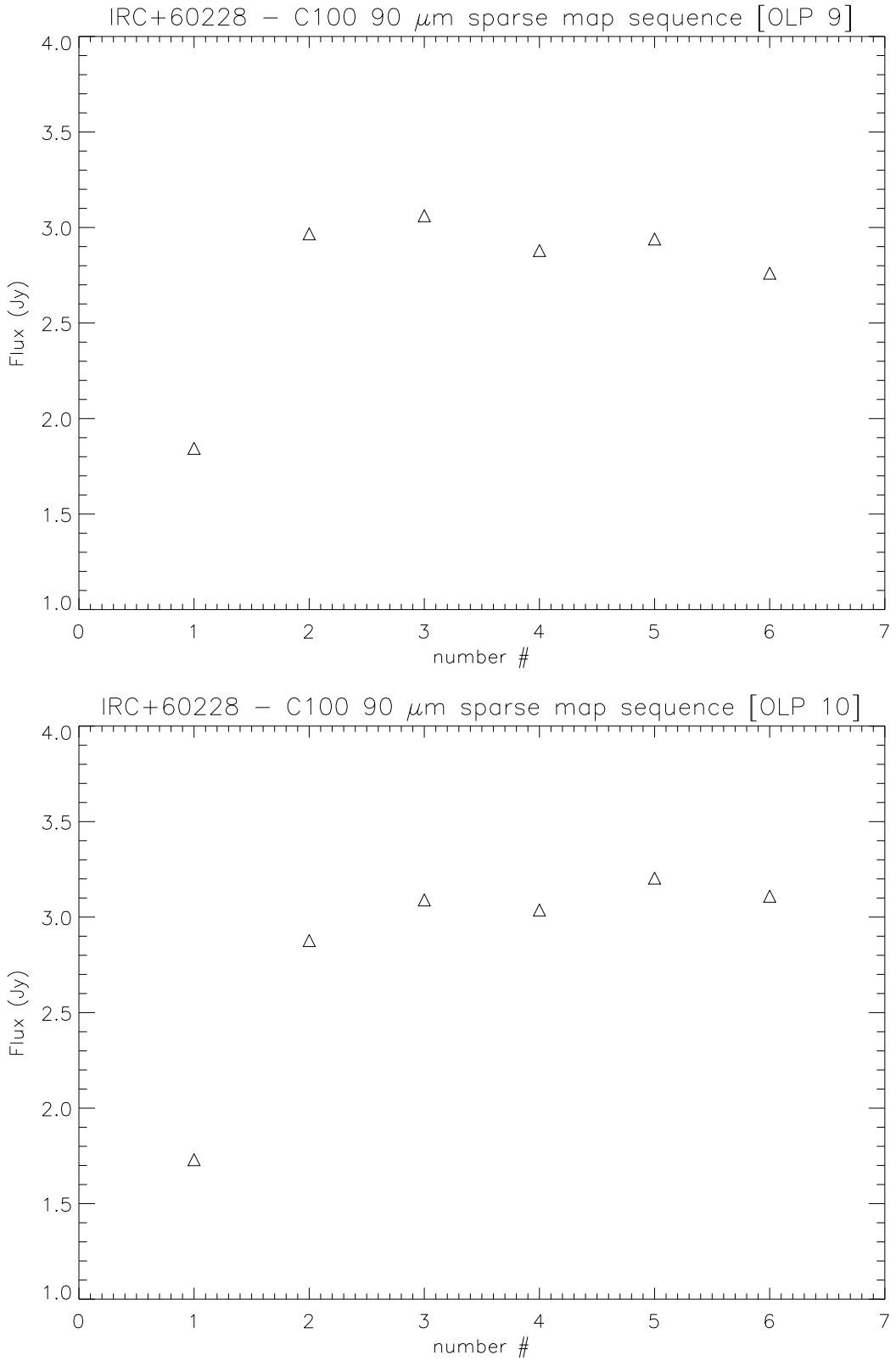

Figure 5.39: Flux sequence of the PHT-C sparse map on IRC +60228 at 90 μm. The first point is the dummy measurement with a short exposure which was used to start the true sequence with a FCS exposure. Starting from the 2nd measurement the sequence was background position #1 – source – background position #2 – source – background position #1.

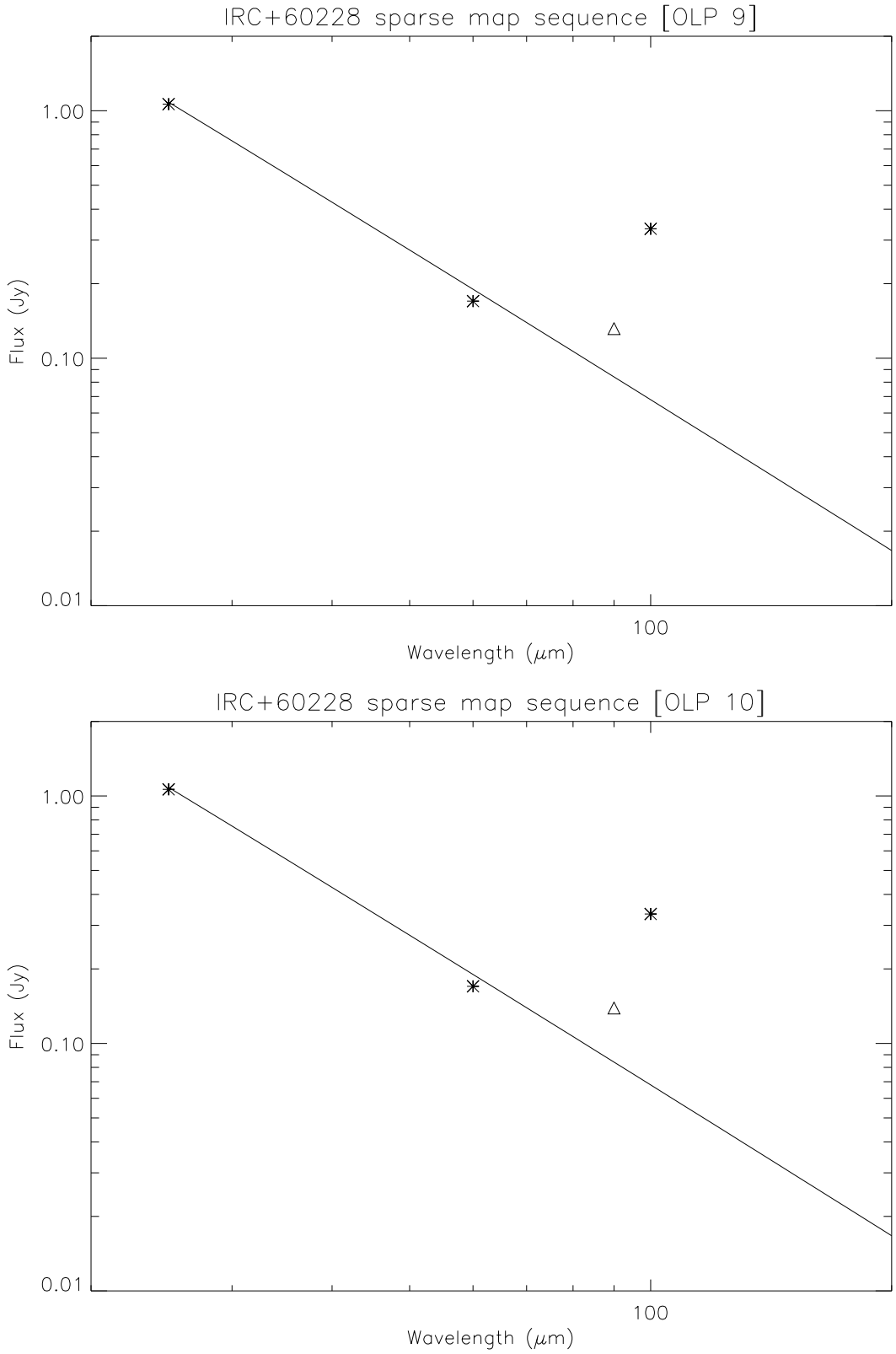

Figure 5.40: Comparison of PHT-C sparse map photometry with the model spectrum of IRC +60228 provided by M. Cohen and with IRAS photometry for OLP 9.0b6 (upper panel) and OLP 10.0b5 (lower panel). All photometric points are color corrected for a 3898 K BB. The meaning of the symbols is the following: solid line: model, asterisk: IRAS, triangle: PHT-C (P37/38/39 AOT).

Evaluation Log

1) point source photometry of IRC +60228

Measurements:

PHT-C1 :	pcae25202509	(P37, dummy, FCS = 90 um)
	pcae25202510	(P38, back1)
	pcap25202511	(P38, source)
	pcae25202512	(P38, back2)
	pcap25202513	(P38, source)
	pcae25202514	(P39, back1, FCS = 90 um)

Colour correction: black body, T = 4048 K

Model: Cohen

Det	cwl (μm)	OLP 9	OLP 10	IRAS	Model	Δ (OLP 9)	Δ (OLP 10)
C1	90.0	0.132	0.139		0.084	56.68	65.38

Chapter 6

Raster Map Photometry

6.1 Consistency Check of Mini-map Photometry

Summary

- Raster mode mini-map photometry was successfully revalidated.
- Calibration accuracies using the PCAS products and achieved by OLP V9 have been consolidated and slightly improved. Calibration accuracies are provided in the general overview in Table 1.9.
- C100 photometry gives reliable photometry ($< 30\,\%$) down to fluxes as low as 50 mJy. However, this may depend on the cirrus confusion level, and hence the absolute surface brightness.
- C200 photometry appears to become unreliable below a flux level of 100 mJy. The absolute level may depend on the actual cirrus confusion noise of this field.
- In case of extended sources the PSF factors used for flux reconstruction must be adjusted accordingly.

6.1.1 Point Source Photometry from PHT22 Mini-Maps: The SED of HR 7980

Motivation

For HR 7980 there exist mini-maps in all C100 filters and in three out of five C200 filters (120 to 170 μm). Therefore, the relative filter-to-filter calibration accuracy can be checked for this case.

Method

We compare the background subtracted, color corrected flux values of OLP V9.01 and OLP V10.0b5 results against the model prediction.

Results

The comparison of OLP 9.01 and OLP 10.0b5 photometry with the model is given in part 1 of the evaluation log. Fig. 6.1 displays the photometric results extracted from the mini-map PCAS product. The C100 photometry is as accurate as 10 % for all filters, except the 105 μm one. But here the photometry by OLP 10 is now improved and as good as 25 %. The C200 photometry is better than 25 %. The IRAS 100 μm FSC flux has only medium quality.

Conclusions

- This test case shows that the good absolute photometric accuracy found for PCAS products holds for all C100 filters and for three out of five C200 filters.
- The C100 absolute photometric accuracy is < 25 %, for filters shortward of 100 μm even < 10 %.
- The C200 absolute photometric accuracy is < 25 %.

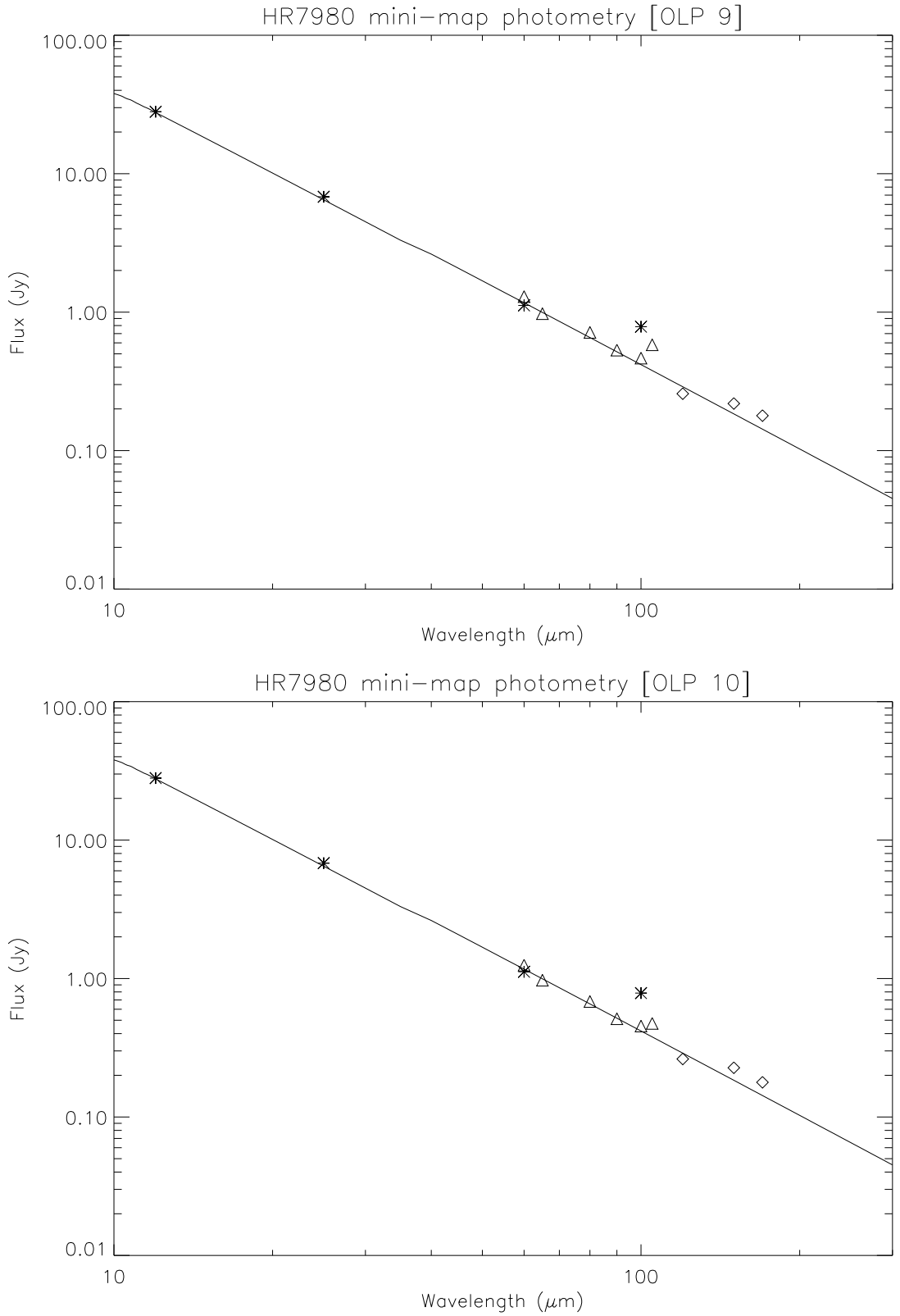

Figure 6.1: Comparison of PHT-C mini-map photometry with the model spectrum (plus extension out to 300 μm) of HR 7980 provided by M. Cohen and with IRAS photometry for OLP 9.01 (upper panel) and OLP 10.0b5 (lower panel). All photometric points are color corrected for a 3850 K BB. The meaning of the symbols is the following: solid line: model, asterisk: IRAS, triangle: PHT-C100 (P22 AOT), diamond: PHT-C200 (P22 AOT).

Evaluation Log

1) point source photometry of HR 7980 from mini-maps

Measurements:

PHT-C100:	pcas72701415 (P22 minimap)	FCS = 60 um
	pcas72701412 (P22 minimap)	FCS = 65 um
	pcas72701409 (P22 minimap)	FCS = 80 um
	pcas72701418 (P22 minimap)	FCS = 90 um
	pcas72701406 (P22 minimap)	FCS = 100 um
	pcas72701403 (P22 minimap)	FCS = 105 um
PHT-C200:	pcas73401709 (P22 minimap)	FCS = 120 um
	pcas73401603 (P22 minimap)	FCS = 150 um
	pcas73401706 (P22 minimap)	FCS = 170 um

Colour correction: black body, T = 3850 K

Model: Cohen

Det	cwl (μm)	OLP 9	OLP 10	IRAS	Model	Δ (OLP 9)	Δ (OLP 10)
C1	60.0	1.295	1.248	1.118	1.169	10.80	6.80
C1	65.0	0.975	0.973		0.995	-2.02	-2.27
C1	80.0	0.714	0.683		0.655	8.96	4.14
C1	90.0	0.532	0.512		0.517	2.81	-0.96
C1	100.0	0.466	0.454	0.785	0.418	11.40	8.52
C1	105.0	0.581	0.474		0.379	53.41	25.18
C2	120.0	0.258	0.262		0.289	-10.96	-9.29
C2	150.0	0.219	0.227		0.184	18.78	23.14
C2	170.0	0.179	0.178		0.143	25.07	24.62

6.1.2 Point Source Photometry from PHT22 Mini-Maps: The SED of HR 1654

Motivation

Also for HR 1654 there exist mini-maps in all C100 filters and in three out of five C200 filters (120 to 170 μm). Therefore, the relative filter-to-filter calibration accuracy can be checked for this case.

Method

We compare the background subtracted, color corrected flux values of OLP V9.01 and OLP V10.0b5 results against the model prediction.

Results

The comparison of OLP 9.01 and OLP 10.0b5 photometry with the model is given in part 1 of the evaluation log. Fig. 6.2 displays the photometric results extracted from the mini-map PCAS product. The C100 photometry is as accurate as 15 % for all filters, for the filters shortward of 100 μm even better than 10 %. The C200 photometry is better than 15 %, too.

Conclusions

- This test case shows that the good absolute photometric accuracy found for PCAS products holds for all C100 filters and for three out of five C200 filters.
- The C100 absolute photometric accuracy is < 15 %, for filters shortward of 100 μm even < 10 %.
- The C200 absolute photometric accuracy is < 15 %.

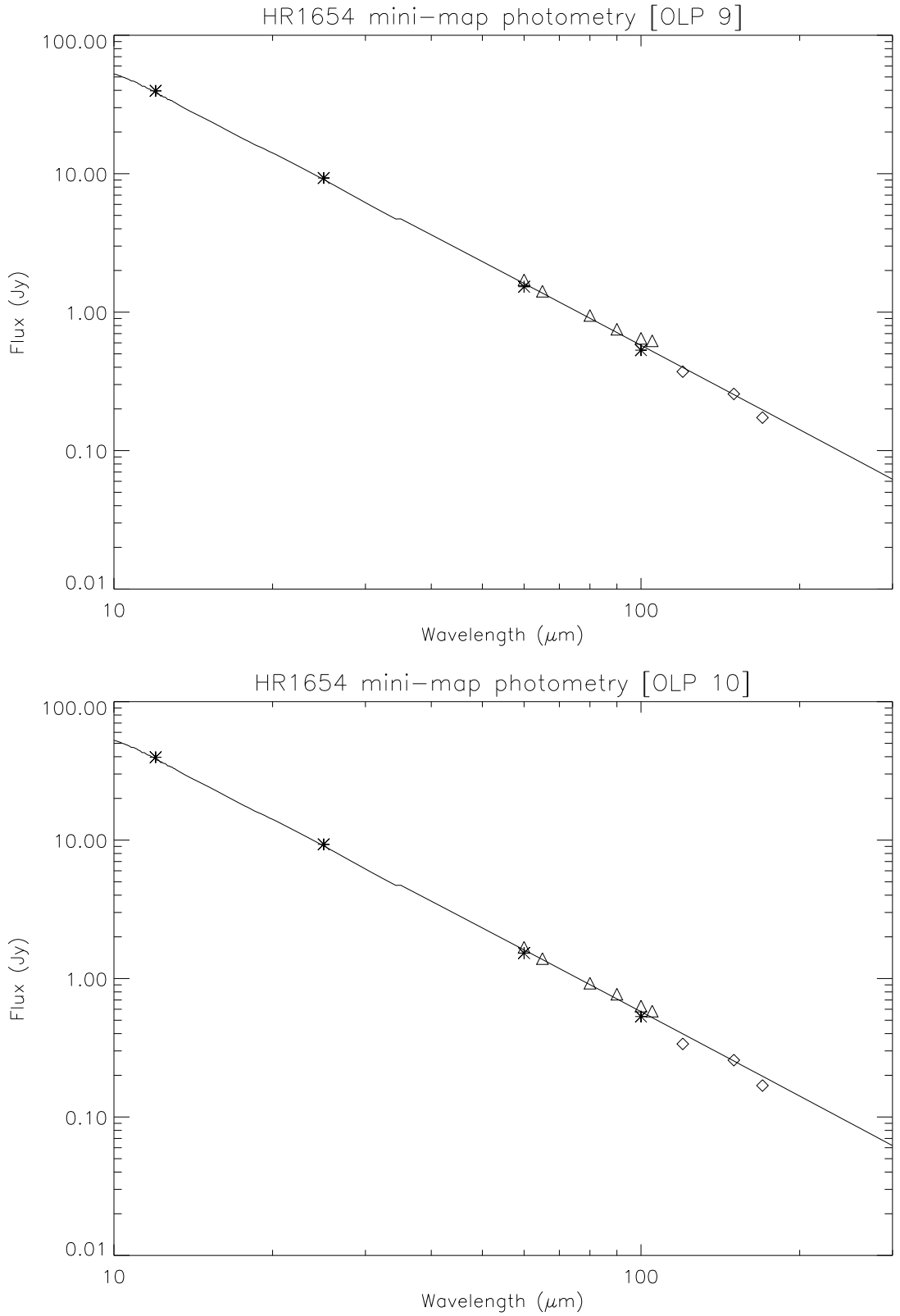

Figure 6.2: Comparison of PHT-C mini-map photometry with the model spectrum (plus extension out to 300 μm) of HR 1654 provided by M. Cohen and with IRAS photometry for OLP 9.01 (upper panel) and OLP 10.0b5 (lower panel). All photometric points are color corrected for a 4000 K BB. The meaning of the symbols is the following: solid line: model, asterisk: IRAS, triangle: PHT-C100 (P22 AOT), diamond: PHT-C200 (P22 AOT).

Evaluation Log

1) point source photometry of HR 1654 from mini-maps

Measurements:

PHT-C100:	pcas65701315 (P22 minimap)	FCS = 60 um
	pcas65701312 (P22 minimap)	FCS = 65 um
	pcas65701309 (P22 minimap)	FCS = 80 um
	pcas65701318 (P22 minimap)	FCS = 90 um
	pcas65701306 (P22 minimap)	FCS = 100 um
	pcas65701303 (P22 minimap)	FCS = 105 um
PHT-C200:	pcas65002709 (P22 minimap)	FCS = 120 um
	pcas65002103 (P22 minimap)	FCS = 150 um
	pcas65002406 (P22 minimap)	FCS = 170 um

Colour correction: black body, T = 4000 K

Model: Cohen

Det	cwl (μm)	OLP 9	OLP 10	IRAS	Model	Δ (OLP 9)	Δ (OLP 10)
C1	60.0	1.710	1.682	1.527	1.610	6.19	4.47
C1	65.0	1.416	1.393		1.372	3.23	1.54
C1	80.0	0.946	0.925		0.903	4.68	2.44
C1	90.0	0.752	0.770		0.713	5.57	8.07
C1	100.0	0.647	0.632	0.531	0.576	12.24	9.72
C1	105.0	0.621	0.581		0.522	18.94	11.37
C2	120.0	0.372	0.337		0.399	-6.73	-15.44
C2	150.0	0.257	0.257		0.254	1.17	1.46
C2	170.0	0.173	0.169		0.197	-12.14	-14.35

6.1.3 Point Source Photometry from PHT22 Mini-Maps: The SED of HR 7310

Motivation

HR 7310 is a factor 5 – 6 fainter than the previous two stars HR 7980 and HR 1654. There exist mini-maps in the C100 100 μm filter and in the same three out of five C200 filters (120 to 170 μm) as for the other two stars. Therefore, the relative filter-to-filter calibration accuracy can be checked for this case.

Method

We compare the background subtracted, color corrected flux values of OLP V9.0b6/9.01 and OLP V10.0b5 results against the model prediction.

Results

The comparison of OLP 9.0b6/9.01 and OLP 10.0b5 photometry with the model is given in part 1 of the evaluation log. Fig. 6.3 displays the photometric results extracted from the mini-map PCAS product. The C100 photometry is as accurate as 30 % for the 100 μm one. The IRAS 100 μm FSC flux is only an upper limit. The C200 photometry is better than 25 % only for the 120 μm filter. Expected source fluxes below 100 mJy which occur for this source at wavelengths longer than 120 μm cannot be measured reliably any more.

Conclusions

- This test case shows some limits of the PCAS photometric method.
- At 100 μm the photometric accuracy is better than 30 %.
- For C200 mini-map photometry a lower flux limit of 0.1 Jy is found below which photometry is not reliable any more.

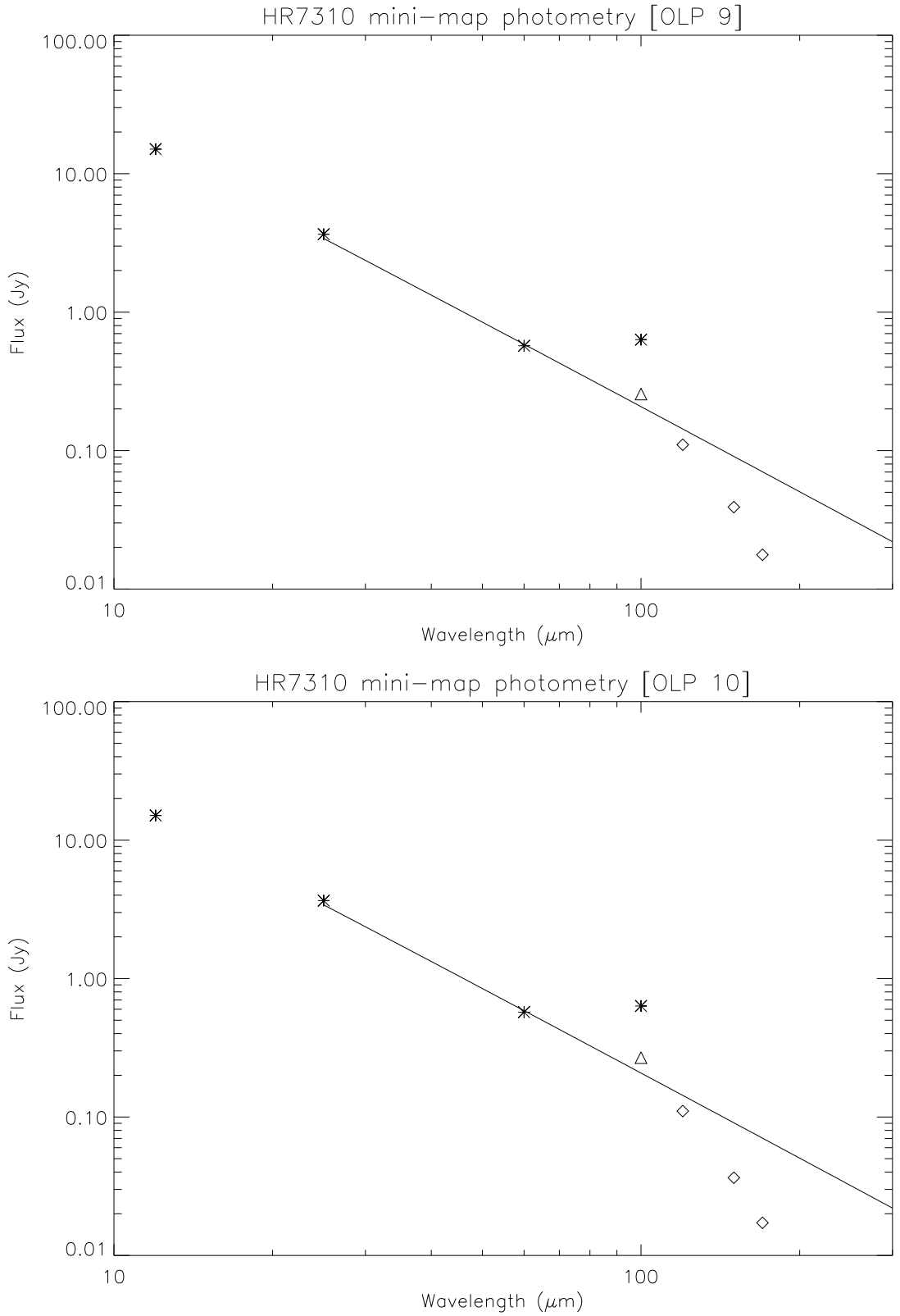

Figure 6.3: Comparison of PHT-C mini-map photometry with the model spectrum (plus extension out to 300 μm) of HR 7310 provided by M. Cohen and with IRAS photometry for OLP 9.0b6/9.01 (upper panel) and OLP 10.0b5 (lower panel). All photometric points are color corrected for a 4852 K BB. The meaning of the symbols is the following: solid line: model, asterisk: IRAS, triangle: PHT-C100 (P22 AOT), diamond: PHT-C200 (P22 AOT).

Evaluation Log

1) point source photometry of HR 7310 from mini-maps

Measurements:

PHT-C100:	pcas74800404 (P22 minimap)	FCS = 100 um
PHT-C200:	pcas60100803 (P22 minimap)	FCS = 120 um
	pcas60101009 (P22 minimap)	FCS = 150 um
	pcas60100906 (P22 minimap)	FCS = 170 um

Colour correction: black body, T = 4852 K

Model: Cohen

Det	cwl (μm)	OLP 9	OLP 10	IRAS	Model	Δ (OLP 9)	Δ (OLP 10)
C1	100.0	0.256	0.268	0.634	0.208	23.27	29.16
C2	120.0	0.110	0.110		0.143	-22.94	-22.97
C2	150.0	0.039	0.036		0.091	-56.98	-59.90
C2	170.0	0.018	0.017		0.070	-74.84	-75.52

6.1.4 Point Source Photometry from PHT22 Mini-Maps: The SED of Sirius (HR 2491)

Motivation

Sirius is one of the two primary calibrators. However, due to its limited visibility it was not used for establishment of the FCS calibration. Therefore, the C100 mini-map photometry of Sirius considered here provides an independent check of the calibration accuracy and also of the measurement reproducibility.

Method

We compare the background subtracted, color corrected flux values of OLP V9.0b6 and OLP V10.0b5 results against the model prediction by Cohen and IRAS photometry.

Results

The comparison of OLP 9.0b6 and OLP 10.0b5 photometry with the model is given in part 1 of the evaluation log. Fig. 6.4 displays the photometric results extracted from the mini-map PCAS product. The C100 photometry is as accurate as 10 %. The IRAS 100 μm PSC flux has only medium quality and shows a positive offset of 70 %.

Conclusions

- This test case shows the good absolute photometric accuracy for PCAS products, with the C100 photometry being < 10 %.

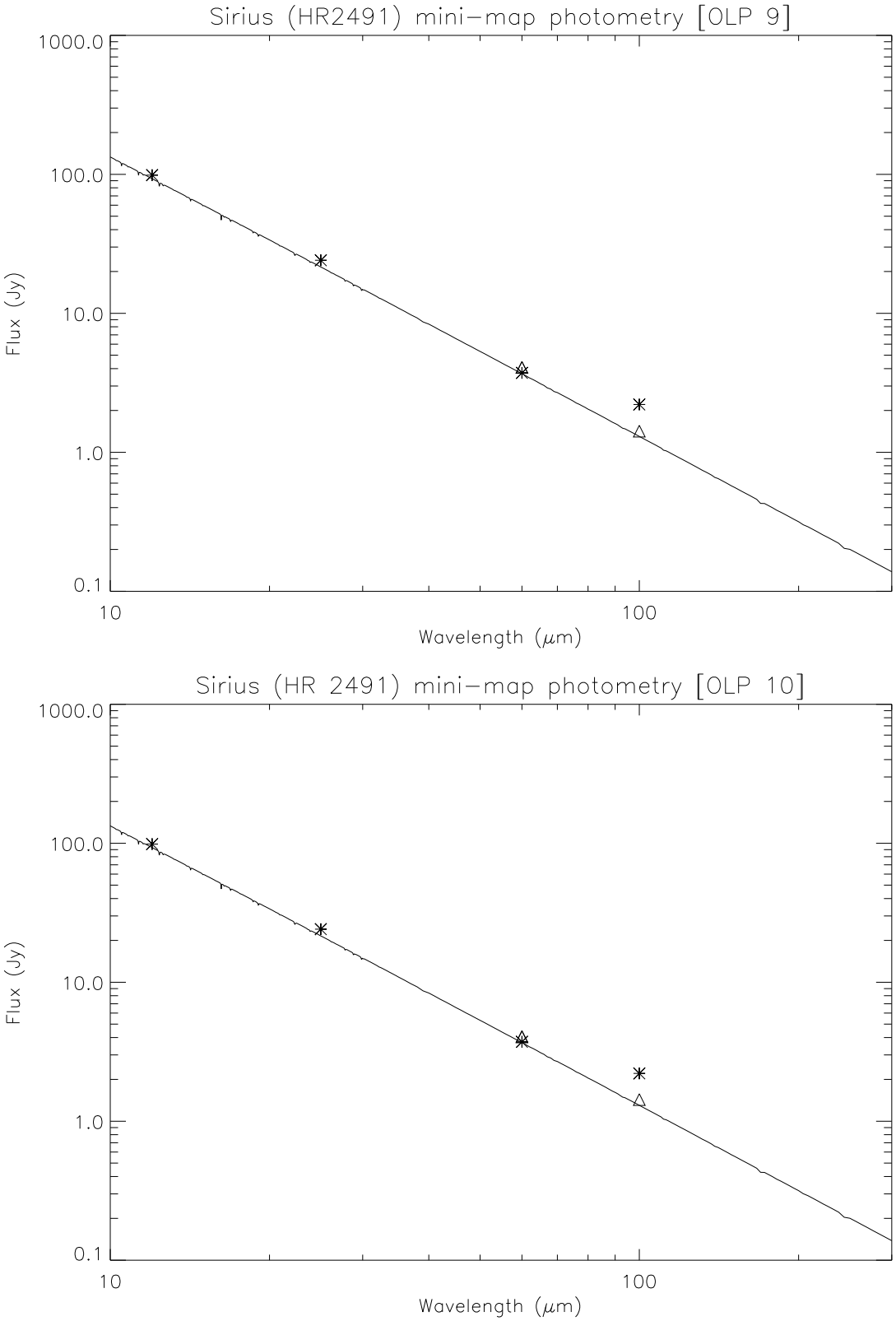

Figure 6.4: Comparison of PHT-C mini-map photometry with the model spectrum (plus extension out to 300 μm) of Sirius (HR 2491) provided by M. Cohen and with IRAS photometry for OLP 9.0b6 (upper panel) and OLP 10.0b5 (lower panel). All photometric points are color corrected for a 10000 K BB. The meaning of the symbols is the following: solid line: model, asterisk: IRAS, triangle: PHT-C100 (P22 AOT).

Evaluation Log

1) point source photometry of Sirius (HR 2491) from mini-maps

Measurements:

PHT-C100:	pcas70705603 (P22 minimap)	FCS = 60 um
	pcas70705604 (P22 minimap)	FCS = 100 um
	pcas72301711 (P22 minimap)	FCS = 60 um (b)

Colour correction: black body, T = 10000 K

Model: Cohen

Det	cwl (μm)	OLP 9	OLP 10	IRAS	Model	Δ (OLP 9)	Δ (OLP 10)
C1	60.0	4.090	4.076	3.728	3.680	11.16	10.79
C1b	60.0	4.078	4.041	3.728	3.680	10.82	9.81
C1	100.0	1.420	1.431	2.208	1.302	9.07	9.88

6.1.5 Point Source Photometry from PHT22 Mini-Maps: The SED of Uranus

Motivation

This is a check-out of the C200 mini-map photometry for the brightest celestial standard, Uranus. For these measurements, the FCS heating power set-ups were such, that they were outside the calibrated range.

Method

We compare the color corrected flux values of both OLP V9.0b6 and OLP V10.0b8 results against the model predictions by Abbas and Griffin & Orton, respectively.

Results

The comparison of the OLP9.0b6 and OLP10.0b8 photometry with the model is given in part 1 of the evaluation log section. We estimate the absolute photometric accuracy per detector assembly for this target as the deviation from the model flux. Fig. 6.5 shows the PHT photometric data points in comparison to the model for OLP 9.0b6 and OLP 10.0b8, respectively. Despite the fact that in OLP10 default responsivities are used in this absolute photometry mode, we note that the absolute calibration accuracy is similar to the one of OLP 9, being better than 7 %.

Conclusions

- The C200 absolute photometry in the bright flux range is as accurate as 7 %.
- The C200 default responsivity calibration does not show any degradance in performance w.r.t. the actual responsivity calibration.

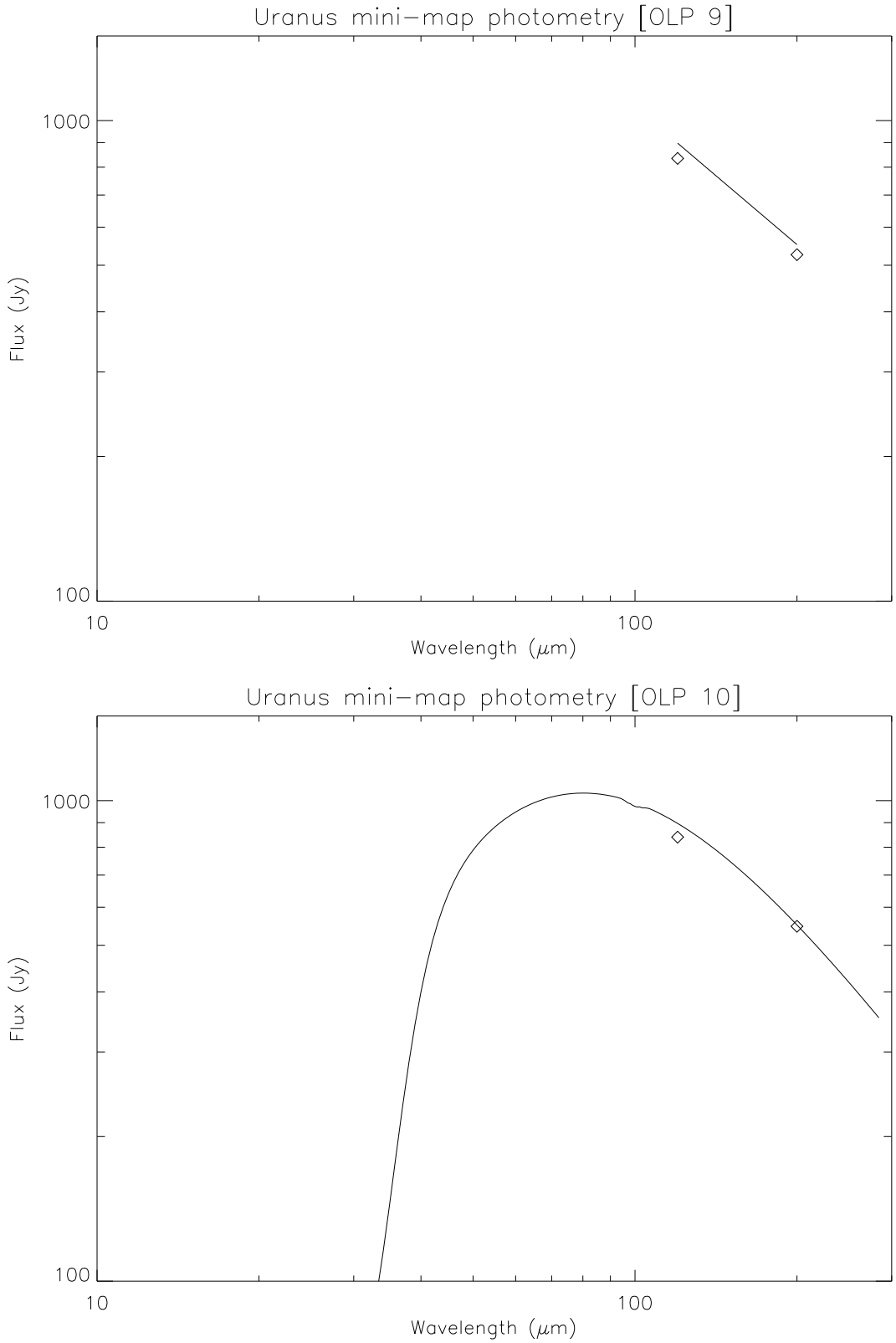

Figure 6.5: Comparison of PHT-C200 mini-map photometry with the spectrum of Uranus provided by M. Griffin & G. Orton (used for OLP 10) and M. Abbas (used for OLP 9) for OLP 9.0b6 (upper panel) and OLP 10.0b8 (lower panel). All photometric points are color corrected for a 60 K BB. The meaning of the symbols is the following: solid line: model, diamond: PHT-C200 (P25 AOT).

Evaluation Log

1) P22 mini-map photometry

Measurements:
PHT-C200: pcas55204908 (minimap) FCS=120 um
pcas55204704 (minimap) FCS=200 um

Colour correction: black body, T = 60 K

Model: Griffin & Orton (OLP 10) – Abbas (OLP 9)

Det	cwl (μm)	OLP 9	OLP 10	Model	Δ (OLP 9)	Δ (OLP 10)
C2	120.0	834.132	839.537	896.663	-7.07	-6.37
C2	200.0	526.040	547.647	551.134	-4.70	-0.63

6.1.6 Point Source Photometry from PHT22 Mini-Maps: The 180 μm flux of α Ari (HR 617)

Motivation

HR 617 (α Ari) is one of the brightest calibration stars. There exists a mini-map in the C200 180 μm filter which can be used to check out the calibration accuracy in this filter.

Method

We compare the background subtracted, color corrected flux values of OLP V9.01 and OLP V10.0b5 results against the model prediction.

Results

The comparison of OLP 9.01 and OLP 10.0b5 photometry with the model is given in part 1 of the evaluation log. Fig. 6.6 displays the photometric results extracted from the mini-map PCAS product. The C200 photometry at a flux level of 250 mJy is as good 30 %. The IRAS 100 μm FSC flux is only an upper limit.

Conclusions

- This test case shows that the good absolute photometric accuracy found for PCAS products holds for C200 filters down to 0.25 mJy with an accuracy of 30 %.

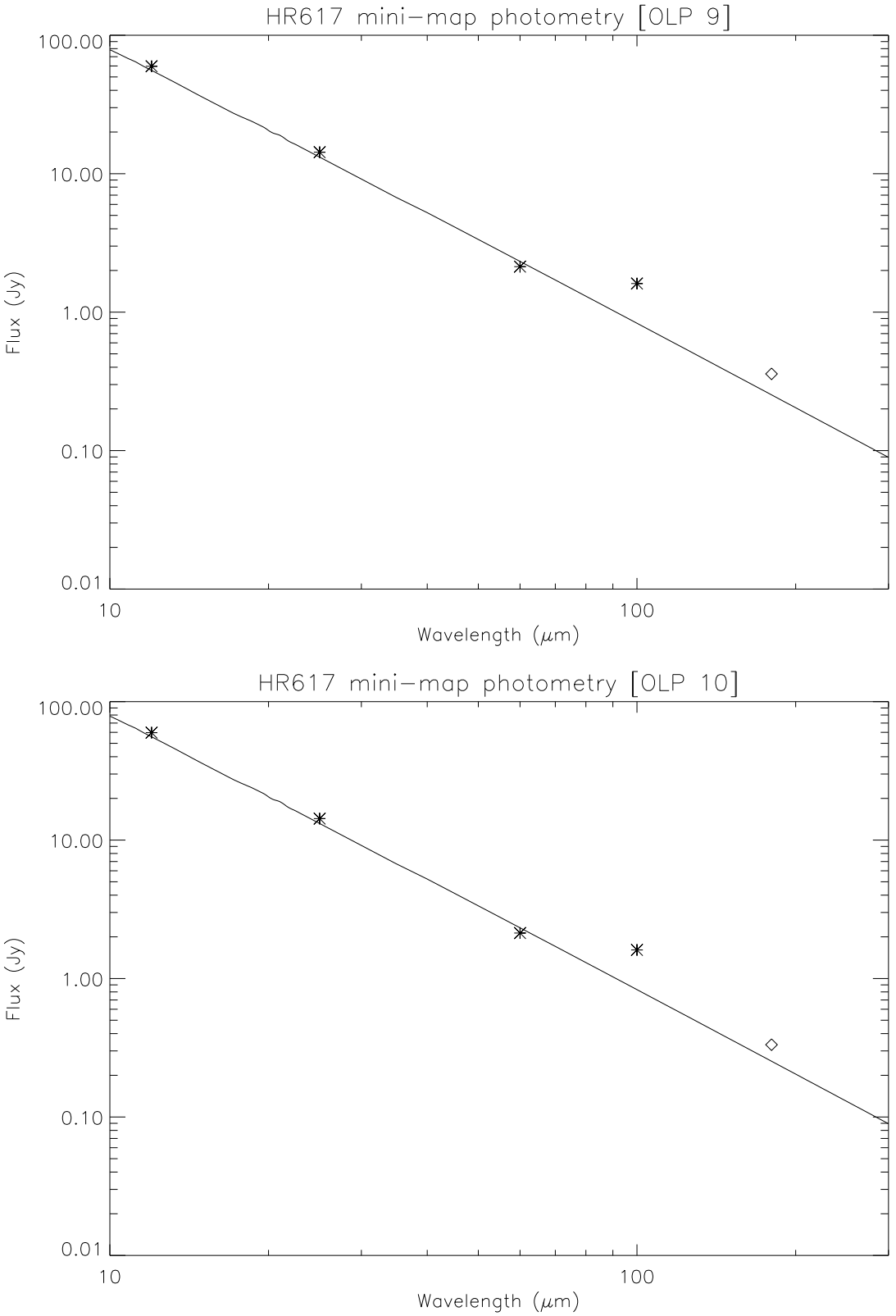

Figure 6.6: Comparison of PHT-C mini-map photometry with the model spectrum (plus extension out to 300 μm) of HR 617 provided by M. Cohen and with IRAS photometry for OLP 9.01 (upper panel) and OLP 10.0b5 (lower panel). All photometric points are color corrected for a 4000 K BB. The meaning of the symbols is the following: solid line: model, asterisk: IRAS, diamond: PHT-C200 (P22 AOT).

Evaluation Log

1) point source photometry of HR 617 from mini-maps

Measurements:
PHT-C200: pcas79001902 (P22 minimap) FCS = 180 um

Colour correction: black body, T = 4000 K

Model: Cohen

Det	cwl (μm)	OLP 9	OLP 10	IRAS	Model	Δ (OLP 9)	Δ (OLP 10)
C2	180.0	0.358	0.333		0.253	41.75	31.63

6.1.7 Point Source Photometry from PHT22 Mini-Maps: The 90 μm flux of HR 6464

Motivation

HR 6464 is a faint calibration star in the C100 range. There exists a mini-map in the C100 90 μm filter which can be used to check out the calibration accuracy in this filter.

Method

We compare the background subtracted, color corrected flux values of OLP V9.0b6 and OLP V10.0b5 results against the model prediction.

Results

The comparison of OLP 9.01 and OLP 10.0b5 photometry with the model is given in part 1 of the evaluation log. Fig. 6.7 displays the photometric results extracted from the mini-map PCAS product. An absolute photometric accuracy of 30 % is achieved for a source flux close to 100 mJy. For this test case we verified the photometric quality by considering only the results from pixel #5, the central pixel of the C100 array. The comparison of OLP 9.01 and OLP 10.0b5 photometry with the model is given in part 2 of the evaluation log. Fig. 6.8 displays the photometric results. This test suggests that for this faint source flux restriction to pixel 5 may improve the final photometric accuracy which is better than 10 % in this case. The IRAS 100 μm FSC flux has only medium quality.

Conclusions

- This test case shows that the good absolute photometric accuracy found for PCAS products holds for C100 filters down to 0.12 Jy with an accuracy of 30 %.
- Special evaluation of the central pixel #5 may suggest that for faint source fluxes the photometric accuracy can be further improved by restricting the analysis to pixel 5 only. In this case an accuracy of < 10 % was achieved.

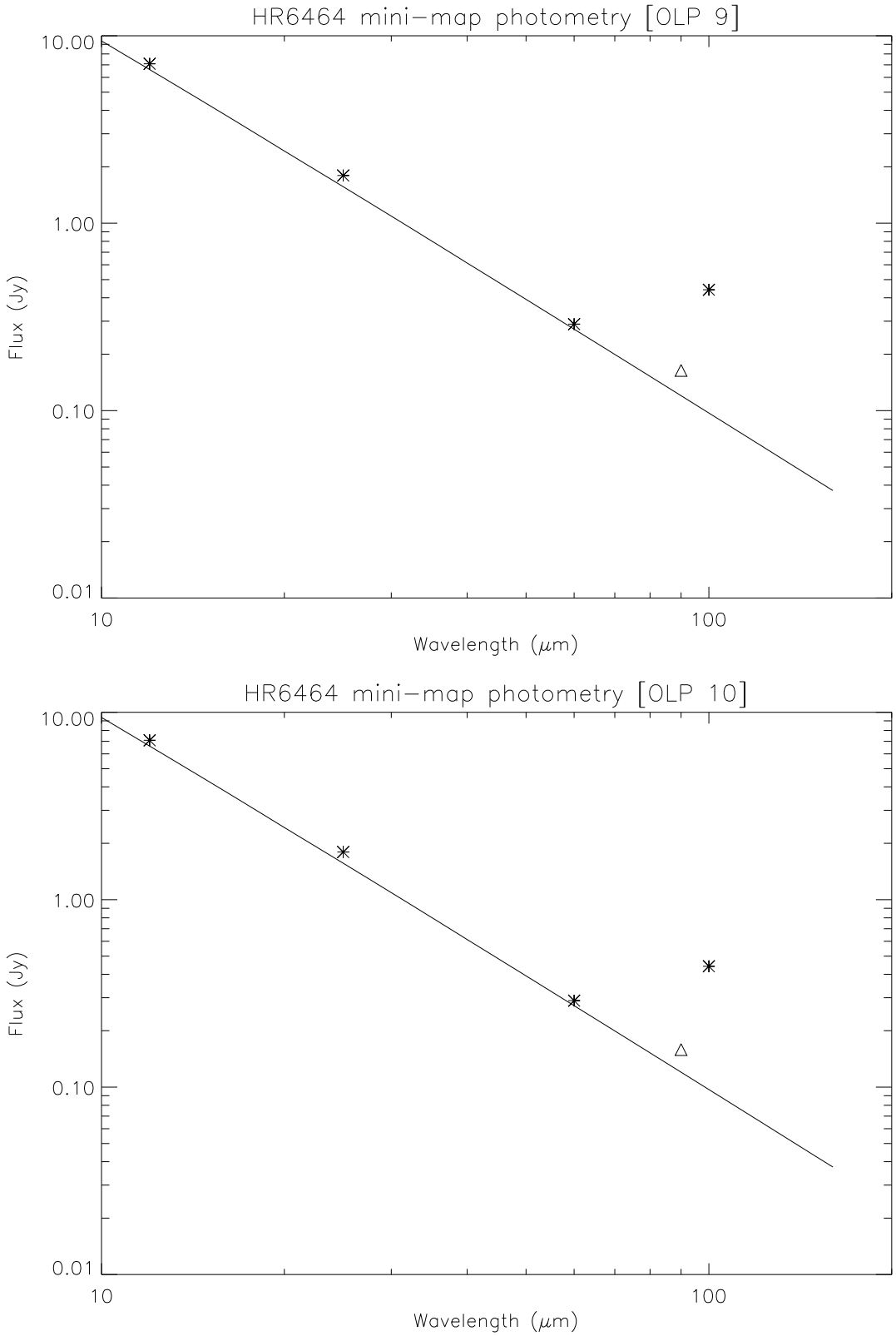

Figure 6.7: Comparison of PHT-C mini-map photometry with the model spectrum of HR 6464 provided by P. Hammersley and with IRAS photometry for OLP 9.0b6 (upper panel) and OLP 10.0b5 (lower panel). All photometric points are color corrected for a 3893 K BB. The meaning of the symbols is the following: solid line: model, asterisk: IRAS, triangle: PHT-C100 (P22 AOT).

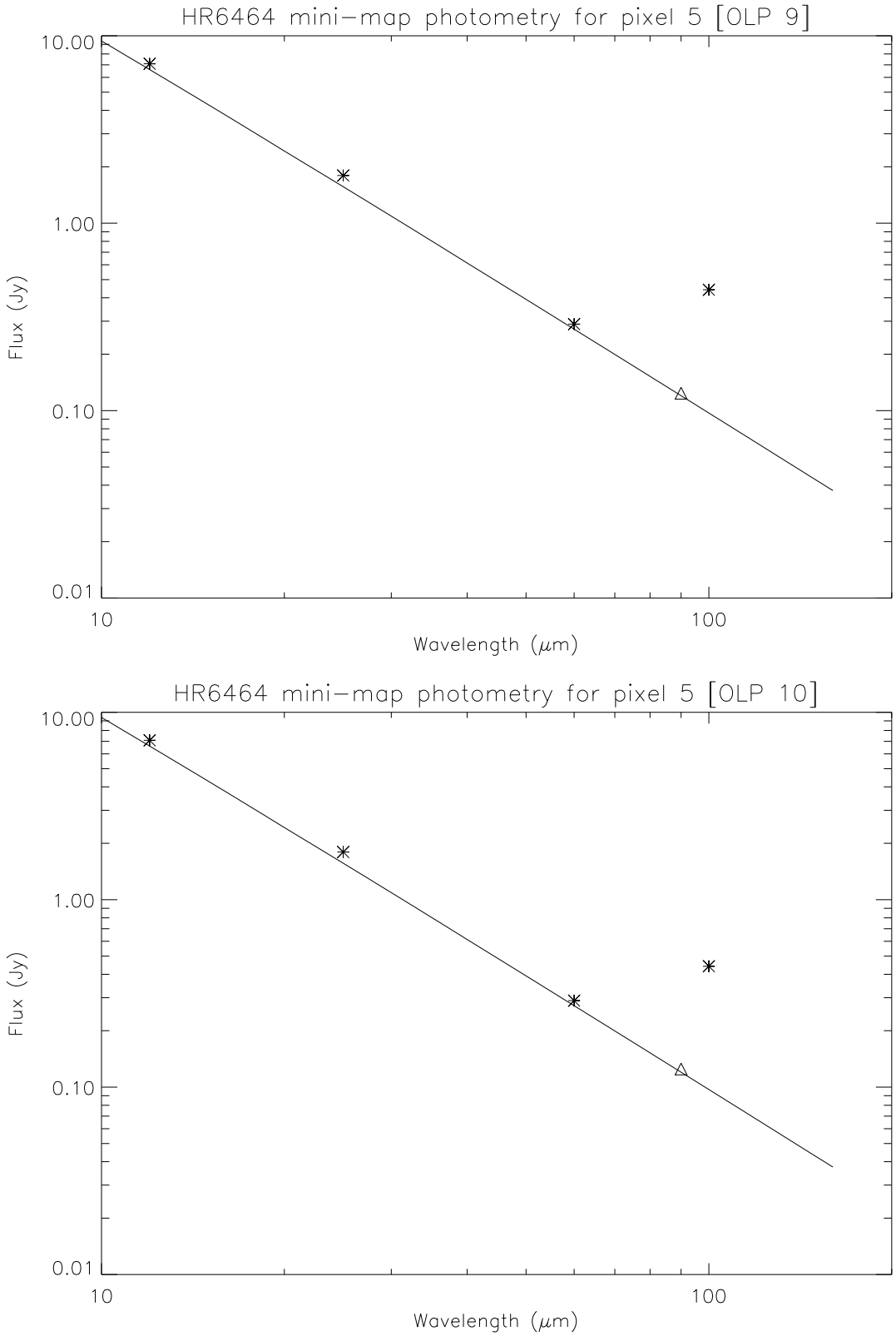

Figure 6.8: Comparison of PHT-C100 mini-map photometry using only the central array pixel (#5) with the model spectrum of HR 6464 provided by P. Hammersley and with IRAS photometry for OLP 9.0b6 (upper panel) and OLP 10.0b5 (lower panel). All photometric points are color corrected for a 3893 K BB. The meaning of the symbols is the following: solid line: model, asterisk: IRAS, triangle: PHT-C100 (P22 AOT).

Evaluation Log

1) point source photometry of HR 6464 from mini-maps

Measurements:
PHT-C100: pcas78300465 (P22 minimap) FCS = 90 um

Colour correction: black body, T = 3893 K

Model: Hammersley

Det	cwl (μm)	OLP 9	OLP 10	IRAS	Model	Δ (OLP 9)	Δ (OLP 10)
C1	90.0	0.164	0.159		0.120	36.36	32.03

2) point source photometry of HR 6464 from mini-map using pixel 5 only

Measurements:
PHT-C100: pcas78300465 (P22 minimap) FCS = 90 um

Colour correction: black body, T = 3893 K

Model: Hammersley

Det	cwl (μm)	OLP 9	OLP 10	IRAS	Model	Δ (OLP 9)	Δ (OLP 10)
C1	90.0	0.124	0.125		0.120	3.11	4.07

6.1.8 Point Source Photometry from PHT22 Mini-Maps: The 60 μm flux of HR 7557 (HD 187642, α Aql)

Motivation

HR 7557 is an intermediately bright calibration star in the C100 range. There exists a mini-map in the C100 60 μm filter which can be used to check out the calibration accuracy in this filter.

Method

We compare the background subtracted, color corrected flux values of OLP V9.0b6 and OLP V10.0b5 results against the model prediction.

Results

The comparison of OLP 9.0b6 and OLP 10.0b5 photometry with the model is given in part 1 of the evaluation log. Fig. 6.9 displays the photometric results extracted from the mini-map PCAS product. The agreement of the 60 μm photometry with the model is better than 10 %.

Conclusions

- This test case demonstrates the good absolute photometric accuracy (better than 10 %) achievable with PCAS products.

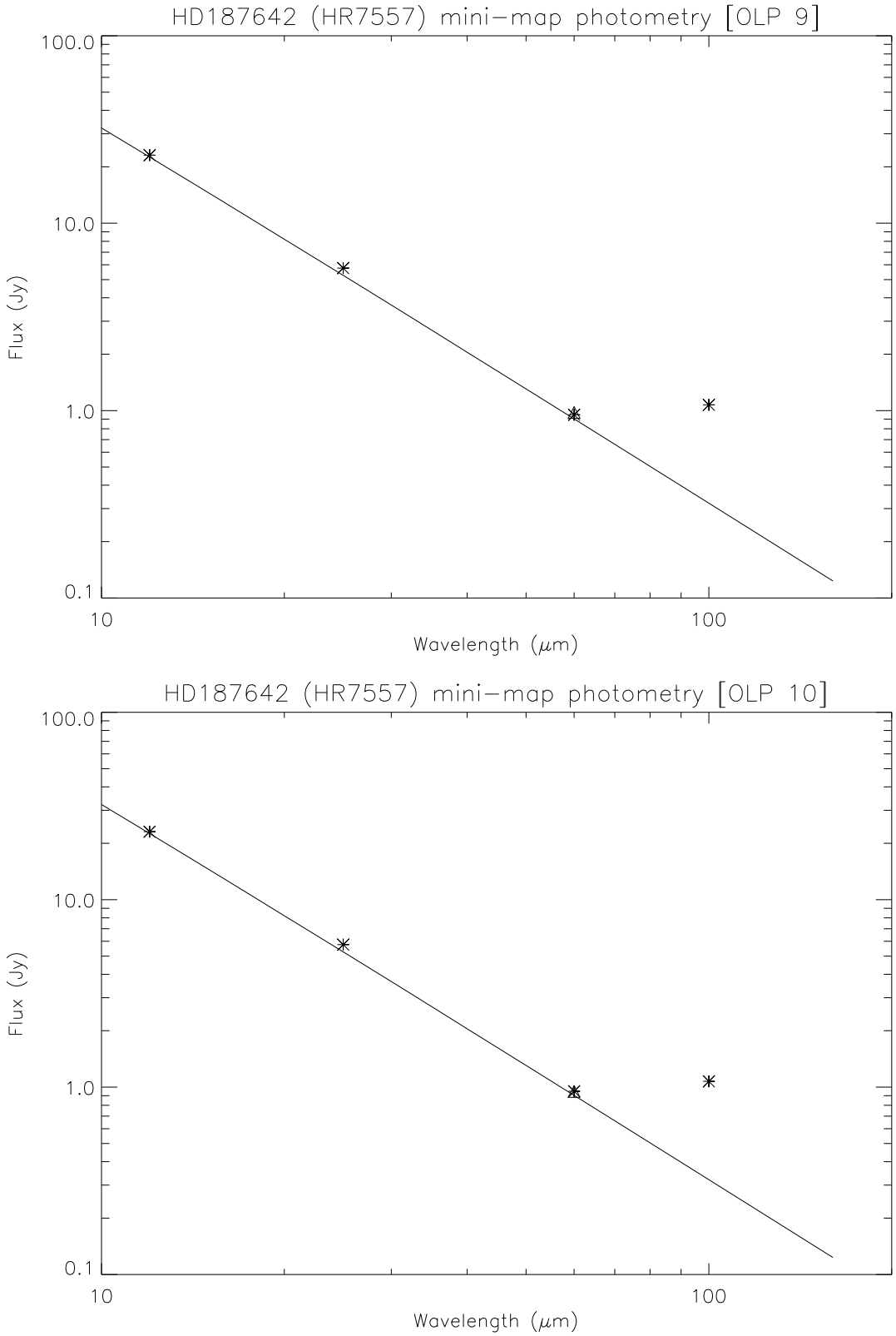

Figure 6.9: Comparison of PHT-C mini-map photometry with the model spectrum of HR 7469 (HD 187642) provided by P. Hammersley and with IRAS photometry for OLP 9.0b6 (upper panel) and OLP 10.0b5 (lower panel). All photometric points are color corrected for a 7596 K BB. The meaning of the symbols is the following: solid line: model, asterisk: IRAS, triangle: PHT-C100 (P22 AOT).

Evaluation Log

1) point source photometry of HR 7557 (HD 187642) from mini-maps

Measurements:
PHT-C100: pcas72400584 (P22 minimap) FCS = 60 um

Colour correction: black body, T = 7596 K

Model: Hammersley

Det	cwl (μm)	OLP 9	OLP 10	IRAS	Model	Δ (OLP 9)	Δ (OLP 10)
C1	60.0	0.977	0.949	0.950	0.903	8.20	5.05

6.1.9 Point Source Photometry from PHT22 Mini-Maps: The 60 μm flux of HR 7469 (HD 185395)

Motivation

HR 7469 is a faint calibration star in the C100 range. There exists a mini-map in the C100 60 μm filter which can be used to check out the calibration accuracy in this filter.

Method

We compare the background subtracted, color corrected flux values of OLP V9.0b6 and OLP V10.0b5 results against the model prediction.

Results

The comparison of OLP 9.0b6 and OLP 10.0b5 photometry with the model is given in part 1 of the evaluation log. Fig. 6.10 displays the photometric results extracted from the mini-map PCAS product. The C100 photometry is accurate as 30 % for this extremely low flux level of less than 50 mJy. The IRAS 60 and 100 μm FSC fluxes are only upper limits.

Conclusions

- This test case shows that the good absolute photometric accuracy found for PCAS products holds for the C100 60 μm filter down to 50 mJy with an accuracy of 30 %.

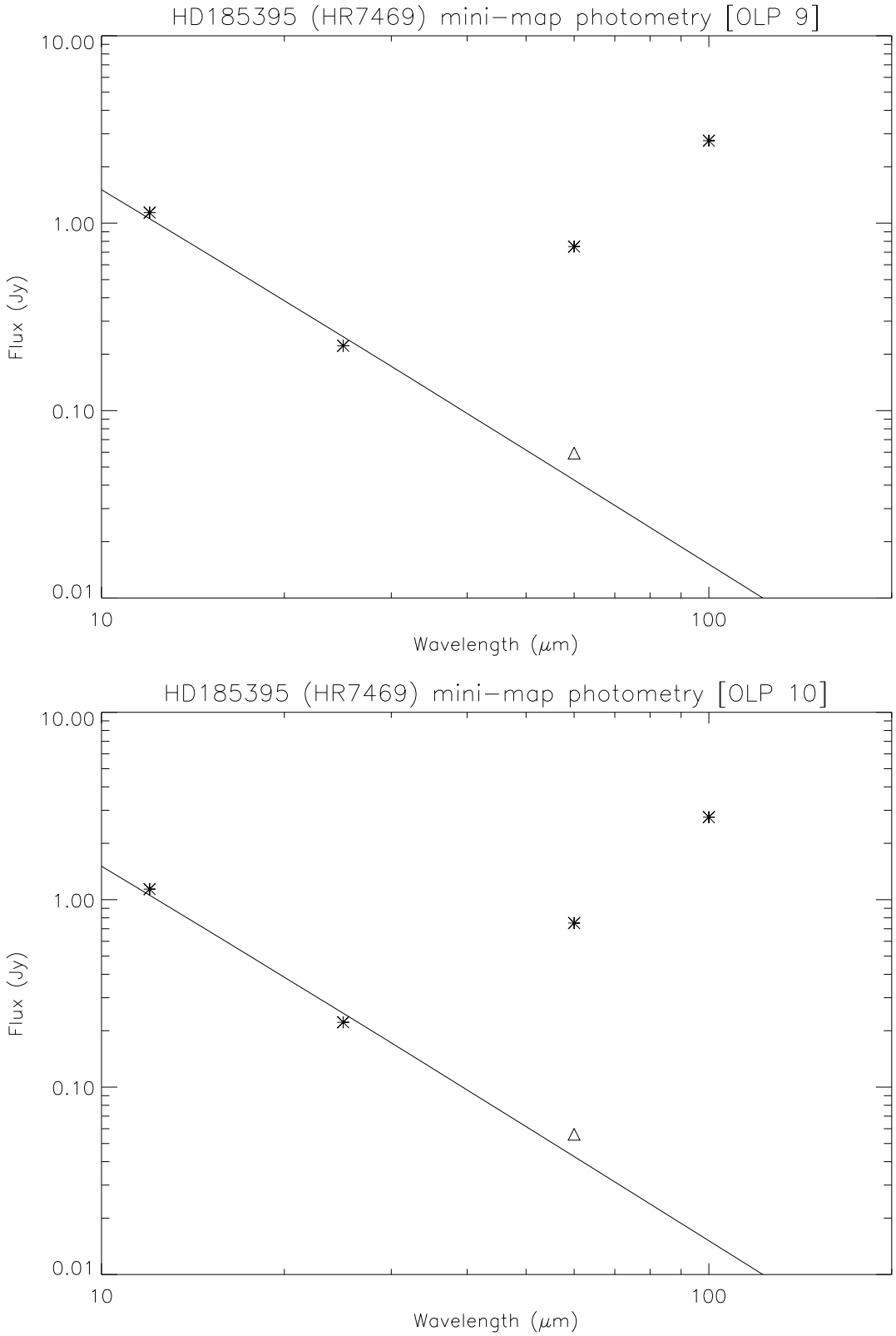

Figure 6.10: Comparison of PHT-C mini-map photometry with the model spectrum of HR 7469 (HD 185395) provided by P. Hammersley and with IRAS photometry for OLP 9.0b6 (upper panel) and OLP 10.0b5 (lower panel). All photometric points are color corrected for a 3893 K BB. The meaning of the symbols is the following: solid line: model, asterisk: IRAS, triangle: PHT-C100 (P22 AOT).

Evaluation Log

1) point source photometry of HD 185395 (HR 7469) from mini-maps

Measurements:
PHT-C100: pcas69301251 (P22 minimap) FCS = 60 um

Colour correction: black body, T = 6622 K

Model: Hammersley

Det	cwl (μm)	OLP 9	OLP 10	IRAS	Model	Δ (OLP 9)	Δ (OLP 10)
C1	60.0	0.059	0.056	0.750	0.043	39.26	31.48

6.1.10 Point Source Photometry from PHT22 Mini-Maps: The 60 μm flux of HD 185144

Motivation

HD 185144 is a faint calibration star in the C100 range. There exists a mini-map in the C100 60 μm filter which can be used to check out the calibration accuracy in this filter.

Method

We compare the background subtracted, color corrected flux values of OLP V9.0b6 and OLP V10.0b5 results against the scaled model predictions predictions by Hammersley and IRAS photometry.

Results

The comparison of OLP 9.0b6 and OLP 10.0b5 photometry with the model is given in part 1 of the evaluation log. Fig. 6.11 displays the photometric results extracted from the mini-map PCAS product. The C100 photometry is accurate as 20 % for this low flux level of less than 100 mJy. The IRAS 60 and 100 μm FSC fluxes are only upper limits.

Conclusions

- This test case verifies the good absolute photometric accuracy found for PCAS products and gives for the C100 60 μm filter an accuracy of better than 20 % for an expected flux level of 100 mJy.

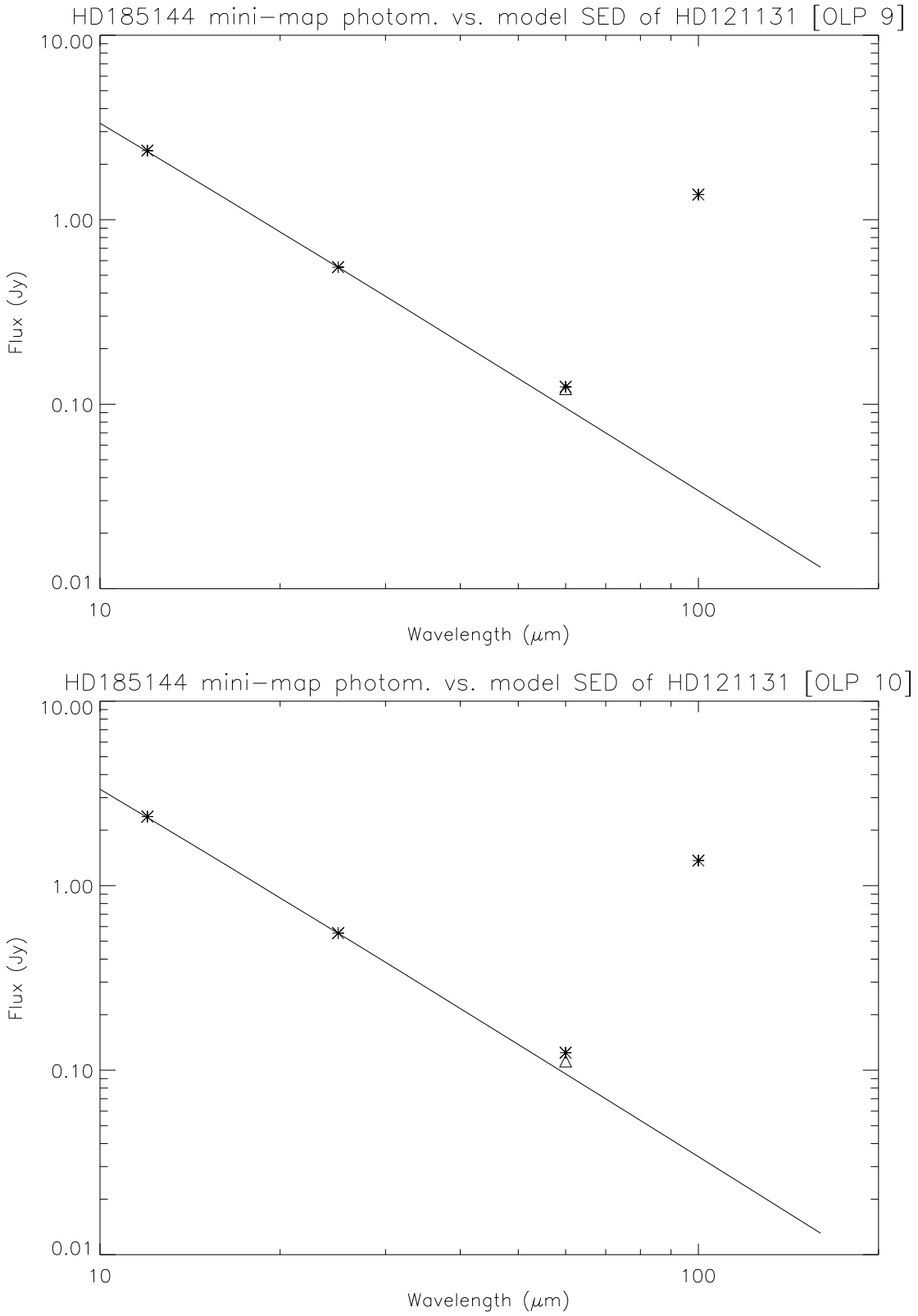

Figure 6.11: Comparison of PHT-C mini-map photometry of HD 185144 (K0V, m_v = 4.70 mag) with the scaled model of HD 121131 (K1V, m_v = 8.34 mag) provided by P. Hammersley and with IRAS photometry for OLP 9.0b6 (upper panel) and OLP 10.0b5 (lower panel). All photometric points are color corrected for a 5103 K BB. The meaning of the symbols is the following: solid line: model, asterisk: IRAS, triangle: PHT-C200 (P22 AOT).

Evaluation Log

1) point source photometry of HD 185144 from mini-maps versus scaled HD121131 model.

Measurements:
PHT-C100: pcas69500449 (P22 minimap) FCS = 60 um

Colour correction: black body, T = 5103 K

Model: Hammersley (HD121131) scaled with V-mag 4.70mag(star)/8.34mag(ref)

Det	cwl (μm)	OLP 9	OLP 10	IRAS	Model	Δ (OLP 9)	Δ (OLP 10)
C1	60.0	0.121	0.112	0.124	0.095	26.90	17.25

6.1.11 Point Source Photometry from PHT22 Mini-Maps: The FIR SED of Vega (HR 7001)

Motivation

Vega is one of the two primary calibrators. However, in the FIR it shows an excess due to a cool disk component. We derive the photometry for this disk component and investigate the temperature range of the disk.

Method

We compare the background subtracted, color corrected flux values of OLP V9.0b6 and OLP V10.0b5 results against IRAS photometry and the model of a modified black body.

Results

Fig. 6.12 displays the photometric results extracted from the mini-map PCAS product. For the derivation of the 60 μm flux not a point source footprint but a 22 arcsec Gaussian footprint was used in order to account for the extended emission of the disk [14]. There is practically no difference between OLP 9 and OLP 10 photometric results. The 60 μm point is relatively consistent with IRAS (within 20 %), though somewhat lower (this is somewhat dependent on the source beam model). The model gives a good fit to the ISOPHOT measurements.

Conclusions

- This test case verifies the good absolute photometric accuracy found for PCAS products by a good consistency with IRAS photometry.
- For an extended source like Vega, the PSF factors in the PCAS evaluation have to be adjusted.

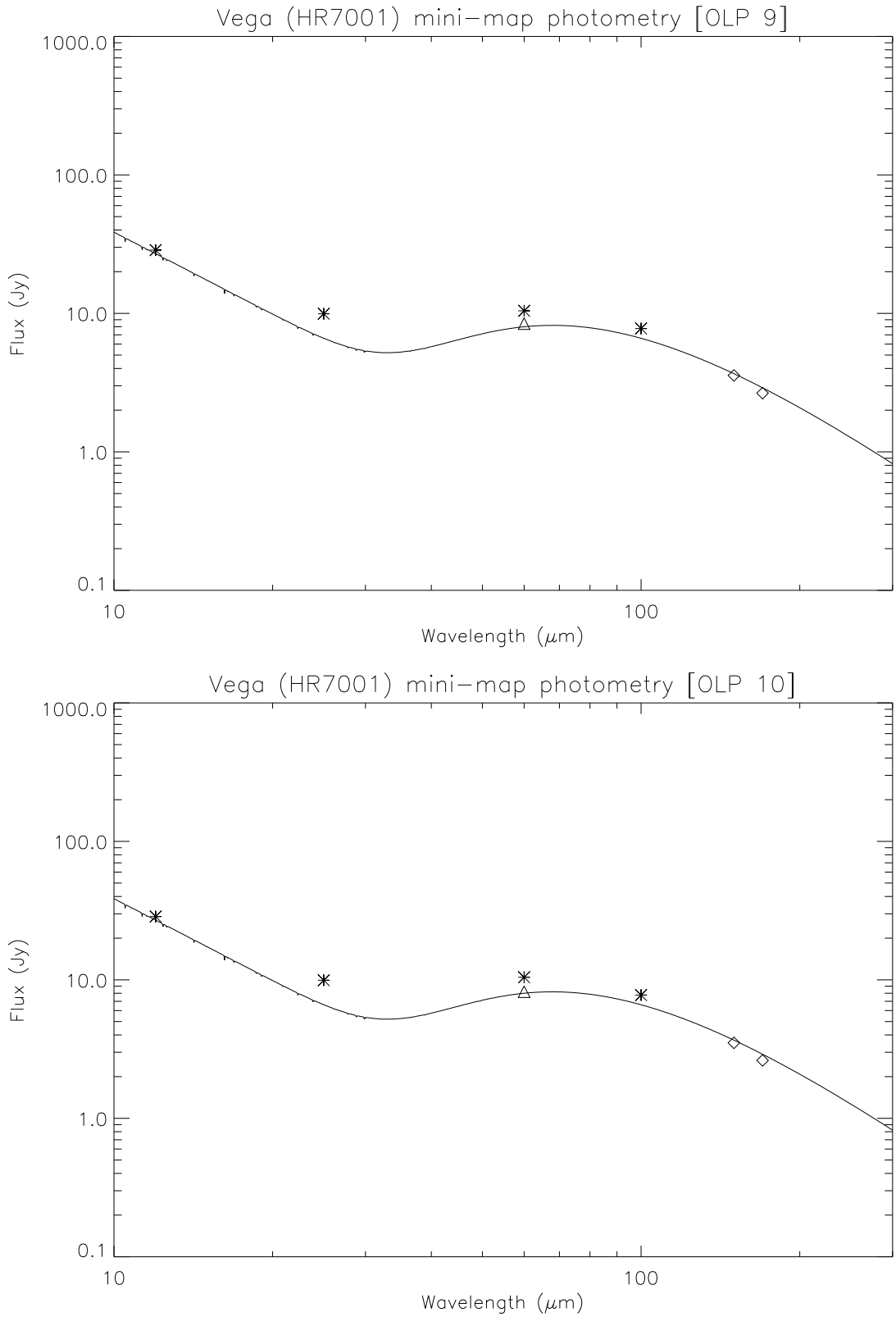

Figure 6.12: Comparison of PHT-C mini-map photometry with the model spectrum of Vega (HR 7001) provided by M. Cohen plus a FIR excess by a 50 K modified BB ($\varepsilon \propto \lambda^{-1}$) and with IRAS photometry for OLP 9.0b6 (upper panel) and OLP 10.0b5 (lower panel). The photometric points are color corrected for a 10000 K BB at 12 μm, 2:1 mixture of 10000 K BB and 80 K modified ($\varepsilon \propto \lambda^{-1}$) BB at 25 μm and 50 K modified BB for $\lambda > 30\,\mu$m. The meaning of the symbols is the following: solid line: model, asterisk: IRAS, triangle: PHT-C100 (P22 AOT), diamond: PHT-C200 (P22 AOT).

Evaluation Log

1) FIR photometry of Vega (HR 7001) from mini-maps

Measurements:
PHT-C100: pcas71500582 (P22 minimap) FCS = 60 um
PHT-C200: pcas44300846 (P22 minimap) FCS = 150, 170 um

Colour correction: mod. bb, em.=1, T = 50 K

Model: Cohen & FIR excess

Det	cwl (μm)	OLP 9	OLP 10	IRAS	Model	Δ (OLP 9)	Δ (OLP 10)
C1	60.0	8.429	8.216	10.445	8.004	5.31	2.64
C2	150.0	3.564	3.509		3.669	-2.86	-4.37
C2	170.0	2.654	2.619		2.900	-8.47	-9.69

6.1.12 Point Source Photometry from PHT22 Mini-Maps: The FIR SED of HD 169142

Motivation

HD 169142 is a FIR excess star. ISOPHOT could not resolve its disk at 60 μm [38].

Method

We compare the background subtracted, color corrected flux values of OLP V9.0b6 and OLP V10.0b5 results against IRAS photometry and the model of a modified black body with the parameters given in [38]. The IRAS 100 μm FSC flux is only an upper limit.

Results

The comparison of OLP 9.0b6 and OLP 10.0b5 photometry with the model is given in part 1 of the evaluation log. Fig. 6.13 displays the photometric results extracted from the mini-map PCAS product. The model fits the two IRAS points as well as the ISOPHOT 150 and 170 μm photometry. The 120 mum point appears in this model a bit low, while the 200 mum point gives an offset. Whether this has any physical background or is a calibration issue is out of scope of this investigation.

Conclusions

- This test case of an IR excess star shows a relatively good consistency with IRAS. Whether the deviations from the simple reference model have any physical background is out of scope of this investigation.

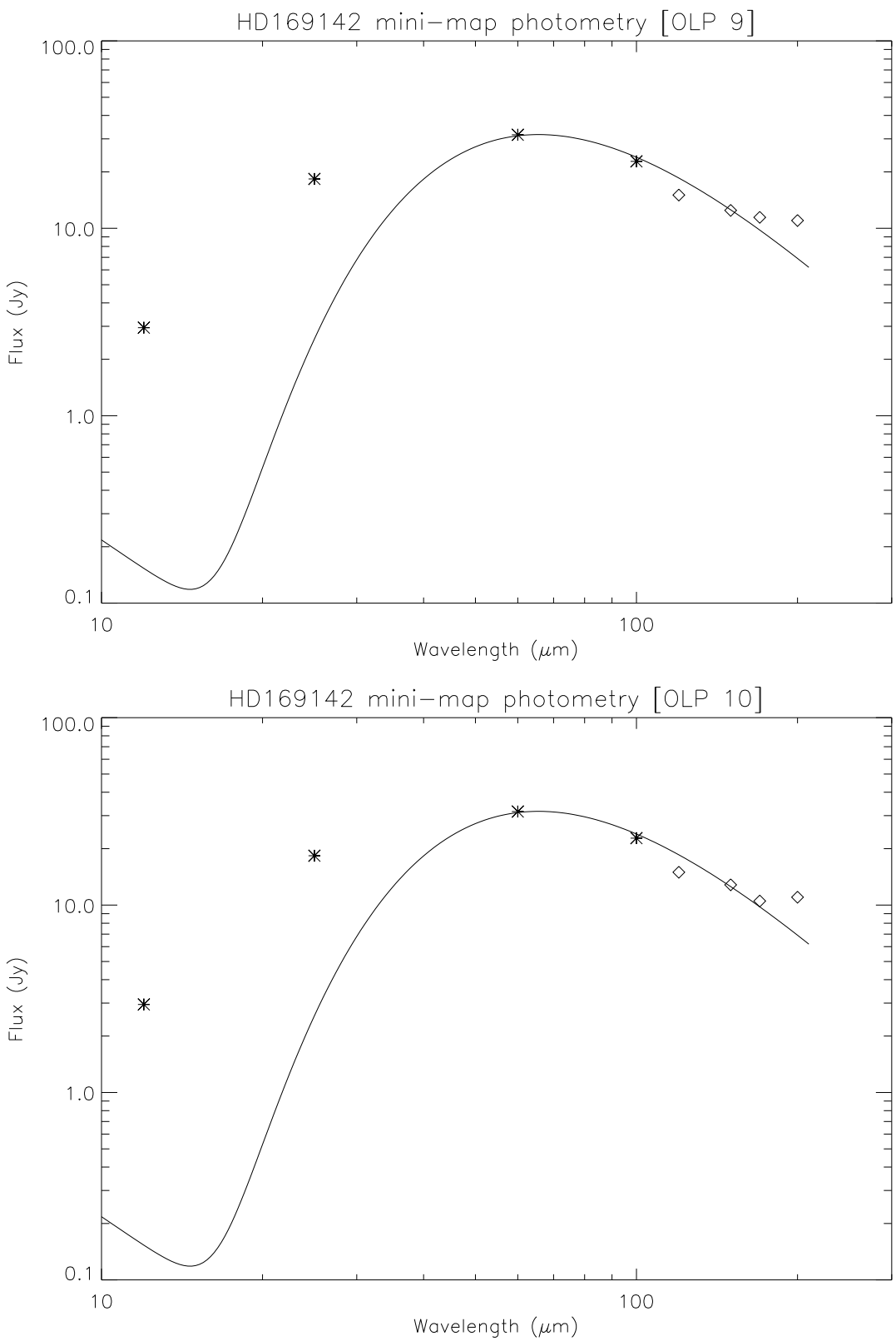

Figure 6.13: Comparison of PHT-C mini-map photometry with the scaled model spectrum of HD 109615) provided by P. Hammersley plus a FIR excess by a 55 K modified BB ($\varepsilon \propto \lambda^{-1}$) and with IRAS photometry for OLP 9.0b6 (upper panel) and OLP 10.0b5 (lower panel). No color correction is applied for $\lambda < 30\,\mu$m and the photometric points are corrected for a 50 K modified BB for $\lambda > 30\,\mu$m. The meaning of the symbols is the following: solid line: model, asterisk: IRAS, diamond: PHT-C200 (P22 AOT).

Evaluation Log

1) FIR photometry of HD 169142 from mini-maps

Measurements:
PHT-C200: pcas84001413 (P22 minimap) FCS = 120, 150, 170, 200 um

Colour correction: mod. bb, em.=1, T = 50 K

Model: Hammersley & 55 K modified ($\varepsilon \propto \lambda^{-1}$) BB

Det	cwl (μm)	OLP 9	OLP 10	IRAS	Model	Δ (OLP 9)	Δ (OLP 10)
C2	120.0	15.045	14.970		18.540	-18.85	-19.26
C2	150.0	12.463	12.826		12.549	-0.68	2.21
C2	170.0	11.439	10.511		9.785	16.90	7.41
C2	200.0	11.003	11.014		6.906	59.33	59.49

6.1.13 Point Source Photometry from PHT22 Mini-Maps: The FIR SED of HD 216956 (Formalhaut)

Motivation

HD 216956 (Formalhaut) is a FIR excess star.

Method

We compare the background subtracted, color corrected flux values of OLP V9.0b6 and OLP V10.0b5 results against IRAS photometry and the model of a modified black body with the parameters given in [38].

Results

The comparison of OLP 9.0b6 and OLP 10.0b5 photometry with the model is given in part 1 of the evaluation log. We derived fluxes assuming both a point source footprint and a 22 arcsec Gaussian footprint (C1e). Assuming a similar extension of the Formalhaut disk as for Vega (cf. 6.1.11) increases the 60 μm flux by about 1.4 Jy and makes it more consistent with IRAS photometry. Figs. 6.14 and 6.15 display the corresponding photometric results extracted from the mini-map PCAS product.

Conclusions

- This test case of an IR excess star shows a relatively good consistency with IRAS. The derived ISOPHOT flux depends somewhat on the assumed source extension, a point source model provides a lower flux limit.

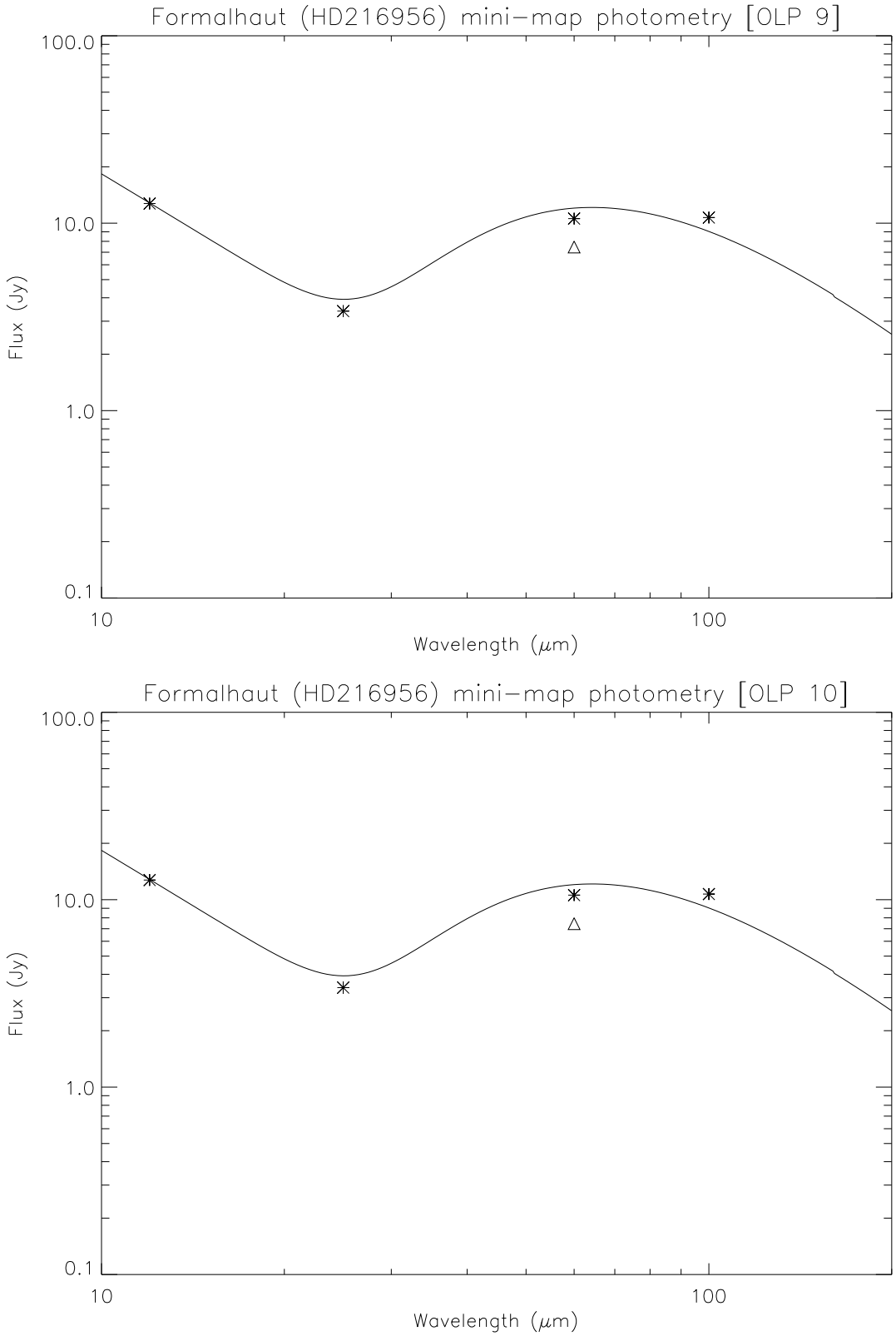

Figure 6.14: Comparison of PHT-C mini-map photometry of HD 216956 (Formalhaut) with the scaled model spectrum of HD 158485 (HR 6514) provided by P. Hammersley plus a FIR excess by a 55 K modified BB ($\varepsilon \propto \lambda^{-1}$) and with IRAS photometry for OLP 9.0b6 (upper panel) and OLP 10.0b5 (lower panel). A point source footprint was assumed in reconstructing the flux from the raster map. The photometric data points are corrected for a 8390 K BB for $\lambda < 30\,\mu$m and for a 50 K modified BB for $\lambda > 30\,\mu$m. The meaning of the symbols is the following: solid line: model, asterisk: IRAS, triangle: PHT-C100 (P22 AOT).

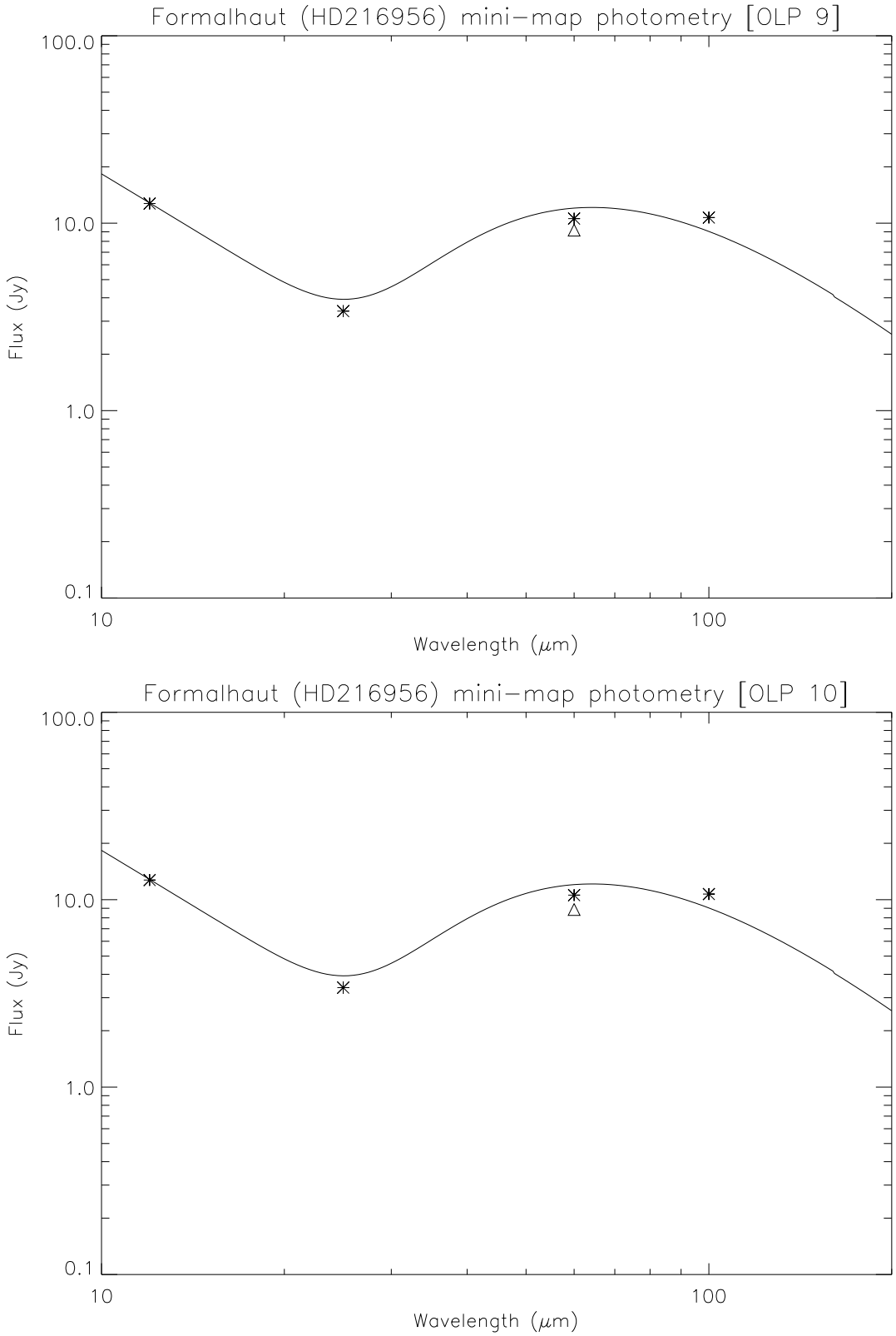

Figure 6.15: Comparison of PHT-C mini-map photometry of HD 216956 (Formalhaut) with the scaled model spectrum of HD 158485 (HR 6514) provided by P. Hammersley plus a FIR excess by a 55 K modified BB ($\varepsilon \propto \lambda^{-1}$) and with IRAS photometry for OLP 9.0b6 (upper panel) and OLP 10.0b5 (lower panel). A 22 arcsec Gaussian footprint was assumed in reconstructing the flux from the raster map. The photometric data points are corrected for a 8390 K BB for $\lambda < 30\,\mu$m and for a 50 K modified BB for $\lambda > 30\,\mu$m. The meaning of the symbols is the following: solid line: model, asterisk: IRAS, triangle: PHT-C100 (P22 AOT).

Evaluation Log

1) FIR photometry of HD 216956 (Formalhaut) from mini-maps

Measurements:
PHT-C100: pcas71800269 (P22 minimap) FCS = 60 um

Flux reconstruction: point source and 22" Gaussian footprint (C1e)

Colour correction: mod. bb, em.=1, T = 50 K

Model: Hammersley & 55 K modified ($\varepsilon \propto \lambda^{-1}$) BB

Det	cwl (μm)	OLP 9	OLP 10	IRAS	Model	Δ (OLP 9)	Δ (OLP 10)
C1	60.0	7.462	7.449	10.576	12.035	-3.92	-38.10
C1e	60.0	9.182	8.866	10.576	12.035	18.22	-26.33

6.1.14 Point Source Photometry from PHT22 Mini-Maps: The SED of the Quasar PG 1700+518

Motivation

These measurements were selected for comparison with chopped photometry on the same source.

Method

We compare the background subtracted flux of OLP V9.0b6 and OLP V10.0b8 results against IRAS photometry. The IRAS 100 μm FSC flux is an upper limit at around 1 Jy.

Results

The comparison of OLP 9.0b6 and OLP 10.0b8 photometry with IRAS is given in part 1 of the evaluation log. Default responsivity calibration was applied for the C200 measurements. Fig. 6.16 displays the photometric results extracted from the mini-map PCAS product. The OLP 10 SED looks smoother, as the 200 μm point has come up. The consistency with IRAS 60 μm photometry is very good. The good photometry at wavelengths longer than 100 μm shows the superior behaviour of the mini-map photometry.

Conclusions

- A good consistency of 60 μm mini-map photometry with IRAS is found.
- The mini-map technique allows good photometric results at wavelenghts beyond 60 μm considerably deeper than IRAS FSC.

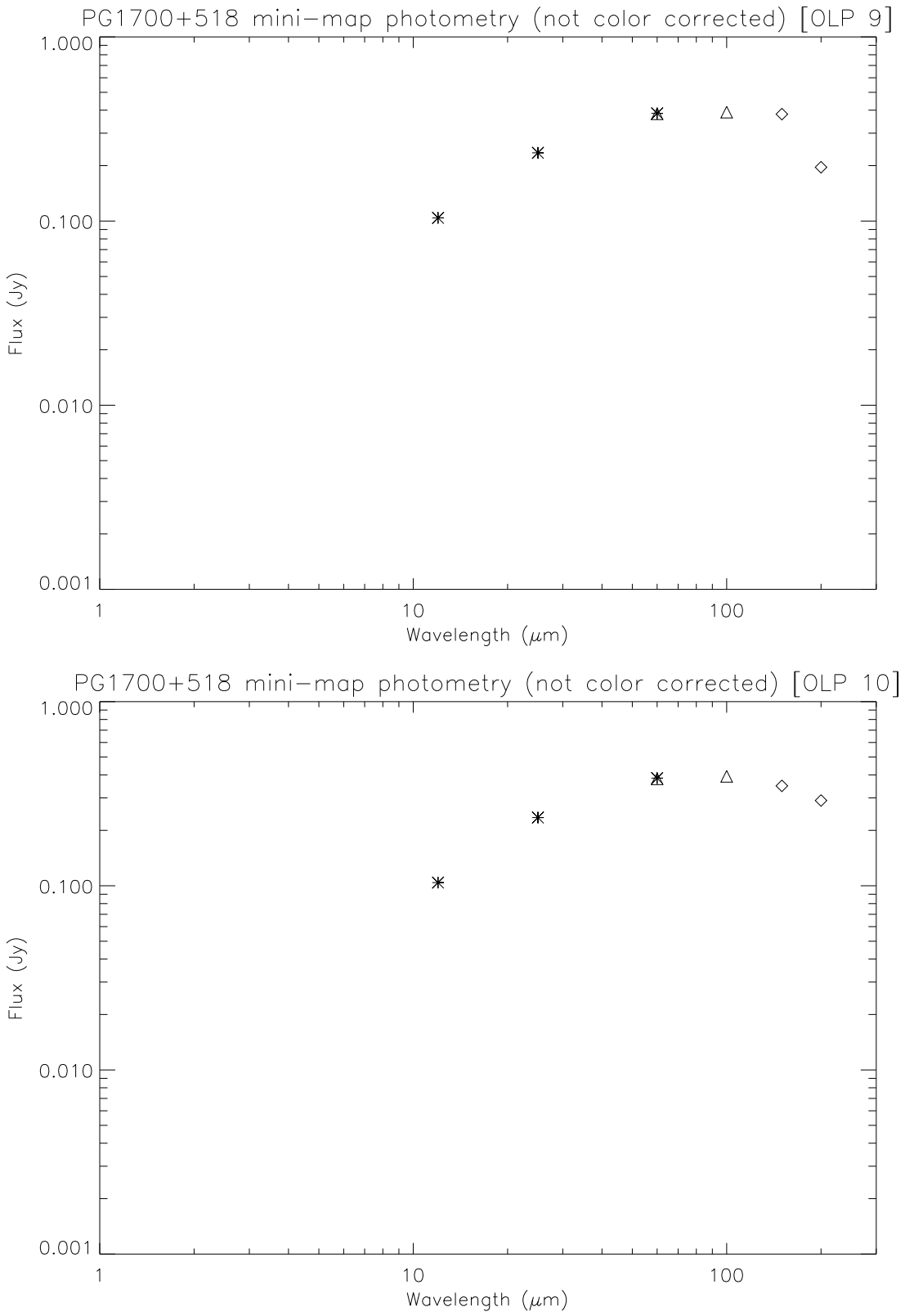

Figure 6.16: Comparison of PHT-C mini-map photometry of PG 1700+518 with IRAS photometry for OLP 9.0b6 (upper panel) and OLP 10.0b8 (lower panel). No color correction was applied. The meaning of the symbols is the following: asterisk: IRAS, triangle: PHT-C100 (P22 AOT), diamond: PHT-C200 (P22 AOT).

Evaluation Log

1) Photometry of PG 1700+518 from mini-maps

Measurements:
PHT-C100: pcas51800420 (P22 minimap) FCS = 60, 100 um
PHT-C200: pcas51800419 (P22 minimap) FCS = 150, 200 um

Det	cwl (μm)	OLP 9	OLP 10	IRAS	Model	Δ (OLP 9)	Δ (OLP 10)
C1	60.0	0.382	0.381	0.384			
C1	100.0	0.390	0.393				
C2	150.0	0.381	0.349				
C2	200.0	0.196	0.290				

Chapter 7

Nodding Photometry

TBW

Chapter 8

Chopped Photometry

8.1 Chopped Photometry Test Cases with Quasi-simultaneous Staring Mode References and Reproducibility Checks

Summary

- We note further stabilization of the chopped photometry processing, in particular for the P2 detector. However, accuracies, in particular the relative filter-to-filter calibration, are still poorer than for staring mode photometry.
- The P1 chopped photometry accuracy was found to be in the range of better than 25 %. The reproducibility is better than 15 %.
- The P2 chopped photometry accuracy was found to be in the range of better than 30 %. The reproducibility is better than 10 %.
- The P3 chopped photometry accuracy was found to be better than 25 % for bright sources. For faint sources fluxes seem to be systematically too low by 50 %. The reproducibility is better than 15 %.
- The C100 chopped photometry accuracy was found to be in the range of better than 30 %. The reproducibility is better than 15 %.
- The C200 chopped photometry accuracy was found to be better than 40 % for sources brighter than 1 Jy. No reproducibility assessment was possible due to noticable cirrus confusion of the target field.
- Cirrus confusion is a limitation in photometric accuracy at 100 μm for sources fainter than 0.2 Jy on backgrounds brighter than $4 - 5\,\mathrm{MJy\,sr^{-1}}$ and 170 μm for sources fainter than 1 Jy on backgrounds brighter than $5\,\mathrm{MJy\,sr^{-1}}$.

8.1.1 PHT03 and PHT22 Multi-filter Chopped Photometry: The SED of IRAS 03068-5346

Motivation

Like for the validation of staring mode observations the measurements on the IR galaxy IRAS 03068-5346 were designed to check out the processing of multi-filter chopped mode for all PHT-P and PHT-C filters. For reference photometry in nodding mode was taken for some filters and IRAS photometry is available.

Method

We compare the background subtracted flux values of both OLP V9.0b6 and OLP V10.0b5 results against the IRAS photometry . Furthermore, we compare the derived background surface brightness with COBE/DIRBE photometry.

Results

The comparison of the OLP9.0b6 and OLP10.0b5 photometry with IRAS is given in part 1 of the evaluation log section. Fig. 8.1 shows the derived SED for IRAS 03068-5346. There are still very low fluxes for the 12 and 15 μm filters for unknown reasons. The 25 μm flux is now consistent with IRAS, however, the 20 μm flux is still too high introducing a negative spectral shape for this wavelength range. C100 60 and 100 μm photometry, as well as P3 60 μm photometry is quite consistent with IRAS photometry (for the color correction performed), within 20 %. In general the resulting SED does not look as smooth as similar ones from staring mode observations (e.g. 5.1.8).
The comparison of the OLP9.0b6 and OLP10.0b5 surface brightness photometry with COBE/DIRBE is given in part 2 of the evaluation log section. Fig. 8.2 shows the derived sky background SED at the position of IRAS 03068-5346 (not color corrected). In the 7 to 25 μm range we see a reasonable background SED shape which is also consistent on absolute level with COBE/DIRBE photometry. The only filter that sticks out is the 12.8 μm filter, as is the case for staring mode observations. The C100 background photometry shows a negative outlier for the 65 μm filter and some positive offset at 80, 90, and 100 μm, otherwise the consistency with COBE/DIRBE and the SED shape is quite reasonable in the FIR.

Conclusions

- For P1 chopped photometry there is still the open point, why the processing of the 12 and 15 μm filter measurements fails to produce reasonable fluxes. This is in contrary to the PIA behaviour.
- P2 chopped photometry still shows some inconsistency, in particular with regard to the relative filter-to-filter calibration of the 20 and 25 μm filters. The 25 μm differential source flux is now consistent with IRAS.
- P3 chopped photometry is relatively consistent with IRAS.
- C100 60 and 100 μm chopped photometry is consistent with IRAS within 5 % (for the assumed flux model and applied color correction factors). 90 and 105 μm fluxes agree well with the 100 μm flux. 65 and 80 μm fluxes show an offset which might be linked to an absolute calibration issue as reflected in the background level determination.
- In C200 chopped photometry the invidual filters do not reflect a smooth SED.
- PHT-P surface brightness photometry is well matched with COBE/DIRBE photometry. An exception is the 12.8 filter measurement which sticks out in the same way as for staring mode background measurements. The 20 μm background looks fine now.
- For C100 the surface brightness consistency with COBE/DIRBE is only good for the 60 μm and 105 μm filters. There is a strange behaviour of the 65 μ filter measurement which shows a significant drop off instead of showing a high positive excess found for staring mode background measurements.

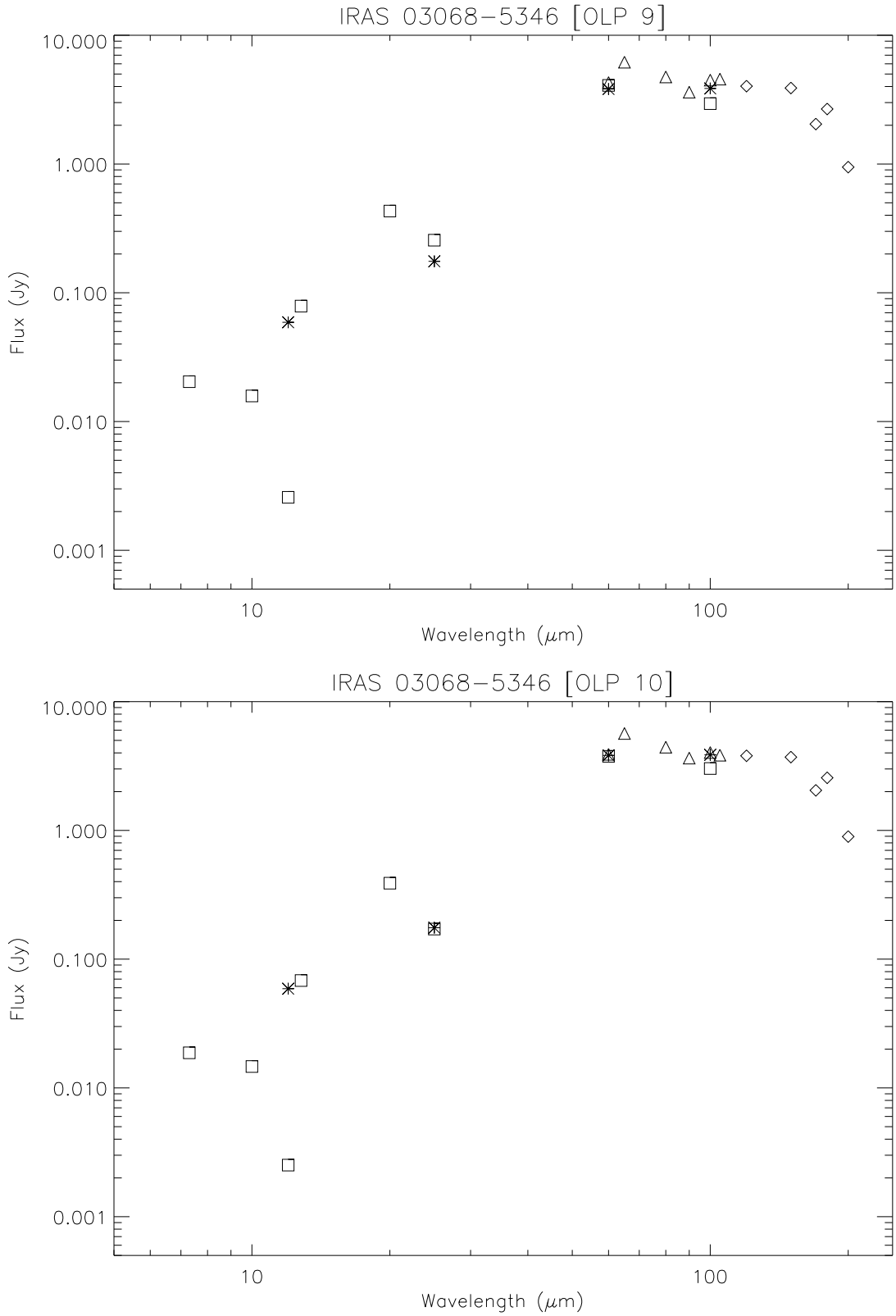

Figure 8.1: Comparison of PHT-P and PHT-C chopped photometry, using the full ISOPHOT filter set, with IRAS photometry both for OLP 9.0b6 (upper panel) and OLP 10.0b5 (lower panel). Color correction has been applied (modified BBs $\propto \lambda^{-2}$ with T1 = 140 K and T2 = 40 K). The meaning of the symbols is the following: asterisk: IRAS, square: PHT-P (P03 AOT), triangle: C100 (P22 AOT), diamond: C200 (P22 AOT).

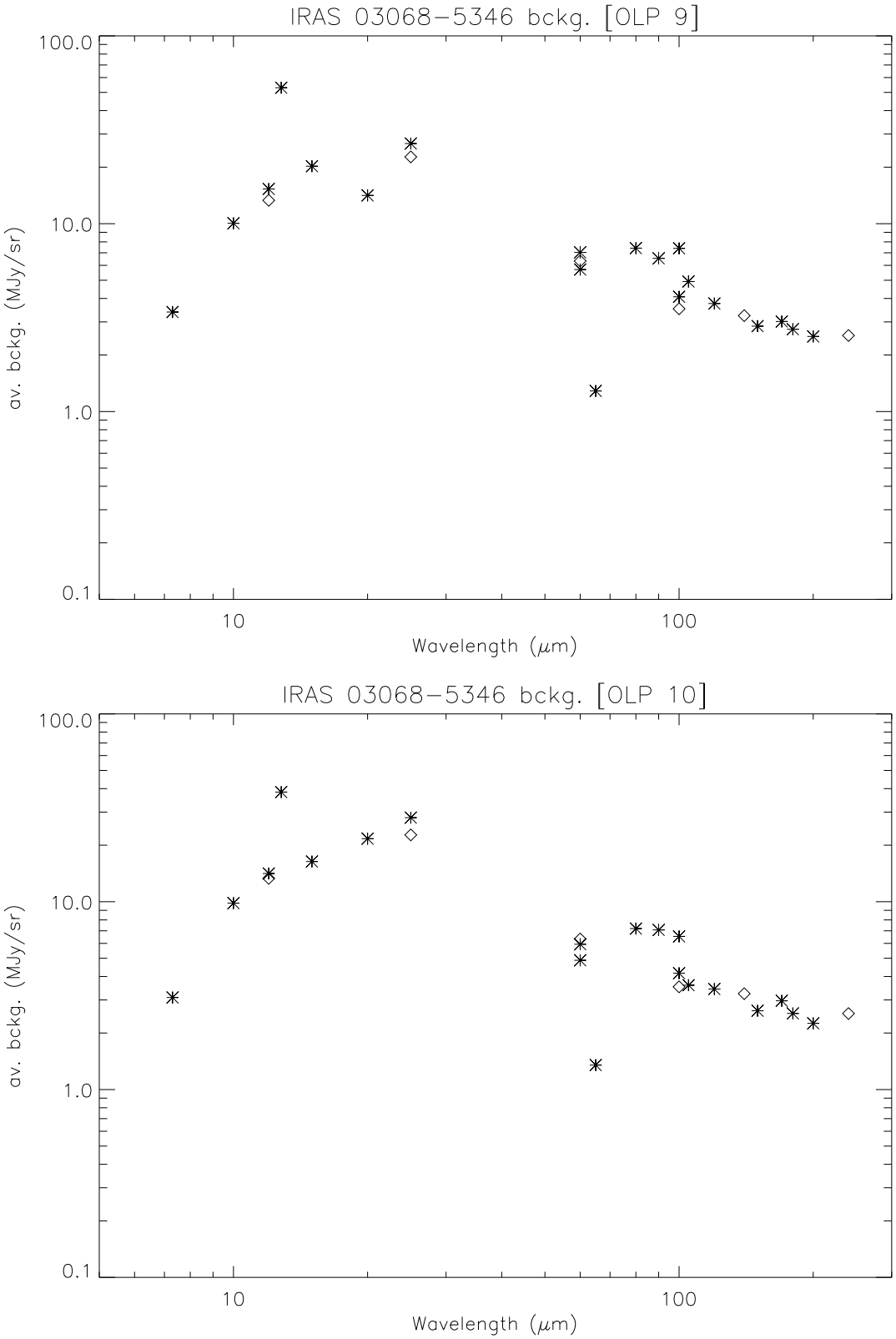

Figure 8.2: Comparison of surface brightness from chopped PHT photometry of the background beam for IRAS 03068-5346 with COBE, both for OLP 9.0b6 (upper panel) and OLP 10.0b5. Asterisk: PHT-P and PHT-C photometry, diamond: COBE.

- Like for staring measurements the C200 surface brightness values reflect a relatively smooth SED and match quite well with the COBE/DIRBE photometry.

Evaluation Log

1) Chopped Point Source Photometry

Measurements:

PHT-P1:	ppap81101701	FCS = 12 um
PHT-P2:	ppap81101701	FCS = 25 um
PHT-P3:	ppap81101802	FCS = 100 um
PHT-C1:	pcap81101906	FCS = 90 um
PHT-C2:	pcap81102008	FCS = 170 um

Colour correction: mod. bb, em.=2, T1 = 140 K (P1, P2), T2 = 40 K (P3, C1, C2)

Det	cwl (μm)	OLP 9	OLP 10	IRAS
P1	7.3	0.020	0.019	
P1	10.0	0.016	0.015	
P1	12.0	0.003	0.003	0.059
P1	12.8	0.079	0.068	
P1	15.0	0.000	0.000	
P2	20.0	0.431	0.389	
P2	25.0	0.256	0.171	0.176
P3	60.0	4.079	3.759	3.822
C1	60.0	4.288	3.898	3.822
C1	65.0	6.174	5.658	
C1	80.0	4.744	4.429	
C1	90.0	3.609	3.640	
P3	100.0	2.944	3.026	3.862
C1	100.0	4.480	4.023	3.862
C1	105.0	4.563	3.838	
C2	120.0	4.023	3.798	
C2	150.0	3.891	3.706	
C2	170.0	2.043	2.047	
C2	180.0	2.674	2.561	
C2	200.0	0.946	0.896	

2) Background photometry from off-source beam

Det	λ	OLP9 (MJy/sr)	OLP10 (MJy/sr)	COBE (MJy/sr)
P1	7.3	3.39	3.09	
P1	10.0	10.06	9.83	
P1	12.0	15.31	14.13	13.32
P1	12.8	52.97	38.34	
P1	15.0	20.24	16.37	
P2	20.0	14.15	21.66	
P2	25.0	26.72	28.02	22.69
P3	60.0	5.70	4.88	6.33
C1	60.0	7.04	5.94	6.33
C1	65.0	1.29	1.35	
C1	80.0	7.41	7.20	
C1	90.0	6.54	7.08	
P3	100.0	4.08	4.17	3.52
C1	100.0	7.39	6.54	3.52
C1	105.0	4.92	3.59	
C2	120.0	3.76	3.43	
C2	150.0	2.85	2.63	3.24
C2	170.0	3.02	2.97	
C2	180.0	2.74	2.54	
C2	200.0	2.51	2.25	2.54

8.1.2 Comparison of PHT03 and PHT22 Chopped and Staring Mode Photometry of Standard Stars from the Empirical Signal Correction Calibration Program

Motivation

A large calibration program had been set up to establish the empirical signal loss correction factors in chopped measurements from a comparison of chopped and nodding/staring photometry in the same instrumental set-up, on the same source and on the same revolution (as one block of measurements, to minimize differences in detector responsivities.) We have selected a few of these measurements to verify the end product of the chopped photometric calibration, as produced by OLP. This does not only include the signal correction, but also the signal derivation itself and the flux calibration using the chopped FCS measurement. We have selected test cases with more than one filter per detector in order to see the relative wavelength behaviour of the correction.

Method

All targets are standard stars for which flux models are available. In all cases ISOPHOT reference photometry, either in simple staring mode or in nodding technique are available. This allows to determine the absolute accuracy w.r.t. the model and in case of a discrepancy to cross-check how the consolidated staring mode photometry behaves.

Results

For HR 6817 the comparison of the OLP V9.01 and OLP V10.0b5 photometry with the model is given in part 1a of the evaluation log. Fig. 8.3 shows the chopped P1 photometry on HR 6817. Both OLP versions yield practically identical results. For the 3.3 μm filter the flux is off by a factor of 7 due to the FCS calibration which gives R=0.134 A/W and hence only 0.12 $\times$ the default responsivity. In the other two filters an absolute accuracy of better than 10 % is achieved.
The background photometry from the off-source beam is listed in part 1b of the evaluation log. Fig. 8.4 shows the comparison with COBE/DIRBE photometry. For OLP 10 the 7.3 μm background value has come closer to the SED indicated by COBE/DIRBE. The 3.3 and 3.6 μm values are still quite some factor off. This is presumably due to the case of the high contrast between on-source and off-source beam for these measurements. The off-source signal level is never reached.
For HR 6132 the comparison of the OLP V9.01 and OLP V10.0b5 photometry with the model is given in part 2a of the evaluation log. Fig. 8.5 shows the chopped P2 photometry on HR 6132. Both for the 20 and 25 μm filters two different apertures were used, namely the 120 arcsec and the 180 arcsec ones. These are non-standard apertures for these filters. Like for the OLP 9.01 the resulting fluxes are still too high, however the relative spectral shape is much better reflected. The values of the smaller 120 arcsec aperture are within 50 % of the model.
The background photometry from the off-source beam is listed in part 2b of the evaluation log. Fig. 8.6 shows the comparison with COBE/DIRBE photometry. For OLP 10 the 25 μm background values have come much closer to the SED indicated by COBE/DIRBE.
For HR 1457 the comparison of the OLP V9.01 and OLP V10.0b5 photometry with the model is given in part 3a of the evaluation log. Fig. 8.7 shows the chopped P3 photometry on HR 6132. There is not much difference between OLP 9 and OLP 10 results. The consistency with the model and IRAS is better than 25 %. At 100 μm both the IRAS and the ISOPHOT flux are below the model.
The background photometry from the off-source beam is listed in part 3b of the evaluation log. Fig. 8.8 shows the comparison with COBE/DIRBE photometry. Again OLP 9 and OLP 10 results are quite similar. The 60 mum background flux is about a factor of 2 higher than suggested from COBE, while the 100 mum flux shows a good correspondence.
For HR 5340 the comparison of the OLP V9.01 and OLP V10.0b5 photometry with the model is given in part 4a of the evaluation log. Fig. 8.9 shows the chopped C200 photometry on HR 5340. There is not much difference between OLP 9 and OLP 10 results. The consistency with the model is better than 40 %.

The background photometry from the off-source beam is listed in part 4b of the evaluation log. Fig. 8.10 shows the comparison with COBE/DIRBE photometry. Again OLP 9 and OLP 10 results are quite similar. Taking into account that the COBE 140 μm point always tends to be a bit too high, the consistency with the COBE 100 and 240 μm background fluxes is quite good.

Conclusions

- The accuracy of chopped P1 photometry on HR 6817 is better than 10 % (not considering the 3.3 μm measurement). The contrast in the short wavelength P1 filters is too high, so that the corrected signal is far above the one corresponding to the real background flux.
- Fluxes from chopped P2 photometry of HR 6132 are 50 % to a factor of 2 too high, being an exception to the results from other test cases. The measurements were done in non-standard apertures. The photometry of the 120 arcsec aperture is within 50 % of the model now. The relative filter-to-filter calibration at 20 and 25 μm is improved. The relative background SED is much more consistent with COBE.
- Fluxes from chopped P3 photometry of HR 1457 are within 25 % of the model flux, however the surface brightness of the off-beam in the 60 μm measurement is a factor of 2 higher than suggested by COBE/DIRBE, while the 100 μm surface brightness is consistent with COBE/DIRBE.
- The accuracy of chopped C200 photometry on HR 5340 is 40 % absolute and 60 % relative. The background SED is reasonably consistent with COBE photometry.

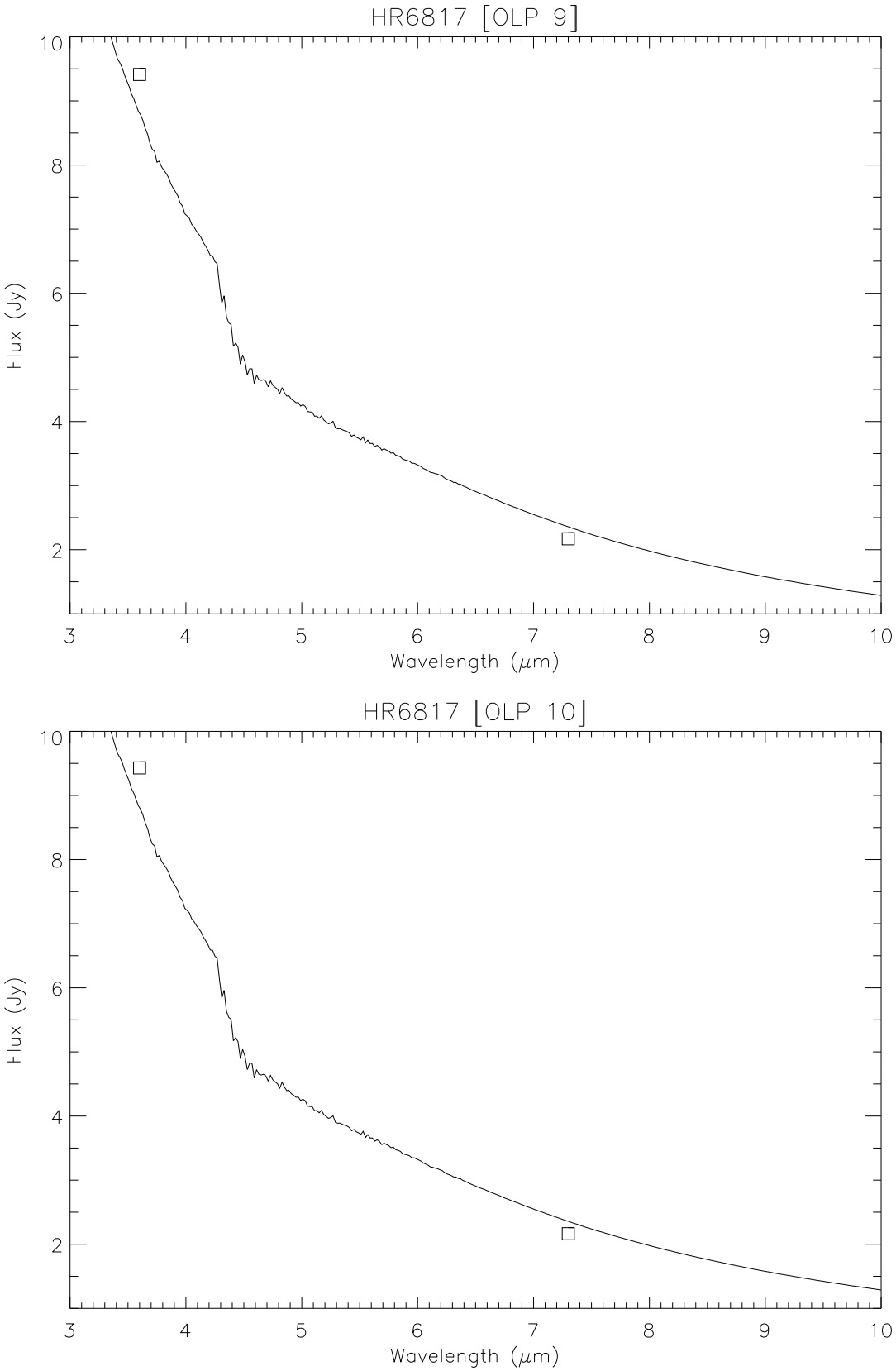

Figure 8.3: Comparison of PHT-P1 chopped photometry with the model spectrum of HR 6817, provided by P. Hammersley, for OLP 9.01 (upper panel) and OLP 10.0b5 (lower panel). The meaning of the symbols is the following: solid line: model, square: PHT-P1.

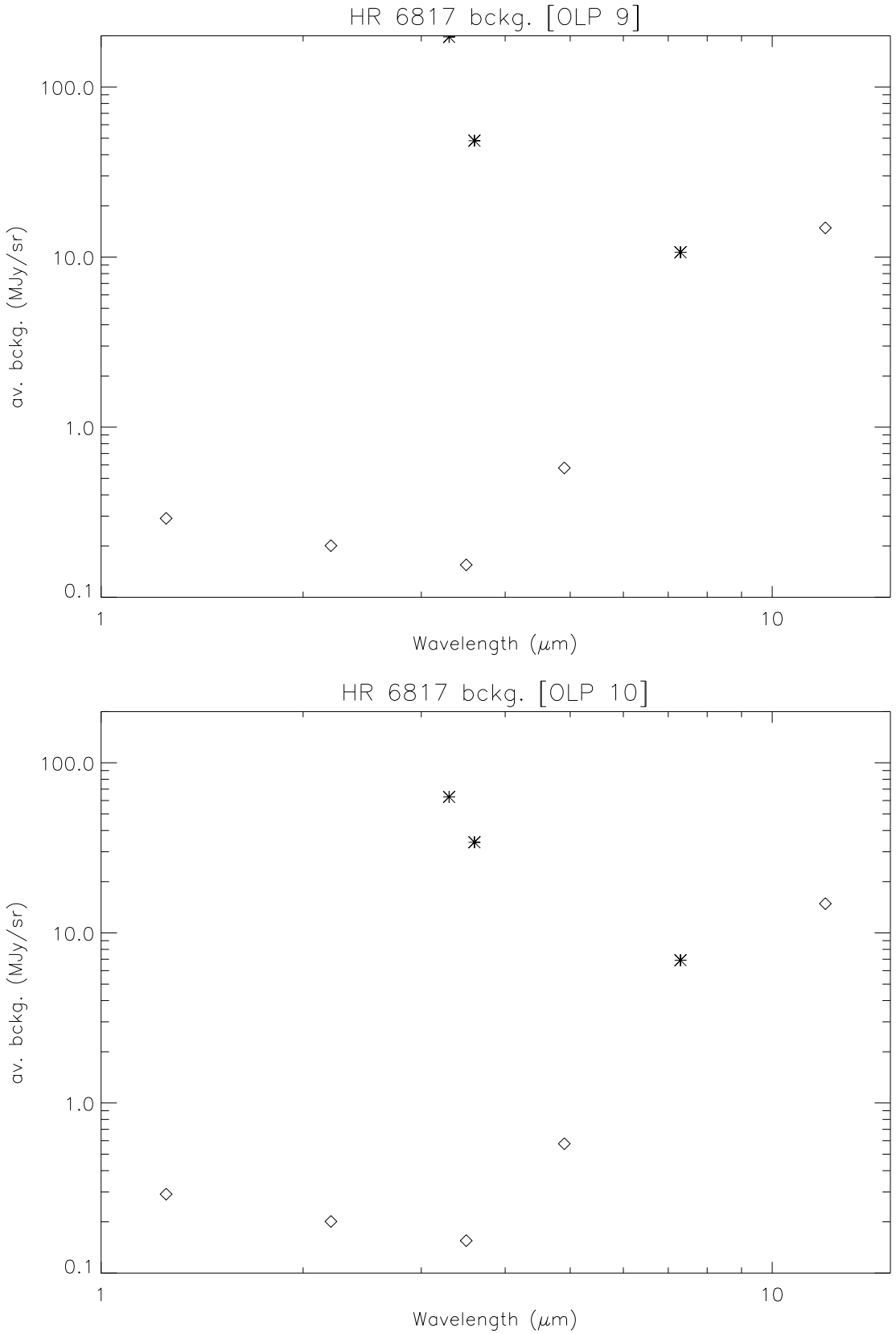

Figure 8.4: Comparison of surface brightness from chopped PHT photometry of the background beam for HR 6817 with COBE, both for OLP 9.01 (upper panel) and OLP 10.0b5. Asterisk: PHT-P and PHT-C photometry, diamond: COBE.

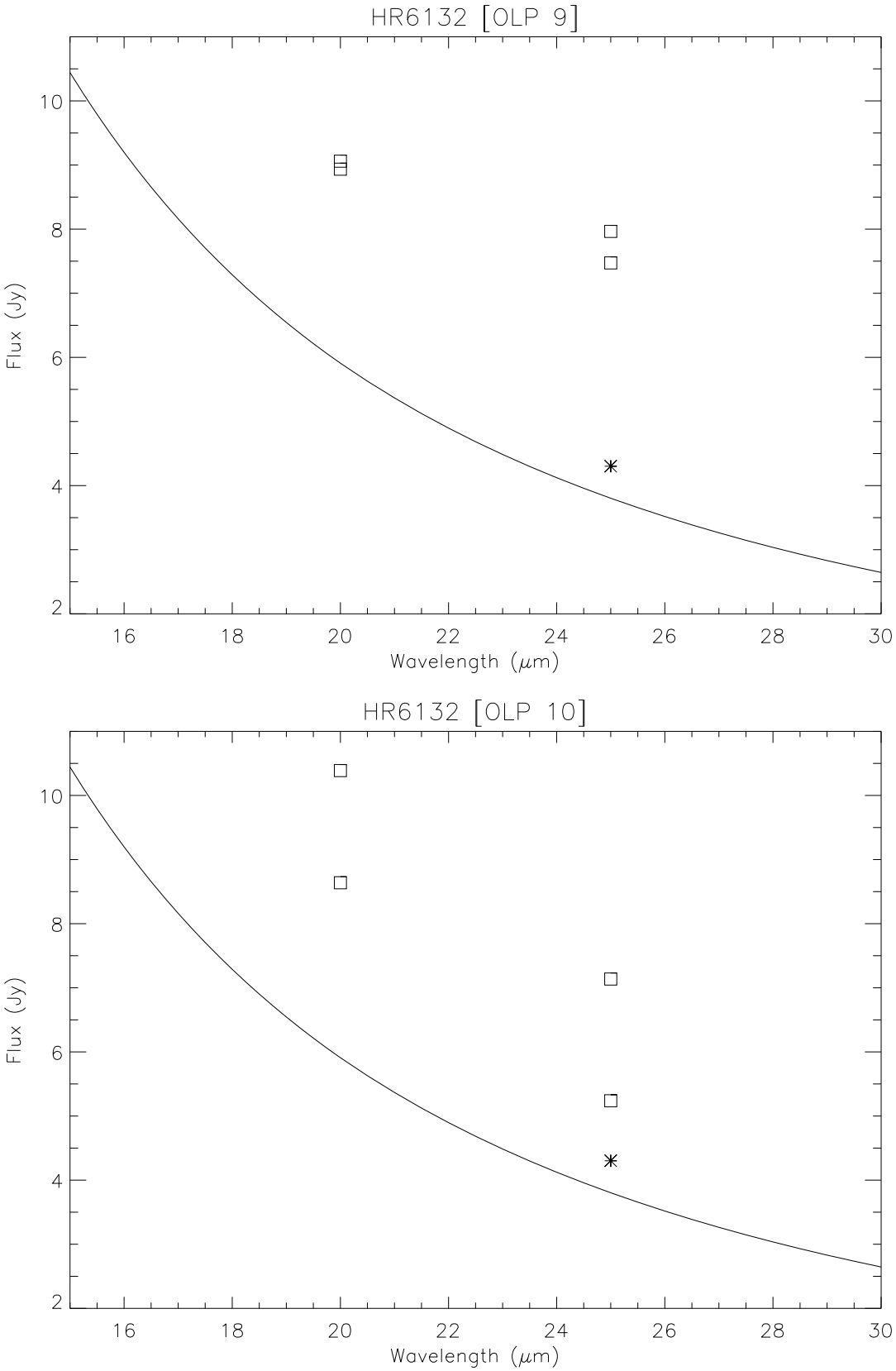

Figure 8.5: Comparison of PHT-P2 chopped photometry with the model spectrum of HR 6132, provided by P. Hammersley, for OLP 9.01 (upper panel) and OLP 10.0b5 (lower panel). The meaning of the symbols is the following: solid line: model, square: PHT-P2, asterisk: IRAS. Measurements were done both in the 120 and 180 arcsec aperture.

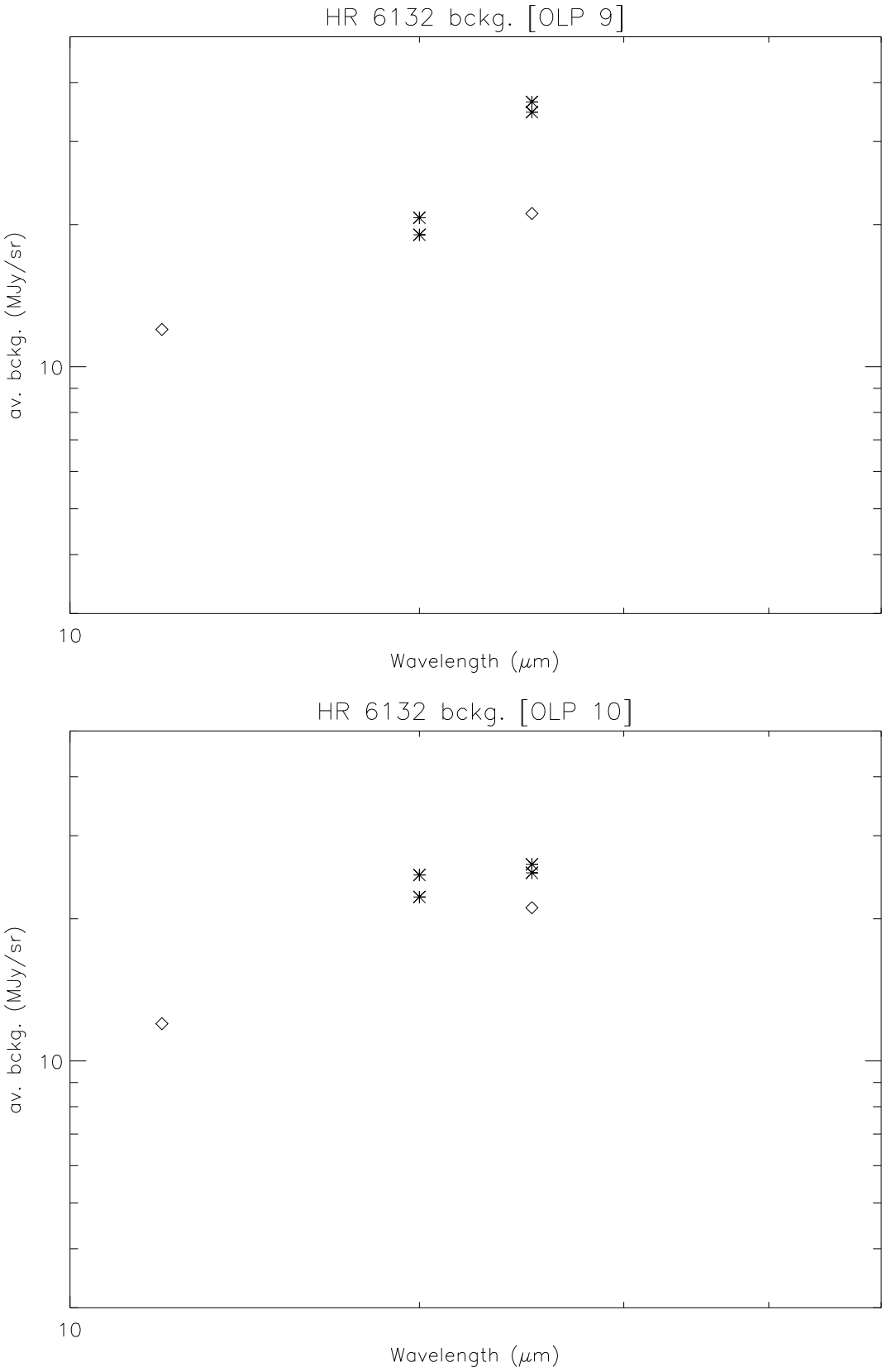

Figure 8.6: Comparison of surface brightness from chopped PHT photometry of the background beam for HR 6132 with COBE, both for OLP 9.01 (upper panel) and OLP 10.0b5. Asterisk: PHT-P and PHT-C photometry, diamond: COBE.

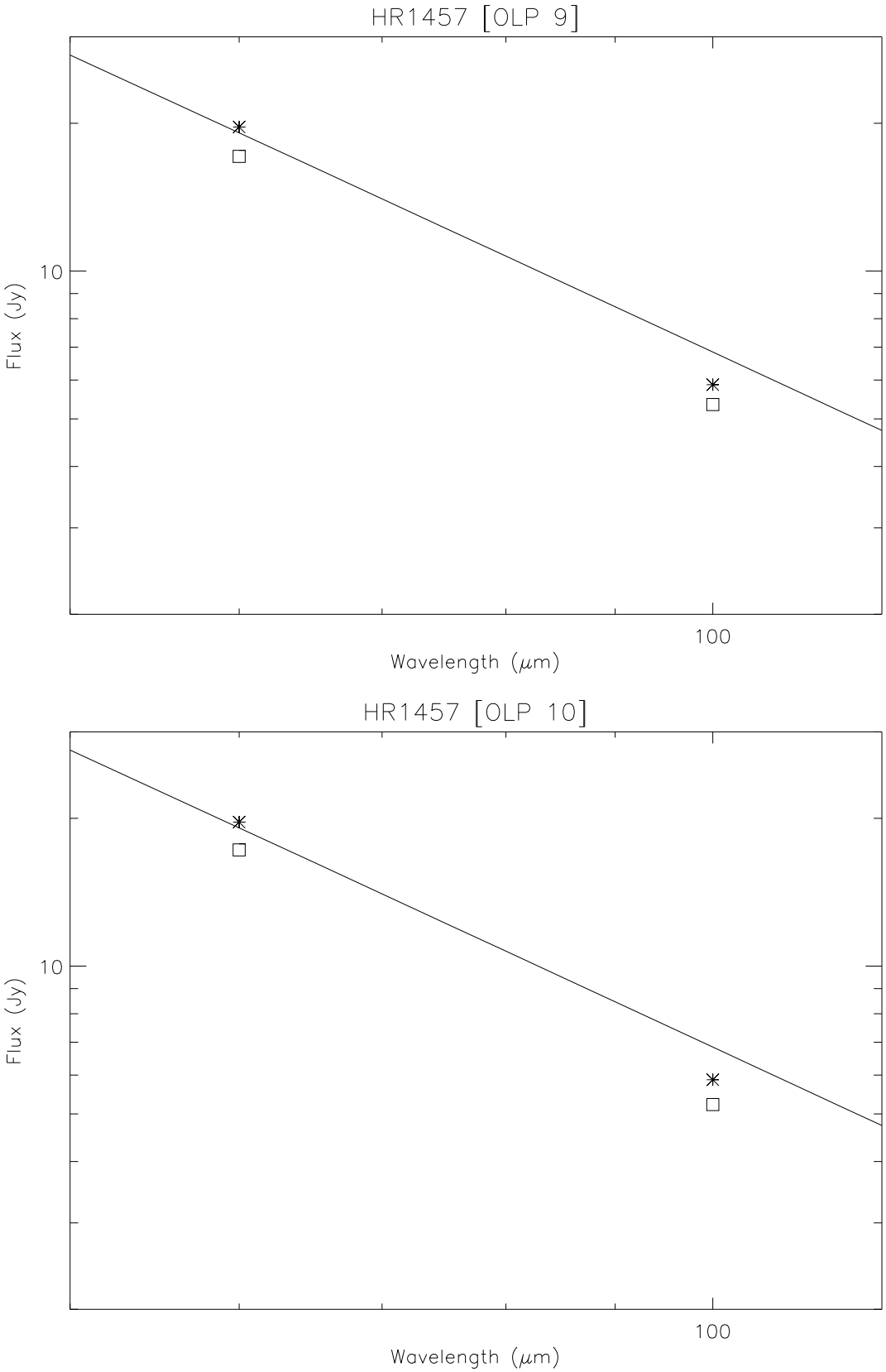

Figure 8.7: Comparison of PHT-P3 chopped photometry with the model spectrum of HR 1457, provided by M. Cohen, for OLP 9.01 (upper panel) and OLP 10.0b5 (lower panel). The meaning of the symbols is the following: solid line: model, square: PHT-P3, asterisk: IRAS.

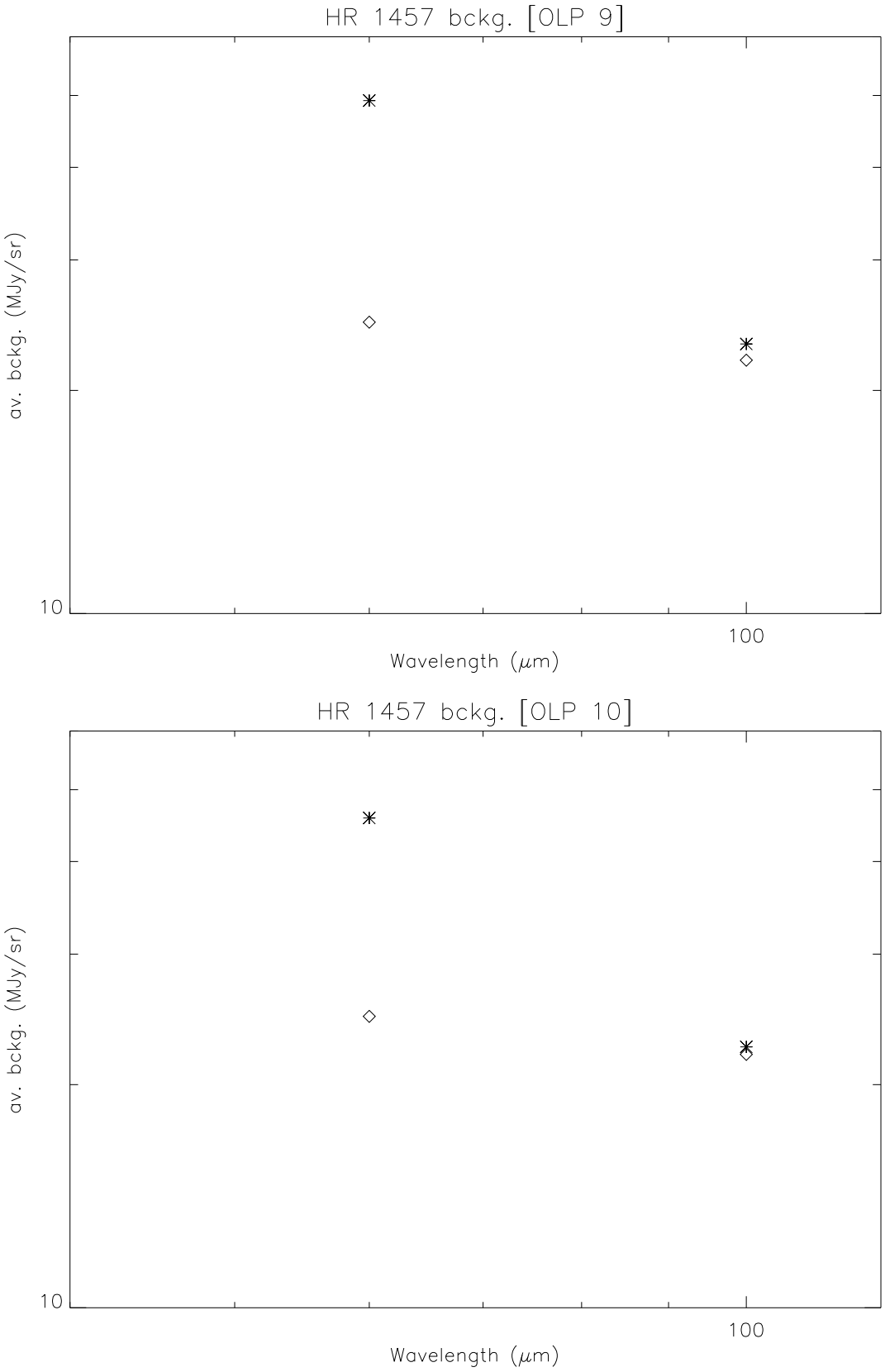

Figure 8.8: Comparison of surface brightness from chopped PHT photometry of the background beam for HR 1457 with COBE, both for OLP 9.01 (upper panel) and OLP 10.0b5. Asterisk: PHT-P and PHT-C photometry, diamond: COBE.

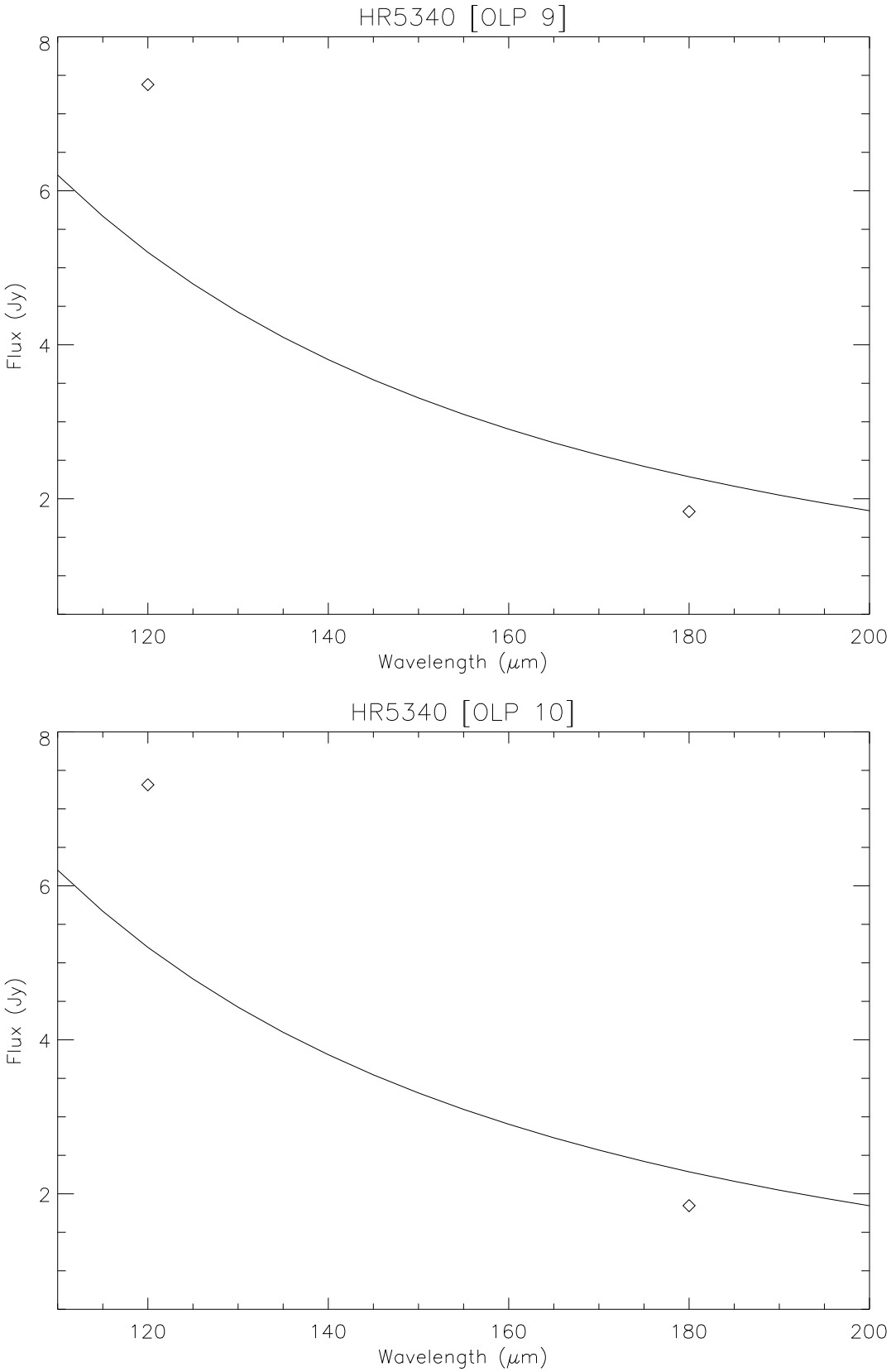

Figure 8.9: Comparison of PHT-C200 chopped photometry with the model spectrum of HR 5340, provided by M. Cohen, for OLP 9.01 (upper panel) and OLP 10.0b5 (lower panel). The meaning of the symbols is the following: solid line: model, diamond: PHT-C200.

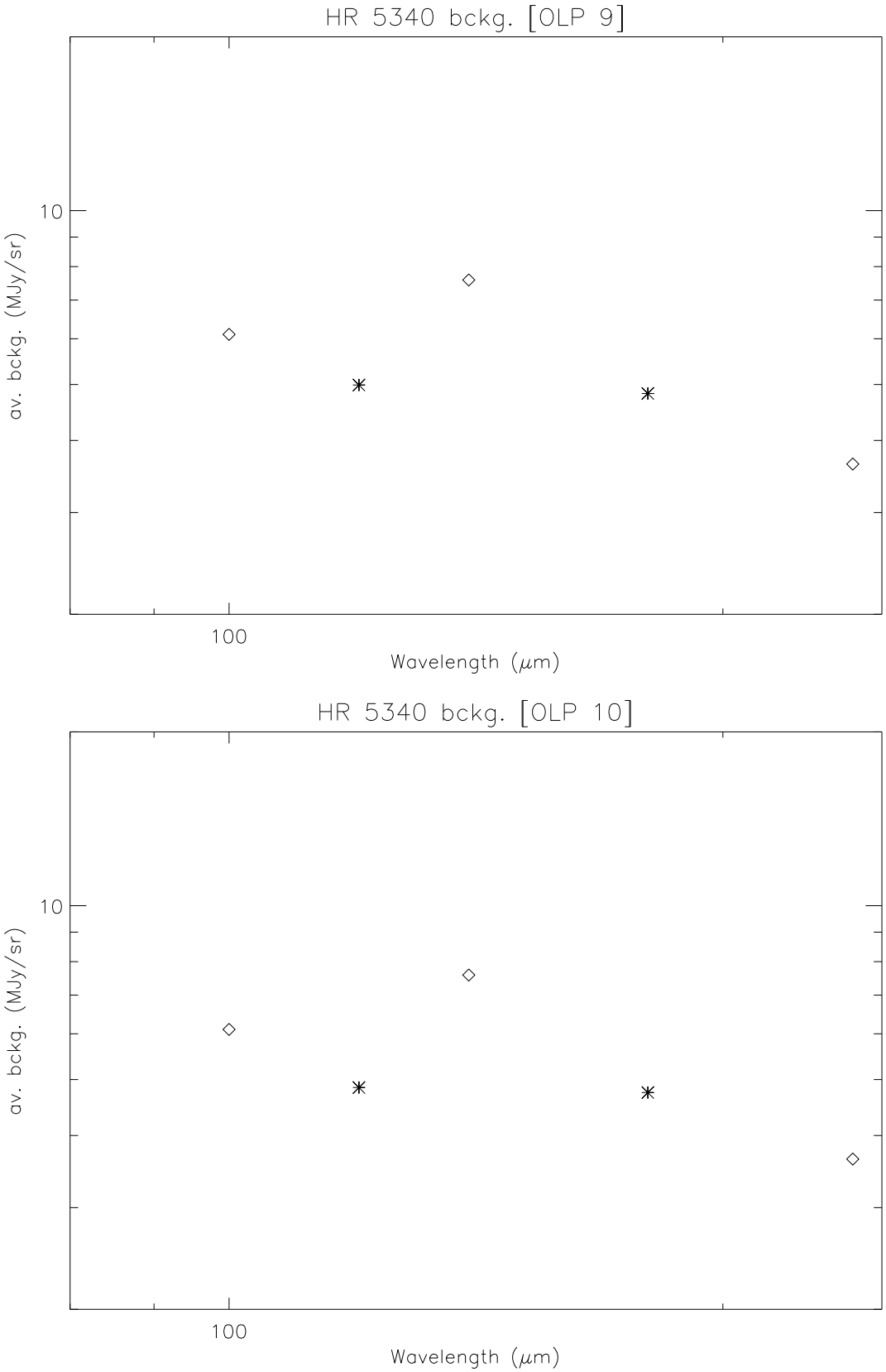

Figure 8.10: Comparison of surface brightness from chopped PHT photometry of the background beam for HR 5340 with COBE, both for OLP 9.01 (upper panel) and OLP 10.0b5. Asterisk: PHT-P and PHT-C photometry, diamond: COBE.

Evaluation Log

1) HR 6817

a) Chopped point source photometry

Measurements:
PHT-P1: ppap78300901
PHT-P1: ppap78301005
PHT-P1: ppap78301107

Colour correction: black body, T = 5000 K

Model: Hammersley

Det	cwl (μm)	OLP 9	OLP 10	Model	Δ (OLP 9)	Δ (OLP 10)
P1	3.3	72.052	71.344	10.251	602.88	595.97
P1	3.6	9.412	9.430	8.809	6.84	7.04
P1	7.3	2.170	2.164	2.358	-7.97	-8.22

b) Background photometry from off-source beam

Det	λ	OLP9 (MJy/sr)	OLP10 (MJy/sr)	COBE (MJy/sr)
P1	3.3	197.05	63.00	
P1	3.6	48.35	34.10	
P1	7.3	10.67	6.91	

2) HR 6132

a) Chopped point source photometry

Measurements:
PHT-P2: ppap76901902 120 arcsec aperture
PHT-P2b: ppap76902011 180 arcsec aperture
PHT-P2: ppap76902106 120 arcsec aperture
PHT-P2b: ppap76902216 180 arcsec aperture

Colour correction: black body, T = 5000 K

Model: Hammersley

Det	cwl (μm)	OLP 9	OLP 10	IRAS	Model	Δ (OLP 9)	Δ (OLP 10)
P2	20.0	8.935	8.639		5.909	51.22	46.20
P2b	20.0	9.060	10.388		5.909	53.33	75.80
P2	25.0	7.473	5.238	4.301	3.803	96.51	37.74
P2b	25.0	7.964	7.137	4.301	3.803	109.43	87.67

b) Background photometry from off-source beam

Det	λ	OLP9 (MJy/sr)	OLP10 (MJy/sr)	COBE (MJy/sr)
P2	20.0	20.68	24.77	
P2b	20.0	19.03	22.25	
P2	25.0	36.39	25.03	21.11
P2b	25.0	34.61	26.10	21.11

3) HR 1457

a) Chopped point source photometry

Measurements:
PHT-P3 : ppap86101202
PHT-P3 : ppap86101306

Colour correction: black body, T = 4000 K

Model: Cohen

Det	cwl (μm)	OLP 9	OLP 10	IRAS	Model	Δ (OLP 9)	Δ (OLP 10)
P3	60.0	17.126	17.249	19.650	19.120	-10.43	-9.79
P3	100.0	5.348	5.225	5.870	6.842	-21.84	-23.63

b) Background photometry from off-source beam

Det	λ	OLP9 (MJy/sr)	OLP10 (MJy/sr)	COBE (MJy/sr)
P3	60.0	49.21	45.79	24.72
P3	100.0	23.11	22.49	21.97

4) HR 5340

a) Chopped point source photometry

Measurements:
PHT-C2: pcap62900722 FCS = 120 um

Colour correction: black body, T = 4000 K

Model: Cohen

Det	cwl (μm)	OLP 9	OLP 10	Model	Δ (OLP 9)	Δ (OLP 10)
C2	120.0	7.380	7.313	5.201	41.90	40.60
C2	180.0	1.835	1.847	2.286	-19.74	-19.21

b) Background photometry from off-source beam

Det	λ	OLP9 (MJy/sr)	OLP10 (MJy/sr)	COBE (MJy/sr)
C2	120.0	4.99	4.84	
C2	180.0	4.82	4.75	

8.1.3 PHT03 and PHT22 Chopped Photometric Results for the Faint Point Source Detection Limit Program

Motivation

In order to determine the optimal observing strategies for faint point sources a dedicated engineering program had been performed. This resulted in recommendations for the most sensitive and photometrically accurate faint source observation modes [27]. This program was largely done using AOTs so that the resulting OLP fluxes can be checked for their accuracies.

Method

Both chopped and staring (sparse map, nodding mode was not yet available at that time) mode OLP 9 and OLP 10 results are compared with each other. All targets are faint standard stars for which M. Cohen has provided extensions of the SED out to 300 μm, so that comparison with the model prediction is possible.

Results

For IRC+60228 the comparison of the OLP V9.01 and OLP V10.0b5 photometry with the model is given in part 1a of the evaluation log. Fig. 8.11 shows the chopped C100 photometry on IRC+60228. Both OLP versions yield practically identical results. The resulting fluxes are about 70 % above the model flux. We have, however, to note that the chopped photometry is in very good agreement with sparse map photometry performed on the star (see Sect. 5.3.5) which yields a flux of 139 mJy. Therefore, one can question whether the model extrapolation is right. The IRAS 100 μm FSC flux is only an upper limit. Thus, we do not consider this test case for the determination of photometric accuracies. According to [39] the 1 σ cirrus confusion value is estimated to be 14 mJy (using formulae 6, 7 and 8 with B = 4 MJy sr^{-1}, q = 1.6 from 150 arcsec chop throw and $\gamma = 0.13$), thus cirrus confusion can account for about 20 – 30 % photometric uncertainty.
The background photometry from the off-source beam is listed in part 1b of the evaluation log. Fig. 8.12 shows the comparison with COBE/DIRBE photometry. The 90 μm point is a bit higher than would be suggested from the COBE SED, however, local cirrus contributions have to be taken into account for this wavelength.
For HR 5981 the comparison of the OLP V9.01 and OLP V10.0b5 photometry with the model is given in part 2a of the evaluation log. Fig. 8.13 shows the chopped P3 and C100 photometry, both at 60 μm on HR 5981. The chopping direction is the same for both measurements, since they were executed on the same revolution. The 52 arcsec aperture was used for the P3 measurement which is comparable in size to one C100 pixel. Both OLP versions yield quite similar results. The P3 60 μm flux is significantly below the model (by 70 – 80 %), while the C100 60 μm flux gives a very good agreement with the model. This is in contradiction with the sparse map photometry result (see Sect. refsect:hr5981smfaint for which the P3 flux gives a good correspondence with the model, while the C100 flux is a factor of 2 too high. Cirrus confusion can be excluded in this case, since due to the same chop direction and similar aperture size the same impact would be expected for both measurements.
The background photometry from the off-source beam is listed in part 2b of the evaluation log. Fig. 8.14 shows the comparison with COBE/DIRBE photometry. With regard to the COBE 60 μm point, the background surface brightness derived from the P3 measurement is too low, while the one derived from the C100 measurement is too low.

Conclusions

- The P3 chopped photometry gives too low fluxes (by 80 %), hence it is not reliable on this flux level of expected 150 mJy. Cirrus confusion cannot explain this behaviour, since a similar set-up C100 measurement produces a different result.
- The C100 chopped photometry yields discrepant accuracies for the two test stars. While for HR 5981 a good consistency with the model was found (in contradiction with the sparse map results), in the case of IRC+60228 the flux was 70 % above the

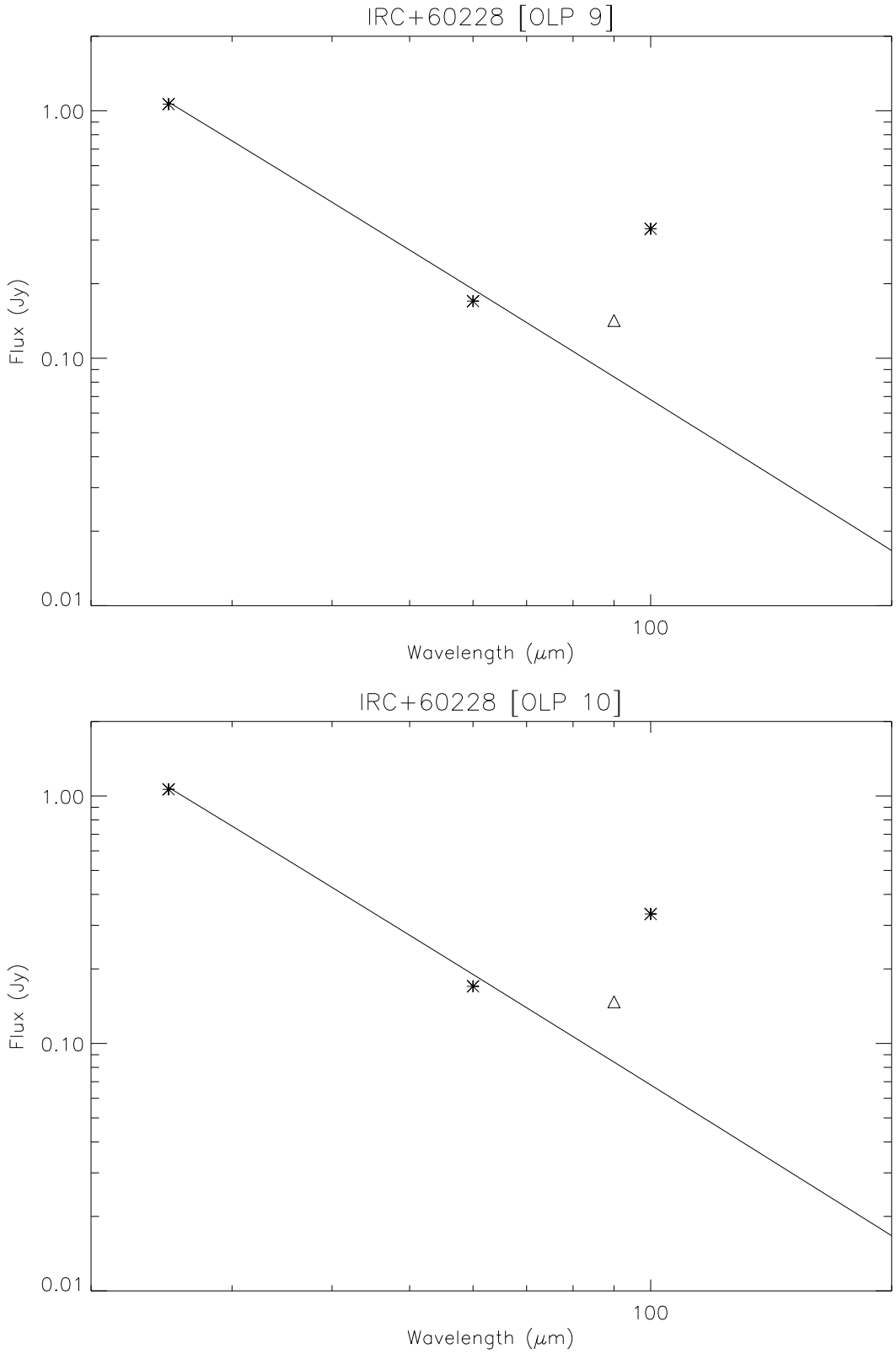

Figure 8.11: Comparison of PHT-C100 chopped photometry with the model spectrum of IRC+60228, provided by M. Cohen, for OLP 9.01 (upper panel) and OLP 10.0b5 (lower panel). The meaning of the symbols is the following: solid line: model, asterisk: IRAS, triangle: PHT-C100.

model. Since in this latter case there is a good agreement with the sparse map result,

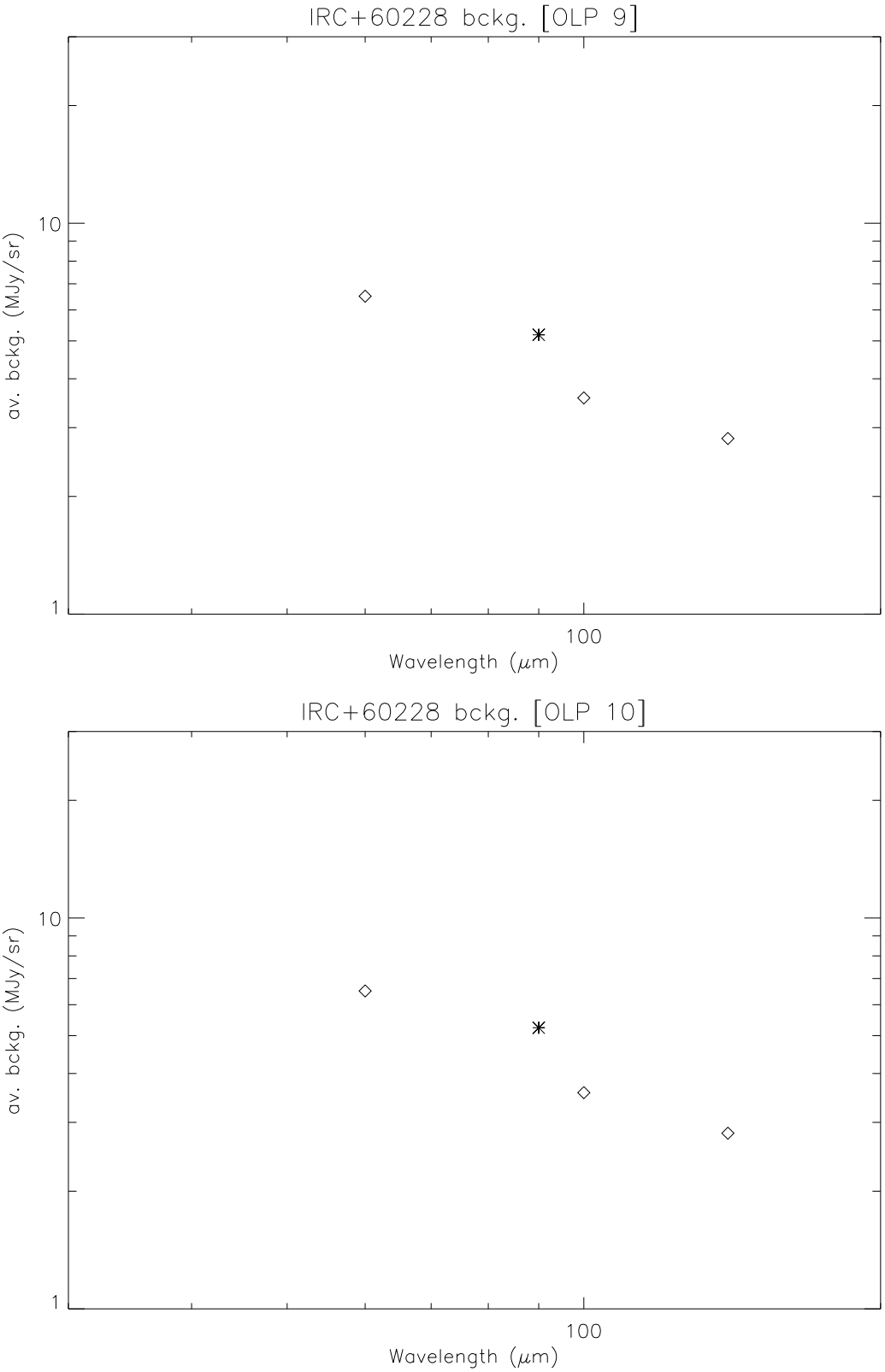

Figure 8.12: Comparison of surface brightness from chopped PHT photometry of the background beam for IRC+60228 with COBE, both for OLP 9.01 (upper panel) and OLP 10.0b5. Asterisk: PHT-C photometry, diamond: COBE.

the value of the model extrapolation may be questioned.

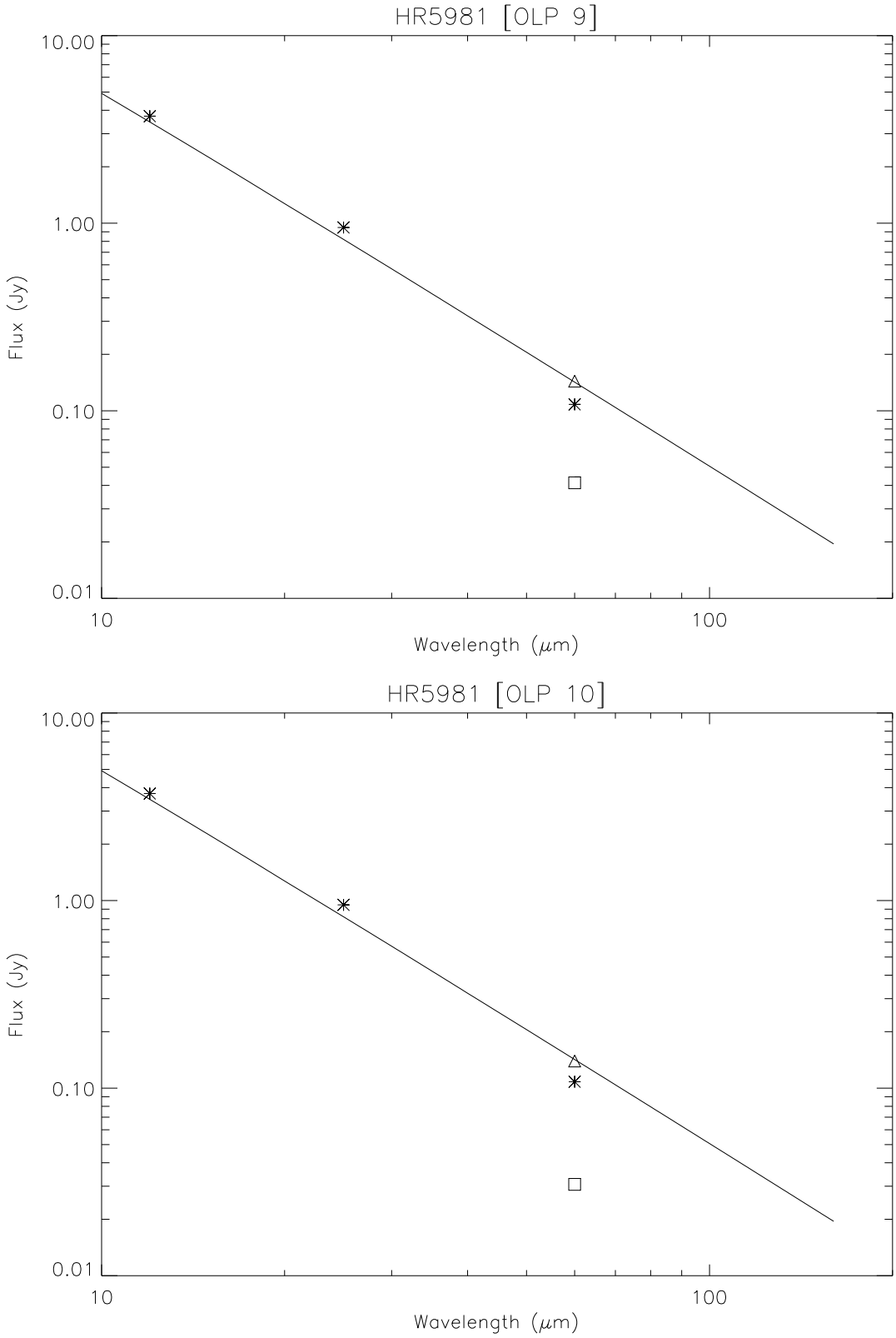

Figure 8.13: Comparison of PHT-P3 and -C100 chopped photometry with the model spectrum of HR 5981, provided by P. Hammersley, for OLP 9.01 (upper panel) and OLP 10.0b5 (lower panel). The meaning of the symbols is the following: solid line: model, asterisk: IRAS, square: PHT-P, triangle: PHT-C100.

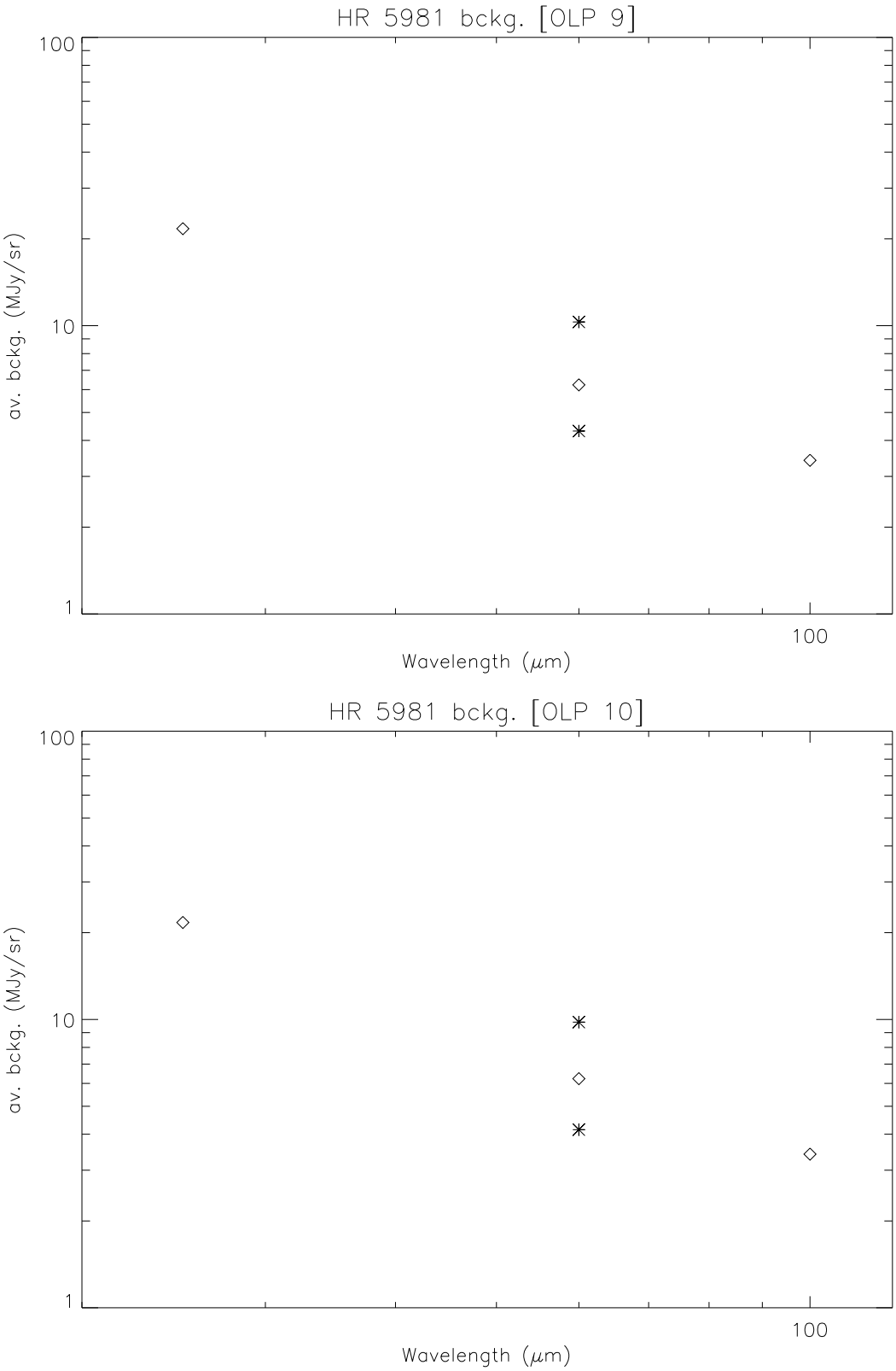

Figure 8.14: Comparison of surface brightness from chopped PHT photometry of the background beam for HR 5981 with COBE, both for OLP 9.01 (upper panel) and OLP 10.0b5. Asterisk: PHT-P and PHT-C photometry, diamond: COBE.

Evaluation Log

1) IRC 60228

a) Chopped point source photometry

Measurements:
PHT-C1 : pcap25202408 FCS = 90 um

Colour correction: black body, T = 3898 K

Model: Cohen

Det	cwl (μm)	OLP 9	OLP 10	IRAS	Model	Δ (OLP 9)	Δ (OLP 10)
C1	90.0	0.142	0.147		0.084	69.02	75.29

b) Background photometry from off-source beam

Det	λ	OLP9 (MJy/sr)	OLP10 (MJy/sr)	COBE (MJy/sr)
C1	90.0	5.18	5.24	

2) HR 5981

a) Chopped point source photometry

Measurements:
PHT-P3 : ppap39200626 FCS = 60 um
PHT-C1 : pcap39200413 FCS = 60 um

Colour correction: black body, T = 4048 K

Model: Hammersley

Det	cwl (μm)	OLP 9	OLP 10	IRAS	Model	Δ (OLP 9)	Δ (OLP 10)
P3	60.0	0.041	0.031	0.108	0.142	-70.94	-78.40
C1	60.0	0.144	0.140	0.108	0.142	1.25	-1.83

b) Background photometry from off-source beam

Det	λ	OLP9 (MJy/sr)	OLP10 (MJy/sr)	COBE (MJy/sr)
P3	60.0	4.31	4.15	6.23
C1	60.0	10.30	9.79	6.23

8.1.4 PHT03 and PHT22 Chopped Photometry of Stars Observed by the MFAINT and CFAINT Programs

Motivation

The faint stars observed repeatedly by the monitoring program MFAINT have also been observed several times in chopped mode by the program CFAINT. MFAINT used the most recommended observation modes (nodding for P1, P2, and P3 and mini-map for C100 and C200). We compare here the results of the measurement set performed on revolution 748. This includes more filters than were later used for the monitoring program.

Method

Both colour corrected nodding and chopped photometry are compared with each other and against the model predictions by Cohen or Hammersley. For detailed results of the noddig photometry cf. Sect. 7. We compare also the flux values of OLP V9.0b10/V9.01 and OLP V10.0b5. Furthermore, we compare the derived background surface brightness with COBE/DIRBE photometry.

Results

For HD 172323 the comparison of the OLP V9.0b10 and OLP V10.0b5 photometry with the model is given in part 2a of the evaluation log. Fig. 8.15 shows the chopped P1 photometry on HD 172323. Both OLP versions yield practically identical results. The resulting fluxes correspond within 25 % with the model flux. This is corrobotated by a monitoring sequence as described in Sect. 8.1.5.
The background photometry from the off-source beam is listed in part 2b of the evaluation log. There is a quite good consistency with the COBE value.
For HR 7310 the comparison of the OLP V9.0b10 and OLP V10.0b5 photometry with the model is given in part 1a of the evaluation log. Fig. 8.16 shows the chopped P2, P3 and C100 photometry on HR 7310. The P2 photometry is improved with OLP 10 and is better than 30 %. For P3 and C100 photometry there is practically no change. At 60 μm the P3 flux is below the model, while the C100 flux is above the model. However, the 180 arcsec aperture was used for the P3 measurements which causes a completely different source-to-background contrast. At 100 μm the chopped photometry flux is 25 % above the model, but is consistent with the flux derived from mini-map photometry (see Sect. 6.1.3). According to [39] the 1 σ cirrus confusion value for 100 μm is estimated to be 13 mJy (using formulae 4, 7 and 8 with B = 5 MJy sr^{-1}, q = 1.6 from 150 arcsec chop throw and γ = 0.19), thus cirrus confusion can account for about 10 – 20 % photometric uncertainty. Therefore, it is unlikely that the discrepancies at 60 μm can be explained by cirrus confusion noise.
The background photometry from the off-source beam is listed in part 1b of the evaluation log. Fig. 8.17 shows the comparison with COBE/DIRBE photometry. There is now a quite good consistency with COBE/DIRBE.
For HR 6705 the comparison of the OLP V9.0b10 and OLP V10.0b5 photometry with the model is given in part 3a of the evaluation log. There are two measurements sets for 90 – 105 μm photometry which used different chopper frequencies. The results of the staring mode pendants are given in Sect. 5.1.2, see part 2 of the evaluation log there. Fig. 8.18 shows the chopped C100 and C200 photometry on HR 6705. The C100 photometry is improved with OLP 10 and is better than 30 %. The chopped photometry yields better photometry than the corresponding staring mode photometry. According to [39] the 1 σ cirrus confusion value for 100 μm is estimated to be 12 mJy (using formulae 4, 7 and 8 with B = 4.5 MJy sr^{-1}, q = 1.0 from 90 arcsec chop throw and an increase by 20 % since the rectangular chop provided only one reference position), thus cirrus confusion can account for about 2 % photometric uncertainty. The 170 μm flux is considerably below the model flux. According to [39] a minimum 1 σ cirrus confusion value for 170 μm is estimated to be 62 mJy (using formulae 6, 7 and 8 with B = 6 MJy sr^{-1}, q = 1.0 from 90 arcsec chop throw and an increase by 20 % since the rectangular chop provided only one reference position; this is strictly valid only for one pixel, but the photometry is performed with the array aperture), thus cirrus confusion can account for at least 20 – 30 % photometric uncertainty. A strong indication for cirrus confusion of this measurement comes from the monitoring program, see Sect. 8.1.5.

The background photometry from the off-source beam is listed in part 3b of the evaluation log. Fig. 8.19 shows the comparison with COBE/DIRBE photometry. The C100 background fluxes are a factor of 2 higher than the COBE photometry and the two measurements also reflect some internal scatter with impact on the relative SED shape; on the other hand staring measurements indicate that the local background is somewhat higher than averaged over the COBE beam (about $7\,\mathrm{MJy\,sr^{-1}}$). The $170\,\mu$m flux fits quite well to the COBE photometry.

Conclusions

- The test case on HD 172323 shows that the P1 chopped photometry accuracy of about 25 % is maintained.
- The P2 photometry is improved with an accuracy better than 30 % for the test case HR 7310.
- P3 photometry of sources fainter than 1 Jy does not give a reliable result. The reason for that is not yet completely clarified.
- C100 photometry of the test source HR 6705 which is brighter than 1 Jy has an accuracy of better than 30 % and also a reasonable relative spectral calibration. For the fainter source HR 7310 the $100\,\mu$m chopped photometry flux is consistent with the mini-map photometry. Cirrus confusion noise can account for $20-30$ % photometric uncertainty for sources of 200 mJy on a background of $4-5\,\mathrm{MJy\,sr^{-1}}$.
- Cirrus confusion noise very likely limits the photometric accuracy of rectangular chopped measurements of sources fainter than 1 Jy for backgrounds brighter than $6\,\mathrm{MJy\,sr^{-1}}$.

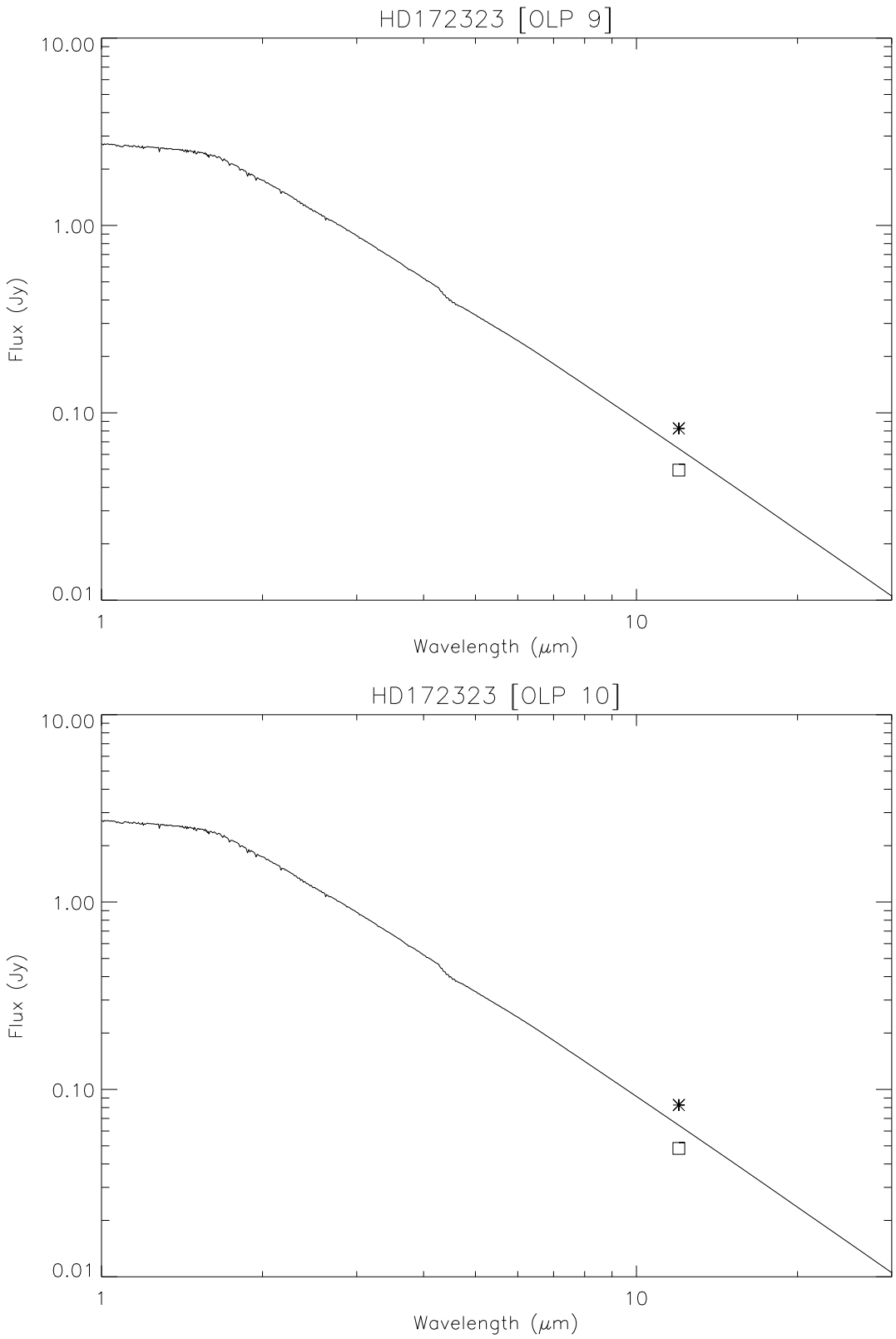

Figure 8.15: Comparison of PHT-P1 chopped photometry with the model spectrum of HD 172323, provided by P. Hammersley, for OLP 9.0b10 (upper panel) and OLP 10.0b5 (lower panel). The meaning of the symbols is the following: solid line: model, asterisk: IRAS, square: PHT-P.

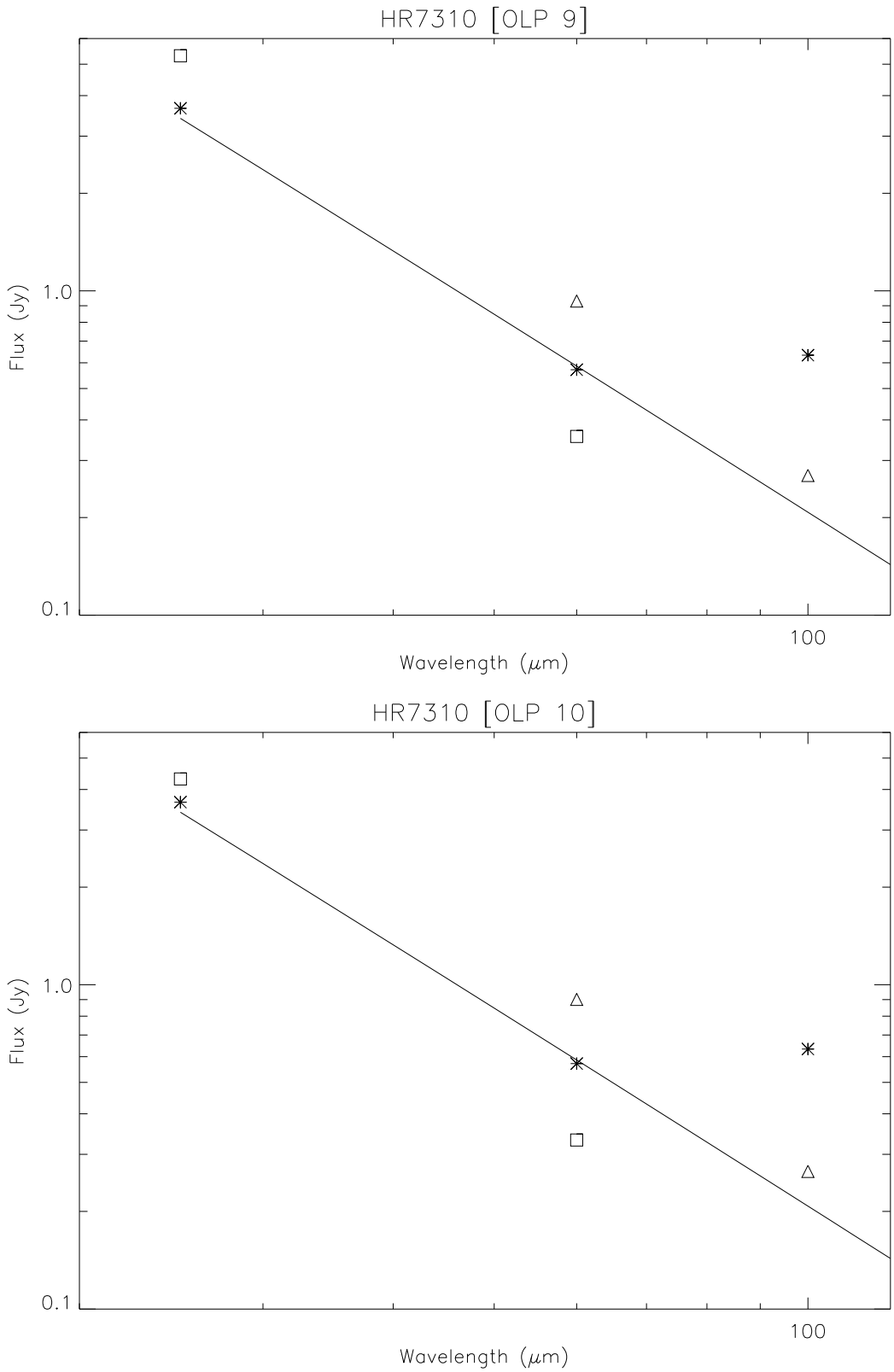

Figure 8.16: Comparison of PHT-P2, -P3 and -C100 chopped photometry with the model spectrum of HR 7310, provided by M. Cohen, for OLP 9.0b10 (upper panel) and OLP 10.0b5 (lower panel). The meaning of the symbols is the following: solid line: model, asterisk: IRAS (100 μm: upper limit), square: PHT-P, triangle: PHT-C100.

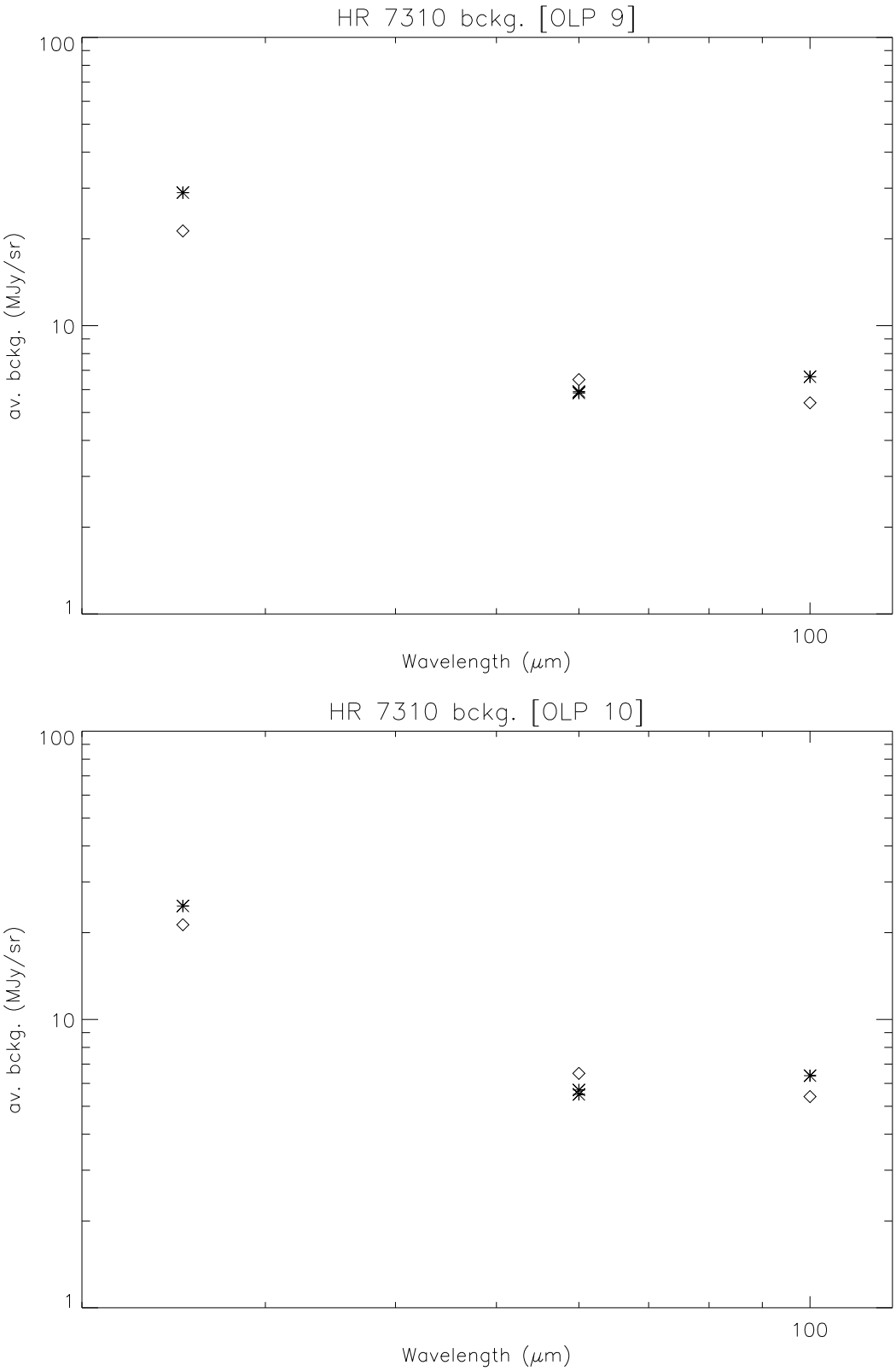

Figure 8.17: Comparison of surface brightness from chopped PHT photometry of the background beam for HR 7310 with COBE, both for OLP 9.0b10 (upper panel) and OLP 10.0b5. Asterisk: PHT-P and PHT-C photometry, diamond: COBE.

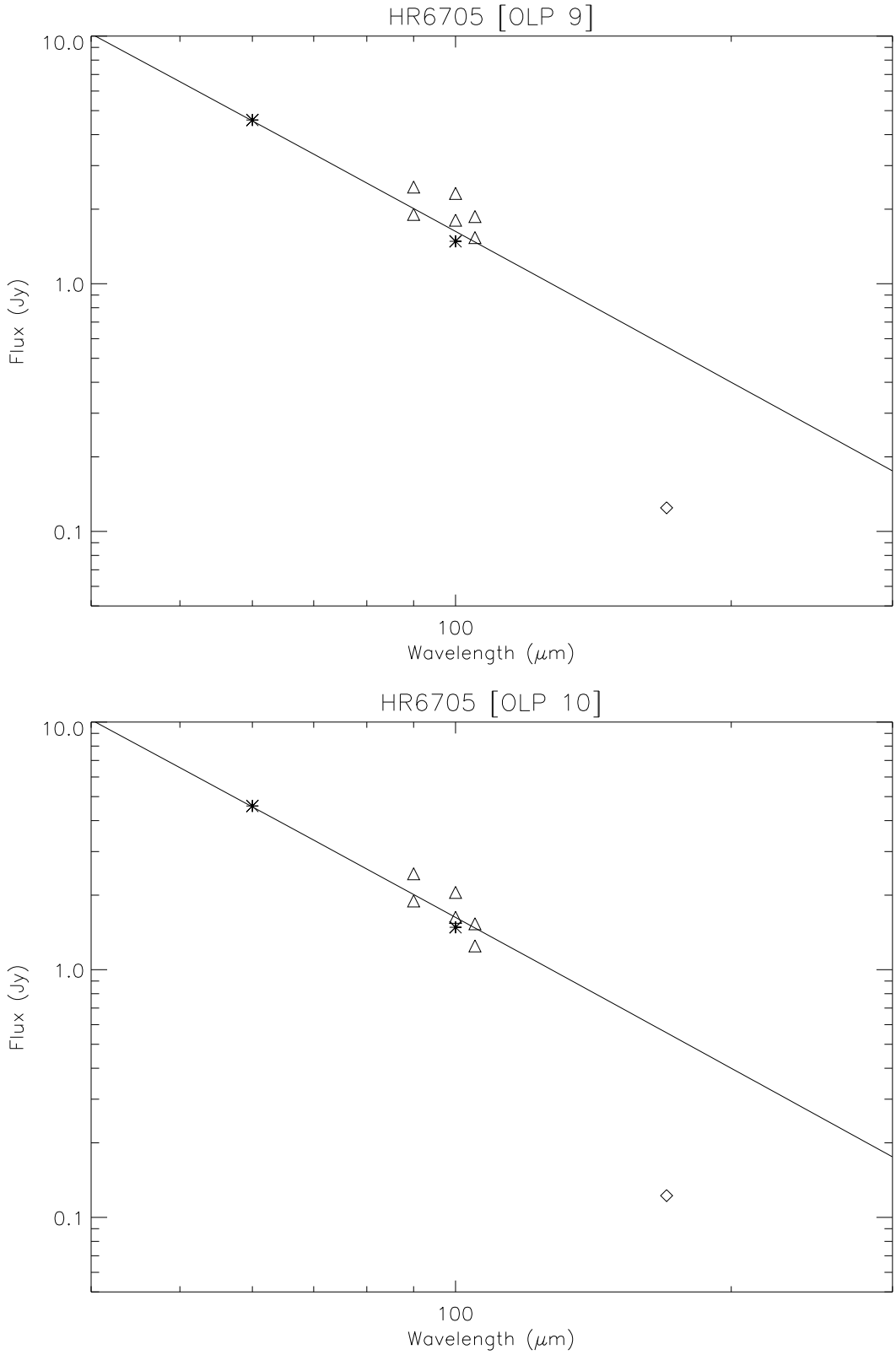

Figure 8.18: Comparison of PHT-C100 and -C200 chopped photometry with the model spectrum of HR 6705 (γ Dra), provided by M. Cohen, for OLP 9.0b10 (upper panel) and OLP 10.0b5 (lower panel). The meaning of the symbols is the following: solid line: model, asterisk: IRAS, triangle: PHT-C100, diamond: PHT-C200.

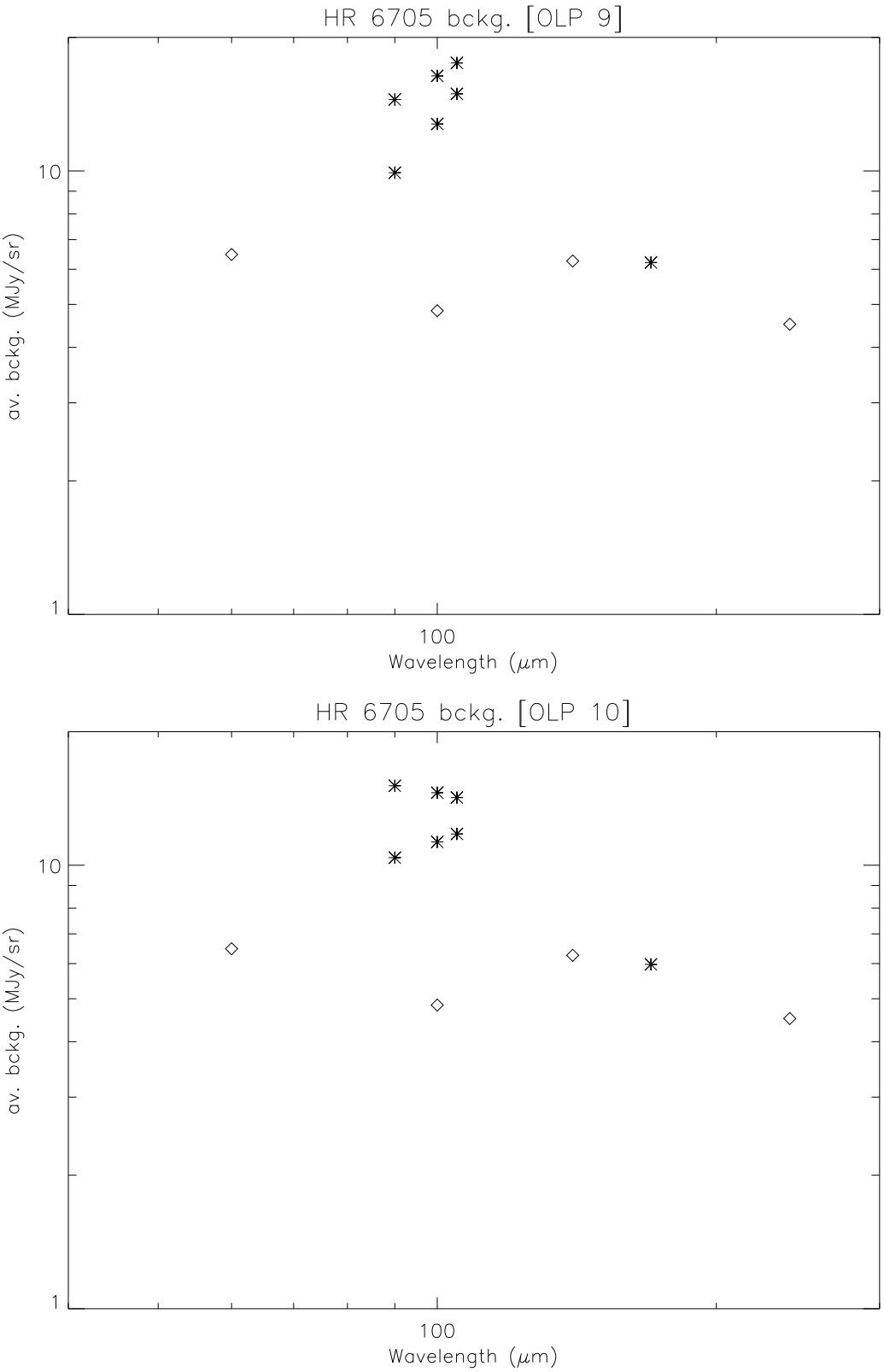

Figure 8.19: Comparison of surface brightness from chopped PHT photometry of the background beam for HR 6705 with COBE, both for OLP 9.0b10 (upper panel) and OLP 10.0b5. Asterisk: PHT-C photometry, diamond: COBE.

Evaluation Log

1) HR 7310

a) Chopped point source photometry

Measurements:
PHT-P2 : ppap74800610 FCS = 25 um
PHT-P3 : ppap74800303 FCS = 60 um
PHT-C1 : pcap74800505 FCS = 60 um

Colour correction: black body, T = 4852 K

Model: Cohen

Det	cwl (μm)	OLP 9	OLP 10	IRAS	Model	Δ (OLP 9)	Δ (OLP 10)
P2	25.0	5.309	4.311	3.656	3.403	56.00	26.69
P3	60.0	0.356	0.332	0.571	0.586	-39.29	-43.34
C1	60.0	0.931	0.901	0.571	0.586	58.76	53.79
C1	100.0	0.270	0.266	0.634	0.208	29.83	27.94

b) Background photometry from off-source beam

Det	λ	OLP9 (MJy/sr)	OLP10 (MJy/sr)	COBE (MJy/sr)
P2	25.0	28.94	24.75	21.31
P3	60.0	5.84	5.50	6.50
C1	60.0	5.90	5.69	6.50
C1	100.0	6.65	6.38	5.40

2) HD 172323

a) Chopped point source photometry

Measurements:
PHT-P1 : ppap74800801 FCS = 12 um

Colour correction: black body, T = 5719 K

Model: Hammersley

Det	cwl (μm)	OLP 9	OLP 10	IRAS	Model	Δ (OLP 9)	Δ (OLP 10)
P1	12.0	0.049	0.048	0.083	0.064	-23.15	-24.73

b) Background photometry from off-source beam

Det	λ	OLP9 (MJy/sr)	OLP10 (MJy/sr)	COBE (MJy/sr)
P1	12.0	15.06	14.24	12.05

3) HR 6705

a) Chopped point source photometry

Measurements:
PHT-C1 (a): pcap67100803 FCS = 90 um
PHT-C1 (b): pcap67100912 FCS = 90 um
PHT-C2 : pcap74801212 FCS = 170 um

Colour correction: black body, T = 4000 K

Model: Cohen

Det	cwl (μm)	OLP 9	OLP 10	IRAS	Model	Δ (OLP 9)	Δ (OLP 10)
C1	90.0	2.457	2.440		2.012	22.10	21.28
C1	100.0	2.316	2.052	1.483	1.627	42.35	26.12
C1	105.0	1.868	1.532		1.474	26.71	3.96
C1b	90.0	1.905	1.895		2.012	-5.31	-5.82
C1b	100.0	1.806	1.627	1.483	1.627	10.98	0.02
C1b	105.0	1.536	1.248		1.474	4.19	-15.33
C2	170.0	0.124	0.122		0.556	-77.62	-77.99

b) Background photometry from off-source beam

Det	λ	OLP9 (MJy/sr)	OLP10 (MJy/sr)	COBE (MJy/sr)
C1	90.0	9.91	10.40	
C1b	90.0	14.48	15.11	
C1	100.0	12.76	11.28	4.84
C1b	100.0	16.37	14.57	4.84
C1	105.0	14.92	11.76	
C1b	105.0	17.51	14.21	
C2	170.0	6.21	5.97	

8.1.5 Reproducibility Assessment of PHT03 and PHT22 Chopped Mode Photometry from CFAINT Program

Motivation

We evaluate here a data set which was obtained for establishing the reproducibility of the chopped photometry mode. This data set helps to investigate the stability of the chopped mode processing. For P1 (12 μm), P3 (60 μm), C100 (100 μm) and C200 (170 μm) the measurement was repeated 6 times, for P2 (25 μm) only 3 times for technical reasons.

Method

We compare the differential source flux against the model prediction by Cohen or Hammersley and the surface brightness of the off-beam against COBE/DIRBE photometry (from weekly maps). This is done for OLP V9.0b10.

Results

Fig. 8.20 shows the reproducibility for P1 on the star HD 172323. The source flux agrees with the model prediction within 25 %. For OLP 10 the surface brightness of the off-beam is consistent with COBE/DIRBE within 15 %. There is no parallel trend in the scatter of differential flux and off-beam surface brightness. For OLP 10 the average flux is 0.056 Jy $\pm$ 0.009 Jy, giving a 1 σ reproducibility accuracy of 16 %. For the off-beam we get 14.5 MJy sr^{-1} $\pm$ 0.8 MJy sr^{-1}, giving a 1 σ reproducibility accuracy of 5 %.
Fig. 8.21 shows the reproducibility for P2 on the star HR 5986. For OLP10 the resulting source flux agrees now with the model prediction within 30 %. The surface brightness of the off-beam is systematically higher than the COBE/DIRBE photometry. There is some correlation between the differential on-source and the off-source flux. The average flux is 0.63 Jy $\pm$ 0.047 Jy, giving a 1 σ reproducibility accuracy of 7 %. For the off-beam we get 33.0 MJy sr^{-1} $\pm$ 3.0 MJy sr^{-1}, giving a 1 σ reproducibility accuracy of 9 %.
Fig. 8.22 shows the reproducibility for P3 on the star HR 7310. For OLP10 The resulting source flux is between 30 and 50 % lower than the model flux. There is some systematic trend in the source flux. During the monitoring period the focal plane rotated by 127 deg. However, the background flux in the off-beam is not anti-correlated with the resulting source flux, so that the measurement itself cannot confirm that structure in the background impacts on the resulting source flux. The background flux is about 15 % below the COBE/DIRBE photometry. The average source flux is 0.365 Jy $\pm$ 0.045 Jy, giving a 1 σ reproducibility accuracy of 12 %. For the off-beam we get 5.6 MJy sr^{-1} $\pm$ 0.1 MJy sr^{-1}, giving a 1 σ reproducibility accuracy of 1.5 %.
Fig. 8.23 shows the reproducibility for C100 again on the star HR 7310, but this time in the 100 μm filter where the star is 2.8 times fainter. The resulting on-source fluxes correspond with the model to better than 30 %. The off-beam surface brightness shows some scatter which is not correlated to the trend of the resulting source flux. For three off-source measurements there is a good consistency with COBE/DIRBE. The average flux is 0.236 Jy $\pm$ 0.029 Jy, giving a 1 σ reproducibility accuracy of 12 %. For the off-beam we get 6.5 MJy sr^{-1} $\pm$ 0.9 MJy sr^{-1}, giving a 1 σ reproducibility accuracy of 14 %.
Fig. 8.24 shows a remarkable strong trend. In the first measurement the resulting source flux is a factor 4.5 less than the model flux. For the second and third measurement the flux is within 20 % of the model flux. For the last three measurements the flux is a factor of 1.6 greater than the model flux. On the other hand the background flux decreases rather smoothly (in contrary to the COBE/DIRBE photometry) from 5.9 to 5.1 MJy sr^{-1}. A surface brightness of 6 MJy sr^{-1} corresponds to 6 Jy total flux in the 4 C200 pixels. A variation by 1 MJy sr^{-1}, i.e. 15 %, leads to 0.9 Jy variation in flux in the C200 array which is approximately the order of variation of the differential flux. The focal plane rotates by 128 deg between first and last measurement, so that background variations could account for this trend. Cirrus confusion noise for the background brightness of 6 MJy sr^{-1} is estimated to have a minimum 1 σ = 0.062 Jy (see Sect. 8.1.4) so that some background gradient with imposed cirrus fluctuations could cause this strong trend.

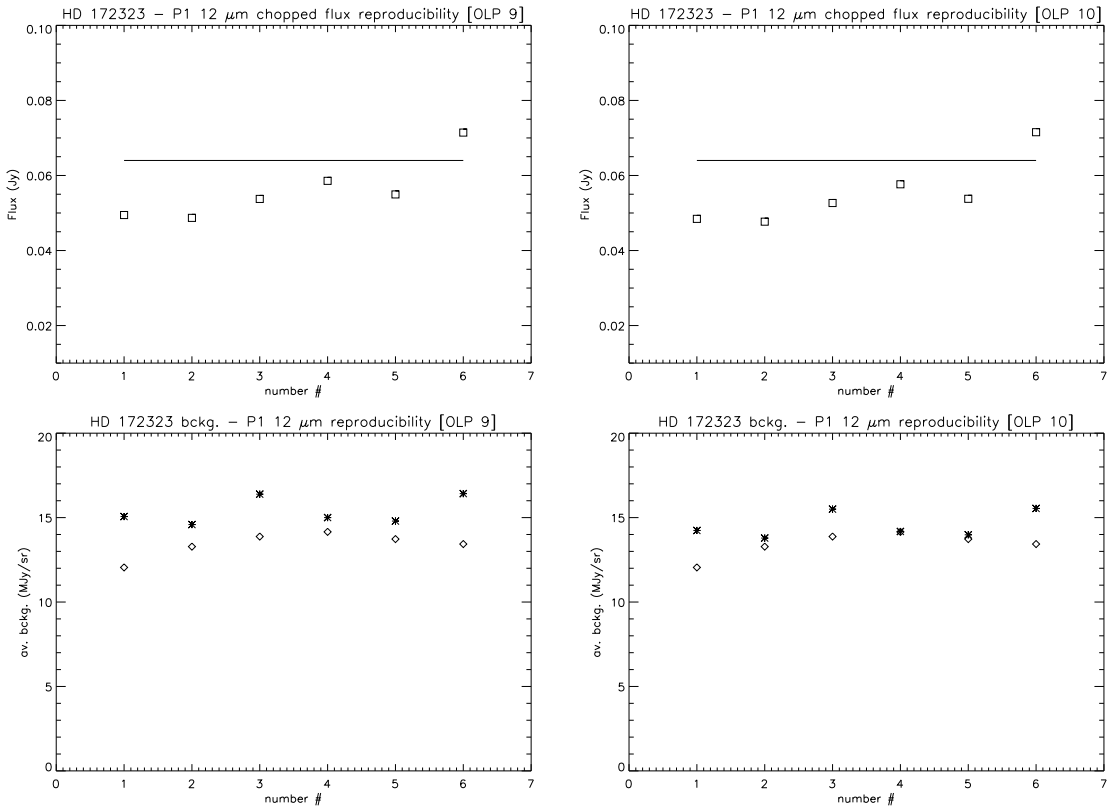

Figure 8.20: Reproducibility of P1 chopped photometry processed with OLP 9.0b10 and OLP 10.0b5 with regard to point source flux derivation and background flux derivation from the off-source beam. The point source fluxes (upper panels, OLP 9.0b10 left and OLP 10.0b5 right) are compared with the flux value of the model of HD 172323, provided by P. Hammersley. The meaning of the symbols is the following: solid line: model flux at 12 μm, square: background subtracted ISOPHOT flux (for info on the revolution refer to the evaluation log). The background fluxes (lower panels, OLP 9.0b10 left and OLP 10.0b5 right) are compared with COBE/DIRBE weekly photometry. The meaning of the symbols is the following: diamond: COBE/DIRBE photometry, asterisk: ISOPHOT background flux.

Conclusions

- For P1, P2, P3 and C100 we find a relative good reproducibility of chopped photometry. For the differential source flux the 1 σ reproducibility is 16, 7, 12 and 12 %, respectively determined from 6 (3 for P2) measurements taken over a period of 126 revolutions. For the surface brightness of the off-beam the 1 σ reproducibility is 5, 9, 1.5 and 14 %, respectively.

- For C200 we find a strong trend with a variation of the differential source flux by a factor of 7.5. This trend may be explained by small scale gradients in the background (on a 3 arcmin step), partially caused by cirrus, when the chop direction rotates with time relative to the sky N-direction (by 128 deg between the first and the last measurement).

- With regard to absolute accuracy of the differential source flux, satisfying results are achieved for P1 ($<$ 25 %), P2 ($<$ 30 %), and C100 ($<$ 30 %). For P3 the derived fluxes are systematically too low (30 - 45 %). For C200 no number can be given due to the strong trend.

- With regard to absolute accuracy of the background surface brightness in the off-beam good consistency with COBE/DIRBE is achieved for P1, P3 and partially C100. For P2 the derived surface brightness is significantly higher than COBE/DIRBE. For C200 the ISOPHOT surface brightness is in general lower than COBE/DIRBE, however the COBE/DIRBE 140 μm surface brightness shows a large scatter, while the ISOPHOT surface brightness displays a smooth behaviour.

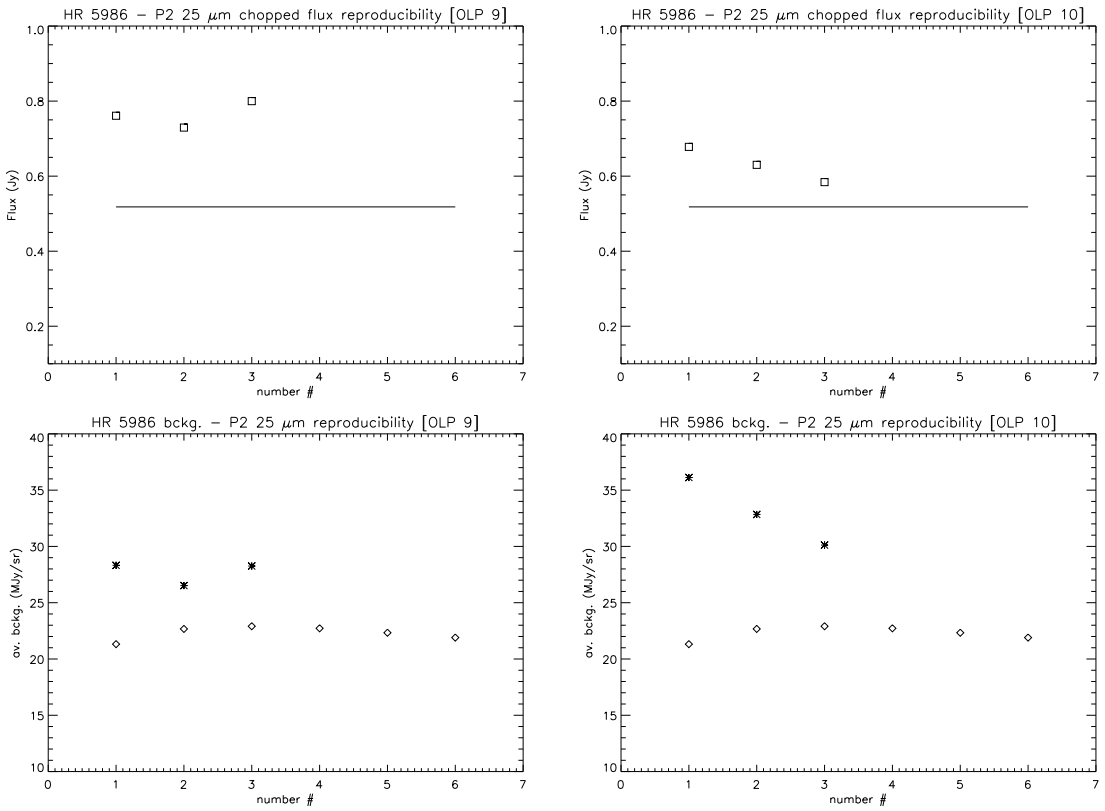

Figure 8.21: Reproducibility of P2 chopped photometry processed with OLP 9.0b10 and OLP 10.0b5 with regard to point source flux derivation and background flux derivation from the off-source beam. The point source fluxes (upper panels, OLP 9.0b10 left and OLP 10.0b5 right) are compared with the flux value of the model of HR 5986, provided by P. Hammersley. The meaning of the symbols is the following: solid line: model flux at 25 μm, square: background subtracted ISOPHOT flux (for info on the revolution refer to the evaluation log). The background fluxes (lower panels, OLP 9.0b10 left and OLP 10.0b5 right) are compared with COBE/DIRBE weekly photometry. The meaning of the symbols is the following: diamond: COBE/DIRBE photometry, asterisk: ISOPHOT background flux.

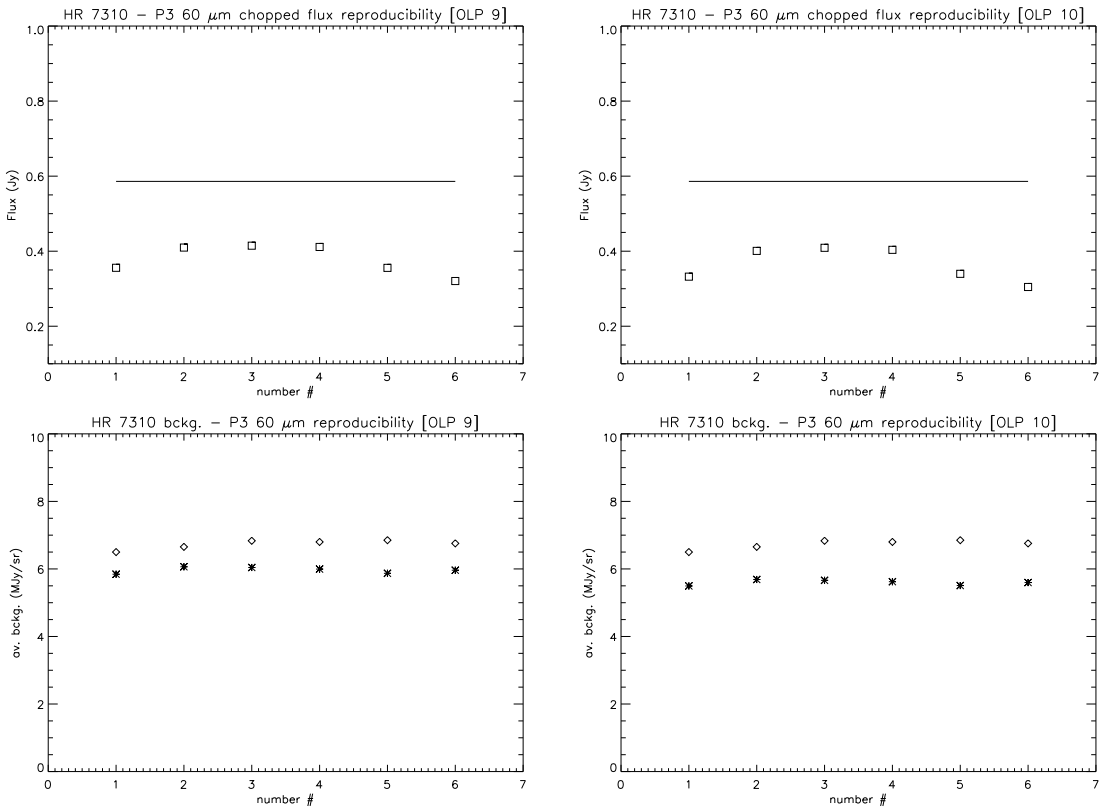

Figure 8.22: Reproducibility of P3 chopped photometry processed with OLP 9.0b10 and OLP 10.0b5 with regard to point source flux derivation and background flux derivation from the off-source beam. The point source fluxes (upper panels, OLP 9.0b10 left and OLP 10.0b5 right) are compared with the flux value of the model of HR 7310, provided by M. Cohen. The meaning of the symbols is the following: solid line: model flux at 60 μm, square: background subtracted ISOPHOT flux (for info on the revolution refer to the evaluation log). The background fluxes (lower panels, OLP 9.0b10 left and OLP 10.0b5 right) are compared with COBE/DIRBE weekly photometry. The meaning of the symbols is the following: diamond: COBE/DIRBE photometry, asterisk: ISOPHOT background flux.

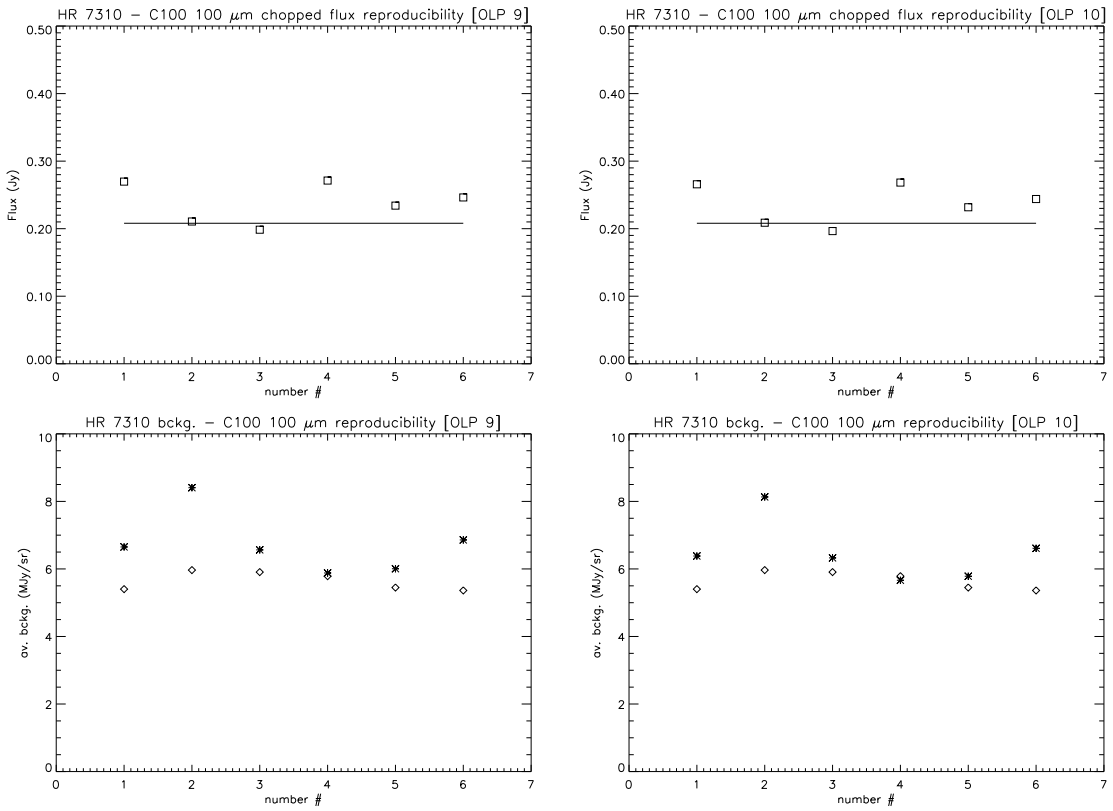

Figure 8.23: Reproducibility of C100 chopped photometry processed with OLP 9.0b10 and OLP 10.0b5 with regard to point source flux derivation and background flux derivation from the off-source beam. The point source fluxes (upper panels, OLP 9.0b10 left and OLP 10.0b5 right) are compared with the flux value of the model of HR 7310, provided by M. Cohen. The meaning of the symbols is the following: solid line: model flux at 100 μm, square: background subtracted ISOPHOT flux (for info on the revolution refer to the evaluation log). The background fluxes (lower panels, OLP 9.0b10 left and OLP 10.0b5 right) are compared with COBE/DIRBE weekly photometry. The meaning of the symbols is the following: diamond: COBE/DIRBE photometry, asterisk: ISOPHOT background flux.

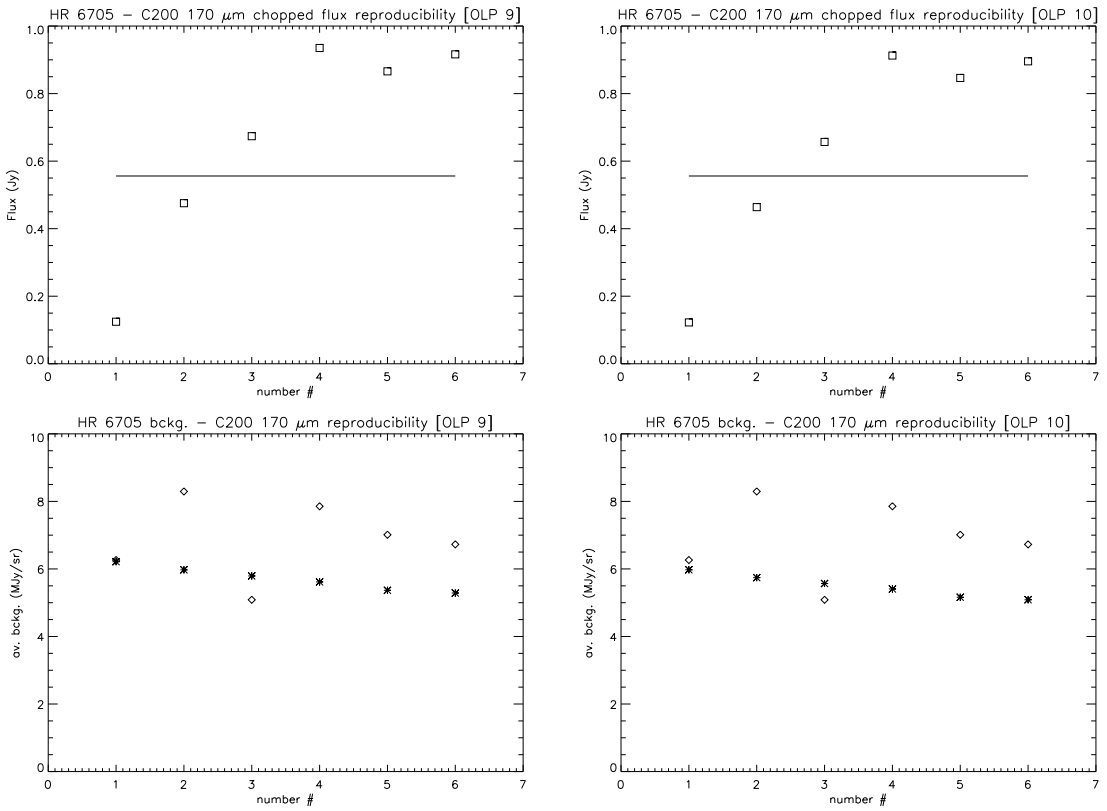

Figure 8.24: Reproducibility of C200 chopped photometry processed with OLP 9.0b10 and OLP 10.0b5 with regard to point source flux derivation and background flux derivation from the off-source beam. The point source fluxes (upper panels, OLP 9.0b10 left and OLP 10.0b5 right) are compared with the flux value of the model of HR 6705, provided by M. Cohen. The meaning of the symbols is the following: solid line: model flux at 170 μm, square: background subtracted ISOPHOT flux (for info on the revolution refer to the evaluation log). The background fluxes (lower panels, OLP 9.0b10 left and OLP 10.0b5 right) are compared with COBE/DIRBE weekly photometry. The meaning of the symbols is the following: diamond: COBE/DIRBE photometry, asterisk: ISOPHOT background flux.

Evaluation Log

1) HD 172323, P1

a) Chopped point source photometry

Measurements:
PHT-P1 : ppap74800801 FCS = 12 um
PHT-P1 : ppap76201302 FCS = 12 um
PHT-P1 : ppap79000801 FCS = 12 um
PHT-P1 : ppap81801801 FCS = 12 um
PHT-P1 : ppap84601901 FCS = 12 um
PHT-P1 : ppap87400601 FCS = 12 um

Colour correction: black body, T = 5719 K

Model: Hammersley

Det	cwl (μm)	OLP 9	OLP 10	IRAS	Model	Δ (OLP 9)	Δ (OLP 10)
P1	12.0	0.049	0.048	0.083	0.064	-23.15	-24.73
P1	12.0	0.049	0.048	0.083	0.064	-24.33	-25.91
P1	12.0	0.054	0.053	0.083	0.064	-16.48	-18.18
P1	12.0	0.059	0.058	0.083	0.064	-8.99	-10.42
P1	12.0	0.055	0.054	0.083	0.064	-14.62	-16.44
P1	12.0	0.071	0.072	0.083	0.064	10.98	11.14

b) Background photometry from off-source beam

Det	λ	OLP9 (MJy/sr)	OLP10 (MJy/sr)	COBE (MJy/sr)
P1	12.0	15.06	14.24	12.05
P1	12.0	14.59	13.79	13.28
P1	12.0	16.39	15.50	13.88
P1	12.0	15.00	14.18	14.15
P1	12.0	14.79	13.98	13.73
P1	12.0	16.42	15.54	13.43

2) HR 5986, P2

a) Chopped point source photometry

Measurements:
PHT-P2 : ppap74801002 FCS = 25 um
PHT-P2 : ppap76201104 FCS = 25 um
PHT-P2 : ppap79000502 FCS = 25 um

Colour correction: black body, T = 6084 K

Model: Hammersley

Det	cwl (μm)	OLP 9	OLP 10	IRAS	Model	Δ (OLP 9)	Δ (OLP 10)
P2	25.0	0.761	0.678	0.527	0.518	46.77	30.76
P2	25.0	0.729	0.630	0.527	0.518	40.68	21.54
P2	25.0	0.800	0.584	0.527	0.518	54.26	12.65

b) Background photometry from off-source beam

Det	λ	OLP9 (MJy/sr)	OLP10 (MJy/sr)	COBE (MJy/sr)
P2	25.0	28.32	36.12	21.32
P2	25.0	26.52	32.84	22.67
P2	25.0	28.26	30.12	22.91

3) HR 7310, P3

a) Chopped point source photometry

Measurements:

PHT-P3 :	ppap74800303	FCS = 60 um
PHT-P3 :	ppap76201506	FCS = 60 um
PHT-P3 :	ppap79000903	FCS = 60 um
PHT-P3 :	ppap81802103	FCS = 60 um
PHT-P3 :	ppap84602003	FCS = 60 um
PHT-P3 :	ppap87400503	FCS = 60 um

Colour correction: black body, T = 4852 K

Model: Cohen

Det	cwl (μm)	OLP 9	OLP 10	IRAS	Model	Δ (OLP 9)	Δ (OLP 10)
P3	60.0	0.356	0.332	0.571	0.586	-39.29	-43.34
P3	60.0	0.410	0.401	0.571	0.586	-30.11	-31.61
P3	60.0	0.415	0.409	0.571	0.586	-29.26	-30.21
P3	60.0	0.411	0.404	0.571	0.586	-29.84	-31.13
P3	60.0	0.356	0.340	0.571	0.586	-39.33	-42.04
P3	60.0	0.321	0.305	0.571	0.586	-45.31	-48.02

b) Background photometry from off-source beam

Det	λ	OLP9 (MJy/sr)	OLP10 (MJy/sr)	COBE (MJy/sr)
P3	60.0	5.84	5.50	6.50
P3	60.0	6.06	5.69	6.65
P3	60.0	6.04	5.66	6.83
P3	60.0	6.00	5.62	6.80
P3	60.0	5.87	5.51	6.85
P3	60.0	5.96	5.60	6.76

4) HR 7310, C100

a) Chopped point source photometry

Measurements:
PHT-C100 : pcap74800505 FCS = 100 um
PHT-C100 : pcap76201508 FCS = 100 um
PHT-C100 : pcap79000904 FCS = 100 um
PHT-C100 : pcap81802104 FCS = 100 um
PHT-C100 : pcap84602004 FCS = 100 um
PHT-C100 : pcap87400504 FCS = 100 um

Colour correction: black body, T = 4852 K

Model: Cohen

Det	cwl (μm)	OLP 9	OLP 10	IRAS	Model	Δ (OLP 9)	Δ (OLP 10)
C1	100.0	0.270	0.266	0.634	0.208	29.83	27.94
C1	100.0	0.211	0.209	0.634	0.208	1.40	0.53
C1	100.0	0.198	0.196	0.634	0.208	-4.44	-5.42
C1	100.0	0.271	0.268	0.634	0.208	30.60	29.17
C1	100.0	0.234	0.232	0.634	0.208	12.72	11.57
C1	100.0	0.246	0.244	0.634	0.208	18.56	17.42

b) Background photometry from off-source beam

Det	λ	OLP9 (MJy/sr)	OLP10 (MJy/sr)	COBE (MJy/sr)
C1	100.0	6.65	6.38	5.40
C1	100.0	8.40	8.13	5.97
C1	100.0	6.56	6.33	5.91
C1	100.0	5.88	5.66	5.79
C1	100.0	6.01	5.78	5.45
C1	100.0	6.86	6.61	5.36

5) HR 6705, C200

a) Chopped point source photometry

Measurements:
PHT-C200 : pcap74801212 FCS = 170 um
PHT-C200 : pcap76201014 FCS = 170 um
PHT-C200 : pcap79000605 FCS = 170 um
PHT-C200 : pcap81800705 FCS = 170 um
PHT-C200 : pcap84600805 FCS = 170 um
PHT-C200 : pcap87400705 FCS = 170 um

Colour correction: black body, T = 4000 K

Model: Cohen

Det	cwl (μm)	OLP 9	OLP 10	IRAS	Model	Δ (OLP 9)	Δ (OLP 10)
C2	170.0	0.124	0.122		0.556	-77.62	-77.99
C2	170.0	0.475	0.464		0.556	-14.54	-16.63
C2	170.0	0.674	0.657		0.556	21.14	18.08
C2	170.0	0.935	0.913		0.556	68.07	64.05
C2	170.0	0.866	0.846		0.556	55.64	52.13
C2	170.0	0.916	0.896		0.556	64.70	60.98

b) Background photometry from off-source beam

Det	λ	OLP9 (MJy/sr)	OLP10 (MJy/sr)	COBE (MJy/sr)
C2	170.0	6.21	5.97	6.26
C2	170.0	5.97	5.74	8.29
C2	170.0	5.79	5.57	5.09
C2	170.0	5.62	5.41	7.86
C2	170.0	5.37	5.16	7.01
C2	170.0	5.29	5.09	6.73

8.2 Chopped Photometry Test Cases with Staring Mode References on other Revolutions

Summary

- P2 chopped photometry has been improved yielding reasonable accuracies.
- P3 chopped photometry on sources brighter than 5 Jy provides reasonable accuracy.
- C100 chopped point source photometry on small extended sources is likely to underestimate fluxes, since only the central pixel of the array is used.

8.2.1 PHT03 and PHT22 Chopped Mode: The FIR Excess SED of Vega

Motivation

We investigate here observations of a general observer's program for which photometry using Interactive Analysis has been published, cf. Ref. [14]. In addition, IRAS photometry at 25, 60, and 100 μm is available.

Method

We compare the color corrected source flux values of both OLP V9.01 and OLP V10.0b5 with model fluxes, IRAS photometry and the photometry derived in [14] (called HWK photometry in the following).
The color correction was dependent on the relative contribution by the stellar photosphere and the IR disc, and hence on the wavelength. We followed the description as given in Ref.[14]:

- from 60 to 100 μm the SED behaves like an 80 K modified BB, $\varepsilon \propto \nu$
- from 20 to 25 μm the SED is a mixture of a 10000 K BB and an 80 K modified BB with a ratio 2:1.

Results

For Vega the assessment of the OLP V9.01 and OLP V10.0b5 photometry is given in part 1 of the evaluation log. Note that the Δs computed w.r.t. the photospheric model of Cohen are only a measure of the excess and not of the calibration accuracy!
Fig. 8.25 shows the chopped P2, P3, C100 and C200 photometry on Vega. The consistency of the P2 25 μm photometry with IRAS photometry is now better than 10 %. Also the P3 60 and 100 μm photometry agree with IRAS photometry within 15 %. The relative spectral shapes deduced from the chopped C100 and C200 photometry remain weird and the behaviour is not understood. The C100 chopped photometry only uses the central pixel of the array. The fluxes are corrected for the PSF fraction outside the pixel. Since the FIR flux of Vega is extended a larger correction has to be applied. At 60 μm the ratio of the central pixel PSF to a 22 arcsec Gaussian is $0.667/0.569 = 1.17$. This scales the C100 60 μm fluxes up to 6.88 and 7.94 Jy and brings them into better agreement with the P3 and IRAS 60 μm photometry.
The background photometry from the off-source beam is listed in part 2 of the evaluation log. Fig. 8.26 shows the comparison with COBE/DIRBE photometry. The P2 25 μm background flux is now closer to COBE/DIRBE, yet a factor of 2 higher. P3 and C100 backround fluxes are at least a factor of 2 higher than COBE/DIRBE, except of the P3 100 μm background value which agrees quite well with the COBE/DIRBE flux. The C200 background fluxes are about in the right range.

Conclusions

- The P2 photometry has been improved for this target and is now in good agreement with the IRAS photometry. The derived surface brightness in the off-beam is not consistent with COBE/DIRBE photometry.
- The P3 photometry shows a good performance, indicating that for brighter sources the flux deficits found in the previous chapters disappear.
- The C100 photomery displays a strange behaviour with a steep flux fall-off towards longer wavelengths. This was already observed for earlier OLP versions and the reason for this is not yet understood. Also the C100 surface brightness photometry of the off-beam is very discrepant from COBE/DIRBE. A correction for the extension of Vega brings the 60 μm fluxes in better accordance with the P3 and IRAS photometry.
- While the C200 surface brightness of the off-beam shows a relatively smooth behaviour which is quite consistent with COBE/DIRBE, the C200 part of the SED appears to

be too oblique and does not fit with the IRAS and P3 photometry. Furthermore the data points show a relatively large scatter.

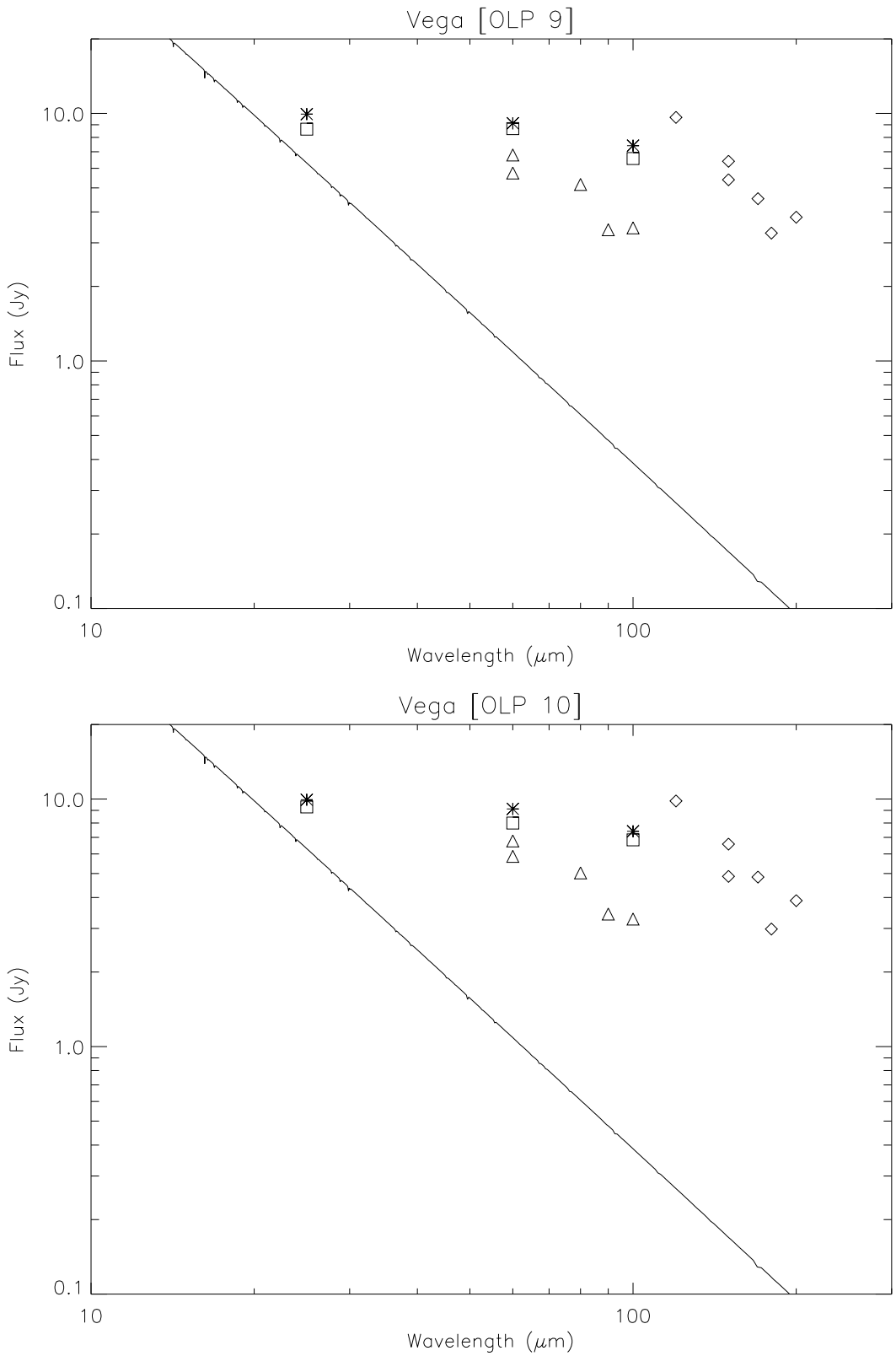

Figure 8.25: Comparison of PHT-P and PHT-C chopped photometry with the photospheric model of Vega by M. Cohen and with IRAS photometry both for OLP 9.01 (upper panel) and OLP 10.0b5 (lower panel). Color correction has been applied according to the description in the method section. The meaning of the symbols is the following: solid line: photospheric model, asterisk: IRAS, square: PHT-P (P03 AOT), triangle: C100 (P22 AOT), diamond: C200 (P22 AOT).

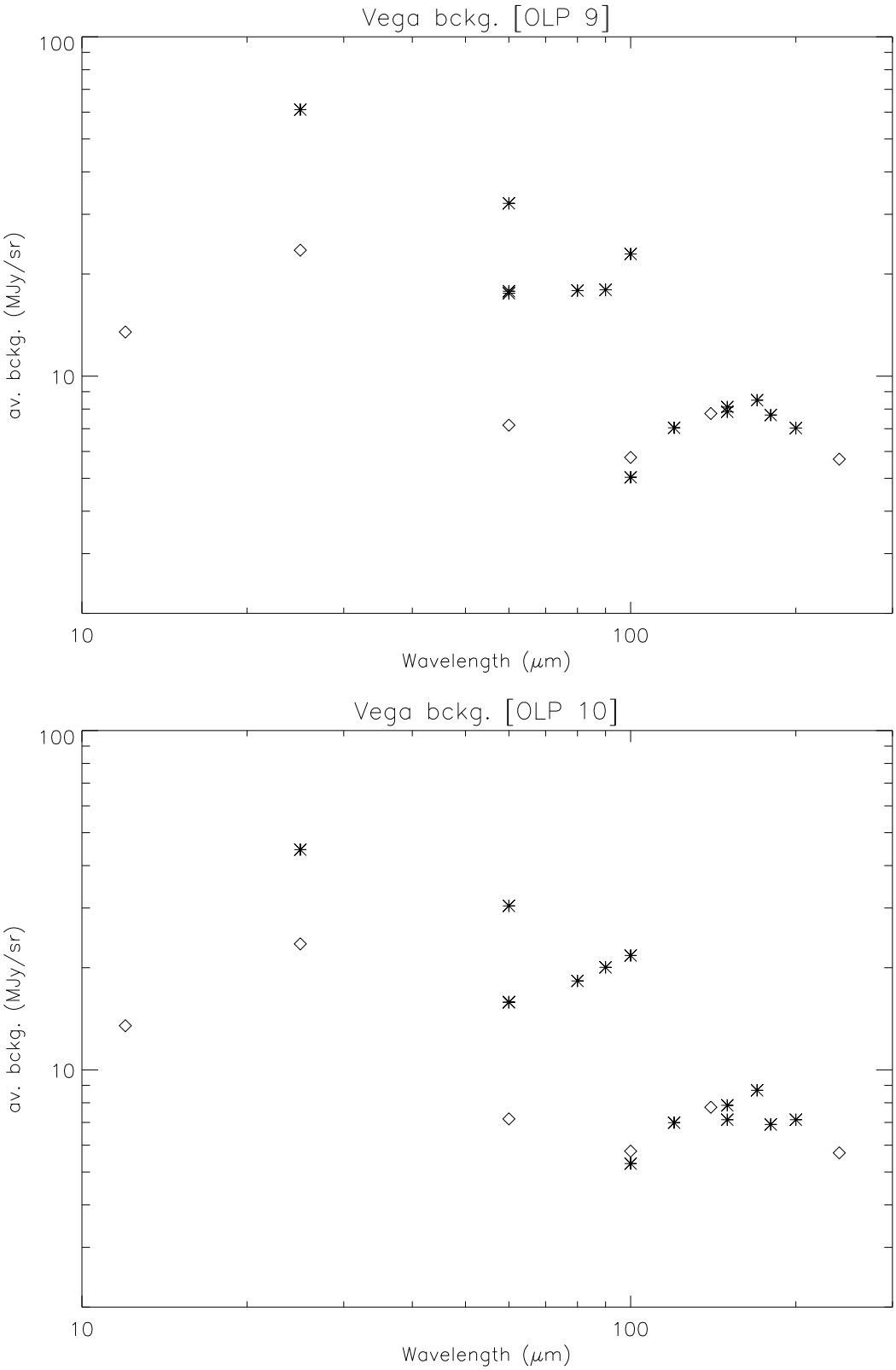

Figure 8.26: Comparison of surface brightness from chopped PHT photometry of the background beam for Vega with COBE, both for OLP 9.01 (upper panel) and OLP 10.0b5 (lower panel). Asterisk: PHT-P and PHT-C photometry, diamond: COBE.

Evaluation Log

1) Chopped Point Source Photometry

Measurements:

PHT-P:	ppap08900788	FCS = 25 um
	ppap08500241	FCS = 100 um
PHT-C:	pcap08900789	FCS = 90 um
	pcap08900790	FCS = 150 um
	pcap10601101	FCS = 60, 170 um

Colour correction: mixture of 10000K BB & 80K modified (em.=1) BB
see text for details

Model: Cohen

Det	cwl (μm)	OLP 9	OLP 10	IRAS	Model	Δ (OLP 9)	Δ (OLP 10)
P2	25.0	8.636	9.292	9.938	6.301	37.06	47.48
P3	60.0	8.678	7.998	9.121	1.087	698.66	636.06
P3	100.0	6.573	6.841	7.408	0.387	1600.66	1670.02
C1	60.0	5.744	5.867	9.121	1.087	428.60	439.96
C1	90.0	3.389	3.431		0.478	608.72	617.56
C2	150.0	5.392	4.871		0.169	3081.46	2773.93
C2	180.0	3.285	2.984		0.117	2706.84	2450.12
C1	60.0	6.793	6.771	9.121	1.087	525.12	523.11
C1	80.0	5.163	5.030		0.607	750.87	728.94
C1	100.0	3.448	3.274	7.408	0.387	791.97	747.18
C2	120.0	9.637	9.821		0.267	3510.43	3579.47
C2	150.0	6.407	6.576		0.169	3680.42	3779.99
C2	170.0	4.523	4.837		0.129	3417.64	3661.47
C2	200.0	3.806	3.885		0.094	3945.92	4029.59

Note: The Δs do not give calibration accuracies here!

2) Background photometry from off-source beam

Det	λ	OLP9 (MJy/sr)	OLP10 (MJy/sr)	COBE (MJy/sr)
P2	25.0	61.02	44.58	23.51
P3	60.0	17.79	15.85	7.17
C1	60.0	17.55	15.81	7.17
C1	60.0	32.30	30.43	7.17
C1	80.0	17.88	18.29	
C1	90.0	17.97	20.05	
P3	100.0	5.04	5.29	5.76
C1	100.0	22.91	21.73	5.76
C2	120.0	7.04	6.99	
C2	150.0	8.11	7.13	7.76
C2	150.0	7.85	7.86	7.76
C2	170.0	8.49	8.71	
C2	180.0	7.68	6.91	
C2	200.0	7.03	7.13	5.69

8.2.2 PHT03 Chopped Mode: The SED of Sirius (HR 2491)

Motivation

We check the improvement in quality for P2 chopped photometry on the bright star Sirius for which also absolute photometry measurements in staring mode are available (cf. Sect. 5.2.2).

Method

We compare the color corrected flux values of both OLP V9.0b6 and OLP V10.0b5 results against the model prediction by Cohen and IRAS photometry.

Results

For Sirius the assessment of the OLP V9.0b6 and OLP V10.0b5 photometry is given in part 1 of the evaluation log. Fig. 8.27 shows the chopped P2 photometry on Sirius. Although there is a slight decrease in accuracy w.r.t. OLP 9, the accuracy is maintained sufficiently good verifying the overall P2 chopped photometry improvement on this high flux level.

Conclusions

- The quality of the P2 chopped photometry accuracy is verified at a high flux level of 20 Jy with an accuracy of better than 15 %.

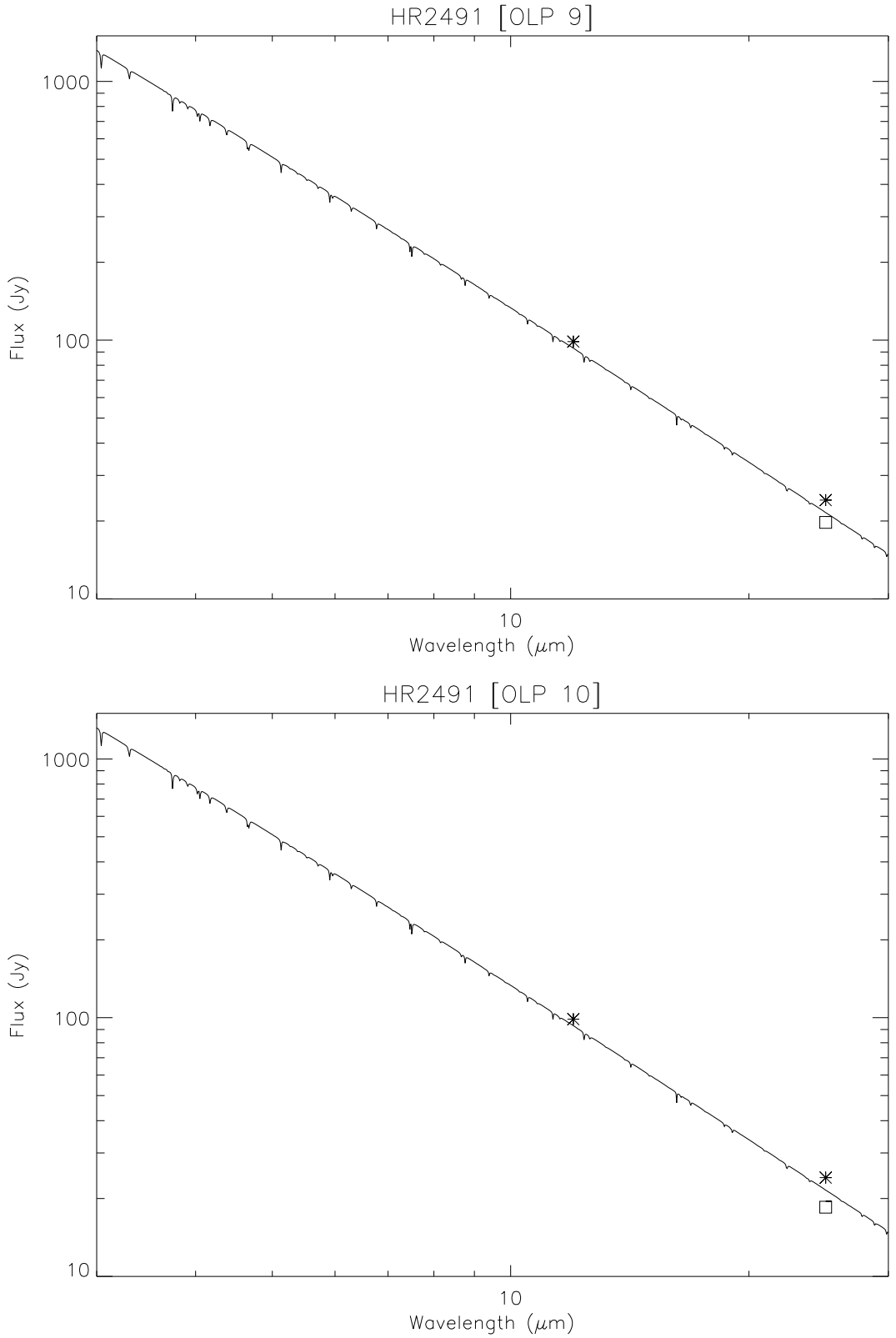

Figure 8.27: Comparison of PHT-P chopped photometry with the composite spectrum of Sirius (HR 2491) provided by M. Cohen and with IRAS photometry for OLP 9.0b6 (upper panel) and OLP 10.0b5 (lower panel). All photometric points are color corrected for a 10000 K BB. The meaning of the symbols is the following: solid line: model, asterisk: IRAS, square: PHT-P (P03 AOT).

Evaluation Log

1) Chopped Point Source Photometry

Measurements:
PHT-P: PPAP72301710 FCS = 25 um

Colour correction: black body, T = 10000 K

Model: Cohen

Det	cwl (μm)	OLP 9	OLP 10	IRAS	Model	Δ (OLP 9)	Δ (OLP 10)
P2	25.0	19.762	18.521	24.092	21.541	-8.26	-14.02

8.2.3 PHT03 Chopped Mode: The SED of HR 337

Motivation

We check the quality for P3 chopped photometry on the bright star HR 337 for which also sparse map photometry measurements in staring mode are available (cf. Sect. 5.3.1).

Method

We compare the color corrected flux values of both OLP V9.0b6 and OLP V10.0b5 results against the model prediction by Cohen and IRAS photometry.

Results

For HR 337 the assessment of the OLP V9.0b6 and OLP V10.0b5 photometry is given in part 1 of the evaluation log. We estimate the absolute photometric accuracy as the deviation from the model flux in the filter in which the FCS calibration was done, and the relative filter-to-filter accuracy as the peak-to-peak variation of the others filters around this offset. Fig. 8.28 shows the chopped P3 photometry on HR 337. The quality of the 100 μm flux (relative calibration) is somewhat worse for OLP 10. We derive an absolute calibration of better than 10 % and a relative filter-to-filter calibration of better than 20 %.

Conclusions

- The quality of P3 chopped photometry is maintained at the bright flux level (several Jy) with an absolute accuracy of better than 10 % and a relative accuracy of better than 20 %.

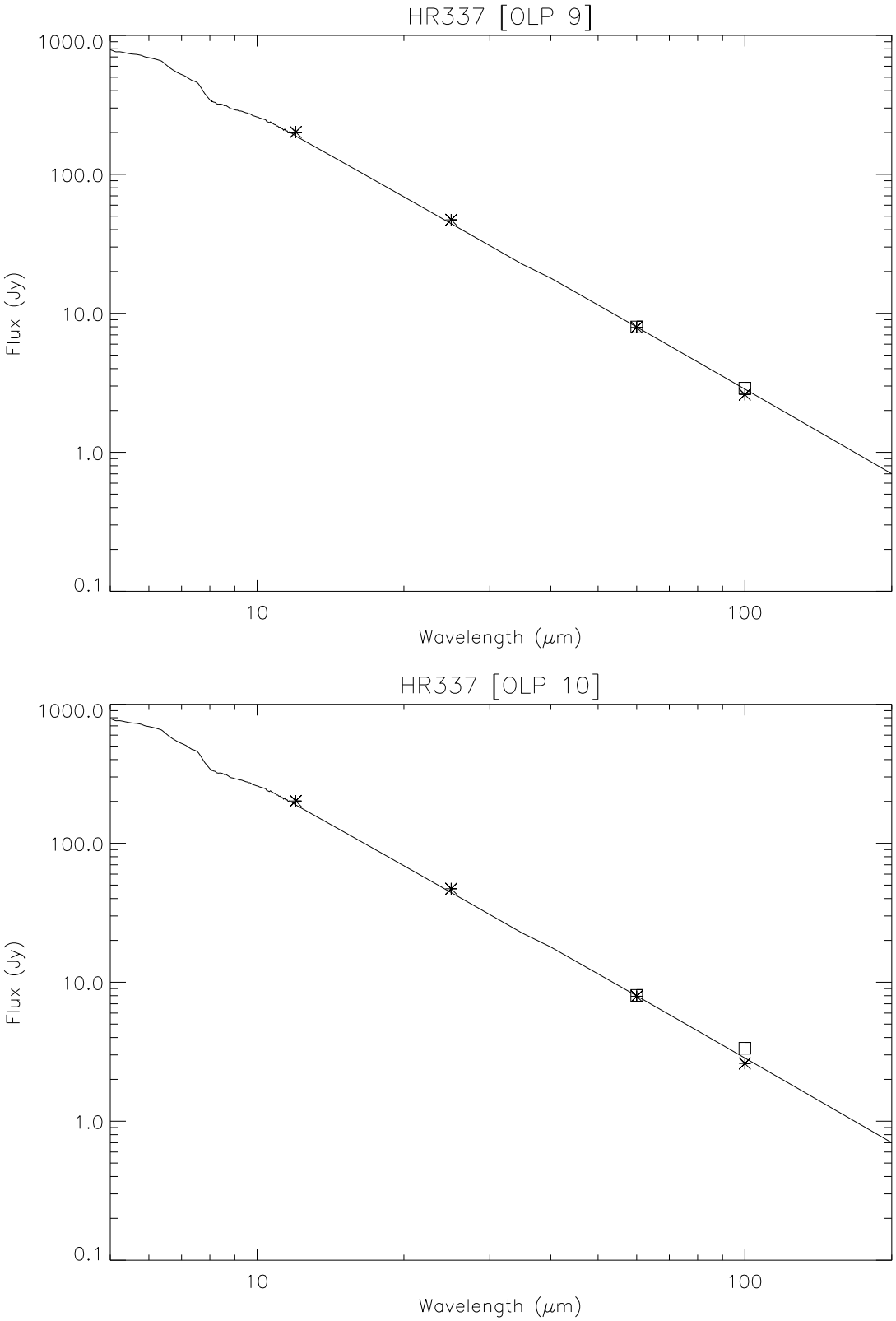

Figure 8.28: Comparison of PHT-P chopped photometry with the composite spectrum of HR 337 plus extrapolation out to 300 μm provided by M. Cohen and with IRAS photometry for OLP 9.0b6 (upper panel) and OLP 10.0b5 (lower panel). All photometric points are color corrected for a 3839 K BB. The meaning of the symbols is the following: solid line: model, asterisk: IRAS, square: PHT-P (P03 AOT).

Evaluation Log

1) Chopped Point Source Photometry

Measurements:
PHT-P3: ppap45002409 FCS = 60 um

Colour correction: black body, T = 3839 K

Model: Cohen

Det	cwl (μm)	OLP 9	OLP 10	IRAS	Model	Δ (OLP 9)	Δ (OLP 10)
P3	60.0	7.975	8.036	7.924	7.972	0.03	0.81
P3	100.0	2.896	3.351	2.603	2.851	1.58	17.55

8.2.4 PHT03 Chopped Mode: The SED of HR 617

Motivation

We check the quality for P3 chopped photometry on the intermediate bright star HR 617 for which also absolute photometry measurements in staring mode (cf. Sect. 5.2.3) and nodding observations are available.

Method

We compare the color corrected flux values of both OLP V9.0b6 and OLP V10.0b5 results against the model prediction by Cohen and IRAS photometry.

Results

For HR 617 the assessment of the OLP V9.0b6 and OLP V10.0b5 photometry is given in part 1 of the evaluation log. We estimate the absolute photometric accuracy as the deviation from the model flux in the filter in which the FCS calibration was done, and the relative filter-to-filter accuracy as the peak-to-peak variation of the others filters around this offset. Fig. 8.29 shows the chopped P3 photometry on HR 617. For OLP 10 both the absolute and the relative calibration accuracy is improved. We derive an absolute accuracy of better than 10 % and a relative filter-to-filter calibration of about 25 %.

Conclusions

- The quality of P3 chopped photometry is maintained at the intermediate bright flux level ($1 - 2$ Jy) with an absolute accuracy of better than 10 % and a relative accuracy of about 25 %.

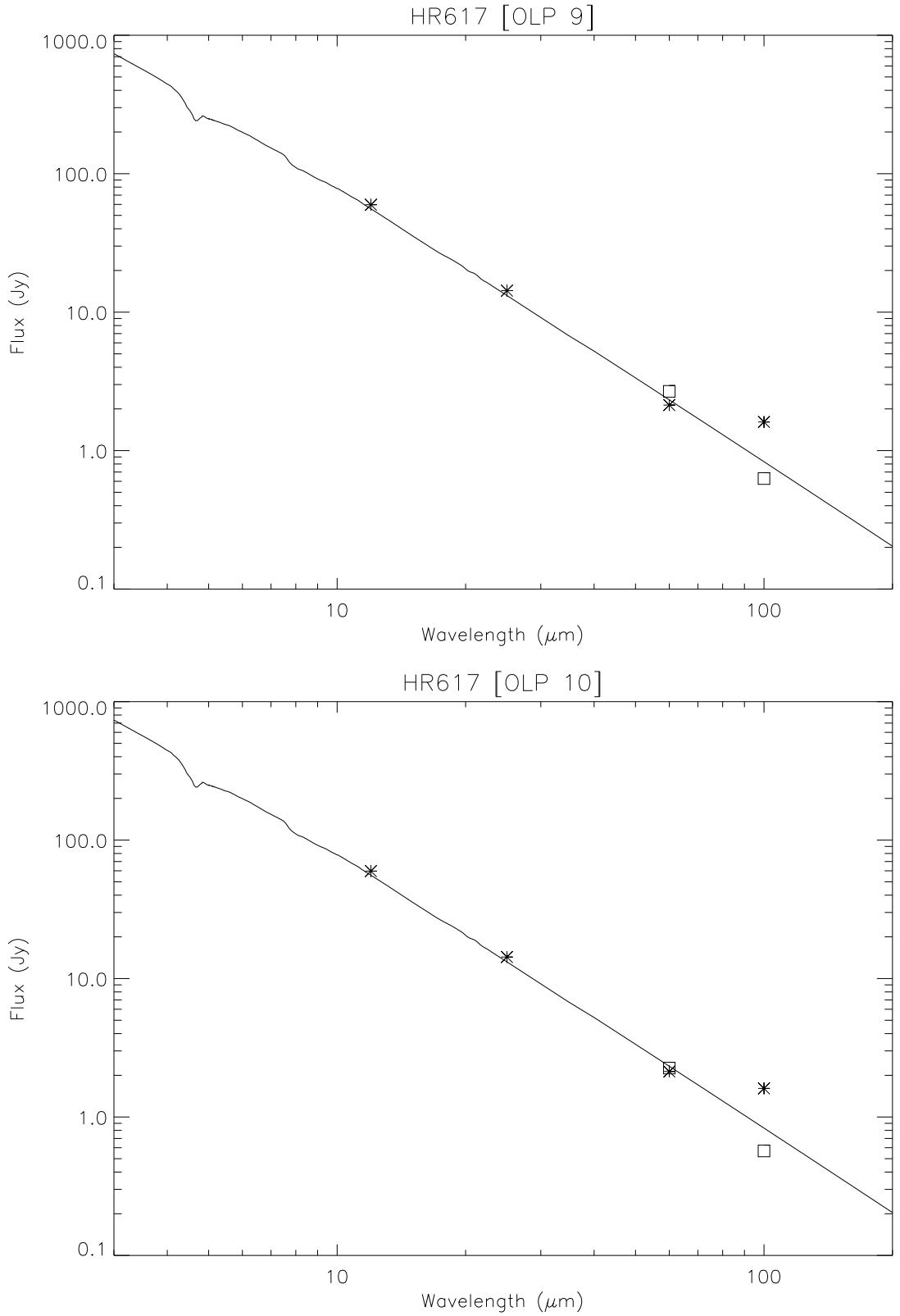

Figure 8.29: Comparison of PHT-P chopped photometry with the composite spectrum of HR 617 plus extrapolation out to 300 μm provided by M. Cohen and with IRAS photometry for OLP 9.0b6 (upper panel) and OLP 10.0b5 (lower panel). All photometric points are color corrected for a 4000 K BB. The meaning of the symbols is the following: solid line: model, asterisk: IRAS, square: PHT-P (P03 AOT).

Evaluation Log

1) Chopped Point Source Photometry

Measurements:
PHT-P3: ppap45002409 FCS = 100 um

Colour correction: black body, T = 4000 K

Model: Cohen

Det	cwl (μm)	OLP 9	OLP 10	IRAS	Model	Δ (OLP 9)	Δ (OLP 10)
P3	60.0	2.678	2.254	2.131	2.325	15.20	-3.04
P3	100.0	0.629	0.568	1.609	0.831	-24.40	-31.63

8.2.5 PHT03 Chopped Mode: The SED of HR 6847

Motivation

We check the quality for P1 multi-filter chopped photometry on the intermediate bright star HR 6847 for which also multi-filter photometry measurements in staring mode (cf. Sect. 5.1.4) are available. There are actually three measurements of the star so that a reproducibility assessment can be done, too.

Method

We compare the color corrected flux values of both OLP V9.0b6 and OLP V10.0b5 results against the model prediction by Hammersley and IRAS photometry.

Results

For HR 6847 the assessment of the OLP V9.0b6 and OLP V10.0b5 photometry is given in parts 1 (Routine Phase measurements) and 2 (Performance Verification Phase measurements) of the evaluation log. The routine phase measurements were done with a 79 arcsec aperture and the performance verification phase measurements in a 23 arcsec aperture. Both apertures are not the standard apertures for most filters in use and in particular for the 12 μm band different behaviour may be explained partially by beam effects. We estimate the absolute photometric accuracy as the deviation from the model flux in the filter in which the FCS calibration was done, and the relative filter-to-filter accuracy as the peak-to-peak variation of the others filters around this offset. Figs. 8.30 and 8.31 show the chopped P1 photometry on HR 6847. The absolute photometric accuracy in the 3.6 mum filter is very good (better than 10 %) and the reproducibility is very good (the three measurements yield the same 3.6 μm fluxes within 3 %.). For the relatively calibrated filters (these measurements are performed first in the measurement sequence) there are some ambiguous results. For the routine phase measurement the relative filter calibration is as good as 25 %. For the performance verification phase measurements, the 12 μm fluxes are reproducibly off by about a factor of 1.8. This might be due to impact of transient effects. The use of a small aperture with strong asymmetries of the beam profile and in addition some dependence on the operational detector temperature (P1 was not temperature controlled and the temperature environment during the PV Phase was different) may be linked to this behaviour.

Conclusions

- The in general good performance of chopped P1 photometry on intermediate bright objects is confirmed for this test case.
- We find a quite good reproducibility ($\pm$ 3 %) for the absolute calibration accuracy.
- Discrepancies of the relative caibration of the 12 μm filter could be linked to the use of different apertures introducing different transient behaviour.

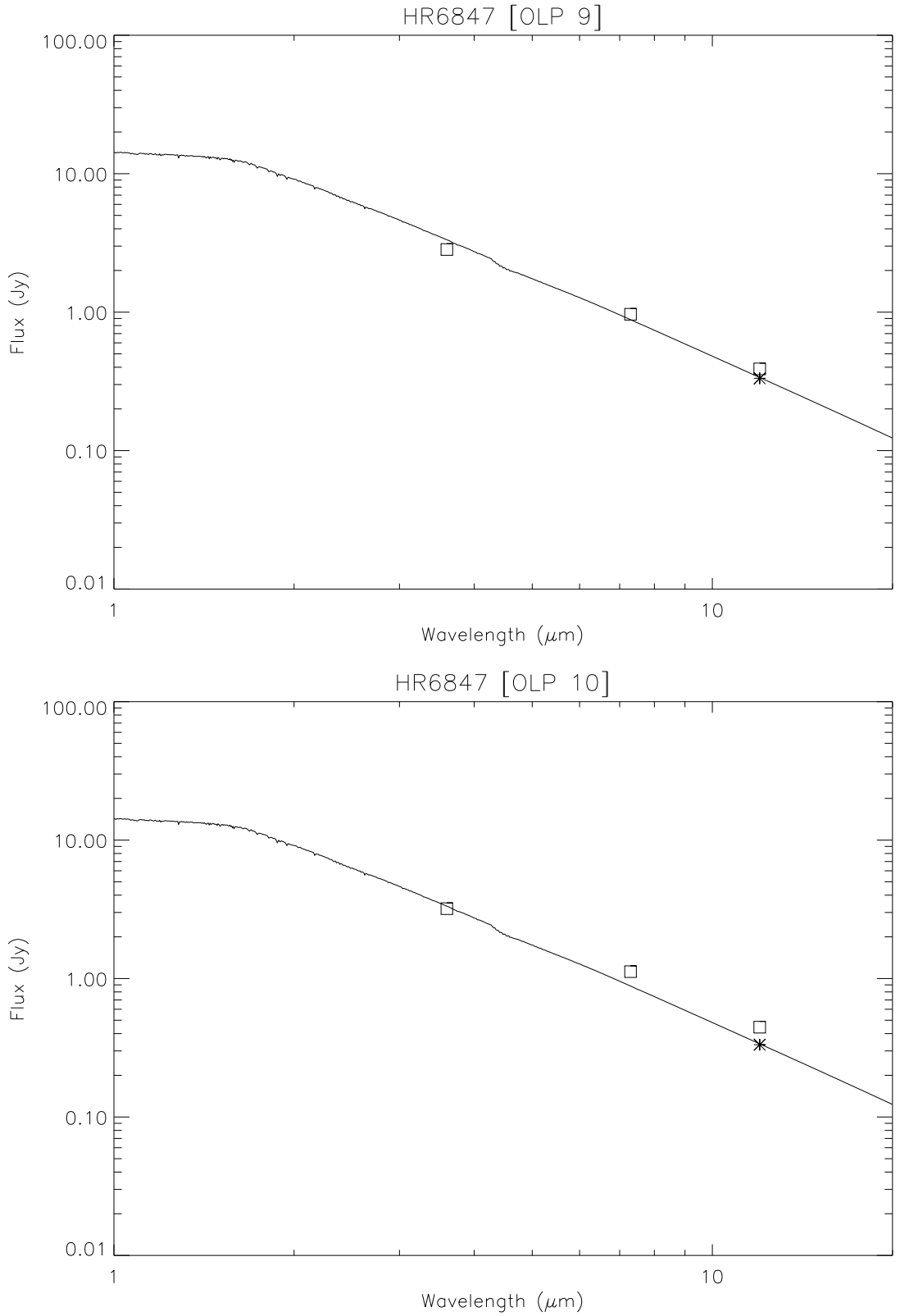

Figure 8.30: Comparison of PHT-P chopped photometry with the model of HR 6847 provided by P. Hammersley and with IRAS photometry for OLP 9.0b6 (upper panel) and OLP 10.0b5 (lower panel). All photometric points are color corrected for a 4000 K BB. The meaning of the symbols is the following: solid line: model, asterisk: IRAS, square: PHT-P (P03 AOT).

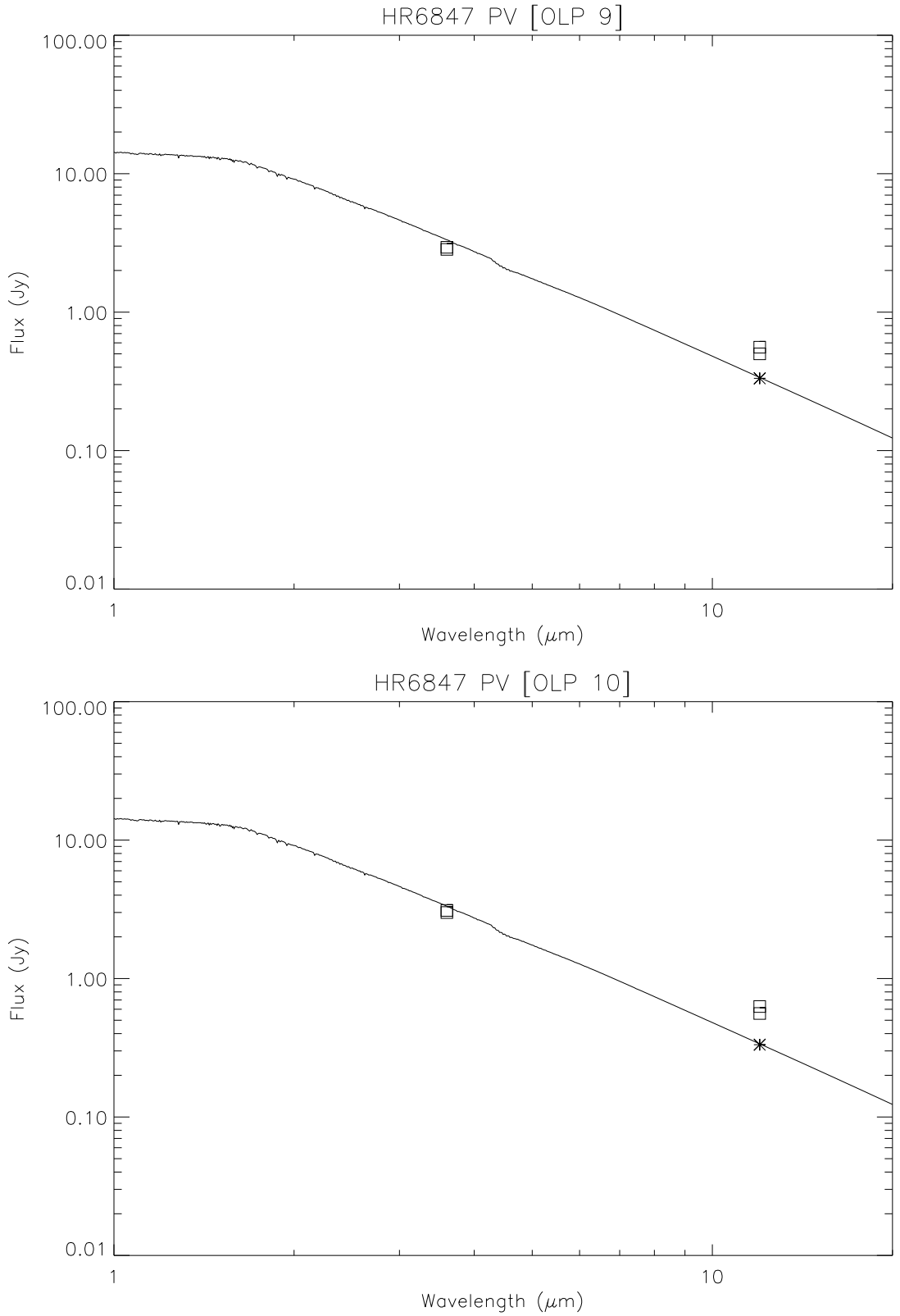

Figure 8.31: Comparison of PHT-P chopped photometry taken during the Performance Verification Phase with the model of HR 6847 provided by P. Hammersley and with IRAS photometry for OLP 9.0b6 (upper panel) and OLP 10.0b5 (lower panel). All photometric points are color corrected for a 4000 K BB. The meaning of the symbols is the following: solid line: model, asterisk: IRAS, square: PHT-P (P03 AOT).

Evaluation Log

1) Chopped Point Source Photometry (Routine Phase), 79 arcsec aperture

Measurements:
PHT-P1: ppap70601103 FCS = 3.6 um

Colour correction: black body, T = 5720 K

Model: Hammersley

Det	cwl (μm)	OLP 9	OLP 10	IRAS	Model	Δ (OLP 9)	Δ (OLP 10)
P1	3.6	2.835	3.198		3.333	-14.93	-4.04
P1	7.3	0.966	1.122		0.883	9.43	27.06
P1	12.0	0.389	0.445	0.333	0.337	15.32	31.94

2) Chopped Point Source Photometry (Performance Verification Phase), 23 arcsec aperture

Measurements:
PHT-P1 : ppap07402407 FCS = 3.6 um
PHT-P1b: ppap07601507 FCS = 3.6 um

Colour correction: black body, T = 5720 K

Model: Hammersley

Det	cwl (μm)	OLP 9	OLP 10	IRAS	Model	Δ (OLP 9)	Δ (OLP 10)
P1	3.6	2.841	2.998		3.333	-14.77	-10.04
P1b	3.6	2.940	3.105		3.333	-11.78	-6.84
P1	12.0	0.500	0.559	0.333	0.337	48.13	65.82
P1b	12.0	0.558	0.628	0.333	0.337	65.43	86.17

8.2.6 PHT03 and PHT22 Chopped Mode: The SED of HR 7469

Motivation

We check the quality for P2 and C100 multi-filter chopped photometry on the faint star HR 7469 for which also multi-filter photometry measurements in staring mode (cf. Sect. 5.1.5) and mini-map photometry at 60 μm (cf. Sect. 6.1.9) are available.

Method

We compare the color corrected flux values of both OLP V9.0b6 and OLP V10.0b5 results against the model prediction by Hammersley and IRAS photometry.

Results

For HR 7469 the assessment of the OLP V9.0b6 and OLP V10.0b5 photometry is given in part 1 of the evaluation log. Fig. 8.32 shows the chopped P2 and C100 photometry on HR 7469. We note an improvement of the accuracy of chopped P2 photometry for OLP 10 to better than 10 %. This is also a much better performance than was found for the staring mode on-off photometry. We also note a good performance of the C100 chopped photometry. Both IRAS 60 and 100 μm FSC fluxes are upper limits for this source. The ISOPHOT 60 μm flux is within 10 % of the model. This is in contrast to several somewhat brighter test cases for which always too high fluxes are derived. This may indicate that some refinement of the signal loss correction may be possible. Another difference with these measurements is, that the FCS calibration was done in the 90 μm filter instead of the 60 μm filter. The 90 mum flux can be affected by cirrus confusion: According to [39] the 1 σ cirrus confusion value for 90 μm is estimated to be 28 mJy (using formulae 6, 7 and 8 with B = 8 MJy sr^{-1}, q = 1.6 from 150 arcsec chop throw and $\gamma = 0.33$), thus cirrus confusion noise is stronger than the expected source flux.

Conclusions

- P2 chopped photometry performance has been improved with an absolute accuracy of better than 10 %.
- The C100 chopped photometry performance of this faint star is clearly limited by cirrus confusion at 90 μm. The 60 μm photometry accuracy derived from the comparison with the model is better than 10 %, much better than found for other test cases of similar brightness.

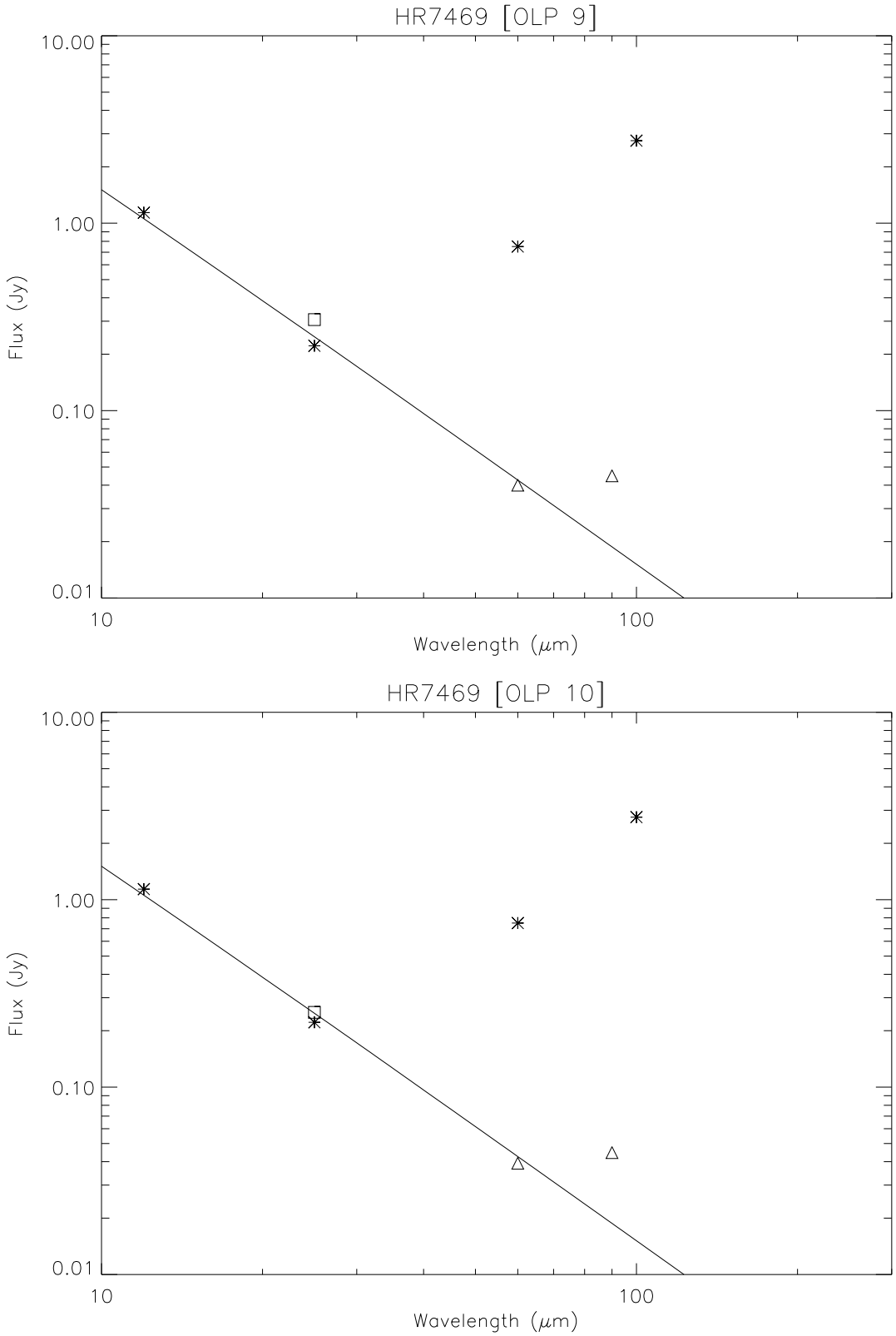

Figure 8.32: Comparison of PHT-P chopped photometry with the model of HR 7469 provided by P. Hammersley and with IRAS photometry for OLP 9.0b6 (upper panel) and OLP 10.0b5 (lower panel). All photometric points are color corrected for a 6622 K BB. The meaning of the symbols is the following: solid line: model, asterisk: IRAS, square: PHT-P (P03 AOT), triangle: PHT-C100 (P22 AOT).

Evaluation Log

1) Chopped Point Source Photometry

Measurements:
PHT-P : PPAP54801897 FCS = 25 um
PHT-C100: PCAP54801898 FCS = 90 um

Colour correction: black body, T = 6622 K

Model: Hammersley

Det	cwl (μm)	OLP 9	OLP 10	IRAS	Model	Δ (OLP 9)	Δ (OLP 10)
P2	25.0	0.306	0.251	0.222	0.248	23.46	1.08
C1	60.0	0.040	0.039	0.750	0.043	-6.10	-7.86
C1	90.0	0.045	0.045		0.019	139.21	138.51

8.2.7 PHT03 and PHT22 Chopped Mode: The SED of HR 7557

Motivation

We check the quality for P2, C100 and C200 multi-filter chopped photometry on the star HR 7557 for which also mini-map photometry at 60 μm (cf. Sect. 6.1.8) is available.

Method

We compare the color corrected flux values of both OLP V9.0b6 and OLP V10.0b5 results against the model prediction by Hammersley and IRAS photometry.

Results

For HR 7557 the assessment of the OLP V9.0b6 and OLP V10.0b5 photometry is given in part 1 of the evaluation log. Fig. 8.33 shows the chopped P2 and C100 photometry on HR 7557. The P2 chopped photometry gives an excellent agreement with the model flux. The C100 photometry in both the 60 and the 90 μm filter is a factor $2-3$ below the model.The resulting C200 fluxes are negative. Inspection of the C100 PCAP data product shows that the derived flux uncertainty at 60 μm is as high as the flux itself. In contrary the 60 μm mini-map flux is very accurate and consistent with the model. But the 60 μm mini-map shows an increased surface brightness structure south of the star (Fig. 8.34). The roll angle of the observation was 90 deg, hence the chop direction was N – S and the signal in one of the reference beams could be very likely affected by this source. The FCS measurement at this early mission phase had a length of only 16 s. The actual responsivity for the central pixel 5 is higher by 30 % than the default responsivity, so that part of the flux loss might also be explained by an inaccurate responsivity calibration. The background around this source is relatively high, so that general cirrus confusion plays a significant role at 90 μm: According to [39] the 1 σ cirrus confusion value for 90 μm is estimated to be 104 mJy (using formulae 6, 7 and 8 with B = 20 MJy sr^{-1}, q = 1.6 from 150 arcsec chop throw and γ = 0.59). For 170 μm the 1 σ cirrus confusion value is estimated to be $\sim$ 250 mJy according to [39] (using formulae 6, 7 and 8 with B = 20 MJy sr^{-1} and increasing the noise by 20 % for only one reference position). This cirrus noise is larger than the expected source flux and since also the 90 μm C100 measurement gives a reduced source flux a negative flux result is likely to happen. The C200 chop reference position was south of the source exactly in the direction of the possibly confusing source. This might explain the relatively high negative flux values.

Conclusions

- The test case confirms the good performance of P2 chopped photometry with OLP 10.
- The C100 chopped photometry gives a factor $2-3$ too low fluxes. The comparison with the mini-map photometry at 60 μm indicates a possible confusion of one of the background reference beams. At 90 μm the general cirrus confusion noise derived for the background can explain the flux loss.
- The C200 chopped photometry gives quite negative fluxes. The cirrus confusion noise estimate is higher than the expected source fluxes. The one reference beam was located in the direction of a possibly confusing source.

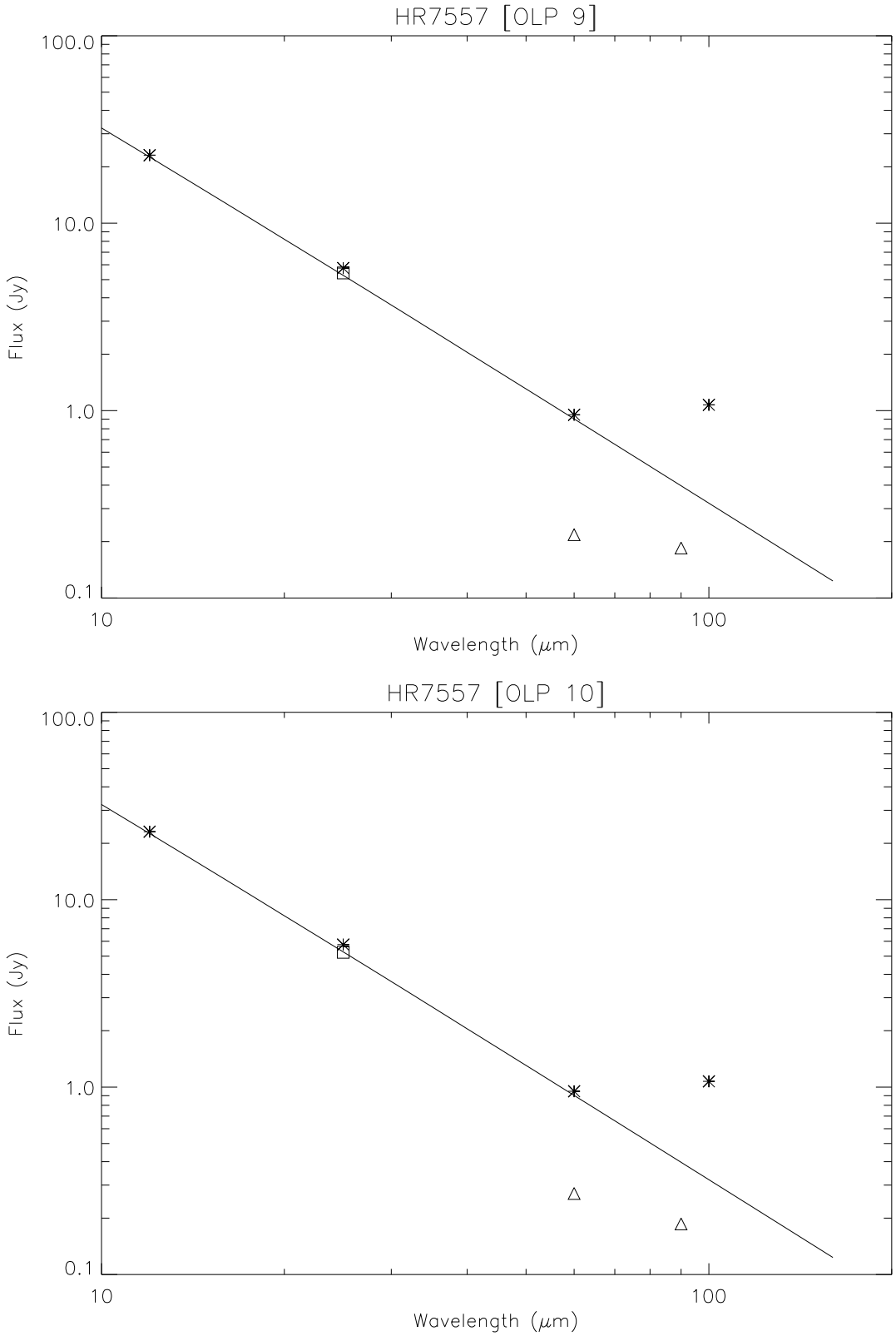

Figure 8.33: Comparison of PHT-P and PHT-C100 chopped photometry with the model of HR 7557 provided by P. Hammersley and with IRAS photometry for OLP 9.0b6 (upper panel) and OLP 10.0b5 (lower panel). All photometric points are color corrected for a 7596 K BB. The meaning of the symbols is the following: solid line: model, asterisk: IRAS, square: PHT-P (P03 AOT), triangle: PHT-C100 (P22 AOT).

Evaluation Log

1) Chopped Point Source Photometry

Measurements:
PHT-P : PPAP13001001 FCS = 25 um
PHT-C100: PCAP13001002 FCS = 90 um
PHT-C200: PCAP13001003 FCS = 150 um

Colour correction: black body, T = 7596 K

Model: Hammersley

Det	cwl (μm)	OLP 9	OLP 10	IRAS	Model	Δ (OLP 9)	Δ (OLP 10)
P2	25.0	5.427	5.241	5.759	5.268	3.01	-0.52
C1	60.0	0.218	0.271	0.950	0.903	-75.88	-70.03
C1	90.0	0.185	0.186		0.397	-53.42	-53.09
C2	150.0	-1.410	-1.563		0.141	-1102.55	-1211.78
C2	180.0	-1.174	-1.400		0.092	-1379.84	-1626.70

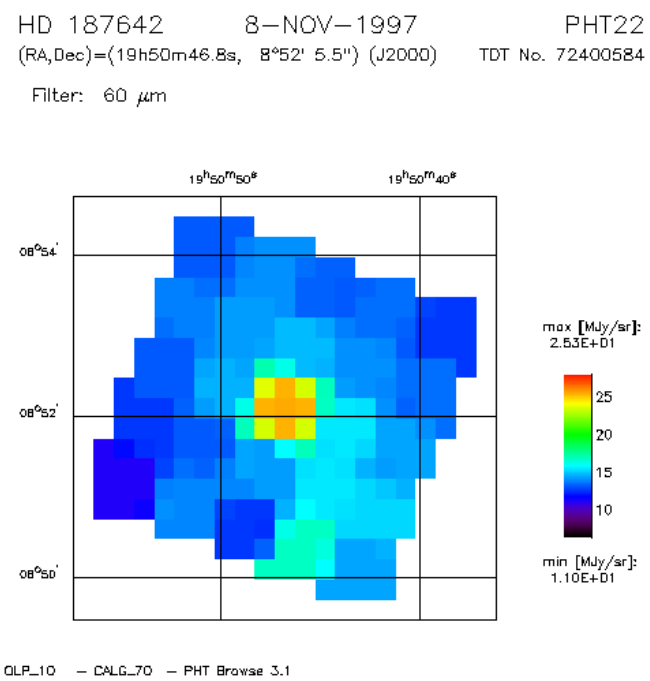

Figure 8.34: 60 μm mini-map of HR 7557. There is a structure south of the source. The chop direction was N – S, the background positions of the central pixel 5 are outside the map ($\pm$ 2.5 arcmin north and south of the star).

8.2.8 PHT22 Chopped Mode: The SED of HD 216956 (Formalhaut)

Motivation

We check the quality for C100 multi-filter chopped photometry on the FIR excess star HD 216956 for which also mini-map photometry at 60 μm (cf. Sect. 6.1.13) is available.

Method

We compare the color corrected flux values of both OLP V9.0b6 and OLP V10.0b5 results against IRAS photometry and the model of a modified black body with the parameters given in [38].

Results

For HD 216956 the assessment of the OLP V9.0b6 and OLP V10.0b5 photometry is given in part 1 of the evaluation log. Fig. 8.35 shows the chopped C100 photometry on HD 216956. There is a good consistency with the IRAS photometry, at 60 μm the agreement is better than 2 %. The chopped ISOPHOT flux is somewhat higher than the one derived from the mini-maps. We estimate an absolute photometric accuracy of about 20 %.

Conclusions

- Chopped C100 photometry of a 10 Jy source gives an absolute accuracy of about 20 %. The flux unceratinty of this source is increased by the unknown beam factor due to the extension of the source.

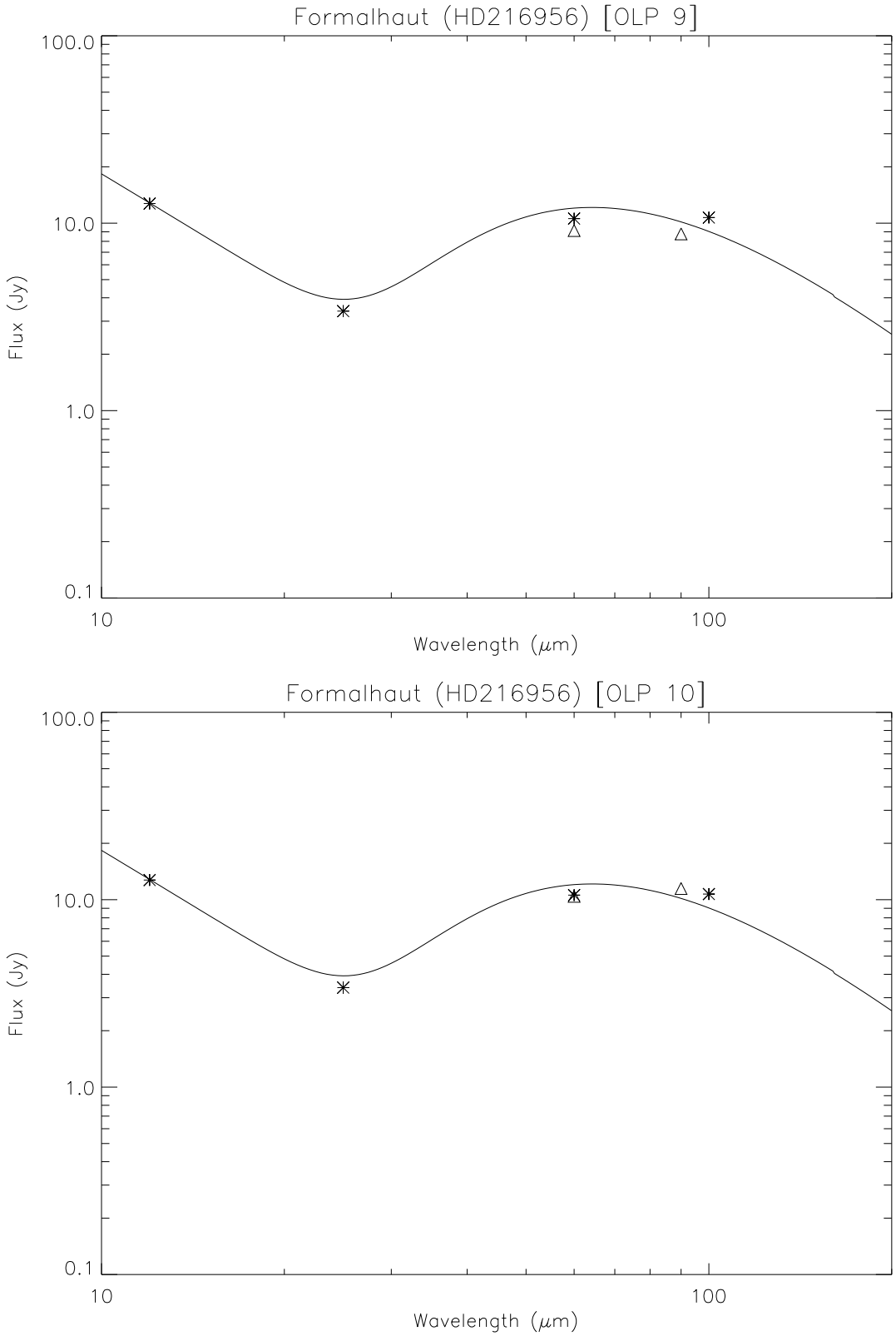

Figure 8.35: Comparison of PHT-C100 chopped photometry of HD 216956 (Formalhaut) with the scaled model spectrum of HD 158485 (HR 6514) provided by P. Hammersley plus a FIR excess by a 55 K modified BB ($\varepsilon \propto \lambda^{-1}$) and with IRAS photometry for OLP 9.0b6 (upper panel) and OLP 10.0b5 (lower panel). A point source footprint was assumed in reconstructing the flux from the measurement with the central pixel of the C100 array. The photometric data points are corrected for a 8390 K BB for $\lambda < 30\,\mu$m and for a 50 K modified BB for $\lambda > 30\,\mu$m. The meaning of the symbols is the following: solid line: model, asterisk: IRAS, triangle: PHT-C100 (P22 AOT).

Evaluation Log

1) Chopped Point Source Photometry

Measurements:
PHT-C100: PCAP16402729 FCS = 90 um

Flux reconstruction: point source footprint

Colour correction: mod. bb, em.=1, T = 50 K

Model: Hammersley & 55 K modified ($\varepsilon \propto \lambda^{-1}$) BB

Det	cwl (μm)	OLP 9	OLP 10	IRAS	Model	Δ (OLP 9)	Δ (OLP 10)
C1	60.0	9.134	10.423	10.576	12.035	-24.10	-13.40
C1	90.0	8.767	11.473		10.160	-13.71	12.92

8.2.9 PHT03 and PHT22 Chopped Mode: The SED of the Quasar PG 1700+518

Motivation

We check the quality for P1, P2, P3, C100 and C200 multi-filter chopped photometry on the quasar PG 1700+518 for which also mini-map photometry from $60-200\,\mu$m (cf. Sect. 6.1.14) is available.

Method

We compare the color corrected flux values of both OLP V9.01 and OLP V10.0b8 results against IRAS photometry.

Results

For PG 1700+518 the assessment of the OLP V9.01 and OLP V10.0b8 photometry is given in part 1 of the evaluation log. Fig. 8.36 shows the chopped multi-filter photometry on PG 1700+518. P1, P2, P3 and C200 detectors are default responsivity calibrated. The default responsivity calibration improves the P1 fluxes considerably, however the $12\,\mu$m flux us a factor of 2.5 higher than the IRAS flux. The P2 flux matches for OLP 10 within 20 % with IRAS. The P3 fluxes are a factor of 3 too high. The measurement was very close to the end of the science window in revolution 92, so that in fact a responsivity three times higher than the default one may be correct. This is suggested by the subsequent C200 measurement for which also an increase of the actual responsivity by a factor of about 2 is indicated. The C100 chopped photometry is quite consistent with IRAS and with the mini-map photometry (at $60\,\mu$m: 18 % with IRAS and mini-map photometry, at $100\,\mu$m: 1 % with mini-map photometry. The C200 fluxes of the measurement on revolution 92 are negative, while the $200\,\mu$m flux of the measurement on revolution 195 is quite consistent with the mini-map photometry. This indicates significant impact by cirrus confusion, a minimum estimate of the $1\,\sigma$ confusion noise is 40 mJy.

Conclusions

- The default responsivity calibration improves the P1 chopped photometry.
- The P2 chopped photometry is consistent with IRAS within 20 %
- The C100 chopped photometry is consistent with IRAS and ISOPHOT mini-map photometry within 20 %.
- The P3 chopped photometry suffers from space weather effects which seem to lead to an exceptionally high responsivity which is far off the default responsivity applied to this measurement, because the FCS heating power was outside the calibrated range.
- C200 chopped photometry suffers significantly from cirrus confusion noise.

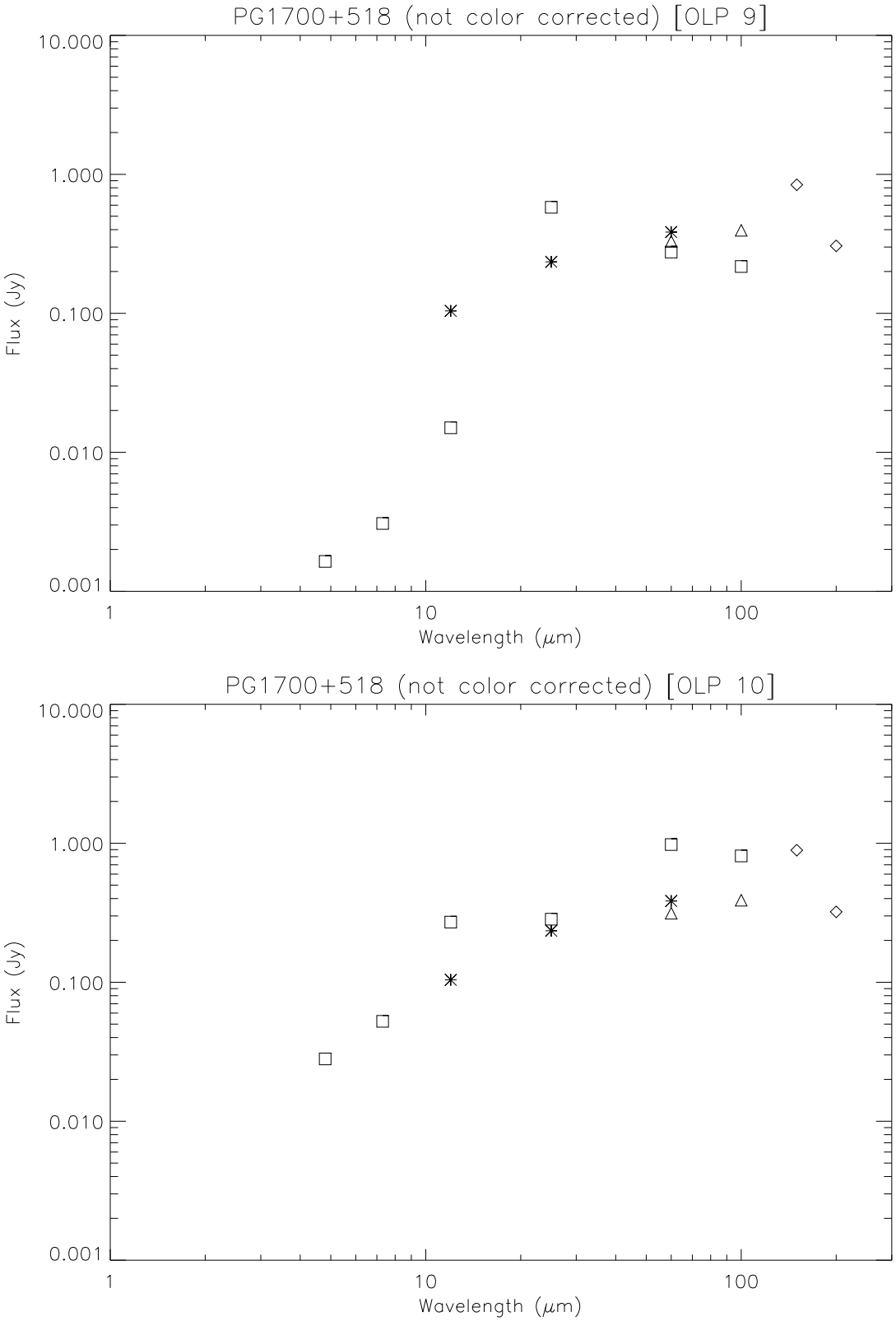

Figure 8.36: Comparison of PHT-P and PHT-C chopped photometry of PG 1700+518 with IRAS photometry for OLP 9.01 (upper panel) and OLP 10.0b8 (lower panel). No color correction was applied. The meaning of the symbols is the following: asterisk: IRAS, square: PHT-P (P03 AOT), triangle: PHT-C100 (P22 AOT), diamond: PHT-C200 (P22 AOT).

Evaluation Log

1) Chopped Point Source Photometry

Measurements:
PHT-P : ppap09202633 FCS = 12, 25, 100 um
PHT-Cb : pcap09202634 FCS = 150 um
PHT-C : pcap19501857 FCS = 60, 150 um

Det	cwl (μm)	OLP 9	OLP 10	IRAS	Model	Δ (OLP 9)	Δ (OLP 10)
P1	4.8	0.002	0.028				
P1	7.3	0.003	0.052				
P1	12.0	0.015	0.271	0.104			
P2	25.0	0.579	0.284	0.235			
P3	60.0	0.276	0.979	0.384			
C1	60.0	0.330	0.314	0.384			
P3	100.0	0.217	0.811				
C1	100.0	0.396	0.389				
C2	150.0	0.842	0.891				
C2b	150.0	-0.101	-0.208				
C2	200.0	0.306	0.321				
C2b	200.0	-0.651	-1.221				

8.3 Chopped Observations of Known Sources

Summary

- For P1 chopped photometry reasonable calibration accuracies are achieved.
- P2 chopped photometry is significantly improved with regard to OLP 9 giving now in general reasonable calibration accuracies better than 30 %.
- C100 photometry for sources fainter than 100 mJy gives currently still insufficient results. The observed offsets for all $60 mu$m observations cannot be explained by cirrus confusion and look rather systematic.
- Cirrus confusion is a limitation in photometric accuracy at 100 μm for sources fainter than 0.2 Jy. For backgrounds brighter than $4 - 5\,\mathrm{MJy\,sr^{-1}}$ the $1\,\sigma$ cirrus confusion noise for triangular chopper configurations ($\pm$ 150 arcsec to both sides of the source is in the order of 15 mJy.

8.3.1 PHT03 and PHT22 Chopped Mode: The SEDs of Stars with Known Fluxes

Motivation

We investigate here the results of chopped photometry for several stars, namely HR 5447, BS 5062, HR 5304, HR 5914 and HR 5986, for which model fluxes are available.

Method

We compare the background subtracted flux values of both OLP V9.0b10/V9.01 and OLP V10.0b5 results against the models by Cohen and Hammersley and IRAS photometry. Furthermore, we compare the derived background surface brightness with COBE/DIRBE photometry.

Results

For HR 5447 the comparison of the OLP V9.0b10 and OLP V10.0b5 photometry with the model is given in part 1a of the evaluation log. Fig. 8.37 shows the chopped P2 and C100 photometry on HR 5447. The P2 photometry is improved with OLP 10 and is better than 30 %. For C100 photometry there is practically no change. Both 60 μm flux values are close to the IRAS FSC value, but a factor 1.7 - 2.4 above the model expectation. At 100 μm the IRAS FSC flux is clearly cirrus confusion limited. The ISOPHOT photometry at 90 μm goes deeper, but very discrepant fluxes are found from the two observations. The orientation of the chop on the sky was 277 deg vs. 93 deg, i.e. a rotation of 184 deg. Since for the C100 observations triangular chopping was applied, the same background positions were seen in both measurements, and hence the scatter is due to internal measurement uncertainty.
For BS 5062 the comparison of the OLP V9.0b10 and OLP V10.0b5 photometry with the model is given in part 2a of the evaluation log. Fig. 8.38 shows the chopped P1, P2 and C100 photometry on BS 5062. The P1 7.3 μm photometry is excellent, while the 12 μm point which is calibrated relative to it is yet far off. The P2 photometry is considerably improved for OLP 10, yet it is a factor of about 2. This is one of the very few test cases which do not confirm the good performance of chopped P2 photometry for OLP 10. The C100 60 μm flux is closer to the model than IRAS, while the 90 μm flux goes off, but is still considerably lower than the IRAS 100 μm upper limit. According to [39] the 1 σ cirrus confusion value for 90 μm is estimated to be 14 mJy (using formulae 6, 7 and 8 with B = 4 MJy sr^{-1}, q = 1.6 from 150 arcsec chop throw and $\gamma = 0.13$) which is as large as the expected source flux. The background photometry from the off-source beam is listed in part 2b of the evaluation log. Fig. 8.39 shows the comparison with COBE/DIRBE photometry. There is a reasonable agreement except for the 12 μm point which does not give any accurate differential flux either.
For HR 5304 the comparison of the OLP V9.01 and OLP V10.0b5 photometry with the model is given in part 3a of the evaluation log. Fig. 8.40 shows the chopped C100 photometry on HR 5304. Both OLP versions show quite similar results. The ISOPHOT fluxes are a factor of 1.8 to 2.5 above the model prediction. According to [39] the 1 σ cirrus confusion value for 100 μm is estimated to be 13 mJy (using formulae 4, 7 and 8 with B = 5 MJy sr^{-1}, q = 1.6 from 150 arcsec chop throw and $\gamma = 0.19$) which is as large as the expected source flux.
The background photometry from the off-source beam is listed in part 3b of the evaluation log. Fig. 8.41 shows the comparison with COBE/DIRBE photometry. There is reasonable agreement.
For HR 5914 the comparison of the OLP V9.01 and OLP V10.0b5 photometry with the model is given in part 4a of the evaluation log. Fig. 8.42 shows the chopped P2 and C100 photometry on HR 5914. The P2 photometry is improved for OLP 10. The 60 μm flux is a factor of 2.4 above the model flux, but also the IRAS flux is higher than the model flux by 50 %. According to [39] the 1 σ cirrus confusion value for 90 μm is estimated to be 15 mJy (using formulae 6, 7 and 8 with B = 4.5 MJy sr^{-1}, q = 1.6 from 150 arcsec chop throw and $\gamma = 0.16$) which is in the order of the expected source flux.
The background photometry from the off-source beam is listed in part 4b of the evaluation log. Fig. 8.43 shows the comparison with COBE/DIRBE photometry. The 25 and 90 μm background fluxes appear a bit too high w.r.t. COBE/DIRBE.

For HR 5986 the comparison of the OLP V9.01 and OLP V10.0b5 photometry with the model is given in part 5a of the evaluation log. Fig. 8.44 shows the chopped P1, P2 and C100 photometry on HR 5986. The P2 photometry is improved for OLP 10. The 60 μm flux is a factor of 3 above the model flux. At 100 μm the IRAS FSC flux is only an upper limit. According to [39] the 1 σ cirrus confusion value for 100 μm is estimated to be 10 mJy (using formulae 4, 7 and 8 with B = 4 MJy sr^{-1}, q = 1.6 from 150 arcsec chop throw and $\gamma = 0.19$) which can have a significant impact on the accuracy of the resulting source flux.
The background photometry from the off-source beam is listed in part 5b of the evaluation log. Fig. 8.45 shows the comparison with COBE/DIRBE photometry. There is reasonable agreement in the shape of the background SED, the ISOPHOT fluxes are, however, 30 – 70 % higher.

Conclusions

- For P1 chopped photometry the calibration accuracy is maintained. Only one multi-filter case (BS 5062) indicates a potential calibration problem for the relatively calibrated filter.
- The P2 chopped photometry is significantly improved with regard to OLP 9 giving now in general reasonable calibration accuracies better than 30 %.
- All 5 test cases are faint in the FIR with 60 μm fluxes below 100 mJy. We observed the general phenomenon, that the ISOPHOT fluxes are in general above the model fluxes by factors 2 – 3. This points to a potential calibration deficiency.
- The 90 or 100 μm fluxes of these 5 test cases are in the order of only 15 to 30 mJy. Here the agreement of the ISOPHOT fluxes with the models is much better than at 60 μm, although only relatively calibrated, however, the derived cirrus confusion noise is always in the same order as the expected source fluxes, thus limiting the achievable photometric accuracy.

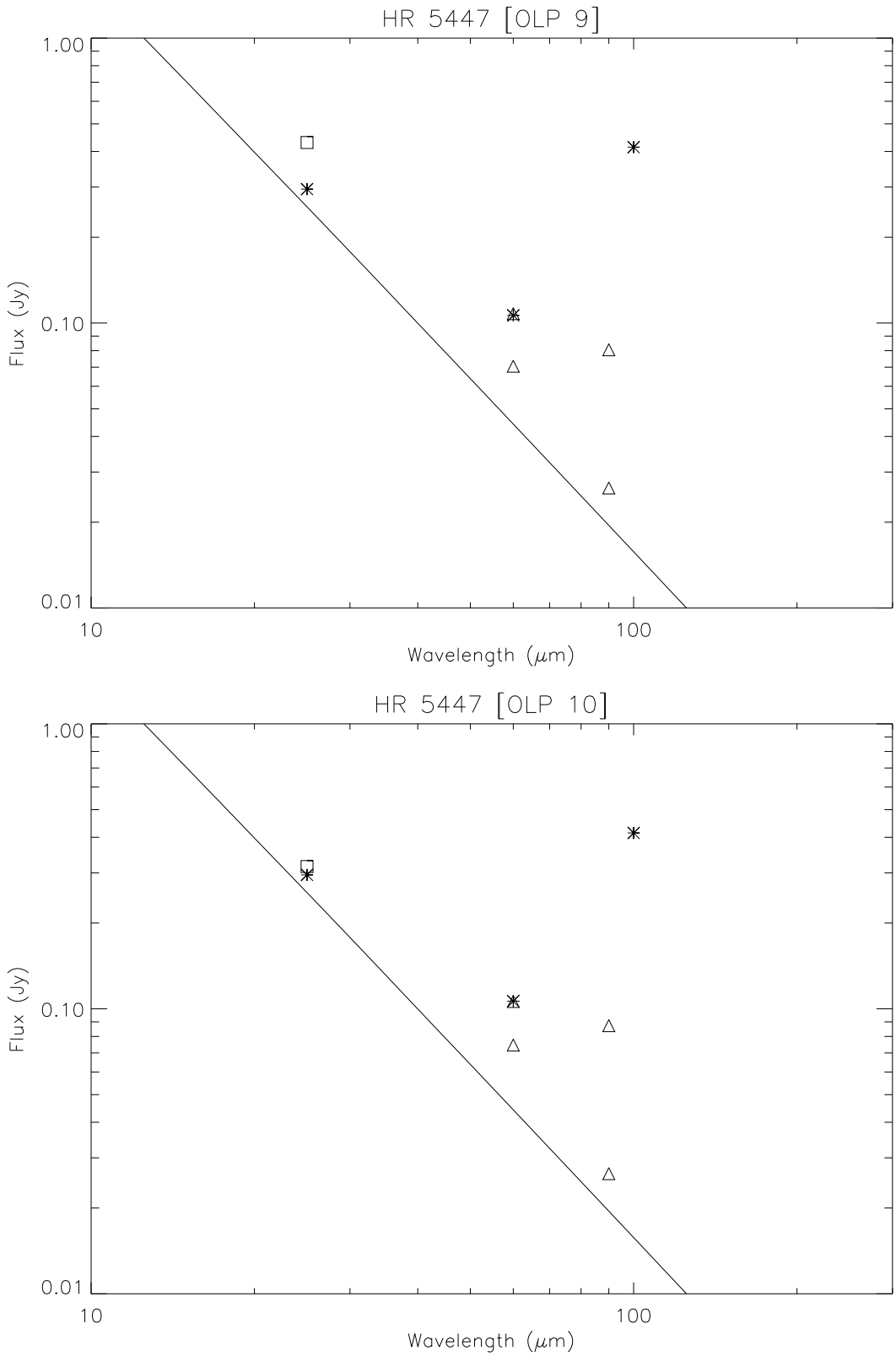

Figure 8.37: Comparison of PHT-P and PHT-C chopped photometry with the model by Hammersley and IRAS photometry both for OLP 9.01 (upper panel) and OLP 10.0b5 (lower panel). The meaning of the symbols is the following: solid line: model, asterisk: IRAS, square: PHT-P (P03 AOT), triangle: C100 (P22 AOT).

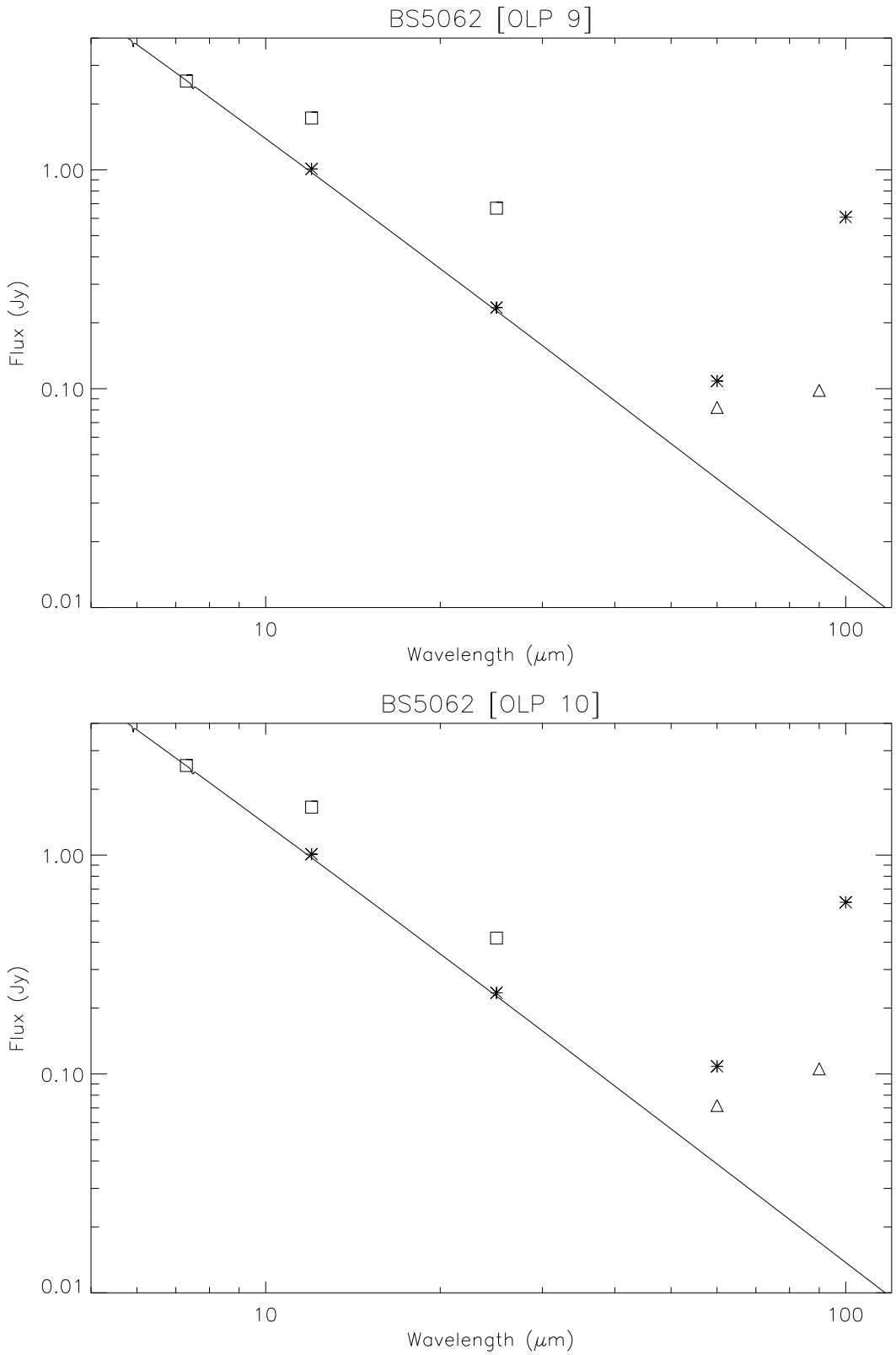

Figure 8.38: Comparison of PHT-P and PHT-C chopped photometry with the model by Hammersley and IRAS photometry both for OLP 9.0b10 (upper panel) and OLP 10.0b5 (lower panel). The meaning of the symbols is the following: solid line: model, asterisk: IRAS, square: PHT-P (P03 AOT), triangle: C100 (P22 AOT).

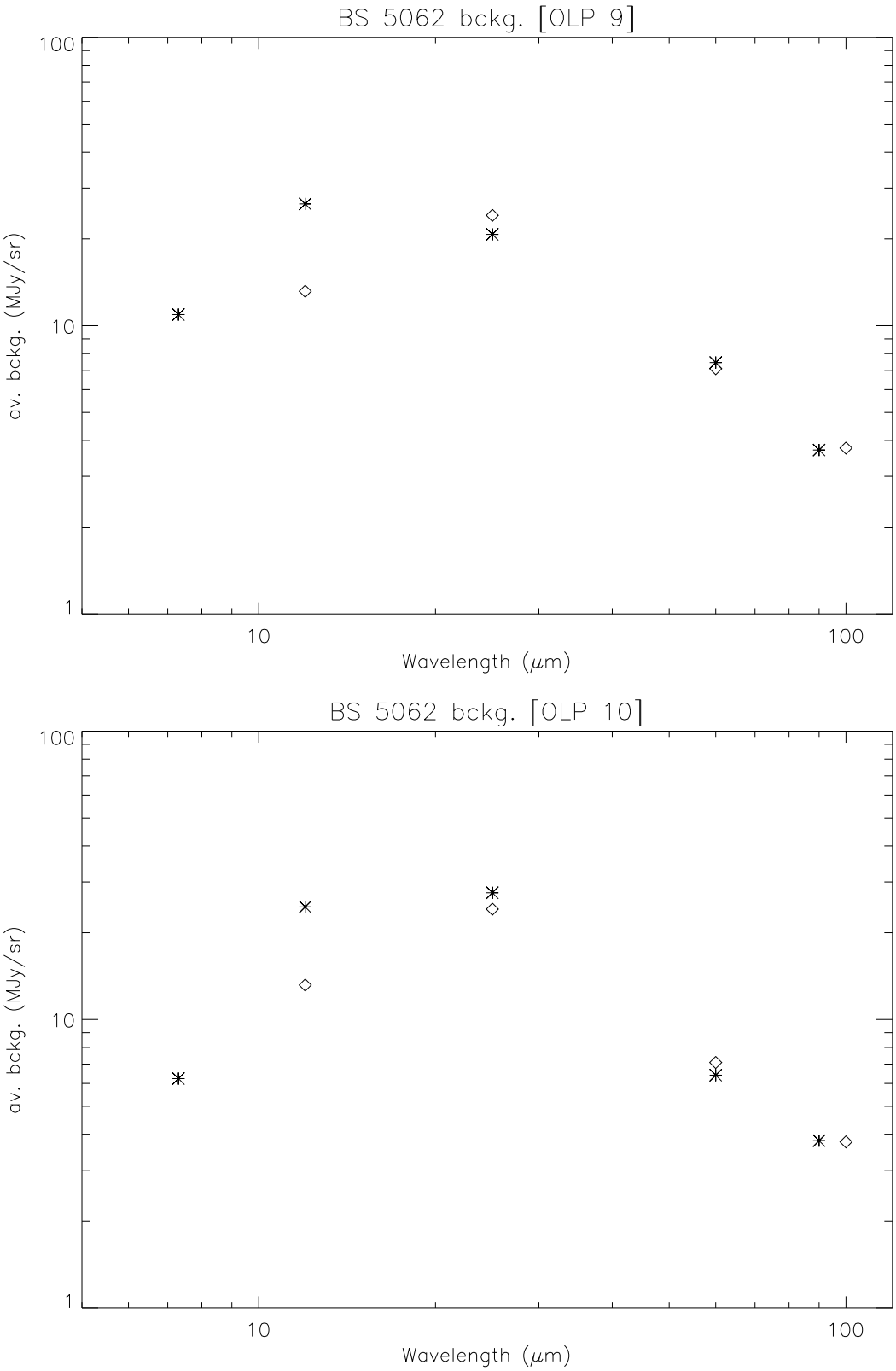

Figure 8.39: Comparison of surface brightness from chopped PHT photometry of the background beam for BS 5062 with COBE, both for OLP 9.0b10 (upper panel) and OLP 10.0b5. Asterisk: PHT-P and PHT-C photometry, diamond: COBE.

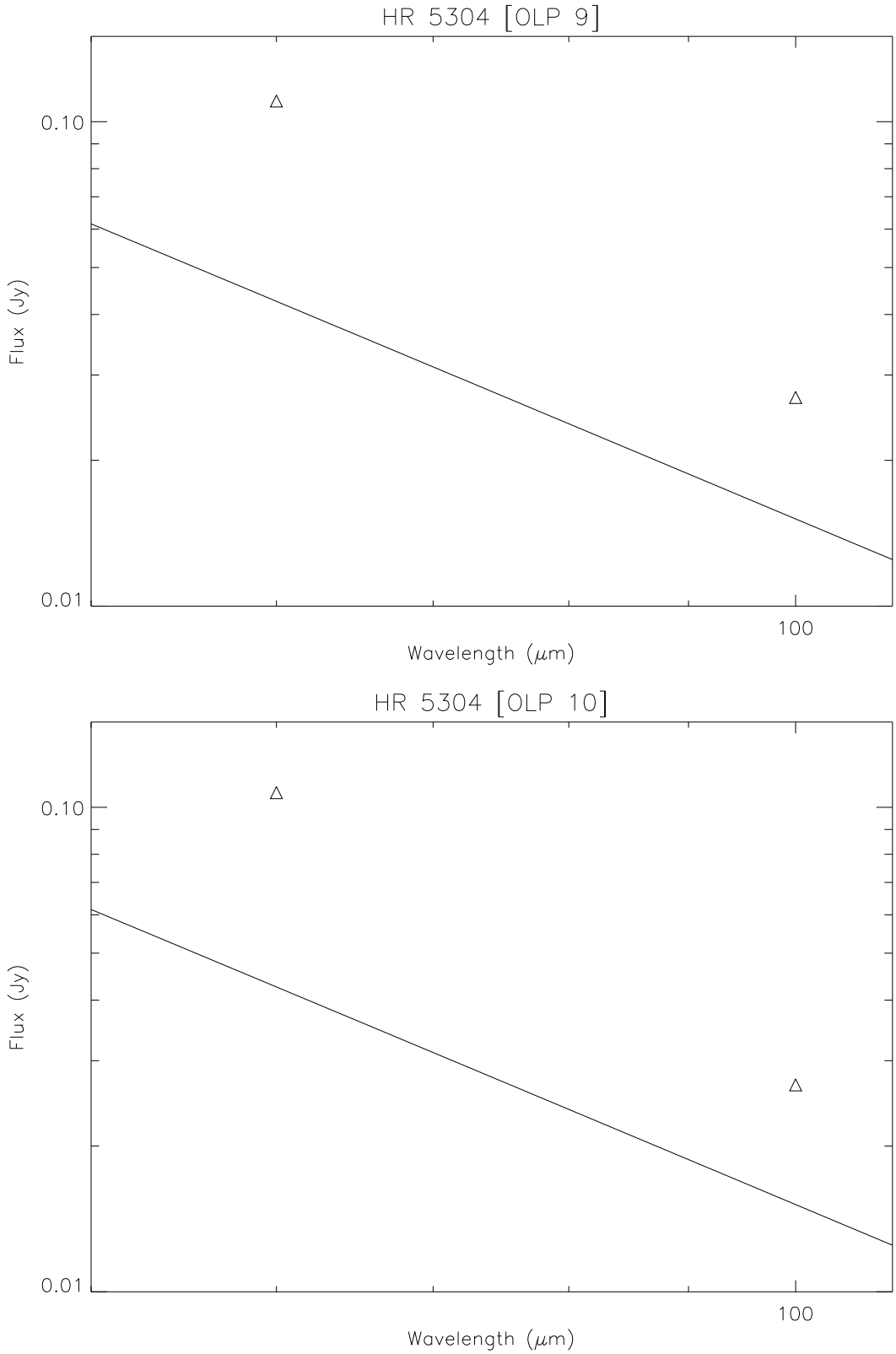

Figure 8.40: Comparison of PHT-C chopped photometry with the model by Cohen both for OLP 9.01 (upper panel) and OLP 10.0b5 (lower panel). The meaning of the symbols is the following: solid line: model, triangle: C100 (P22 AOT).

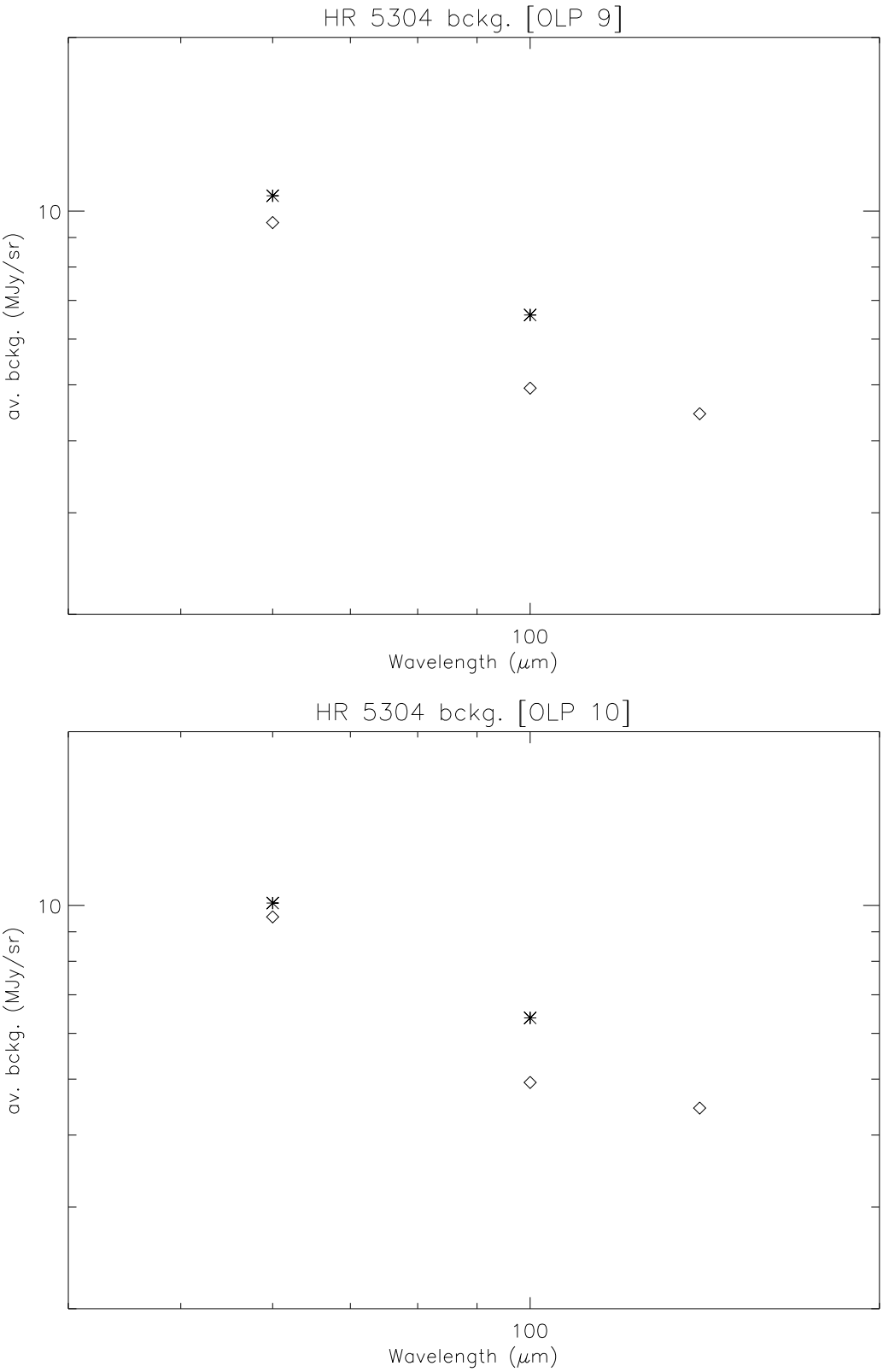

Figure 8.41: Comparison of surface brightness from chopped PHT photometry of the background beam for HR 5304 with COBE, both for OLP 9.01 (upper panel) and OLP 10.0b5. Asterisk: PHT-C photometry, diamond: COBE.

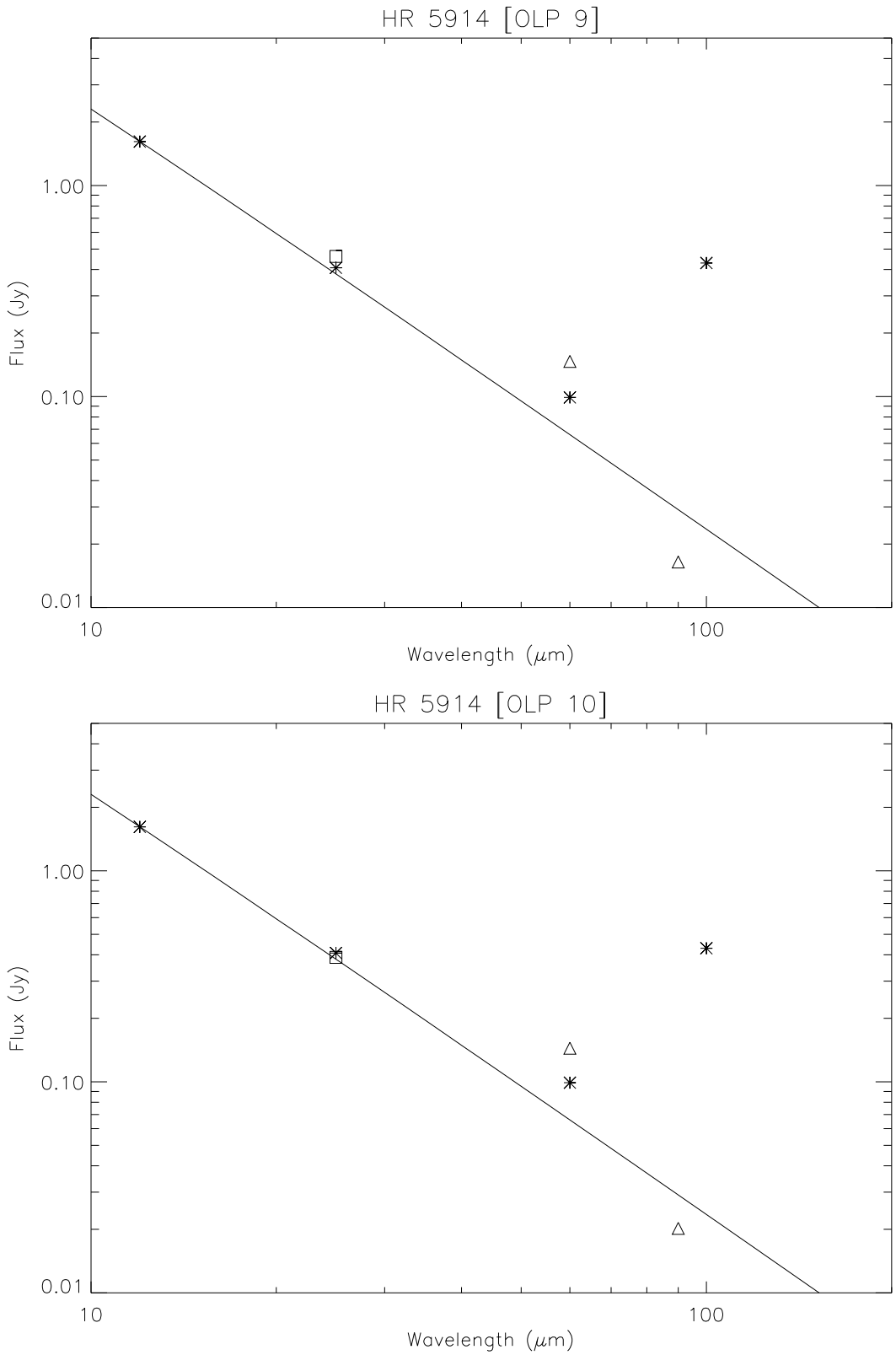

Figure 8.42: Comparison of PHT-P and PHT-C chopped photometry with the model by Cohen and IRAS photometry both for OLP 9.01 (upper panel) and OLP 10.0b5 (lower panel). The meaning of the symbols is the following: solid line: model, asterisk: IRAS, square: PHT-P (P03 AOT),triangle: C100 (P22 AOT).

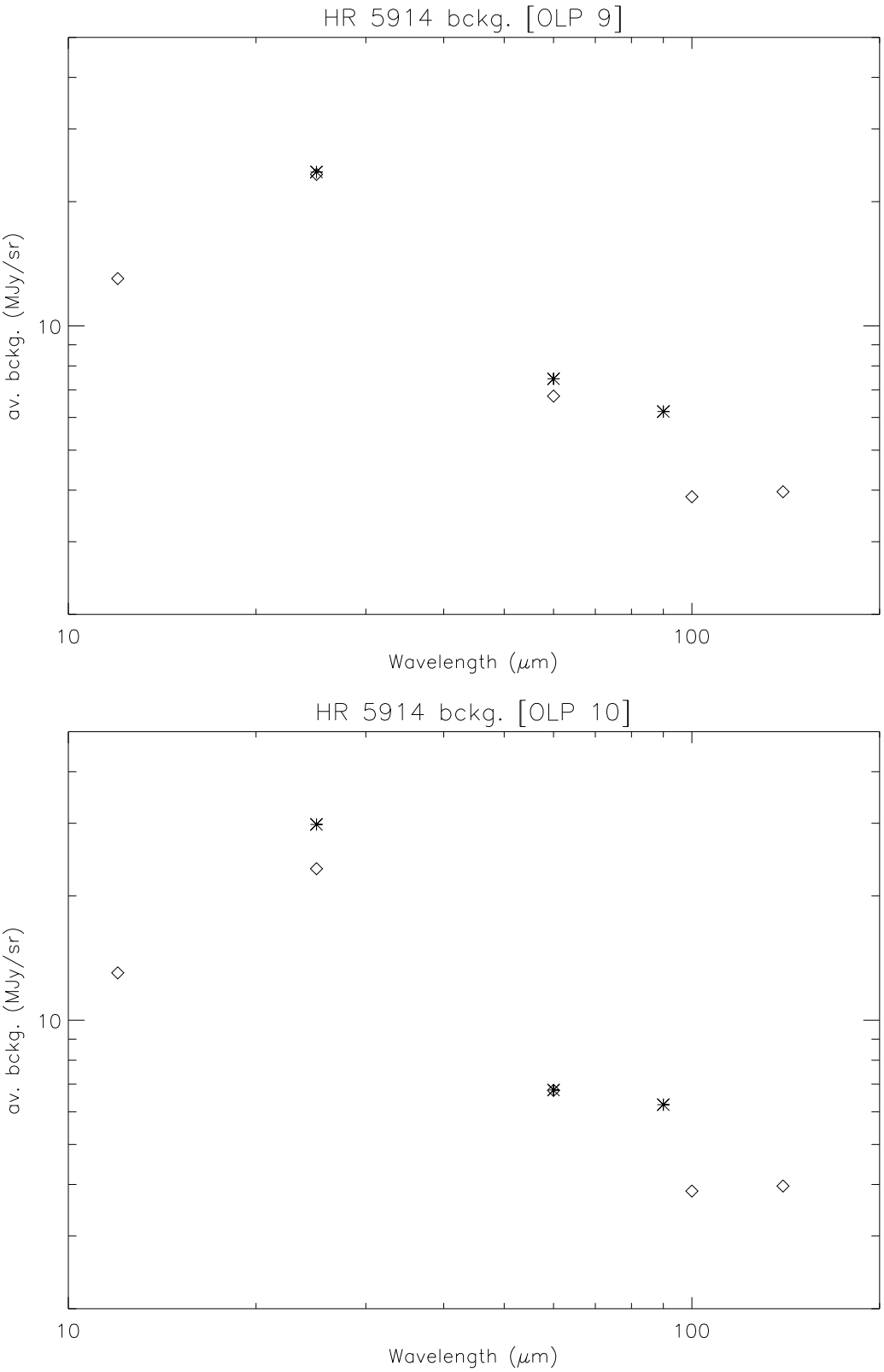

Figure 8.43: Comparison of surface brightness from chopped PHT photometry of the background beam for HR 5914 with COBE, both for OLP 9.01 (upper panel) and OLP 10.0b5. Asterisk: PHT-P and PHT-C photometry, diamond: COBE.

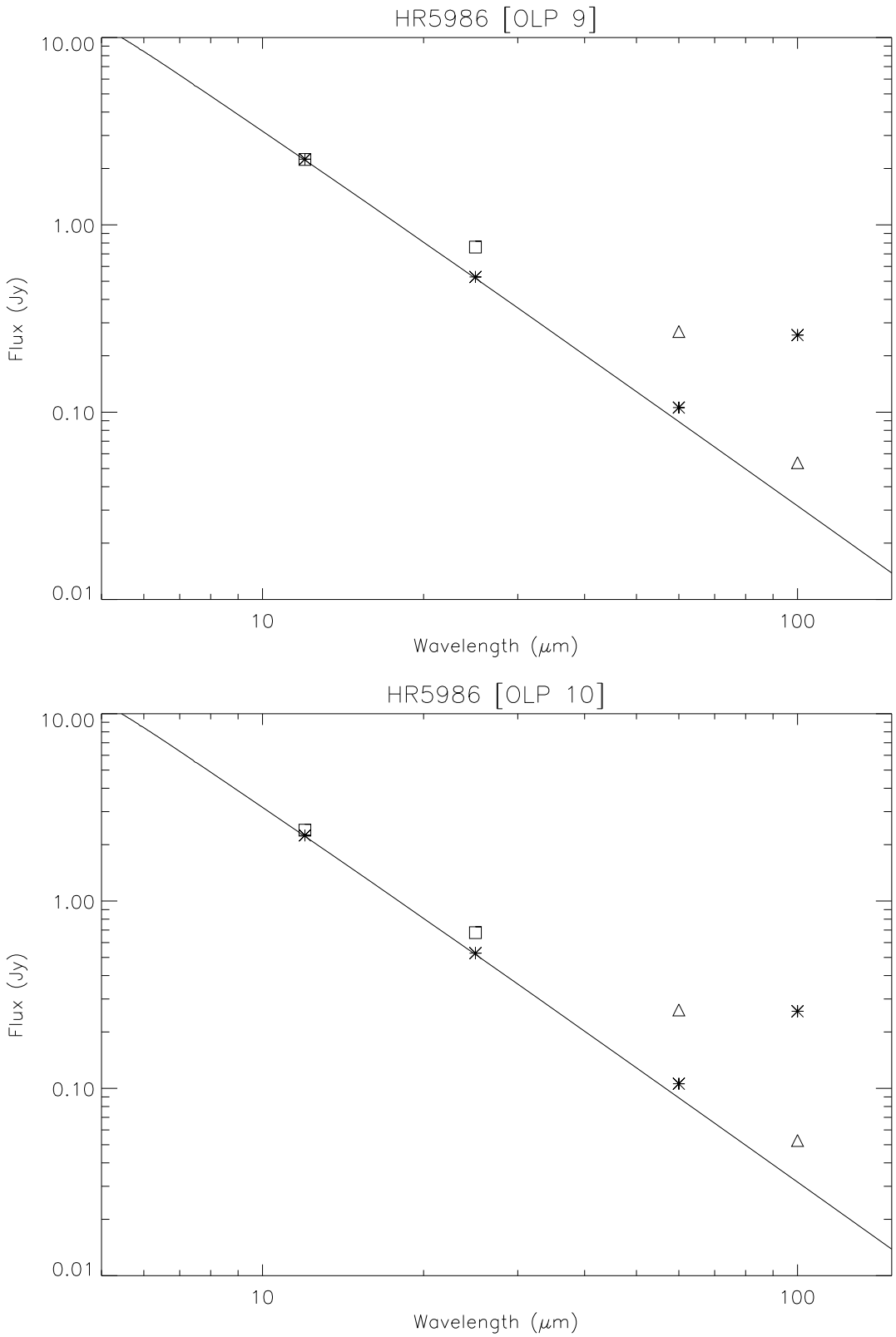

Figure 8.44: Comparison of PHT-P and PHT-C chopped photometry with the model by Hammersley and IRAS photometry both for OLP 9.01 (upper panel) and OLP 10.0b5 (lower panel). The meaning of the symbols is the following: solid line: model, asterisk: IRAS, square: PHT-P (P03 AOT), triangle: C100 (P22 AOT).

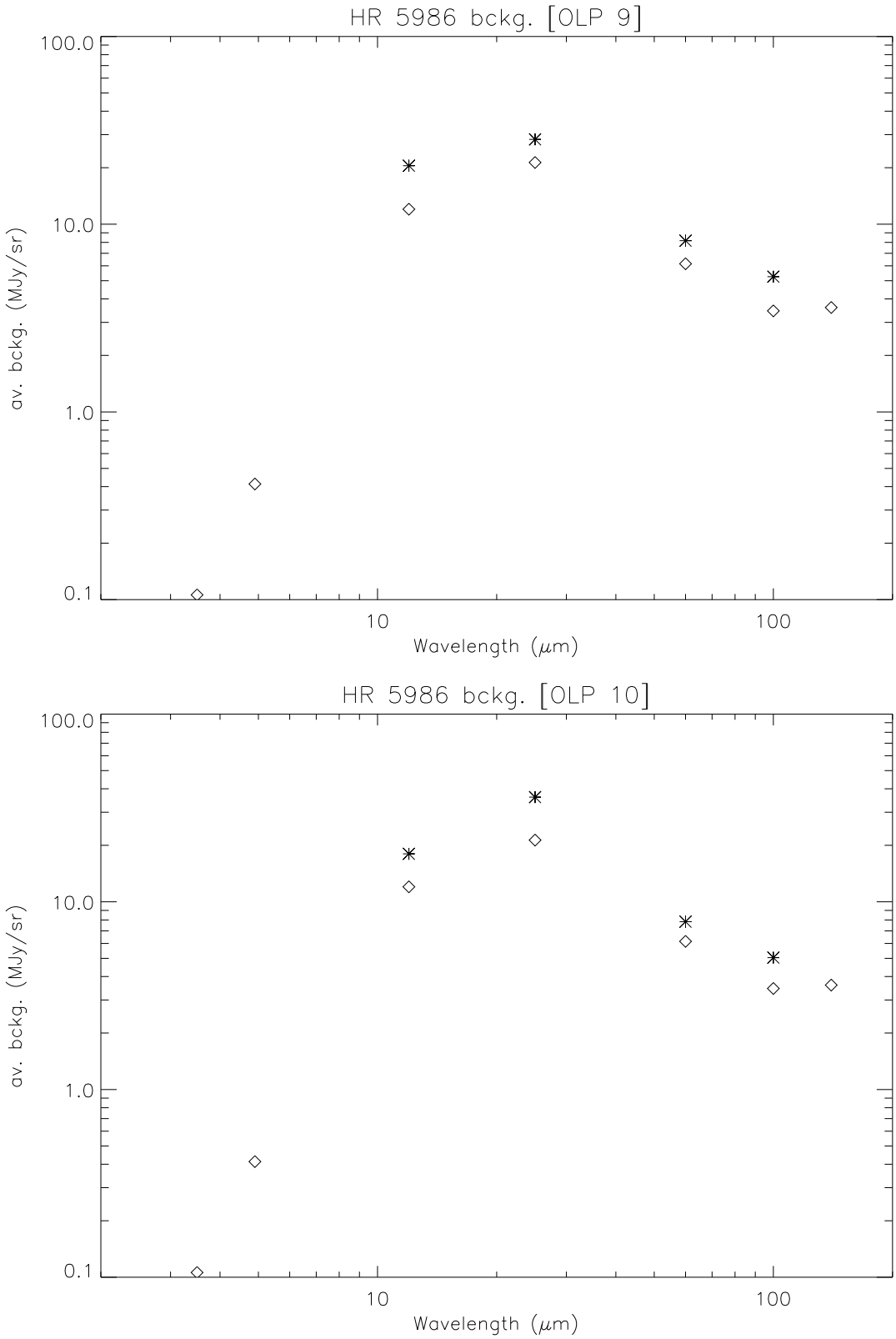

Figure 8.45: Comparison of surface brightness from chopped PHT photometry of the background beam for HR 5986 with COBE, both for OLP 9.01 (upper panel) and OLP 10.0b5. Asterisk: PHT-P and PHT-C photometry, diamond: COBE.

Evaluation Log

1) HR 5447

a) Chopped point source photometry

Measurements:
PHT-P : PPAP26900346 FCS = 25 um
PHT-C100: PCAP08900847 FCS = 90 um
PCAP26900347 FCS = 90 um (b)

Colour correction: black body, T = 6687K

Model: Cohen

Det	cwl (μm)	OLP 9	OLP 10	IRAS	Model	Δ (OLP 9)	Δ (OLP 10)
P2	25.0	0.430	0.316	0.295	0.256	68.15	23.43
C1	60.0	0.108	0.106	0.106	0.044	144.09	139.98
C1b	60.0	0.071	0.075	0.106	0.044	59.59	68.87
C1	90.0	0.081	0.087		0.019	313.29	347.71
C1b	90.0	0.026	0.026		0.019	35.32	35.41

2) BS 5062

a) Chopped point source photometry

Measurements:
PHT-P: ppap19500982 FCS = 7.3, 25 um
PHT-C: pcap19500983 FCS = 90 um

Colour correction: black body, T = 8087K

Model: Hammersley

Det	cwl (μm)	OLP 9	OLP 10	IRAS	Model	Δ (OLP 9)	Δ (OLP 10)
P1	7.3	2.545	2.567		2.559	-0.54	0.33
P1	12.0	1.724	1.656	1.010	0.972	77.44	70.46
P2	25.0	0.668	0.418	0.235	0.227	194.76	84.24
C1	60.0	0.082	0.072	0.108	0.039	111.86	85.10
C1	90.0	0.098	0.106		0.017	476.38	519.25

b) Background photometry from off-source beam

Det	λ	OLP9 (MJy/sr)	OLP10 (MJy/sr)	COBE (MJy/sr)
P1	7.3	10.93	6.23	
P1	12.0	26.45	24.57	13.16
P2	25.0	20.73	27.52	24.14
C1	60.0	7.45	6.41	7.09
C1	90.0	3.70	3.80	

3) HR 5304

a) Chopped point source photometry

Measurements:
PHT-C: PCAP24602245 FCS = 60 um

Colour correction: black body, T = 6143 K

Model: Cohen

Det	cwl (μm)	OLP 9	OLP 10	Model	Δ (OLP 9)	Δ (OLP 10)
C1	60.0	0.110	0.107	0.043	159.11	151.77
C1	100.0	0.027	0.027	0.015	78.09	76.60

b) Background photometry from off-source beam

Det	λ	OLP9 (MJy/sr)	OLP10 (MJy/sr)	COBE (MJy/sr)
C1	60.0	10.63	10.10	9.55
C1	100.0	6.61	6.38	4.93

4) HR 5914

a) Chopped point source photometry

Measurements:
PHT-P: PPAP28100658 FCS = 25 um
PHT-C: PCAP28100659 FCS = 90 um

Colour correction: black body, T = 5676 K

Model: Cohen

Det	cwl (μm)	OLP 9	OLP 10	IRAS	Model	Δ (OLP 9)	Δ (OLP 10)
P2	25.0	0.461	0.389	0.408	0.381	21.02	2.02
C1	60.0	0.147	0.144	0.099	0.066	122.36	118.68
C1	90.0	0.016	0.020		0.029	-43.52	-30.60

b) Background photometry from off-source beam

Det	λ	OLP9 (MJy/sr)	OLP10 (MJy/sr)	COBE (MJy/sr)
P2	25.0	23.61	29.80	23.28
C1	60.0	7.44	6.77	6.76
C1	90.0	6.20	6.24	

5) HR 5986

a) Chopped point source photometry

Measurements:
PHT-P1 : ppap74801108 FCS = 12 um
PHT-P2 : ppap74801002 FCS = 25 um
PHT-C1 : pcap27702221 FCS = 60 um

Colour correction: black body, T = 6084 K

Model: Hammersley

Det	cwl (μm)	OLP 9	OLP 10	IRAS	Model	Δ (OLP 9)	Δ (OLP 10)
P1	12.0	2.234	2.390	2.242	2.216	0.85	7.87
P2	25.0	0.761	0.678	0.527	0.518	46.77	30.76
C1	60.0	0.269	0.262	0.106	0.089	202.72	194.39
C1	100.0	0.054	0.053	0.258	0.032	69.95	66.59

b) Background photometry from off-source beam

Det	λ	OLP9 (MJy/sr)	OLP10 (MJy/sr)	COBE (MJy/sr)
P1	12.0	20.50	18.02	12.02
P2	25.0	28.32	36.12	21.32
C1	60.0	8.17	7.84	6.16
C1	100.0	5.25	5.04	3.45

Chapter 9

Multi-aperture Photometry

TBW

Chapter 10

Chopped High Resolution Mapping

TBW

Chapter 11

Staring Mode Spectroscopy

11.1 Consistency Check of Calibration Method with Calibration Standards

Summary

- Staring mode spectroscopy was successfully revalidated.
- From measurements of standard stars we derive an absolute accuracy of better than $\pm 10\,\%$ and a relative spectral shape accuracy of better than $\pm 20\,\%$ for the large flux ranges of $1 - 8000\,\mathrm{Jy}$ with the SS-array and $0.2 - 1800\,\mathrm{Jy}$ with the SL-array.
- Observations of longer than 1024 s become smoother with the revised and extended dynmaic spectral response calibration.

11.1.1 PHT40 Spectroscopy: Consistency Check of PHT-S Dynamic Response Calibration on Calibration Stars

Motivation

We process on-source and off-source measurements of several calibration stars of different brightness (HR 7001 = Vega, HR 5340, HR 7469, HR 7924, HR 7980, HR 8487) which were used to establish the dynamic relative spectral reponse function surfaces of CALG file PS-DYNAMIC and check whether the input model SED is reproduced.

Method

We compare the stellar SEDs of OLP 10.0b5 with the flux models by Hammersley and with OLP 9.01. Relative differences are plotted. For HR 7980 only the OLP 10.1 data are available.

Results

In Figs. 11.1 to 11.6 we perform the comparison with OLP9 and the model.
For HR 7001 (Vega) OLP 10 and OLP 9 yield identical results. The measured spectrum is on average about 5 % below the model and the relative spectral shape is consistent within ±5 %.
For HR 5340 (α Boo) OLP 10 and OLP 9 yield practically identical results. The absolute accuracy of the SED is on average better than 5 % and the relative spectral shape better than ±10 %.
For HR 7469 OLP 10 and OLP 9 yield practically identical results, there are discrepancies in the order of 5 % at the long wavelength end which are introduced by the two-threshold deglitching. The absolute accuracy of the SED is on average better than 5 % and the relative spectral shape better than ±15 %.
For HR 7924 OLP 10 and OLP 9 yield identical results. The measured spectrum is on average about 10 % above the model and the relative spectral shape consistent within ±20 %.
For HR 8487 differences between OLP 10 and OLP 9 are in the order of 10 %. The absolute accuracy of the SED is on average better than 10 % and the relative spectral shape better than ±20 %.
For HR 7980 the absolute accuracy of the SED is on average better than 5 % and the relative spectral shape better than ±10 %.
We conclude from this analysis that the absolute calibration accuracy is better than 10 % while the relative calibration accuracy (relative spectral shape) is better than 20 % for the flux range 1 – 8000 Jy with SS and 0.2 – 1800 Jy with SL.

Conclusions

- The quality of the dynamic spectral response function calibration for PHT-S is successfully verified by the self-consistency check on calibration standards.
- For some stars we get perfect agreement with the flux model, for other stars some discrepancies remain. From all test cases we derive an absolute calibration accuracy of better than 10 %, the relative accuracy is always better than 20 %. This accuracy holds down to flux levels of 10^{-14} W m^{-2} μm^{-1} (corresponding to a flux density in frequency range of $\sim$ 300 mJy at 10 μm).

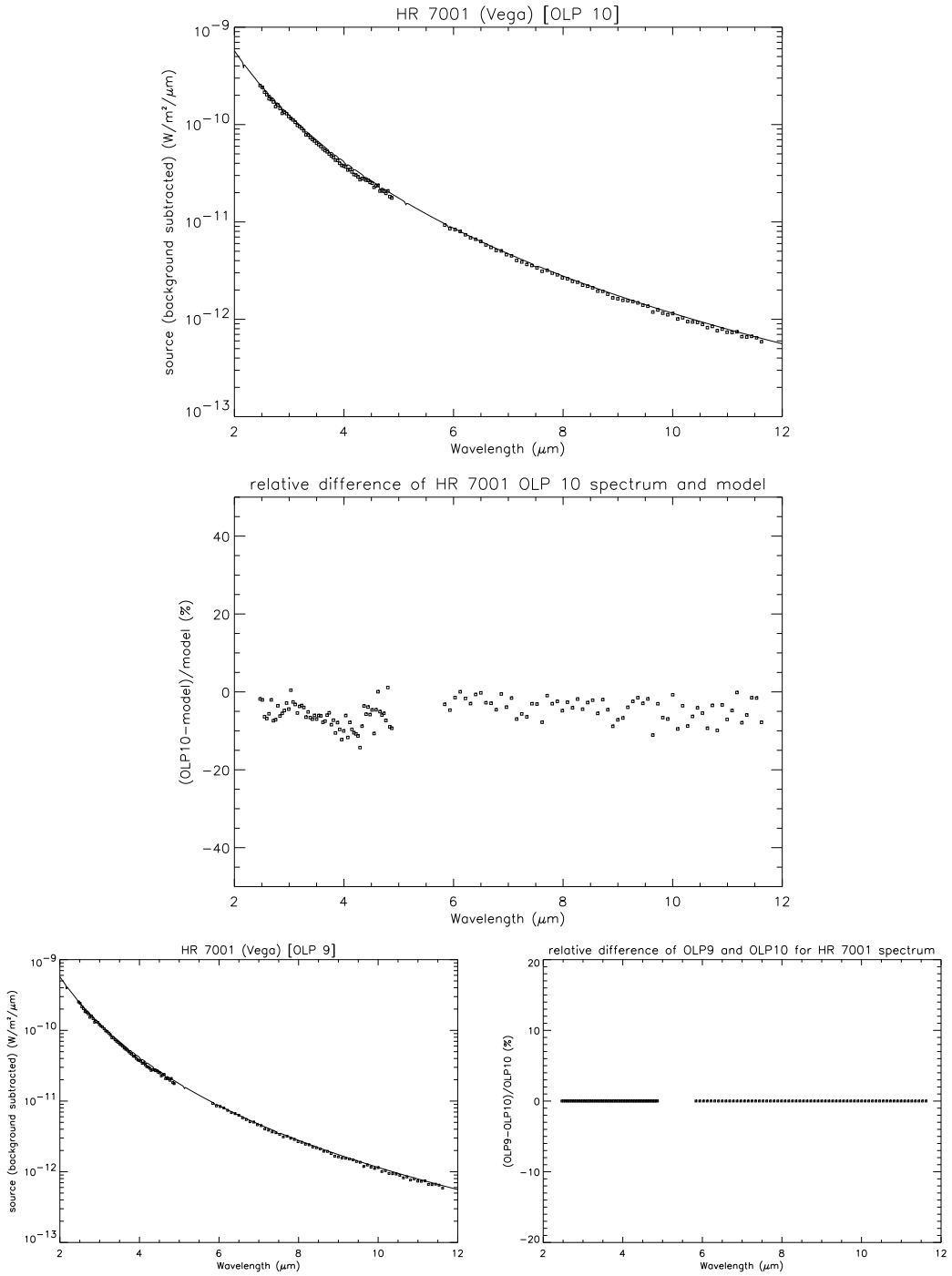

Figure 11.1: Comparison of the spectrum of HR 7001 (Vega, background subtracted) with the flux model by Hammersley. OLP 10.0b5 spectrum (upper panel), relative difference to model (middle panel), OLP 9.01 spectrum (lower left panel) and the relative difference between both OLP versions (lower right panel).

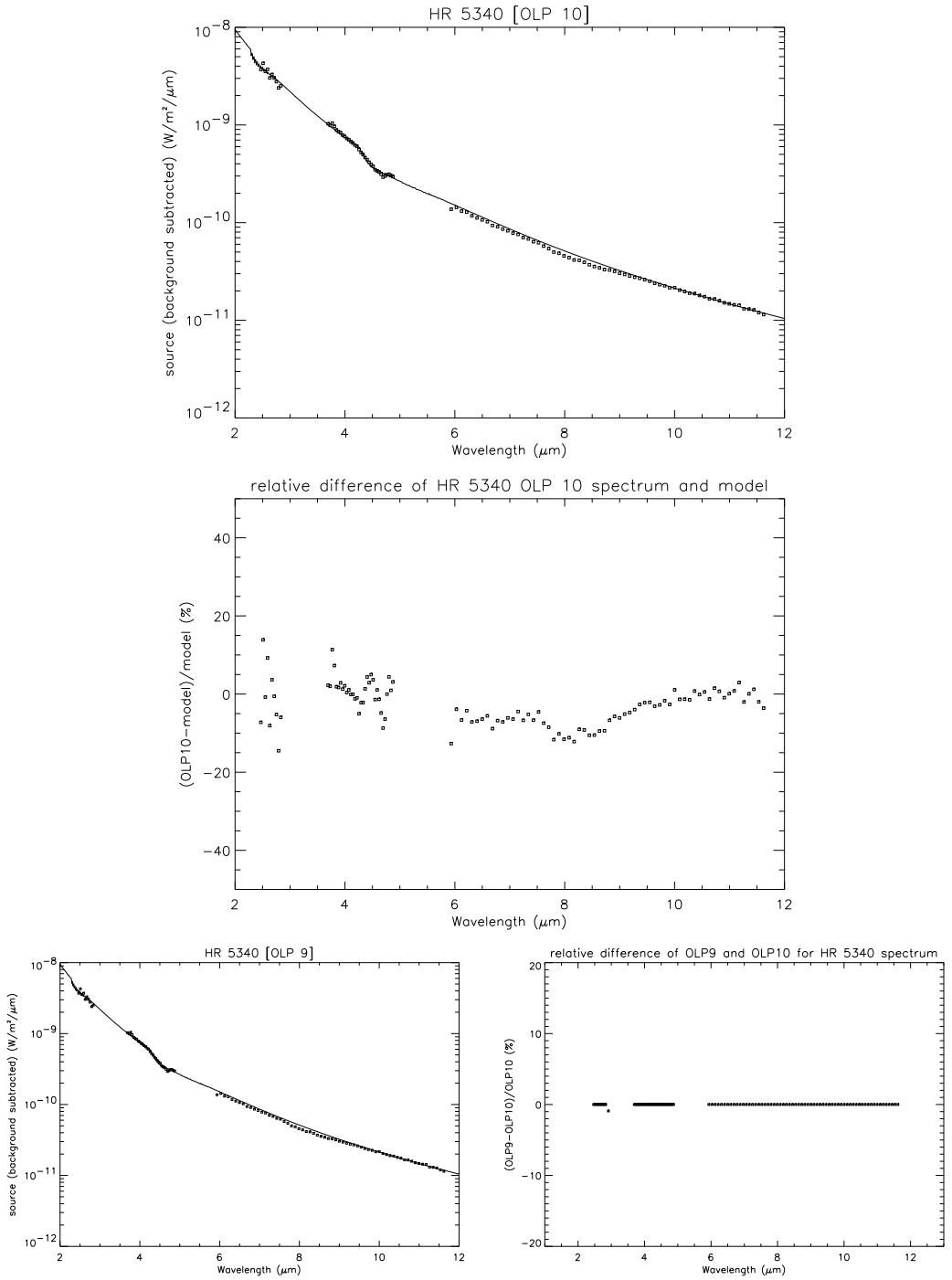

Figure 11.2: Comparison of the spectrum of HR 5340 (α Boo, background subtracted) with the flux model by Hammersley. OLP 10.0b5 spectrum (upper panel), relative difference to model (middle panel), OLP 9.01 spectrum (lower left panel) and the relative difference between both OLP versions (lower right panel).

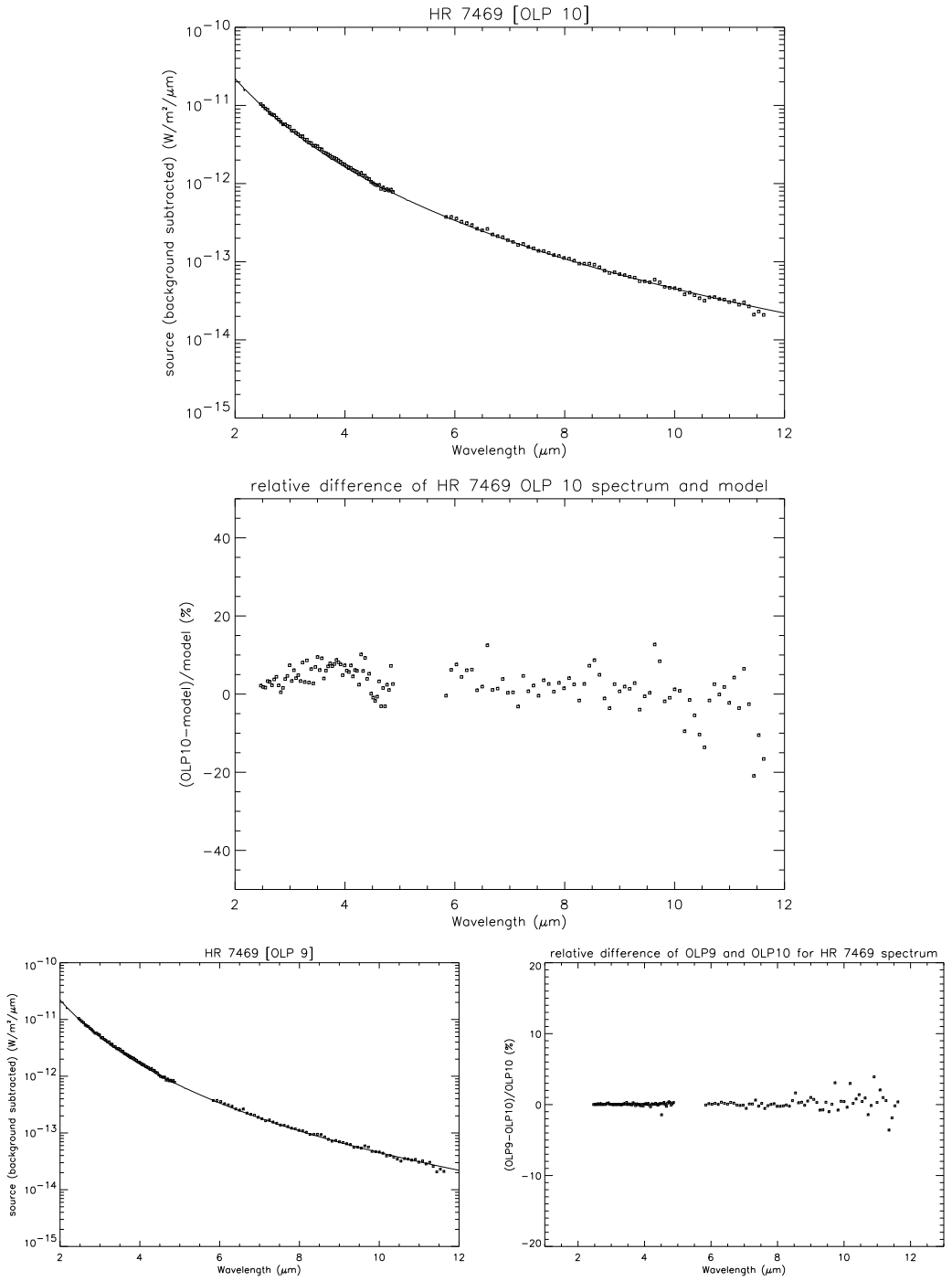

Figure 11.3: Comparison of the spectrum of HR 7469 (background subtracted) with the flux model by Hammersley. OLP 10.0b5 spectrum (upper panel), relative difference to model (middle panel), OLP 9.01 spectrum (lower left panel) and the relative difference between both OLP versions (lower right panel).

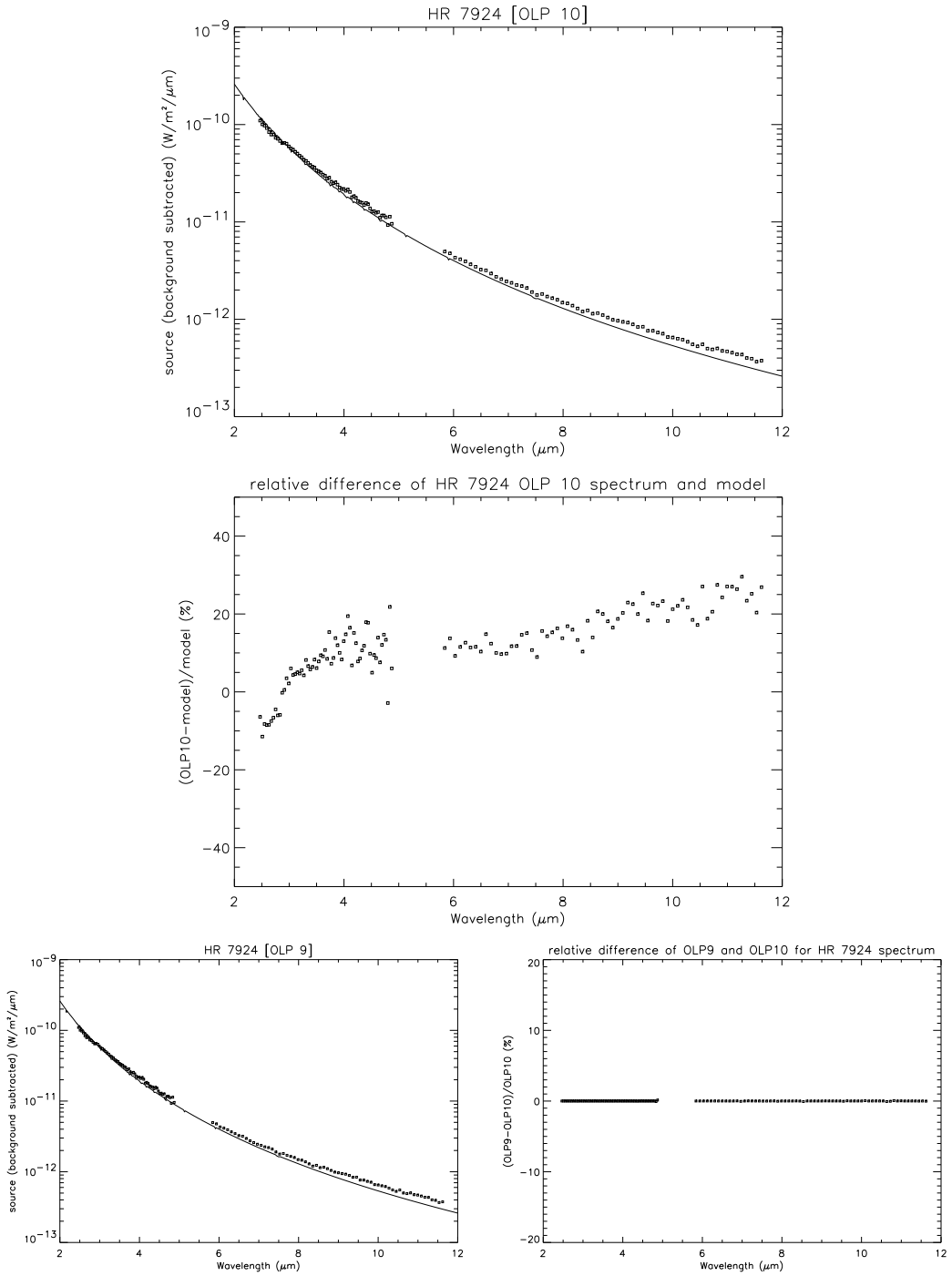

Figure 11.4: Comparison of the spectrum of HR 7924 (background subtracted) with the flux model by Hammersley. OLP 10.0b5 spectrum (upper panel), relative difference to model (middle panel), OLP 9.01 spectrum (lower left panel) and the relative difference between both OLP versions (lower right panel).

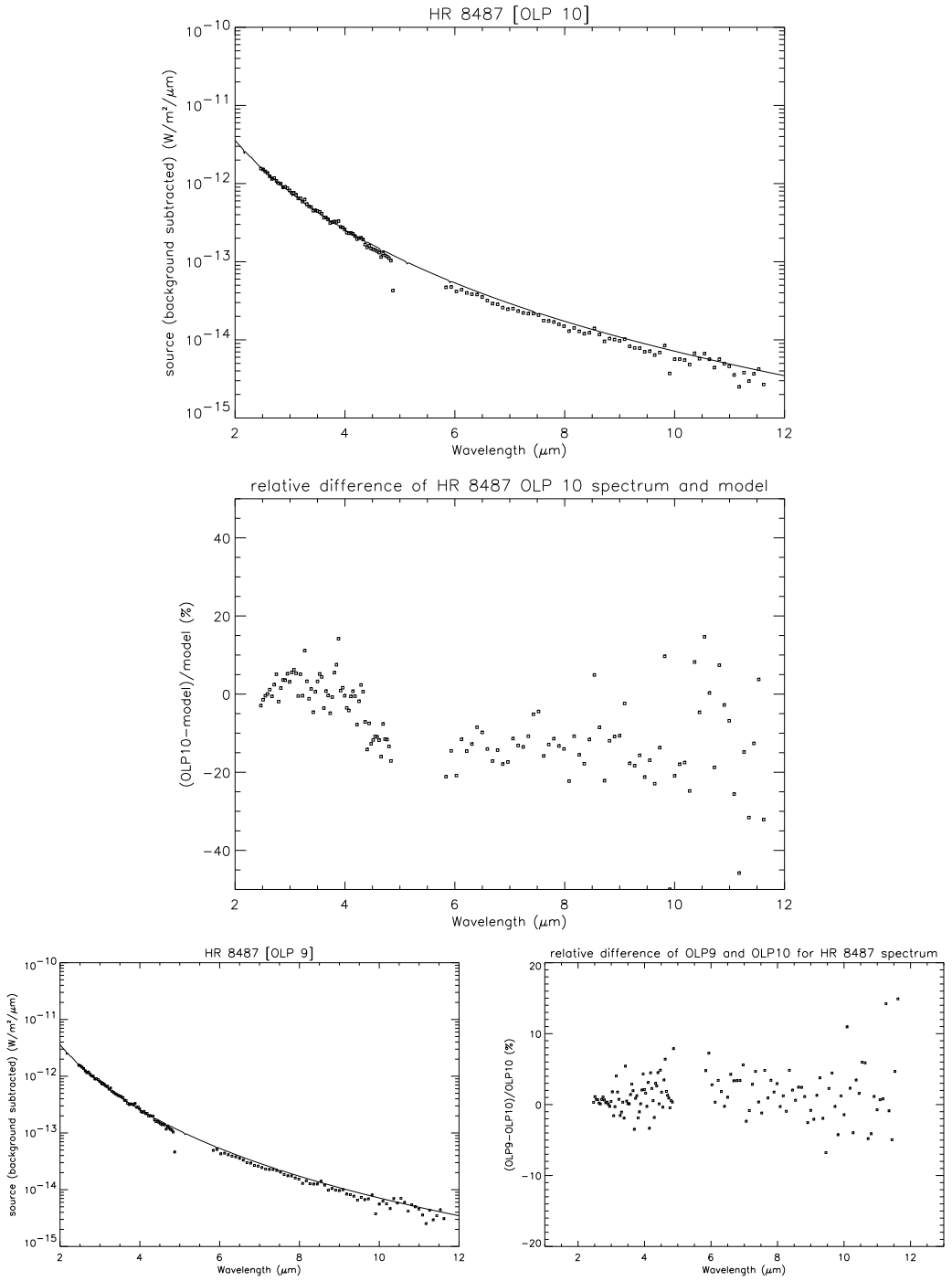

Figure 11.5: Comparison of the spectrum of HR 8487 (background subtracted) with the flux model by Hammersley. OLP 10.0b5 spectrum (upper panel), relative difference to model (middle panel), OLP 9.01 spectrum (lower left panel) and the relative difference between both OLP versions (lower right panel).

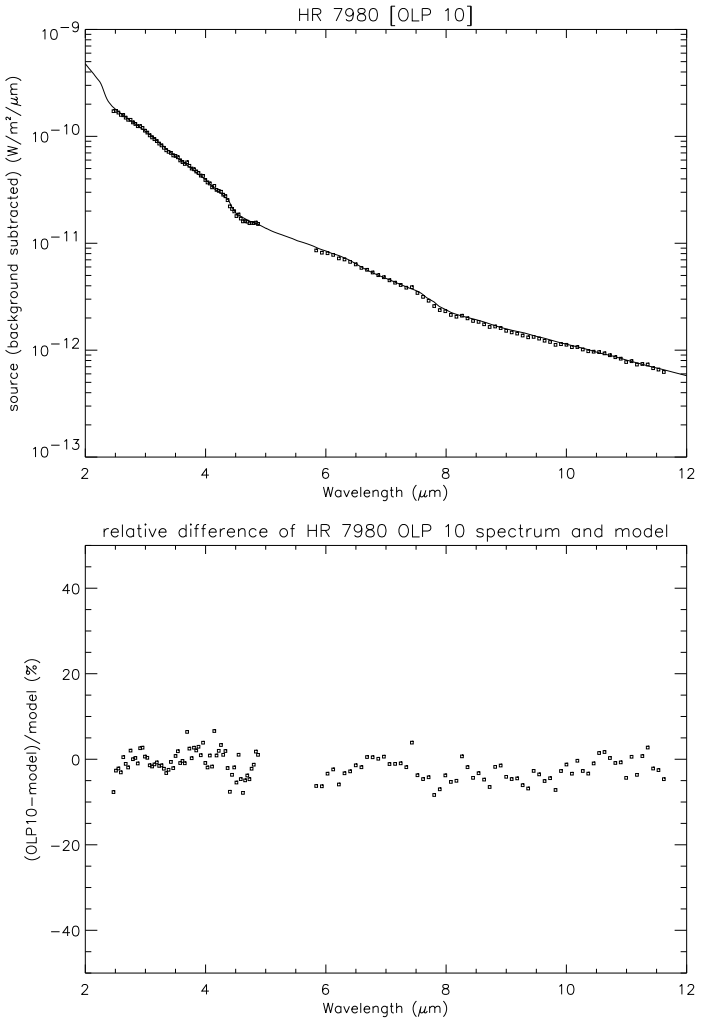

Figure 11.6: Comparison of the spectrum of HR 7980 (background subtracted) with the flux model by Cohen. OLP 10.1 spectrum (upper panel) and relative difference to model (lower panel).

11.1.2 PHT40 Spectroscopy: Consistency Check of PHT-S Dynamic Response Calibration Extension for Measurements Greater Equal 1024 Seconds

Motivation

For OLP 9 the dynamic calibration was established from calibration standards up to 1024 s. For longer measurement times the calibration found for 1024 s was applied beyond. For OLP 10 the dynamic calibration was extended to 4096 s (the longest measurement time in use).

Method

We intercompare OLP9 and OLP10 results of spectra with measurement times longer than 512 s. We compare both on-source and off-source spectra as well as the resulting source spectra. Relative differences are plotted.

Results

Figs. 11.7 to 11.20 show for the faint stars GL 752a, GL 905, LHS 1070, HD 198269, HD 209621, HD 201626 and HD 26 the spectra of the stars and the spectra of the on-source and off-source positions, respectively. We note, that in general the OLP 10 spectra look smoother in particular for the off-source positions and the stellar spectra.

Conclusions

- Spectra of faint stars and sky background with exposure times of longer than 1024 s look smoother with OLP 10 after the extension of the dynamic spectral response calibartion to 4096 s.

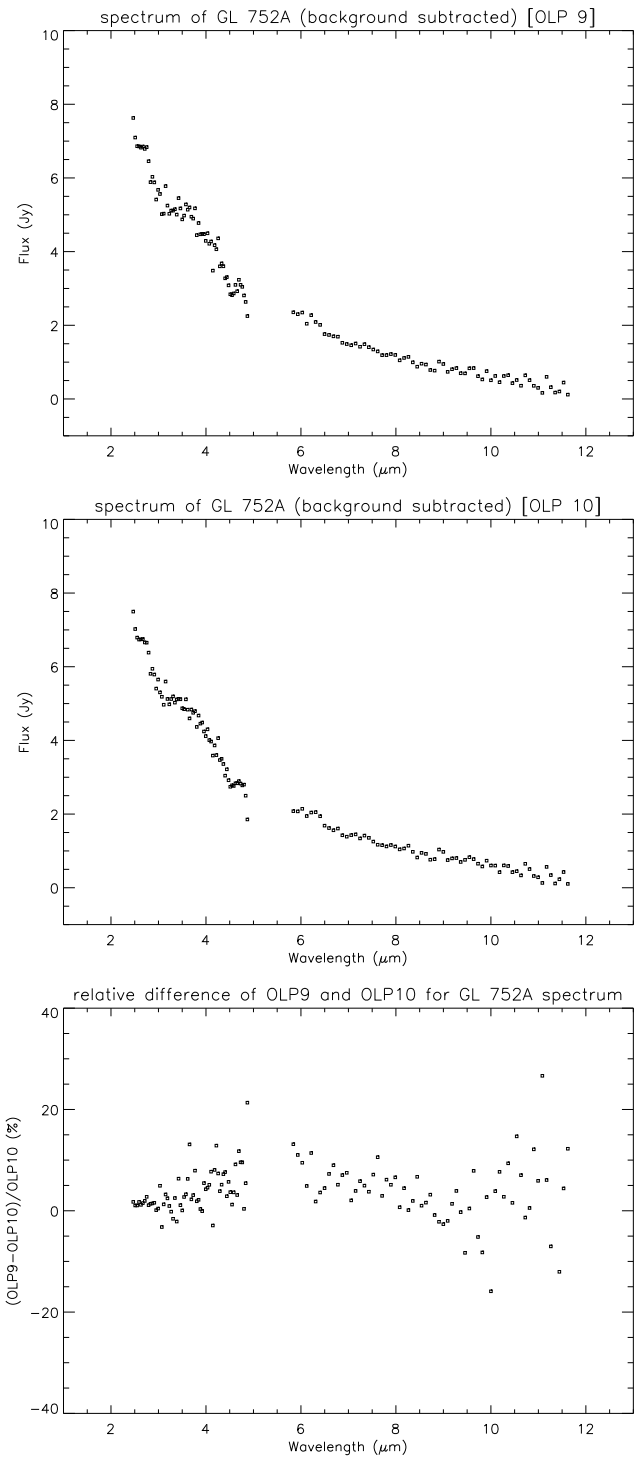

Figure 11.7: Intercomparison of the background subtracted spectra of GL 752A from OLP 9.01 (upper panel) and from OLP 10.0b5 (middle panel) and the relative difference of both versions (lower panel).

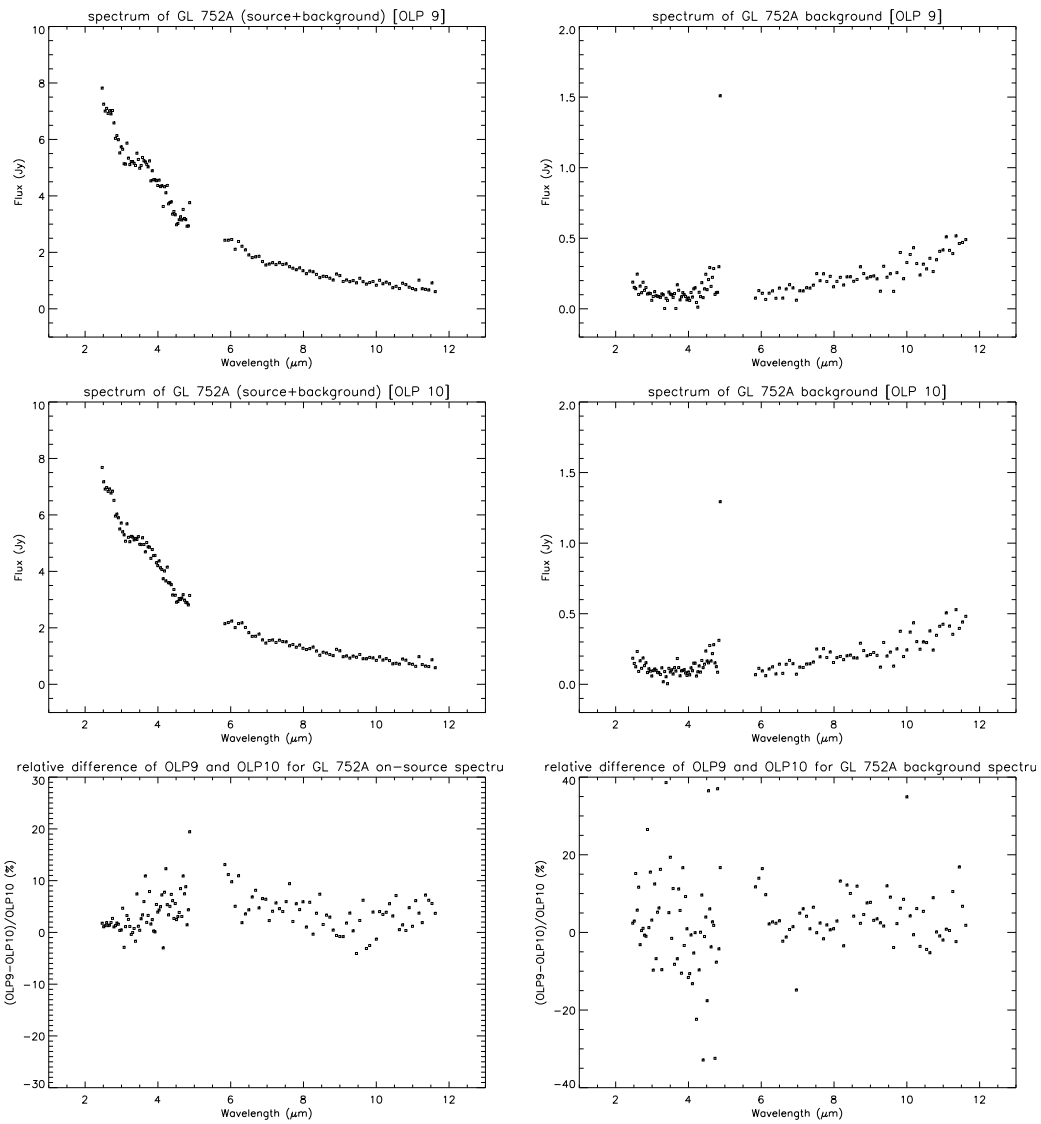

Figure 11.8: Intercomparison of the on-source and off-source spectra of GL 752A from OLP 9.01 (upper panels) and from OLP 10.0b5 (middle panels) and the relative difference of both versions (lower panels).

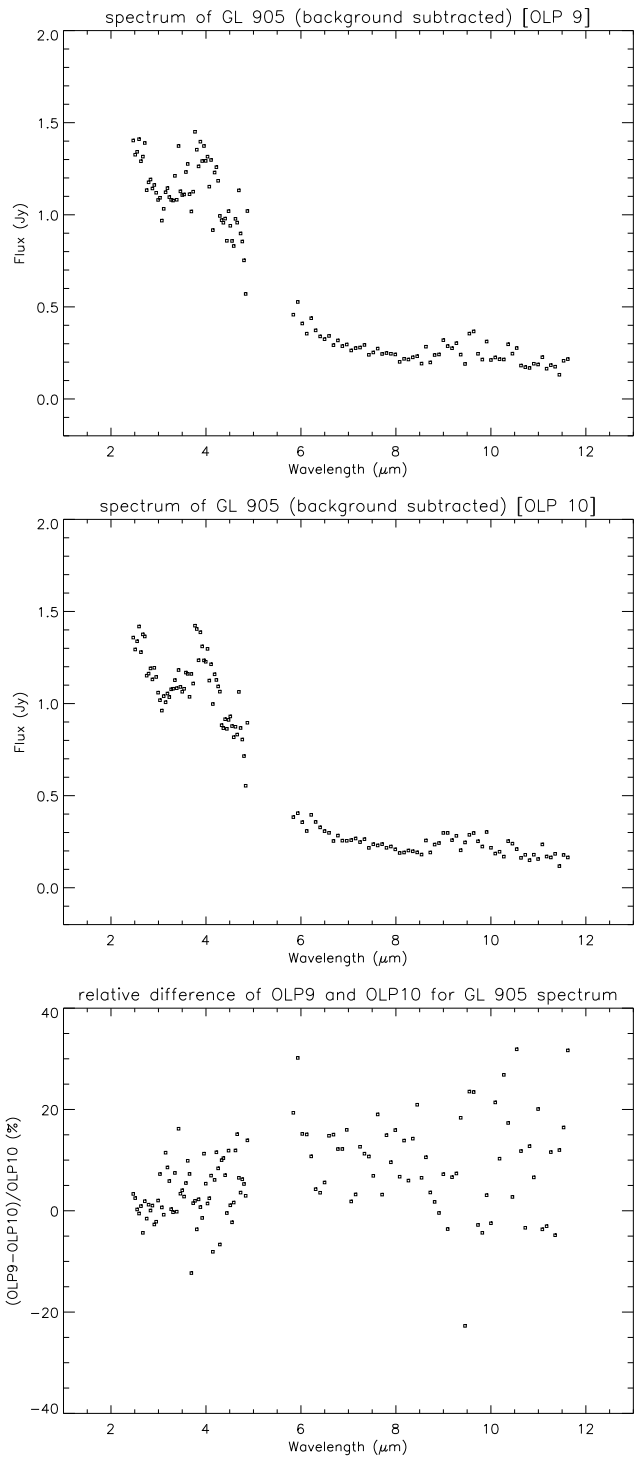

Figure 11.9: Intercomparison of the background subtracted spectra of GL 905 from OLP 9.01 (upper panel) and from OLP 10.0b5 (middle panel) and the relative difference of both versions (lower panel).

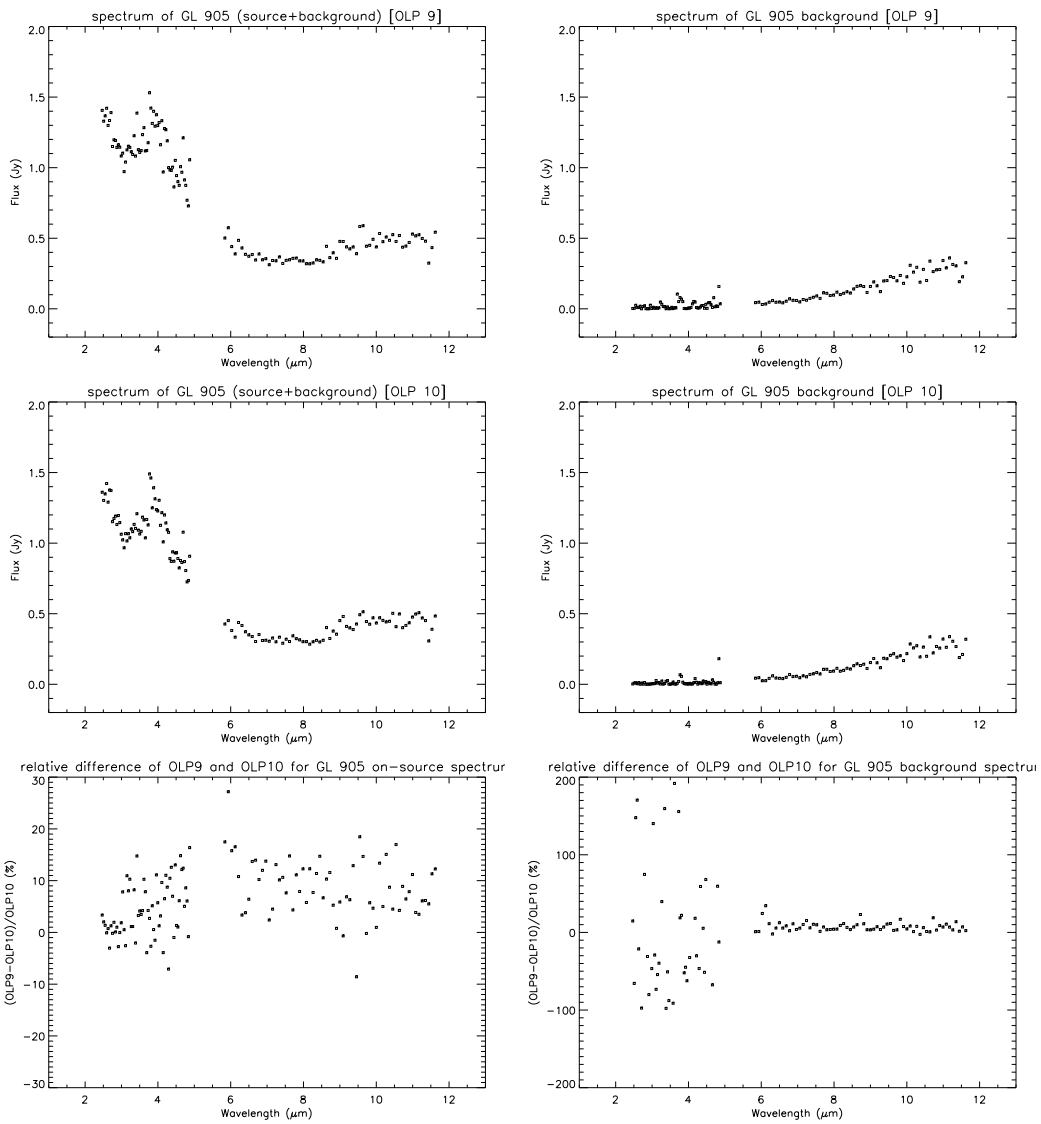

Figure 11.10: Intercomparison of the on-source and off-source spectra of GL 905 from OLP 9.01 (upper panels) and from OLP 10.0b5 (middle panels) and the relative difference of both versions (lower panels).

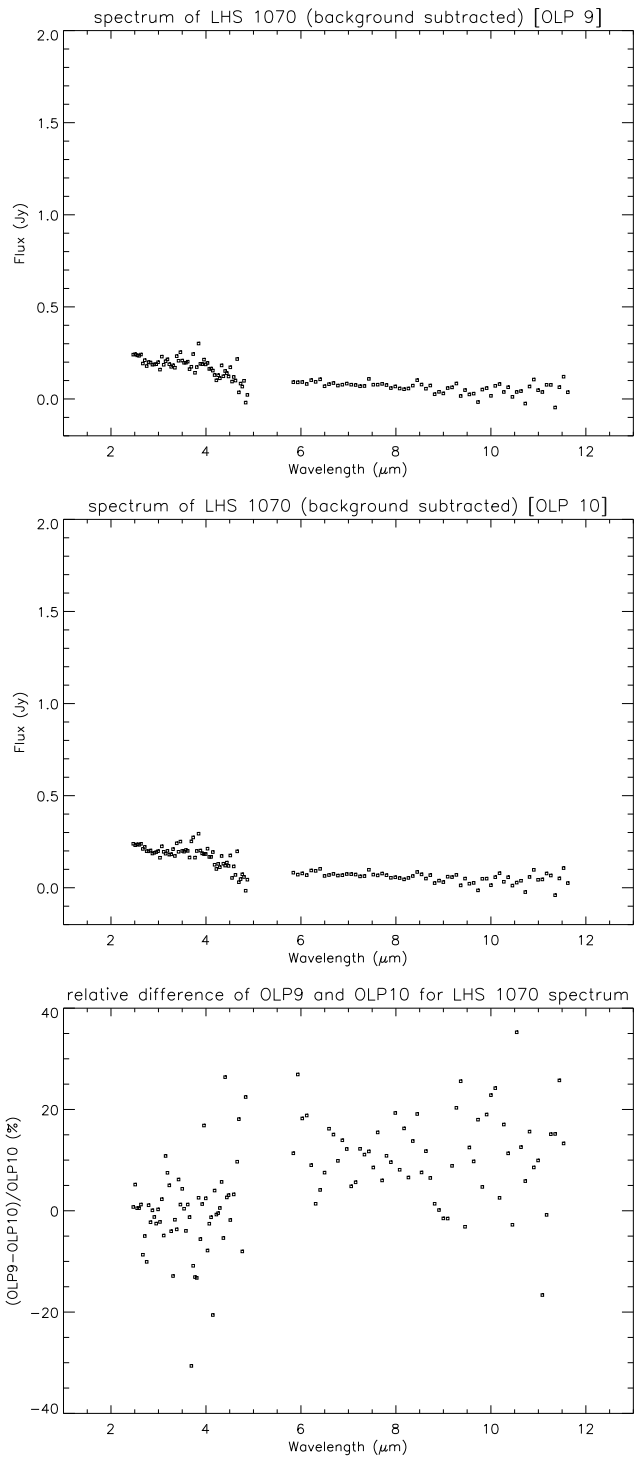

Figure 11.11: Intercomparison of the background subtracted spectra of LHS 1070 from OLP 9.01 (upper panel) and from OLP 10.0b5 (middle panel) and the relative difference of both versions (lower panel).

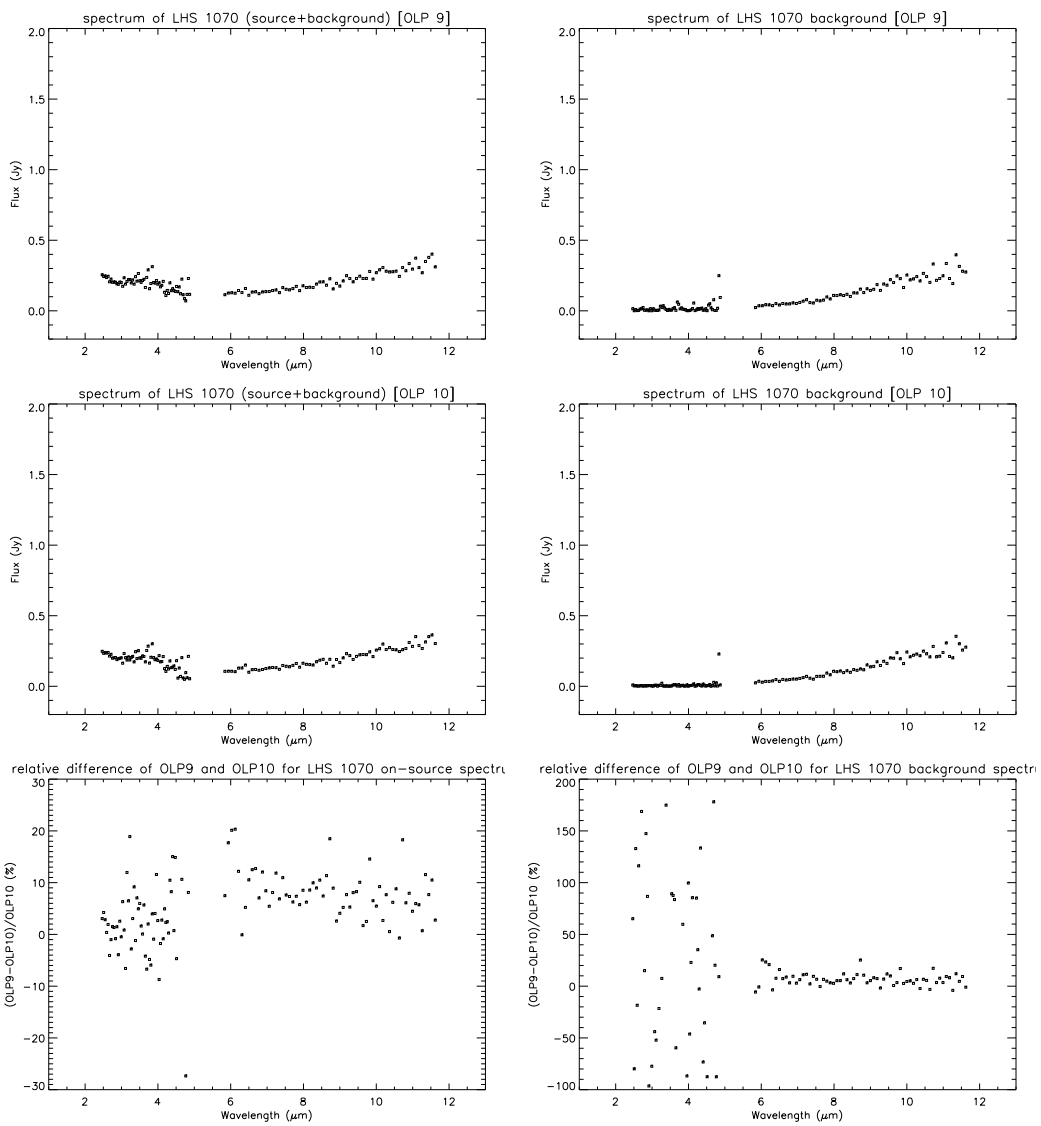

Figure 11.12: Intercomparison of the on-source and off-source spectra of LHS 1070 from OLP 9.01 (upper panels) and from OLP 10.0b5 (middle panels) and the relative difference of both versions (lower panels).

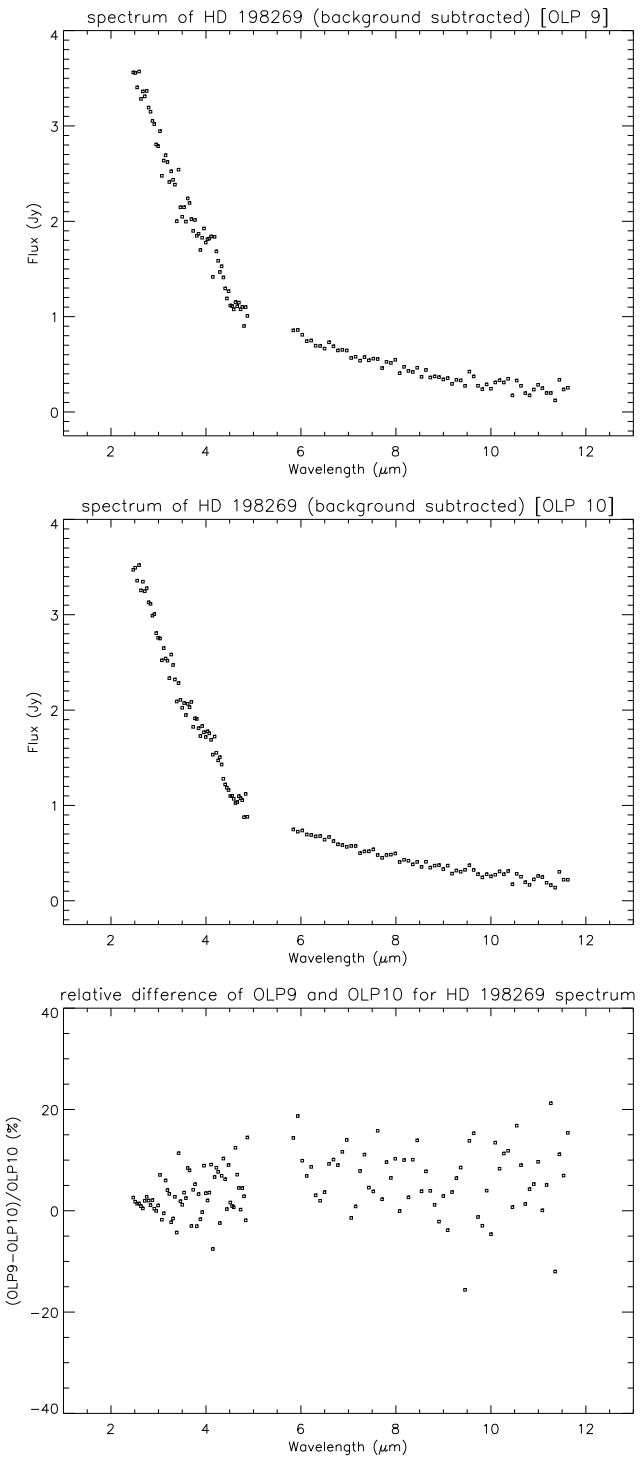

Figure 11.13: Intercomparison of the background subtracted spectra of HD 198269 from OLP 9.01 (upper panel) and from OLP 10.0b5 (middle panel) and the relative difference of both versions (lower panel).

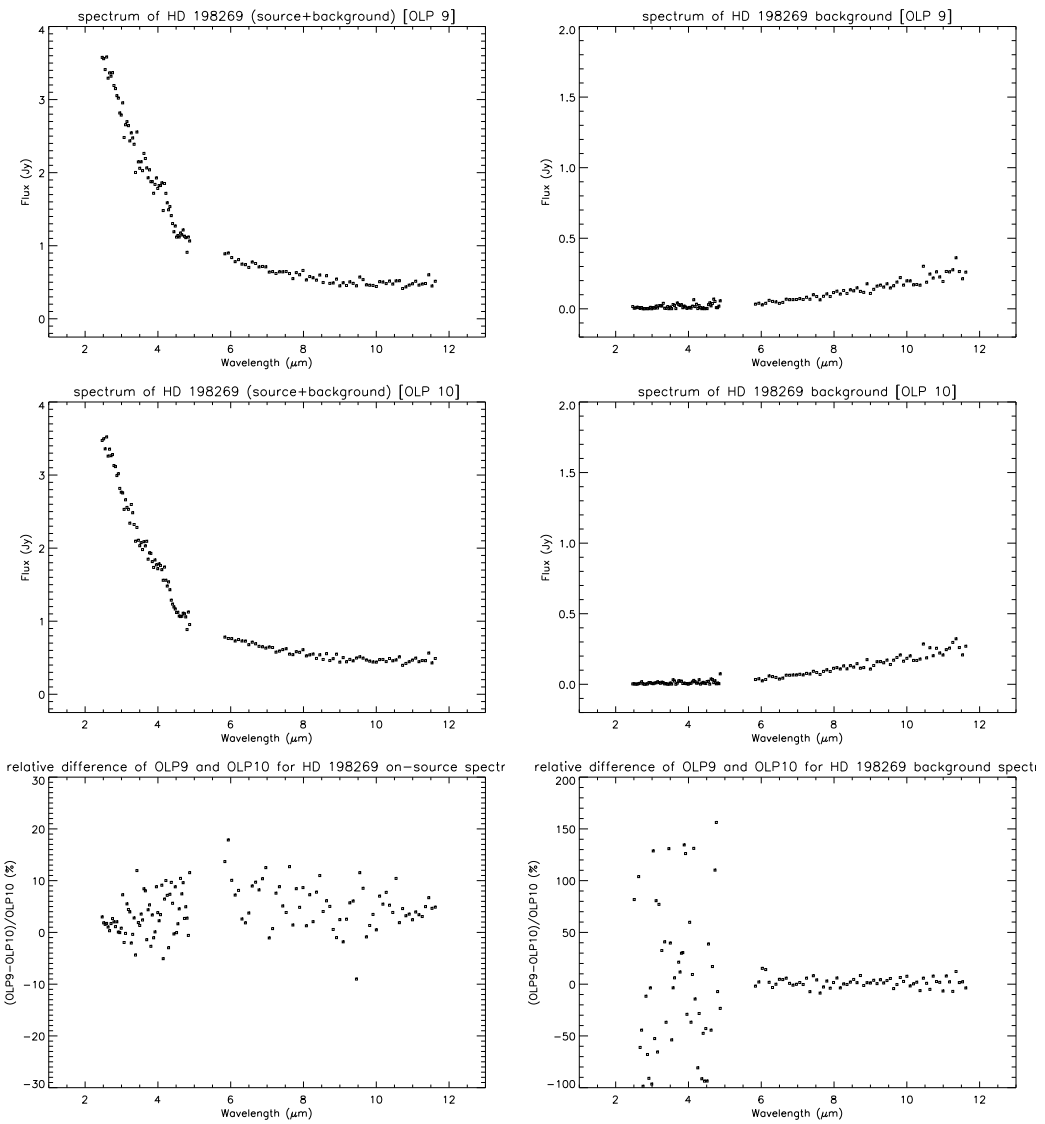

Figure 11.14: Intercomparison of the on-source and off-source spectra of HD 198269 from OLP 9.01 (upper panels) and from OLP 10.0b5 (middle panels) and the relative difference of both versions (lower panels).

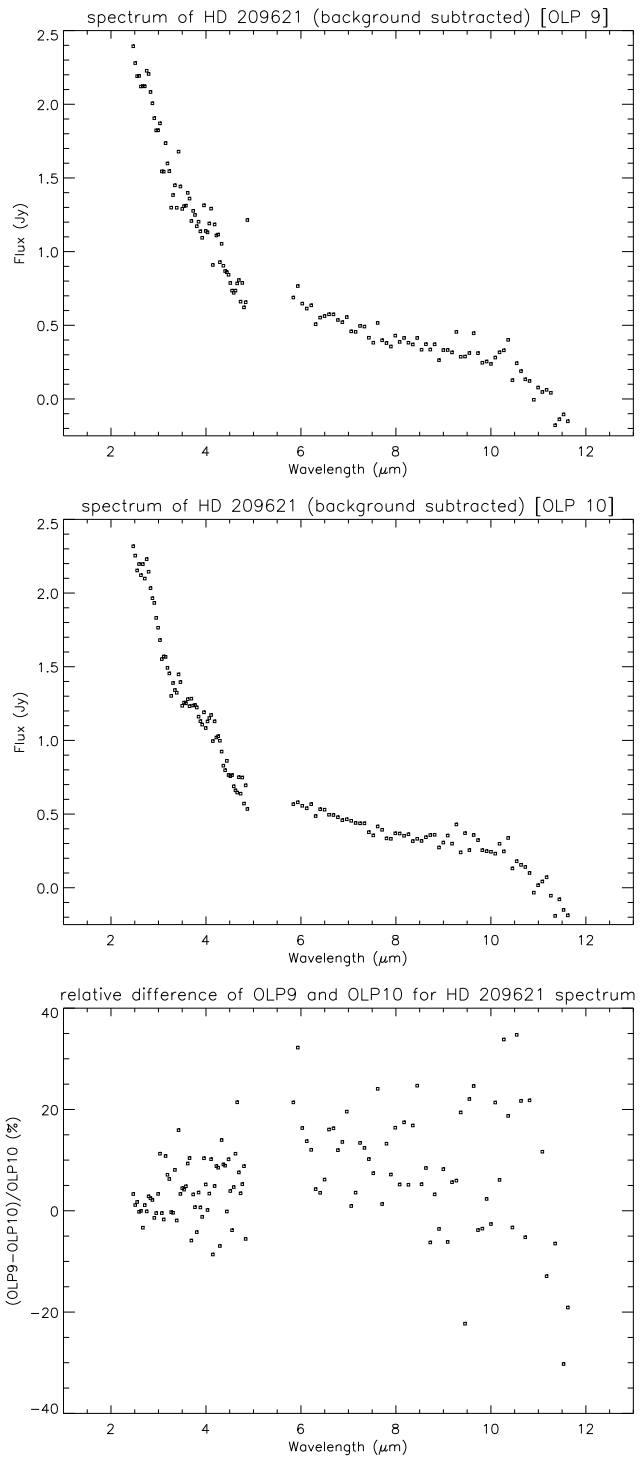

Figure 11.15: Intercomparison of the background subtracted spectra of HD 209621 from OLP 9.01 (upper panel) and from OLP 10.0b5 (middle panel) and the relative difference of both versions (lower panel).

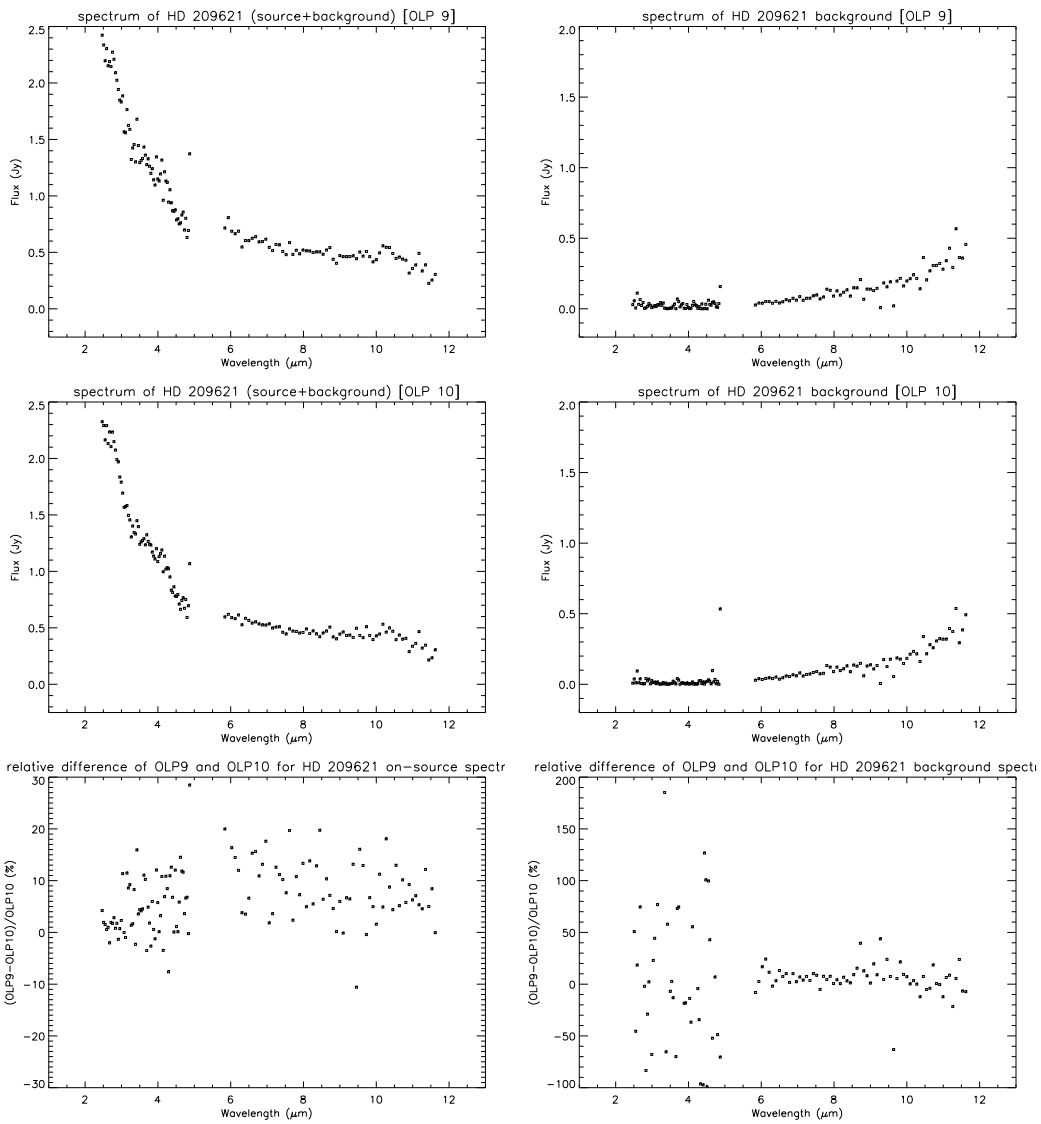

Figure 11.16: Intercomparison of the on-source and off-source spectra of HD 209621 from OLP 9.01 (upper panels) and from OLP 10.0b5 (middle panels) and the relative difference of both versions (lower panels).

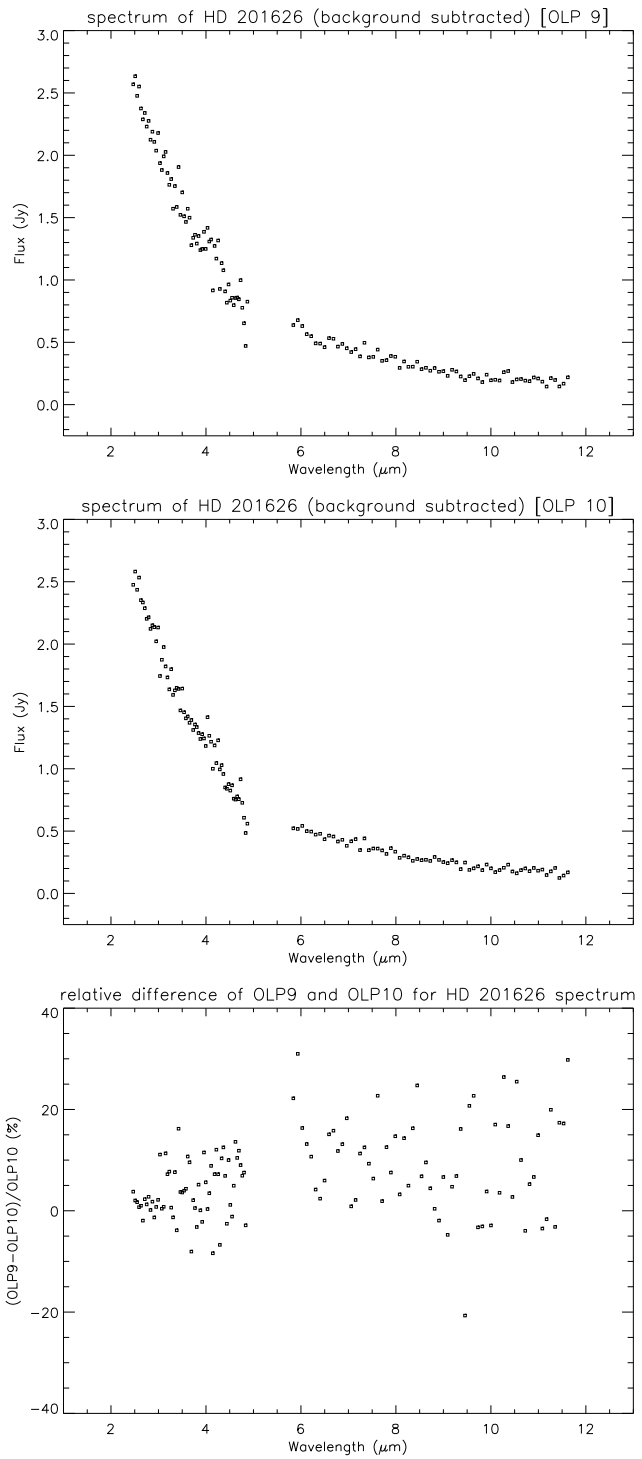

Figure 11.17: Intercomparison of the background subtracted spectra of HD 201626 from OLP 9.01 (upper panel) and from OLP 10.0b5 (middle panel) and the relative difference of both versions (lower panel).

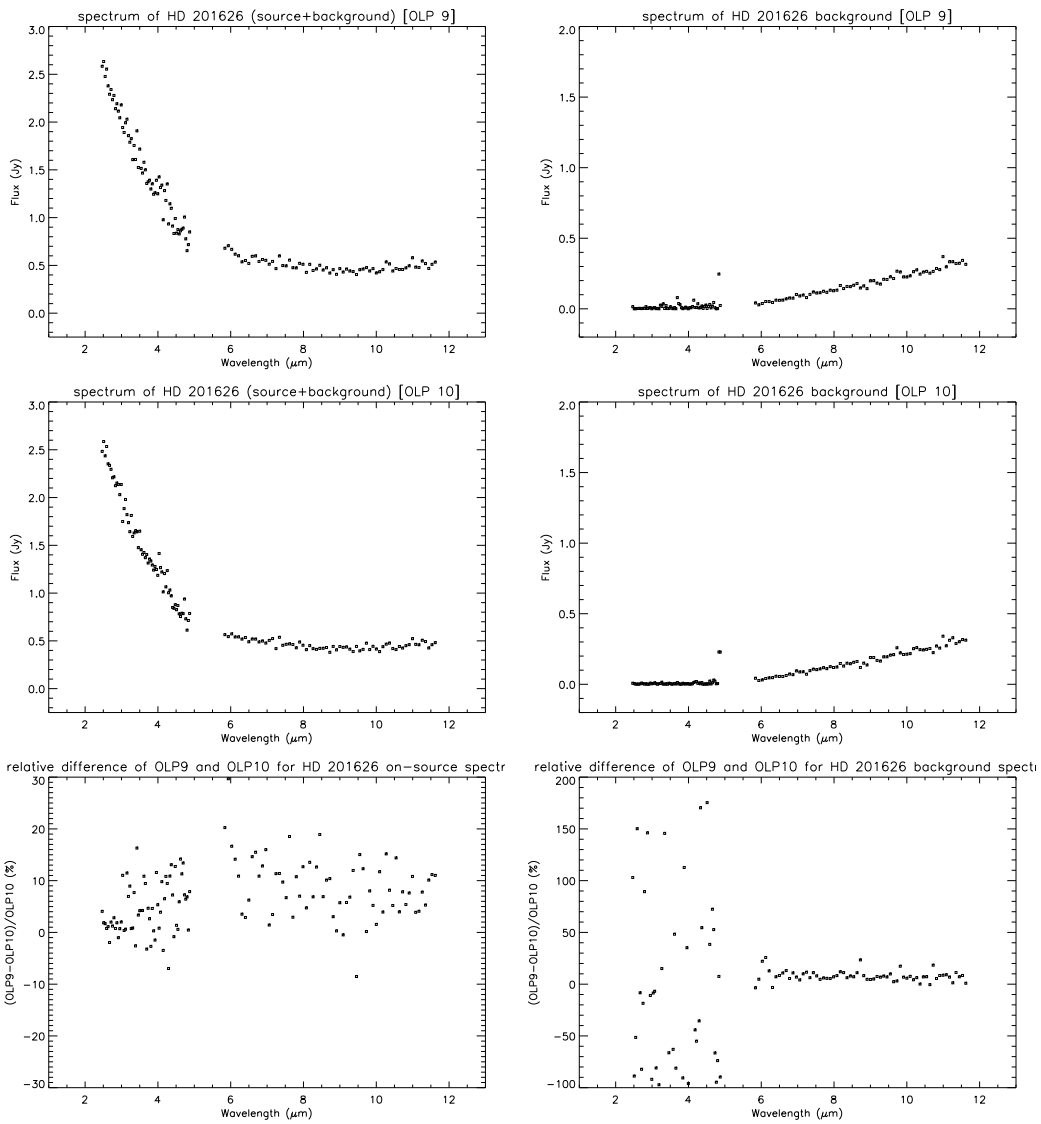

Figure 11.18: Intercomparison of the on-source and off-source spectra of HD 201626 from OLP 9.01 (upper panels) and from OLP 10.0b5 (middle panels) and the relative difference of both versions (lower panels).

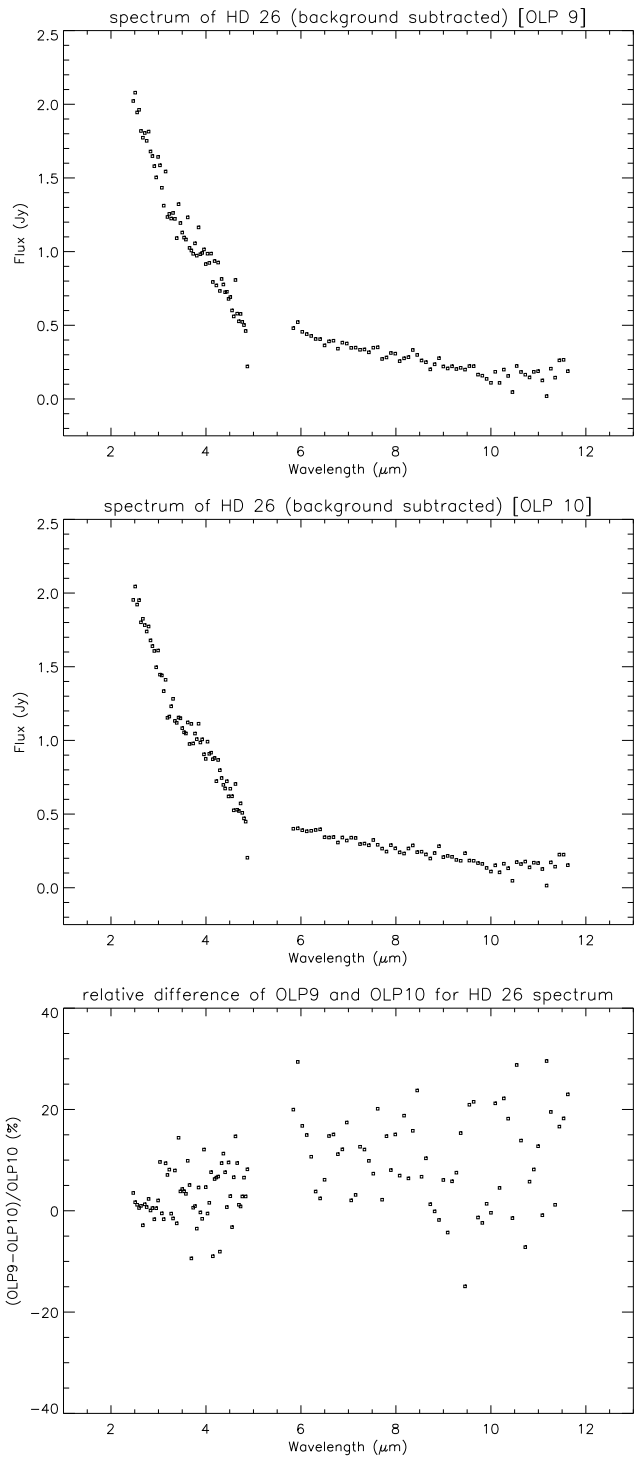

Figure 11.19: Intercomparison of the background subtracted spectra of HD 26 from OLP 9.01 (upper panel) and from OLP 10.0b5 (middle panel) and the relative difference of both versions (lower panel).

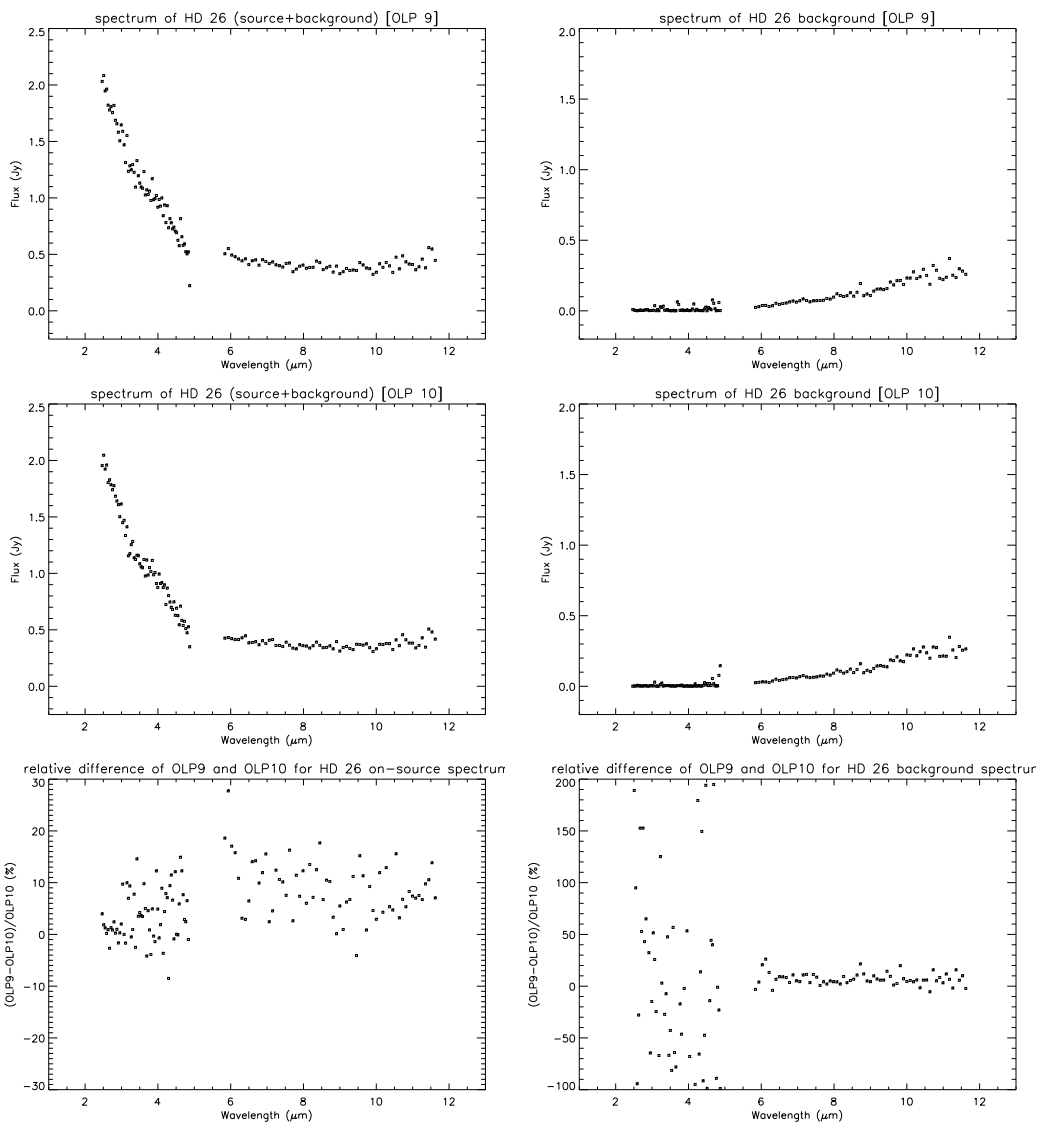

Figure 11.20: Intercomparison of the on-source and off-source spectra of HD 26 from OLP 9.01 (upper panels) and from OLP 10.0b5 (middle panels) and the relative difference of both versions (lower panels).

11.2 Comparison with Stellar Models for Non-calibration Stars

Summary

- Staring mode spectroscopy was successfully revalidated.
- From measurements of bright stars we derive an absolute accuracy of better than ±10 % and a relative spectral shape accuarcy of better than ±20 %.

11.2.1 PHT40 Spectroscopy: MIR Spectra of Stars from Staring On and Off PHT-S Measurements

Motivation

We found four stars in the data base with similar spectral type as standard stars but different brightness. It is therefore possible to test absolute and relative accuracy of the new ISOPHOT-S dynamic calibration on different brightness levels than standard stars used to establish the calibration. The properties of the four stars are compiled in Table 11.1:

Table 11.1: Properties of stars used for verification of staring ISOPHOT-S spectra

Name	**Spectral Type**	**Apparent Brightness** (mag)	**Reference Star**	**Spectral Type**	**Apparent Brightness** (mag)
BS 6056	M0.5III	$m_v = 2.74$	HD 25025 (=γ Eri)	M0.5III	$m_v = 2.931$
BS 8679	M0III	$m_v = 4.01$	HD 95578 (=61 Leo)	M0III	$m_v = 3.079$
BS 337	M0III	$m_v = 2.06$	BS 337 (=β And)	M0III	$m_v = 2.06$
BS 617	K2III	$m_v = 2.00$	BS 617 (=α Ari)	K2III	$m_v = 2.00$

Method

We scale the model spectra of HD 25025 and HD 95578 according to the apparent brightness ratio in the V band. BS 337 and BS 617 are calibration stars, however, the measurements considered here are not in the calibration data base. We compare the absolute fluxes and relative shapes of the OLP 10.0b5 ISOPHOT-S spectra with the scaled model spectra and with OLP 9.01. Relative differences are plotted.

Results

In Figs. 11.21 to 11.24 we perform the comparison with OLP9 and the model.
For BS 6056 OLP 10 and OLP 9 yield identical results. The measured spectrum is on average about 10 % above the model and the relative spectral shape is consistent within ±15 %.
For BS 8679 differences between OLP 10 and OLP 9 are not more than a few per cent. The measured spectrum is somewhat oblique w.r.t. the scaled model. The average absolute accuracy is in the order of 10 % and the relative spectral shape coincides within ±20 %.
For BS 337 OLP 10 and OLP 9 yield identical results. The absolute accuracy is better than 5 %, the relative spectral shape is better than ±10 %.
For BS 617 OLP 10 and OLP 9 yield identical results. The absolute accuracy is better than 5 %, the relative spectral shape is better than ±15 %.
We derive similar calibration accuracies as before, i.e. an absolute calibration accuracy of better than 10 % and a relative calibration accuracy (relative spectral shape) of better than 20 %.

Conclusions

- The quality of the dynamic spectral response function calibration for PHT-S is successfully verified by the consistency check on bright stars.
- We confirm the calibration accuracy being in the range better than 10 % for absolute calibration and better than 20 % for the relative shape of the SED.

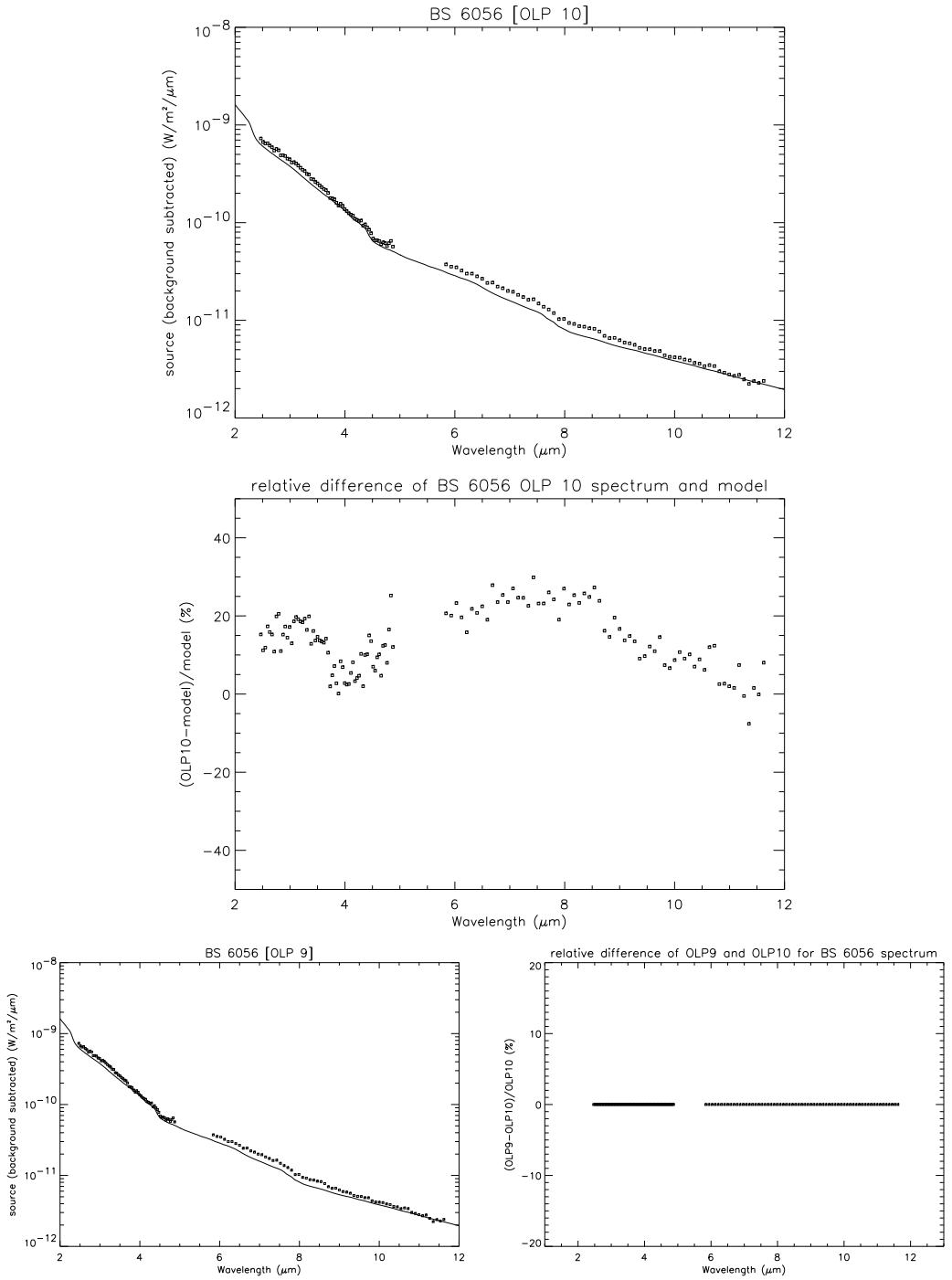

Figure 11.21: Comparison of the spectrum of BS 6056 (background subtracted) with the scaled flux model of HD 25025. OLP 10.0b5 spectrum (upper panel), relative difference to model (middle panel), OLP 9.01 spectrum (lower left panel) and the relative difference between both OLP versions (lower right panel).

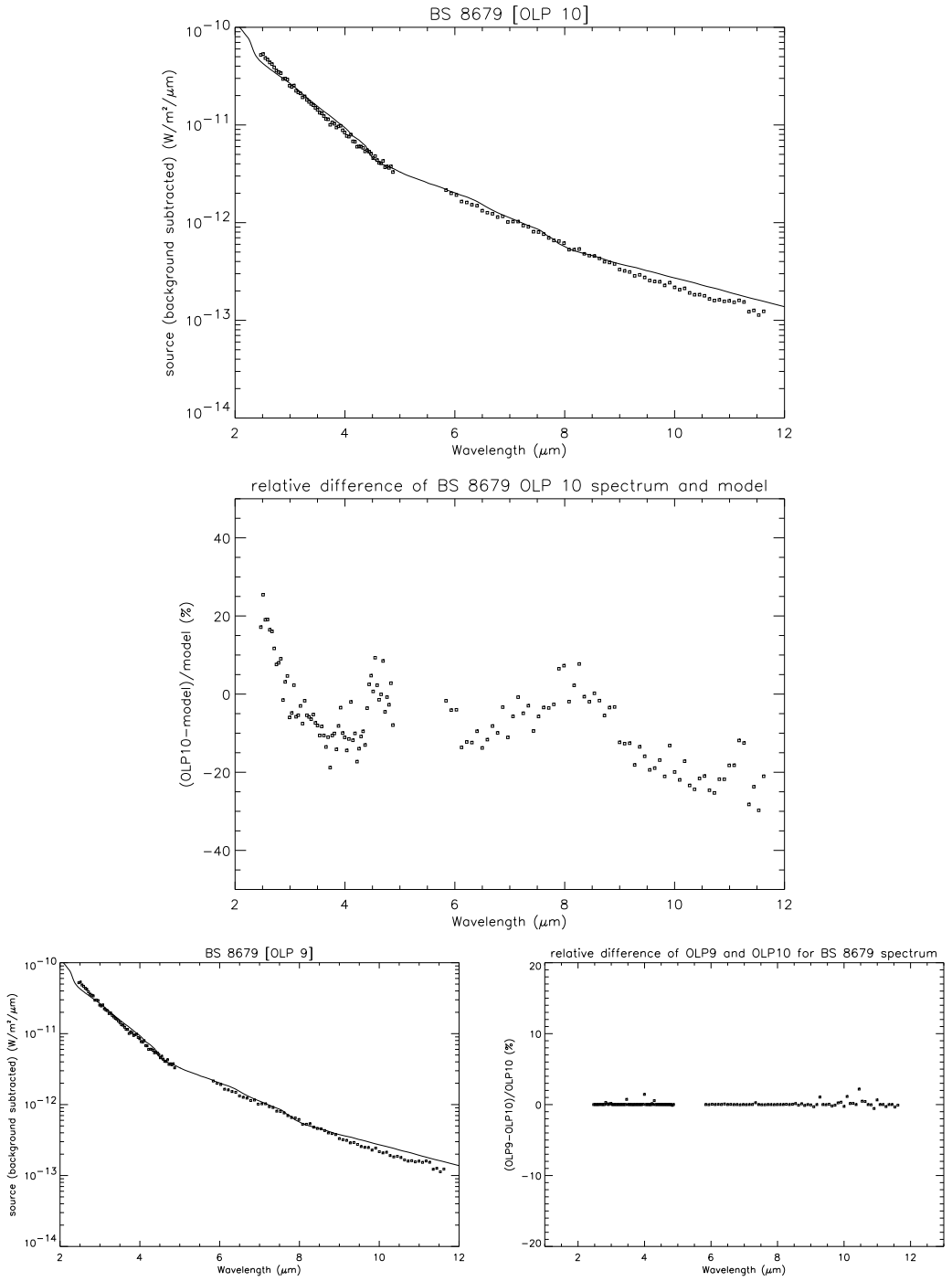

Figure 11.22: Comparison of the spectrum of BS 8679 (background subtracted) with the scaled flux model of HD 95578. OLP 10.0b5 spectrum (upper panel), relative difference to model (middle panel), OLP 9.01 spectrum (lower left panel) and the relative difference between both OLP versions (lower right panel).

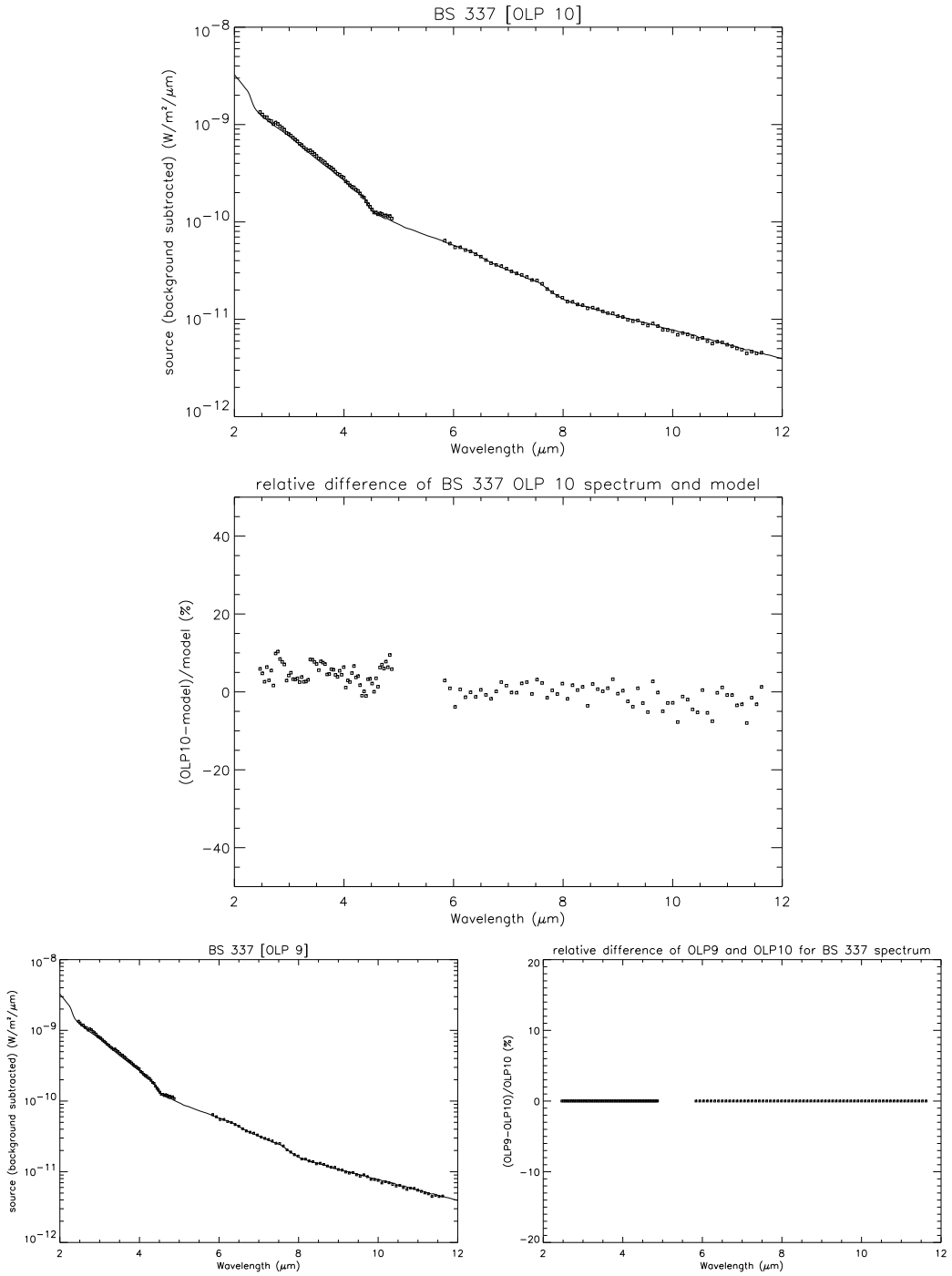

Figure 11.23: Comparison of the spectrum of BS 337 (background subtracted) with the model by Cohen. OLP 10.0b5 spectrum (upper panel), relative difference to model (middle panel), OLP 9.01 spectrum (lower left panel) and the relative difference between both OLP versions (lower right panel).

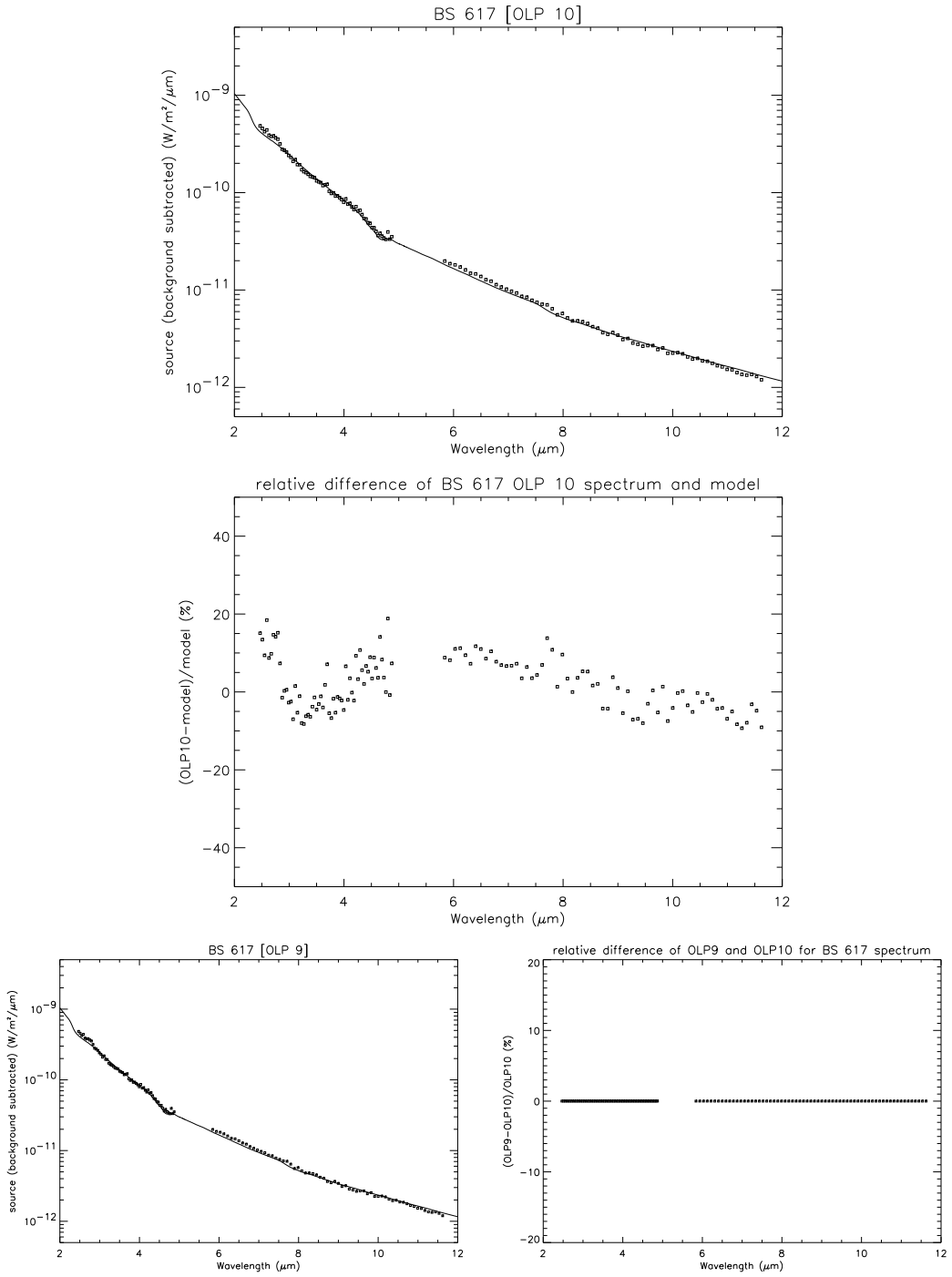

Figure 11.24: Comparison of the spectrum of BS 617 (background subtracted) with the model by Cohen. OLP 10.0b5 spectrum (upper panel), relative difference to model (middle panel), OLP 9.01 spectrum (lower left panel) and the relative difference between both OLP versions (lower right panel).

11.3 Comparison with Ground-based Spectroscopy

Summary

- Staring mode spectroscopy was successfully revalidated.
- The comparison of ISOPHOT-S spectra of galaxies and PN with groundbased 8 - 13 micron spectroscopy shows reasonable consistency, having in mind the different beam sizes on these partly extended objects.
- Repeated spectra give reasonable coincidence in the spectral features. For one case where this is not the case, it could be shown that the combined effect of off-pointing and the relative beam profile shape may explain the discrepancy.

11.3.1 PHT40 Spectroscopy: MIR Spectra of Galaxies from Staring PHT-S Measurements

Motivation

We investigate here the spectra of the three galxies NGC 253, Circinus and NGC 6946. These galaxies have SED shapes different from the ones of standard stars for which the dynamic PHT-S spectral response function was derived. There is groundbased $8-13$ micron spectroscopy available (cf. Ref. [8]).

Method

We compare the absolute fluxes and relative shapes of the ISOPHOT-S spectra with the groundbased spectroscopy. Note that we compare an aperture size of $24 \times 24\,\mathrm{arcsec}^2$ for ISOPHOT-S with 5 arcsec aperture size of the groundbased measurements. We expect therefore, that the ISOPHOT-S flux is higher, since it contains a larger fraction of the galaxies. In particular for NGC 6946, which the observer specified as an extended object, we converted the extended source flux into a point source flux by applying the effective solid angle. The galaxies are active galaxies with strong line emission. Due to the mixture of emission regions the relative line ratios may be different.

Results

Figs. 11.25 to 11.27 show the comparison of the OLP 10 product with OLP 9. Both versions give identical results. As expected, the PHT-S spectra show higher fluxes than the groundbased spectra due to the larger aperture size. For NGC 253 and NGC 6946 both types of spectra reveal the PAH emission.

Conclusions

- The comparison of ISOPHOT-S spectra of galaxies with groundbased 8 - 13 micron spectroscopy shows reasonable consistency, having in mind the different beam sizes on these active galaxies providing different mixture of activity areas.
- There is no or no significant difference between the versions 9 and 10.

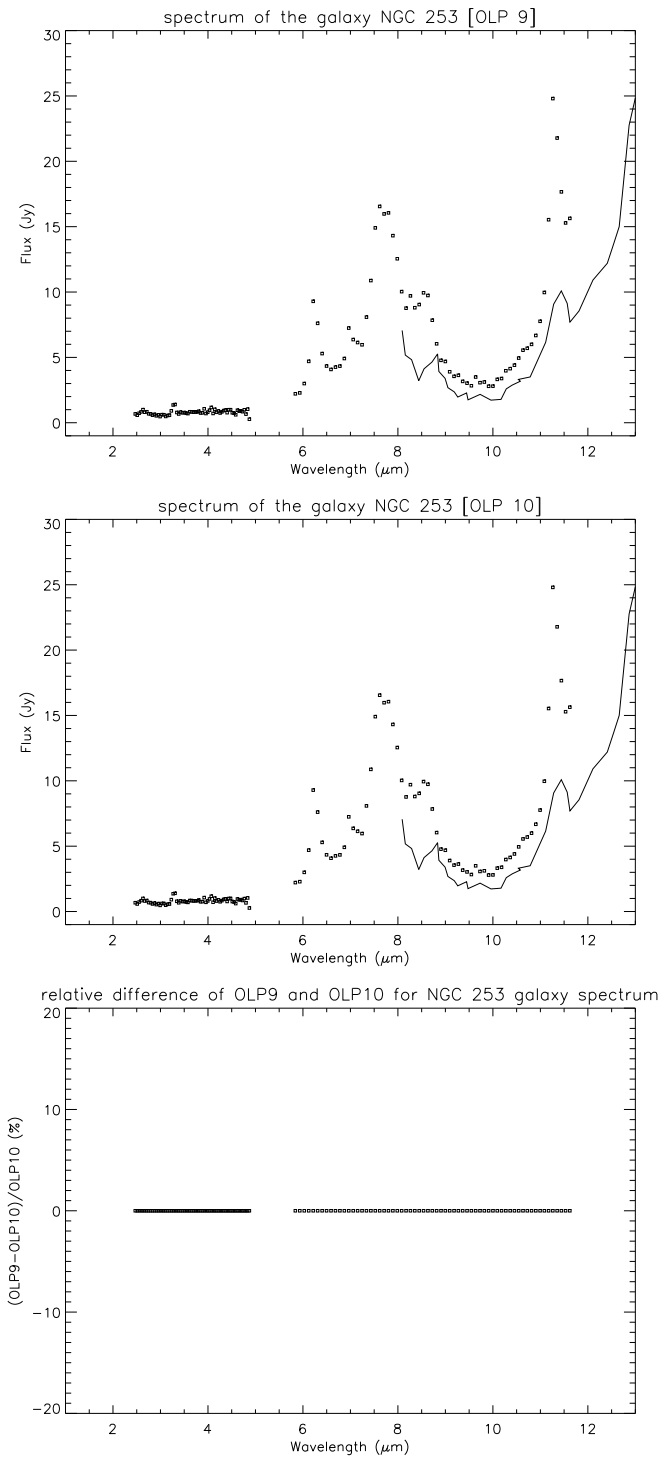

Figure 11.25: Comparison of the spectrum of NGC 253 with groundbased 8 - 13 micron spectroscopy for OLP 9.01 (upper panel), OLP 10.0b5 (middle panel) and the relative difference of both versions (lower panel).

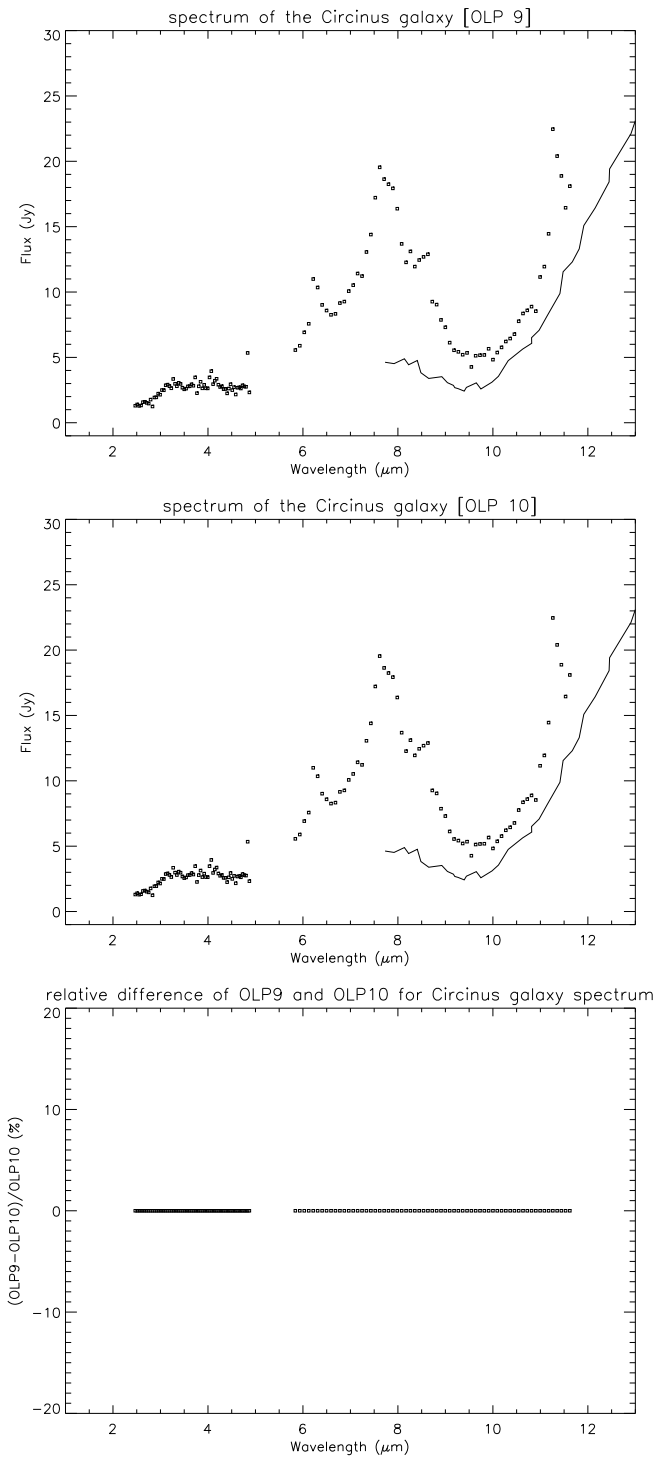

Figure 11.26: Comparison of the spectrum of the Circinus galaxy with groundbased 8 - 13 micron spectroscopy for OLP 9.01 (upper panel), OLP 10.0b5 (middle panel) and the relative difference of both versions (lower panel).

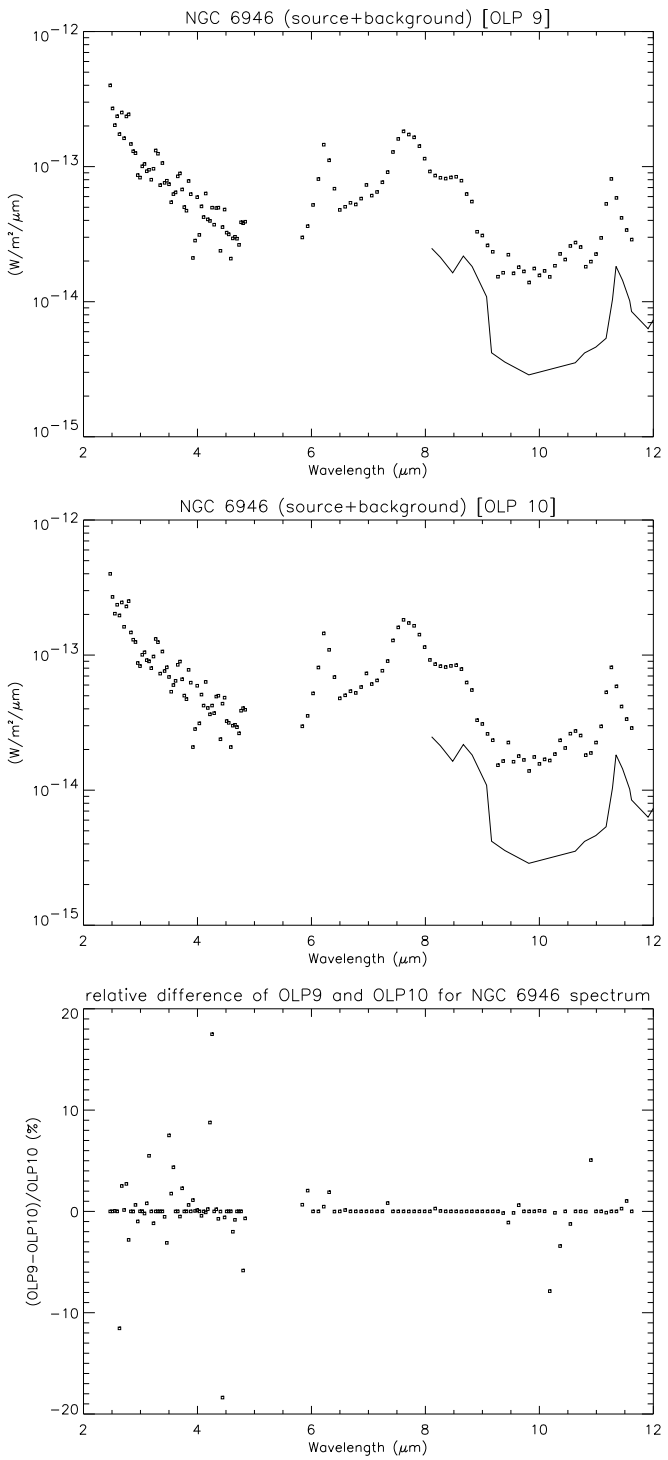

Figure 11.27: Comparison of the spectrum of the galaxy NGC 6946 with groundbased 8 - 13 micron spectroscopy for OLP 9.01 (upper panel), OLP 10.0b5 (middle panel) and the relative difference of both versions (lower panel). For comparison with the groundbased spectrum the extended source data product was converted to a point source data product by applying the effective solid angle of the PHT-S aperture.

11.3.2 PHT40 Spectroscopy: MIR Spectra of Planetary Nebulae from Staring PHT-S Measurements

Motivation

We investigate here the spectra of several Planetary Nebulae. These objects have different SED shapes than the standard stars from which the dynamic PHT-S spectral response function was derived. Some objects have very strong ionic lines, others show a pronounced continuum. There is groundbased $8 - 13$ micron (cf. Refs. [34], [35], [36]) and IRAS LRS (cf. Ref. [37]) available.

Method

We compare the absolute fluxes and relative shapes of the ISOPHOT-S spectra with the groundbased spectroscopy. Note that we compare an aperture size of $24 \times 24\,\mathrm{arcsec}^2$ for ISOPHOT-S with 5 arcsec aperture size of the groundbased measurements. We expect therefore, that the ISOPHOT-S flux is higher, if the PN is not compact. We can also compare ratios of the line peak fluxes.

Results

For all spectra there is no difference between the OLP 9 and OLP 10 results.
Figs. 11.28 and 11.29 show two PNs with strong silicate emission features. The spectra of HB 12 and VY 2-2 are in good consistency with the groundbased spectrum with regard to continuum level and features.
The highly excited PN NGC 6302 shows strong emission lines of [NeVI]7.642 μm and [SIV]10.51 μm (Fig. 11.30). The PHT-S lines are sharpest due to the somewhat better spectral resolution and hence have the highest peak flux.
NGC 6572 (fig. 11.31) shows strong emission lines. The ratio of the [SIV]10.51 μm / [ArIII]8.99 μm lines is ~ 2.5 for both the groundbased and ISOPHOT-S spectrum. The raising continuum of the ISOPHOT-S spectrum, in line with the IRAS LRS spectrum indicates extended emission (then, in principle the point source calibration is not applicable).
The match of the compact PN IC 4997 with the groundbased spectrum is quite good. The signals in the SS channel reflect detector noise.
For BD+30 3639 we have two spectra (figs. 11.33 and 11.34). The reproducibility of the continuum level and the peaks of the PAH features is quite good (the [ArII]6.99 μm line shows a slightly larger discrepancy, but that may be due to the fact that the line is centered in one pixel for spectrum 2, but appears broader due to location inbetween 2 pixels in spectrum 1.). The source is clearly extended. Spectrum 2 had a less well matching of the read-out timing for the SS channel.
For NGC 5315 (Figs. 11.35 and 11.36) the PAH features come out clearly and the emission lines are sharp. The read-out timing of the SS channel was not matched to the incoming flux, so that this part suffers from digitization noise and is not very reliable. There are significant differences in the line strengths between spectrum 1 and spectrum 2. The roll angle difference between the two epochs is 172 deg so that nearly the same region should be located inside the PHT-S aperture. The comparison with the SIMBAD position shows an offset of nearly 16 arcsec and since the aperture is rotated the asymmetry in the beam profile can fully account for this flux difference, in particular, since the source is not centered.

Conclusions

- The comparison of ISOPHOT-S spectra of PN with groundbased 8 - 13 micron spectroscopy shows reasonable consistency, having in mind the different beam sizes on these partly extended objects.
- Repeated spectra show either a quite good reproducibility (in the case of BD+30 3639) or the discrepancies can be explained by a combination of off-pointing and beam effects (in the case of NGC 5315).
- Optimization of the read-out for one channel (selectable via the AOT input parameters) leads to digitization noise and hence no reasonable data in the other channel.

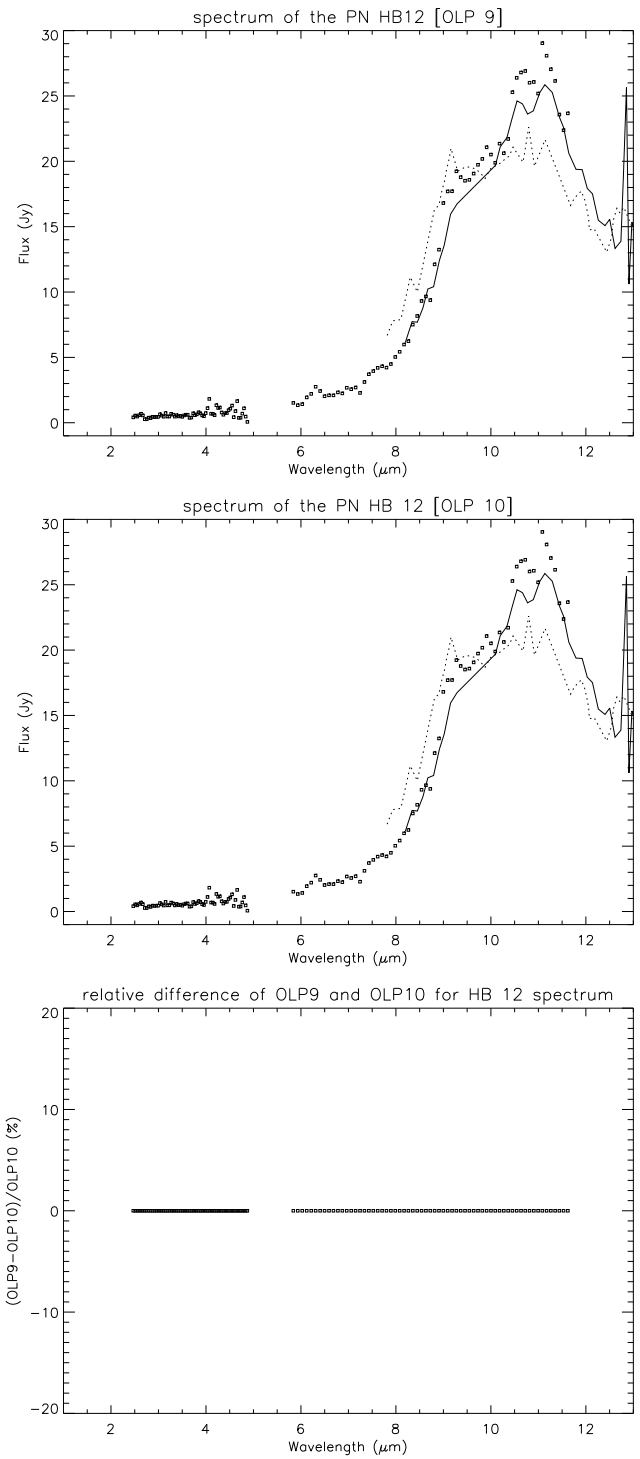

Figure 11.28: Comparison of the spectrum of HB 12 with groundbased 8 - 13 micron spectroscopy (solid line) and IRAS LRS spectroscopy (dashed line) for OLP 9.01 (upper panel) and OLP 10.0b5 (middle panel) and the relative difference of both versions (lower panel).

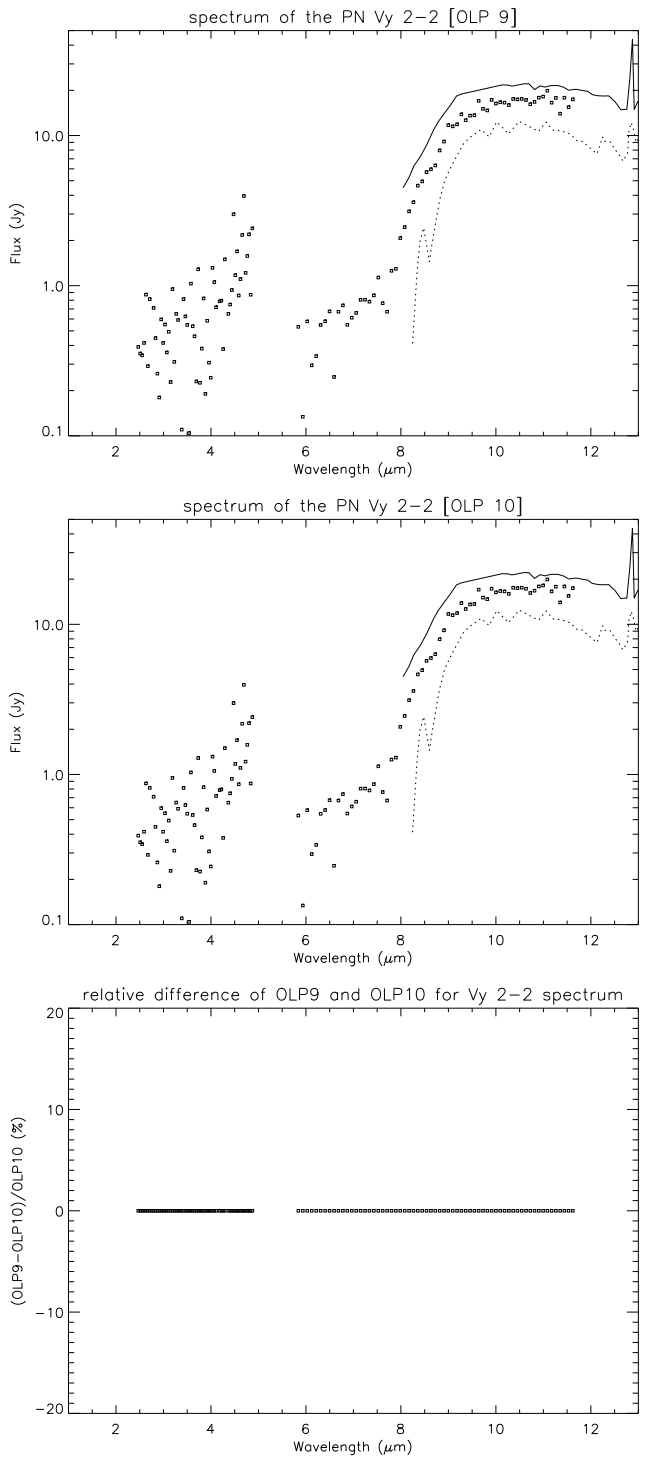

Figure 11.29: Comparison of the spectrum of VY 2-2 with groundbased 8 - 13 micron spectroscopy (solid line) and IRAS LRS spectroscopy (dashed line) for OLP 9.01 (upper panel) and OLP 10.0b5 (middle panel) and the relative difference of both versions (lower panel).

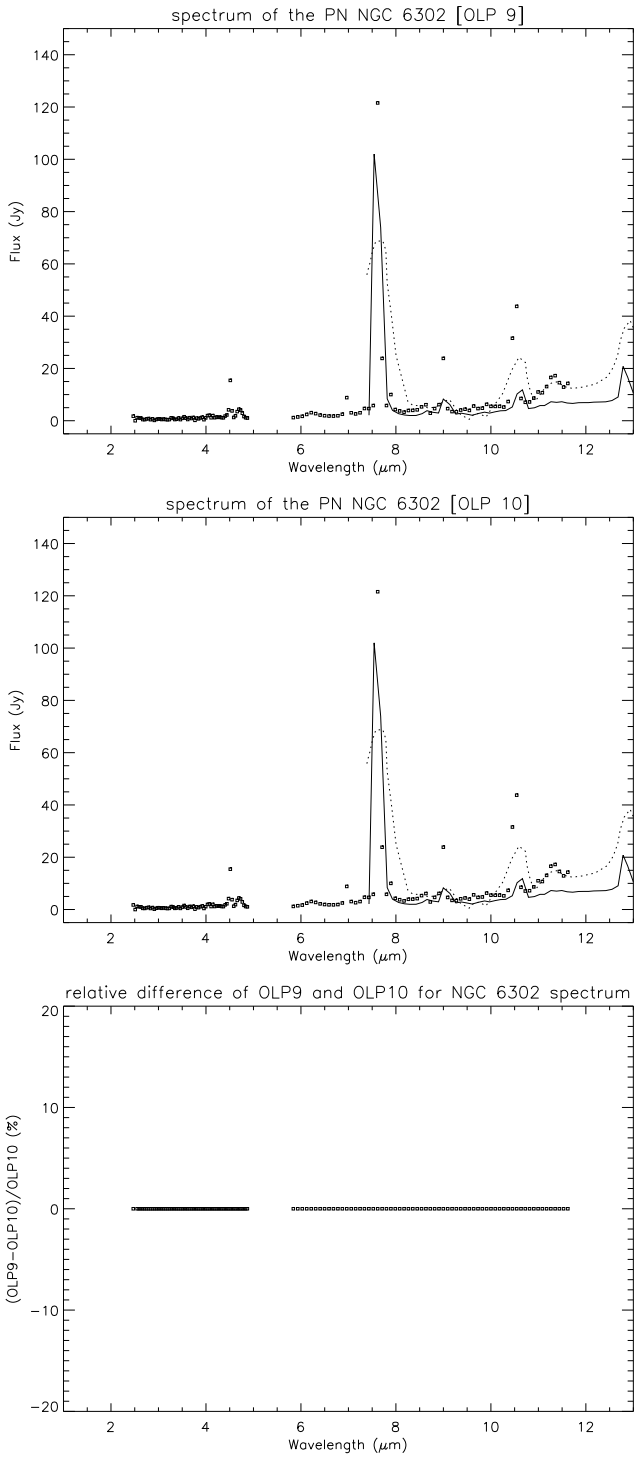

Figure 11.30: Comparison of the spectrum of NGC 6302 with groundbased 8 - 13 micron spectroscopy (solid line) and IRAS LRS spectroscopy (dashed line) for OLP 9.01 (upper panel) and OLP 10.0b5 (middle panel) and the relative difference of both versions (lower panel).

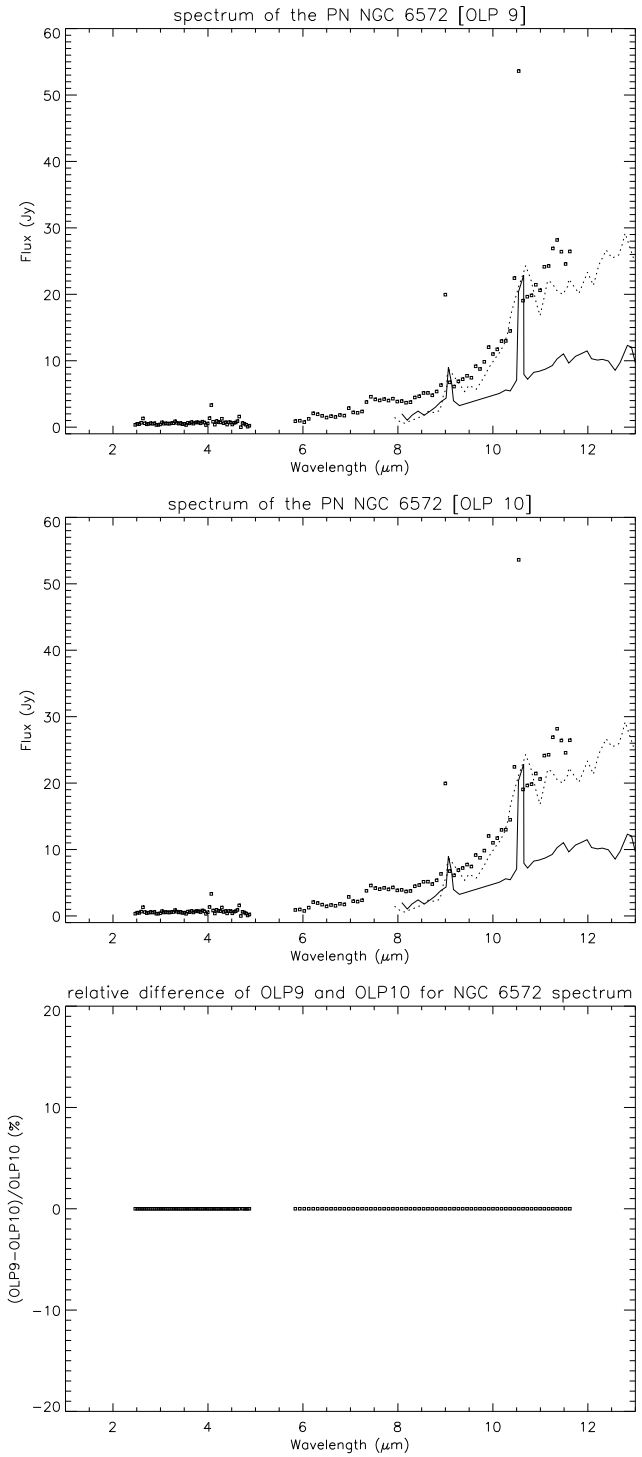

Figure 11.31: Comparison of the spectrum of NGC 6572 with groundbased 8 - 13 micron spectroscopy (solid line) and IRAS LRS spectroscopy (dashed line) for OLP 9.01 (upper panel) and OLP 10.0b5 (middle panel) and the relative difference of both versions (lower panel).

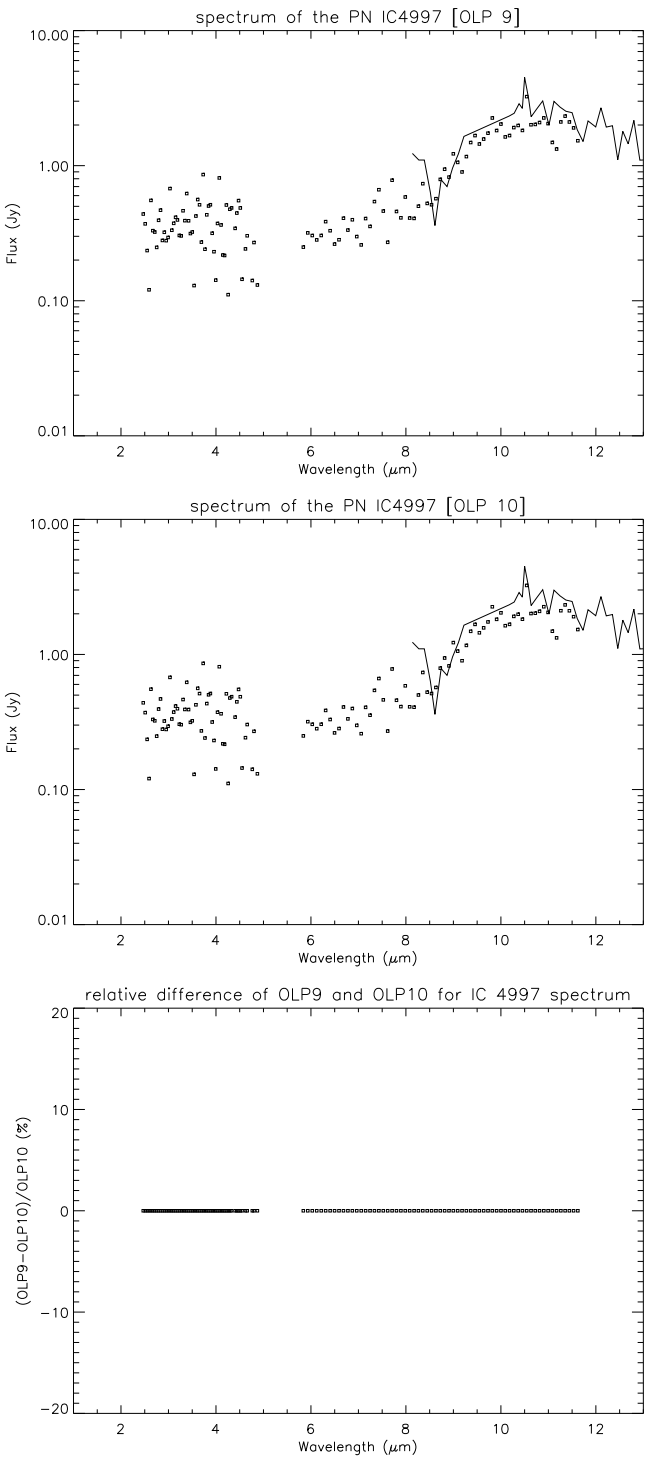

Figure 11.32: Comparison of the spectrum of IC 4997 with groundbased 8 - 13 micron spectroscopy (solid line) for OLP 9.01 (upper panel) and OLP 10.0b5 (middle panel) and the relative difference of both versions (lower panel).

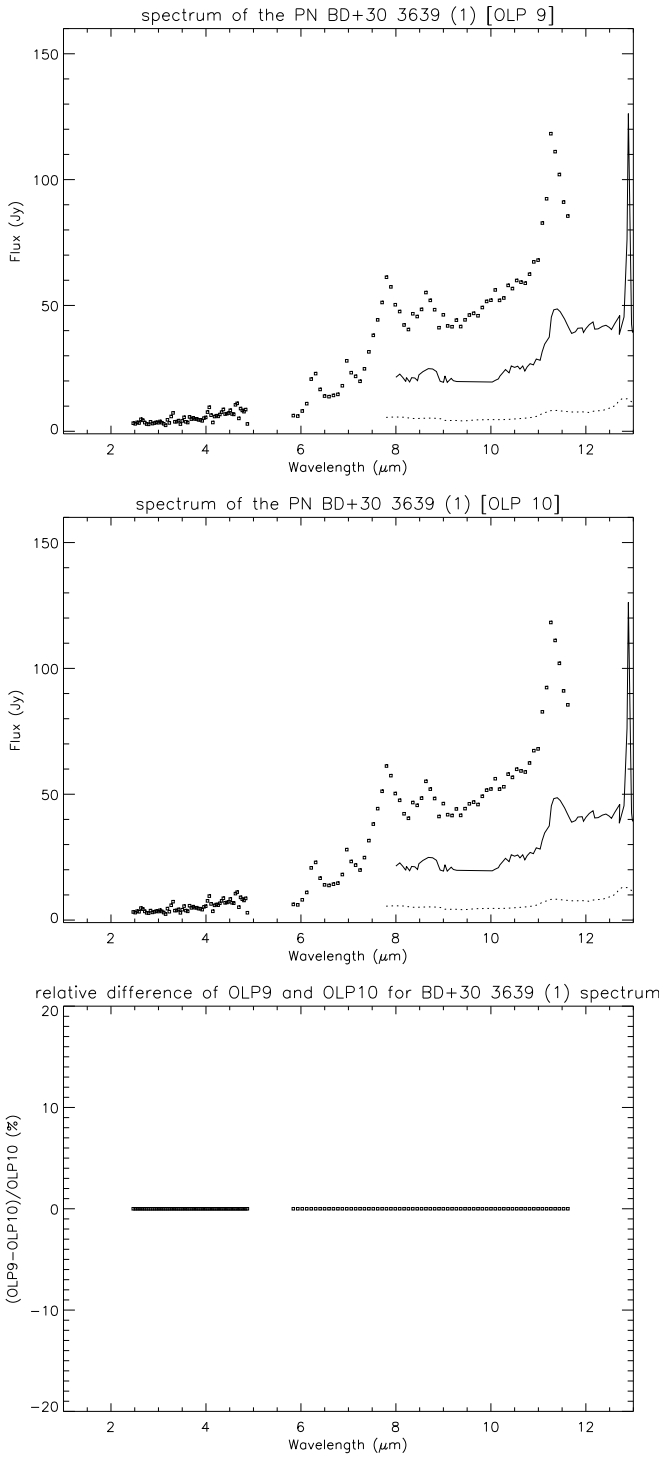

Figure 11.33: Comparison of the spectrum of BD+30 3639 (1) with groundbased 8 - 13 micron spectroscopy (solid line) and IRAS LRS spectroscopy (dashed line) for OLP 9.01 (upper panel) and OLP 10.0b5 (middle panel) and the relative difference of both versions (lower panel).

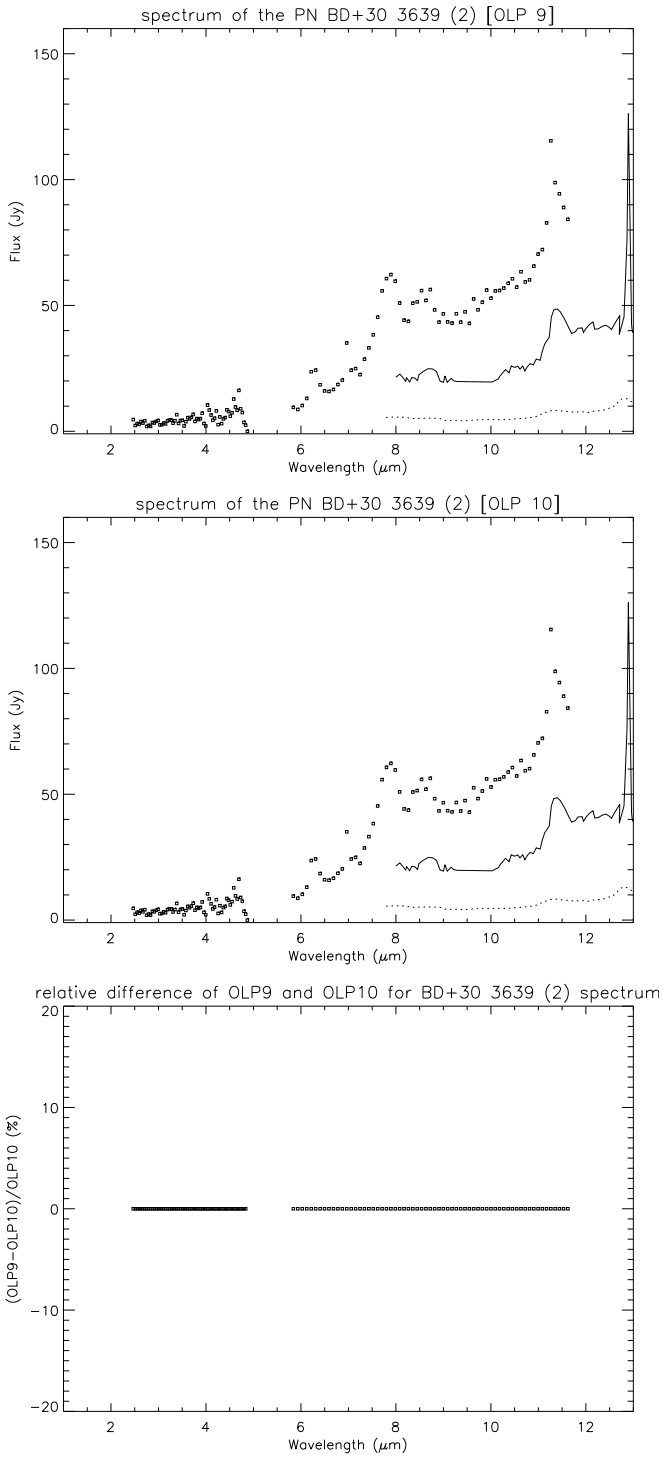

Figure 11.34: Comparison of the spectrum of BD+30 3639 (2) with groundbased 8 - 13 micron spectroscopy (solid line) and IRAS LRS spectroscopy (dashed line) for OLP 9.01 (upper panel) and OLP 10.0b5 (lower panel) and the relative difference of both versions (lower panel).

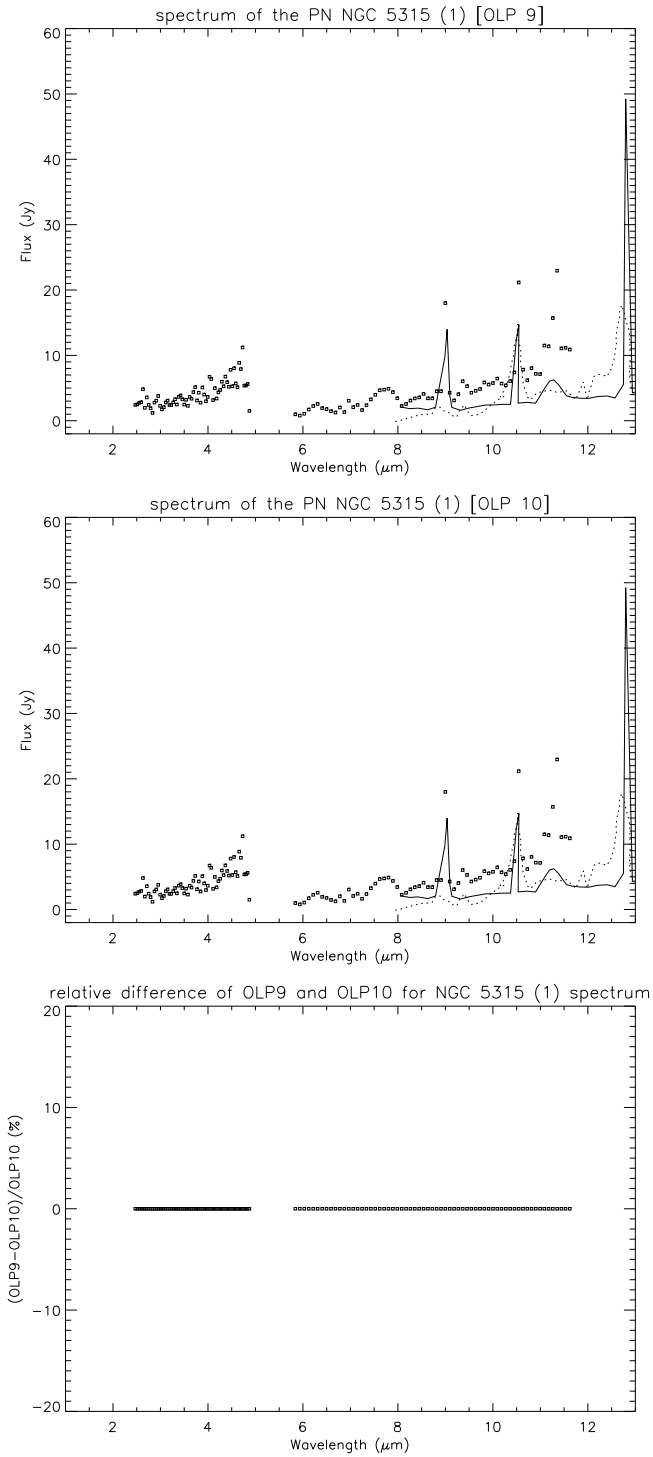

Figure 11.35: Comparison of the spectrum of NGC 5315 (1) with groundbased 8 - 13 micron spectroscopy (solid line) and IRAS LRS spectroscopy (dashed line) for OLP 9.01 (upper panel) and OLP 10.0b5 (middle panel) and the relative difference of both versions (lower panel).

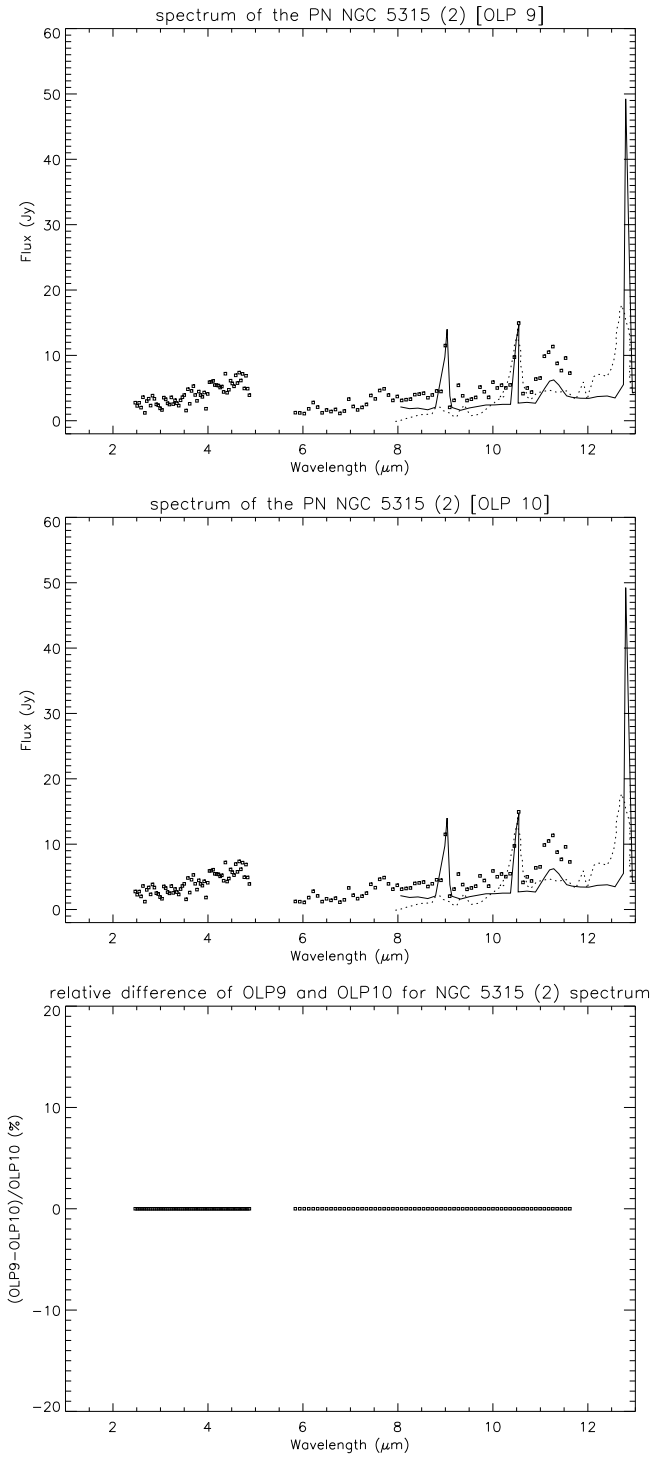

Figure 11.36: Comparison of the spectrum of NGC 5315 (2) with groundbased 8 - 13 micron spectroscopy (solid line) and IRAS LRS spectroscopy (dashed line) for OLP 9.01 (upper panel) and OLP 10.0b5 (lower panel) and the relative difference of both versions (lower panel).

11.4 Comparison with IRTS spectra

Summary

- Staring mode spectroscopy was successfully revalidated.
- We find a quite good consistency with IRTS/MIRS spectra for bright stars where the background is still negligible (due to the large entrance aperture of IRTS). For the cross-calibration standard HR 7980 (ω Cap) the agreement is very good over a large wavelength range and only for the longest wavelengths there are some deviations. Overall the agreement is very good for the SS wavelength range and better than 30 % for the SL wavelength range.

11.4.1 PHT40 Spectroscopy: Cross-calibration of IRTS and ISOPHOT-S on HR 7980 (ω Cap)

Motivation

The IRTS Mid-Infrared Spectrometer (MIRS) covered a similar wavelength range as ISOPHOT-S. It had a somewhat lower spectral resolution (about 30 at 10 μm) and an entrance aperture of 8' $\times$ 8'. HR 7980 (ω Cap) was observed for cross-calibration purposes. The IRTS spectra were kindly provided to us by Dr. Issei Yamamura.

Method

We compare the absolute fluxes and relative shapes of the OLP 10.1 ISOPHOT-S spectrum with the IRTS spectra and with the model by Cohen. The background contribution is negligible.

Results

Fig. 11.37 shows the comparison of the two spectra with the model by Cohen. There is an excellent agreement between the ISOPHOT-S spectrum, the IRTS spectrum and the Cohen model for the wavelength range 2.5 to $\sim$9 μm. Beyond this wavelength the IRTS spectrum shows some features which are neither reflected by the ISOPHOT-S spectrum nor by the model. The agreement of the ISOPHOT-S spectrum with the model is better than 10 % for the whole ISOPHOT-S wavelength range (see Sect. 11.1.1).

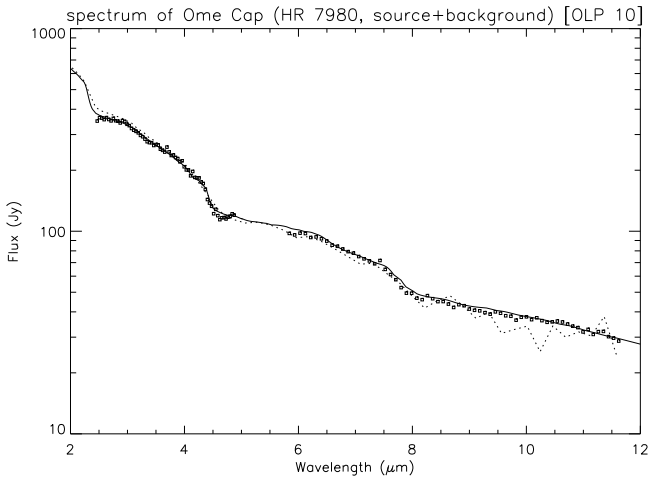

Figure 11.37: Comparison of the OLP 10.1 spectrum of HR 7980 with the IRTS spectrum kindly provided by the IRTS Team (dashed line) and the model by Cohen (solid line).

Conclusions

- There is a good cross-calibration accuracy between ISOPHOT-S and the IRTS/MIRS verified on the standard star HR 7980 (ω Cap). Only for the longest wavelengths (9 to 11.5 μm) the IRTS spectrum shows some features which are neither seen in the ISOPHOT-S spectrum nor the model by Cohen. These deviations are less than 30 %.

11.4.2 PHT40 Spectroscopy: Spectra of the Carbon Star U Cam and the S-type Star S Cas

Motivation

The IRTS Mid-Infrared Spectrometer (MIRS) covered a similar wavelength range as ISOPHOT-S. It had a somewhat lower spectral resolution (about 30 at 10 μm) and an entrance aperture of $8' \times 8'$. We identified several bright star spectra which were measured by both instruments. The IRTS spectra were kindly provided to us by Dr. Issei Yamamura.

Method

We compare the absolute fluxes and relative shapes of the OLP 10.0b5 ISOPHOT-S spectra with the IRTS spectra and with OLP 9.01. Relative differences to OLP 9.01 are plotted. The background contribution is negligible.

Results

For both spectra there is no difference between OLP 9 and OLP 10 results. Figs. 11.38 and 11.39 show the comparison of the PHT-S spectra with the IRTS/MIRS spectra.
The consistency for the spectrum of U Cam is quite good, the major spectral features are visible in both spectra. PHT-S displays some finer absorption features which are not visible in the IRTS spectrum. The absolute levels deviate at most $\sim$20 %.
The consistency for the spectrum of S Cas is less good. PHT-SL appears to be systematically higher (about 30 %) and there are also some noticable differences in features. The general spectral shape with the steady incline of flux with wavelength is, however, reflected by both spectra.

Conclusions

- Spectrophotometry of bright stars from IRTS/MIRS and ISOPHOT-S gives consistency of better than 30 %.

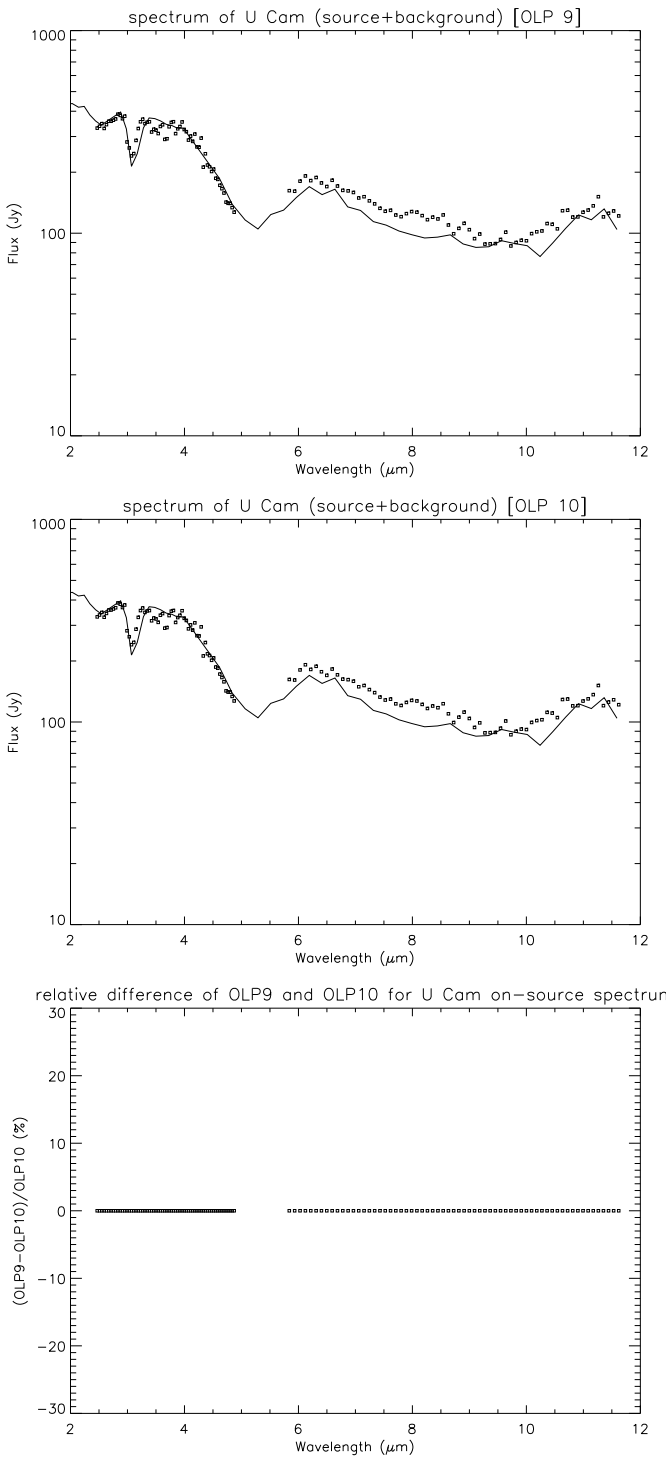

Figure 11.38: Comparison of the spectrum of the carbon star U Cam with the IRTS spectrum kindly provided by the IRTS Team for OLP 9.01 (upper panel) and OLP 10.0b5 (middle panel) and the relative difference of both versions (lower panel).

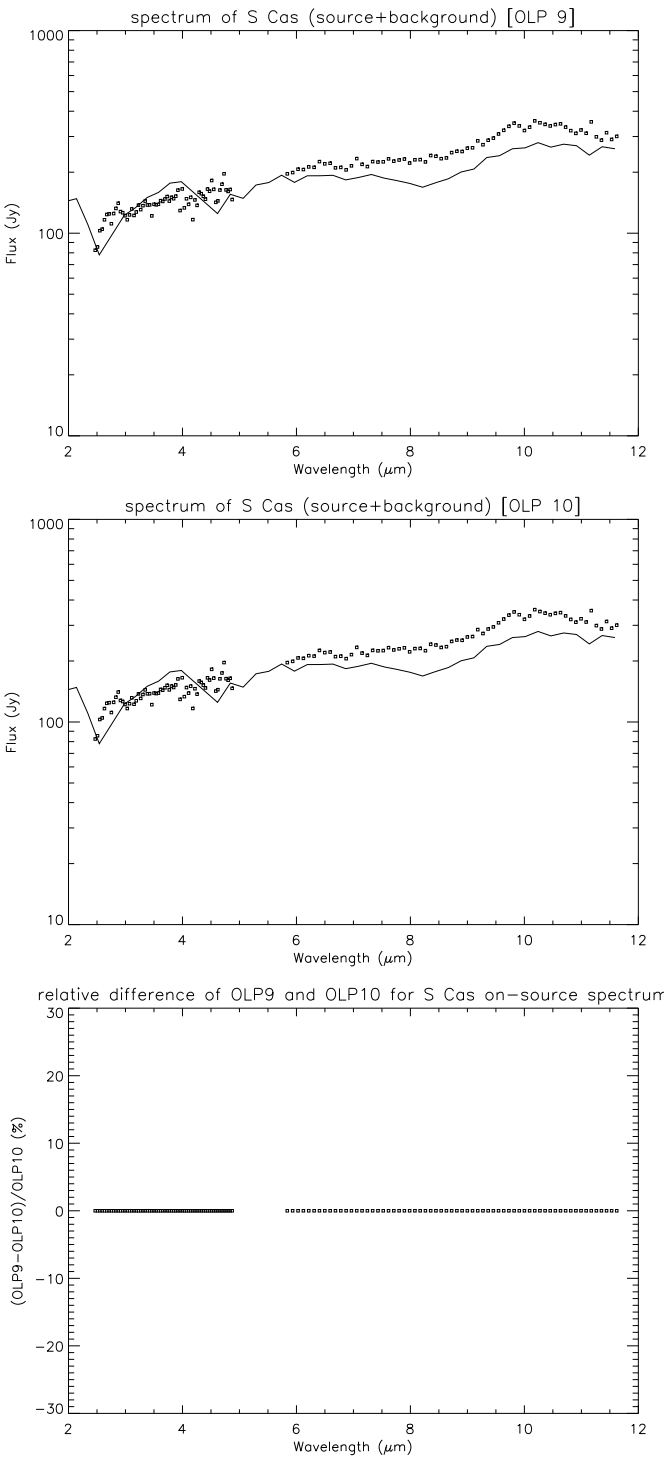

Figure 11.39: Comparison of the spectrum of the S-type star S Cas with the IRTS spectrum kindly provided by the IRTS Team for OLP 9.01 (upper panel) and OLP 10.0b5 (middle panel) and the relative difference of both versions (lower panel).

11.5 Measurements out of Calibrated Range

Summary

- Staring mode spectroscopy was successfully revalidated.
- Test cases with the detector temperature outside the valid range indicate accuracies in the range $\pm 20 - \pm 40\,\%$. The different detector temperature has a stronger impact on the relative spectral shape than on the absolute level.

11.5.1 PHT40 Spectroscopy: Stellar Spectra with Measurement Conditions outside the Calibrated Range

Motivation

The dynamic spectral response function calibration only works perfect as long as the detector temperature is within a certain range. Otherwise the transient behaviour changes and the method cannot fully compensate for that. When applying the dynamic spectral response function calibration the software checks for the detector temperature and issues a warning, if the specified range is not met:

```
COMMENT ************************************************
COMMENT !!!WARNING!!!
COMMENT Detector temperature outside valid range
COMMENT ************************************************
```

This means that according to the caveat in Sect. 2.14 the detector temperature was outside the range $2.7\,\mathrm{K} < \mathrm{T} < 3.1\,\mathrm{K}$ and hence the transient behaviour of the detector signals was different from the ones of the calibration stars leading to a less good match by the dynamic spectral response calibration. In particular measurements of the Performance Verifaction Phase (revolution ≤ 78) are affected, because the one instrument per revolution operations caused a different effective temperature of the Optical Support Structure on which the ISOPHOT Focal Plane Unit was mounted. PHT-S had non-temperature controlled detectors and thus the detector temperature floated with the one of the FPU.

Method

We compare the stellar SEDs of measurements with the detector temperature warning flag set with the flux models by Cohen and assess the deviations from the ideal case.

Results

There is no difference between the OLP 9 and OLP 10 spectra for the two brighter stars HR 2491 and HR 6705. For HR 6817 the difference between OLP 9 and OLP 10 spectra is on the 5 % level.
Figs. 11.40 to 11.42 display the results including the inter-comparison of OLP9 and OLP 10 andd the comparison with the model spectra.
For HR 2491 (Sirius) there are some systematic deviations from the model. The absolute accuracy is quite good, the relative spectral shape is still within the maximum range of ±20 %, however, this usually applies to fainter stars (see Table 1.4).
The measurements of HR 6705 and HR 6817 were taken during the PV phase. Here larger deviations from the model spectrum can be found, up to 35 %, mostly affecting the relative spectral shape.

Conclusions

- Spectra with the detector temperature outside the valid range show a reduced consistency with the model fluxes with an accuracy of better than ±40 %. Mostly the relative spectral shape is affected due to different transient behaviour of the individual pixels.

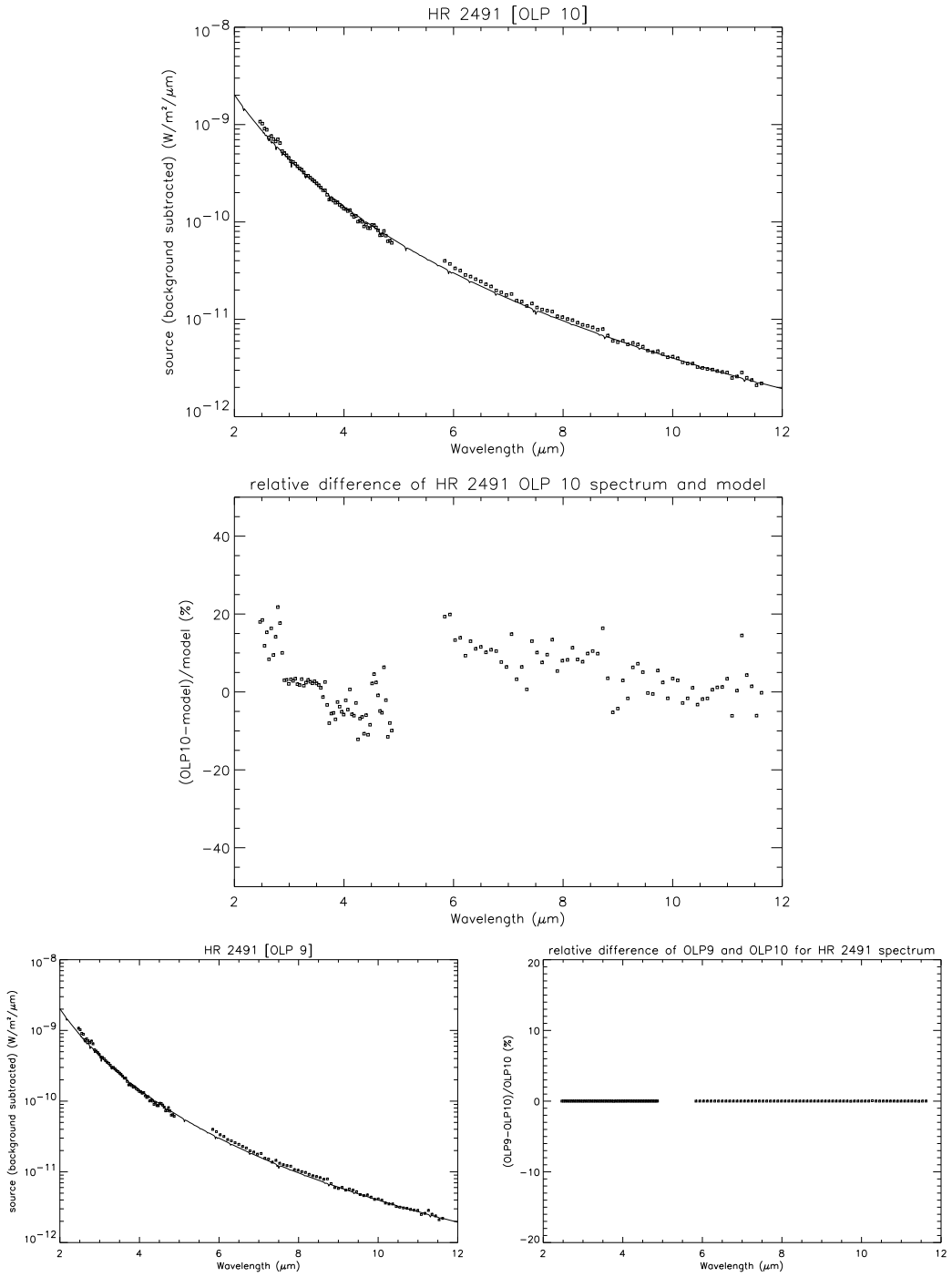

Figure 11.40: Comparison of the spectrum of HR 2491 (Sirius) with the flux model by Cohen. OLP 10.0b5 spectrum (upper panel), relative difference to model (middle panel), OLP 9.01 spectrum (lower left panel) and the relative difference between both OLP versions (lower right panel).

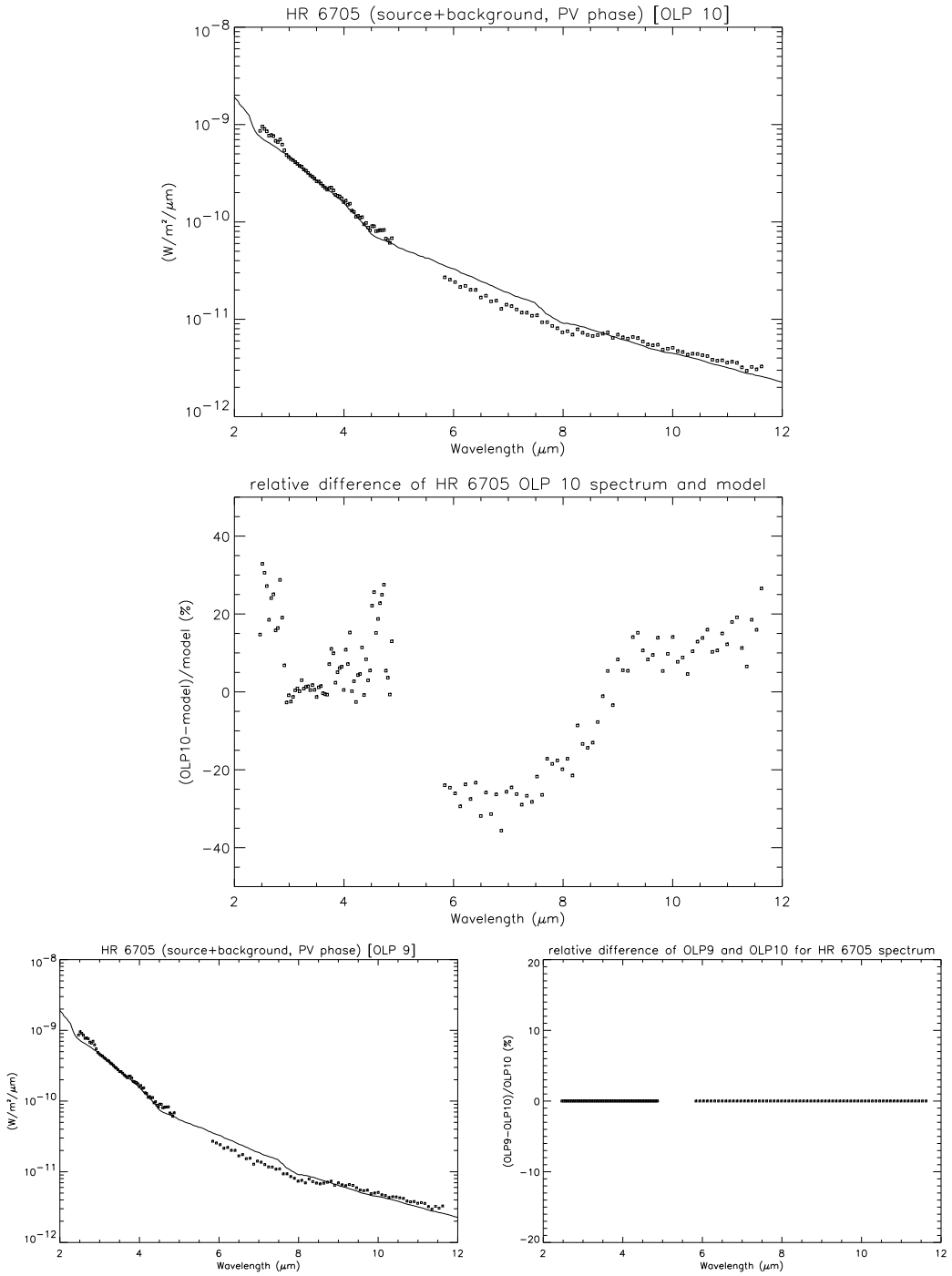

Figure 11.41: Comparison of the spectrum of HR 6705 (γ Dra) with the flux model by Cohen. OLP 10.0b5 spectrum (upper panel), relative difference to model (middle panel), OLP 9.01 spectrum (lower left panel) and the relative difference between both OLP versions (lower right panel).

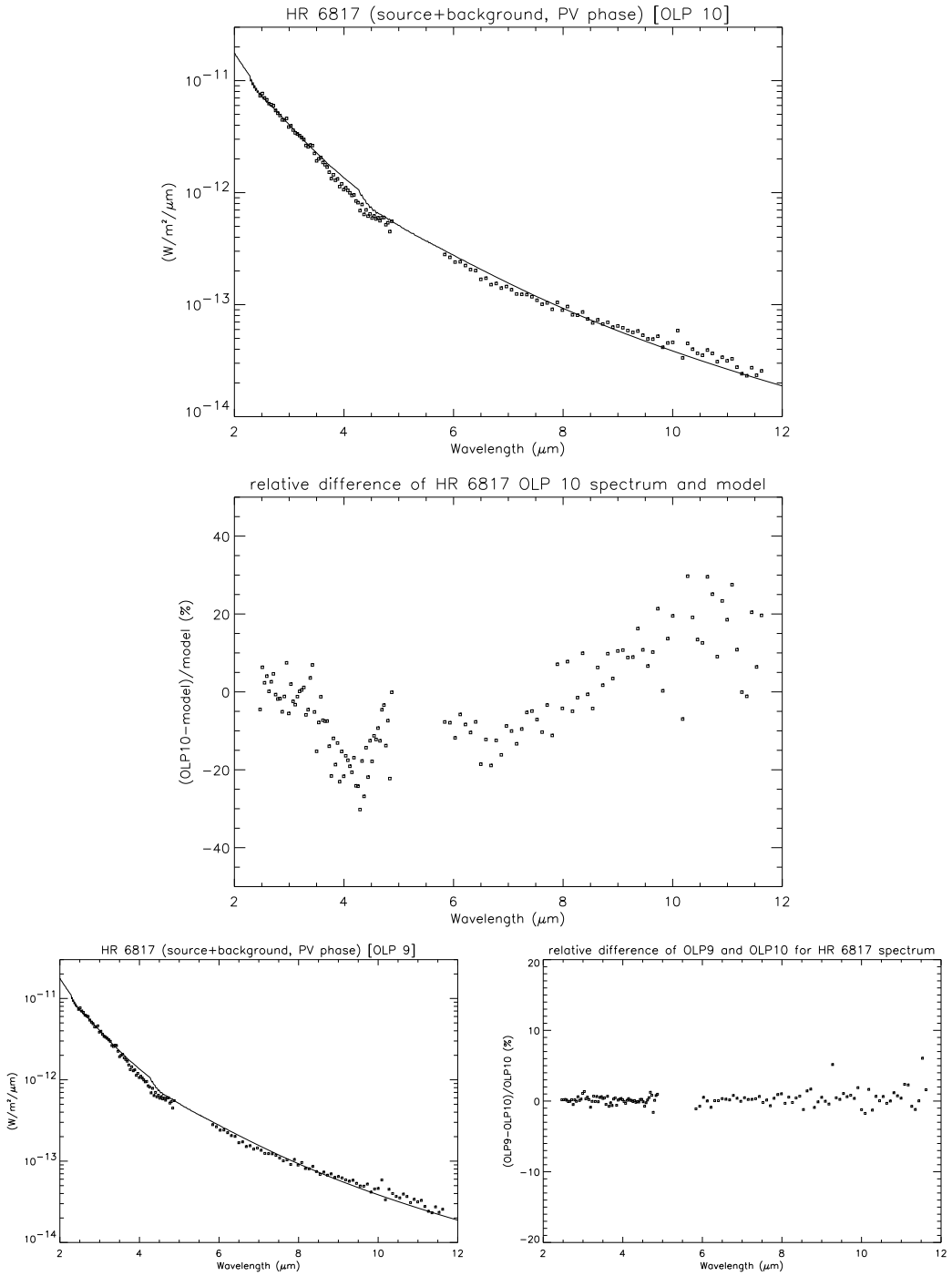

Figure 11.42: Comparison of the spectrum of HR 6817 with the flux model by Hammersley. OLP 10.0b5 spectrum (upper panel), relative difference to model (middle panel), OLP 9.01 spectrum (lower left panel) and the relative difference between both OLP versions (lower right panel).

Chapter 12

Chopped Mode Spectroscopy

12.1 Consistency Check of Calibration Method with Calibration Standards

Summary

- Chopped mode spectroscopy was successfully revalidated.
- From measurements of standard stars we derive an absolute accuracy of better than $\pm 10\,\%$ for the flux range of $2 - 15$ Jy with the SS-array and $0.4 - 4$ Jy with the SL-array. Some pixels show outliers outside this accuracy range.
- A better deglitching making use of the bi-weight mean algorithm as applied for chopped photometry would make the spectra smoother.

12.1.1 PHT40 Spectroscopy: Consistency Check of Chopped PHT-S Relative Spectral Response Function on Calibration Stars for Different Chopper Modes

Motivation

We process measurements of two calibration stars (HR 6817 and HR 6847) which were used to establish the Relative Spectral Response Function (RSRF) for chopped PHT-S measurements and check whether the input model SED is reproduced. Both calibration stars were measured both in rectangular chopped and triangular chopped mode. This allows to assess the consistency of the processing of the two chopper modes.

Method

We compare the results of both OLP 9.0b6 and OLP 10.0b5 with the flux models by Hammersley et al. 1998 [11].

Results

In Figs. 12.1 to 12.4 we perform an individual comparison of both OLP versions with the flux model.
For HR 6817 measured in rectangular chopped mode, one can see that OLP 9 and OLP 10 results are in essence identical. Individual pixels show differences up to ±10 %. The consistency with the model is about 5 % absolute and better than ±10 % in relative spectral shape, excluding some outliers.
For HR 6817 measured in triangular chopped mode, one can see that OLP 9 and OLP 10 results are in essence identical. Individual pixels show differences up to ±10 %. The consistency with the model is better than 5 % absolute and better than ±10 % in relative spectral shape, excluding some outliers.
For HR 6847 measured in rectangular chopped mode, one can see that OLP 9 and OLP 10 results are in essence identical. Individual pixels show differences up to ±20 %, in particular for the faint flux level at the long wavelength end. The consistency with the model is about 10 % absolute and better than ±10 % in relative spectral shape, excluding some outliers.
For HR 6847 measured in triangular chopped mode, one can see that OLP 9 and OLP 10 results are in essence identical. Individual pixels show differences up to ±10 %, in particular for the faint flux level at the long wavelength end. The consistency with the model is better than 10 % absolute and better than ±10 % in relative spectral shape, excluding some outliers.

Conclusions

- The two OLP versions give very similar results; slight changes are expected by the two-threshold deglitching on ramp level and the slightly different averaging scheme of signals on a plateau.
- There is no significant difference in the results recognizable between rectangular and triangular chopped mode.
- The absolute accuracy was found to be better than 10 % and the relative spectral shape better than ±10 %.
- There are occasional outliers. A better deglitching making use of the bi-weight mean algorithm as applied for chopped photometry would make the spectra smoother.

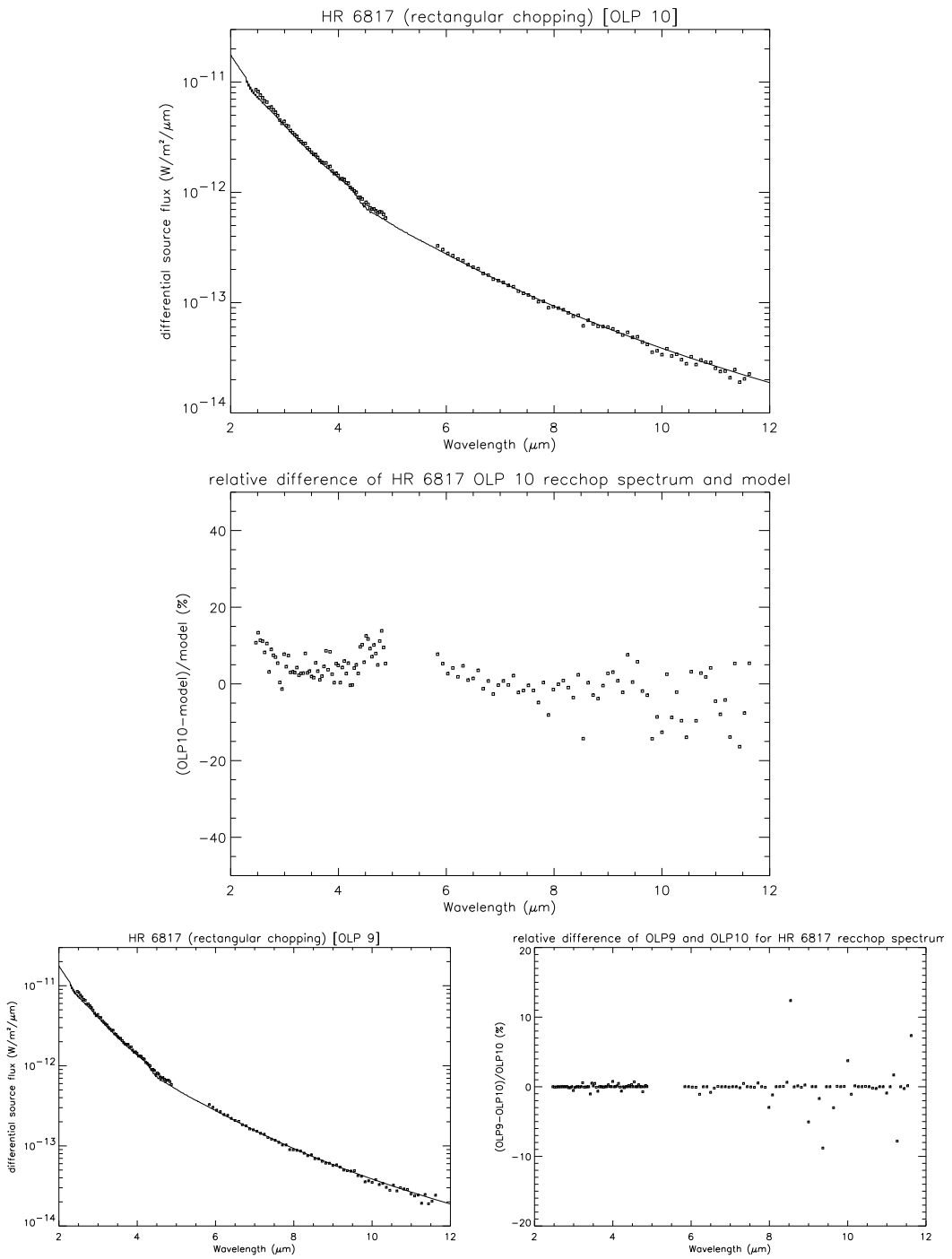

Figure 12.1: Comparison of the spectrum of HR 6817 obtained in PHT-S rectangular chopped mode with the flux model by Hammersley. OLP 10.0b5 spectrum (upper panel), relative difference to model (middle panel), OLP 9.0b6 spectrum (lower left panel) and relative difference between both OLP versions (lower right panel).

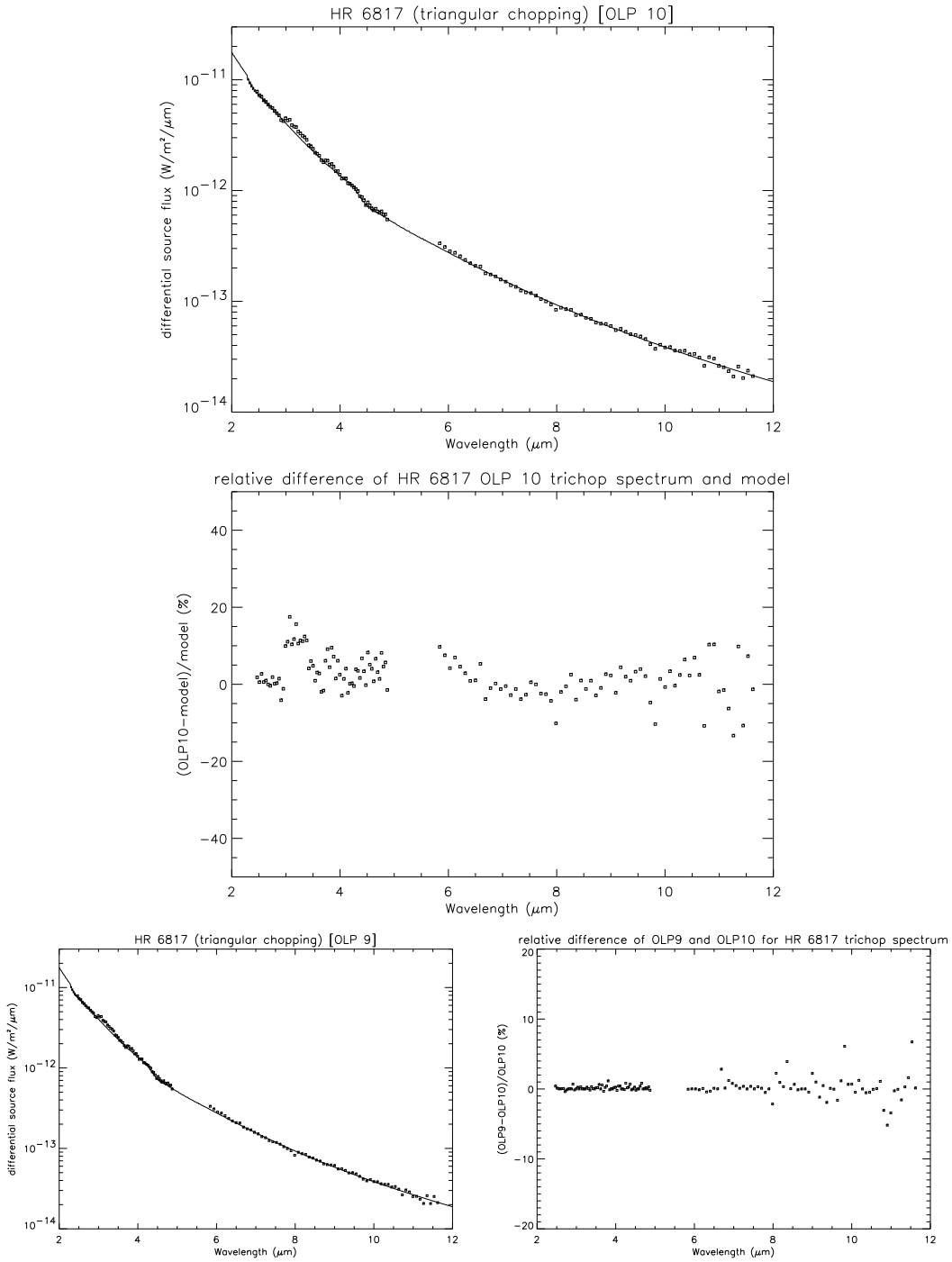

Figure 12.2: Comparison of the spectrum of HR 6817 obtained in PHT-S triangular chopped mode with the flux model by Hammersley. OLP 10.0b5 spectrum (upper panel), relative difference to model (middle panel), OLP 9.0b6 spectrum (lower left panel) and relative difference between both OLP versions (lower right panel).

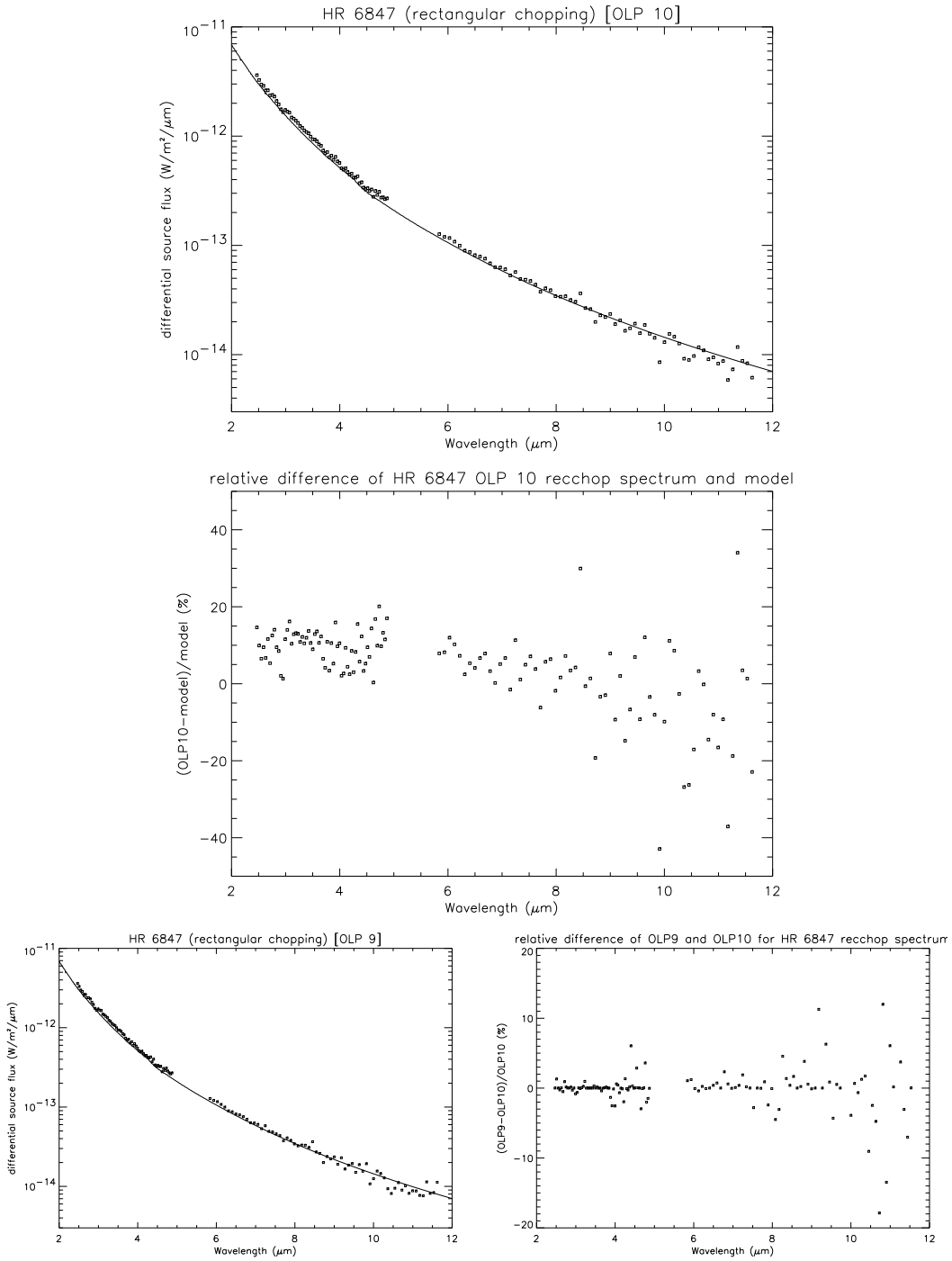

Figure 12.3: Comparison of the spectrum of HR 6847 obtained in PHT-S rectangular chopped mode with the flux model by Hammersley. OLP 10.0b5 spectrum (upper panel), relative difference to model (middle panel), OLP 9.0b6 spectrum (lower left panel) and relative difference between both OLP versions (lower right panel).

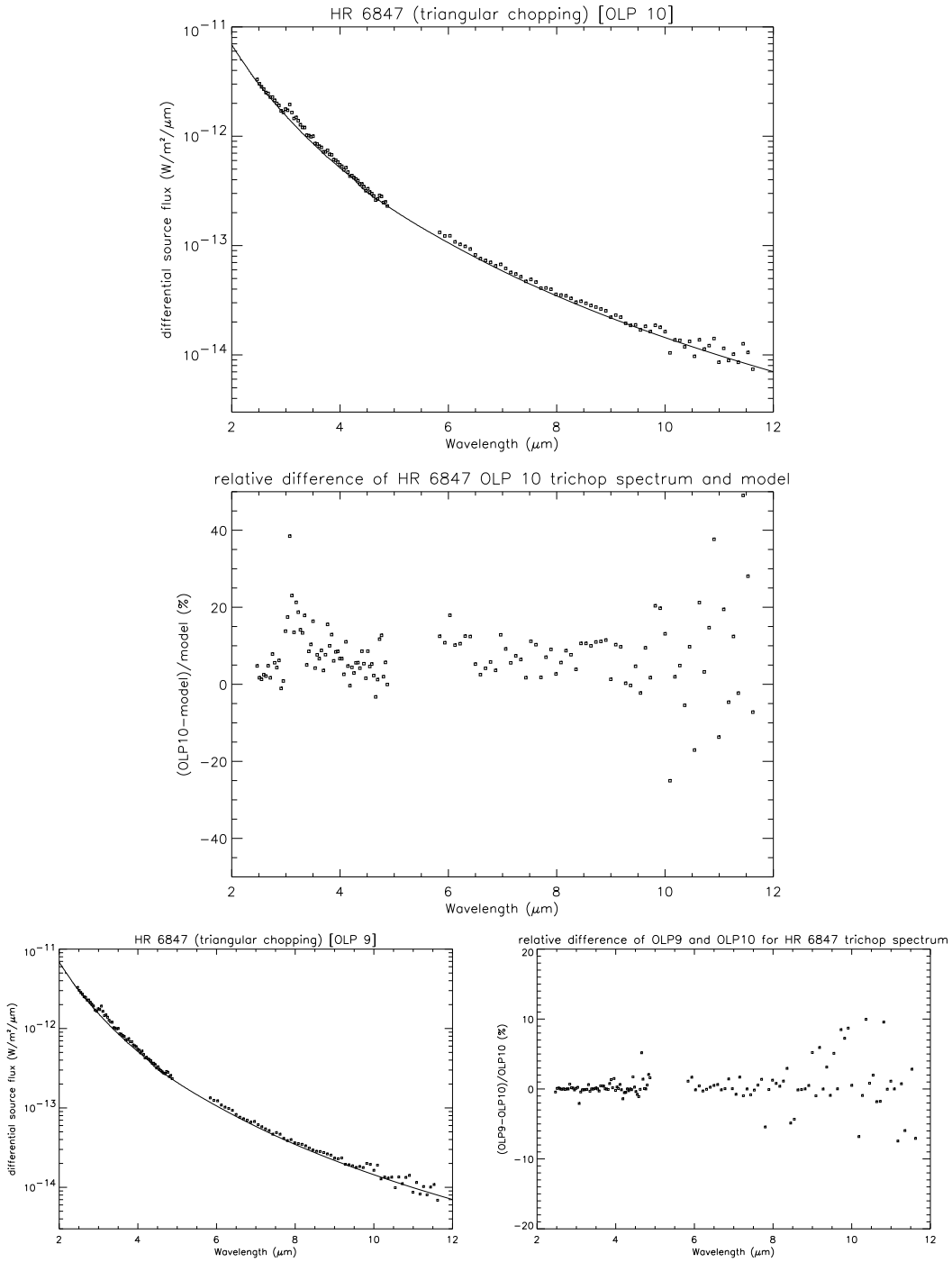

Figure 12.4: Comparison of the spectrum of HR 6847 obtained in PHT-S triangular chopped mode with the flux model by Hammersley. OLP 10.0b5 spectrum (upper panel), relative difference to model (middle panel), OLP 9.0b6 spectrum (lower left panel) and relative difference between both OLP versions (lower right panel).

12.2 Comparison with Stellar Models for Non-calibration Stars

Summary

- Chopped mode spectroscopy was successfully revalidated.
- For the faint source test cases we find sensitivity limits, when the quality of the calibration accuracy breaks down, of $7 \times 10^{-14}\,\mathrm{W\,m^{-2}\,\mu m^{-1}}$ to $10^{-13}\,\mathrm{W\,m^{-2}\,\mu m^{-1}}$ for PHT-SS, corresponding to 400–500 mJy at $4\,\mu$m, and $8 \times 10^{-15}\,\mathrm{W\,m^{-2}\,\mu m^{-1}}$ to $10^{-14}\,\mathrm{W\,m^{-2}\,\mu m^{-1}}$ for PHT-SL, corresponding to $\sim$150 mJy at $7.5\,\mu$m, for an on-source exposure time of 512 s. These limits should scale approximately with the square root of the on-source exposure time.

12.2.1 PHT40 Spectroscopy: MIR Spectra of the Stars HD 23763, HR 7428 and HD 23441 from Chopped PHT-S Measurements

Motivation

We found three stars in the data base with similar spectral type as standard stars but different brightness. It is therefore possible to test absolute and relative accuracy of the ISOPHOT-S chopped calibration on different brightness levels than the ones of standard stars used to establish the calibration. The properties of the three stars are compiled in Table 12.1:

Table 12.1: Properties of stars used for verification of chopped ISOPHOT-S spectra

Name	**Spectral Type**	**Apparent Brightness** (mag)	**Comment**	**Reference Star**	**Spectral Type**	**Apparent Brightness** (mag)
HD 23763	A1V	m_k = 6.567		Sirius (HR 2491)	A1V	m_k = -1.39
HR 7428 (HD 184398)	K2II-III+A0V Sp(IR) K2II-III Ca-	m_v = 6.37	RS CVn binary	HR 6688	K2III	m_v = 3.747
HD 23441	A0Vn	m_v = 6.43	Pleiades 859	Vega (HR 7001)	A0V	m_v = 0.033

For a reference of the spectral types of HR 7428, cf. [20], and of HD 23441, cf. [22]. HR 7428 has an IRAS 12 μm flux of 1.82 Jy, cf. [21] (=1.26 Jy for T=4000 K BB).

Method

The model spectra of Sirius, HR 6688 and Vega are scaled according to the apparent brightness ratio in the K or V band. The absolute fluxes and relative shapes of the ISOPHOT-S spectra of both OLP 9.0b6 and OLP 10.0b5 are comapred with the scaled model spectra.

Results

In Figs. 12.5 to 12.7 we perform an individual comparison of both OLP versions with the flux model. One can see that the results are practically identical.
For HD 23763 the PHT-SS fluxes out to 4 μm fulfill the criterium with absolute acccuracy $\sim$ 10 % and relative accuracy <10 %. Below a flux level of 7×10^{-14} W m^{-2} μm^{-1}, corresponding to 400 mJy at 4 μm, a larger scatter with higher uncertainties occurs. For PHT-SL there is good performance up to 7.5 μm. Below a flux level of 8×10^{-15} W m^{-2} μm^{-1}, corresponding to 150 mJy at 7.5 μm there is again a larger scatter with higher uncertainties. These appear to be sensitivity limits. The on-source exposure time was 512 s.
HR 7428 is a factor of 10 brighter than HD 23763. There is a systematic constant offset between the measurement and the scaled model, so that it remains open whether this is totally due to calibration or also due to some uncertainty in the brightness ratio. The releative spectral shape is better than $\pm$10 %.
HD 23441 is a similar case as HD 23763. Here, below a flux level of 10^{-13} W m^{-2} μm^{-1}, corresponding to 500 mJy at 4 μm, the good calibration quality is lost for PHT-SS. For PHT-SL the limit is at 10^{-14} W m^{-2} μm^{-1}, corresponding to 160 mJy at 7 μm. Again the on-source exposure time was 512 s.

Conclusions

- The two OLP versions give very similar results; slight changes are expected by the introduction of the two-threshold deglitching on ramp level for OLP10.
- These faint source test cases probe sensitivity limits for this measurement mode which are 7×10^{-14} W m^{-2} μm^{-1} to 10^{-13} W m^{-2} μm^{-1}, corresponding to 400–500 mJy at 4 μm, and 8×10^{-15} W m^{-2} μm^{-1} to 10^{-14} W m^{-2} μm^{-1}, corresponding to $\sim$150 mJy at 7.5 μm, for an on-source exposure time of 512 s.

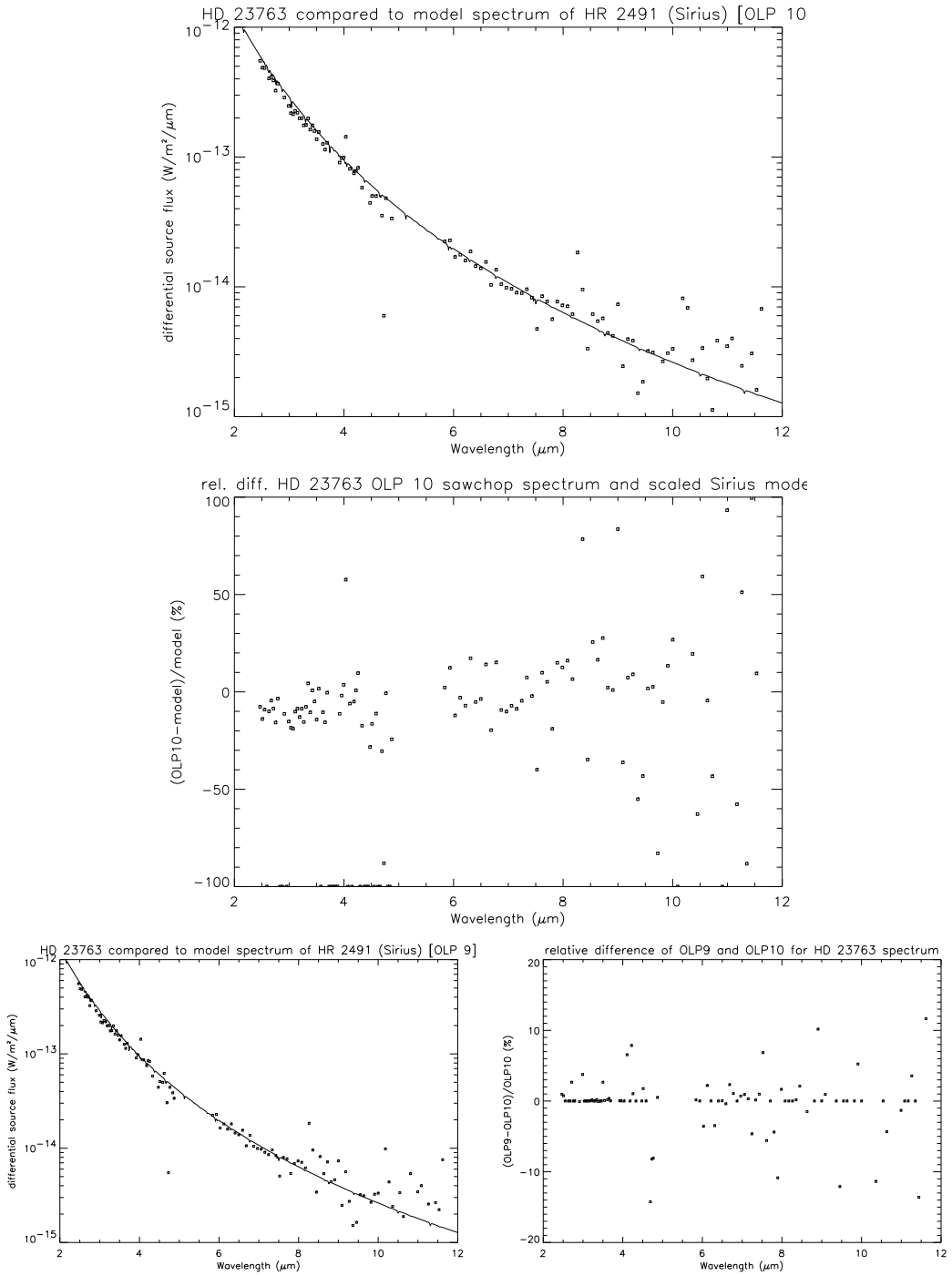

Figure 12.5: Comparison of the spectrum of the A1V star HD 23763 obtained in PHT-S sawtooth chopped mode with the model of Sirius scaled with the K-magnitude ratio of (6.567 mag / -1.39 mag) for both OLP 9.0b6 (upper panel) and OLP 10.0b5 (middle panel) and the relative difference of both versions (lower panel).

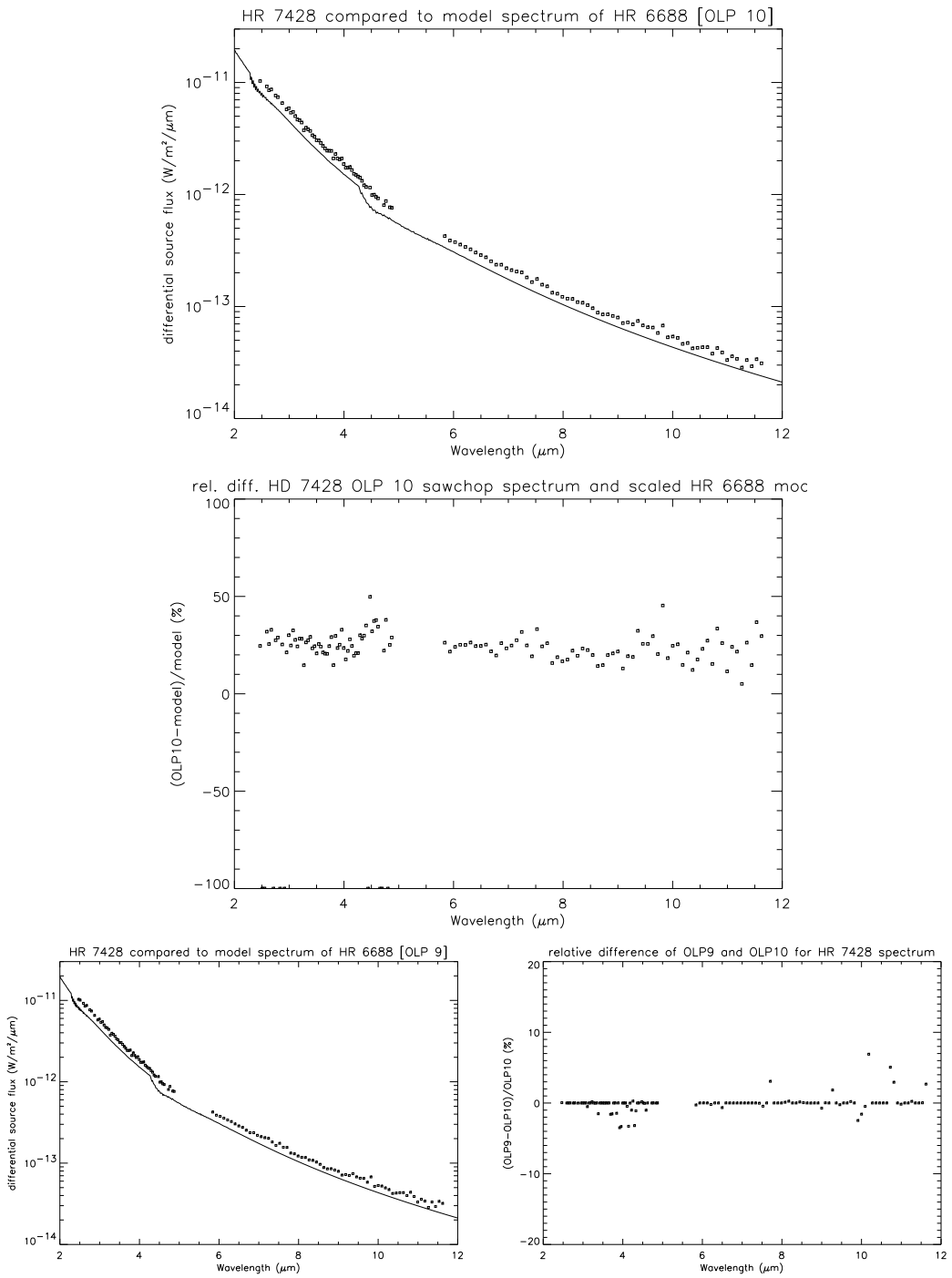

Figure 12.6: Comparison of the spectrum of the RS CVn binary HR 7428 (spectral type: K2II-III+A0V) obtained in PHT-S rectangular chopped mode with the model of HR 6688 (spectral type: K2III) scaled with the V-magnitude ratio of (6.37 mag / 3.747 mag) for both OLP 9.0b6 (upper panel) and OLP 10.0b5 (middle panel) and the relative difference of both versions (lower panel).

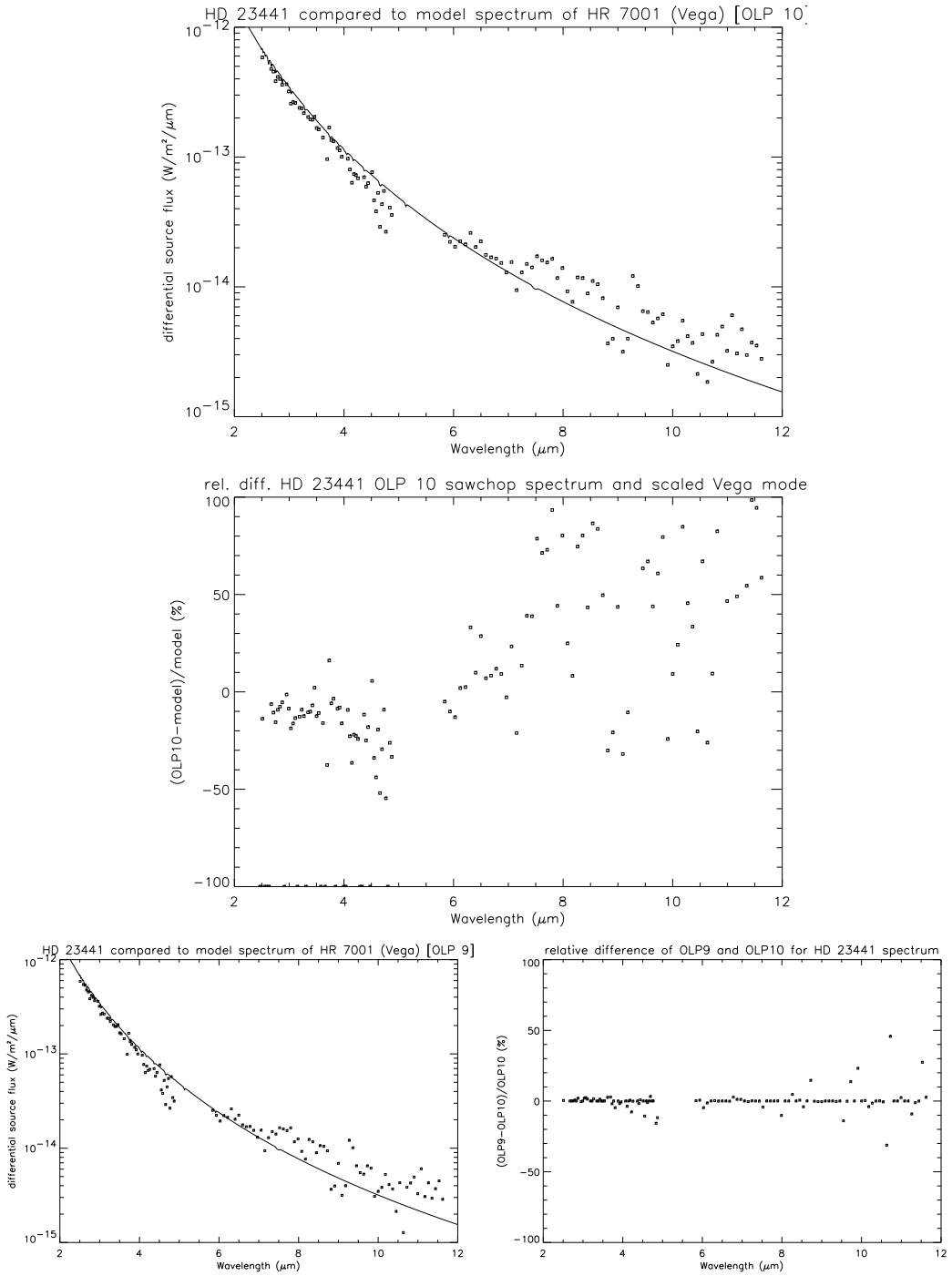

Figure 12.7: Comparison of the spectrum of the A0Vn star HD 23441 obtained in PHT-S sawtooth chopped mode with the model of Vega scaled with the V-magnitude ratio of (6.43 mag / 0.033 mag) for both OLP 9.0b6 (upper panel) and OLP 10.0b5 (middle panel) and the relative difference of both versions (lower panel).

12.3 Comparison with Ground-based Spectroscopy

Summary

- Chopped mode spectroscopy was successfully revalidated.
- There is a quite good consistency with ground-based spectroscopy, in particular w.r.t. spectral features. A 1-to-1 correspondence, in particular in absolute level, does not have to be expected due to the quite different beam sizes and the extension of several targets.
- The galaxy spectra confirm the findings for stellar spectra that sensitivity limits of accurate spectrophotometry for typically 512 s on-source exposure time are around $7 \times 10^{-14}\,\mathrm{W\,m^{-2}\,\mu m^{-1}}$ for PHT-SS, corresponding to around 400 mJy at 4 μm and $7 \times 10^{-15}\,\mathrm{W\,m^{-2}\,\mu m^{-1}}$ to $10^{-14}\,\mathrm{W\,m^{-2}\,\mu m^{-1}}$ for PHT-SL, corresponding to 150 – 210 mJy at 8 μm.
- A better deglitching making use of the bi-weight mean algorithm as applied for chopped photometry would make the spectra smoother.

12.3.1 PHT40 Spectroscopy: MIR Spectra of a Symbiotic Star and a Nova from Chopped PHT-S Measurements

Motivation

In order to to increase the variety of object types for which PHT-S spectra are checked we included the spectrum of a symbiotic star, AG Peg, and the spectrum of a Nova, Nova Her91, in our test case list. For both targets groundbased 8 - 13 micron spectroscopy is available (cf. Refs. [12] and [13], respectively). The comparison for the Nova is of qualitative nature, as changes in the SED between the epoch of the groundbased measurement (1991, 67 days after the eruption) and the epoch of the ISOPHOT-S measurement (1996) are quite likely.

Method

We compare the absolute fluxes and relative shapes of the ISOPHOT-S spectra of both OLP 9.0b6 and OLP 10.0b5 with the groundbased spectroscopy. Note that we compare an aperture size of 24x24 arcsec^2 for ISOPHOT-S with 5 arcsec aperture size of the groundbased measurements.

Results

In Figs. 12.8 to 12.9 we perform an individual comparison of both OLP versions with the flux model.
For AG Peg, both OLP versions show practically identical results and there is a good agreement with the ground-based spectroscopy.
Due to the low flux level of Nova Her91, the measurement is at the detection limit of both PHT-S channels and hence very noisy. The on-source exposure time was 1024 s, so upper flux limits of 6×10^{-14} W m^{-2} μm^{-1} for PHT-SS, corresponding to 320 mJy at 4 μm and 6×10^{-15} W m^{-2} μm^{-1} for PHT-SL, corresponding to 130 mJy at 8 μm should apply.

Conclusions

- The two OLP versions give very similar results. Changes are expected due to the introduction of two-threshold deglitching on ramp level for OLP 10.
- For the symbiotic star AG Peg we find a good consistency with ground-based $8 - 13\,\mu$m spectroscopy.
- The Nova Her91 was too faint to give a meaningful spectrum. Upper flux limits of 320 mJy at 4 μm and 130 mJy at 8 μm were derived for the on-source exposure time of 1024 s.

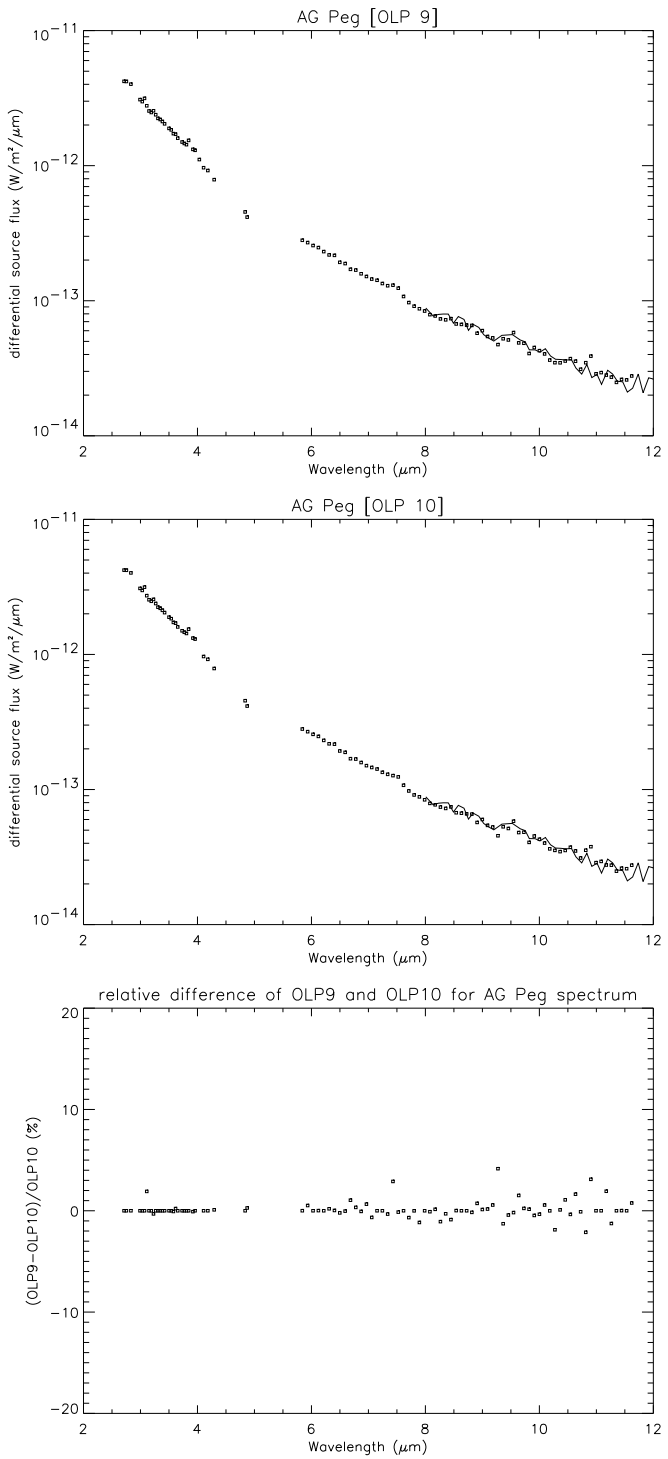

Figure 12.8: Comparison of the spectrum of the symbiotic star AG Peg obtained in PHT-S triangular chopped mode with the groundbased $8-13$ micron spectroscopy by Roche et al. 1983 for both OLP 9.0b6 (upper panel) and OLP 10.0b5 (middle panel) and the relative difference of both versions (lower panel).

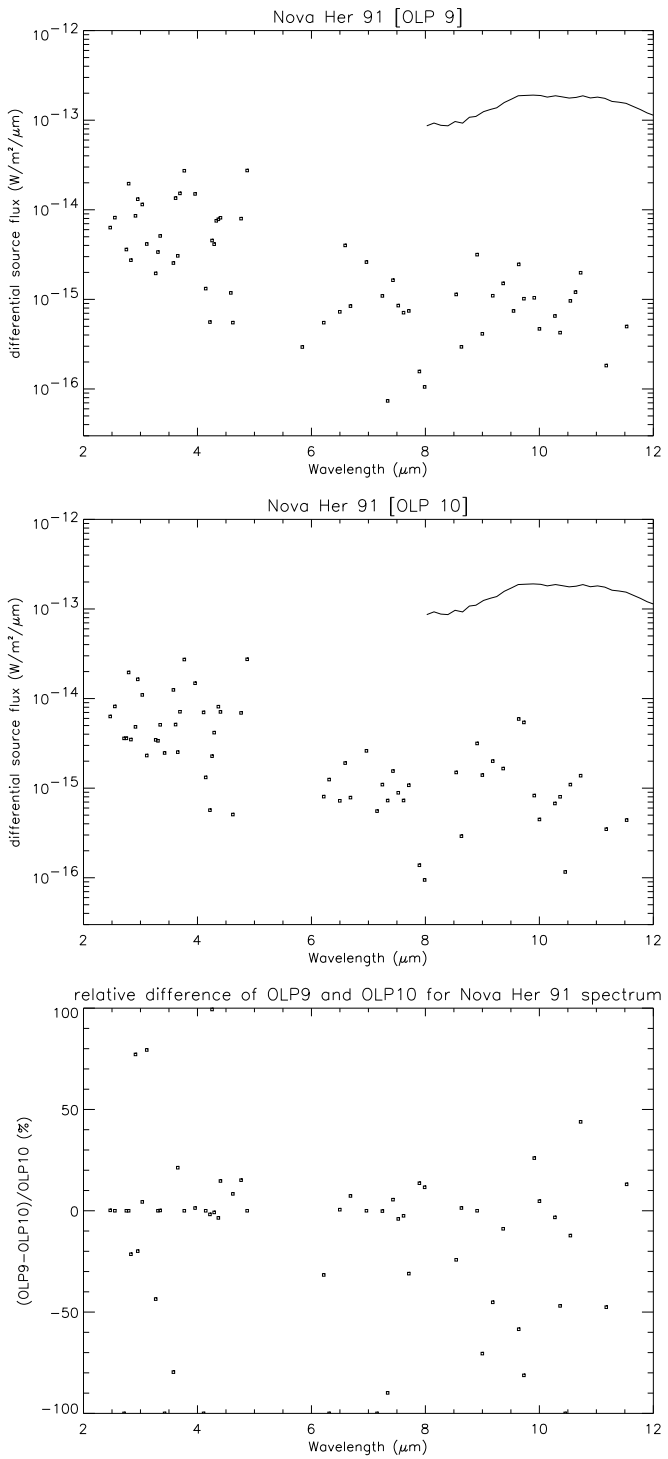

Figure 12.9: Comparison of the spectrum of Nova Her91 obtained in PHT-S rectangular chopped mode in 1996 with the groundbased $8 - 13$ micron spectroscopy by Smith et al. 1995, obtained in 1991, 67 days after its maximum for both OLP 9.0b6 (upper panel) and OLP 10.0b5 (middle panel) and the relative difference of both versions (lower panel).

12.3.2 PHT40 Spectroscopy: MIR Spectra of Galaxies from Chopped PHT-S Measurements

Motivation

There is a set of chopped PHT-S measurements of galaxies with fluxes in the range 10^{-14} to $10^{-12}\,\mathrm{W/m^2/\mu m}$. These galaxies have different SED shapes than the standard stars from which the chopped PHT-S spectral response function was derived. There is groundbased $8 - 13$ micron spectroscopy available (cf. Ref. [8]). We selected a range of galaxies from featureless continuum to spectra with PAH features and strong 10 μm silicon absorption.

Method

We compare the absolute fluxes and relative shapes of the ISOPHOT-S spectra of both OLP 9.0b6 and OLP 10.0b5 with the groundbased spectroscopy. Note that we compare an aperture size of 24x24 arcsec^2 for ISOPHOT-S with 5 arcsec aperture size of the groundbased measurements. Note, that in previous reports there appeared to be an inconsistency for NGC 5253 with the groundbased spectrum showing a higher flux than the ISOPHOT-S spectrum. This could be traced back to a wrong flux level scaling (a factor 10 too high) in Roche et al. (1991) by looking up the spectrum of the source in Aitken et al. (1982, MNRAS 199, 31P).

Results

In Figs. 12.10 to 12.27 we perform an individual comparison of both OLP versions with the groundbased spectroscopy. The spectra are ordered with increasing PAH and silicate absorption feature strength. NGC 1068 is by far the brightest object of the sample considered here. NGC 1068, NGC 4151, NGC 5506, Mrk 231 and 3C 273 are the only galaxies with 2.5 – 4 μm fluxes being above $7 \times 10^{-14}\,\mathrm{W\,m^{-2}\,\mu m^{-1}}$ and hence above the sensitivity limit for PHT-SS. For all the other galaxies the PHT-SS channel displays only noise. The PHT-SL spectra show a very good agreement in the relative spectral shape with the groundbased spectroscopy. In some cases the PHT-SL spectrum shows a significantly higher flux indicating the extension of the source (3C 273 is a variable source). NGC 5506, NGC 4051 and NGC 5253 show a noticable [SIV]10.6 μm-line. NGC 4102 and Mrk 331 show pronounced PAH features, NGC 4418, NGC 6240 and Arp 220 a strong slicate absorption feature.

Conclusions

- The two OLP versions give very similar results; slight changes are expected due to the two-threshold deglitching on ramp level.
- The galaxy spectra confirm the findings for stellar spectra that sensitivity limits of accurate spectrophotometry for typically 512 s on-source exposure time are around $7 \times 10^{-14}\,\mathrm{W\,m^{-2}\,\mu m^{-1}}$ for PHT-SS, corresponding to around 400 mJy at 4 μm and $7 \times 10^{-15}\,\mathrm{W\,m^{-2}\,\mu m^{-1}}$ to $10^{-14}\,\mathrm{W\,m^{-2}\,\mu m^{-1}}$ for PHT-SL, corresponding to 150 – 210 mJy at 8 μm.
- A better deglitching making use of the bi-weight mean algorithm as applied for chopped photometry would make the spectra smoother.

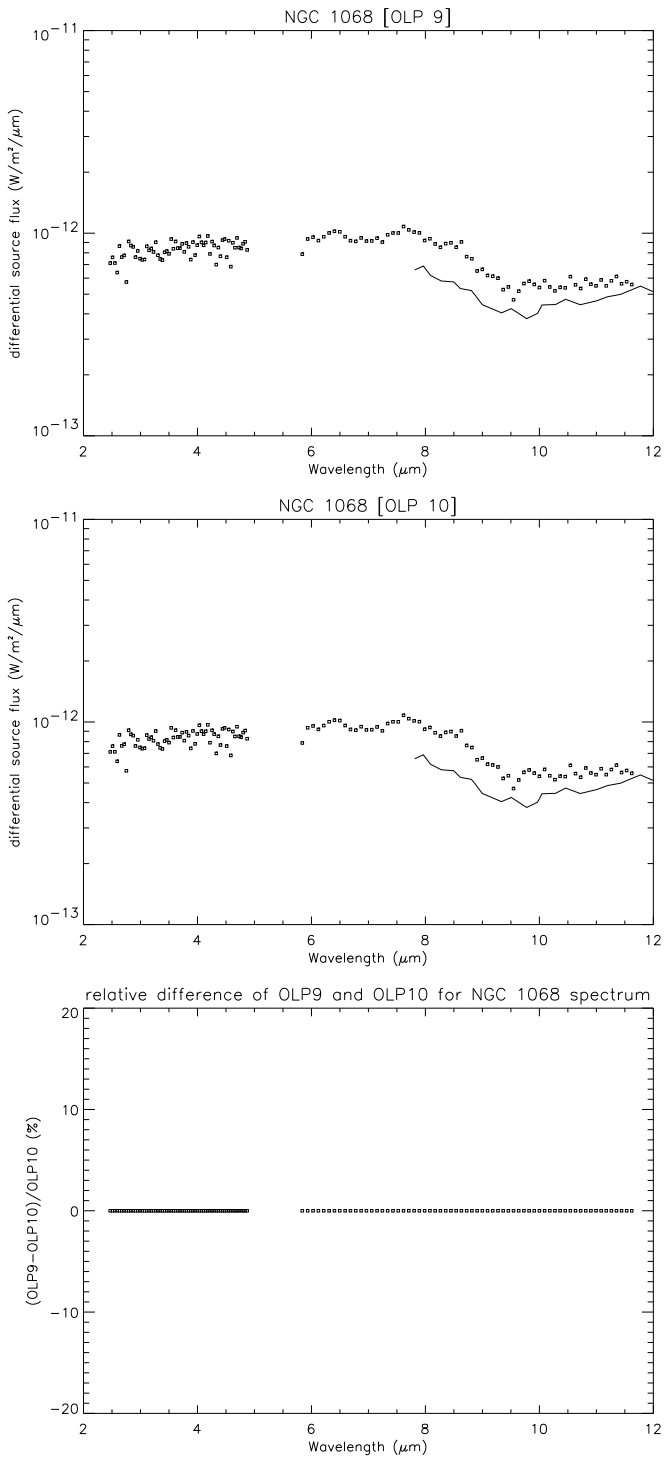

Figure 12.10: Comparison of the spectrum of NGC 1068 obtained in rectangular chopped mode (dots) with groundbased $8-13$ micron spectroscopy (solid line) by Roche et al. 1991 for both OLP 9.0b6 (upper panel) and OLP 10.0b5 (middle panel) and the relative difference of both versions (lower panel).

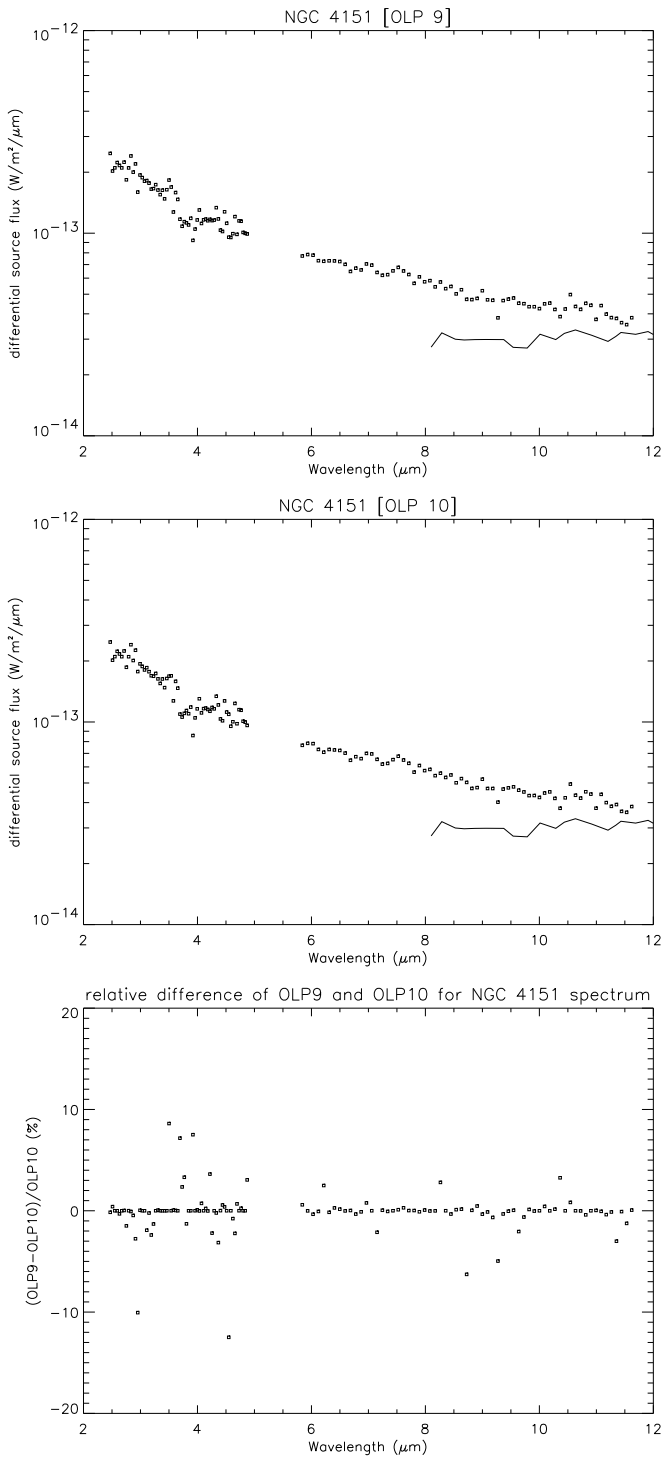

Figure 12.11: Comparison of the spectrum of NGC 4151 obtained in rectangular chopped mode (dots) with groundbased $8-13$ micron spectroscopy (solid line) by Roche et al. 1991 for both OLP 9.0b6 (upper panel) and OLP 10.0b5 (middle panel) and the relative difference of both versions (lower panel).

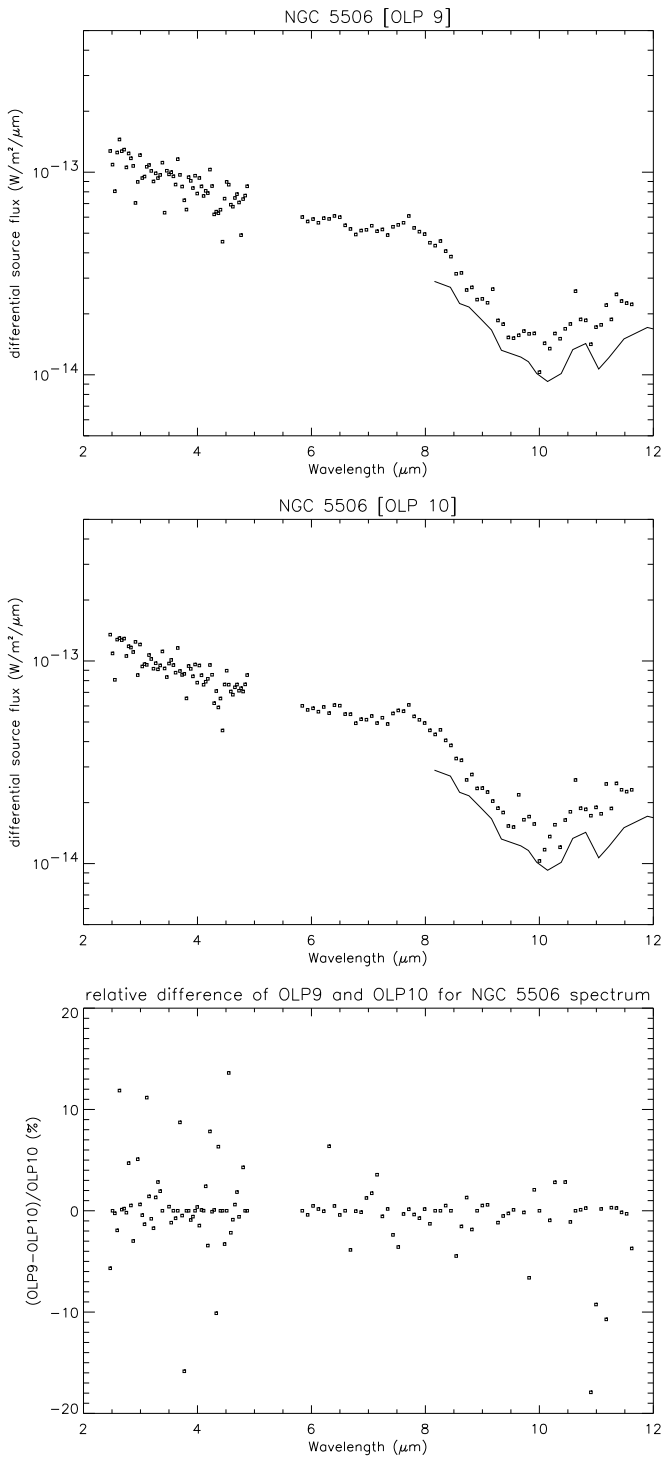

Figure 12.12: Comparison of the spectrum of NGC 5506 obtained in rectangular chopped mode (dots) with groundbased $8-13$ micron spectroscopy (solid line) by Roche et al. 1991 for both OLP 9.0b6 (upper panel) and OLP 10.0b5 (middle panel) and the relative difference of both versions (lower panel).

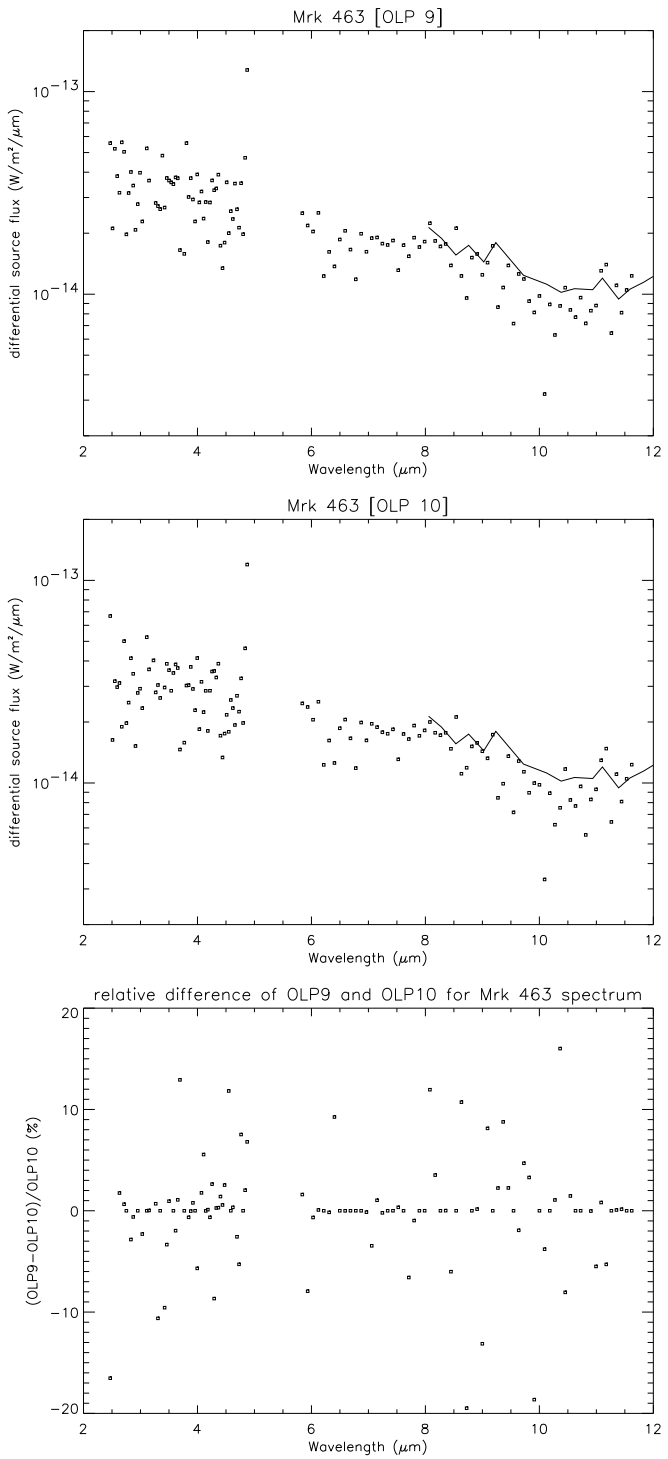

Figure 12.13: Comparison of the spectrum of Mrk 463 obtained in rectangular chopped mode (dots) with groundbased 8 – 13 micron spectroscopy (solid line) by Roche et al. 1991 for both OLP 9.0b6 (upper panel) and OLP 10.0b5 (middle panel) and the relative difference of both versions (lower panel).

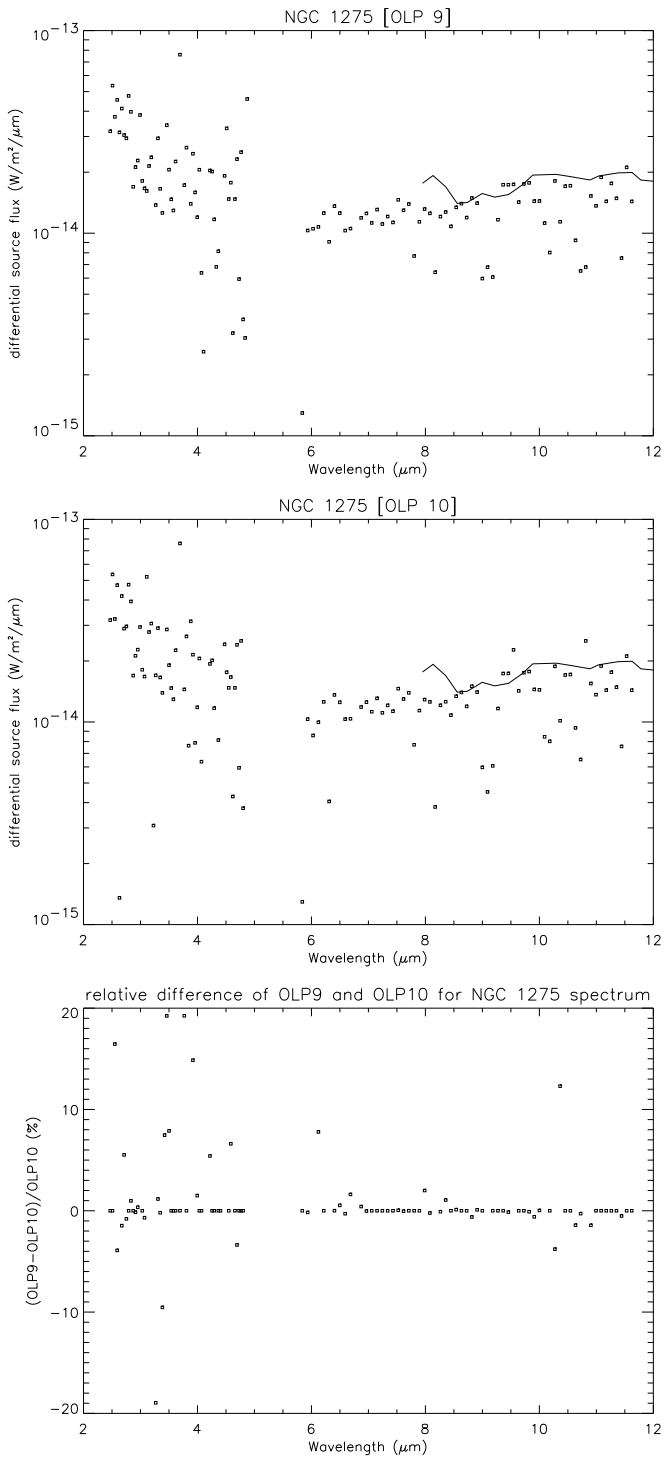

Figure 12.14: Comparison of the spectrum of NGC 1275 obtained in rectangular chopped mode (dots) with groundbased $8-13$ micron spectroscopy (solid line) by Roche et al. 1991 for both OLP 9.0b6 (upper panel) and OLP 10.0b5 (middle panel) and the relative difference of both versions (lower panel).

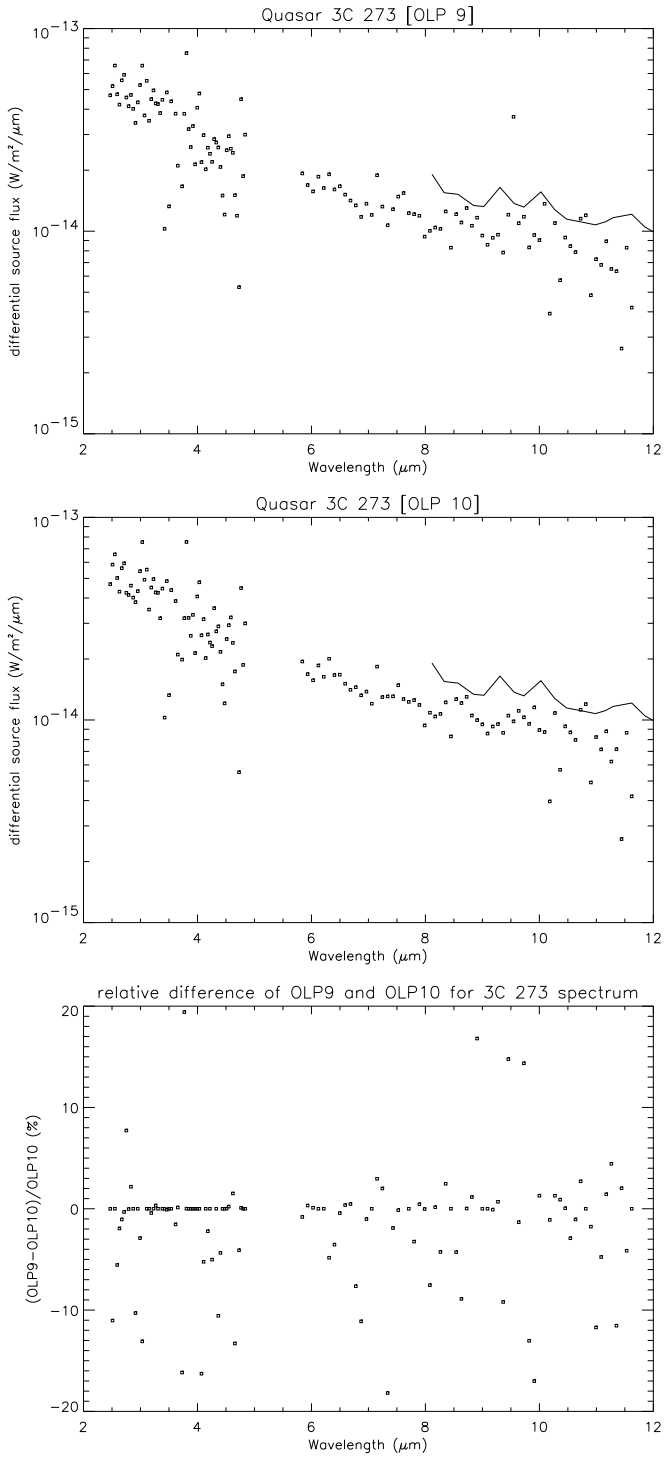

Figure 12.15: Comparison of the spectrum of 3C 273 obtained in rectangular chopped mode (dots) with groundbased 8 – 13 micron spectroscopy (solid line) by Roche et al. 1991 for both OLP 9.0b6 (upper panel) and OLP 10.0b5 (middle panel) and the relative difference of both versions (lower panel).

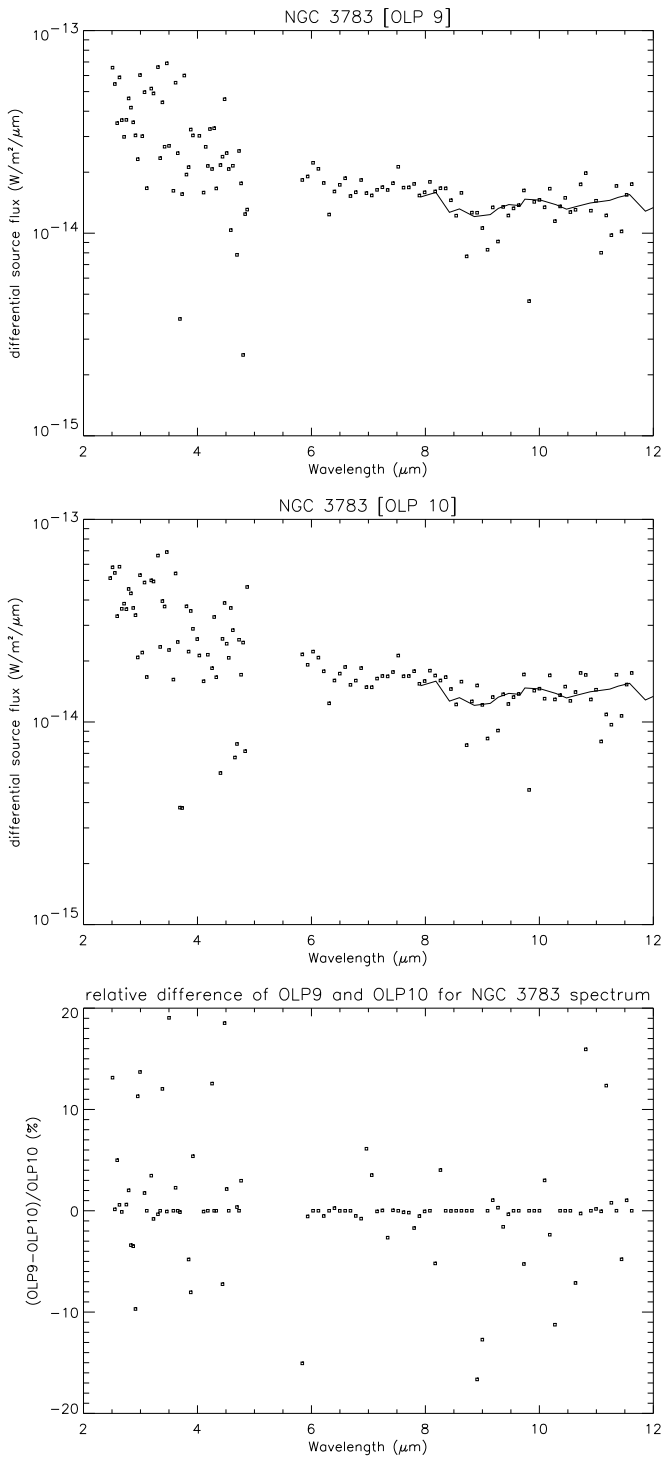

Figure 12.16: Comparison of the spectrum of NGC 3783 obtained in rectangular chopped mode (dots) with groundbased $8-13$ micron spectroscopy (solid line) by Roche et al. 1991 for both OLP 9.0b6 (upper panel) and OLP 10.0b5 (middle panel) and the relative difference of both versions (lower panel).

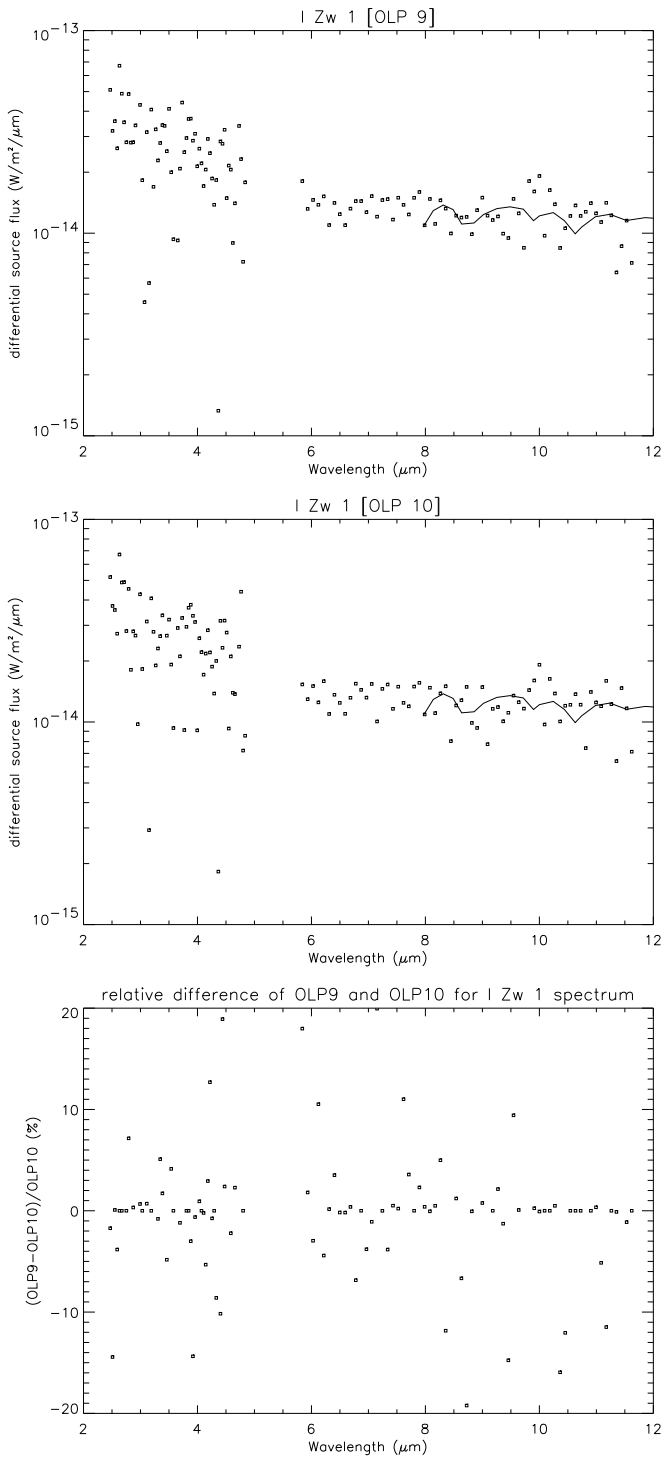

Figure 12.17: Comparison of the spectrum of I Zw 1 obtained in rectangular chopped mode (dots) with groundbased 8 – 13 micron spectroscopy (solid line) by Roche et al. 1991 for both OLP 9.0b6 (upper panel) and OLP 10.0b5 (middle panel) and the relative difference of both versions (lower panel).

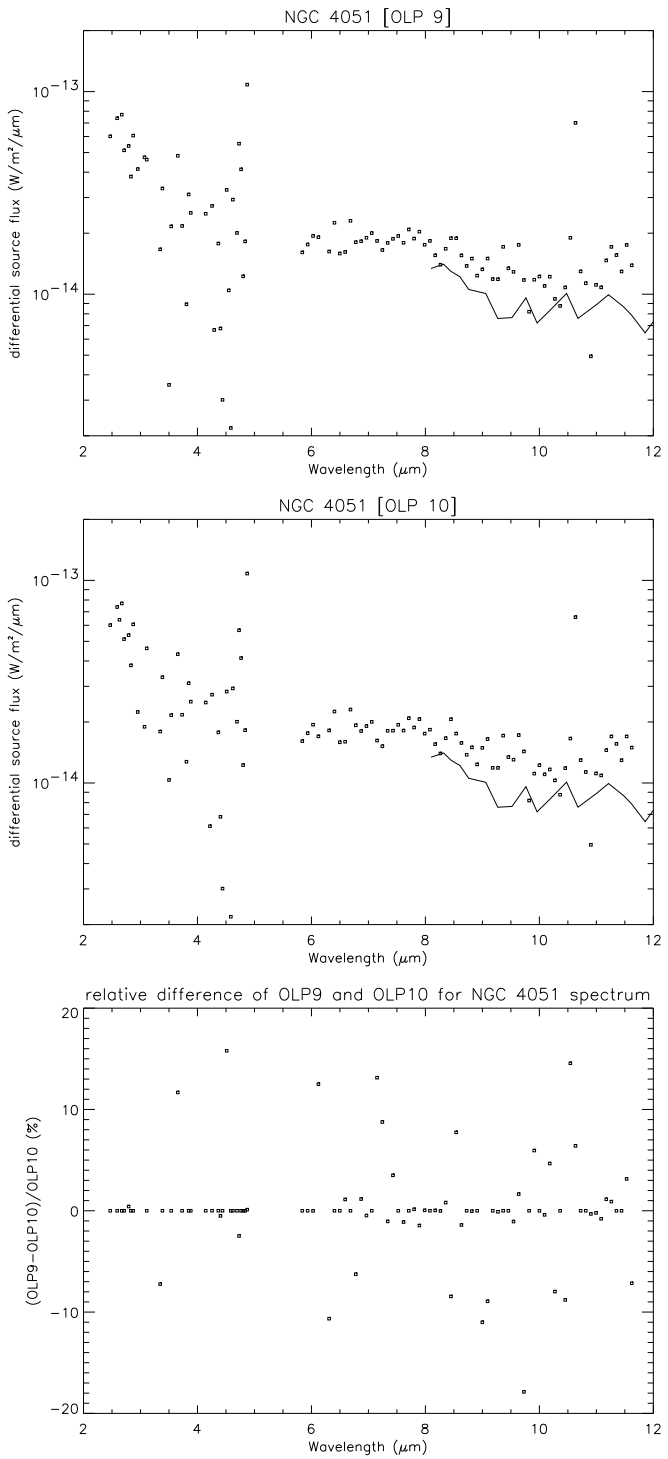

Figure 12.18: Comparison of the spectrum of NGC 4051 obtained in rectangular chopped mode (dots) with groundbased $8-13$ micron spectroscopy (solid line) by Roche et al. 1991 for both OLP 9.0b6 (upper panel) and OLP 10.0b5 (middle panel) and the relative difference of both versions (lower panel).

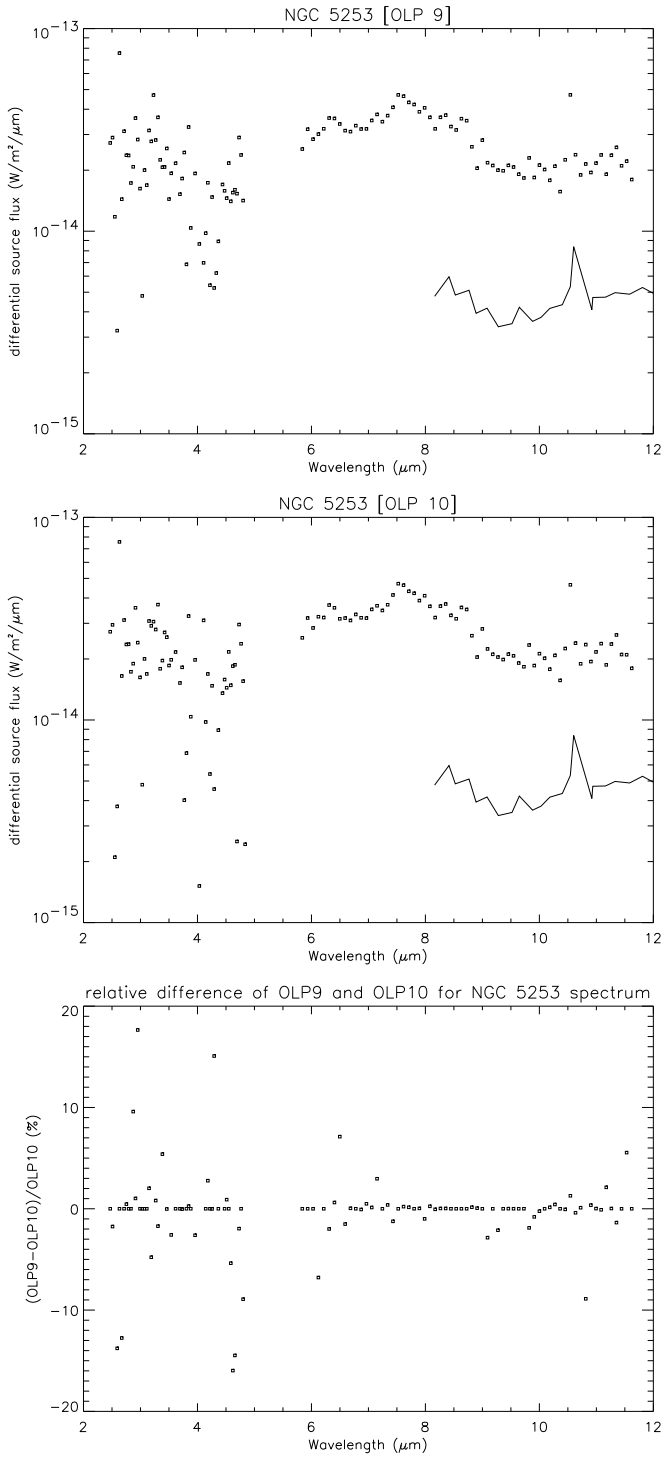

Figure 12.19: Comparison of the spectrum of NGC 5253 obtained in rectangular chopped mode (dots) with groundbased $8-13$ micron spectroscopy (solid line) by Aitken et al. 1982 for both OLP 9.0b6 (upper panel) and OLP 10.0b5 (middle panel) and the relative difference of both versions (lower panel).

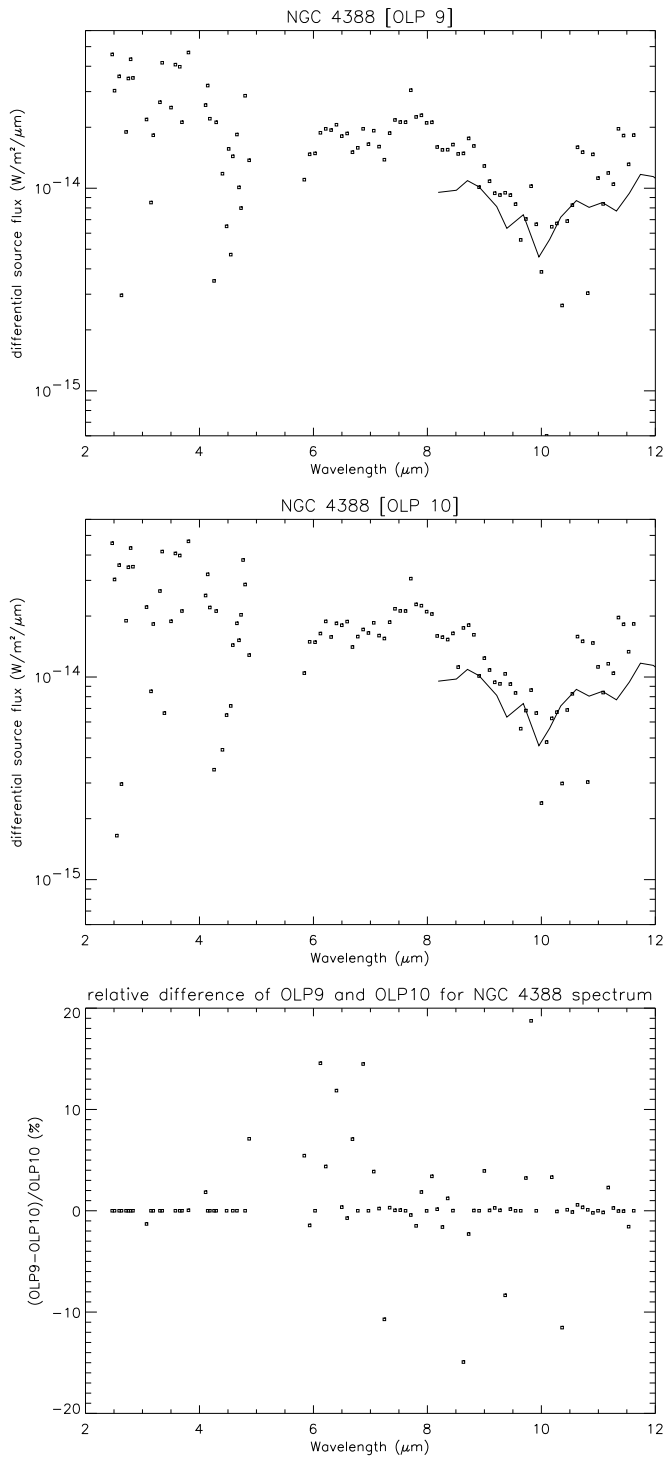

Figure 12.20: Comparison of the spectrum of NGC 4388 obtained in rectangular chopped mode (dots) with groundbased $8-13$ micron spectroscopy (solid line) by Roche et al. 1991 for both OLP 9.0b6 (upper panel) and OLP 10.0b5 (middle panel) and the relative difference of both versions (lower panel).

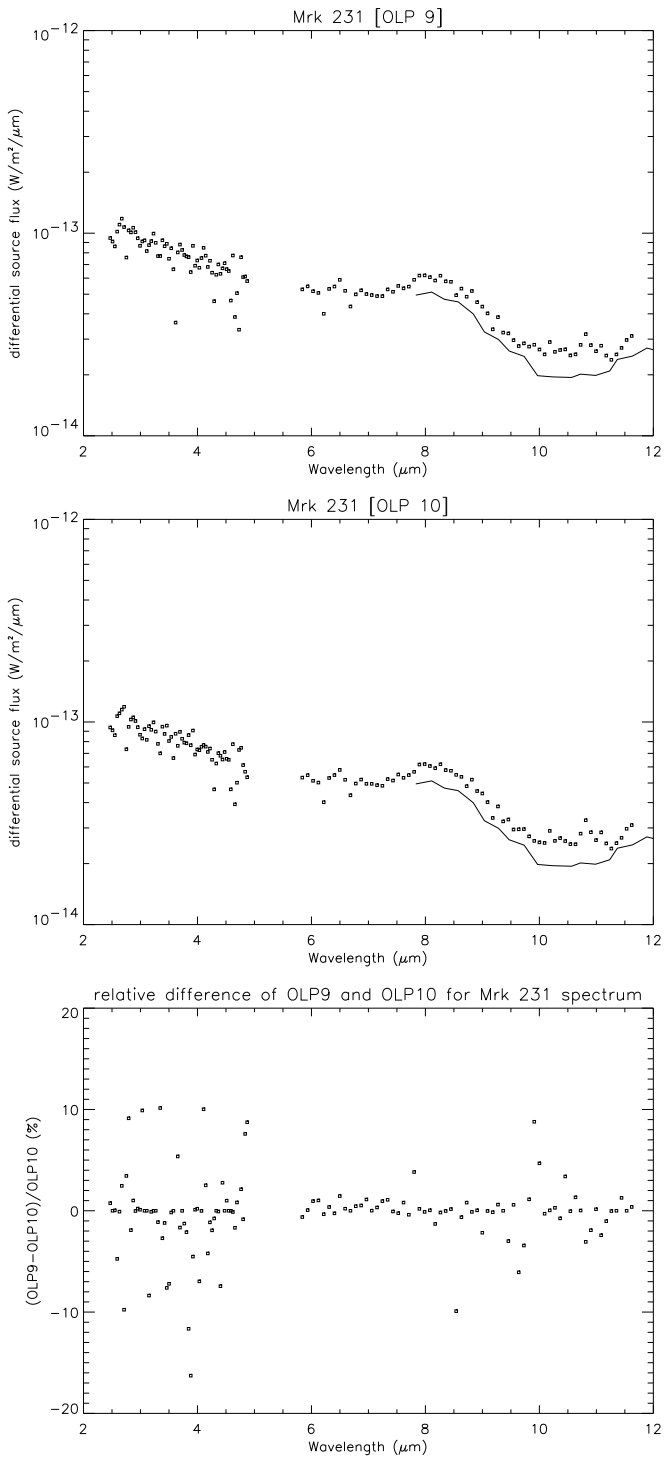

Figure 12.21: Comparison of the spectrum of Mrk 231 obtained in rectangular chopped mode (dots) with groundbased 8 – 13 micron spectroscopy (solid line) by Roche et al. 1991 for both OLP 9.0b6 (upper panel) and OLP 10.0b5 (middle panel) and the relative difference of both versions (lower panel).

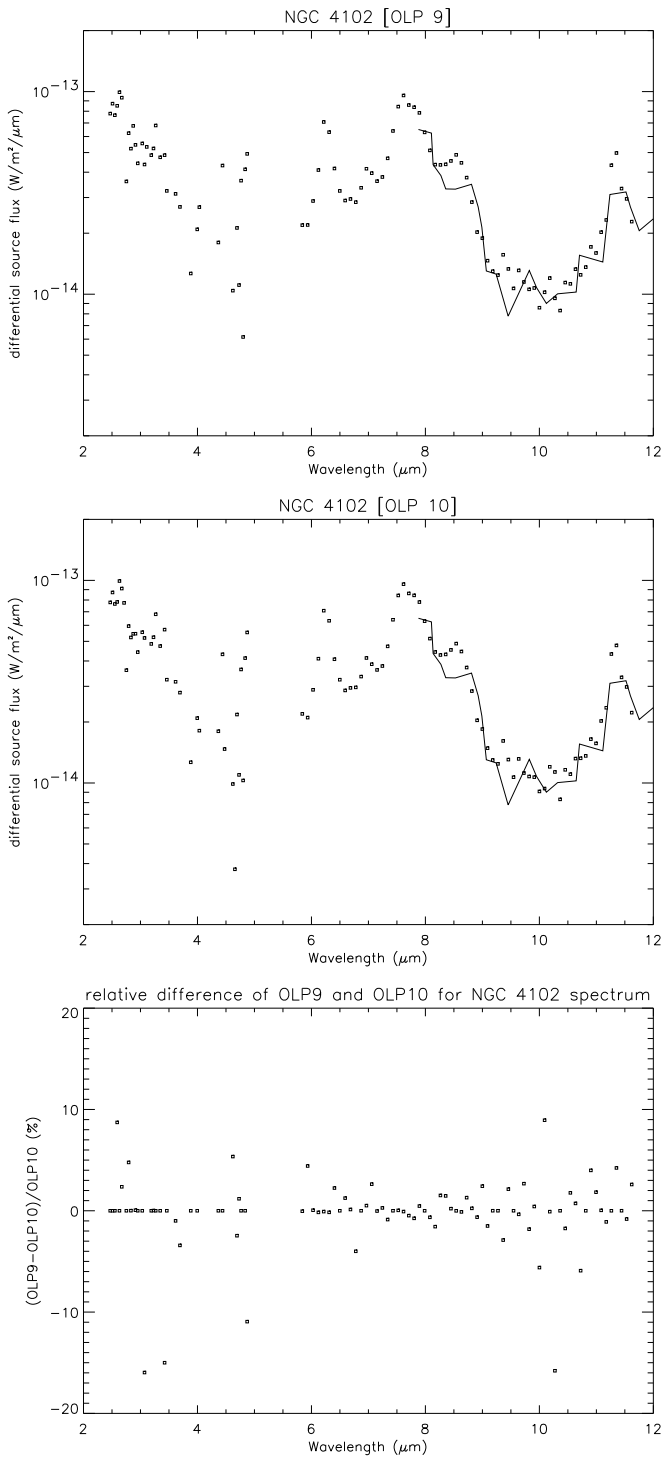

Figure 12.22: Comparison of the spectrum of NGC 4102 obtained in triangular chopped mode (dots) with groundbased $8-13$ micron spectroscopy (solid line) by Roche et al. 1991 for both OLP 9.0b6 (upper panel) and OLP 10.0b5 (middle panel) and the relative difference of both versions (lower panel).

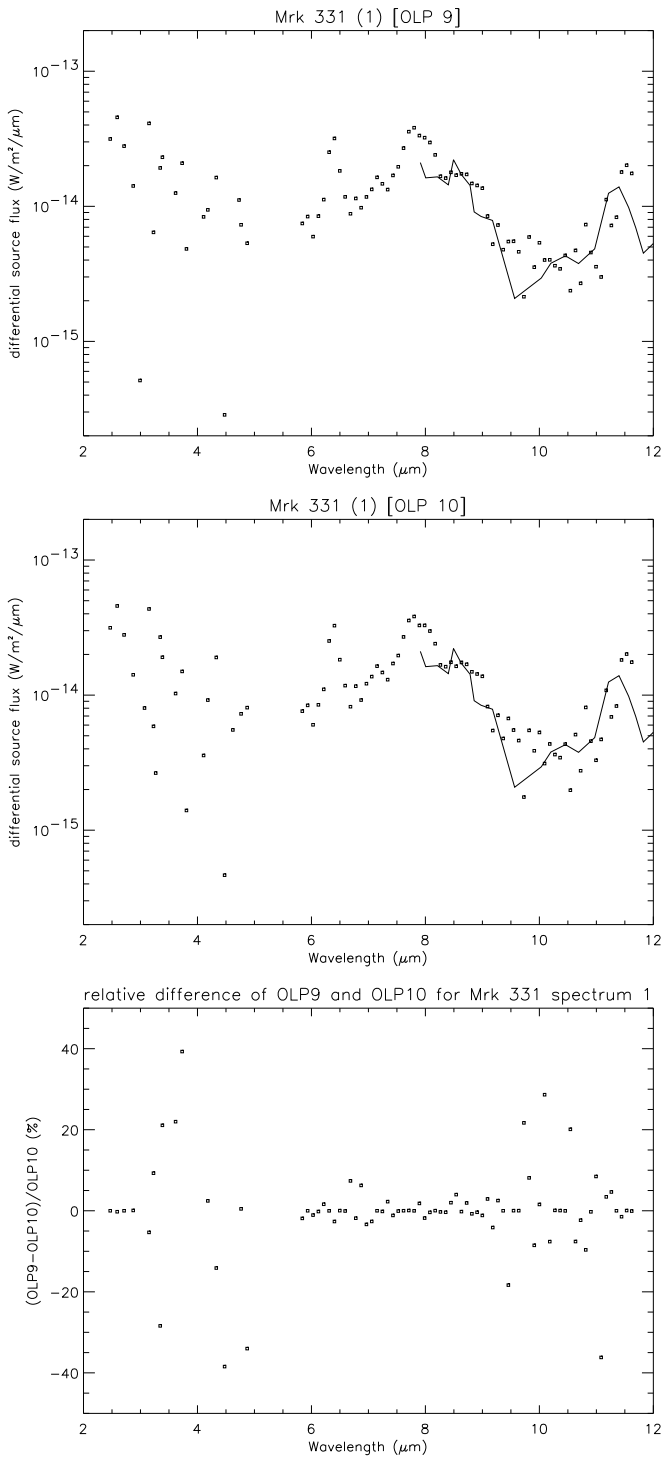

Figure 12.23: Comparison of the spectrum of Mrk 331 (1 = TDT37901644) obtained in triangular chopped mode (dots) with groundbased $8-13$ micron spectroscopy (solid line) by Roche et al. 1991 for both OLP 9.0b6 (upper panel) and OLP 10.0b5 (middle panel) and the relative difference of both versions (lower panel).

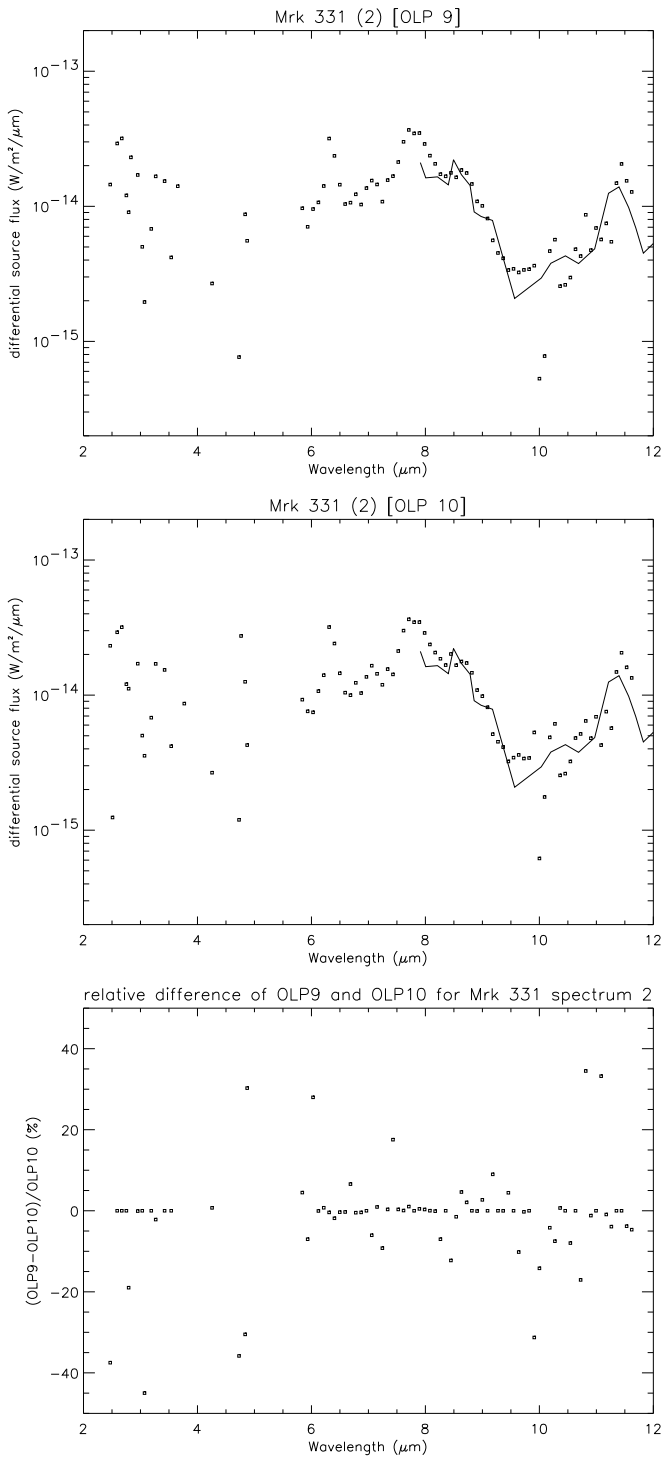

Figure 12.24: Comparison of the spectrum of Mrk 331 (2 = TDT56500644) obtained in triangular chopped mode (dots) with groundbased $8-13$ micron spectroscopy (solid line) by Roche et al. 1991 for both OLP 9.0b6 (upper panel) and OLP 10.0b5 (middle panel) and the relative difference of both versions (lower panel).

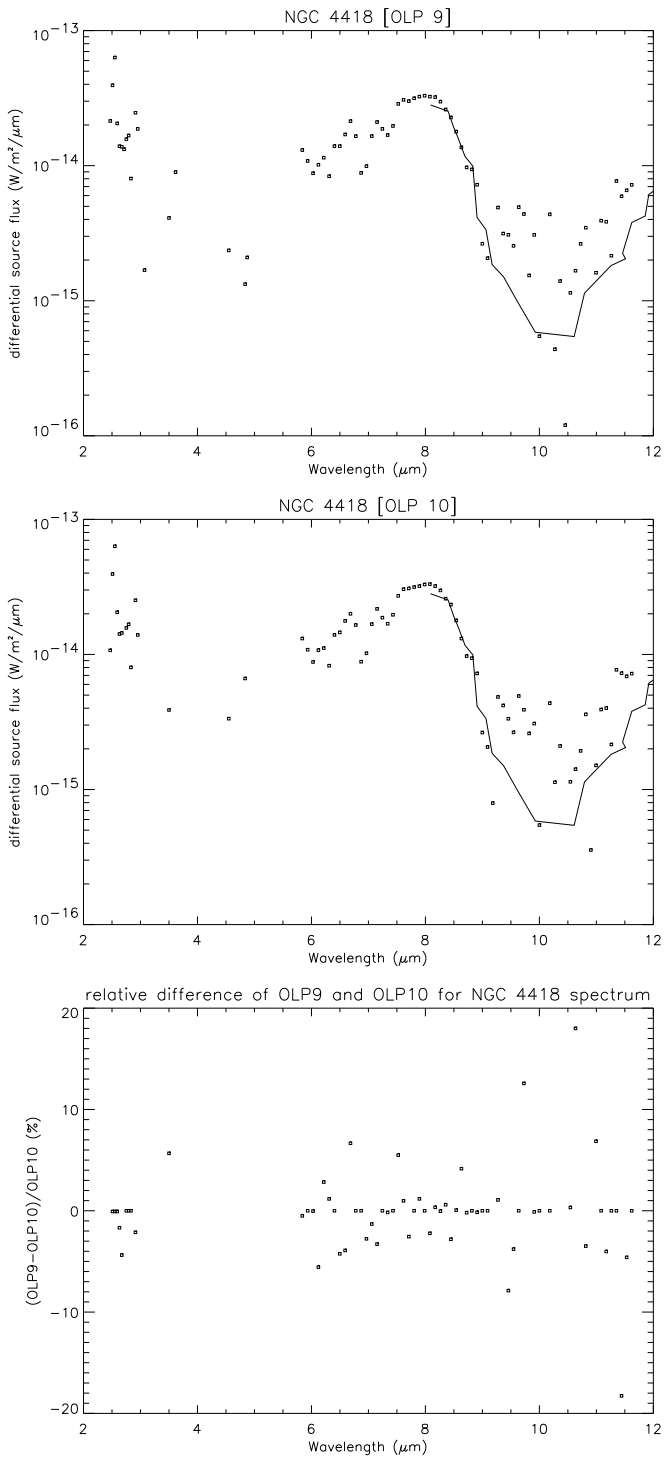

Figure 12.25: Comparison of the spectrum of NGC 4418 obtained in triangular chopped mode (dots) with groundbased $8-13$ micron spectroscopy (solid line) by Roche et al. 1991 for both OLP 9.0b6 (upper panel) and OLP 10.0b5 (middle panel) and the relative difference of both versions (lower panel).

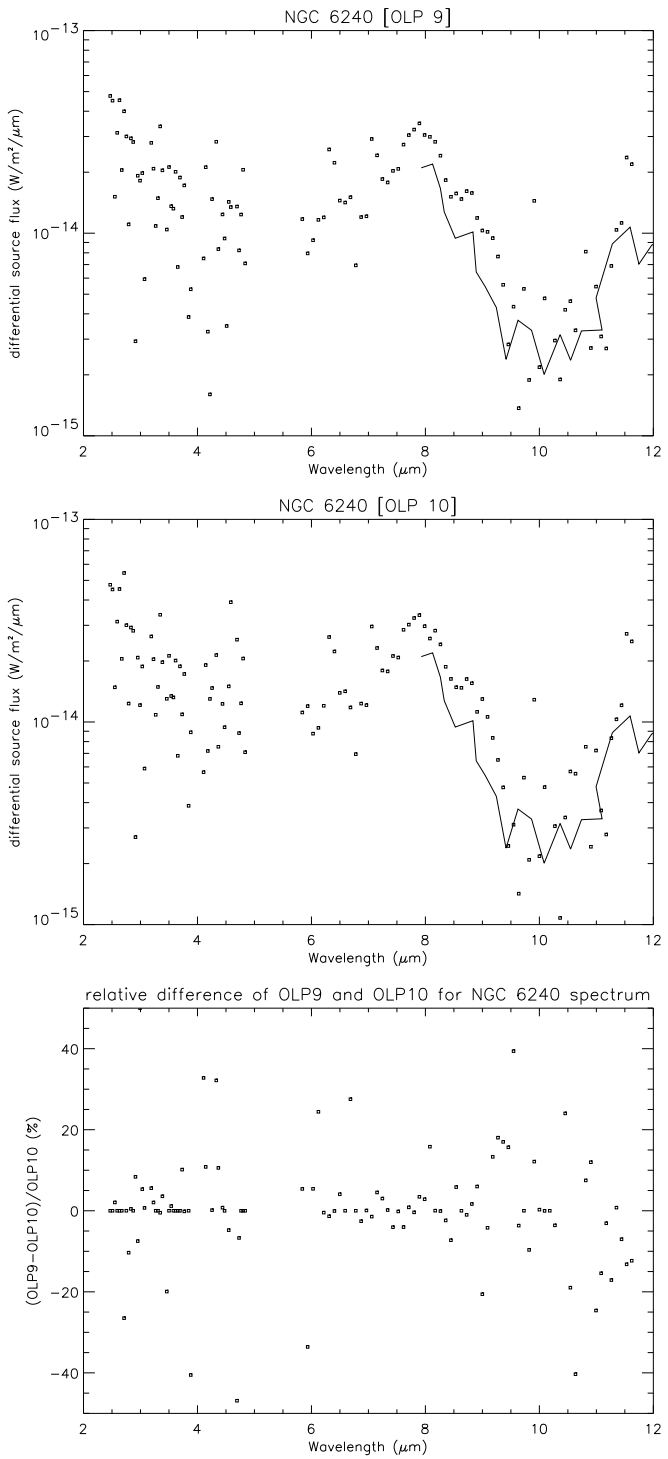

Figure 12.26: Comparison of the spectrum of NGC 6240 obtained in rectangular chopped mode (dots) with groundbased $8-13$ micron spectroscopy (solid line) by Roche et al. 1991 for both OLP 9.0b6 (upper panel) and OLP 10.0b5 (middle panel) and the relative difference of both versions (lower panel).

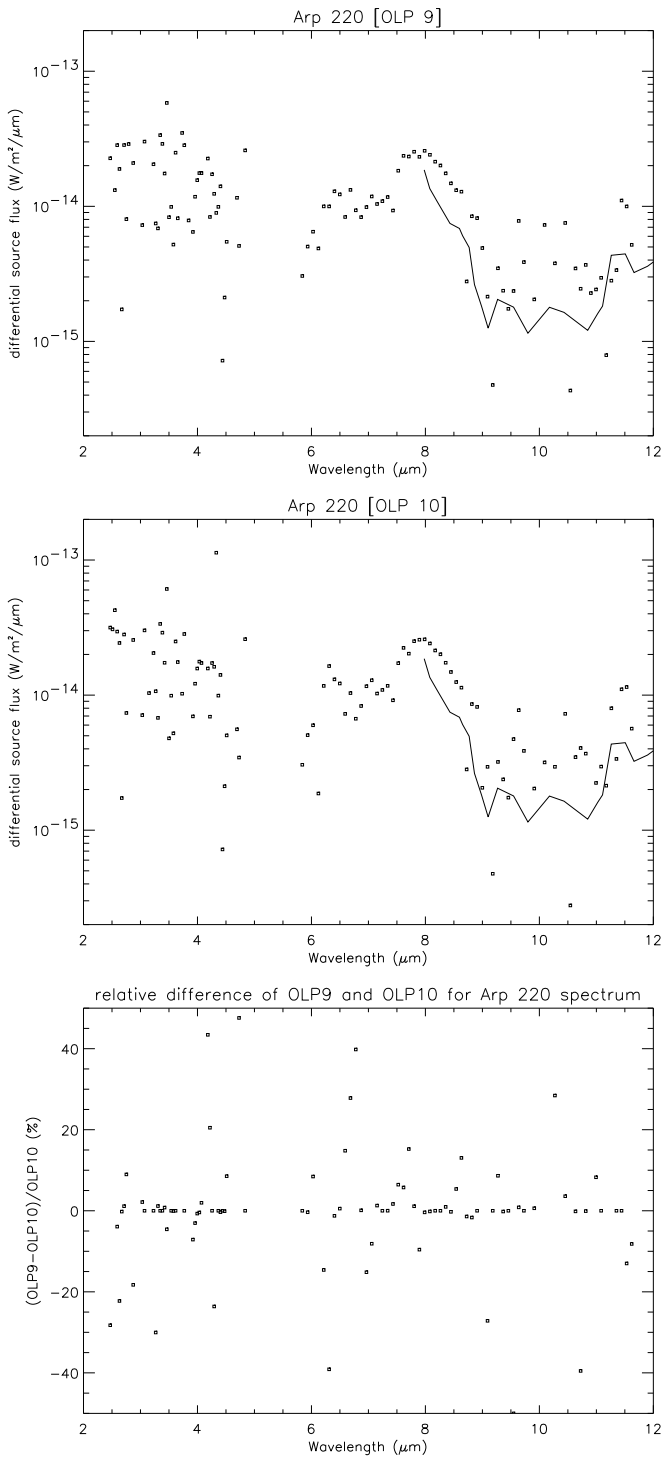

Figure 12.27: Comparison of the spectrum of Arp 220 obtained in rectangular chopped mode (dots) with groundbased 8 – 13 micron spectroscopy (solid line) by Roche et al. 1991 for both OLP 9.0b6 (upper panel) and OLP 10.0b5 (middle panel) and the relative difference of both versions (lower panel).

Chapter 13

Raster Mode Spectroscopy

TBW

Chapter 14

Conclusions and Outlook

The Scientific Validation of the ISOPHOT OLP 10.0 version has demonstrated and achieved the following:

- Further consolidation with improved photometric accuracy for staring mode observations, including faint source photometry from mini-maps.
- More detailed assessment of the photometric accuracy of absolute and multi-filter staring modes, including lower flux limits for accurate on-off photometry.
- Further consolidation of the correction for non-linearity of signals due to flux dependence of detector responsivity.
- Upgraded FCS power tables.
- Validation of the chopped photometry calibration, including assessment of accuracy limitations, mainly due to FIR cirrus confusion .
- Improvement of the flat-field accuracy of P22 raster maps with greater equal 20 raster points by a statistical flat-field method .
- The installation of a more efficient glitch removal and improvement of the flat-field accuracy of P32 oversampled maps .
- The introduction of a processing to determine a background subtracted source flux normalized to the flux in the 180 arcsec aperture for suitable multi-aperture photometry (P04) measurements to determine a relative source profile .
- The provision of better interfaces to the overall ISO Data Archive structure, e.g. by calculating the on-source positions for rectangular chopped measurements and using world coordinates for mapping products.

A summary schedule for the OLP 10 upgrade and scientific validation is outlined in Table 14.1. With this OLP version the standard ISOPHOT data products contained in the ISO Legacy Archive were generated.

Table 14.1: Schedule for PHT OLP 10.0 Upgrades, Scientific Validation and Documentation.

Software and Cal-G file implementation	Nov & Dec-2000
Software and calibration file delivery (1)	11-Dec-2000
OLP 10.0 test plan	13-Dec-2000
Software and calibration file delivery (2)	09-Jan-2001
Scientific Validation Period 1 (OLP 10.0b3)	17-Jan - 02-Feb-2001
Software and calibration file delivery (3)	02-Feb-2001
Scientific Validation Period 2 (OLP 10.0b5)	13-Feb - 14-Mar-2001
Software and calibration file delivery (4)	14-Mar-2001
Scientific Validation Period 3 (OLP 10.0b7)	23-Mar - 16-Apr-2001
Software and calibration file delivery (5)	06&12-Apr-2001
Scientific Validation Period 4 (OLP 10.0b8)	23-Apr - 03-May-2001
Software delivery (6)	26-Apr-2001
Scientific Validation Period 5 (OLP 10.0b9)	09 - 23-May-2001
Software delivery (7)	23&24-May-2001
Scientific Validation Period 6 (OLP 10.0b11)	25 - 31-May-2001
Final software upgrades	01-June-2001
Scientific Validation Period 7 (OLP 10.0b12)	05-June-2001
ISOPHOT OLP 10.0 Release	05-June-2001
ISOPHOT OLP 10.1 Release	20-Nov-2001
ISOPHOT Legacy Archive Release	28-Feb-2002
ISOPHOT Handbook, Version 2.0	31-Mar-2002
Version 1.0 of PHT Scientific Validation Report	09-Apr-2002
PHT Calibration Accuracies V5.0 (adapted to OLP10) & PHT Calibration Accuracies per Submode	$\sim$ May-2002

The ISOPHOT Data Centre at MPIA and the UK ISO Data Centre at RAL will continue to improve the general calibration and the quality of specific ISOPHOT data products during the upcoming five year period of the ISO Active Archive Phase. The activities will comprise:

- Refinement of the current calibration files, like time and orbit phase dependent dark signals and default responsivities.
- Introduction of new calibration items, like the contribution of by-passing sky light to the FCS signals (for all surface brightness observations which do not contain a cold FCS measurement).
- Scientific assessment of photometry in non-standard apertures and establishment of correction factors with regard to the standard apertures.
- Tests of signal transient corrections (interactive and automatic).
- Bulk processing of data sets with improved calibration or for easier access of photometric information and import into the Archive.
  Projects in realization are:
  1) All PHT40 chopped PHT-S measurements with improved deglitching by application of the bi-weight mean method applied already to chopped photometry measurements.
  2) Inclusion of point source photometry information in the PGAI product header for PHT22 raster maps of centered point sources (mini-maps) by application of the PCAS evaluation method (PSF weighted fit of the fluxes for all distances of a respective pixel relative to the map centre in order to determine the peak flux and the background level and robust averaging of the results for individual pixels).
- Product quality and validation checks.

Bibliography

[1] U. Klaas, K. Wilke, C. Kiss, M. Radovich and P. Richards, "Report on the PHT Scientific Validation for OLP Version 9.0", SAI/2000-014/Rp, Version 2.0, 19-December-2000.

[2] R.J. Laureijs, U. Klaas, P.J. Richards, B. Schulz and P. Ábrahám, "The ISO Handbook, Volume V: PHT – The Imaging Photo-Polarimeter", SAI/99-069/Dc, Version 1.2, 01-July-2001

[3] R.J. Laureijs and U. Klaas, "ISOPHOT Error Budgets", SAI/98-091/Dc, Version 1.0, 21-April-1999 (DERIVE_SPD Processing Steps)

[4] U. Klaas, "Plan for the PHT Scientific (Re-)Validation of PHT OLP Version 10.0", SAI/2000-068/Dc, Version 2.0, 02-February-2001

[5] J. Acosta, "Dynamic Calibration for ISOPHOT-S", IAC / IDC PHT internal calibration report, 03-August-1999

[6] K. Sellgren, L.J. Allamandola, J.D. Bregman, et al., "Emission Features in the 4-13 Micron Spectra of the Reflection Nebulae NGC 7023 and NGC 2023", ApJ 299, 416, 1985

[7] D. Cesarsky, J. Lequeux, A. Abergel, et al., "Infrared Spectrophotometry of M17 with ISOCAM", A&A 315, L305, 1996

[8] P.F. Roche, D.K. Aitken, C.H. Smith and M.J. Ward, "An Atlas of Mid-infrared Spectra of Galaxy Nuclei", MNRAS 248, 606, 1991

[9] J. Acosta-Pulido, "Calibration of ISOPHOT-S Chopped Measurements", IDC PHT Internal Calibration Report, 08-March-1999

[10] R.J. Laureijs, "Point Spread Function Fractions Related to the ISOPHOT C100 and C200 Arrays", IDC PHT Internal Calibration Report, Version 1.0, 29-June-1999

[11] P.L. Hammersley, M. Jourdain De Muizon, M.F. Kessler, P. Bouchet, R.D. Joseph, H. Habing, A. Salama, L. Metcalfe, "Infrared standards for ISO. I. A new calibration of mid infrared photometry", A&AS 128, 207, 1998

[12] P.F. Roche, D.A. Allen, D.K. Aitken, "Symbiotic stars: spectrophotometry at 3-4 and 8-13 um", MNRAS 204, 1009, 1983

[13] C.H. Smith, D.K. Aitken, P.F. Roche, C.M. Wright, "Mid-infrared spectroscopy of galactic novae", MNRAS 277, 259, 1995

[14] I. Heinrichsen, H.J. Walker, and U. Klaas, "Infrared Mapping of the Dust Disc around Vega", MNRAS 293, L78, 1998

[15] U. Klaas, M. Haas, I. Heinrichsen, B. Schulz, "Infrared spectral energy distributions of the interacting galaxies Arp 244, NGC 6240 and Arp 220", 1997, A&A 325, L21

[16] L. Verstraete, J.L. Puget, E. Falgarone, S. Drapatz, C.M. Wright, R. Timmermann, "SWS Spectroscopy of Small Grain Features across the M17-Southwest Photodissociation Front", 1996, A&A 315, L337

[17] D. Cesarsky, J. Lequeux, A. Abergel, M. Perault, E. Palazzi, S. Madden, D. Tran, "Infrared Spectrophotometry of M17 with ISOCAM", 1996, A&A 315, L309

[18] B. Schulz & S. Huth, "Explanatory Supplement for FCS Monitoring Observations", Draft 2.0, 20-June-97 and related diagrams

[19] P. Ábrahám, M. Radovich, L. Schmidtobreick, U. Klaas, T. Kranz, "Analysis of Chopped ISOPHOT Measurements", Version 1.0, PHT/MPIA Calibration Report, 24-November-1999

[20] N. Ginestet, J.M. Carquillat, C. Jaschek, "Spectral classifications in the near infrared of stars with composite spectra", 1999, A&A Supp 134, 473

[21] C.K. Mitrou, J.G. Doyle, M. Mathioudakis, E. Antonopoulou, "The emission of the RS CVn binaries in the IRAS passbands", 1996, A&A Supp 115, 61

[22] C.L. Perry, E.H. Olsen, D.L. Crawford, "A catalog of bright uvbybeta standard stars", 1987, PASP 99, 1184

[23] K. Mattila, D. Lemke, L.K. Haikala, R.J. Laureijs, A. Léger, K. Lehtinen, Ch. Leinert, and P.G. Mezger, "Spectrophotometry of UIR bands in the diffuse emission of the galactic disk", 1996, A&A 315, L353

[24] T. Onaka, and the IRTS team, "IRTS observations of the unidentified infrared bands in the diffuse Galactic light", 1997, Diffuse Infrared Radiation and the IRTS, H. Okuda, T. Matsumoto, and T.L. Roellig (eds.), ASP Conference Series, Vol. 124, 170

[25] I. Heinrichsen, H.J. Walker, U. Klaas, R.J. Sylvester, and D. Lemke, "An infrared image of the dust disc around β Pic", 1999, MNRAS 304, 589

[26] U. Klaas, J.A. Acosta–Pulido, P. Ábrahám, H.O. Castañeda, L. Cornwall, F. Garzon, P. Hammersley, I. Heinrichsen, U. Kinkel, D. Lemke, J. Schubert, and M. Wells, "ISOPHOT-S: Capabilities and Calibration", Proc. First ISO Workshop on Analytical Spectroscopy, p. 113, ESA SP-419, December 1997

[27] U. Klaas, P. Ábrahám, M. Haas, U. Herbstmeier, and R.J. Laureijs, "General ISOPHOT Observing Strategies for Faint Sources", SAI/97-013/Wb, Version 1.3, 28-February-1997

[28] P. Ábrahám, U. Klaas, M. Haas, U. Herbstmeier, M. Linden, and D. Lemke, "Detection Limit and Observing Strategy for Very Faint Point Sources: Test Observations with P3, C100, and C200", Version 2.0, PHT/MPIA Calibration Report, 29-April-1997

[29] B.T. Soifer, L. Boehmer, G. Neugebauer, D.B. Sanders, "The *IRAS* Bright Galaxy Sample. IV. Complete *IRAS* Observations", 1989 AJ 98, 766

[30] B. Schulz, Linearization of ISOPHOT-P and C detector signals in OLP8", IDC PHT Internal Calibration Report, Version 1.0, 29-Sep-1999

[31] T. Müller & J.S.V. Lagerros, "Asteroids as far-infrared photometric standards for ISOPHOT", 1998, A&A 338, 340

[32] U. Herbstmeier, P. Abraham, D. Lemke, R.J. Laureijs, U. Klaas, K. Mattila, Ch. Leinert, Ch. Surace, M. Kunkel, "Small-scale structures in the far-infrared background", 1998, A&A 332, 739

[33] C. Gabriel, M. Haas, I. Heinrichsen, and W.-M. Tai, "The ISOPHOT Interactive Analysis - PIA User's Manual", 2000 (for PIA V9.0)

[34] D.K. Aitken & P.F. Roche, "8–13 μm spectroscopy of compact planetary nebulae and emission line objects", 1982, MNRAS 200, 217

[35] P.F. Roche, D.K. Aitken, & B. Whitmore, "8–13 μm spectral observations of eight moderately extended planetary nebulae", 1983, MNRAS 204, 101

[36] P.F. Roche & D.K. Aitken, "The infrared spectral properties of planetary nebulae", 1986, MNRAS 221, 63

[37] S.R. Pottash, A. Preite–Martinez, F.M. Olnon, Mo Jing–Er, S. Kingma, "IRAS spectra of planetary nebulae. III", A&A 161, 363, 1986

[38] H.J. Walker & I. Heinrichsen, "ISOPHOT Observations of Dust Disks around Main Sequence (Vega-Like) Stars", Icarus 143, 147, 2000

[39] C.S. Kiss, P. Ábarahám, U. Klaas, M. Juvela, D. Lemke, "Sky confusion noise in the far-infrared: Cirrus, galaxies and the cosmic far-infrared background", A&A 379, 1161, 2001

Acknowledgement
During the ISO Post Operations Phase (1998 – 2001) the ISOPHOT Data Centre at MPIA was supported by Deutsches Zentrum für Luft- und Raumfahrt e.V. (DLR) with funds of Bundesministerium für Bildung und Forschung, grant no. 50 QI 9801 3. During the ISO Active Archive Phase (2002 – 2006) the ISOPHOT Data Centre is supported by Deutsches Zentrum für Luft- und Raumfahrt e.V. (DLR) with funds of Bundesministerium für Bildung und Forschung, grant no. 50 QI 0201.